REPORT NO.
UCB/EERC-90/13
SEPTEMBER 1989

EARTHQUAKE ENGINEERING RESEARCH CENTER

THE EFFECTS OF TECTONIC MOVEMENTS ON STRESSES AND DEFORMATIONS IN EARTH EMBANKMENTS

by

JONATHAN D. BRAY
RAYMOND B. SEED
H. BOLTON SEED

Report to the National Science Foundation

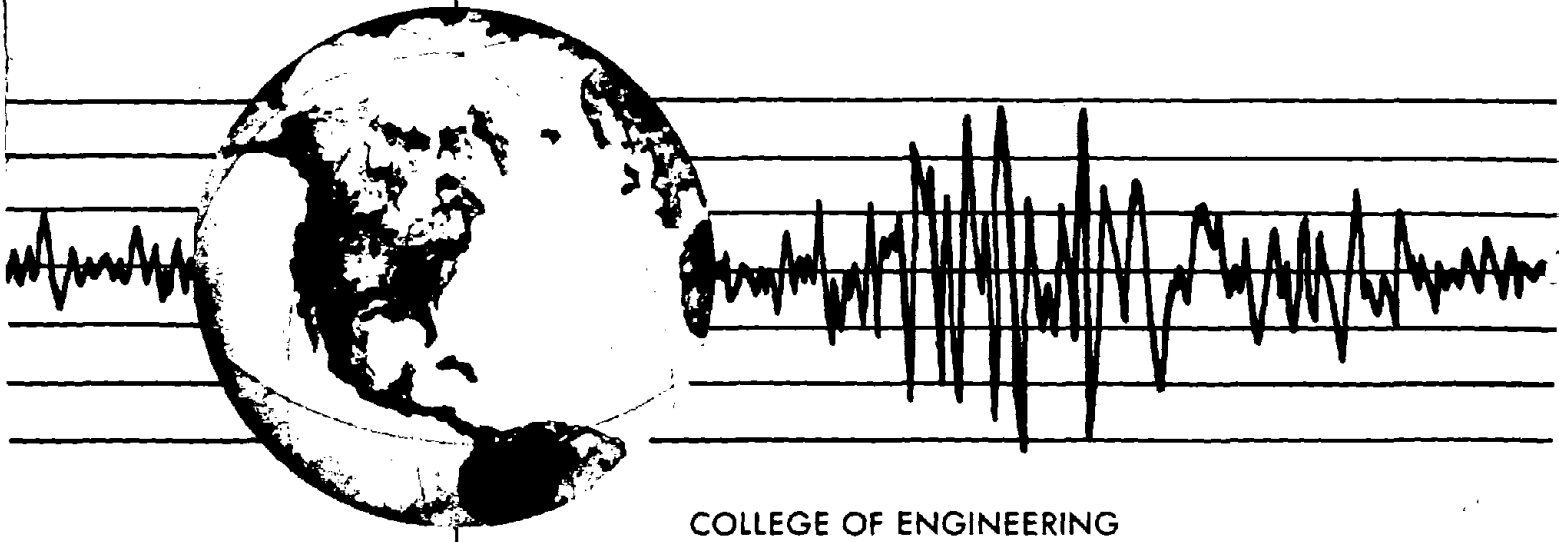

COLLEGE OF ENGINEERING

UNIVERSITY OF CALIFORNIA AT BERKELEY

For sale by the National Technical Information Service, U.S. Department of Commerce, Springfield, Virginia 22161

See back of report for up to date listing of EERC reports.

50272-101

REPORT DOCUMENTATION PAGE	1. REPORT NO. NSF/ENG-90007	2.	3. PB92-192996

4. Title and Subtitle
The Effects of Tectonic Movements on Stresses and Deformations in Earth Embankments

5. Report Date
September 1989

6.

7. Author(s)
Jonathan D. Bray, Raymond B. Seed, and H. Bolton Seed

8. Performing Organization Rept. No.
UCB/EERC-90/13

9. Performing Organization Name and Address
Earthquake Engineering Research Center
University of California, Berkeley
1301 So. 46th Street
Richmond, Calif. 94804

10. Project/Task/Work Unit No.

11. Contract(C) or Grant(G) No.
(C)
(G) MSM-8847137

12. Sponsoring Organization Name and Address
National Science Foundation
1800 G Street, N.W.
Washington, D.C. 20550

13. Type of Report & Period Covered

14.

15. Supplementary Notes

16. Abstract (Limit: 200 words)

To isolate critical parameters for a more in-depth study of their influence on how a soil mass responds to an underlying base rock fault displacement, previous investigations involving physical model tests and numerical analyses of the fault rupture propagation phenomenon are reviewed and evaluated. This literature review is extended to evaluate two closely related topics: anchor pull-out behavior and mining subsidence, in the hope that soil rupture behavior analogous to that observed during fault rupture propagation could be studied. Results from previous small-scale model studies involving testing of dry sands are found to provide particularly valuable insights, though the applicability of these studies to saturated clay soils is limited. In addition, this study presents the results of a program of base deformation testing using 1 g small-scale models composed of a weak saturated clay mixture, which demonstrated failure behavior in close agreement with that observed in the field. It was found that the height of the shear zone in the soil above the base rock fault rupture was controlled primarily by the amount of base movement and the stress-strain behavior of the soil. The numerical analyses suggest that the finite element method can be successfully applied to this class of problem provided that the soil's nonlinear stress-dependent stress-strain behavior is properly modeled. The results of these studies have led to the development of analytical techniques for modeling fault rupture propagation through overlying clays. Recommendations are developed for design provisions to minimize the potentially adverse effects of earthquake fault rupture propagation on dam stability and integrity.

17. Document Analysis a. Descriptors

b. Identifiers/Open-Ended Terms

c. COSATI Field/Group

18. Availability Statement:	19. Security Class (This Report)	21. No. of Pages
Release Unlimited	unclassified	448
	20. Security Class (This Page) unclassified	22. Price

(See ANSI-Z39.18) See Instructions on Reverse OPTIONAL FORM 272 (4-77)
(Formerly NTIS-35)
Department of Commerce

THE EFFECTS OF TECTONIC MOVEMENTS ON STRESSES AND DEFORMATIONS IN EARTH EMBANKMENTS

by

Jonathan D. Bray, Raymond B. Seed

and H. Bolton Seed

REPORT NO. UCB/EERC-90/13

September, 1989

Earthquake Engineering Research Center

University of California

Berkeley, California

ABSTRACT

Although much attention has been devoted to understanding the dynamic response of earth embankments to seismic loadings, relatively little effort has been devoted to improving our understanding of fault rupture propagation through soils. In particular, the effect of a base rock fault displacement on the integrity and serviceability of the saturated clay core of an overlying earth dam has not been explored fully. Yet, a number of earth dams have been constructed over potentially active faults. Since dam failures can be catastrophic events, it is prudent to attempt to gain an understanding of the phenomenon of base fault rupture propagation through overlying clays. This understanding would also assist engineers in siting and designing buildings and other critical facilities constructed in regions where clayey foundation soils overlie active faults.

It would seem appropriate to first review case histories which describe how earth dams respond to base rock fault displacements. Unfortunately, however, no well-documented case studies exist for this special case. Geologic studies of fault rupture, however, do provide insights into how soils respond to fault movements. For example, the changing surface expression of the Patton Bay Fault movement during the Great Alaskan Earthquake of 1964 indicates that different overlying soil deposits produce different types, orientations and magnitudes of surface displacement.

Although field investigations provide information which suggests a number of general trends, the case histories available exhibit variability because of the complexities of the geologic materials and processes involved. To isolate critical parameters for a more in-depth study of their influence on how a soil mass responds to an underlying base rock fault displacement, previous investigations involving physical model tests and numerical analyses of the fault rupture

propagation phenomenon have been reviewed and evaluated. In addition, the review of literature was extended to evaluate two closely related topics: anchor pull-out behavior and mining subsidence, in the hope that soil rupture behavior analogous to that observed during fault rupture propagation could be studied. Results from previous small-scale model studies involving testing of dry sands were found to provide particularly valuable insights, though the applicability of these studies to saturated clay soils is limited.

In addition to these reviews of case histories and previous research efforts, this study presents the results of a program of base deformation testing using 1 g small-scale models composed of a weak saturated clay mixture. A 3:1 mixture of kaolinite and sodium montmorillonite produces a material with undrained shear strengths on the order of 10-100 psf and well-scaled stress deformation behavior for small-scale model testing without the need for a centrifuge apparatus. The 1 g small-scale models tested demonstrated failure behavior in close agreement with that observed in the field. It was found that the height of the shear zone in the soil above the base rock fault rupture was controlled primarily by the amount of base movement and the stress-strain behavior of the soil.

The results from numerical analyses suggest that the finite element method can be successfully applied to this class of problem provided that the soil's nonlinear stress-dependent stress-strain behavior is properly modeled. Linear elastic and linear elastic-perfectly plastic constitutive models produced inconsistent results when employed in the finite element method, but nonlinear models provided significantly better predictions of observed behavior. The results of these studies have led to the development of analytical techniques for modeling fault rupture propagation through overlying clays.

Finally, lessons learned from previous studies and case histories of fault rupture propagation through earth dams; case histories and previous studies of

earthquake fault rupture propagation through soils; previous studies of two closely related topics: anchor pull-out and mining subsidence; 1 g small-scale model tests of fault rupture propagation through saturated clay; and finite element analyses of fault rupture propagation through saturated clay have been synthesized to develop recommendations for design provisions to minimize the potentially adverse effects of earthquake fault rupture propagation on dam stability and integrity.

ACKNOWLEDGEMENTS

The authors wish to thank Mr. Clarence Chan for his advice regarding the clay-box model tests, and Professor R. L. Taylor for the use of his graphics post-processor from the finite element analysis program PCFEAP. The tremendous support provided by Elizabeth Turner was also instrumental to completing this research project, and her support is greatly appreciated.

The authors are indebted to the National Science Foundation, whose 3 year graduate fellowship support for the first author made this research effort possible. Additional support was provided by the National Science Foundation under Grant No. MSM-8847137, and this support is gratefully acknowledged.

TABLE OF CONTENTS

LIST OF TABLES

LIST OF FIGURES

LIST OF SYMBOLS

B	-	Width of base
B	-	Bulk modulus (used in conjunction with the Duncan et al. (1984) hyperbolic soil model in Chapters Seven and Eight)
C	-	Undrained shear strength of saturated cohesive soil
c'	-	Effective stress strength envelope cohesion intercept, or effective soil cohesion
C_u	-	Coefficient of uniformity of soil = d_{60}/d_{10}
d	-	Diameter of soil particle
d_{10}	-	Soil particle size for which 10% by weight of soil particles are smaller
d_{60}	-	Soil particle size for which 60% by weight of soil particles are smaller
d_{85}	-	Soil particle size for which 85% by weight of soil particles are smaller
d_{90}	-	Soil particle size for which 90% by weight of soil particles are smaller
d_b	-	Vertical upward displacement of base section
d_f	-	Vertical upward displacement of base section at failure
D	-	Depth
D_S	-	Depth of soil
d_b/D_S	-	Normalized vertical base displacement
D/B	-	Ratio of the depth of the anchor to the width of the anchor plate
$(D/B)_{CRIT}$	-	Value of D/B that distinguishes when an anchor behaves as a shallow or deep anchor
e	-	Void ratio

E	-	Young's Modulus of Elasticity
E_i	-	Initial tangential Young's Modulus of Elasticity
E_t	-	Instantaneous tangential Young's Modulus of Elasticity
E_{ur}	-	Young's Modulus of Elasticity for unloading and reloading
h_f	-	Vertical height of shear rupture zone in soil overlying displaced base section
h_f/d_b	-	Normalized vertical height of shear rupture zone in soil overlying displaced base section
H	-	Height
K	-	Young's Modulus number
K_b	-	Bulk modulus number
K_o	-	Coefficient of lateral earth pressure at rest: $K_o = \sigma_3'/\sigma_1'$
K_{ur}	-	Unloading/reloading Young's Modulus number
L	-	Length
m	-	Bulk modulus exponent
M_L	-	Local magnitude of earthquake (Richter Magnitude)
n	-	Young's Modulus exponent
p'	-	Vertical effective stress
P_a	-	Atmospheric pressure (1 bar)
PI	-	Plasticity index of soil
R_f	-	Failure ratio
S_u	-	Undrained shear strength of saturated clay
SL	-	Stress level: $SL = (\sigma_1 - \sigma_3)/(\sigma_1 - \sigma_3)_f$
SS	-	Stress state: $SS = SL \cdot \sqrt[4]{\sigma_3'/P_a}$
$SS_{max\ past}$	-	Maximum past stress state
u	-	Porewater pressure

v	-	Angle of dilation: $\sin v = -(\dot{\epsilon}_1 + \dot{\epsilon}_3)/(\dot{\epsilon}_1 - \dot{\epsilon}_3)$
v_{ps}	-	Plane strain angle of dilation
w_c	-	Water content of soil
z	-	Depth below the ground surface
β	-	Orientation of the failure plane in a soil mass relative to the major principal stress direction in degrees: $\beta = 45° - \phi'/2$
ϵ	-	Axial failure strain
$\dot{\epsilon}_1$	-	Major principal strain rate
$\dot{\epsilon}_3$	-	Minor principal strain rate
ϵ_a	-	Axial failure strain
ϵ_f	-	Axial failure strain at failure (maximum deviatoric stress)
λ	-	Geometric scale ratio
γ	-	Unit weight of soil
γ_d	-	Dry unit weight of soil
γ_m	-	Moist unit weight of soil
$\Delta\phi'$	-	Reduction in friction angle per log-cycle increase in σ_3'
ν	-	Poisson's ratio
σ_1	-	Major principal total stress
σ_1'	-	Major principal effective stress
σ_3	-	Minor principal total stress
σ_3'	-	Minor principal effective stress
$(\sigma_1 - \sigma_3)$	-	Deviatoric stress
$(\sigma_1 - \sigma_3)_f$	-	Deviatoric stress required to cause failure
$(\sigma_1 - \sigma_3)_{ult}$	-	Theoretical asymptote of the hyperbolic function
ϕ	-	Soil friction angle
ϕ'	-	Effective stress soil friction angle
ϕ_{ps}	-	Plane strain soil friction angle

θ - Angle between the stress characteristics and the velocity characteristics: $\theta = 1/2(\phi - \nu)$

CHAPTER ONE:
INTRODUCTION

Over the past three decades, much attention has been devoted to understanding the dynamic response of earth embankments to seismic loadings. Relatively little effort, however, has been devoted to improving our understanding of the effects of a base rock fault movement on the stability and safe performance of an earth dam. In particular, the effects of a base rock fault displacement on the integrity and serviceability of the saturated clay core of an overlying earth dam have not been explored fully. Moreover, the phenomenon of fault rupture propagation through overlying soil deposits is not yet well understood.

Although engineers generally try to avoid building dams over potentially active faults, a number of earth dams have been constructed over potentially active faults. A partial list of earth dams known to be built over potentially active faults is presented in Table 1-1. In fact, in seismic zones, it is becoming increasingly difficult to avoid faults in the foundation as feasible alternate dam sites may not exist. Also, potentially active faults may not be discovered at the chosen dam site until a comprehensive site investigation is performed or until excavation of the dam's foundation is initiated; after which point much time and money has already been devoted to building the dam at the selected site. For example, the existence of potentially active faults was not suspected at the Cedar Springs Dam site in San Bernadino County, California until construction of the earth dam foundation was initiated. Similarly, faults located at the proposed location of the Auburn Dam in Placer County, California were not judged to be potentially active until a considerable amount of time and money had been expended in site investigations and in the preliminary design of the dam.

Table 1-1: EXAMPLES OF EARTH DAMS BUILT OVER POTENTIALLY ACTIVE FAULTS

Dam	Location (County & State)	Height (ft)	Fault
Cedar Springs	San Bernadino, Calif.	236	Cleghorn
Calaveras	Alameda, Calif.	210	near Calaveras
Austrian	Santa Clara, Calif.	185	near San Andreas
Los Angeles	Los Angeles, Calif.	150	near San Fernando
Coyote	Santa Clara, Calif.	140	Calaveras
Henshaw	San Diego, Calif.	123	Elsinore
Temescal	Alameda, Calif.	116	Hayward
Hebgen	Gallatin, Montana	90	near Hebgen
Lower Karori	New Zealand	82	Wellington
Quail Lake	Los Angeles, Calif.	45	San Andreas
Lower Howell	Santa Clara, Calif.	39	San Andreas
Lake Ranch	Santa Clara, Calif.	38	San Andreas
Upper Howell	Santa Clara, Calif.	36	San Andreas
Palmdale	Los Angeles, Calif.	34	San Andreas
Harold	Los Angeles, Calif.	30	San Andreas

Since dam failures can be catastrophic events, it is prudent to attempt to gain an understanding of the phenomenon of fault rupture propagation through earth embankments. This understanding would also assist engineers in siting and designing critical buildings, utility and transportation systems, and other types of facilities constructed in regions where soils overlie potentially active faults.

The phenomenon of fault rupture propagation through overlying soils is quite complex, and is not well understood at this time. The National Research Council Panel on Earthquake Problems Related to the Siting of Critical Facilities expressed this strong concern (National Academy of Sciences, 1980):

> The problem [fault rupture propagation through soils] is worthy of more general study . . . The Panel believes there is no question that our understanding of surface faulting features and how they might affect a given site could be enhanced by further model studies, theoretical approaches, and field studies of historical and Quaternary faulting and its relationship to other geologic processes.

Hence, there is a need to improve our current level of understanding of fault rupture propagation through soils and the resulting potentially hazardous effects of tectonic movements on the stability of earth dams.

How would an earth dam respond to a fault offset in its foundation? One might suspect that the dam might crack, but how much? How extensive would shear or tension zones be? Would uncontrollable leakage of the reservoir water impounded behind the earth embankment initiate? Might this lead to uncontrolled internal erosion? These types of potential concerns can be be divided into six basic categories as exemplified by the following six critical questions which must be addressed when designing an earth dam to be located over a potentially active fault:

(1) What is the extent of the likely shear rupture zone with increasing magnitudes of base deformation?

(2) What will be the extent of tension zones or zones of potential hydraulic fracturing with increasing magnitudes of base deformation?

(3) How much reservoir water could leak through disturbed core and filter zones or through a disturbed foundation, and might this result in uncontrolled internal erosion?

(4) How might the base deformation damage the slopes and crest of the earth dam?

(5) Given the potential hazards associated with fault rupture propagation through an earth dam, what are the characteristics of the dam core material which can best mitigate these hazards?

(6) What other steps or design features are necessary for the safe construction of a dam over a potentially active fault?

This study represents an attempt to further develop the knowledge and understanding of the fault rupture propagation phenomenon, and hence, is a necessary step in developing answers to these critical questions.

As mentioned, the attempt to gain insight into the complex fault rupture propagation phenomenon is a difficult task. A number of variables can significantly influence the nature of fault rupture propagation through soils. Any real soil deposit is likely to be significantly nonhomogeneous. Existing planes of weakness or rigid inclusions within a weaker soil mass will certainly cause the fault rupture pattern observed in the field to deviate from any fault rupture pattern predicted by theories based on the assumption of homogeneous soil masses. Additionally, the soil may be saturated or partially saturated, it may exhibit varying degrees of anisotropy, it may be cohesionless or cohesive, and it may display contractive or dilative volume-change tendencies during shear rupture. Time effects may be significant. Earthquake shaking, in conjunction with the movement

across the fault, may alter the response of the overlying soil deposit. The geometry of the soil mass overlying the base rock fault (e.g. level or unlevel ground; shallow or deep soil deposit; soil types and conditions; and the three dimensional shape and internal geometry of the earth mass or embankment) may influence the fault rupture propagation process. Of course, the type of fault movement and the orientation of the fault relative to the earth structure will exert considerable influence on the behavior of the soil during fault rupture propagation.

This investigation will concentrate on studying the effects of variations in the most significant of these variables, and will accept that some limits will persist in the level of accuracy and reliability which can be achieved in analyses of the fault rupture propagation phenomenon. Nonetheless, the study of fault rupture propagation through soil can provide invaluable lessons regarding the design of earth embankments over potentially active faults.

The first stage of these studies consisted of a review and evaluation of previous studies and case histories which describe how earth dams respond to base rock fault displacements. No well-documented case studies exist, however, for this special case. Hence, the literature review was increased in scope to include a review and evaluation of geologic field studies, physical small-scale model studies, and numerical analyses of fault rupture propagation. The literature review was also extended to include the review and evaluation of prior studies dealing with two closely related topics, anchor pull-out behavior and mining subsidence, in the hope that soil behavior analogous to that displayed during fault rupture propagation through soils could be observed. This reasonably comprehensive review of the fault rupture propagation phenomenon, presented in Chapters Two through Five, provided valuable insights into the earth dam/fault rupture problem.

Still, shortcomings in the adequacy of our current level of understanding persisted. Although the field investigations provide information which may suggest

general behavioral or phenomenological trends, the surface faulting case histories exhibit considerable variability because of the complexities of the geologic materials, stratification and processes involved. Moreover, the results from most previous physical model studies and numerical (analytical) model studies employed dry sands; although these provide valuable insights, the applicability of these results to saturated clay soils is limited. The core is the critical component of an earth dam. Since the majority of earth dams possess cores constructed of nearly saturated clayey materials, this study focussed on development of an improved understanding of the phenomenon of base fault rupture propagation through overlying clays.

In Chapter Six, the results from a program of base deformation testing on a series of 1 g small-scale physical models composed of a weak saturated clay mixture are presented. Previous studies had shown that a 3:1 mixture of kaolinite and sodium montmorillonite would produce a material with controllable undrained shear strengths on the order of 10-100 psf and well-scaled stress deformation behavior for small-scale model testing without the need for a centrifuge apparatus. The 1 g small-scale models tested demonstrated failure behavior in close agreement with that observed in the field and provided key insights into the phenomenon of fault rupture propagation through saturated clay.

To isolate critical parameters for a more in-depth study of their influence on how a saturated clay soil responds to a base rock fault displacement, numerical analyses were then performed, and these are described in Chapters Seven and Eight. Comparison of the results from the numerical analyses with both observations from field case studies as well as with the results of the 1 g small-scale model tests described in Chapter Six, suggests that the finite element method can be successfully applied to the fault rupture propagation problem provided that the soil's nonlinear, stress-dependent stress-strain behavior is adequately modeled. Linear elastic and linear elastic-perfectly plastic constitutive models produced

inconsistent results when employed in conjunction with the finite element method, but relatively simple nonlinear soil behavior models provided significantly better predictions of observed behavior. The results of the 1 g small-scale model tests described in Chapter Six and the results of previous well-documented model studies of anchor pull-out were used as a basis for the evaluation of the accuracy and the reliability of the analytical procedures applied in this study. Additionally, the general trends of soil behavior during fault rupture propagation observed in field case histories and previous model studies were used to validate the applicability of the analytical procedures employed in this study. Good agreement between the numerical analyses, the 1 g small-scale model study, and case histories and previous studies of fault rupture propagation provides strong support for the accuracy and usefulness of the analytical methods employed in this research.

The results of this research have led to the development of analytical techniques for modeling fault rupture propagation through overlying clays, and to the development of recommendations for design provisions to minimize the resulting potentially adverse effects on dam stability and integrity. These are discussed and summarized in Chapter Nine, which also presents recommendations for further research in this area.

CHAPTER TWO:
REVIEW AND EVALUATION OF PREVIOUS STUDIES OF FAULT RUPTURE PROPAGATION THROUGH EARTH DAMS

2.1 Introduction

The phenomenon of fault rupture propagation through overlying soils is quite complex, and is not well understood at this time. To provide insights into this class of problem, an extensive review of literature was performed to identify previous work in this area. Because of the limited number of works concentrating on this class of problem, the literature review was increased in scope to identify related field case histories, physical model studies, and numerical analyses which might improve our understanding of how movement on a bedrock fault might propagate through overlying soils. Hence, literature in the fields of seismology, geology, mining engineering, numerical modeling, and geotechnics was reviewed. The results of this review of literature and an evaluation of prior field and model studies of fault rupture propagation, as well as related areas of study, and the principal lessons to be learned from them are presented in the following four chapters.

Chapter Two is organized into four sections. Following this introduction, previous studies of the effects of fault rupture on the performance of earth dams are reviewed in Section 2.2. Next, earth dam fault offset case histories are described and reviewed in Section 2.3. Section 2.4 summarizes the lessons to be learned from these previous studies and case histories of fault rupture propagation through earth dams. As discussed, the literature review was extended in Chapter Three to investigate available earthquake surface rupture case histories. Additionally, physical and numerical model studies of the fault rupture propagation phenomenon are reviewed and evaluated. The principal lessons to be

learned from the surface rupture case histories and the model studies of fault rupture propagation are also described. Considerable effort has been devoted in the past to improving our understanding of the anchor pull-out problem. Chapter Four presents illustrative studies in this area in the hope that soil behavior analagous to how soil responds to an earthquake fault movement in its foundation might be observed Likewise, the mining subsidence/earthquake fault analogy is explored. Finally, in Chapter Five, key findings from the overall review and evaluation of all of these case histories and studies are summarized, and shortcomings in our current knowledge that warrant further field, laboratory and analytical study are identified. Chapters Two, Three, Four, and Five thus comprise a reasonably comprehensive review of the current state of knowledge regarding fault rupture propagation through soils, as well as related areas of study.

2.2 Previous Studies of the Effects of Fault Rupture on the Performance of Earth Dams

2.2.1 General:

Although much attention has been devoted to understanding the dynamic response of earth embankments to seismic loadings, relatively little effort has been devoted to improving our understanding of the effects of fault rupture on the stability of earth dams. In fact, a comprehensive review of literature found only seven works which directly addressed this problem. These works are summarized herein and critical insights as well as potentially dangerous misconceptions from these works are described.

2.2.2 Louderback (1937):

Louderback (1937) provided the first comprehensive study of the effects of faulting on dams in his classical paper, "Characteristics of Active Faults in the

Central Coast Ranges of California, with application to the Safety of Dams". This paper demonstrated Louderback's keen perception. He began, "In the search for reservoir sites in the Coast Ranges of Central California, engineers since the early days of such activity, have found the most satisfactory topographic features in fault-line valleys." His paper attempted to answer the critical question that he posed in the introduction, "Can a safe dam be built in a fault-line valley of a presumably active fault, and, if so, what conditions should be fulfilled?" Louderback's paper was organized into three main sections: the observed effects of faulting on dams as a result of the 1906 and 1868 earthquakes in the San Francisco Bay area, a general discussion of the character of active faults and their movement, and the application of the 1930's state-of-the-art knowledge in this field to the design of Coyote Dam.

After investigating the effects of the 1906 rupture along the San Andreas fault (principally a strike-slip fault movement) on four dams - the San Andreas Dam, the Upper Crystal Springs Dam, the Lower Crystal Springs Dam, and the Old San Andreas Dam - Louderback concluded that ". . . the conditions involved were so special that very little critically important evidence was obtained . . ." The specifics of this event will not be discussed here as the facts will be fully described in Section 2.3.2. At this time it is important to note that Louderback emphatically concluded:

> It may be stated definitely that up to the present no satisfactory observational data have been obtained, along these California fault lines of comparatively recent disturbance, on the behavior of dams simultaneously affected by fault displacement across a critical section and earthquake shock, and, as far as the writer is aware, no such data have been obtained in any other locality.

Because of the risk to the safety of life and property, Louderback felt compelled to continue his search for the answer to his question, can a safe dam be to be built over an active fault? Hence, for the majority of his paper, Louderback,

an eminent professor of geology, summarized the current understanding of fault movement in the hope that this general knowledge would assist the practicing engineer in designing dams to be built over potentially active faults. He confined his study to the major fault zones in the San Francisco Bay area - the San Andreas, the Hayward, and the Calaveras faults. All of these faults display principally strike-slip motion, so his discussion was applicable only to similar fault movements. The characteristics of thrust and normal fault movements were not examined.

First, Louderback stressed the importance of determining whether existing faults at the dam site were active or not. If a fault repeatedly offset overlying deposits during Quaternany time (e.g. a young alluvium), it must be characterized as active and future movements would be inevitable. Although the fault zones studied often displayed broad shear zones that could extend over a mile or more in width, the greater part of any fault movement was limited to a single narrow zone.

Louderback continued by noting that fault displacements would probably occur along existing fractures and would most likely occur along those most recently disturbed. Yet, the possibility of movements along other "inactive" fractures could not be ignored. The 1906 San Francisco fault movement provided the principal evidence for Louderback's assertions. Drawing from this experience, he recommended that dams be designed for a direct horizontal offset of 15 feet along a single shear zone and a distributed horizontal displacement of 20 feet across a wider shear zone. The magnitude of vertical displacements along these strike-slip faults should be determined by investigating offsets in the dam site area. Louderback proposed an allowance for a maximum vertical displacement of 10 feet (as a graben or wedge-block depression), although he felt 5 feet would probably provide sufficient safety.

In addition to these movements along the fault plane, Louderback expressed concern over movements normal to the faults. Buckling of fences and

sagging of telephone lines across the San Andreas fault trace demonstrated that " . . . there was evidently a definite compression normal to the fault line." The slight compressional effect observed would not likely cause an earth dam to fail, (although it could shear or crush a rigid structure), but a tensional effect could lead to disastrous results. Although evidence for such a tensional effect was meager, Louderback felt that the possibility of an open fissure could not be excluded. In fact, Louderback recommended that the design consider the possibility of a permanent opening not exceeding 12 to 18 inches in width in the dam. He supported his concern for the development of a tensional effect across a strike-slip fault with the eyewitness accounts of a fault fracture that reportedly gaped open during the 1906 earthquake, swallowed a cow, and then closed again leaving only the cow's tail visible above the surface. Furthermore, Louderback cited historic records of fault fissures that remained open after movement on the Hayward fault in 1868, and geologic records which showed pebbles of an overlying formation in the fault gouge in the Hayward fault shear zone. Louderback did not acknowledge the possibility that these open fractures might be secondary ground movements from liquefaction or gravitional landsliding. Finally, Louderback noted that the spreading effect which created subsidence zones would be accounted for by the vertical displacement criterion already described.

With respect to dam design, Louderback recommended constructing outlet pipes and spillways parallel to developed zones of localized movement to preclude the certainty of rupturing these systems if they were placed across active fault traces. Nevertheless, cracking or rupturing of these water control systems should be expected. He added "The impervious member of the dam should be so designed that rupture and differential displacement will not jeopardize the structure." The design of Coyote Dam, which will be discussed next, provided an example of what Louderback believed to be an "acceptable" dam core design.

Furthermore, Louderback warned that the dam must be designed to withstand the other hazards of earthquake events, such as earthquake shaking, landsliding, and wave action. Moreover, faults, being lines of weakness, must not jeopardize the static stability of the earth dam.

In the final section of his paper, Louderback described the reasoning used by the State-appointed consulting board to oversee the design and construction of the Coyote Dam over the combined general shear zones of the Hayward and Calaveras faults. The maximum height cross-section of the Coyote Dam is shown in Figure 2-1. The dam's principal features to guard against instability as a result of base fault movement were:

1. The fault movement must not completely rupture the dam's impervious element. "This precludes the use of a rigid type of dam, a concrete water face, or a core wall of concrete or a narrow puddle." The use of compacted earth materials was considered preferable.
2. The dam core should be wide enough to accommodate differential movement. To protect against a 20 foot strike-slip offset, the core was designed to be as wide as six times the vertical head at any height and 60 feet wide at the crest. Side slopes were 2H:1V. The impervious member was protected on the upstream and downstream side by wide rock and gravel fill zones with flat outside slopes.
3. A zone of gravel was placed directly against the core so that if a fissure opened in the dam, the gravel would fall into the void, seal it and prevent further erosion.
4. A liberal freeboard protected against differential vertical displacements.

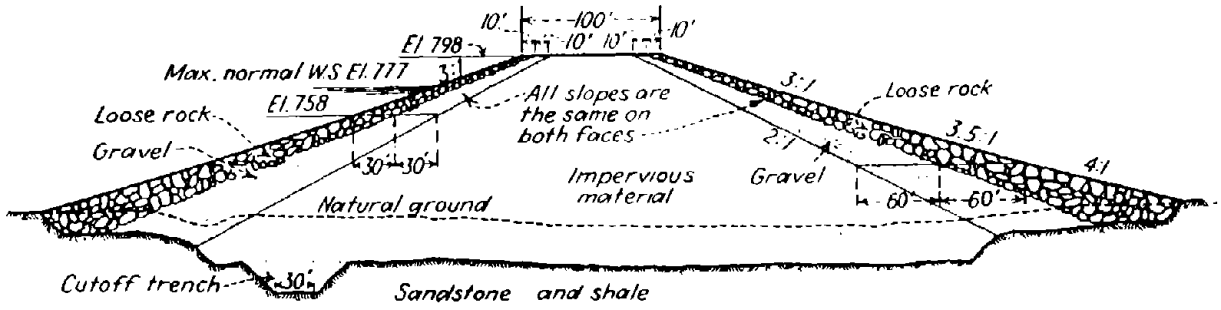

Figure 2-1: CROSS SECTION OF THE COYOTE DAM (after Tibbetts, 1936)

5. The spillway and outlet works were sited so as not to traverse the primary shear zones.
6. The fault's crush and gouge zones were excavated and backfilled to ensure cut-off of groundwater flow.

Louderback, a member of this consulting board, believed adherence to these principles provided Coyote Dam with the capability to safely withstand a fault movement across it. Therefore, Louderback answered that yes, a safe dam can be built across an active fault and he explained in detail the conditions which must be fulfilled in this case to ensure the safety of Coyote Dam.

2.2.3 Sherard (1966 & 1967):

The State of California Department of Water Resources employed James L. Sherard to develop recommendations for the design of an earth dam to withstand the hazards of earthquakes. Sherard's 1966 final report as well as a follow-up 1967 article in the ASCE Geotechnical Journal, summarized his findings (Sherard, 1966; Sherard, 1967). Although his study concentrated primarily on the effects of seismic shaking, Sherard recognized the hazards of fault movement in a dam's foundation and he provided guidance for mitigation of the associated potential hazards. Sherard felt that a safe dam could usually be built over a potentially active fault. Large movements on a fault passing transversely through a dam, however, presented special difficulties. In cases where a rupture across the dam cross-section could form, he recommended that every effort should be made to find an alternate dam site.

Sherard's primary concern was the development of concentrated leaks in the dam. Like Louderback, Sherard expressed concern over the possibility of faults gaping open momentarily during slippage. Sherard noted, however, that no evidence supported this concern. In fact, he quoted Dr. Clarence Allen, an

experienced engineering geologist, who said, "Everything we know about faulting indicates that it is a compressional phenomenon involving shearing, not tension." Sherard felt that the stretching of a dam because of the orientation of a fault to the axis of the dam was a more reasonable concern (See Figure 2.2). "A few feet of displacement on a fault of this kind [one which stretches the longitudinal axis of the dam] may create a more serious situation than a movement of 10 or 15 feet which does not have an appreciable component acting to stretch the dam."

After summarizing his experience observing surface fault ruptures (through soils, though not through dams or embankments), Sherard emphasized the variability of fault rupture propagation. Usually most of the differential movement was concentrated along a distinct shear plane. However, a number of cases reinforced Sherard's concern for designing for a more complex pattern of movement. Movement could be distributed over a wide gouge zone. Subsidiary faults away from the main fault rupture may displace a significant amount. Rock joints or cracks in rock might be pulled open an inch or two. Records of changes in a region's groundwater flow pattern after an earthquake suggested that joints in the foundation rock may open and close as a result of base rock movement. Hence, the post-earthquake effectiveness of grout curtains must be questioned. Although Sherard admitted that several of the experts who reviewed his report believed he overemphasized these secondary crustal deformations, Sherard felt that a conservative dam designer should anticipate these movements. Two of his expert reviewers remarked that an isolated movement of a foot or two would not modify the design of earth dams with which they were familiar.

Sherard's report also described the need for, and the conduct of, a geologic evaluation of the region surrounding a potential dam site. If a fault was discovered at the site, it was prudent to study the surface geology over an area within a radius of 10 miles or more. Trenching, tunneling, inclined boring, and aerial photography

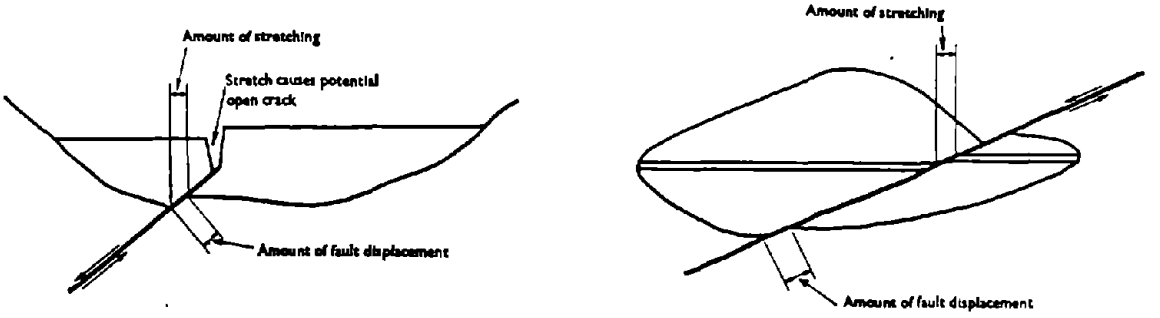

Figure 2-2: FAULT MOVEMENTS WHICH CAN STRETCH A DAM (after Sherard et al., 1974)

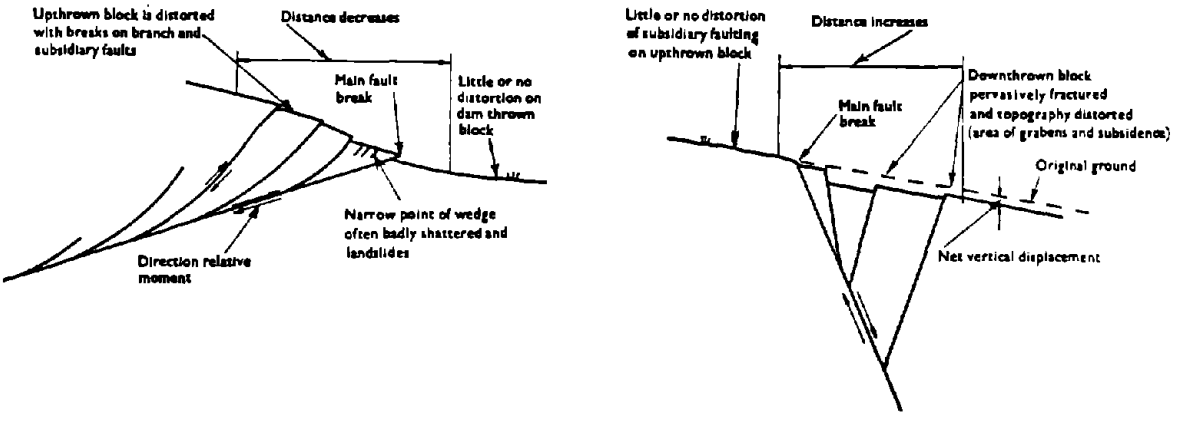

(A) Thrust Fault

(B) Normal Fault

Figure 2-3: CHARACTERISTICS OF THRUST AND NORMAL FAULTS (after Sherard et al., 1974)

were considered essential parts of the geological study. To assist the engineer in preliminary design, Sherard recommended utilizing these design assumptions: (1) rupture and increased permeability of the grout curtain if tension cracks or opening of joints were expected, (2) 2 feet of movement in any direction on active secondary faults (less than a mile long) and inactive major faults (10 miles long or more), and (3) a minimum of 10 feet of movement in the direction geologic evidence suggested for major faults not judged to be inactive. Furthermore, Sherard advised, "Because the water pressure is an important factor in the majority of these modes of failure; it seems reasonable to deduce that the risk of complete failure may increase rapidly with the [dam's] height, probably at least with the square." Accordingly, he added, " . . . the degree of conservatism justified should be considered to depend to a great extent on the dam height."

Of the techniques Sherard recommended utilizing to mitigate the hazards of earthquake faulting, he continually emphasized four principal defensive design measures. First, the inherent resistance to erosion of the foundation materials was the most critical factor to consider in the design of the dam built over an active fault. Erodible soil or weak rock should be avoided, excavated, or improved in situ. Special attention should be devoted to determining the erosion resistance of the fault gouge material. The zoning of the earth embankment was another important concern. Any earth dam in an earthquake area should be expected to develop concentrated leaks. Hence, all of these dams should have at least a cohesionless chimney filter and drainage system along the downstream face of the core which extended the full height of the dam. A homogeneous dam designed with a downstream horizontal drain or toe drain was inadequate. A single, wide transition or filter zone (wider than the anticipated fault offset) consisting of a well-graded mixture of sand and gravel was considered to be one of the best lines of defense available. After fault offset, this zone would remain continuous and the

"self-healing" properties of the sand-gravel mixture would plug concentrated leaks. To provide a secondary line of defense, the core material should possess some inherent resistance to the damaging effects of concentrated leakage. Drawing upon his pioneering work concerning the erosion resistance of earth materials, Sherard considered "good" core materials to be either a well-graded mixture of sand, gravel, and clayey fines where D_{85} is coarser than 1 inch, or a highly plastic, tough clay with a plasticity index greater than 20. Low plasticity clays (PI < 8), silts of medium to high plasticity, and medium to fine uniform sands with cohesionless fines were "poor" core materials. Finally, Sherard's last important design consideration was to reinforce the top of the earth dam section. Sherard found the top of the dam to be most vulnerable because it was the thinnest part of the dam and the place where the core was most likely to be damaged by cracks which could remain open due to low confining stresses.

In his study, Sherard focused the engineer's attention on the need to recognize and design against the hazards of earthquakes, including the specific hazard of fault movement in the foundation of an earth dam. Because examples of how full-scale earth dams responded to fault offsets in their foundation did not exist, Sherard's study relied primarily on the engineering judgment he developed by observing surface fault ruptures, testing the erosion resistance of earth materials, and his considerable personal experience in designing earth dams.

2.2.4 Sherard, Cluff, and Allen (1974):

In 1974, Sherard joined with Cluff and Allen to publish a landmark study of the effects of faulting on the design of earth dams (Sherard et al., 1974). In their article "Potentially Active Faults in Dam Foundations", these authors presented the most comprehensive examination of this subject to date. The paper reviewed cases of fault movement near dams, described the special design details of existing dams

built over potentially active faults, summarized the authors' observations of surface fault breaks, provided guidance in the conduct of geological studies of fault activity, and, finally, recommended critical features to incorporate in the future design of earth dams to be built over potentially active faults.

Sherard, Cluff, and Allen had considerable experience in the fields of earth dam design, seismicity, and geology. It was their opinion that in some highly seismic regions, such as California, the occurrence of faults in dam foundations was the rule rather than the exception. In fault-controlled geology, rivers often followed faults because faulting produced zones of weak, crushed rock. Hence, Sherard et al. stressed the need to perform a comprehensive geologic investigation of every dam site within an earthquake region to identify faults and to characterize their level of activity. They suggested a two-phase investigation program. Initially, the regional geology and seismicity over an area extending up to 100-200 miles from the dam site should be studied. In the second phase, detailed geological mapping should be conducted at all locations where faults might exist. The authors emphasized the usefulness of aerial photography in both phases of the investigation. Additionally, they stressed the importance of studying the character of identified faults a considerable distance from the dam site. A fault which showed no signs of recent movement at the dam site may have displayed conclusive evidence of recent movement away from the site.

Although a number of dams had been built over faults, the authors found no instance where a fault in the foundation of a dam had displaced during an earthquake. They did, however, review a number of cases described as "near misses". These case histories will be addressed in detail in Section 2.3. They are the 1906 San Francisco earthquake, 1959 Hebgen earthquake, and the All-American Canal offset in 1940. In addition to these cases, the authors reviewed the failure of Baldwin Hills reservoir in 1963. Without the occurrence of a strong

earthquake, a fault in the Baldwin Hills Dam's foundation moved a few inches, breaking the compacted clay reservoir lining. A concentrated leak along the fault eventually eroded the cohesionless fine sand and silt deposits comprising the dam's foundation. Once initiated, the piping phenomenon continued until the dam failed. They noted that the Baldwin Hills reservoir failure illustrated the importance of controlling the flow of water through an earth dam and of preventing the movement of soil in areas where concentrated leaks may develop.

Without actual dam foundation faulting case histories, Sherard et al. relied upon their experience observing the occurrence of surface fault ruptures during strong earthquakes to predict how fault movements may disrupt a dam. Their review of fault rupture behavior provided salient lessons to the dam designer. Fault breaks usually occurred on existing fractures. Normally, sufficient prior evidence existed to conclude that these faults were potentially active. Of the three types of faulting: thrust, normal, and strike-slip, thrust faulting was believed to be most dangerous to an earth dam. Strike-slip faults were considered to be the least dangerous. Of course, as Sherard described in his earlier papers, the orientation of the fault to the axis of the dam was at least as important as the fault type. Nevertheless, the authors found that the fault type determined the amount and location of movement on secondary features. As shown in Figure 2-3, thrust faults may distort the upthrown block but leave the downthrown block relatively undisturbed, whereas normal faulting produced secondary fracturing primarily above the downthrown block. Strong earthquakes may deform the ground surface to distances of a few miles or tens of miles from the main fault. These secondary crustal deformations were more frequent with thrust faults and less likely with strike-slip faults. The engineer should anticipate at least small adjustments on faults or fractures located in seismic areas. Moreover, since these small fractures are difficult to identify, they should be assumed to exist in any region close to a

major fault. Furthermore, sufficient evidence existed to conclude that filling a reservoir may trigger strong earthquakes ("reservoir-induced seismicity"). The possibility of widespread ground movements precluded the use of concrete dams in seismic regions, as only an inch or two of differential movement at a critical location could be unacceptable. On the other hand, the authors believed that a conservatively designed earth dam could be safely constructed over potentially active faults.

Sherard et al. cited two reasons for their confidence in their ability to design a safe dam to be built over a potentially active fault. First, history indicated that the practical maximum fault offset was on the order of 20 to 25 feet. Furthermore, the average displacement along a fault for this worst case was less than 50% of the maximum displacement, or less than 10 feet. For the majority of cases where faults moved, the magnitude of the displacement or offset along most of the fault was much less than this. Since the critical zones of an earth dam could be made much thicker than these expected offsets, they felt that dams could be safely designed to withstand the hazards associated with earthquake faulting. Finally, theory and experience demonstrated that leakage through a dam could be controlled by proper zoning of the earth dam materials. The authors emphatically concluded,

> There is no doubt concerning these conclusions . . . as long as the flow entering the downstream rockfill zone is controlled (choked) by the permeability of the finer transition material upstream, the flowing water entering the [downstream] rockfill zone cannot cause threat of instability. . . . even if a large open crack develops in the impervious core the maximum leakage will be limited by the permeability of the transition material to a volume which can be controlled safely.

The cohesionless transition zone and the downstream rockfill zone comprised the two main elements of a safe dam over an active fault. The authors maintained that the properties of the impervious core material were much less

important. In fact, a "safe dam can be made using a core material of any type." Figure 2-4 illustrates what Sherard et al. believed to be the two critical elements of a "fundamentally safe" earth dam. The gradation of the crack-proof well-graded sand-gravel mixture is also provided. These design recommendations were based on the authors' assertions that cracks cannot exist in a cohesionless material and that a well-graded material will eventually heal itself or plug any concentrated leak through it.

The authors noted, however, that the quality of the foundation materials and the width and freeboard of the dam crest could not be overlooked. Their "fundamentally safe" dam had to be constructed on a stable foundation not susceptible to erosion. Additionally, the earth zones at the crest must be wide enough to permit the expected offset without becoming discontinuous. Finally, sufficient freeboard must be available to allow for the development of cracks in the top of the dam, where confining pressures are quite low, without permitting an overtopping failure mode to initiate. Depending on the cohesiveness of the earth materials, adequate freeboard was defined as within the range of 10 - 30 m.

In developing these design recommendations, Sherard et al. reviewed the concepts employed in the design of a number of dams built over known active faults. Of these dams, the authors felt that the Cedar Springs Dam shown in plan and cross-section view in Figure 2-5 possessed all of the critical elements of a safe dam built over an active fault. During construction of the dam foundation, several faults were discovered and found to be potentially active. Because of this discovery, the dam was redesigned to improve its ability to withstand the hazards associated with earthquake faulting. The dam height and reservoir storage volume were reduced to minimize risk. The axis of the dam was moved upstream so that the entire core section was seated on the intact sound granite rock between faults. Most importantly, the embankment dam cross-section was modified to produce a

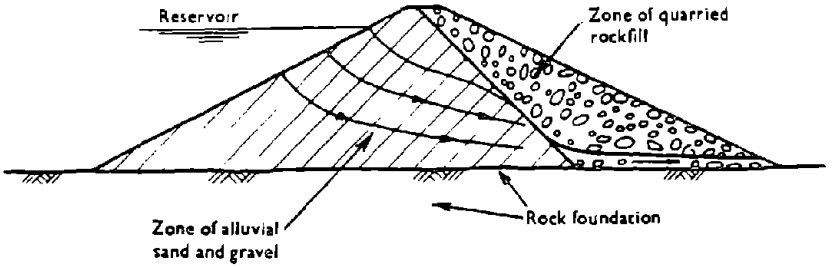

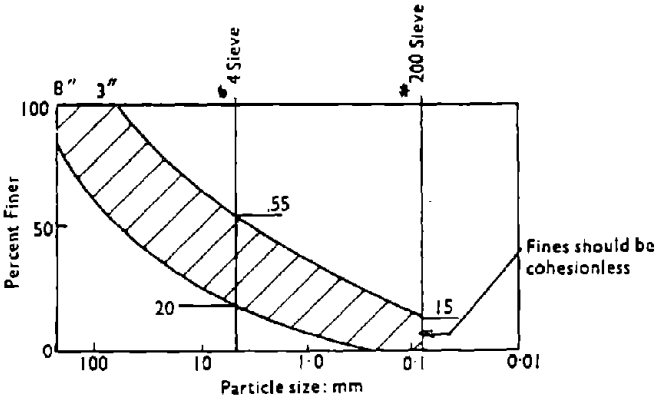

Figure 2-4: EXAMPLE OF A FUNDAMENTALLY SAFE EARTH DAM AND THE RANGE OF GRADATIONS OF THE "SELF-HEALING" WELL-GRADED SAND-GRAVEL MIXTURE USED AS A CORE OR TRANSITION ZONE (after Sherard et al., 1974)

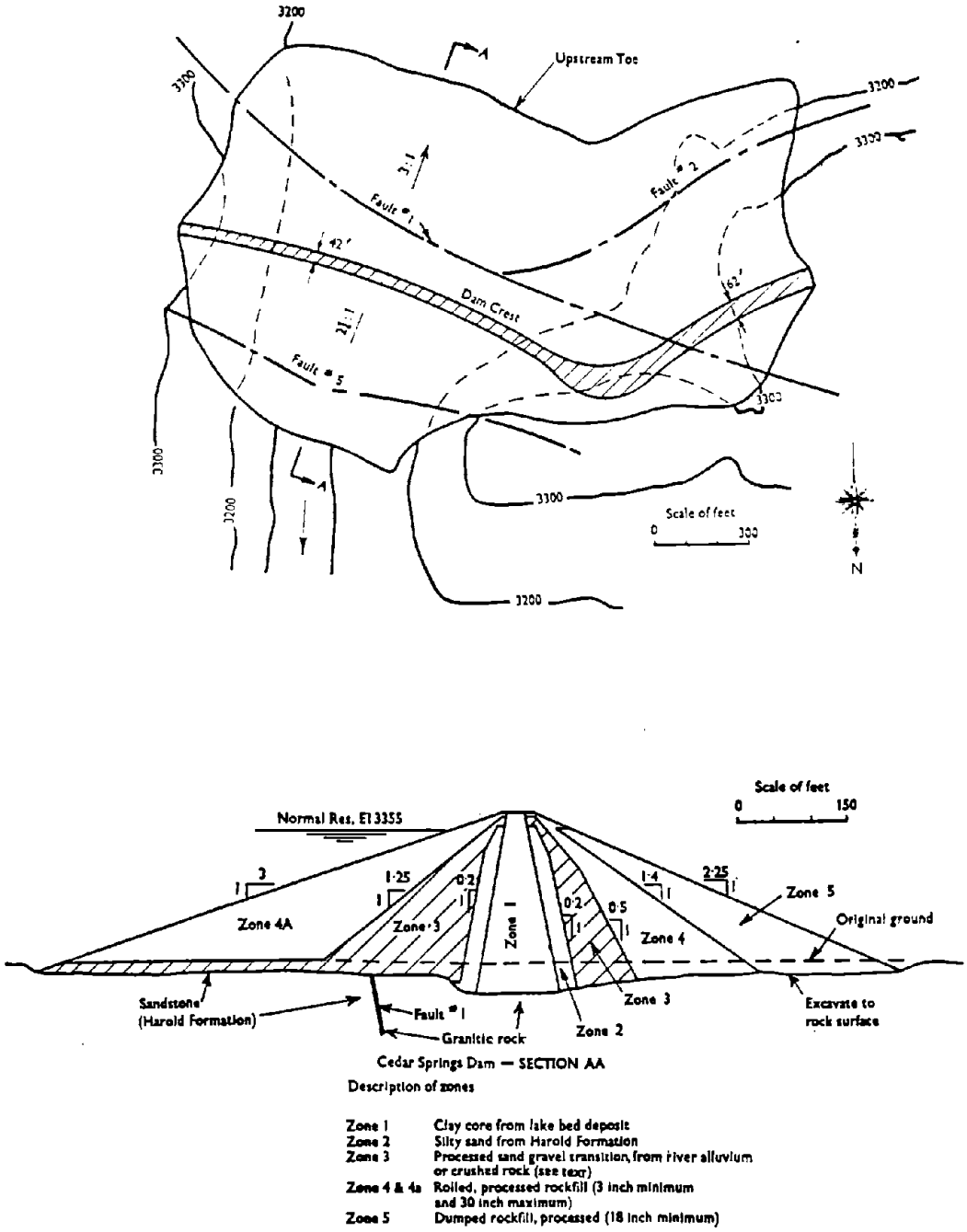

Figure 2-5: CEDAR SPRINGS DAM: PLAN VIEW AND TYPICAL CROSS SECTION WITH FAULT LOCATIONS (after Sherard et al., 1974)

thoroughly zoned dam. Thick zones of well-graded, coarse sand-gravel transition material and quarried hard rock exterior shell material both upstream and downstream of the core replaced what was an ordinary zoned dam with a narrow chimney drain. An especially tough, erosion-resistant clay replaced the original locally available core material, a silty sand. The crest width was increased to 40 - 60 feet. The authors believed that the well-graded, sand-gravel Zone 3 was the main line of defense for the reasons previously delineated. The Cedar Springs Dam was felt to be the best existing example of a highly conservative earth dam that could safely withstand the hazard of fault movement.

2.2.5 Swiger (1978):

In an ASCE specialty session on the design of structures for fault displacement, a distinguished panel of engineers and geologists reported the following opinions on if and how an earth embankment dam could be safely built over an active fault (Swiger, 1978). The orientation of the fault relative to the axis of the dam and the type of fault movement anticipated determined whether or not a dam should be constructed over an active fault. A strike-slip fault at any orientation could be designed for by enlarging the core and transition zones. Moderate dip-slip motions on a fault parallel to the dam's axis could also be accommodated. On the other hand, even small dip-slip motions which crossed the dam from upstream to downstream would be difficult to design for and it was extremely doubtful if larger dip-slip motions with this orientation could be accommodated. The expert panel believed that the defensive design measures incorporated in the design of Cedar Springs Dam included the critical elements of a safe dam design. The consensus of opinion was that it was not practical to design gravity dams on sites where even as little as an inch or so of movement was

expected, and that an arch dam could not be safely designed for a site where any significant movement was expected.

2.2.6 Cheney, Shen, and Ghorayek (1984):

Cheney et al. (1984) presented the findings of a preliminary centrifuge model study which investigated the performance of a hypothetical 18 foot high prototype homogeneous earth embankment dam ruptured by a strike-slip fault perpendicular to the axis of the dam. A series of eight tests were conducted on two different dam cross sections built of compacted Yolo loam, a silty sandy clay of moderate plasticity, which was compacted to $w_c \approx 17\%$ and $\gamma_d \approx 110$ lb/ft^3. Dams of Group A, with a crest length to base width ratio (L/B) of 0.8, and a model height of 3.6 inches were tested at 60 g's. Group B dams, with L/B = 1.0 and a height of 2.7 inches, were tested at 80 g's. Water was not impounded behind the dam cross sections during these model tests.

The trends established by the results of these tests were informative. A linear relationship between the magnitude of uni-directional base offset and the magnitude of resulting crest offset seemed to exist for the models tested. Furthermore, a given amount of base displacement (or "offset") was required before the shear fracture reached the surface of the dam. Moreover, crack openings in the embankment were larger near the base than at the crest of the dam. Surprisingly, the failure modes from the two test groups were dramatically different. The crack propagated through the Group A dams at a 45° angle to a horizontal plane through the base of the dam. On the other hand, the crack propagated through Group B dams with an essentially vertical orientation. The authors hypothesized that the 45° angle crack pattern indicated diagonal tension cracking, whereas the vertical or 90° angle crack pattern indicated transverse shear cracking. It was judged that further testing would be required to determine if the

different crack patterns for Group A and B models were a result of varying the L/B ratios, different initial stresses, dissimiliar soil properties at the two acceleration levels, or another unknown variable.

2.2.7 Sohn (1987):

In his dissertation, Sohn (1987) presented the results from a series of 6 centrifuge tests on earth dam models 3.4 inches in height ruptured by a strike-slip fault orthogonally bisecting the dam, as well as the results of 3-D finite element analyses of the corresponding 17 foot high prototype embankment dam. Unlike the earlier work by Cheney et al. (1984), Sohn impounded water behind the model dam to observe if water passed through the dam cross section after base movement. The model embankment was again constructed of compacted Yolo loam. The crest length to base width ratio of all the dam models was approximately 0.8:1. Tests were conducted at accelerations of 60 g's, 80 g's and 100 g's.

The centrifuge model tests produced two types of crack patterns. At the base of the embankment, a direct shear mechanism produced a nearly vertical crack which traversed the full width of the dam cross-section. A diagonal tension crack pattern oriented 45° to the strike of the basement fault developed later at the surface of the embankment. For the amount of offset created (which was up to 30% of the height of the dam), the base and surface crack patterns did not intersect. Because the surface tension cracks were not continuous, no conduit for water was produced. The base "direct shear" cracks, however, were continuous along the base of the dam, but the plastic nature of the silty clay and the higher confining stress within the embankment combined to seal off any open leakage channel. No water escaped through the dam cross-section in any of the 6 tests conducted.

The incremental finite element analysis utilized a bounding surface time-independent plasticity constitutive law to model nonlinear soil behavior. The 3-D, 600-node finite element analysis showed that the shear failure initiated at the base of the dam at the location of the fault and propagated up to the surface as base deformation increased. As in the centrifuge model, tension zones developed at the surface at an orientation of about 45° to the strike of the fault and disappeared within the embankment. The two crack patterns developed independently and did not intersect until a large amount of base deformation took place. The analysis was not judged to be fully reliable on a local scale once the failure condition (shear or tensile) was reached.

2.2.8 Leps (1989):

In his work, "The Influence Of Possible Fault Offsets on Dam Design," Leps (1989) outlines the current guidance on the design of dams to be constructed over potentially active faults. After briefly reviewing previous studies of this subject, Leps describes the key philosophical features of a prudent defensive design of an earth dam which crosses a potentially active fault by examining the defensive measures actually employed in the design of nine existing or proposed dams. Leps suggests that the prime objective of these defensive measures should be to ensure that leakage through the dam is controlled and that the progressive erosion of dam materials does not occur.

His review of dams designed to withstand fault offset highlighted some important points. The branch of the Calaveras fault which passes through the Coyote Dam described previously in Section 2.2.2 has probably displaced a few inches in 40 years, without undermining the stability of the dam. The primary defensive measures employed in the design of Palmdale Dam (See Figure 2-6), Cedar Springs Dam (See Figure 2-5), and the proposed earth core/rockfill Auburn

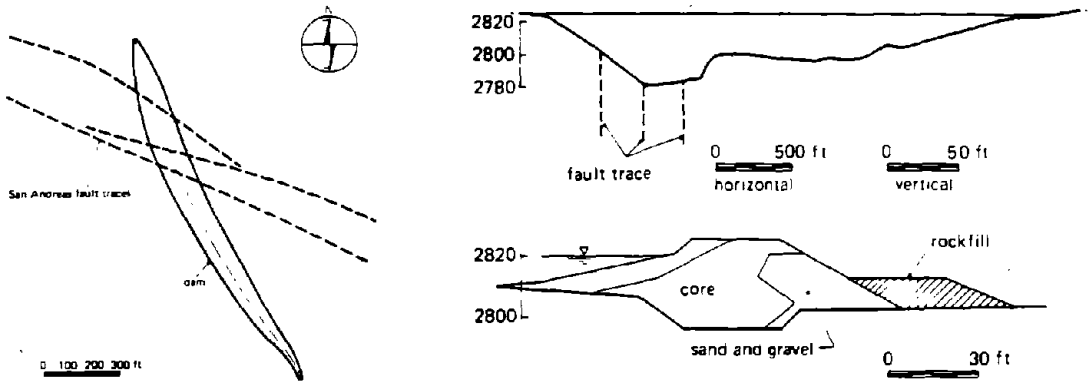

Figure 2-6: PALMDALE DAM IN PLAN VIEW, PROFILE AND CROSS SECTION (after Leps, 1989)

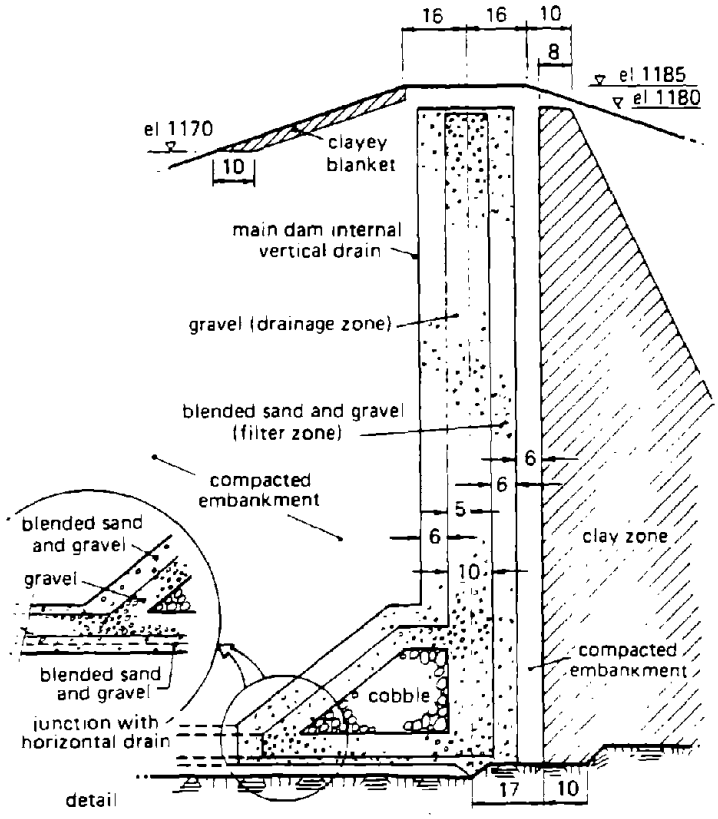

Figure 2-7: SECTION AND DETAILS OF THE DRAINAGE SYSTEM OF THE LOS ANGELES DAM (after Leps, 1989)

Dam were thick gravelly sand transition zones and large rockfill drain zones, both situated downstream from the impervious cores of the dams. These measures were intended to control the quantity of water that could reasonably flow through a core cracked by a fault offset in the foundation.

The "filtered chimney drain backed up at foundation level by a special cobble zone leakage collector and outfall finger drains" in the design of the Los Angeles Dam intrigued Leps. The details of the special drainage system installed in the Los Angeles Dam are illustrated in Figure 2-7. Leps pointed out,

> Note that the cobble zone backup for the conventional, thick, chimney drain is considered to be the most important defensive design detail for this particular dam, aimed at providing safe control of leakage which could begin at a severe, local, transverse, vertical, fault offset, by backing up the sheared chimney drain with a self-adjusting, non-destructible [drainage] zone. . . . The broad-based and amply sized cobble drain is visualized as being so cohesionless as to be able to adjust completely [to a foundation fault offset] and thus plug off any possible gap at the base of the chimney drain.

In fact, a "self-healing aseismic plug" composed of successive zones of material ranging from cobble size to sand-gravel size particles appearing very similar in concept to the detail shown in Figure 2-7 was utilized as a downstream buttress to improve the safety of the existing concrete gravity dam at Lake Henshaw. A branch of a potentially active fault was discovered crossing this dam site and this repair was deemed necessary. Finally, as previous authors noted, defensive design details should include ample crest width and adequate foundation treatment.

2.2.9 The Potential Error of Pure Reasoning and Other Lessons to be Learned:

A primary finding from the review of these studies is that, to date, no full-scale earth dam/foundation fault rupture case history exists to guide engineers in the design of embankment dams built over active faults. This finding will be

explored in further detail in the next section. Without direct evidence in this area, the authors of the studies discussed thus far have had to rely primarily on applying reasoning based on their experience designing earth dams and on observations of surface fault ruptures not passing through dams. Pure reasoning, however, does not always lead to valid conclusions.

Just 5 years after publication of the Sherard et al. (1974) landmark study "Potentially Active Faults in Dam Foundations," Sherard reported the findings from his investigation of the development of sinkholes in dams composed of coarse, broadly graded soils (Sherard, 1979). After noting that a number of sinkholes developed in dams built only with these soils, Sherard concluded that the broadly graded coarse soils were internally unstable with regard to erosion because the fine fraction of the soil mixture was not compatible with the coarse particles; in fact, they do not satisfy the widely used filter criteria: (d_{15}) coarser material / (d_{85}) finer material < 5. Figure 2-8 illustrates this point. The solid line represents the gradation curve of a soil which falls within the ranges of gradation of the well-graded, coarse sand-gravel mixture originally recommended by Sherard et al. (1974) as being especially suitable for use as a transition or core zone in an earth dam designed to withstand a fault offset. Such soils were believed to be "self-healing". Yet, if this soil mixture is equally divided into coarse and fine fractions (e.g. the dotted lines in Figure 2-8), it is apparent that the coarse fraction cannot even prevent movement of the soil's fine fraction. Sherard (1979) now described this type of soil mixture as coarser particles floating in a matrix of fines. In fact, if these two fractions of this mixture were placed side by side in a dam one would expect the finer particles to migrate through the coarser fraction zone. Furthermore, it has long been standard practice to avoid constructing the critical filter sections of an earth dam with well-graded materials since segregation of fine and coarse fractions during construction may produce an ineffective filter. Seed

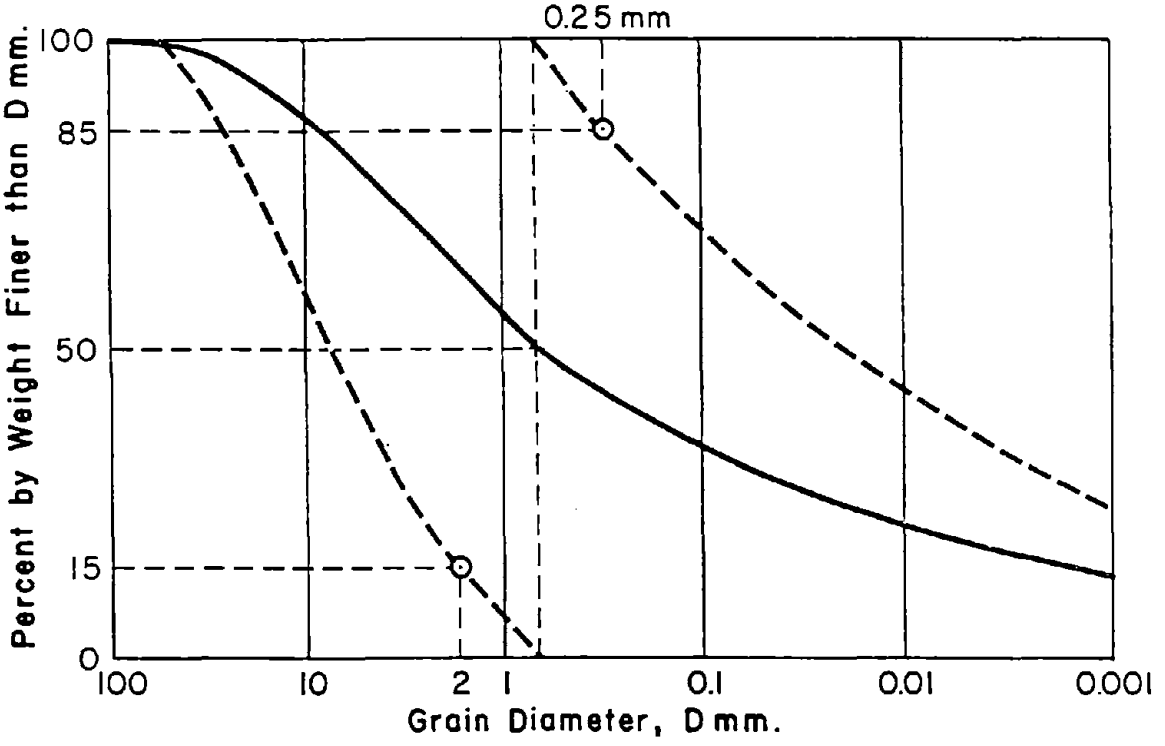

$$\frac{(d_{15})\text{ coarse fraction}}{(d_{85})\text{ fine fraction}} \approx \frac{2}{0.25} \approx 8 > 5$$

Figure 2-8: INTERNAL INSTABILITY OF A COARSE, BROADLY GRADED SOIL (after Seed, 1987)

(1987) recommended using uniformly graded filter materials with $C_u = d_{60}/d_{10} \approx 4$, and Sherard (1979) admits that filter material gradations should not usually possess values of $C_u > 20$, although he believes a criteria based on the d_{90} size of the soil would serve as a better indication of possible segregation problems.

Nevertheless, the well-graded soil originally proposed by Sherard to be an excellent core or transition material possessed a C_u value of on the order of 100 to 1000. Hence, segregation of this soil during construction would be probable, thereby reducing its effectiveness. In conclusion, clear evidence of soil particle migration in dams built of well-graded, coarse soil mixtures and the possibility of soil particle segregation during construction outweigh any prior arguments which reasoned that these soils would make excellent core or transition zones in earth dams built over active faults because of their inherent "self-healing" properties. Such soils may actually "self-destruct" if not surrounded by soils with properties which could prevent soil migration from these zones. This serves to point out the dangers associated with potential errors derived from the use of "pure reasoning" as a means of extrapolating previous experience for application to new conditions not directly reflective of that previous experience.

These studies also produced a number of important lessons for the design of dams built over potentially active faults. To date, all of the earth embankment dams built across known potentially active fault valleys possess thick core sections composed of tough, plastic clay materials. The boards of consultants for these projects thus appear to have reached the consensus opinion that the character of the impervious core was indeed important and that a tough, plastic clay core material improves the ability of an earth dam to withstand the hazards associated with potential fault rupture. The need for conservatism was repeatedly stressed. Sites with potentially active faults, especially when a dangerous combination of fault type and orientation existed, should be avoided. If a dam was necessary at a

faulted site, multiple lines of defense should be employed. It is not prudent to rely upon only one key defensive design measure. Instead, freeboard should be increased, reservoir height minimized, and crest width enlarged. The foundation material must be stable if subjected to the full water pressure of the reservoir. Outlet works and the spillway should be sited to minimize potential damage.

Thick upstream crackstopper zones and thick downstream transition and drainage zones are essential. In particular, the use of a rockfill zone at the downstream face of the earth dam minimizes the likelihood of a piping failure. Concentrated leaks must be expected and safely controlled. Finally, conservatism requires that rigid dams should not be constructed over active faults.

In reviewing the surface fault rupture phenomenon, the authors cited thus far have emphasized the need for a comprehensive geologic investigation at and away from the dam site. The designer should anticipate at least small differential movement on secondary fault features and existing planes of weakness in the bedrock. Contrary to what Louderback suggests, there is no reliable evidence of strike-slip faults gaping open during slippage. Further study is necessary, however, before Louderback's concern on this issue can be dispelled. It seems reasonable that tension gapes are soil surface manifestations that may not exist at depth, but this too remains unproven. Finally, the lessons to be learned from previous physical models (centrifuge) and one numerical analysis (finite element) of fault rupture through earth dams are somewhat unclear. These studies did, however, highlight one major shortcoming in our current knowledge of earth dam performance: the need to study what conditions are necessary for water in the reservoir to initiate traveling through the dam along shear zones or fractures that develop as a result of a fault offset in the dam's foundation.

2.3 Full-Scale Earth Dam Case Histories

2.3.1 General:

Case histories usually provide the most reliable source of information with regard to how physical events occur, and the use of case histories as a basis for the develoment of both insights and engineering judgment has long been a cornerstone of geotechnical practice. Furthermore, there is no guarantee that physical or numerical models adequately represent the prototype case to be studied in all important aspects, or if known deviations can be properly accounted for. Therefore, any effort to determine how earth dams respond to movement on faults in their foundation should ideally begin with a review of full-scale earth dam/fault rupture case histories.

A review of literature revealed only four full-scale earth dam/fault rupture case histories. In this section, these case histories will be examined. As previous authors have already noted, however, these case histories do not provide much useful information. Nonetheless, since they present the only source of field experience in this area, review of these full-scale case histories is warranted. It is important to clearly identify what can or cannot be learned from these case histories. At times, these case studies have been used to justify the claim that earth dams designed by current procedures will inherently possess the ability to safely adjust to foundation fault offsets. While the importance of lessons which can be learned from case histories cannot be overemphasized, the potential dangers associated with unwarranted extrapolation of lessons not justified by the field experience must also be guarded against.

2.3.2 Dams Ruptured by the 1906 San Francisco Earthquake:

Six earth embankments were ruptured during the 1906 San Francisco earthquake (Lawson et al., 1908; Ambraseys, 1960). As noted by Louderback

(1937) and Sherard et al. (1974), these cases did not contain much detailed information to help the engineer design an earth dam to safely withstand a foundation fault offset.

The San Andreas Dam, located approximately 15 miles south of San Francisco, and shown in both plan view and cross section in Figure 2-9, was not actually offset by the active trace of the San Andreas fault. The fault passed through a rock knoll which served as a central abutment for the larger rolled earth saddle dam to the west of the fault and the small rolled earth saddle dam to the east. Whereas the fault produced a clean break of roughly 7 feet distributed over a width of only 50 feet in the destroyed brick waste weir tunnel 125 yards downstream of the San Andreas Dam, the 7 foot right-lateral strike-slip offset in the rocky central abutment was distributed over a 200 foot wide distorted zone (See Figure 2-9). About 550 yards south of the dam, the fault produced a 10 foot offset in a fence. Hence, in the proximity of the San Andreas Dam, the strike-slip fault offset within a relatively narrow zone was on the order of 7 to 10 feet. But the faulting did not cut through the earth sections of the dam, so little could be learned from this field case. This case did, however, illustrate the importance of not siting water outlet works or spillways across active traces of faults. Additionally, this case demonstrated the potential complexity of the fault rupture phenomenon. Within a short distance, the character of the expression of the surface fault rupture varied considerably.

The Upper Crystal Springs Dam shown in Figure 2-10, located approximately 6 miles south of the San Andreas Dam, was not functioning as a dam when the 1906 San Andreas fault offset occurred. Instead, the earth embankment was serving as a causeway across the Crystal Springs reservoir. The Upper Dam was submerged within the reservoir created by the construction of the Lower Crystal Springs Dam downstream. The road and fence along what had been

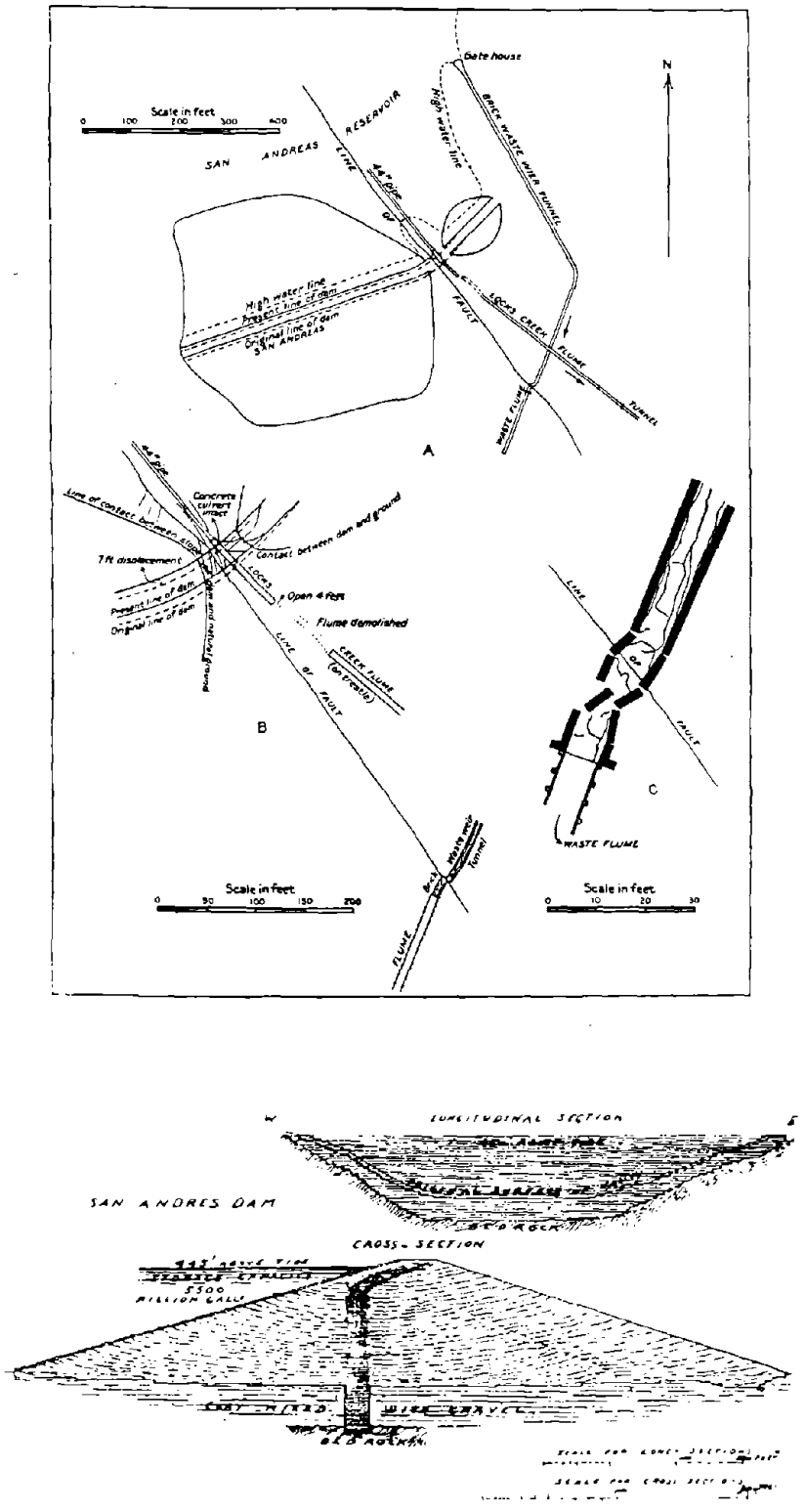

Figure 2-9: SAN ANDREAS DAM: PLAN VIEW SHOWING INTERSECTION BY FAULT AND CROSS SECTION (after Lawson, 1968 and Schussler, 1909)

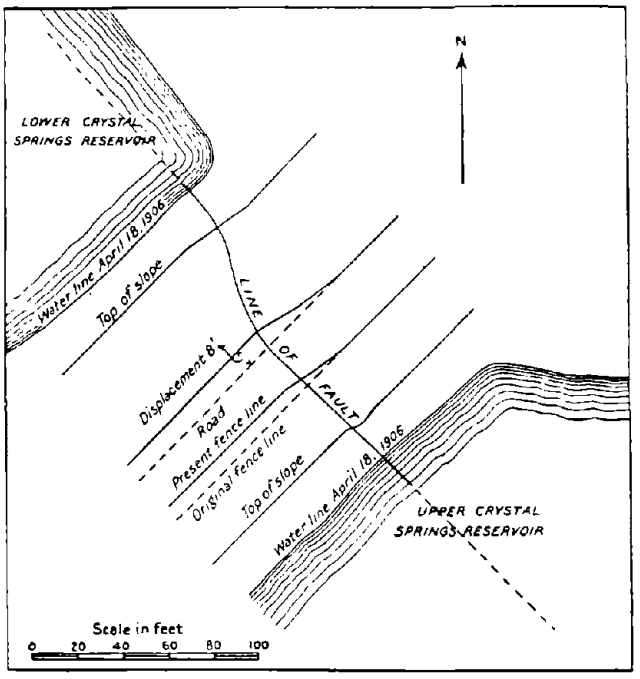

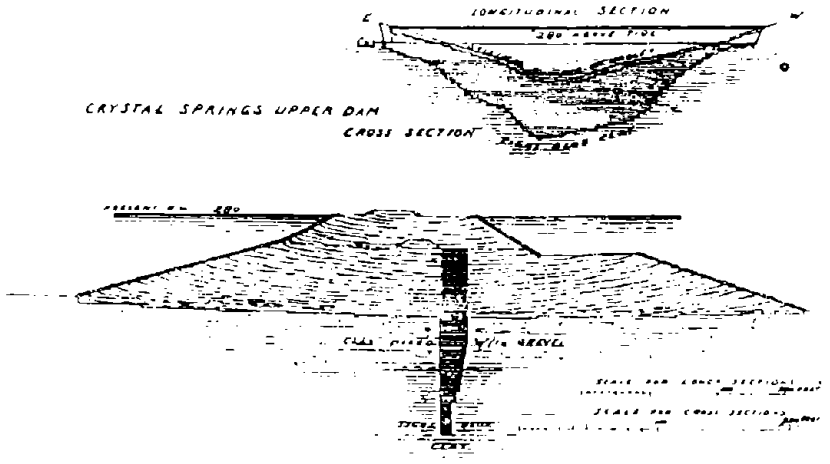

Figure 2-10: LOWER CRYSTAL SPRINGS DAM: PLAN VIEW SHOWING INTERSECTION BY FAULT AND CROSS SECTION (after Lawson, 1908 and Schussler, 1909)

the crest of the earth dam were offset approximately 8 feet by the fault. The distorted zone was about 40 feet wide. The fault was nearly perpendicular to the axis of the embankment, and passed within 20 feet of the east abutment on the embankment's north side and within 60 feet of the east abutment on the south side. At this location, the crest of the constructed earth embankment was only about 20 feet above its rock foundation.

Transverse and longitudinal cracks were observed in the top of the embankment. Settlement of the saturated earth fill may have produced the longitudinal cracks which were about 6 inches wide and up to 4 feet deep. The transverse cracks appeared in the distorted zone produced by the fault offset, but they were less well defined. Ambraseys (1960) indicated that an inspector of the dam believed these transverse cracks parallel to the fault trace were shear cracks. Because of the special nature of this case history, it was impossible to predict how this embankment would have performed if it had been functioning as a dam and not a causeway. Moreover, since the earth section traversed by the fault was shallow, it was difficult to say how a larger earth embankment section would have responded to a similar strike-slip fault offset.

The Old San Andreas Dam was a small abandoned earth dam submerged beneath the Crystal Springs reservoir when the 1906 San Francisco earthquake produced a 7 foot offset in the crest of the embankment. Little was known of this dam. In fact, it was not rediscovered until 1931 when the Crystal Springs reservoir was lowered to inspect the Lower Crystal Springs gravity dam. Like the Upper Crystal Springs Dam, the offset of the Old San Andreas Dam offered no direct evidence of the performance of an operational earth dam during a fault offset. Once again, like the earlier Upper Crystal Springs Dam case history, this case history indicated that the zone of disturbance for a shallow earth embankment aligned normal to a strike-slip fault offset was relatively narrow.

Three other earth dams located approximately 25 miles southeast of the Upper Crystal Springs Dam were offset or nearly offset by the San Andreas fault during the 1906 San Francisco earthquake. Little was known of the construction of these earth structures. Again, because of the special circumstances of these events, little useful information was gained. The Lake Ranch Dam's main section was not offset by the San Andreas fault. Instead, the fault intersected a small 3 foot high subsidiary dike. The reservoir water was said to have run over the dike at the location of the fault offset. The eastern end of the Upper Howell Dam was offset by the strike-slip movement of the San Andreas fault, but this case is relatively poorly documented. Cracks which extended through the full depth of the dam were found at the point where the fault trace intersected the dam axis. The dam did not fail. The Lower Howell dam, however, did fail. A 10 inch diameter outlet pipe which crossed the fault ruptured, and the earth embankment materials began to erode at this location. A breach 4 to 6 feet wide allowed water to escape downstream. Surprisingly, the fault produced "very little" displacement at this point. Ambraseys (1960) stated, "Whether the dam itself would have been seriously damaged by the earthquake if this pipe had not broken could not be determined." This case history did demonstrate that it is not prudent to locate outlet pipes across potentially active fault traces, especially when the pipe is buried within the earth embankment itself.

The review of the performance of the earth dams ruptured by the San Andreas fault during the 1906 San Francisco earthquake failed to uncover a well-documented example of the performance of an earth dam built subjected to a foundation fault offset. If the fault trace crossed the earth embankments at all, it did so at locations near abutments where the dam cross-section was small. Furthermore, two of the earth embankments reviewed were not functioning as dams during the fault offset. One clear lesson from these case histories was the

importance of properly locating water outlet works. Otherwise, as Louderback concluded, little practical information can be learned from these full-scale earth dam/fault rupture case histories.

2.3.3 The All-American Canal Embankment (1940):

A break of over 40 miles on the Imperial Fault displaced the All-American Canal 15 feet during the 1940 El Centro earthquake (M_L = 6.7). The All-American Canal was still under construction and hence, was not carrying water at the time of the fault offset. The two sides of the canal were relatively small homogeneous earth embankments, so this case history would have been of limited interest even if the canal was not dry. As shown in Figure 2-11, the fractured zone produced in the canal's earth embankments by the 15 foot offset on this right-lateral strike-slip fault was fairly narrow.

Upon closer examination of the fractured zone as it crossed the left bank of the canal, as shown in Figure 2-12, it was apparent that the fault offset produced multiple shear cracks through the earth embankment. Movement was concentrated, however, on two of these shear cracks, with the majority of movement occurring on the shear crack farthest from the photographer. The observed cracks were vertical or nearly vertical, and were roughly perpendicular to the axes of the canal embankments (and parallel to the base fault orientation). To the north and south of the All-American Canal the fault trace could be seen as a well-defined single surface rupture. Richter (1958) suggested that it was possible that the All-American Canal itself helped to produce the widening of the surface expression of the fault rupture which occurred at its location. It was difficult to prove if this hypothesis was true or not, but it seems difficult to image that an earth structure of on the order of only 20 feet high would significantly affect the surface rupture pattern of a fault which cuts through an alluvial valley which is on the

Figure 2-11: ALL-AMERICAN CANAL OFFSET DURING THE 1940 EL CENTRO EARTHQUAKE (after Sherard et al., 1974)

Figure 2-12: CLOSE-UP OF THE FRACTURE ZONE ACROSS THE LEFT ALL-AMERICAN CANAL EMBANKMENT

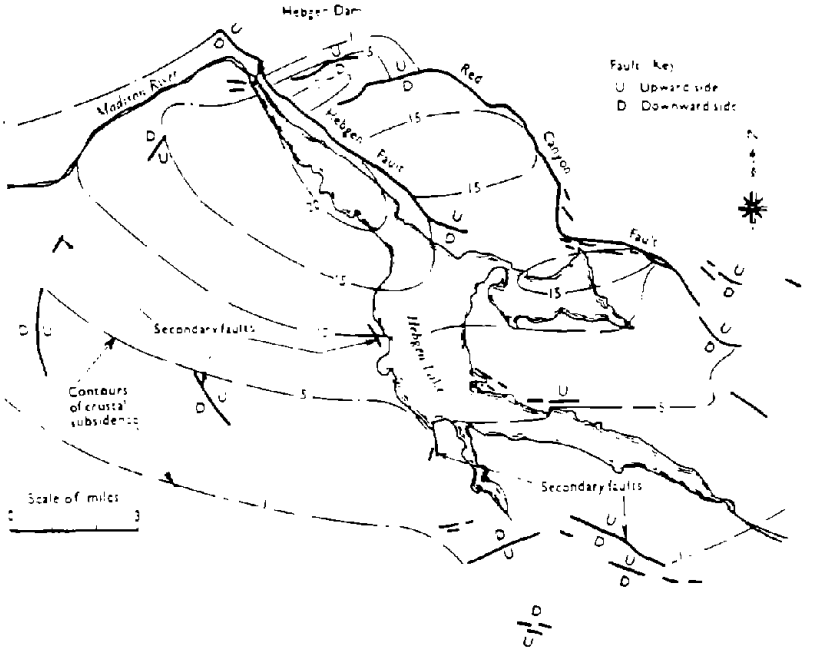

Figure 2-13: FAULT SURFACE BREAKS AND CRUSTAL DEFORMATIONS NEAR HEBGEN DAM AFTER THE 1959 EARTHQUAKE (after Sherard et al., 1974)

order of 400 to 700 feet deep at this location. In conclusion, the fracturing of the All-American Canal produced some interesting questions regarding changes in the expression of earthquake generated surface ruptures, but little of this information can be directly applied toward improving our understanding of how earth dams respond to offsets in foundation faults.

2.3.4 Hebgen Dam (1959):

The 1959 Hebgen Lake earthquake (M_L = 7.1) produced large surface ruptures and crustal deformations in the vicinity of Hebgen Dam. The nearest differential fault offset, however, was located about 900 feet from the eastern abutment of the Hebgen Dam embankment. As illustrated in Figure 2-13, the bedrock below the entire length of the dam subsided more or less uniformly about 10 feet. The bedrock below the reservoir subsided at least this amount so the top of the crest of the dam remained above the top of the water impounded behind it. Some water escaped over the crest of Hebgen Dam, however, due to earthquake wave action (seiches).

Hebgen Dam was a 90 foot high earthfill and rockfill dam with a central concrete core wall which extended through the full height of the dam. The concrete core wall, which varied from 3 to 16 feet in thickness from top to bottom, separated an upstream low permeability earth fill section and a downstream section composed of a loose rock fill drainage layer below a rock and earth fill layer. Ground vibrations were the principal cause of damage to the Hebgen Dam embankment, producing up to 5.4 feet of vertical settlement in the earth fill sections. Re-alignment of the abutments and other minor effects from bedrock movements, however, may have also contributed to the damage. For example, the concrete core wall of the dam was cracked in 16 places and bowed into a gentle "S" curve. Although the core wall cracked and leaked in a number of areas, Hebgen

Dam remained stable, indicating that dams can withstand the sudden onset of increased (and localized) internal seepage. The spillway was damaged too, as it had been sited over loose saturated materials brought into the valley area by an old landslide.

Since significant differential movement did not take place across the dam's foundation, it was not known how this earth dam would have responded to a fault offset in its foundation. It was surprising that this relatively brittle dam with its massive concrete core wall suffered only minor damage from the large sudden drop of its rock foundation. Yet, this emphasized the widely accepted fact that differential settlement, not uniform settlement, was the primary concern in the performance of earth structures. It was also clear, however, that uniform bedrock movements which reduced or eliminated the effective freeboard of the dam must be guarded against. Finally, this case study also served to reconfirm the fact that unsatisfactory foundation materials should be removed or improved in situ. Therefore, Hebgen Dam provided some useful engineering lessons, but not with respect to designing for a distinct fault offset in the foundation of an earth dam.

2.3.5 Baldwin Hills Dam Failure (1963):

The failure of the Baldwin Hills Dam has been investigated by several highly respected geotechnical engineers and geologists and the exact cause and sequence of the failure are still not known with certainty. Findings from this case history remain controversial. A number of sides to this controversy and an informative discussion between panel members are presented in the proceedings from a recent international workshop on dam failures held at Purdue University in 1985 (Leonards, 1987). Wilson summarizes the controversy in writing,

> There appears to be general agreement that vertical offsetting along a fault which crossed the floor of the reservoir was responsible for rupturing the drainage system and permitting the water to enter the foundation soils. There is not general agreement, however, on whether or not there were fault movements immediately prior to failure, which in turn ruptured the clay lining, or whether the clay lining was ruptured first and the resulting introduction of full reservoir pressure into the fault plane was responsible for additional offsetting.

No attempt to resolve this controversy will be made here. Still, the review of the failure of the Baldwin Hills Dam, notwithstanding the uncertainties involved, provides some important lessons.

It was widely accepted that an earthquake event did not displace the faults in the foundation of the Baldwin Hills Dam. Whether differential movement across the fault was produced by fault creep, areal subsidence, compression of foundation soils, or another mechanism, the fact remained that differential movement under a brittle reservoir lining and drainage system allowed water to escape into the weak, erodible foundation material. The reservoir lining system was composed of a 3-inch-thick asphaltic pavement over a 10 foot compacted clay earth liner. The seepage collection system under the reservoir lining system was a 4-inch-thick lightly cemented pea-gravel drain layer with 4-inch clay tile drain pipes underneath. Before installation of the seepage collection system, the existing compacted in-place foundation materials were sealed with a quarter inch thick asphaltic membrane. Once a leak along the fault developed, the stage was set for the progressive erosion of the foundation materials and the ensuing piping failure of Baldwin Hills Dam.

Two relevant lessons are provided by this case history. If a potentially active fault is located at the dam site, it should be expected to eventually move. If the foundation soils are easily erodible, they must either be improved in situ or removed. It is not prudent to rely solely on a reservoir lining and seepage collection system, even if designed to be flexible, to prevent water from entering a

weak foundation. Casagrande's multiple lines of defense concept suggests that, once a reservoir lining and seepage collection system has been designed not to crack, the engineer must then assume it will crack and incorporate adequate features into his design to safely handle this situation. Moreover, a brittle reservoir lining and seepage collection system with a clay layer which permits arching of the soil above erosion tunnels should not be used in areas subjected to possible differential movement. This system proved to be inadequate under the special circumstances of the Baldwin Hills Dam failure, and hence, should not be employed in future earth dams where significant differential movement is expected.

2.3.6 Lessons to be Learned from Full-Scale Earth Dam Case Histories

Dams ruptured by the 1906 San Francisco earthquake, the All-American Canal, Hebgen Dam, and the Baldwin Hills Dam failure comprise all of the known instances where earth embankments were offset or nearly offset by distinct fault movements. A review of these case histories shows, however, that none of these full-scale earth dam/fault rupture case histories provides conclusive evidence of how a substantial earth dam would respond to a fault offset in its foundation. Specific lessons can be inferred from the facts of these case histories, so review of them is justified. The most important lesson to be learned from this review, however, is that no well-documented case histories directly addressing the issue of dam performance when subjected to foundation fault offset exist. The successful performance of earth embankments during the 1906 San Francisco earthquake and Hebgen Dam during the 1959 Hebgen earthquake does not imply that these dams could have survived a fault offset directly through their foundation. On the other hand, the unsatisfactory performance of the Baldwin Hills Dam and Reservoir does suggest that a similar design should not be employed over a potentially active

fault. Finally, it may again be concluded that multiple lines of defense should be built into any dam constructed over a potentially active fault.

For shallow earth embankments, the surface ruptures produced by strike-slip fault offsets normal to the axis of the embankment appeared to be fairly narrow. These cases, however, also illustrated the variability of the surface expressions of a bedrock fault rupture. These case studies suggest that parallel shear fractures alongside main breaks through the earth structure should be expected, but evidence from centrifuge testing of model embankments suggests that other shear and cracking patterns are also possible. Uniform bedrock movements are less critical than differential bedrock displacements. Sufficient freeboard must be provided in cases where the bedrock under the reservoir might increase in elevation relative to the earth dam structure. Erodible foundation materials should be improved in situ or removed, as a designer cannot permanently guarantee that water will not eventually enter the foundation. Finally, the spillway and outlet works should not be located across potentially active fault traces or on unstable ground.

In conclusion, no well-documented case histories exists where an operational earth dam was significantly offset by an earthquake-generated fault offset. These "near miss" case histories merely serve to once again highlight some of the potential problems in designing an earth dam over a potentially active fault.

2.4 Summary and Findings

In Chapter Two, seven previous studies of fault rupture through earth dams were reviewed. In addition, four case histories which comprise all of the known instances where earth embankments were offset or nearly offset by distinct fault movements were described and evaluated. These studies and case histories of fault

rupture propagation through earth dams brought forth a number of salient observations.

Casagrande's concept of multiple lines of defense should be employed in the design of all dams built over potentially active faults. Experts agreed that particular attention must be devoted to controlling the hazards of concentrated leaks through the dam and its foundation. The stability of the foundation must be guaranteed. A thick, ductile core protected upstream by thick 'crackstopper' zones and downstream by thick filter and transition zones were considered desirable. These zones must be backed up by a drainage system that extends the full height and length of the dam. All zones must be wider than the maximum anticipated potential fault offset. The crest width and the freeboard of the dam should be maximized, whereas the required reservoir capacity should be minimized. Of course, if possible, a dam site traversed by potentially active faults should be avoided. Spillways and outlet control works should not traverse potentially active fault traces. Finally, the experts concluded that rigid dam structures such as concrete gravity dams should not be constructed over potentially active faults.

Pure reasoning was shown to have limitations. In 1974, Sherard reasoned that a broadly graded gravel-sand mixture was the best material to use in the core of an earth dam built over a potentially active fault because of the material's "self-healing" tendency. Just five years later, when investigating the development of sinkholes in earth dams constructed of broadly graded soils, Sherard concluded that these materials were prone to soil migration even without base differential movement, and hence, broadly graded soils were potentially unstable with regard to internal erosion.

A proper geologic investigation must be conducted in the early planning stages of any dam sited in a seismic region. The study should include a geologic survey of a large area surrounding the dam site and a detailed study of fault traces

and secondary fractures which cross the dam site. Some amount of movement on these fault traces and secondary fractures should be anticipated.

On the other hand, the review of previous studies and case histories of fault rupture through earth dams identified critical shortcomings in our current level of understanding of this phenomenon. Most importantly, no well-documented case history exists which describes how earth dams respond to base rock fault displacements. A review of the available case histories shows that none of these full-scale earth dam/fault rupture case histories provides conclusive evidence of how a substantial earth dam would respond to a fault offset in its foundation. Furthermore, results from model tests of earth dams of substantial height offset by fault movements are not available. To date only homogeneous prototype earth embankments less than 20 feet high have been modeled in the laboratory, and the results from these model tests have been inconclusive. Moreover, no reliable analyses have been performed to study the effects of tectonic movements on stresses and deformations in earth dams. Finally, the hydraulic conductivity along newly formed shear fractures in earth materials is not known.

Given the shortcomings in our current state of knowledge regarding the effects of tectonic movements on stresses and deformations in earth dams, the literature review was extended to investigate the fault rupture propagation phenomenon in general. Specifically, surface fault rupture field studies and physical and numerical model studies which provide insight into how fault ruptures propagate through soils will be examined in the next chapter.

CHAPTER THREE:
REVIEW AND EVALUATION OF PREVIOUS STUDIES OF EARTHQUAKE FAULT RUPTURE PROPAGATION

3.1 Introduction

The literature review was extended to investigate available earthquake surface rupture case histories to improve our current level of understanding of how fault ruptures propagate through soil. Knowledge of how fault ruptures propagate through soil would provide valuable insight into the likely effects of tectonic movements on stresses and deformations in earth dams built across potentially active faults. Since full-scale field case histories usually provide the most reliable source of information on how physical events occur, earthquake surface rupture field studies available in geologic reports and publications are reviewed and evaluated first in Section 3.2, and lessons to be learned from field studies regarding fault rupture propagation are noted. Then, in Section 3.3, studies involving laboratory model testing and numerical analyses of fault rupture propagation are examined in order to gain further insight and to isolate critical parameters for a more in depth study of their influence on how a soil responds to a base rock fault displacement. Finally, the results of this review and evaluation of previous field studies and physical and numerical model studies of the fault rupture propagation phenomenon are summarized in Section 3.4.

3.2 Earthquake Fault Rupture Propagation Field Studies

3.2.1 Earthquakes and Fault Rupture Propagation:

Without well-documented case histories which describe how earth dams respond to bedrock fault displacements, it is necessary to investigate geologic studies of surface fault ruptures to gain insight into how soils respond to fault

movements. Considerable effort has been devoted to the study of the surface expression of fault ruptures. Unfortunately, however, much of this work has concentrated on areas where the depth of overburden was minimal. Although it is necessary to find a location where younger deposits exist so that the recency of fault activity can be assessed, it is not economical to trench where the depth of overburden is excessive. To this writer's knowledge, no one has deliberately dug a trench of substantial depth (i.e. greater than 50 feet) with the goal of learning how bedrock fault ruptures propagate through deep deposits of soil. Still, the review of surface fault rupture case studies may improve our understanding of the fault rupture propagation phenomenon, and hence, may provide the dam engineer with some understanding at least of the general patterns of behavior of soils overlying bedrock faults which displace. Such studies may also provide some basis for evaluation of the efficacy and reliability with which various numerical analysis techniques model key aspects of fault rupture propagation through soils.

Bonilla (1970) presents a good, comprehensive review of the surface faulting phenomenon. He describes the primary features of most known cases of surface faulting in the United States prior to 1970. A review of his work, as well as general discussions by other experienced seismic geologists, brought forth a number of salient points (Richter, 1958; Bonilla, 1970; Cluff et al., 1970; Oakeshott, 1973; Sherard et al., 1974; Taylor and Cluff, 1977; Bonilla, 1988(a); Bonilla, 1988(b); Bonilla 1988(c); Cluff, 1988; Wells et al., work in progress). There have been more than 100 documented cases of earthquake surface faulting observed during the last 150 years. Although our understanding of these earthquake events is not complete because of the complexities of the geologic materials and processes involved, important lessons have been learned that can be incorporated into the design of earth dams to be built over potentially active faults.

There are three principal types of faults: thrust, normal, and strike-slip. They are illustrated in Figure 3-1. In reality, earthquake events possess a combination of vertical and horizontal components of movement, and the total displacement is called the oblique-slip. One of these three "types" of faulting, however, usually dominates, and hence, fault offsets are characterized as principally thrust, normal, or strike-slip. The type of fault offset can have a significant impact on the nature of fault rupture propagation through overlying soils.

Researchers have also found that, along with the type of fault movement, the character of surface faulting was influenced by the attitude or inclination of the fault plane, the amount of displacement on the fault, the depth of the earth material overlying the bedrock fault rupture, and the surficial geology or nature and geometry of the overlying earth materials (Cluff et al., 1970; Taylor and Cluff, 1977; Bonilla, 1988(a)). For example, a large magnitude earthquake event which produces a large offset on a deeply buried and shallowly dipping fault plane might not create a surface fault rupture, whereas a lower magnitude earthquake event producing a smaller offset on a deeply dipping, shallow fault plane may create a surface fault rupture. As Sherard et al. (1974) noticed, the orientation of the bedrock fault often determines to a large extent how a fault movement affects an earth structure situated above it. These geologists also found that, in general, the character of the surficial geology, whether intact or fractured rock or stiff or plastic soil, also helped to determine the orientation and magnitude of the surface fault rupture. These characteristics, and the factors which influence them, will be the primary focus of this review of surface fault rupture case histories.

Recent work by Wells et al. (work in progress) provides an insight into the scale of the fault offset problem. They have identified nearly 90 cases of observed surface fault displacements, and have plotted the magnitude of the earthquake

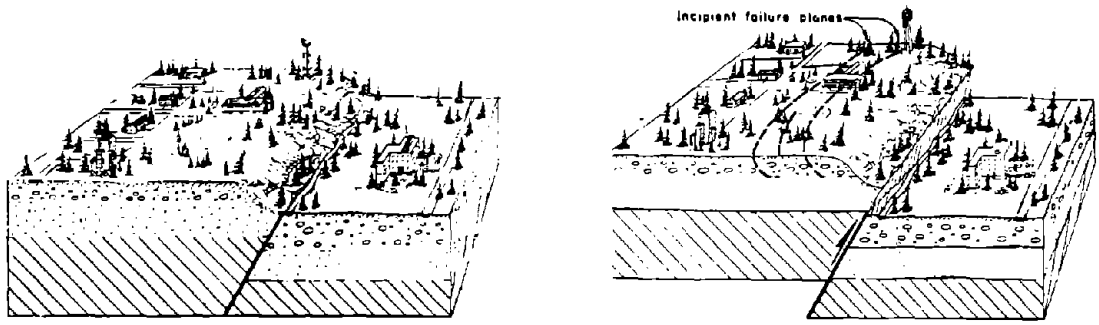

(A) Thrust Fault Sequence

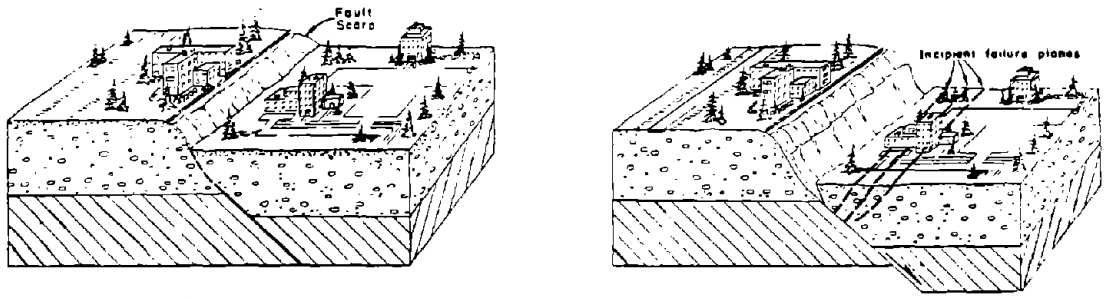

(B) Normal Fault Sequence

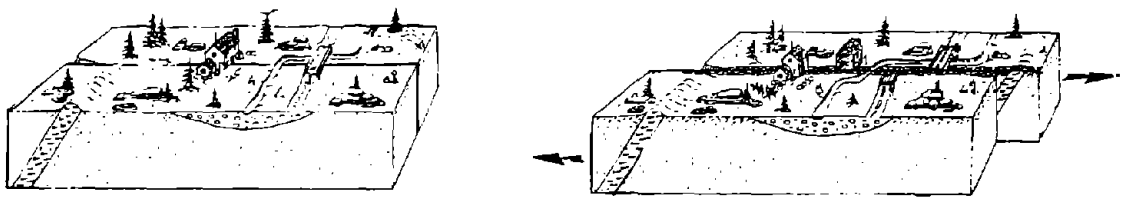

(C) Strike-Slip Fault Sequence

Figure 3-1: TYPES OF FAULT MOVEMENT: THRUST, NORMAL, AND STRIKE-SLIP (after Cluff et al., 1970)

events against the recorded maximum surface displacement for the three principal fault types, as shown in Figure 3-2. Older, but similar, plots of data were presented by Bonilla (1970) and Taylor and Cluff (1977). These records of surface fault ruptures should give the dam engineer confidence in the sense that there appear to be reasonable magnitudes of maximum fault offsets that one would have to consider in the design process. Depending primarily on the magnitude of the earthquake and the type of fault movement, the maximum surface displacement or offset from known earthquake events ranged from less than an inch to at most around 35 feet. Moreover, researchers have found that the average surface fault displacement or offset in any given event was only approximately 50% of the maximum offset at one point along the fault (Sherard et al., 1974; Wells et al., work in progress). In most cases, earth dams would be planned at sites where fault movements were at the lower end of the ranges of displacements given, as dams would not typically be sited across major faults considered capable of producing earthquakes of $M_L > 7$. Thus, in most cases, the dam engineer would have to incorporate defensive design features that would accommodate only a few inches to at most 5 to 10 feet of differential movement. Of course, the site specific value of expected fault offset could be assessed only after a comprehensive geologic study of the dam site and the surrounding region was conducted. This data, however, provides the engineer with preliminary estimates of anticipated fault offsets based on earthquake magnitude and fault type, and at least a sense of the scale of the problem.

In most cases, the majority of fault movement appears to occur along a single rupture plane, with the remainder of the movement being distributed over a wider distorted zone (Bonilla, 1970; Taylor and Cluff, 1977) The rupture plane appears most likely to be aligned, at least roughly, with the most recently displaced

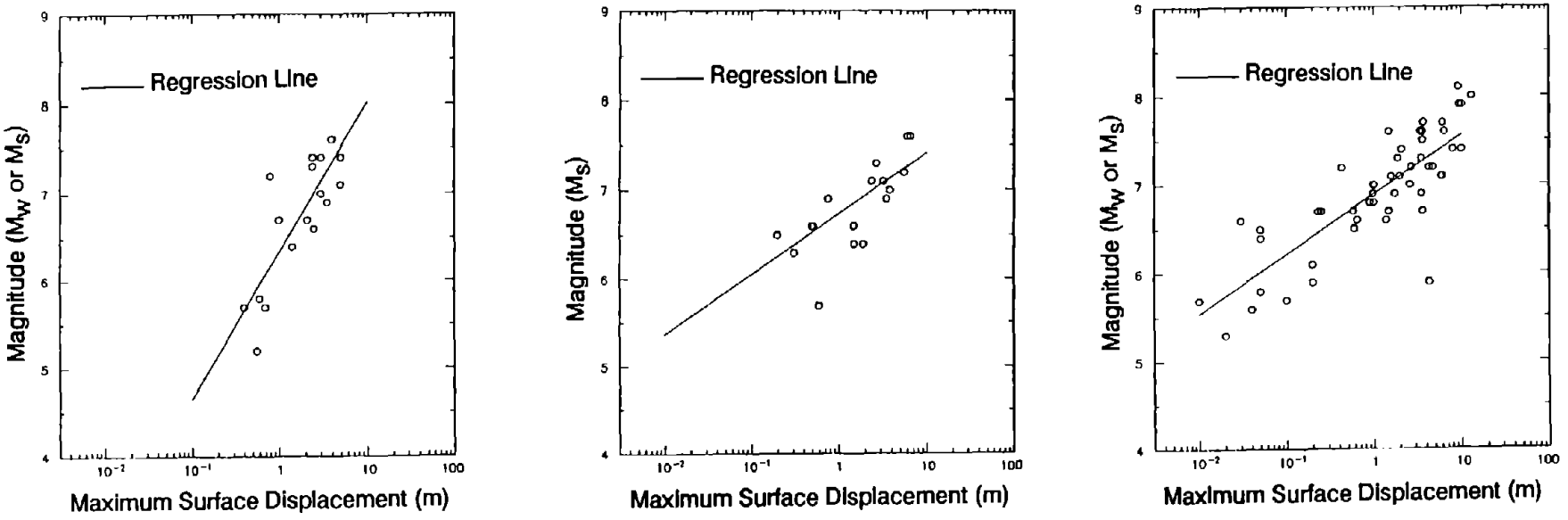

(A) Thrust Fault

(B) Normal Fault

(C) Strike-Slip Fault

Figure 3-2: MAXIMUM SURFACE DISPLACEMENTS VS. EARTHQUAKE MAGNITUDE FOR THREE TYPES OF FAULT MOVEMENTS (after Wells et al., work in progress)

fault strand. After investigating the surface faulting associated with the 1906 San Francisco earthquake, Lawson (1908) concluded:

> The width of the zone of surface rupturing varied usually from a few feet up to 50 feet or more . . . The displacement appears thus not always to have been confined to a single line of rupture, but to have been distributed over a zone of varying width. Generally, however, the greater part of the dislocation within this zone was confined to the main line of rupture, usually marked by a narrow ridge of heaved and torn sod.

Yerkes (1974) found that for the 1971 San Fernando earthquake, "The displacement on the fault occurred across a zone about 350 feet wide, but nearly all of the lateral displacement occurred in a zone about 100 feet wide." Taylor and Cluff (1977) concluded, "Surface faulting is generally confined to a narrow fault-traces in a wider zone of disturbance." Oakeshott (1973) disagreed, "Note that the exception is the simple, single fracture. This is true of all active faults I have followed; the simple, single trace is rare; the complex, discontinuous traces are the rule." Overall, however, it appears that a general consensus had been reached to the effect that the greater part of the fault offset usually occurs within a narrow zone. The rest of the movement may be distributed across a wider distorted zone.

On one hand, the majority of differential movement across a fault zone is likely to be concentrated on a single break so that the problem is likely to be localized. On the other hand, the remainder of the movement could occur on secondary fractures or faults some distance away from the main trace so that the dam engineer cannot afford to focus exclusively only on the main fault trace. In fact, researchers warned of tilting or warping of bedrock adjacent to faults that displaced. Bonilla (1970) presented data which confirmed that significant movement occurred on secondary fault features. As shown in Figure 3-3, displacement on secondary fractures could be as much as 20% of the amount of displacement on the main fault as far away as 8 miles from the main fault. Thus, in

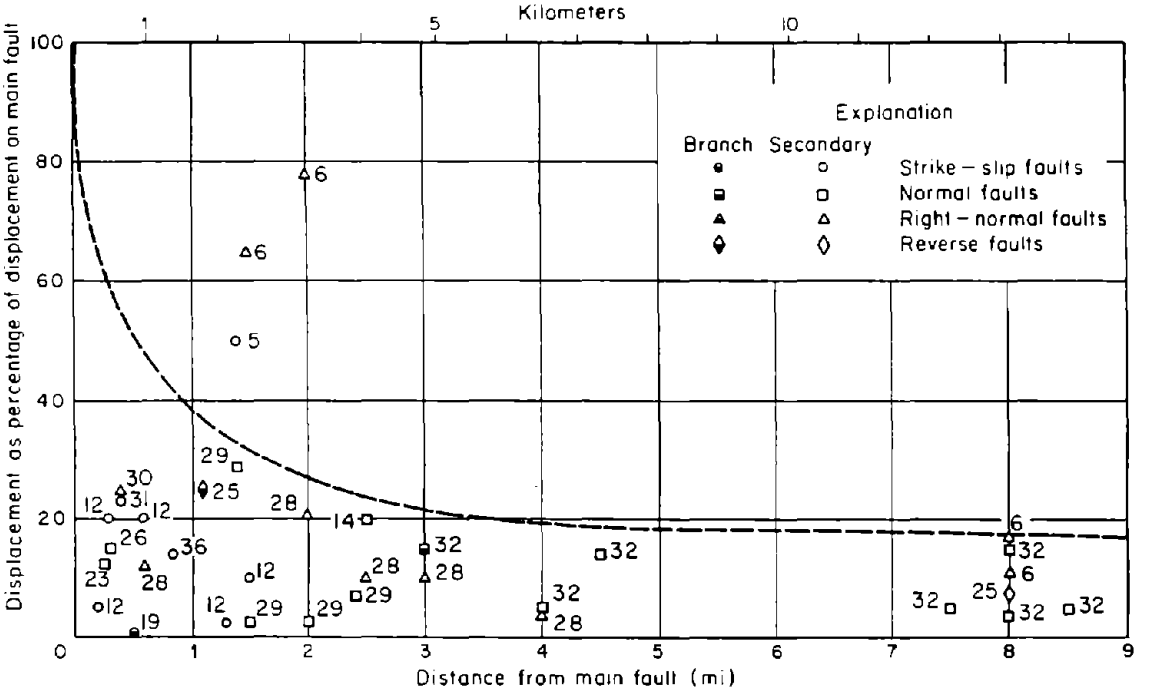

Figure 3-3: SECONDARY FAULT DISPLACEMENT AS RELATED TO DISTANCE FROM THE MAIN FAULT (after Bonilla, 1970)

seismic regions, movement on inactive faults, bedding planes, or existing fractures cannot be ignored. Moreover, an analysis of over 1200 active fault strands by Bonilla and Lienkaemper (work in progress) found that about 14 percent of these strands seemed to die out or actually died out even though the earthquake faulting occurred "recently". This led the authors to conclude that a "fault strand overlain by an apparently undisturbed deposit is not necessarily older than the deposit". Therefore, any existing plane of weakness might be suspect when evaluating the potential for ground movement at a dam site.

Finally, given their experience observing and studying the occurrence of surface faulting, these geologists were able to characterize the general behavior of fault rupture (Lawson et al., 1908; Briggs, 1929; Louderback, 1937; Bonilla, 1970; Cluff et al., 1970; Oakeshott, 1973; Sherard et al., 1974; Taylor and Cluff, 1977; Compton, 1985; McCalpin, 1987; Cluff, 1988; Bonilla, 1988(c)). The dip of thrust faults tended to range from 20° to 40°. Usually the dip of these faults became less steep as the bedrock fault rupture propagated up through soil. The upthrown block of thrust faulting was more likely to be warped or fractured. Hence, the zone of ground deformation above the upthrown block was more extensive. Normal faults tended to dip between 55° and 75°, although a number of normal faults dip nearly vertically. In the case of normal faulting, the dip of the fault plane became more steep as the rupture propagated through soil. Due to the development of gravity grabens and the increased likelihood of secondary fractures in the downthrown block, the zone of ground disturbance was typically wider above the downthrown block in normal fault movements. Strike-slip fault planes tended to be close to vertical. Although individual fault traces may fan out or "flower" near the surface in alluvium, the rupture usually continued to propagate in soil along nearly vertical planes. The zone of disturbance for strike-slip faults was typically narrow relative to that associated with other types of fault movement.

Oakeshott (1973) concluded, "Scarps in bedrock are much simpler and less extreme than scarps in colluvial materials. Bedrock scarps much more accurately reflect the true attitude of the fault surface and nature of movement." It was not surprising, then, that it was difficult to find detailed, informative field studies of how bedrock faults propagated through soil. Seismologists and geologists often concentrated on studying the surface expression of faults in bedrock or shallow soil sites since here the true character of the deeper bedrock fault rupture could be observed. Furthermore, a number of geologists suggested that fault ruptures (or offsets) within the bedrock could be "absorbed" in soil near the surface, and hence, the true magnitude of the fault offset could not be determined at surface expressions. On the other hand, gravity grabens often exaggerated the amount of fault displacement below the surface. It seemed reasonable, however, to expect that fault movement should generally dissipate as the rupture propagated through overlying soil deposits.

Much can be learned from reviewing the published discussions of experienced geologists regarding the surface faulting phenomenon. Earthquake faulting is a complex process which includes many unknowns. Each generalization seems to have its own exception. Yet, the guidance provided by these experienced geologists is potentially invaluable to the designer of dams to be built over faults. It is important to know what the "usual" manifestations of fault rupturing are and to anticipate the deviations from the "usual". In the next sections, specific informative surface rupture field studies will be examined to improve our knowledge of this phenomenon.

3.2.2 Indicative Fault Rupture Propagation Field Studies:

(a) Thrust Faulting:

- The 1964 Alaskan Earthquake:

On March 27, 1964, the Alaskan earthquake produced significant regional tectonic deformation along the south-central coastal area of Alaska. This magnitude 8.4 earthquake with its six magnitude 6.0 or higher aftershocks reactivated two high angle thrust faults on Montague Island in Prince William Sound. A map and profile showing the Patton Bay and Hanning Bay faults along with the tectonic displacements in the vicinity of Montague Island is presented in Figure 3-4. The surface faulting accompanying the 1964 Alaskan earthquake has been thoroughly studied by Plafker (1967). His report forms the basis for the review of this spectacular earthquake event.

Extensive down-warping of the upthrown block occurred in the vicinity of the distinct fault breaks. As shown in Figure 3-5, the upthrown block and downthrown block along the Patton Bay fault displaced or offset more than over 20 feet relative to each other across a 1000 foot wide zone. Only 6 to 8½ feet of this differential movement occurred on the 4 foot wide Patton Bay fault. The remaining 12 to 14 feet of relative displacement was taken up by the tremendous down-warping of the upthrown block of bedrock. This down-warping produced a number of tension cracks along pre-existing joints and bedding planes in the bedrock of the upthrown block. Figure 3-6 shows a number of these secondary cracks in the upthrown bedrock at locations where these cracks were exposed. A close-up of a crack near Hanning Bay fault is shown in Figure 3-7. Individual cracks were over 200 feet long. The cracks opened to widths of up to 0.4 feet and to depths of up to 7 feet. These cracks were typically located within 400 feet of the main fault scarps on the upthrown blocks. No newly opened cracks were found on the downthrown blocks. Cracks displaced primarily in extension perpendicular to

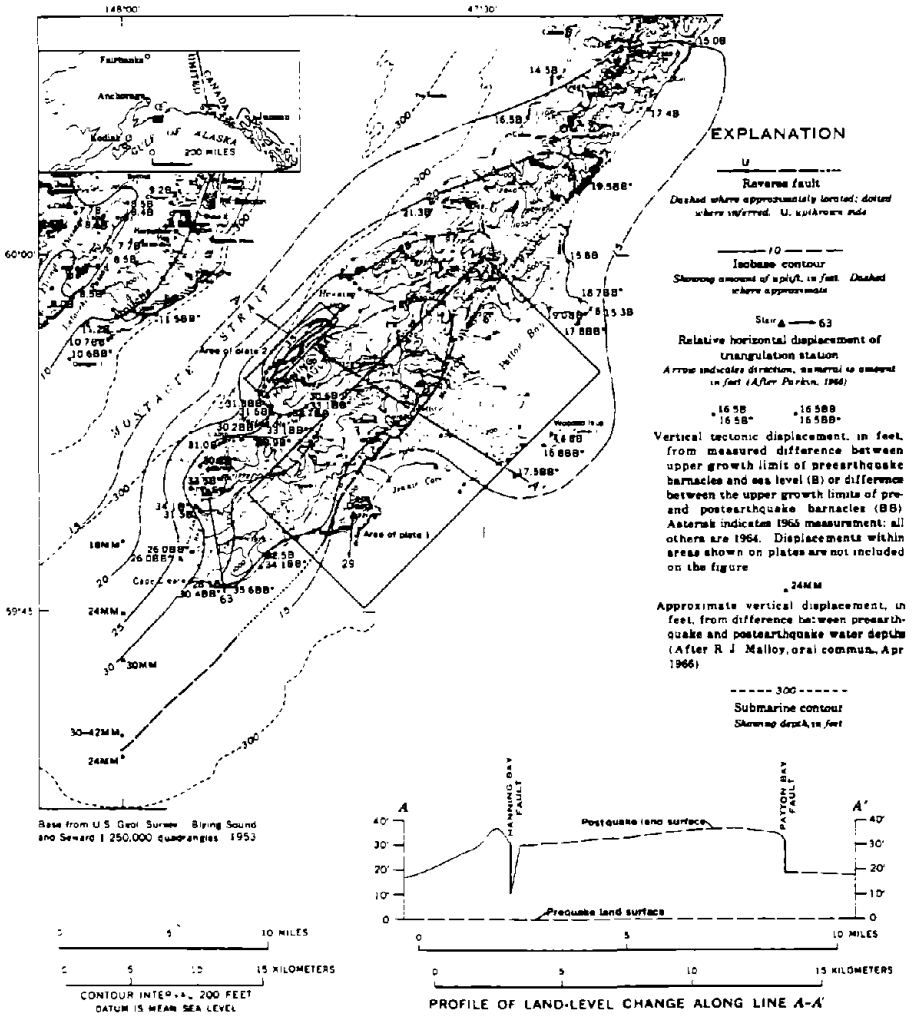

Figure 3-4: MAP AND PROFILE SHOWING FAULTS AND TECTONIC DISPLACEMENTS ON MONTAGUE ISLAND (after Plafker, 1967).

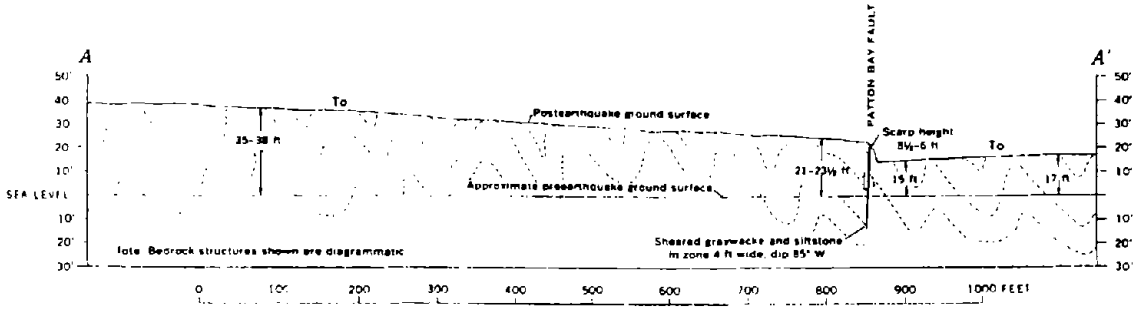

Figure 3-5: CROSS SECTION OF THE DEFORMED REGION IN THE VICINITY OF PATTON BAY FAULT (after Plafker, 1967).

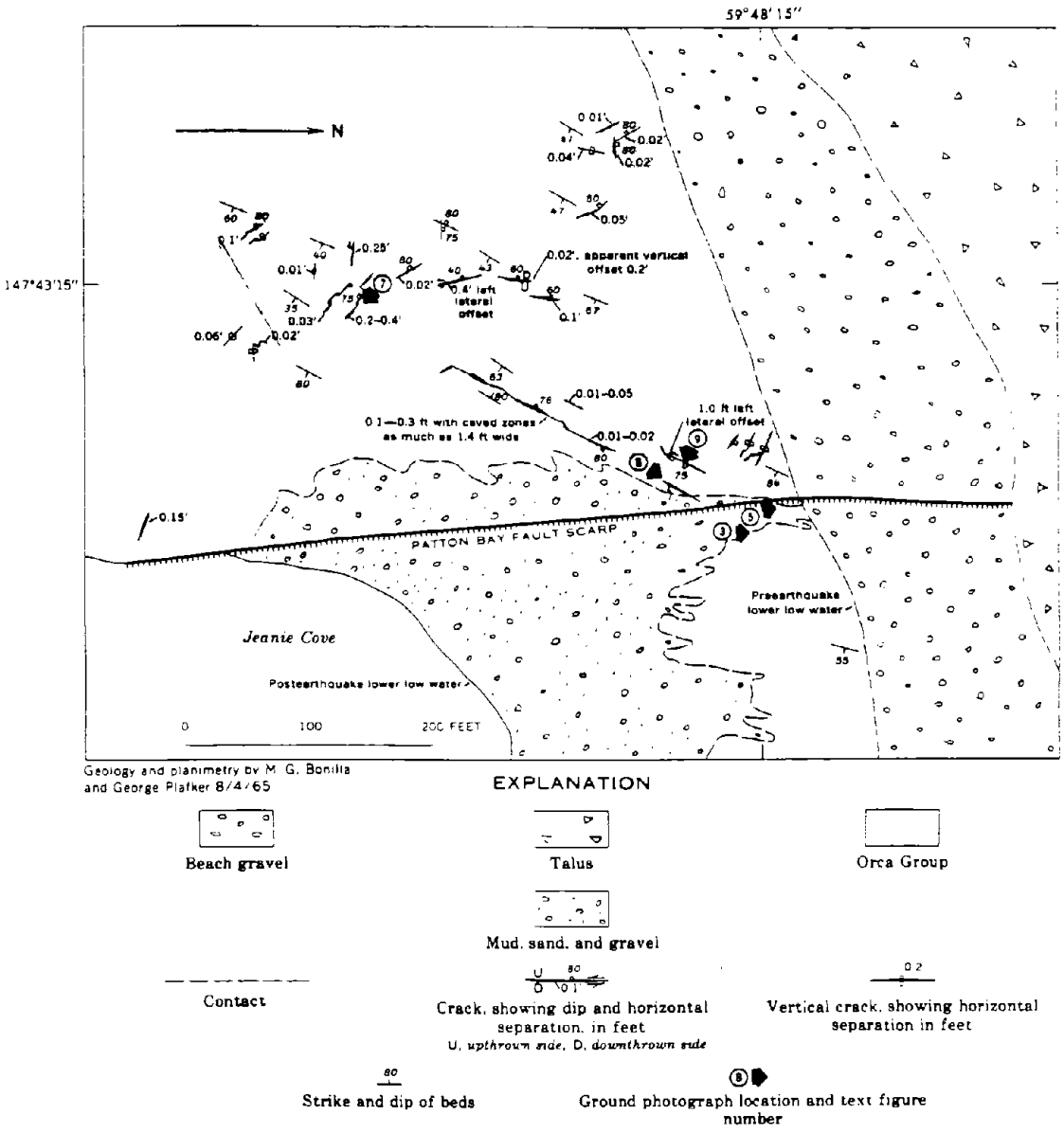

Figure 3-6: SKETCH OF TENSION CRACKS IN THE UPTHROWN BLOCK OF THE PATTON BAY FAULT NEAR JEANIE POINT (after Plafker, 1967).

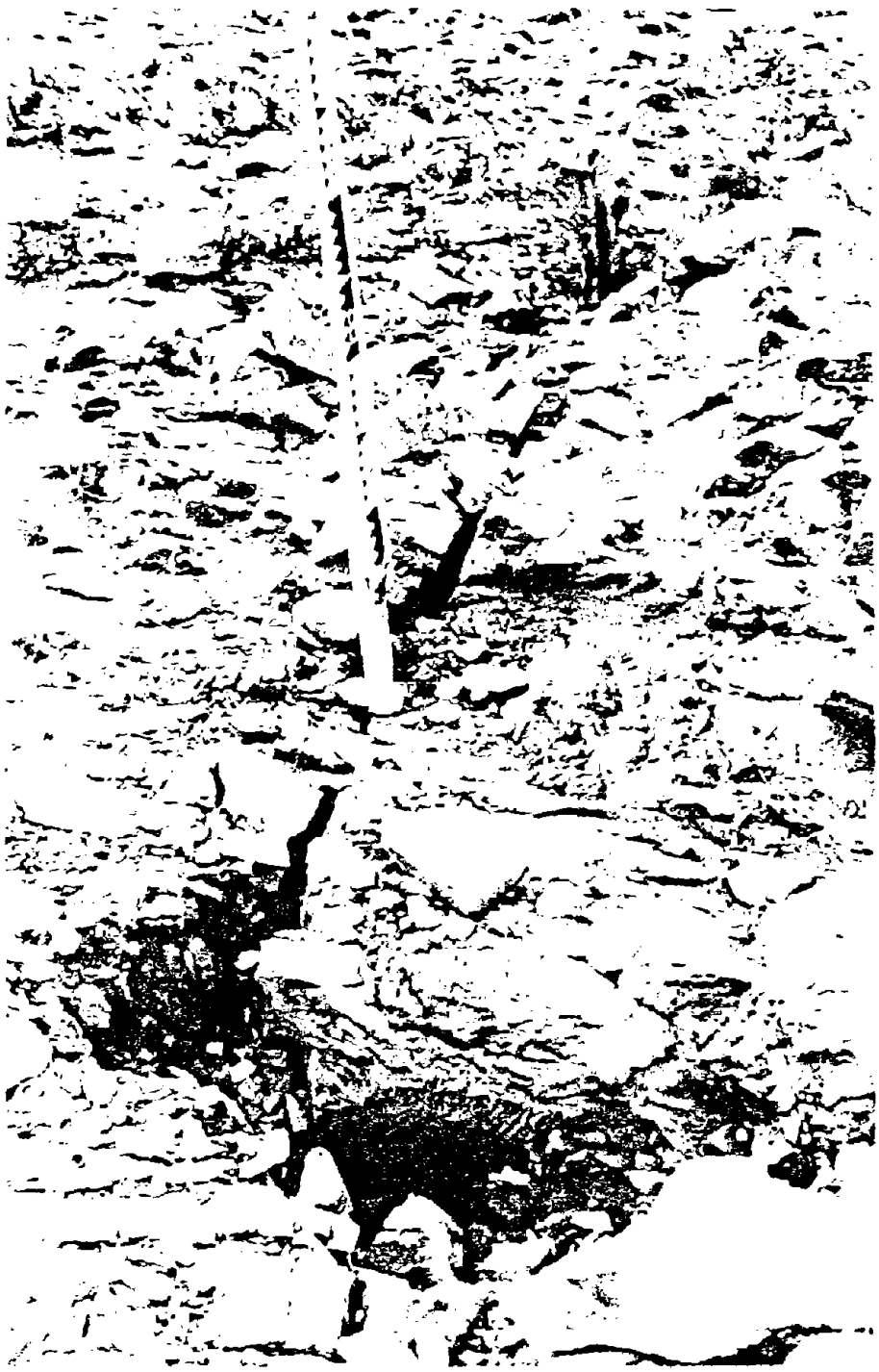

Figure 3-7: TENSION CRACK 2½ INCHES WIDE AND AT LEAST 7 FEET DEEP IN THE WARPED ZONE OF THE UPTHROWN BLOCK OF THE HANNING BAY FAULT (after Plafker, 1967)

the crack face, although a few cracks possessed a shear component also. The 1964 Alaskan earthquake was a powerful example of the dangerous secondary fracture effects which can be produced on the upthrown block of a thrust fault movement.

As shown in Figure 3-5, the 1964 Alaskan earthquake produced a 8 foot offset across the Patton Bay fault, which dips at about 85°, at the shore near Jeanie Point. Figure 3-8 shows this 8 foot scarp in the beach deposits at the bottom of a 500 foot high cliff composed of fractured rock. There was no offset, however, in the continuation of the Patton Bay fault at the top of the cliff. In fact, there was apparently no differential movement across any of the existing faults or fractures at the top of this cliff. Yet, on the backside of the cliff where the elevation dropped 350 feet from the top of the cliff, the fault scarp re-emerged along the continuation of the Patton Bay fault. Over 8 feet of displacement was "absorbed" in the fractured rock between the base and the top of the cliff shown in Figure 3-8. Bonilla (1970) concluded, "Evidently the faulting was distributed and taken up along the numerous joints and minor faults in the rock." This incident provided clear evidence that a fractured medium or granular material could locally absorb significant movements on a distinct bedrock fault plane.

Figure 3-8 illustrates another finding from Plafker's study of the surface faulting on Montague Island. The dip of the Patton Bay fault steepened as the fault traveled up the face of the 500 foot cliff. Plafker believed that the steep dip of 85° to 90° at this location "may represent only a near-surface steepening of the fault plane where it breaks to the surface along the most direct path". Rock outcrops along the trace of the Patton Bay fault showed the fault plane dipping at 65° to 85°. The Hanning Bay fault dipped at 50° to 60° at Fault Cove. When the fault propagated through deposits of glacial till just south of Fault Cove, the dip of the fault plane steepened to around 80°. Although this evidence is far from

Figure 3-8: PATTON BAY FAULT AT THE BEACH AND SEA CLIFF NEAR JEANIE POINT. THE DOTTED LINE AND SOLID LINE DELINEATE THE MAIN FAULT TRACE. THE LEFT SIDE MOVED UP AT THE BASE OF THE CLIFF ROUGHLY 8 FEET RELATIVE TO THE RIGHT SIDE. NO VERTICAL OFFSET EXISTS AT THE TOP OF THE CLIFF (after Plafker, 1967)

conclusive, it suggests that this steeply dipping thrust fault steepened even more as it propagated through fractured surface rock or glacial till.

Plafker complained that it was difficult to measure the inclination of the actual fault planes because bedrock offsets were often expressed at the surface by flexing and fissuring of overlying unconsolidated deposits. It was interesting to follow Plafker as he described the various surface expressions of the Patton Bay fault as it traveled up Montague Island. The changing surface expression of the Patton Bay fault movement during the 1964 Alaskan earthquake indicated that different overlying soil deposits produced unique orientations and magnitudes of surface displacements. A few examples of this phenomenon follow.

Fissures up to 3 feet wide with up to 5 feet of vertical displacement across them defined the fault break at the surface in an area of unconsolidated glacial till and peat vegetation. Approximately a mile away, where the fault intersected a previously flat 100 foot wide muskeg bog, the fault movement tilted the eastern half of the muskeg and produced an anticlinal flexure of its central section. No distinct fissures were observed. Further along the Patton Bay fault, a terrace deposit of stream gravel was displaced into four gently sloping steps 10 to 20 feet wide separated by three large fissures. The ground tilted toward the downthrown block to accommodate a vertical offset of at least 10 to 12 feet. At another point the fault was expressed by a 40 to 60 foot wide swath of trees tilted 20° out of vertical. Here, the net vertical displacement was 14 to 22 feet. Near this location the bedrock fault was exposed in a dry creek bed as a 3 foot wide zone of sheared siltstone. In the flood plain immediately north of this rock outcrop, the 20 foot offset was accommodated by an average 12° downslope tilt of the soil surface over a 100 foot wide area. In a deep valley deposit covered by peat moss over wet soil the fault offset produced a series of small cracks 1 to 4 inches in width in a zone a few hundred feet wide.

It was clear that the local surficial geology significantly influenced the character of the surface rupture. Stiffer till materials exhibited deep, wide fissures in a narrower zone of deformation or tilting; whereas softer, plastic, wet sediments usually accommodated the bedrock fault offset in a broad flexure with smaller and less distinct individual fissures. Of course, not all of the variations in the observed surface expressions of the fault could be attributed solely to soil and ground cover. For example, at one location a broad zone of deformation in the surface materials resulted from the widening of the Patton Bay bedrock fault in this area to roughly 75 feet instead of the normal 3 to 5 foot width. This widening of the bedrock fault zone occurred in a sheared siltstone material. An overwhelming number of observations, however, demonstrated the significant influence of local soil conditions on the character of the surface rupture.

Finally, it was remarkable given the magnitude of the fault movements on Montague Island, that they were not the primary features along which the earthquake occurred. Instead, the epicenter of the main shock was located approximately 90 miles away from the Patton Bay and Hanning Bay fault traces. The epicenter of the nearest major aftershock located along the projection of these fault traces was located more than 120 miles away. The 1964 Alaskan earthquake showed how a large earthquake could produce considerable tectonic deformations over an extensive region.

- The 1971 San Fernando earthquake:

On February 9, 1971, a magnitude 6.5 earthquake occurred on the San Fernando fault near Los Angeles, California. This moderate earthquake produced more than 14 miles of surface faulting, as a block of the western San Gabriel Mountains was thrust out over the San Fernando Valley. Considerable additional subsidiary faulting occurred within the upthrown block. Geologic cross sections

based on well data as well as geologic mapping indicated that the San Fernando Fault was fairly steep at depths greater than 1000 feet (i.e. fault dip greater than 60°; Yerkes, 1973). The estimated orientation of the fault plane at the earthquake's focal depth of around 5 miles was approximately 45° (Bolt, 1972). Numerous observations confirmed, however, that the dip of the San Fernando fault flattened to 30° or less as the fault propagated toward the ground surface through Tertiary sedimentary strata and Quaternary alluvium. For example, at one trench across a 2.3 foot scarp the fault dipped at 32° at depth but near the surface the fault plane bent over to become almost horizontal (Barrows et al., 1973). Since at this location the ground surface was fairly level, this bending over of the low angle thrust fault near the surface was believed to be a result of fault propagation behavior, not gravitational effects. A number of other thrust fault exposures mapped in the San Fernando area exhibited this same tendency to flatten in dip as the fault plane ascended toward the surface. The inclination of another group of thrust faults in this area, however, appeared to remain fairly constant over a considerable depth.

Surface faulting during the 1971 San Fernando earthquake also demonstrated the considerable variability that makes generalizations regarding fault rupture propagation difficult. Figure 3-9 presents two fault trench maps obtained along a subsidiary fault near the San Fernando fault. Trench 2 was located only 85 feet away from Trench 1, along the same fault trace. Whereas at Trench 1, the faulting produced a nearly vertical 3 foot high scarp, at Trench 2, the fault was expressed at the surface by a 3 foot high flexure approximately 60 feet wide. No distinct surface rupture was observed at Trench 2. The variation in these surface expressions of the fault rupture may be partially explained by the variations in earth materials at these two sites. Whereas Trench 1 cut across a segment of the fault bordered by more competent earth materials like siltstone and sandstone,

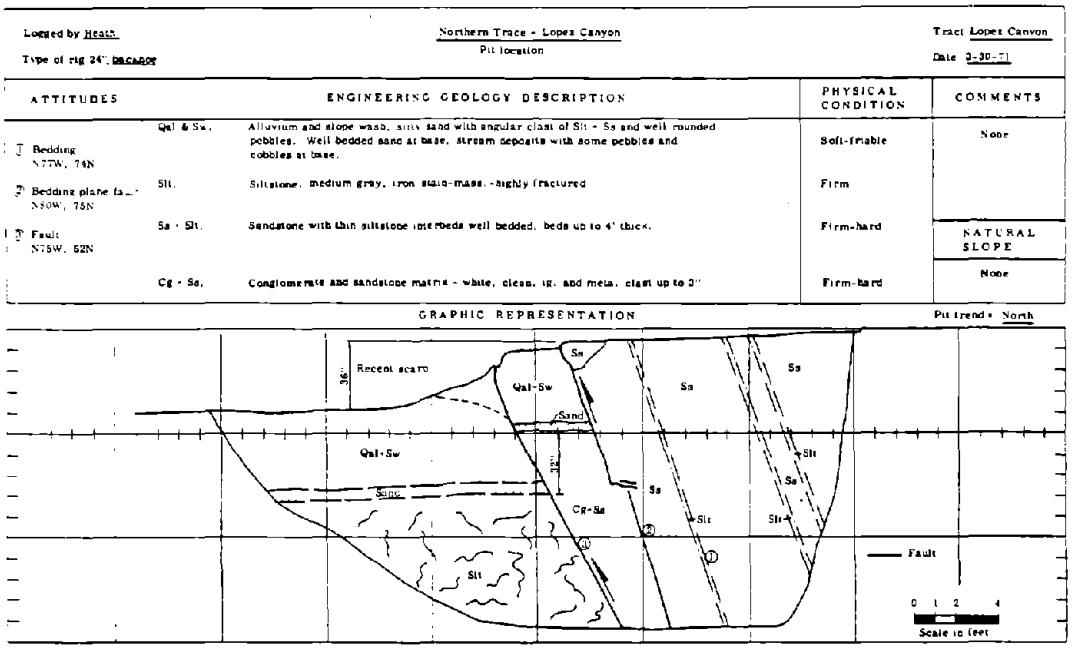

(A) Trench 1

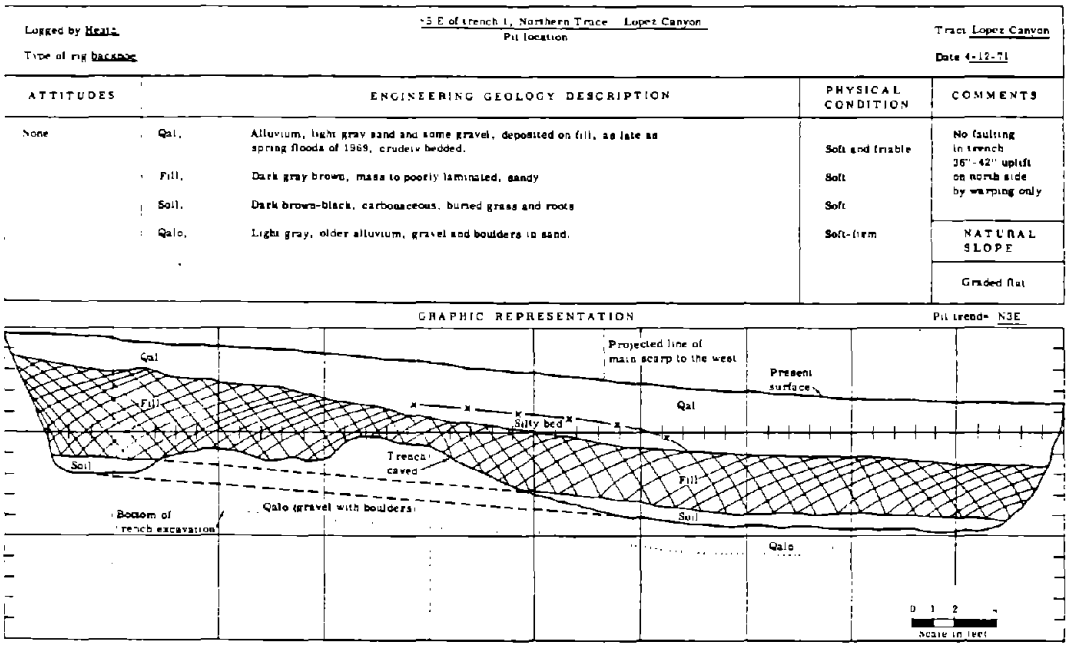

(B) Trench 2

Figure 3-9: GEOLOGIC PIT LOG FOR TRENCHES 1 AND 2 ACROSS A SUBSIDIARY FAULT OF THE 1971 SAN FERNANDO EARTHQUAKE (after Heath and Leighton, 1973)

Trench 2 was located at a site where loose fill and stream deposited alluvium overlay the bedrock fault rupture. Although not the only factor influencing the character of the surface expression of deeper fault ruptures, local soil and rock conditions appeared to be a significant factor.

Movement on the Veterans fault during the 1971 San Fernando earthquake provided another example of the potential importance of surface materials. Differential movement along the bedrock fault plane near the surface was measured to be 6 to 8 inches. The differential movement at the surface decreased to 2 to 3 inches at locations where the Veterans fault was beneath earth fill. Similar to the frustration voiced by Plafker (1967) in the last section, Yerkes (1973) found that it was difficult to identify fault ruptures in "unconsolidated" (soil) materials. Where the fault intersected consolidated (rock-like) materials, the fault ruptures could be seen more easily. Barrows et al. (1973) noted that faults which cut across ridge and canyon topography produced clean vertical offsets in the rock ridges but no visible surface offset in the canyon deposits of soil. Finally, the geologists involved in the post-earthquake investigation warned that it was difficult to determine the activity of faults overlain by loose unconsolidated deposits. Bonilla (1973) concluded,

> Ten out of 16 trenches across 1971 surface ruptures clearly revealed the ruptures, but six trenches yielded no or very equivocal evidence of the ruptures. Fault ruptures can be extremely difficult or impossible to see in massive unbedded material ranging from silt and clay to coarse bouldery sand and gravel.

Oakeshott (1973) agreed, "This confirms experience elsewhere; absence of an obvious fault in a trench does not in itself prove a fault is not there!"

- The 1952 White Wolf, California earthquake:

The 1952 White Wolf, California earthquake (also named the Arvin-Tehachapi earthquake of 1952) produced about 32 miles of discontinuous surface faulting. The width of the fault zone varied from a narrow individual scarp to a complex series of fractures over a mile wide. Oakeshott (1973) explained, "Steep topography, the low near-surface angle of thrusting, interrupted faulting, and lurching make for a highly complex pattern in this fault zone." The magnitude 7.7 earthquake caused left-lateral horizontal movements as well as thrust dip-slip fault movements. A bedrock block at the edge of the Sierra Nevada Mountains was uplifted about 3 to 4 feet and thrust over the alluvium deposits of the San Joaquin Valley. This thrust displacement was accompanied by about 2 feet of left-lateral movement. At the surface along the main rupture zone, movement on low-angle thrust fault planes (i.e. dip angles of 5° to 20°) produced compression ridges or mole-tracks about 3 feet high. Oakeshott (1973) noted that seismological computations estimated that the dip of the fault rupture plane in the bedrock at depth was around 60° to 66° . The uplifting of the mountain block appeared to create a fault rupture which bent over and decreased in dip as the rupture propagated toward the surface.

Another noteworthy observation was made by Buwalda and St. Amand (1955). "We have the dilemma that the faults indicated at the tunnels show displacements of at least several feet while the moletracks which are presumably their continuation on the hill above show relatively small offsets both horizontally and vertically." The differential movement on the fault plane which was readily detected in a concrete lined buried railroad tunnel was distributed and largely absorbed in the fractured, weathered bedrock and soil between the tunnel and the ground surface. This appeared to be further clear evidence that differential

movement across fault ruptures can dissipate as the fault rises up on toward the ground surface through overlying soils.

- The 1980 Algeria earthquake:

A large magnitude earthquake in Algeria in 1980 produced significant tectonic deformations over a wide area. Displacements or offsets on the primary thrust fault reached 8 to 12 feet in places. The fault plane decreased in dip as the fault rupture propagated toward the surface. Distinct breaks or compression ridges along the surface marked the trace of the thrust faults. Significant secondary tectonic deformation in the upthrown block accompanied this major thrust fault movement. Severe normal faulting took place in a region of local extension in the hanging wall above the thrust fault plane. This extension zone in the upthrown block was approximately a half a mile to a mile behind the compression zone created at the trace of the thrust faults. The geologic cross-section shown in Figure 3-10 attempted to explain the development of the compression and extension zones at the surface.

- The 1945 Mikawa, Japan earthquake:

The magnitude 7.1 1945 Mikawa, Japan earthquake produced about 7 feet of differential displacement across a very narrow thrust fault in bedrock. A Japanese researcher reported that there was extensive damage on the upthrown block but negligible damage in the downthrown block of this thrust fault movement. A long section of the fault plane was later exposed in a quarry pit. This fault rupture through bedrock materials near the surface was a clean, narrow, continuous break between the two adjacent rock masses (Department of Water Resources, 1974). Within the rock materials the fault plane dipped at 50° to 70°. Where the bedrock was not exposed, the fracture propagated through overlying

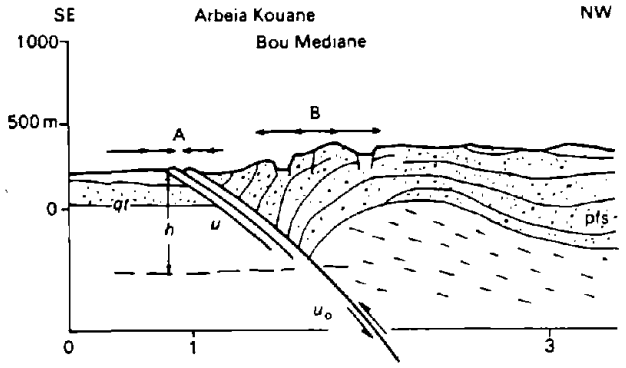

Figure 3-10: GEOLOGIC CROSS SECTION ACROSS THE THRUST FAULT PRODUCING THE 1980 ALGERIA EARTHQUAKE. THE COMPRESSION ZONE (A) IS LOCATED ALONG THE TRACE OF THE THRUST FAULTS. THE EXTENSION ZONE (B) IS LOCATED IN THE HANGING WALL OF THE THRUST FAULT (after Ambraseys and Jackson, 1984)

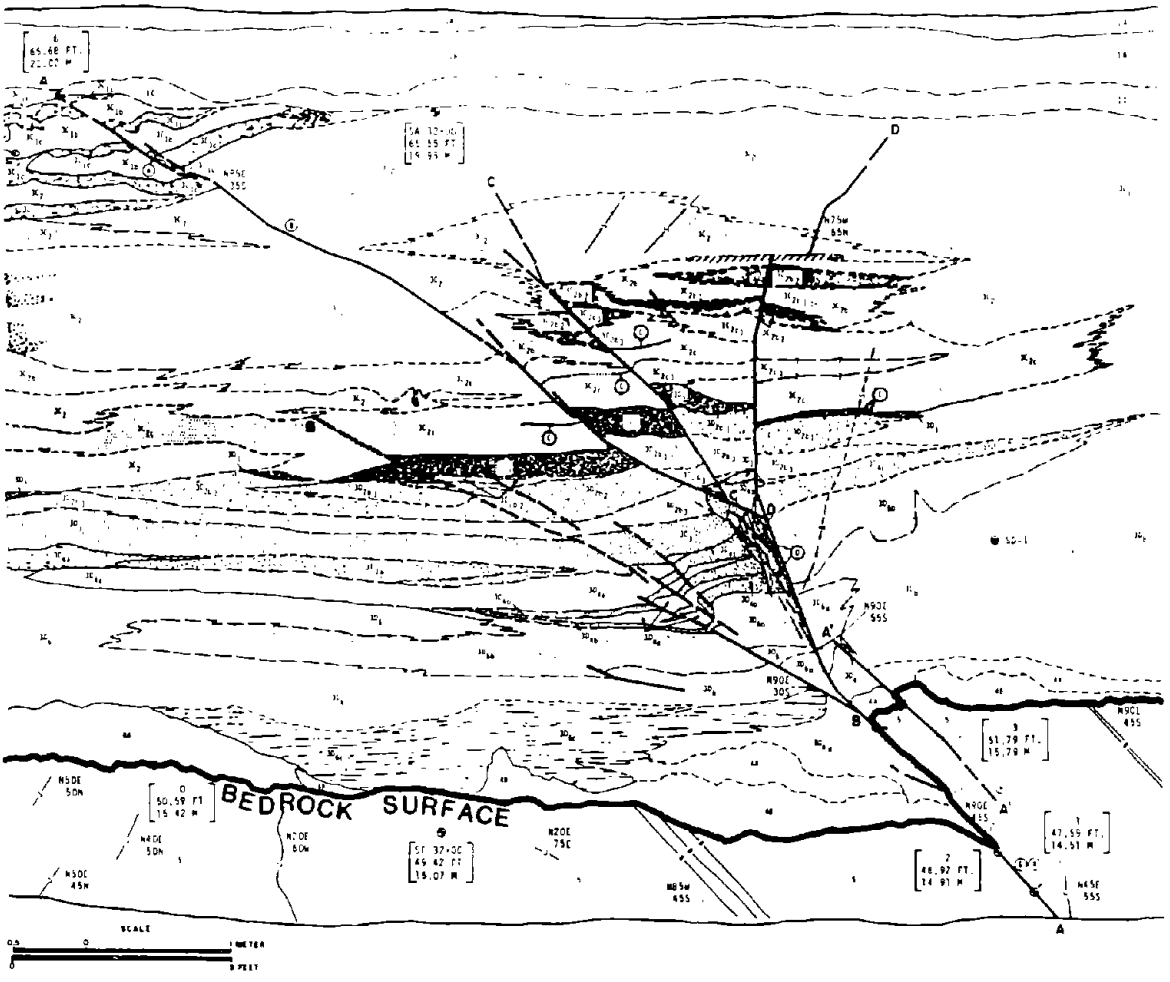

Figure 3-11: ARROYO FAULT EXPOSURE AT POINT CONCEPTION, CALIFORNIA (after Roth et al., 1982)

soil deposits at a flatter dip. At the surface of the soil deposits, the dip of the fault plane was reduced to 15° to 20° (Richter, 1958).

- Fault Exposures at Point Conception, California

A comprehensive geoseismic investigation performed in conjunction with siting a proposed Liquified Natural Gas (LNG) terminal near Point Conception, California produced data on a number of low-angle thrust faults (the most significant of these being the Arroyo fault) which propagated up through 10 to 20 feet of alluvium (Dames & Moore, 1980). Detailed maps were prepared for each trench excavated across the fault traces. The orientation of each fault plane in the bedrock and in the Quaternary terrace deposits was listed. Of the 20 exposures of thrust fault traces where the fault plane attitude could be detected in the bedrock and in the soil deposits above, 12 of these fault planes decreased significantly in dip as the fault rupture propagated from the bedrock through the overlying soil toward the surface. In these cases, a decrease in the fault plane attitude of at least 10° was considered significant. The remaining 8 fault planes did not increase nor decrease significantly in dip in passing from the bedrock to the overlying soil materials. None of the 20 fault planes exposed in the trenches were significantly steeper in the soil deposits above the bedrock materials. The low-angle bedrock thrust fault ruptures tended to flatten out as they propagated through overlying soil deposits.

The faults observed at this site were narrow individual shear planes or narrow bands of multiple shear planes. The Arroyo fault exposure proved to be the exception (See Figure 3-11). It displayed normal fault movements as well as thrust fault movements. The differential movement across the fault in alluvium at this location occurred on individual shear fractures, not in wider distorted shear zones. The soil and rock a short distance away from these individual shear planes

appeared fairly intact. The fault strands which displaced the soil in a thrust manner (labeled A, B and C) generally flattened as they propagated through the soil. The normal fault strand (labeled D), however, steepened as it propagated through the overlying alluvium. This one fault exposure portrayed the typical fault rupture upward propagation paths of both thrust and normal faulting.

- Study of Basement Rock Block Faulting in Wyoming:

Extensive field studies of the Laramide deformation of the Rocky Mountains foreland in Wyoming carried out during a four year period provided the basis for a comprehensive report of basement rock thrust faulting by Prucha, Graham and Nickelsen (1965). This field study included a review of pertinent published papers and U.S.G.S. geological maps of the Wyoming Province. In their attempt to understand the predominant structural features of this region, the authors developed an hypothesis to explain how fault ruptures in the metamorphic or igneous basement rock propagated up through the overlying sedimentary rocks. They substantiated their hypothesis with the results from the stress field analyses, sandbox model studies, and field studies of the Wyoming province. The results from the field studies will be explored here.

Prucha, Graham, and Nickelsen (1965) advanced the theory that uplift of a basement rock block relative to an adjacent block on a distinct vertical fault would produce a fault plane in the overlying sedimentary rocks that initially would be oriented vertically but toward the surface would bend over to dip at a low angle over the downthrown block. Figure 3-12 illustrates the characteristic profile of these hypothesized upthrust faults, and portrays the authors' postulated sequence of deformation of the sedimentary rock beds overlying the offset basement rock blocks. The authors explained,

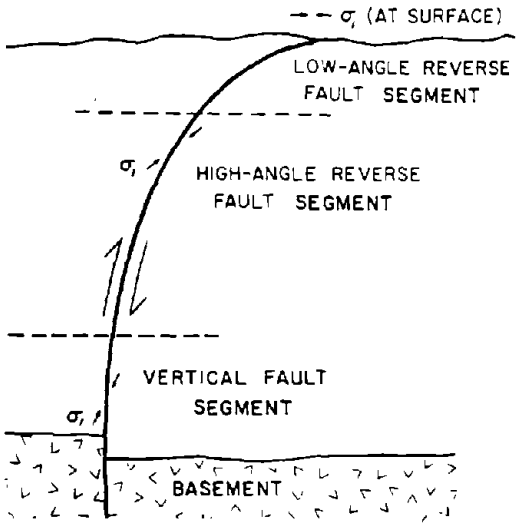

(A) Upthrust Fault Profile

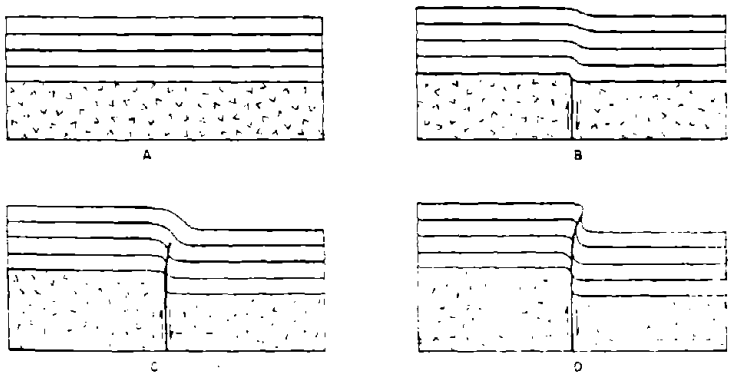

(B) Development of the Upthrust Fault

Figure 3-12: CHARACTERISTIC PROFILE OF THE WYOMING PROVINCE UPTHRUST FAULTS AND POSTULATED SEQUENCE OF FAULT DEVELOPMENT (after Prucha et al., 1965)

> The exact shape of an upthrust fault above the related discontinuity in the basement depends on the thickness of the sedimentary section above the basement, the type of rocks involved, the attitude and magnitude of the discontinuity in the basement, the topographic effects produced by the faulting, and other factors. As a generalization, however, the steep ($> 45^{\circ}$) segments of an upthrust fault constitute the major part of it. Thus, one would expect in nature, as experience confirms, that the steep segments of upthrusts are more commonly found than the flat upper segment. Post-faulting erosion removes the flatter segment of an upthrust first, and this too increases the relative abundance of the steeper parts.

Examination of their postulated sequence of deformation in the sedimentary rock beds overlying the basement fault blocks was also interesting. As shown in Figure 3-12, initially the lower most beds adjusted to the basement rock fault offset by "drape folding" (B). When some limiting strength threshold was reached, these beds failed by faulting (C). Eventually, enough basement rock movement occurred to propagate the fault rupture to the surface (D). As previously noted, sandbox model test results "validated" the authors postulates.

Sound field evidence, however, is always more persuasive than results from model tests. Prucha et al. presented a number of geologic field studies to help validate their hypothesis that vertical basement rock faults decrease in dip as they approach the surface. They interpreted the surface expression of the Long Gulch fault near Bellvue, Colorado as evidence of a plunging upthrust fault plane. As shown in Figure 3-13(A), the Long Gulch fault is expressed at the surface as two distinct segments with divergent dips and strikes. The geometric relations between the high and low angle segments of a plunging upthrust fault plane and an horizontal erosion surface is shown in Figure 3-13(B). Between A and B, the fault appears at the surface as a nearly vertical thrust fault. The trace of segment BC curves to right and it dips at a low angle. The divergent dips and strikes of the Long Gulch fault expressed at the surface are just different manifestations of the same basement rock plunging thrust fault.

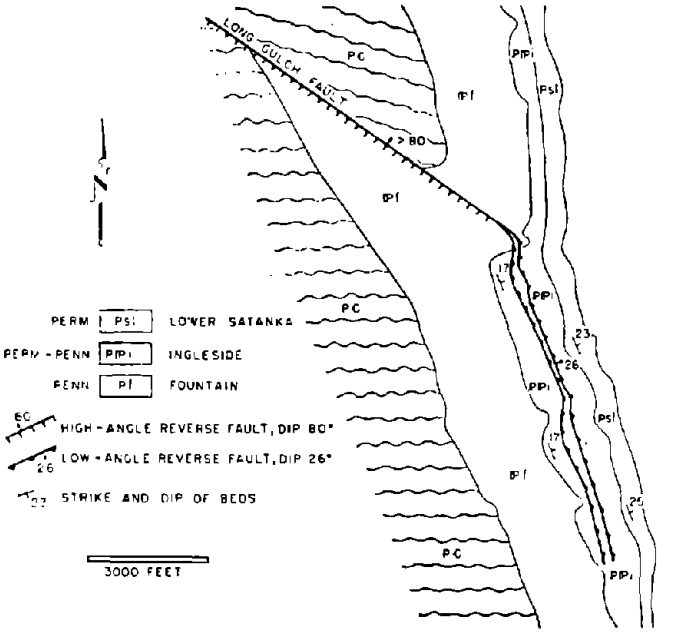

(A) Geologic Map of Area

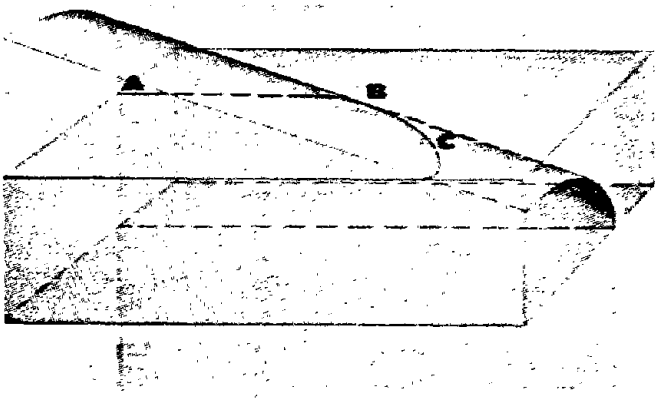

(B) Illustration of How Divergent Surface Expressions Developed

Figure 3-13: FIELD RELATIONS AND GEOMETRIC RELATIONS BETWEEN THE HIGH-ANGLE AND LOW-ANGLE SEGMENTS OF THE LONG GULCH FAULT (after Prucha et al., 1965)

The authors also presented geologic interpretations of other formations. The low-angle segments of the upthrust faults produced the compression structures found in this region. Secondary crustal deformation and faulting occurred above the uplifted basement block in a zone of extension. The postulated folding of the sedimentary beds before the development of a distinct shear plane could be observed at several of the sites studied. They concluded, "The characteristic asymmetry of basins and uplifts, the diversity of structural trends, and the close relation between faulting and folding all are consistent with the concept of structural control by basement block faulting."

Finally, Prucha et al. presented one more interesting view of the fault rupture propagation phenomenon. Two different profiles of thrust faults are shown in Figure 3-14. The fault plane in Diagram A becomes progressively steeper as the rupture approaches the surface. This concave upward thrust fault is produced by regional horizontal compression. This type of fault profile appears to be analogous to the failure surface created by the passive earth failure behind a rigid retaining wall. On the other hand, the fault plane in Diagram B becomes progressively shallower as the rupture approaches the surface. This convex upward thrust fault is produced by the differential vertical uplift of basement rocks as previously described. This type of fault profile appears to be analogous to the failure surface created when a rigid anchor is pulled out of the ground. Prucha, Graham and Nickelsen's simple illustration of the two different tectonic mechanisms that produced these different fault rupture patterns is interesting, and appears to lend itself to these two analogies.

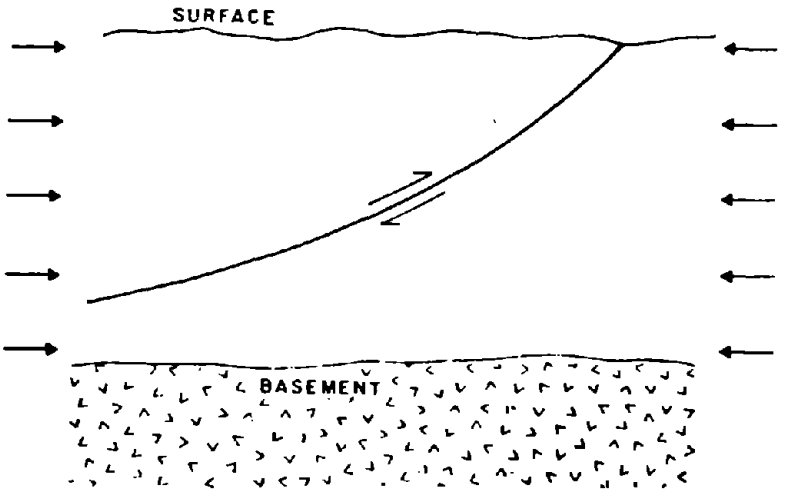

(A) Regional Horizontal Compression

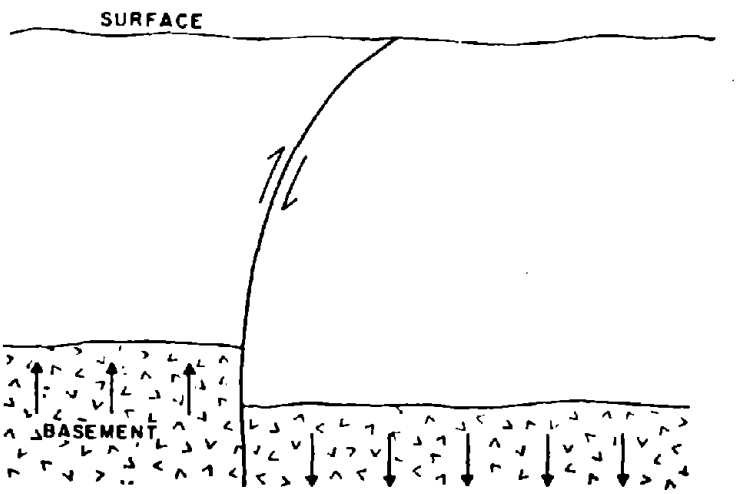

(B) Differential Vertical Uplift

Figure 3-14: PROFILE OF THRUST FAULTS PRODUCED BY REGIONAL HORIZONTAL COMPRESSION AND DIFFERENTIAL VERTICAL UPLIFT (after Prucha et al., 1965)

(b) Normal Faulting:

- The 1954 Dixie Valley-Fairview Peak, Nevada earthquake:

A magnitude 7.1 earthquake centered near Fairview Peak followed four minutes later by a magnitude 6.8 shock near Dixie Valley on December 16, 1954 constituted the 1954 Dixie Valley-Fairview Peak, Nevada earthquake. These earthquake events combined to produce significant surface faulting in an arid region 60 miles long and 20 miles wide. The amount and directions of displacements across the faults in this area were extremely variable. The maximum strike-slip component recorded was 12 feet. Likewise, the maximum normal dip-slip component recorded was 12 feet. The faults usually displaced predominantly in a normal dip-slip manner. Articles by Slemmons (1957) and Oakeshott (1973) provided the basis for this review of the 1954 Dixie Valley-Fairview Peak, Nevada earthquake.

Most of the fault ruptures took place near the contact between an alluvial valley and the bedrock range adjacent to it. Gilbert (1890) found this set of circumstances conducive to the development of gravity graben structures in the alluvial deposits. As shown in Figure 3-15, these graben structures formed when the attitude of the fault plane increased as the rupture propagated into the alluvium. Fault scarps in this case history exhibited all four of the behaviors described by Gilbert. An example is shown in Figure 3-16. Slemmons (1957) observed Gilbert's postulated change in the dip of the fault plane as it left the bedrock and entered into the alluvium. A bedrock fault which dipped at about 55° to 65° increased in dip to 70° to 90° as the fault propagated through alluvium. This tendency for a normal fault to become steeper as it approached the surface seemed to generally hold true at locations away from the bedrock-alluvium contact. At depth, in a firm consolidated alluvium the fault plane was measured at an angle

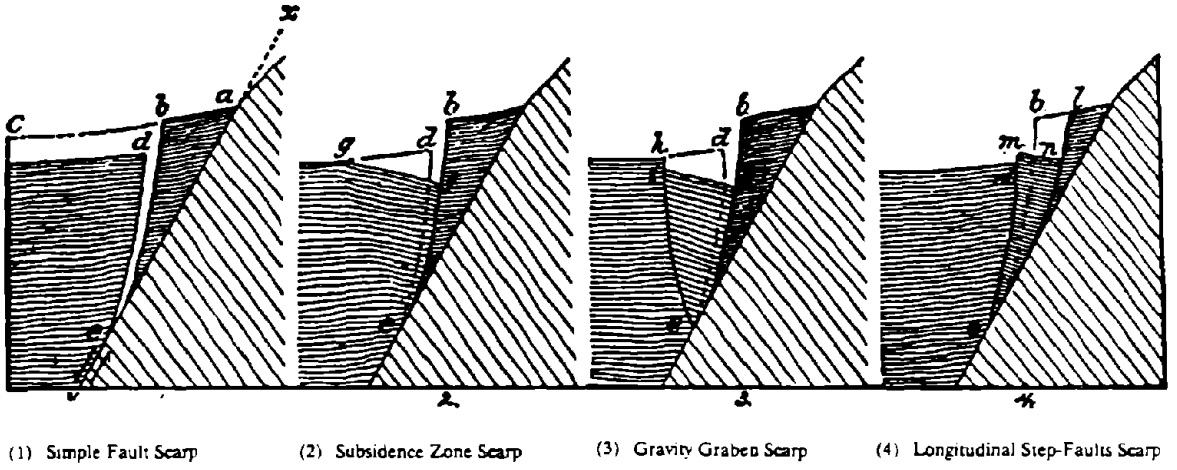

Figure 3-15: GILBERT'S THEORY OF FAULT SCARPS IN ALLUVIUM. DIAGONAL LINES DELINEATE BEDROCK; THIN HORIZONTAL LINES DENOTE ALLUVIUM (after Gilbert, 1890)

Figure 3-16: GRAVITY GRABEN IN DIXIE VALLEY (after Slemmons, 1957)

of dip of 60° . As the fault plane broke to the surface in the looser alluvium above, it steepened to an almost vertical fracture.

The 1954 Dixie Valley-Fairview Peak surface faulting often took the path of least resistance. Slemmons (1957) observed locations where the main scarp left the usual position near the contact between the valley soil deposits and the horst bedrock mountains. Instead, the rupture cut a straight path across the valley between two points on irregular segments along the bedrock-alluvium contact. This tendency to take the most direct route was also demonstrated in the vertical plane when fault ruptures along the alluvium bedrock interface propagated up to the surface through the alluvium at a much steeper dip.

Because of the development of a gravity graben or subsidence zone adjacent to the fault scarp, scarp heights in alluvium, especially on steep slopes, were sometimes much higher than the actual bedrock offset. Gilbert's figures (see Figure 3-15) illustrated the point that local gravity effects could exaggerate the apparent fault offset. Additionally, fault scarps grew when the near vertical face of the original break began to sluff and retreat uphill. At one location, photographs of a fault scarp just 5 days apart showed an increase in the scarp height of about 3 feet. Sluffing and ravelling of the face of the scarp, not additional earthquake faulting, produced this apparent increase in the fault offset.

Without these gravity effects, however, fault offsets in the alluvium were smaller, not larger, than the bedrock fault offsets below. Near Fairview Peak, the scarps were generally 3 or 4 feet high in the alluvium. Where the fault was in bedrock the offset was measured to be about 7 feet. Slemmons (1957) made another interesting observation at this location. As described, the scarp remained about 3 to 4 feet high across this area, except for a quarter mile gap where the surface rupture disappeared beneath an alluvial fan. One plausible explanation for

this observation was the hypothesis that the loose granular materials comprising the alluvial fan locally absorped the vertical fault movement.

Three final points should be made. In general, single, simple fault ruptures appeared at the surface where the fault propagated up through bedrock or well-consolidated alluvial materials. The surface expression of fault ruptures in looser materials was typically much more complex. Secondary deformations occurred predominantly in the normal fault's downthrown block. Finally, precise leveling of U.S. Highway 50 indicated that the Fairview earthquake produced a 25,000 foot wide subsidence zone. Over 20,000 feet of this subsidence zone was located in the downthrown block. The majority of the differential movement occurred across two 300 foot wide fault zones.

- The 1959 Hebgen, Montana earthquake:

The magnitude 7.1 Hebgen, Montana Earthquake of 1959 created a subsidence zone about 15 miles wide and 30 miles long southwest of the Hebgen and Red Canyon faults. Fifty square miles within this subsidence zone in the hanging walls of the normal fault systems subsided over 10 feet. Movement on the Hebgen and Red Canyon faults produced 22 miles of surface ruptures. The main fault scarps were paralleled by numerous secondary breaks in the unconsolidated material above the downthrown block. Withind et al. (1962), Streinbrugge and Cloud (1962), Hadley (1964), Meyers and Hamilton (1964), and Witkind (1964) published detailed accounts of this seismic event.

Simple fault scarps as well as complex graben structures were formed at the surface as a result of the intense bedrock faulting. In either case, bedrock fault planes were usually refracted to steeper orientations in the overlying colluvium. As Gilbert (1890) had described, this change in the dip of the rupture plane produced large open fissures along the main scarps. Figure 3-17 shows the gap created at a

Figure 3-17: GAP OF A SIMPLE FAULT SCARP AS EXPOSED ALONG THE TRACE OF THE HEBGEN FAULT (after Witkind et al., 1962)

simple fault scarp structure. The dip of the exposed rupture surface depended on the kind of surficial material ruptured. Scarps in clayey soils stood nearly vertical, whereas, fault planes in less coherent colluvium materials dipped at lower angles of between 60° and 85°. The investigators believed that the bedrock faults dipped at about 60°. Of course, there were exceptions to these general observations. Where the slope of the ground surface was steep, the fault sometimes did not refract into the colluvium above the bedrock but continued along the bedrock-colluvium interface. The coherent, inclined mass of earth shifted downslope as a unit to take up the displacement on the concealed bedrock fault.

Monoclinal warping and mole-track thrusting provided further evidence of the changing attitude of the fault rupture as it travelled through unconsolidated earth materials. The West Yellowstone basin was a broad plain underlain by a thick deposit of obsidian sand and fine gravel. Witkind et al. (1962) explained,

> Monoclines prodominate at the surface, but are believed to result from extreme near-surface refraction of faults that are normal at greater depth, or from draping over normal faults which do not break the surface . . . Features such as the anomalous dips of fault scarps and the mole-track thrusts are attributed to the combined effects of extreme surficial refraction of bedrock normal faults, which characteristically change dip upward into weak, unconsolidated material, and contemporaneous mutual slump of both walls of the refracted faults.

A diagram illustrating these concepts is shown in Figure 3-18. Differential movement across the mole-track thrust structures at the surface ranged from a few inches to nearly 3 feet. It seemed that larger bedrock fault offsets were dissipated within this unconsolidated soil deposit.

Brune and Allen (1967) calculated that the subsurface displacement or offset along the deep fault rupture which produced the 1959 Hebgen earthquake was more than 40 feet. This calculation was made using dislocation theory. The largest surface rupture produced by the earthquake was only 20 feet. Hence,

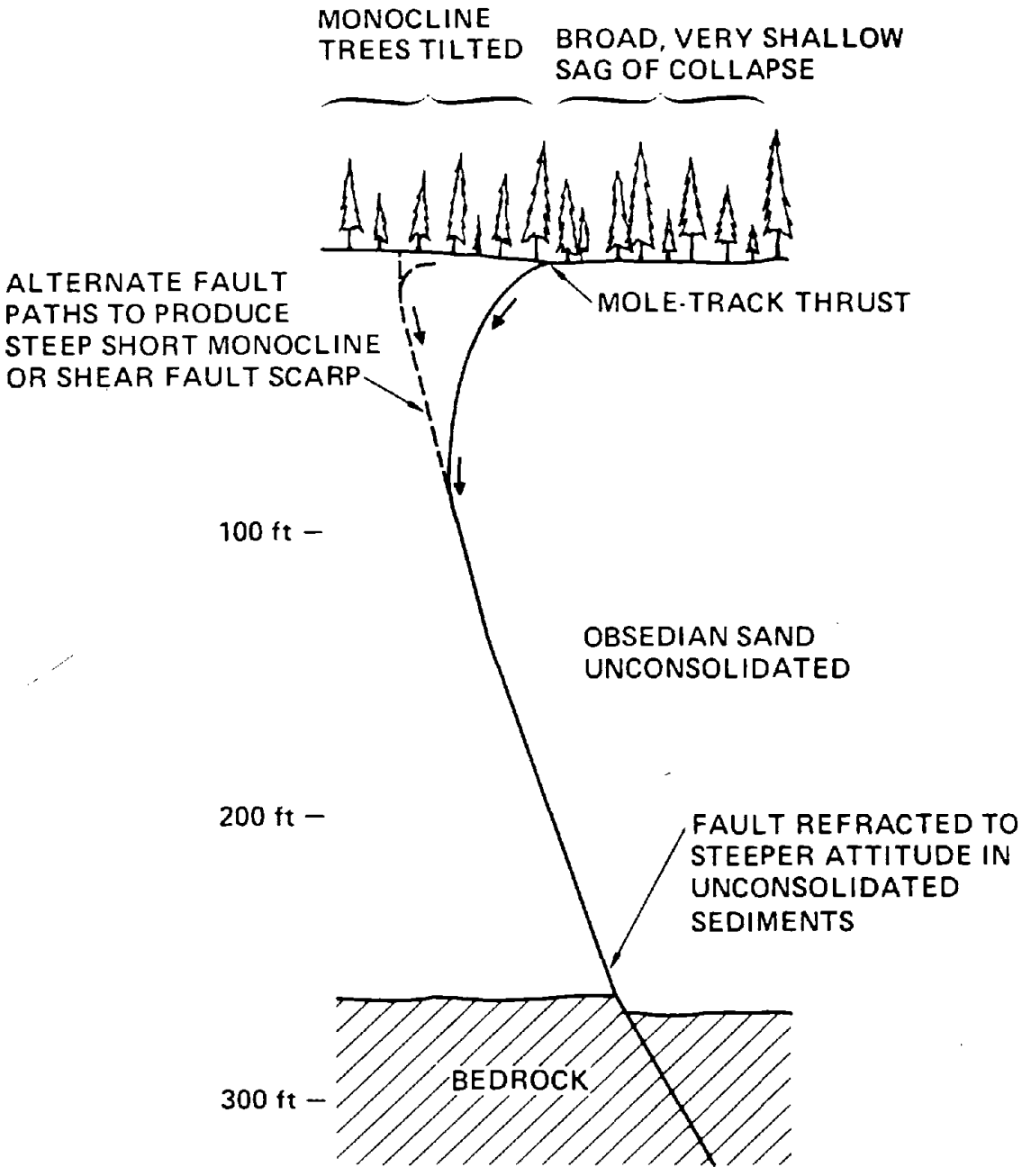

Figure 3-18: FAULT RUPTURE PROPAGATION OF A BEDROCK NORMAL FAULT MOVEMENT THROUGH A DEEP UNCONSOLIDATED DEPOSIT NEAR HEBGEN LAKE, MONTANA (after Lade et al., 1984)

calculations based on dislocation theory suggested that differential movement at the surface could be substantially less than the primary fault rupture displacement at depth. Again, a case could be made that differential movement dissipated as the fault rupture propagated toward the surface through the soils.

- The 1983 Borah Peak earthquake:

The October 28, 1983 Magnitude 7.3 Borah Peak earthquake in central Idaho produced more than 22 miles of surface faults (Taylor et al., 1985; Crone et al., 1987). The downthrown block's valley surface subsided more than 10 feet in some locations. The observed surface ruptures came in many forms. Bedrock faulting created zones of ground breakage as wide as 450 feet, complex gravity grabens, en echelon diagonal scarps, and single scarps nearly 16 feet high. Generally, the fault scarps followed near the mountain bedrock and valley alluvium contact, although at one location, the scarps did deviate from the bedrock-alluvium contact where a more direct path between two points along the bedrock-alluvium contact 2½ miles apart existed.

The average offset along the surface fault features was 3.6 feet. Doser and Smith (1985) estimated that the average coseismic displacement at depth was on the order of 4.6 feet, based on the seismic moment. Stein and Barrientos (1985) estimated the average subsurface displacement to be 7.2 feet, based on modeling of geodetic data. In any case, these calculations suggested that some fraction of the dip-slip offset at depth failed to reach the ground surface. Four separate analyses of teleseismic data from the earthquake's main shock calculated the dip of the fault plane at depth to be on the order of 45° to 60° (National Earthquake Information Service, 1983; Barrientos et al., 1985; Dewey, 1985; Dosier and Smith, 1985). Individual fault planes cutting through the surface alluvial deposits were found to dip significantly more steeply at angles of between 60° and 90°. Often the

cohesive soil near the surface was able to sustain vertical or overhanging scarp faces. Crone et al. (1987) noted,

> The observed surface faulting characterizes the slip at depth only in a general manner. At places, the apparent dip and strike of the fault determined by the relationship of the scarps to the topography are dramatically different than the dip and strike measured in natural and man-made exposures. These discrepancies can be caused by irregularities in the fault plane, multiple fault strands, refraction of the fault in surficial materials, and slumping.

As discussed, the 1983 Borah Peak earthquake produced various patterns of surface ruptures. A 75 to 150 foot wide zone of complex ground breakage is shown together with a close-up shot in Figure 3-19. Crone et al., 1987 offered the plan view and cross section shown in Figure 3-20 as an explanation of this pattern of surface ruptures. The fault scarp cut across a gentle sloping alluvial fan of substantial thickness. Similar to how Witkind et al. (1962) explained the mole-track thrusts formed during the 1959 Hebgen earthquake, Crone et al. (1987) reasoned that the low-angle surface thrust fault in this otherwise extension zone developed because of the change in dip of the principal normal fault plane as it cut through the alluvial deposit. Gravity graben effects produced the secondary synthetic displacements on the smaller fractures between the main scarp and the mole-track.

Local soil conditions played an integral role in the development of different scarp morphologies. Note the contrasting surface expressions of a deeper fault rupture portrayed in Figure 3-21. In the foreground, the fault offset wet, fine grained sediments at a spring. The ground here warped into a broad moncline with virtually no distinct fault scarp. Instead, only tension cracks with little vertical displacement across them formed at the point of maximum flexure. In the background, this same fault offset a dry, brittle, gravelly colluvium. Here, a single distinct scarp accommodated nearly all of the vertical offset. Ductile earth

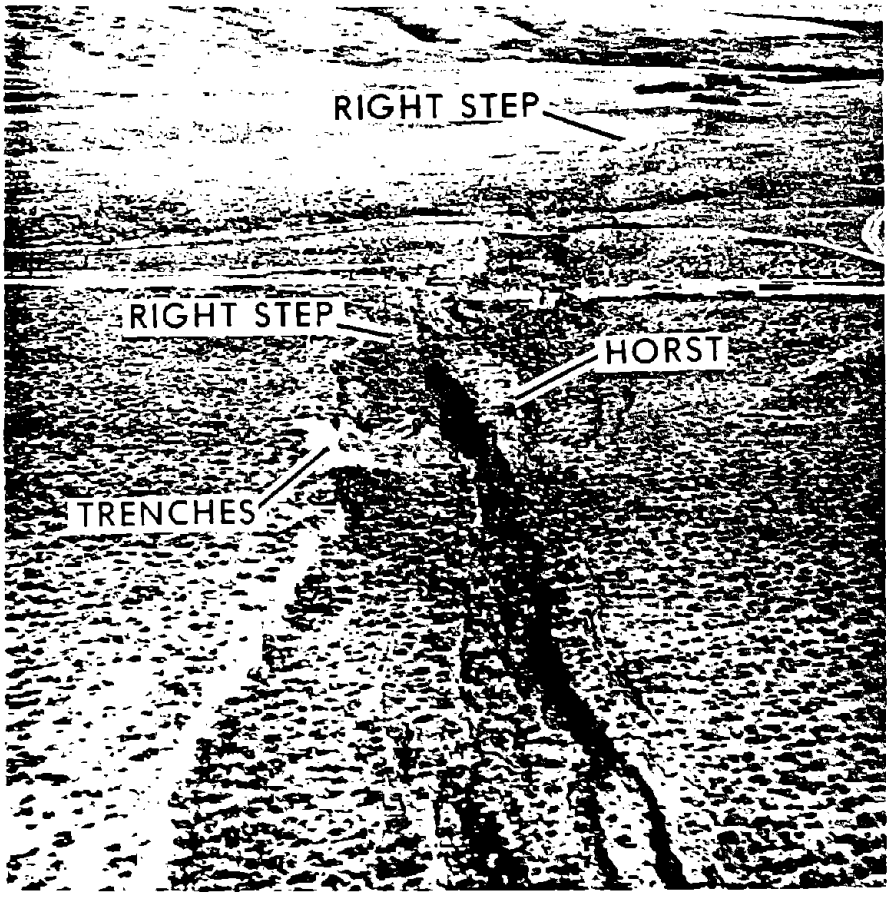

(A) Aerial view

(B) Ground breakage at Doublespring Pass Road

Figure 3-19: AERIAL PHOTOGRAPH AND CLOSE-UP PHOTOGRAPH OF A ZONE OF COMPLEX SURFACE RUPTURES ACROSS DOUBLESPRING PASS ROAD (after Crone et al., 1987)

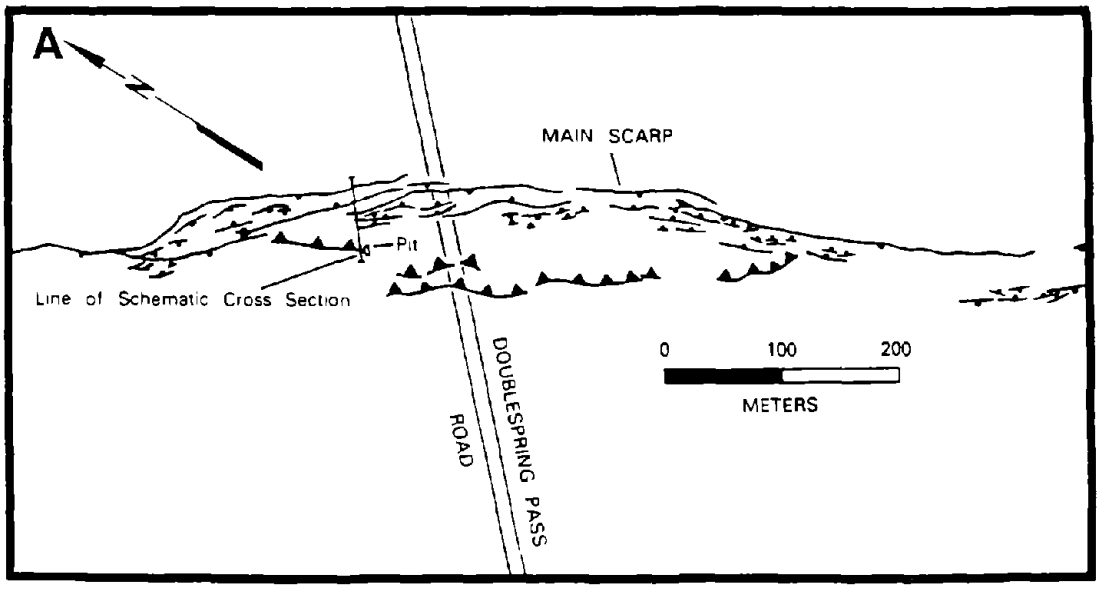

(A) Plan View

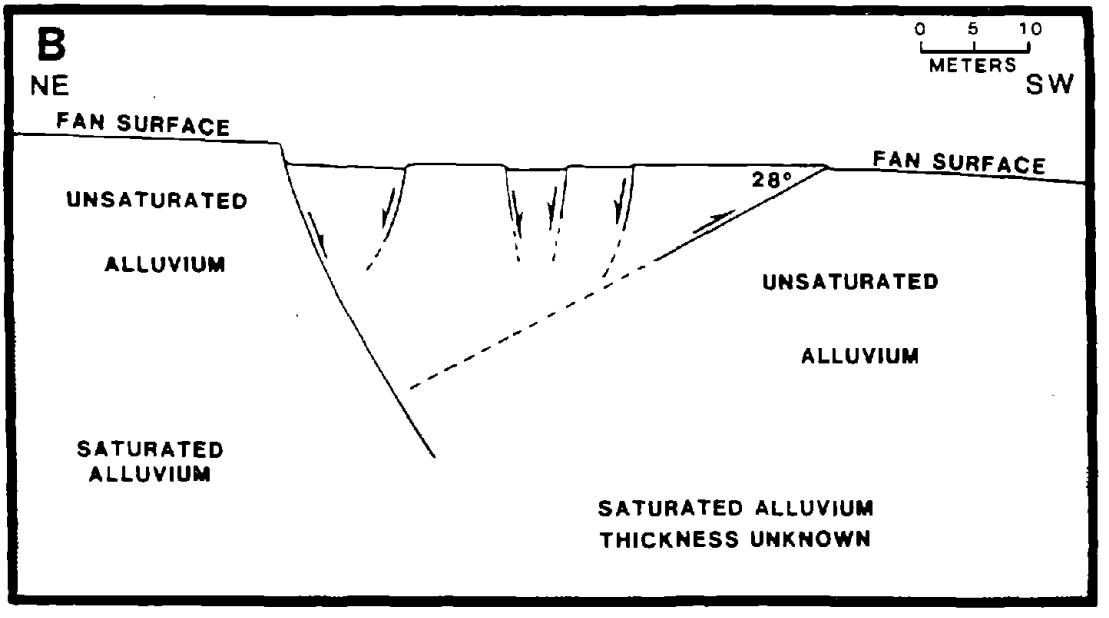

(B) Cross Section

Figure 3-20: MAP OF FAULT SCARPS AND SCHEMATIC CROSS SECTION OF NORMAL AND THRUST FAULTS NEAR DOUBLESPRING PASS ROAD (after Crone et al., 1987)

Figure 3-21: VARIATION IN FAULT SCARP MORPHOLOGY AS SURFICIAL MATERIALS CHANGE FROM COLLUVIUM IN THE BACKGROUND TO WET FINE GRAIN PLASTIC SEDIMENTS IN THE FOREGROUND (after Crone et al., 1987)

materials tended to bend and gradually adjust to differential fault movements. On the other hand, brittle materials broke on sharper individual shear planes.

Two eyewitness accounts of the 1983 Borah Peak earthquake surface faulting were documented by Taylor et al. (1985). These direct observations of the surface fault rupture phenomenon provided a rare opportunity to learn how surface ruptures developed. Mrs. Knox was 1000 ft away from the Arentson Gulch fault when it ruptured. She noted that the surface rupture did not form until the period of strong shaking subsided. The scarp seemed to tear from one end of the landscape to the other end. It took a few seconds for the scarp to elongate about a mile and a half. Two other hunters in a truck only 60 feet from a main fault scarp noticed that the shaking proceeded the ground rupture by 2 or 3 seconds. The ground first dropped around 6 to 10 feet and then about a second later the surface break abruptly appeared. Both sets of eyewitnesses thus observed earthquake shaking, surface deformation and then the subsequent development of a distinct fault scarp.

- The 1915 Pleasant Valley, Nevada earthquake:

The Pleasant Valley, Nevada Earthquake of October 2, 1915 registered as a magnitude 7.6 earthquake. Normal faulting produced 20 to 40 miles of surface ruptures. The characteristics of the fault scarps, as described by Jones (1915), were remarkably similar to those previously described in the review of the 1954 Dixie Valley-Fairview Peak earthquake, the 1959 Hebgen earthquake, and the 1983 Borah Peak earthquake. For example, a gap 9 feet wide opened adjacent to what Gilbert (1890) would have described as a single simple fault scarp. The change in the dip of the fault rupture near the ground surface produced the geometric conditions that allowed for the formation of large open fractures adjacent to the face of the scarp. These open fractures, however, existed at or near the ground

surface and did not appear to penetrate more than a few feet below the lowest adjacent ground surface.

- Studies of the Wasatch Fault Zone:

Although no historical records of surface faulting along the Wasatch fault zone exist, important lessons can be learned from the detailed studies of prior fault movement on distinct fault planes within the Wasatch fault zone. Research by Swan, Schwartz and Cluff (1980) and McCalpin (1987) based primarily on meticulous fault trench maps of sections of the Wasatch fault zone provided some important findings regarding normal fault movements. McCalpin, for example, analyzed 40 trench logs across normal faults.

The overwhelming number of secondary fractures occurred in the normal fault's hanging wall. For example, at one location, the gravity graben structure in the hanging wall contained approximately 100 individual fault planes within an 80 foot wide zone. The geologists believed that the majority of these fractures formed during a single earthquake event. The main fault rupture usually steepened as it approached the surface producing an open fracture, but sometimes the fault rupture continued along the general trend of the fault at depth. The fault plane typically increased in dip by 12° within 5 to 10 feet of the ground surface. The findings from these two studies general agreed well with those made in the previously reviewed fault rupture case histories.

c) Strike-Slip Faulting:

- The 1906 San Francisco earthquake:

The April 18, 1906 San Francisco earthquake, with a magnitude of approximately 8.3, was truly a great earthquake. It tore the earth surface over a length of more than 250 miles. The right-lateral horizontal offset averaged 10 feet along the fault trace, with maximum horizontal and vertical offsets of 21 feet and 3

feet, respectively. This well-documented earthquake event has often been used by geologists and engineers to illustrate the character of strike-slip fault movements. Some of the specifics from this case history have already been discussed in previous sections, such as the reviews of Louderback (1937), of Sherard et al. (1974), and of Dams Ruptured by the 1906 San Francisco Earthquake. Additional important observations and general findings from the Lawson et al. (1908) landmark report of the 1906 San Francisco earthquake will now be presented. This report and a companion report by Reid (1910) provided a comprehensive study of the earthquake fault movements.

There were variations in the surface expressions of the movements along the San Andreas fault, but over the majority of its length the movements were expressed at the surface as a small ridge of earth 3 to 10 feet wide. After walking the northern part of the fault trace, Gilbert observed that the fault break was generally a single line of rupture that remained within a few hundred feet of a straight line connecting its extreme points (See Figure 3-22(A)). After examining a 15 mile section south of Mussel Rock, Anderson summarized,

> The rupture may be traced along every foot of the way when not below the waters of the lakes. It varies in width from 2 or 3 feet to 10 feet, but at times branches out into several furrows that include a space of 100 feet or more in width . . . Sometimes it forms a crack 2 or 3 feet wide and several feet deep, and in other places shows a vertical wall of soil on one side or the other, several feet high. The typical occurrence in turf-covered fields is a long, straight, raised line of blocks of sod broken loose and partly overturned.

Often, lateral cracks oriented diagonally to the trace of the main fault extended away from or across the San Andreas fault trace (See Figure 3-22(B)). At one location, these en echelon shear fractures formed every foot or so and extended away from the main trace for a distance of 100 yards or more. Most cracks or fractures were closed, but some were open a foot or more.

(A) Narrow single rupture

(B) Diagonal cracks across fault trace

Figure 3-22: PHOTOGRAPHS OF THE SAN ANDREAS FAULT RUPTURE (after Lawson et al., 1908)

Specific examples of the character of the surface faulting are presented in Figure 3-23. Near Point Reyes, a 60 foot wide band of multiple fractures offset wheel tracks on a road by 20 feet (See Figure 3-23(A)). Just a mile south of this location, a clean single break of almost 16 feet in a sidewalk defined the active trace of the San Andreas fault. At another location, 6 parallel fractures in a zone 270 feet wide accommodated the horizontal fault movement. Figure 3-23(B) shows the distribution of deformation on one side of the fault near Fort Ross. The deformation of an originally straight fence line, which was carefully surveyed in, clearly shows the drag which occurs along the fault rupture plane. Finally, Banner found a site where the San Andreas fault crossed a mountain road and the unpaved road was "badly shattered by the earthquake". 345 cracks running in every direction were counted within a 3 mile section of the road. Oakeshott (1973) recognized this observation as evidence that great earthquakes may produce secondary ground shattering in the bedrock adjacent to the fault.

Gilbert, in Lawson et al. (1908), categorized the various expressions of the San Andreas fault rupture as the ridge phase, the trench phase and the echelon phase. The ridge phase and the echelon phase have been described in earlier paragraphs. The trench phase described small subsidence zones above the fault trace. The trench phase usually continued only for short distances. More interestingly, Gilbert correlated the occurrence of these categories of surface expressions of fault ruptures with local ground conditions. The echelon phase or diagonal shear cracks occurred chiefly in wet alluvium or wet fine grained soils. Anderson explained, "They appear to have been produced very much like the fracture lines in compression tests of building stones." The ridge phase or single fracture seemed to be more likely to form where the fault cut through rock or stiff earth materials. The trench phase resulted from surface material dropping into voids which either existed before the faulting or were created during the faulting.

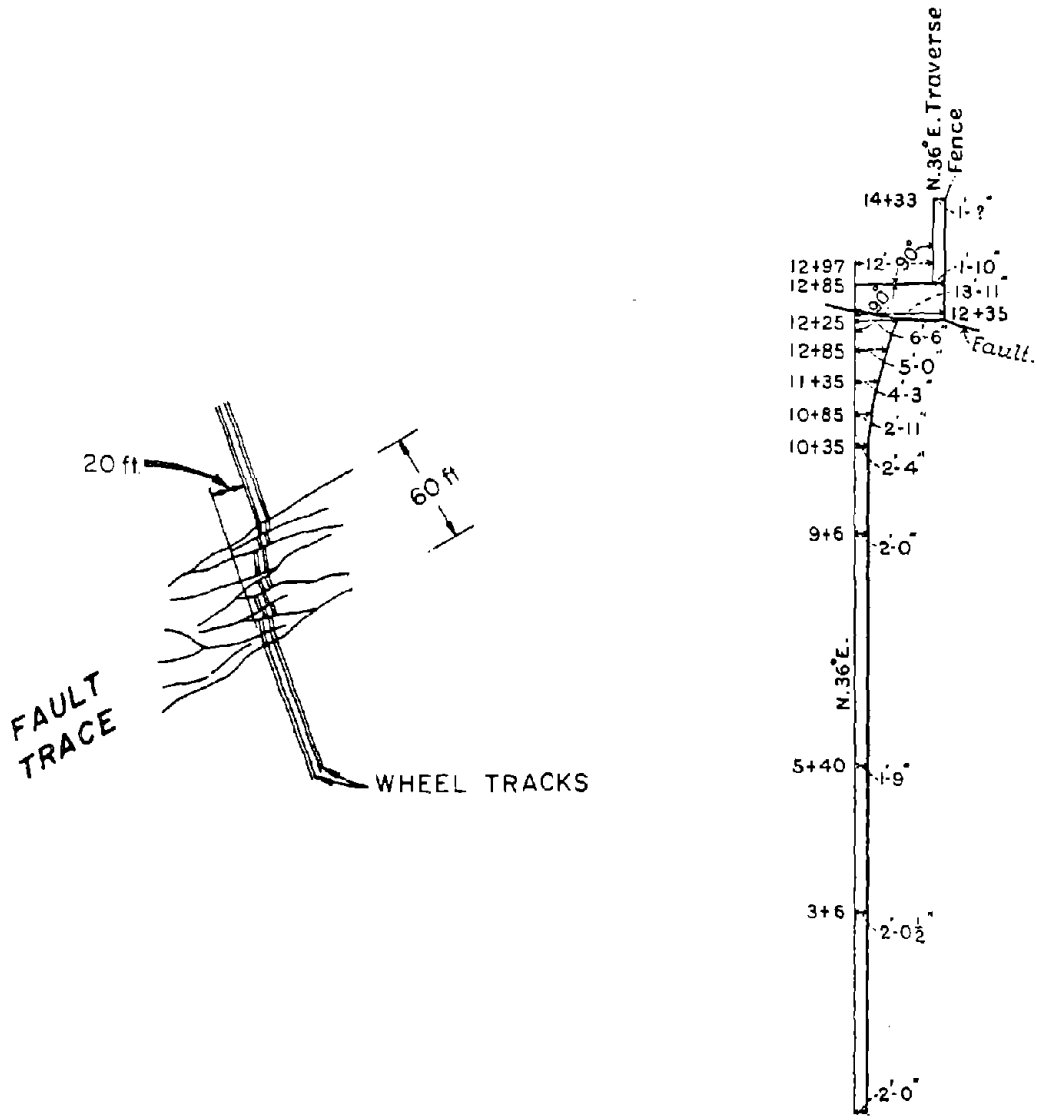

(A) Fault Trace Near Point Reyes (B) Offset of Fence by Fault at Fort Ross

Figure 3-23: EXAMPLES OF SURFACE EXPRESSIONS OF THE 1906 SAN ANDREAS FAULT MOVEMENT (after Lawson et al., 1908)

Gilbert felt that horizontal movement on the bedrock fault plane which probably had minor deviations in its dip and strike could produce small trenches or graben structures. Hence, he suggested that geometric irregularities in the fault plane, not local ground conditions, created the trench phase. In explaining the variations in horizontal displacements measured on fences, roads, and other structures which crossed the fault trace, Lawson claimed,

> Auxiliary cracks, distributed over a zone not uncommonly a few hundred feet wide, took up portions of the displacement; and these auxiliary cracks doubtless escaped observation in many cases. Indeed, owing to the yielding character of the superficial mantle of soil and regolith, it is probable that many of these auxiliary cracks did not appear as ruptures at the surface.

Finally, Reid (1910) offers an exceptionally perceptive insight regarding the influence of surficial geology on the surface expression of the fault rupture:

> In the general descriptions of the fault-trace it is shown that when the rupture occurred there was a zone of varying width between the shifting sides which did not partake of their simple movements, but was more or less distorted by the shearing forces to which it was subjected. The existence of this zone in alluvium or disintegrated rock may be explained even though the fault were a sharply defined crack in the underlying solid rock. Let us suppose that the straight line AOC in the rock (See Figure 3-24) has been broken at the fault and displaced into the two parts A'O' and D'C'. If the alluvium were brittle and with little plasticity, it might be broken and displaced in the same way, but if it were plastic, as it would be if it were to some extent composed of clay, a part of the displacement would be accomplished by shearing distortion, and the offset at the fault-plane would be less than that of the underlying rock. Close to the rock the displacement of the alluvium would be very nearly the same as that of the rock (lines 1 in the figure) at greater distances, however, the distortion in the vertical plane would make itself felt; the offset would be less, and the displacement would be distributed more like the lines 2. The alluvium might be so thick or plastic that it would suffer no break at the surface along the fault-line, the whole displacement being distributed like line 3; this seems to be the condition which produces the *echelon phase* of the fault-trace in very wet alluvium, as described by Mr. Gilbert.

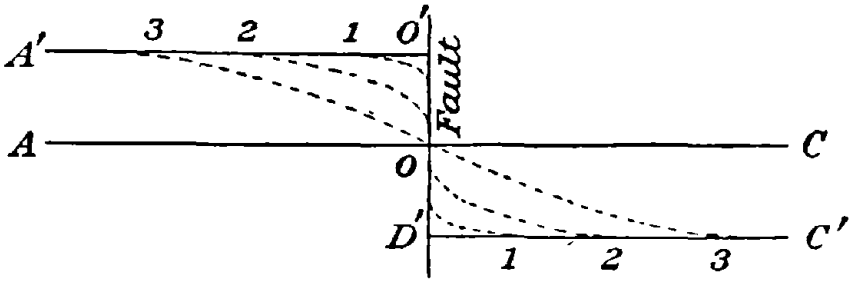

Figure 3-24: VARIATION OF SHEAR FRACTURE AND SHEAR DISTORTION WITH DEPTH IN A THICK, PLASTIC ALLUVIAL DEPOSIT OVER A STRIKE-SLIP FAULT MOVEMENT (after Reid, 1910)

Because of the magnitude of the earth movements during this event, the Coast and Geodetic Survey re-established the triangulation over a large section of the Northern California coast. The surveying of numerous known points throughout the earthquake region brought forth "four laws governing the distribution of the earth movements which occurred on April 18, 1906." In summary, points on opposite sides of the fault moved approximately parallel to the trace of the fault in opposite directions. Points equidistant away from the fault displaced twice as much on the west side than on the east side. "The displacements on each side of the fault were less, the greater the distance of the displaced points from the fault." Furthermore, "In receding from the fault, either to the eastward or to the westward, the displacement decreases more rapidly near the fault than it does further from the fault". The nearest fixed points (i.e. control points that did not move as a result of the 1906 San Francisco earthquake) were located 20 to 90 miles away from the trace of the San Andreas fault.

- The 1940 Imperial Valley earthquake:

This event was previously described in the review of the rupturing of the All-American Canal. The magnitude 7.1 Imperial Valley Earthquake of 1940 produced a 40 mile long continuous surface rupture across a deep alluvial valley. Vertical displacements or offsets along the surface rupture were relatively small (i.e. 0 to 4 feet). On the other hand, the horizontal component of movement generated offsets which varied from a few feet to a maximum of nearly 19 feet. The differential movement occurred across a fairly narrow zone. At one location, a post-earthquake survey found that a line which was originally perpendicular to the trace of the north trending Imperial fault gradually deflected southward as it approached the right-lateral offset from the east. At the fault the eastern segment was offset 9 feet south of its original location. Immediately west of the fault, the

western segment was 6 feet north of the original line. It gradually deflected until it came into alignment with the original line. This gradual deflection of the line could not be seen by the naked eye. Drag effects, which occurred within a 100 to 300 foot zone surrounding the main fault trace, could be readily observed. The deflection of an originally straight line perpendicular to the fault due to local drag effects was actually in the opposite sense of the global elastic rebound deflections previously described. Fault drag bends the offset line back toward the fault trace bringing the ends of the deflected line segments near the fault closer together. Figure 3-25 shows the trace of the Imperial fault as it crossed a citrus grove and a diagram illustrating the effects of fault drag. Richter (1958) noted that drag effects were generally less evident in firmer terrain.

Bonilla (1970) made an interesting observation of the Imperial fault movement which contradicted the idea that the amount of differential movement across a fault should decrease as the fault propagated through deep loose earth deposits. Logs of wells drilled in the vicinity of the Imperial fault suggested that the soil deposits were thicker than 700 feet in this area. The soil profile indicated layers of clay, loam, and sand, and showed that the groundwater level was only 6 feet below the ground surface. Yet, the faulting of 1940 produced a horizontal surficial offset of more than 15 feet at the surface. Three factors may help explain how this much movement propagated to the surface. First, it is entirely possible that the movement at depth was larger than 15 feet. Second, the soil was saturated, and hence, the soil deposit would deform rapidly at relatively constant volume and be essentially incompressible initially. Third, prior movements on the Imperial fault might have already developed a shear plane through the soil deposit with only residual soil shear strengths acting upon it. Some combination of one or more of these conditions could explain the amount of offset observed at the ground surface.

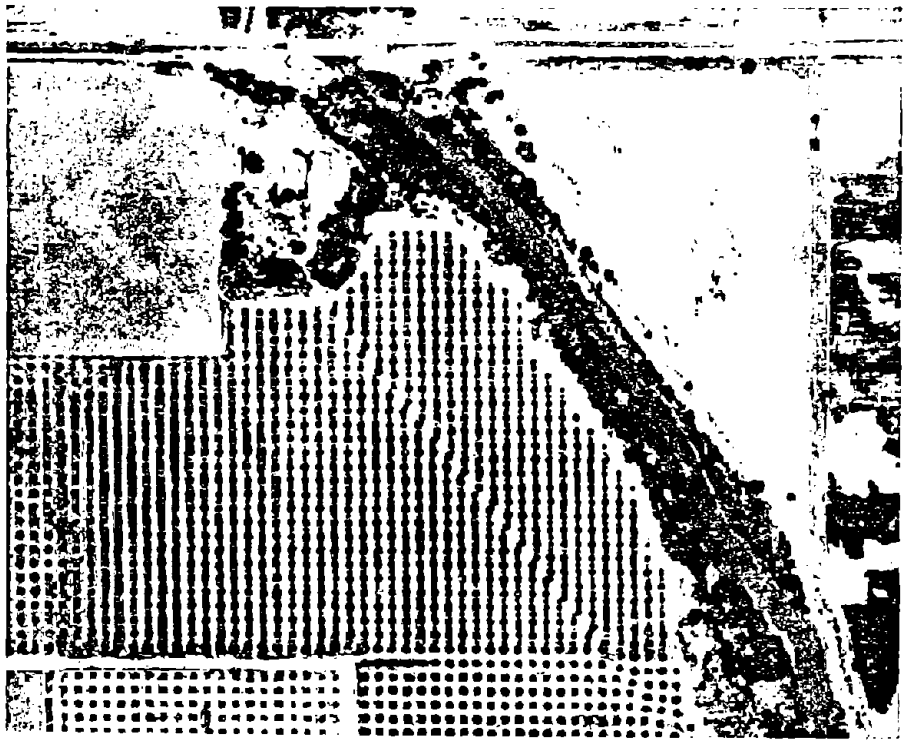

(A) Strike-slip offsetting of trees

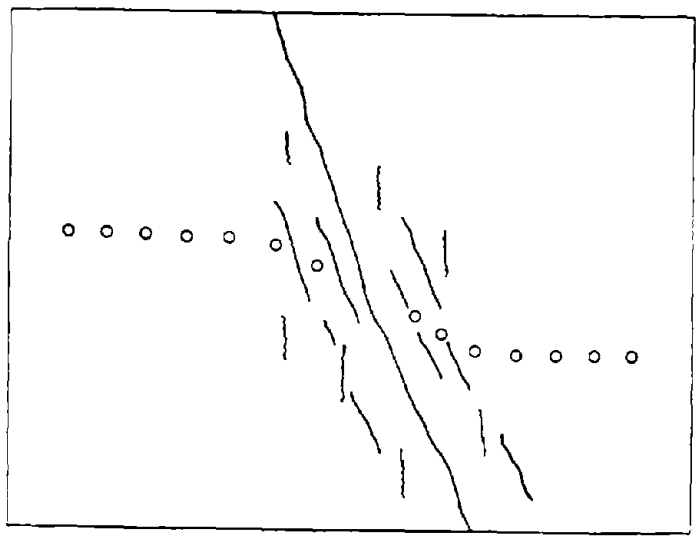

(B) Illustration of drag effects

Figure 3-25: STRIKE-SLIP OFFSETTING OF ORCHARD BY THE IMPERIAL FAULT AND DIAGRAM OF THE OFFSET IN AN ORIGINALY STRAIGHT FENCE (after Richter, 1958)

- The 1868 Hayward Fault earthquake:

The Hayward Earthquake of 1868 was not as well-documented as later earthquake events. Still, review of the Hayward fault movement brought forth a couple of important observations. The 1868 Hayward earthquake was probably a magnitude 7½ event, and produced approximately 30 miles of surface faulting. The maximum probable strike-slip offset at the surface was around 3 feet. Observations were made that the cracks that formed along the trace of the Hayward fault opened and remained open to "very considerable" depths (Lawson et al., 1908). These cracks were about a foot wide. Some observers reported that the cracks extended down to bedrock. In fact, men attempted to sound the bottom of one such crack, but they were unable to do so. Since, the Hayward fault ran within the hill-slopes of the Oakland Hills, it was conceivable that down-slope gravity effects (e.g. landsliding) produced these large open fissures. Moreover, the observers noted that water and sand were ejected from some of the cracks suggesting ground failure due to liquefaction, not faulting. It would not be prudent, however, to dismiss the possibility of cracks opening to reasonable depths because of irregular fault geometry or movement.

Recent field investigations based on exploratory trenches excavated across the Hayward fault provided these observations of this strike-slip fault. The characteristics of the fault often varied along its length. For example, the width of the fault zone varied from 10 to 78 feet along a length of just 800 feet. The individual fault planes within the fault zone were very thin. These fault planes were usually vertical, although they could flower in all directions or bend toward one side near the surface. The strike of these fault planes changed slightly with depth and also varied slightly along the fault trace. Only the most active fault strands reached near the ground surface. Finally, although very small "gopher

holes" were found in the fault zone near the ground surface, these voids did not appear to occur at depth.

- The 1930 Idu, Japan earthquake:

The Idu, Japan earthquake of 1930 presented an excellent example of the dissipation of fault movement as a fault rupture propagated toward the ground surface. A tunnel at a depth of 500 feet was excavated through a geologic profile of volcanic rock overlain by at least 130 feet of sandy clay lake deposits (Nasu, 1931). The strike-slip faulting of the 1930 Idu, Japan earthquake displaced the tunnel 8 feet, but less than 3 feet of offset was measured at the ground surface along the fault trace (Suyehino, 1932; Richter, 1958). Over 5 feet of horizontal movement was apparently dissipated within the 500 feet of material above the tunnel. The majority of the fault rupture was probably absorped in the top 130 feet of sandy clay.

- The 1972 Managua, Nicaragua earthquake:

Niccum et al. (1976) described a unique observation of the interaction of a rigid structure of finite size with the movement on a strike-slip fault which passed beneath the structure. The 1972 Managua, Nicaragua earthquake formed a strike-slip surface rupture with about 7 inches of differential movement across it. The surface rupture was apparently deflected out of its normal alignment by a massive, rigid concrete underground bank vault that appears to have been stronger than the sand and gravel materials in which it was embedded.

- The 1966 Parkfield-Cholame, California earthquake:

The 1966 Parkfield-Cholame earthquake was interesting in three respects. The three moderate earthquakes on the San Andreas fault during the period June 27, 1966 to June 29, 1966 were measured as Magnitude M_L = 5.1, M_L = 5.5, and

M_L = 5.0. It was surprising that these moderate earthquakes produced more than 23 miles of surface faulting. Figure 3-26 shows a segment of this surface faulting. Note that in this alluvium valley the fault movement was expressed as a regular series of en echelon fractures oriented approximately 45° to the strike of the underlying fault plane. Near the USCGS and DWR strong motion station off of Highway 41, the right lateral displacement across the fault was measured to be 1.8 inches 10 hours after the main shock. But on July 8, 1966, just 11 days later, the differential movement across the fault was around 4 inches. Thirty-seven days after the main shock this displacement reached 4.7 inches. It was not known if this additional movement across the fault resulted from rapid post-earthquake fault creep on the San Andreas fault below the valley soil deposits, or whether the additional surface movement represented soil creep behavior of the valley's alluvial deposits. In any case, these measurements suggested that time effects in certain surface rupture events might be important.

3.2.3 Lessons to be Learned from Field Studies Regarding Fault Rupture Propagation:

The aforementioned field studies illustrate the complexity of the fault rupture propagation phenomenon. A number of variables influence the fault rupture process. Given the complexity of the fault rupture propagation phenomenon, it is somewhat surprising that any reasonably consistent patterns of behavior emerged during the review of the case histories, but such trends were observed. Although exceptions to these general patterns of behavior may be found, the preponderance of evidence justifies making a number of salient observations regarding "trends" or typical patterns of behavior. Lessons to be learned from fault rupture field studies regarding fault rupture propagation will be presented under three general headings. They are: (a) movement of the bedrock

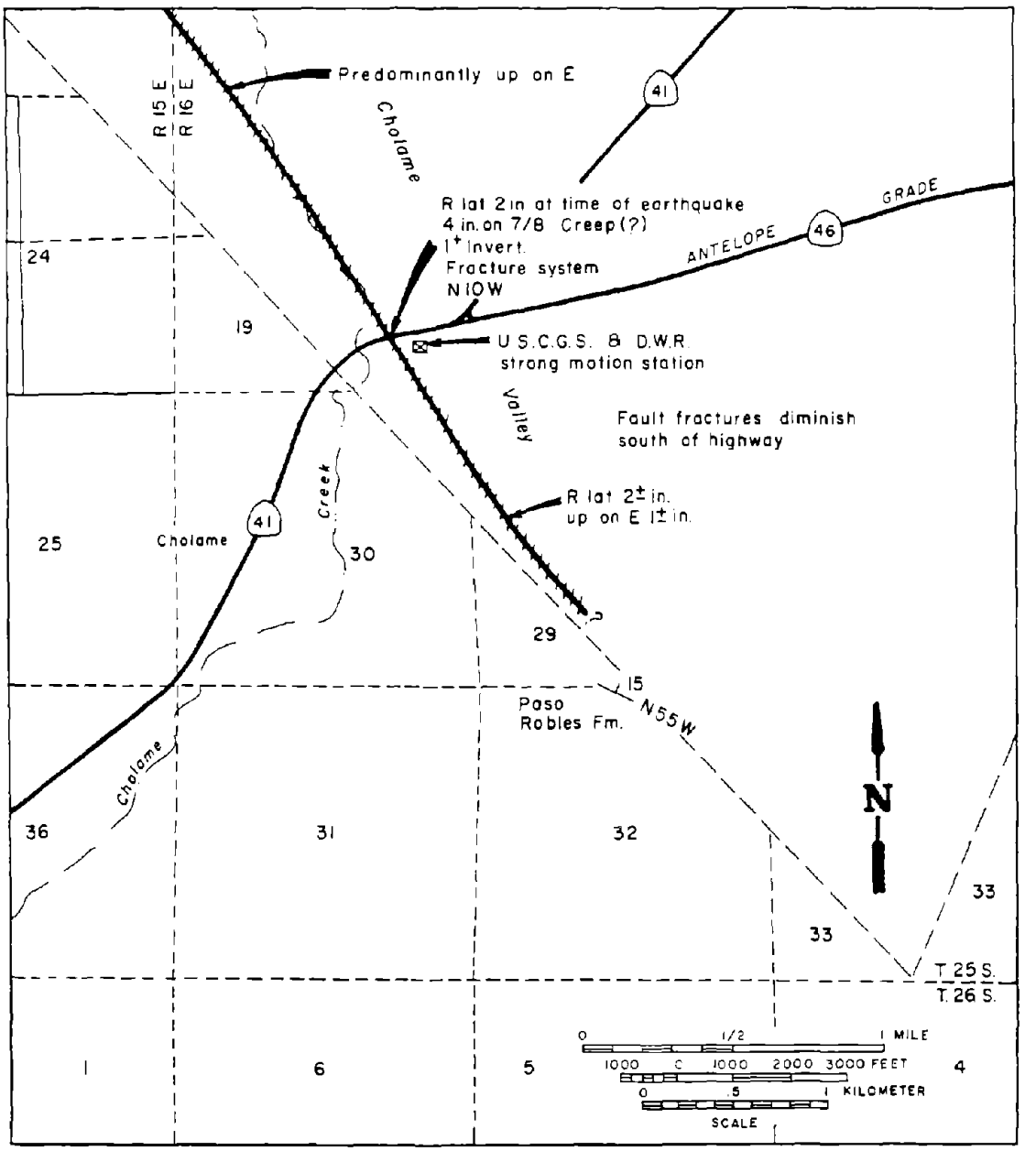

Figure 3-26: MAPPING ALONG THE SAN ANDREAS FAULT ZONE, CHOLAME VALLEY. HEAVY LINES REPRESENT STRIKE OF FAULT; THIN, EN ECHELON LINES REPRESENT GROUND BREAKAGE (after Oakeshott, 1973)

and the soil-bedrock interface during faulting; (b) dissipation of movement as a fault propagates through soil; and (c) path of fault rupture propagation through soil. Moreover, the lessons learned under each of these three headings will be further broken down into those applicable for each of the principal types of fault movements - thrust, normal, and strike-slip faulting. Finally, for the most part, diagrams will be used to illustrate the principal characteristics of the fault rupture propagation phenomenon as described by the observations made of documented case histories of surface fault rupturing.

(a) Movement of the Bedrock and the Soil-Bedrock Interface During Faulting

The principal characteristics of the general behavior of the bedrock and the soil-bedrock interface during faulting are shown in Figures 3-27, 3-28, and 3-29. Down-warping of the upthrown block as it is forced over the downthrown block during thrust faulting typically produces significant secondary deformation in the bedrock of the upthrown block (see Figure 3-27). Movement on secondary faults and opening of tension cracks occurs primarily in the highly disturbed upthrown block. The downthrown block remains fairly intact. No observations were made of the upthrown block peeling the soil up off the downthrown block as it thrust forward, but this does not mean that this did not occur. Initially, the fault propagates into the soil along the same orientation as the bedrock fault plane.

The bedrock behavior pattern is just the opposite during normal faulting (See Figure 3-28). Here, the upthrown block typically remains relatively intact. The majority of secondary deformation occurs in the downthrown block, although there appears to be less distortion or breakage of the downthrown block during normal faulting than of the upthrown block during thrust faulting. The formation of a complex rupture pattern at the ground surface above the downthrown block

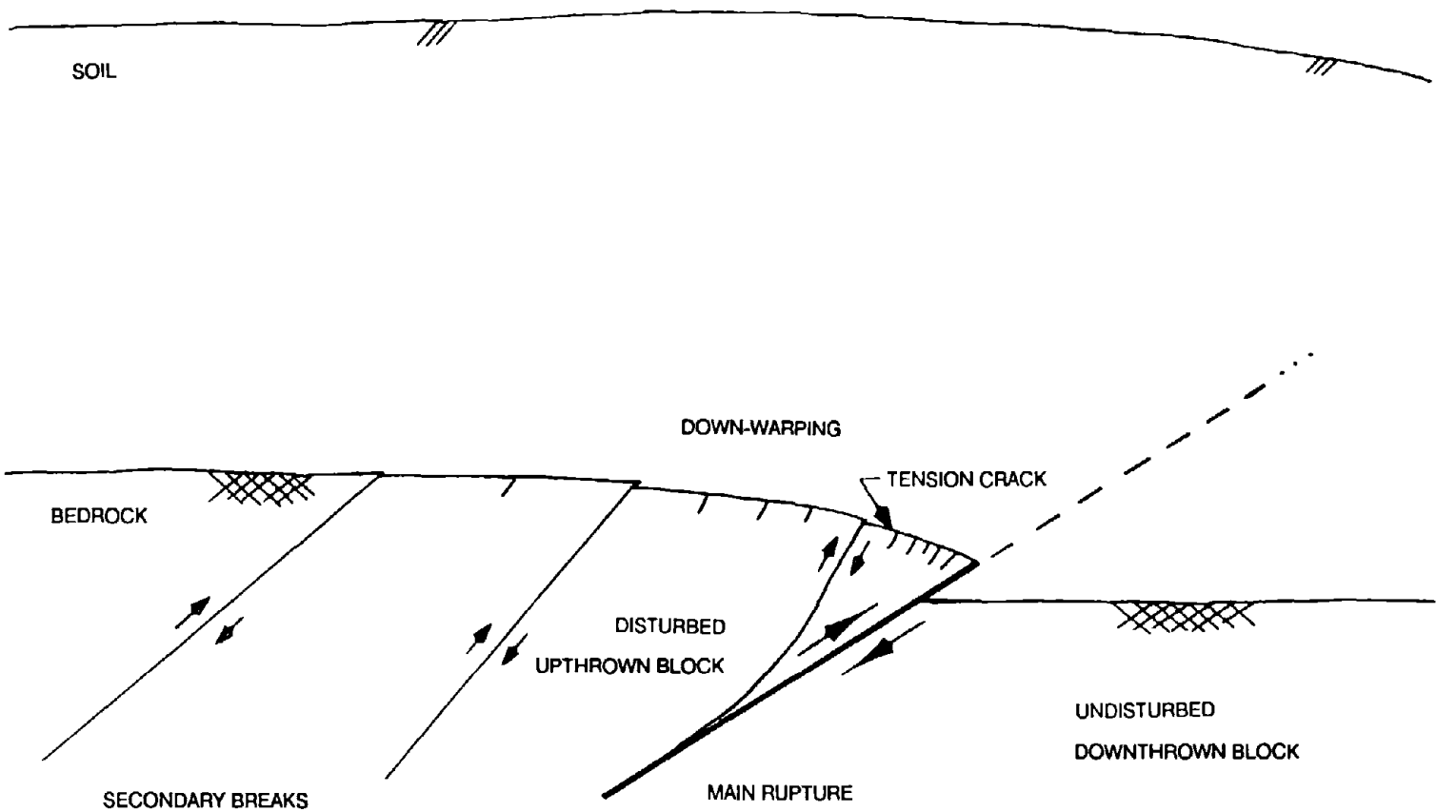

Figure 3-27: GENERAL BEHAVIOR OF BEDROCK AND SOIL-BEDROCK INTERFACE DURING THRUST FAULTING

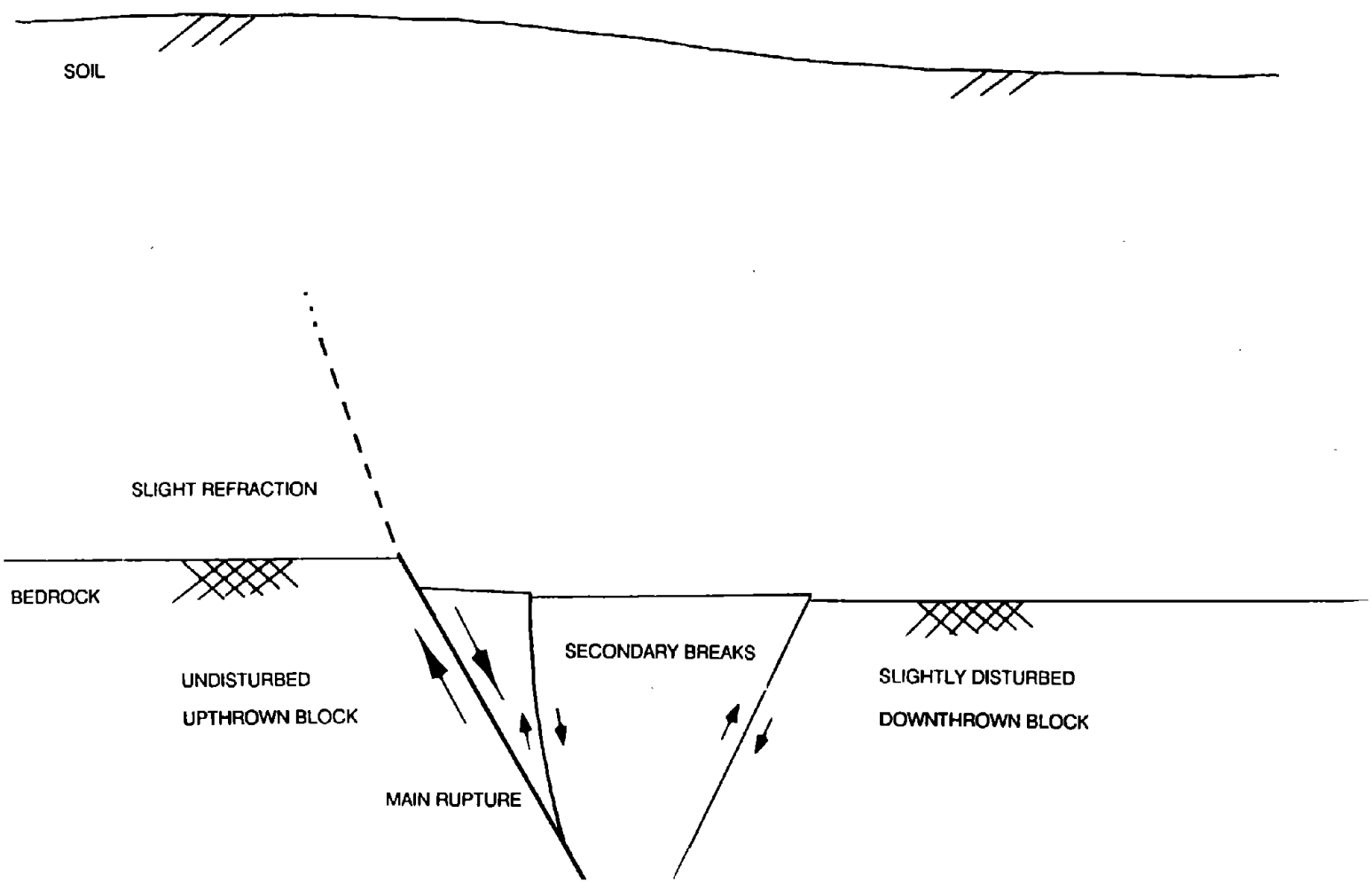

Figure 3-28: GENERAL BEHAVIOR OF BEDROCK AND SOIL-BEDROCK INTERFACE DURING NORMAL FAULTING

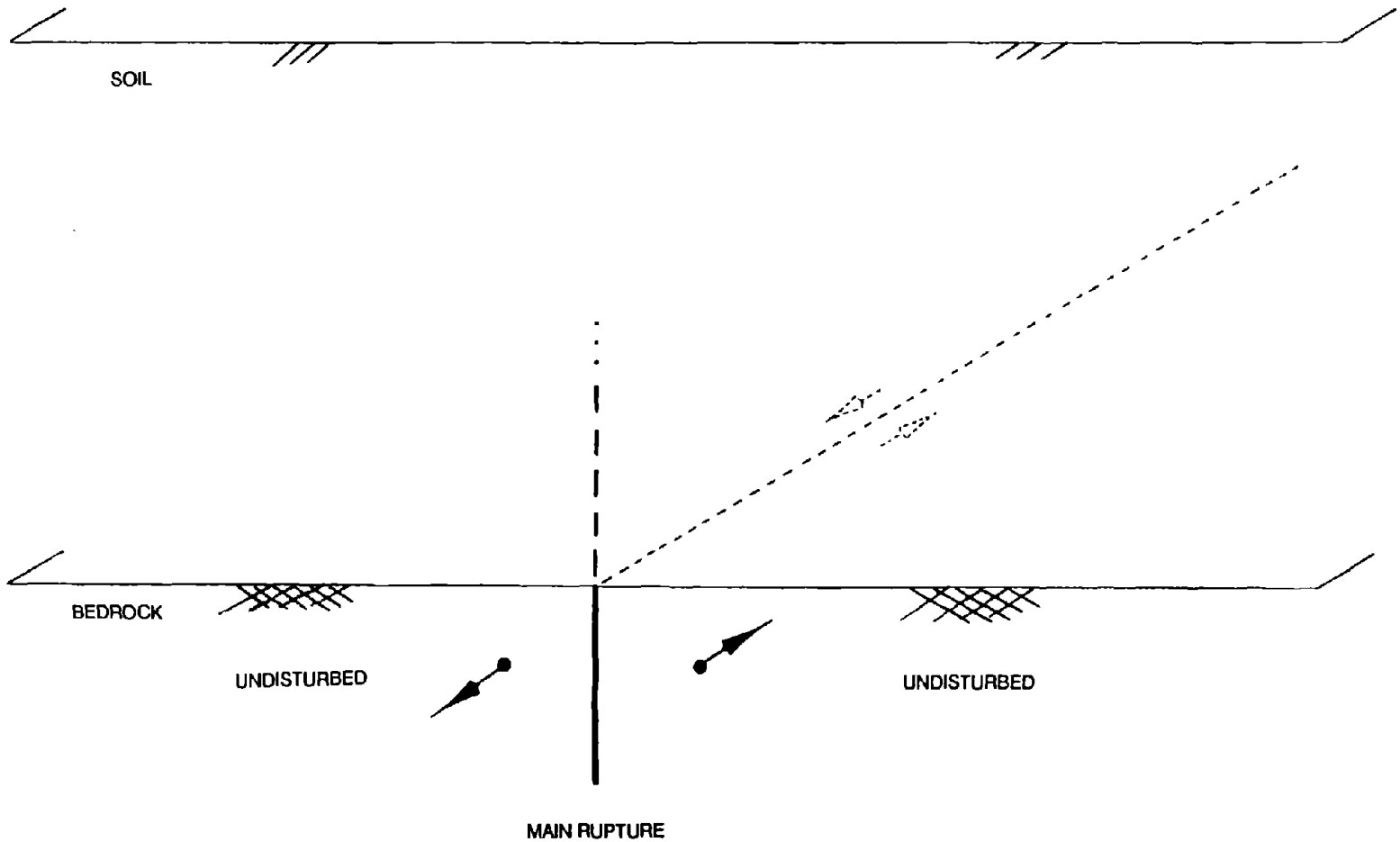

Figure 3-29: GENERAL BEHAVIOR OF BEDROCK AND SOIL-BEDROCK INTERFACE DURING STRIKE-SLIP FAULTING

results principally from the characteristics of fault propagation through alluvium, not because the bedrock itself develops secondary fractures. Again, no observations were made of the upthrown block lifting up the soil above the downthrown block as the downthrown block dropped. Initially, the fault plane refracts slightly or remains at about the same orientation as the fault rupture propagates through the soil above the bedrock.

Strike-slip faulting produces the least amount of subsidiary fault movement and secondary deformation (See Figure 3-29). The rupture zone is often fairly narrow. The bedrock adjacent to the fault is usually fairly undisturbed, although at one location less competent rock was shattered on one side of the San Andreas fault rupture during the 1906 San Francisco earthquake. No observations were made of soil surrounding the bedrock fault loosening during strike-slip fault movement. Usually the fault rupture continues its nearly vertical orientation as it propagates into the soil. Any deviations from a vertical plane at the soil/rock interface are minor.

(b) Dissipation of Movement as a Fault Propagates through Soil:

Differential movement across the fault rupture diminishes as the fault propagates up toward the ground surface. This is true for thrust, normal, and strike-slip faulting. It is true for fault rupture propagation through fractured rock as well as alluvium. An 8 foot fault offset was absorbed in a 500 foot high fractured rock cliff during the 1964 Alaskan earthquake. (The 8 foot baseline offset was roughly 1.5% of the height of the overlying earth materials.) The White Wolf fault offset a tunnel several feet in 1952, but formed only small mole-tracks at the surface. The 1930 Idu, Japan earthquake created an 8 foot offset in a tunnel located at a depth of 500 feet. Less than 3 feet of this differential movement appeared at the surface. Various theories estimated that movement on major

faults at depth during the 1959 Hebgen and 1983 Borah Peak earthquakes were significantly greater than the offsets measured at the ground surface. Within one region, the 1954 Dixie Valley-Fairview Peak earthquake produced a scarp 3 to 4 feet in height which was continuous, except for a quarter mile gap where the fault disappeared under an alluvial fan composed of looser granular materials. These observations strongly support the reasonable preconception that movement across a fault should dissipate as the fault rupture propagates upward since the rupturing of earth materials uses energy (i.e. most soils are somewhat compressible and soils can deform to some degree before developing distinct rupture features).

(c) Path of Fault Rupture Propagation through Soil:

The principal characteristics of the general behavior of the fault rupture as it propagates upward through soil are shown in Figures 3-30, 3-31 and 3-32. The path of the fault rupture depends on a number of variables. Fault rupture propagation within a nonhomogeneous earth mass with established planes of weakness or rigid inclusions would deviate from the general patterns of behavior described herein, as the fault would usually propagate along existing planes of weakness. For instance, the fault traces exposed in the trenches excavated at Point Conception, California predominantly follow the bedrock's bedding planes. The 1972 Managua earthquake's surface rupture deflected around a rigid structure embedded in the more deformable soil deposit.

Besides existing planes of weakness or rigid inclusions, other critical variables may influence the shape of the fault rupture's travel path through an earth mass. Figures 3-30, 3-31, and 3-32 focus on only three of the more important variables - the type of fault movement, the character of the overlying homogeneous soil deposit, and the attitude of the fault plane. Some of the variables not taken into account in these diagrams are the effects of a sloping ground surface, extreme

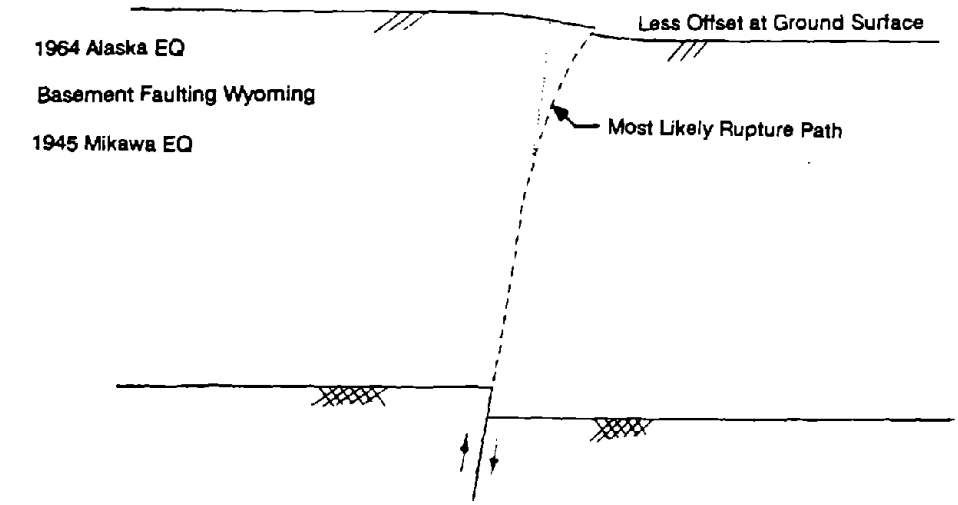

(A) "Stiff" Earth Materials - Steep Dip

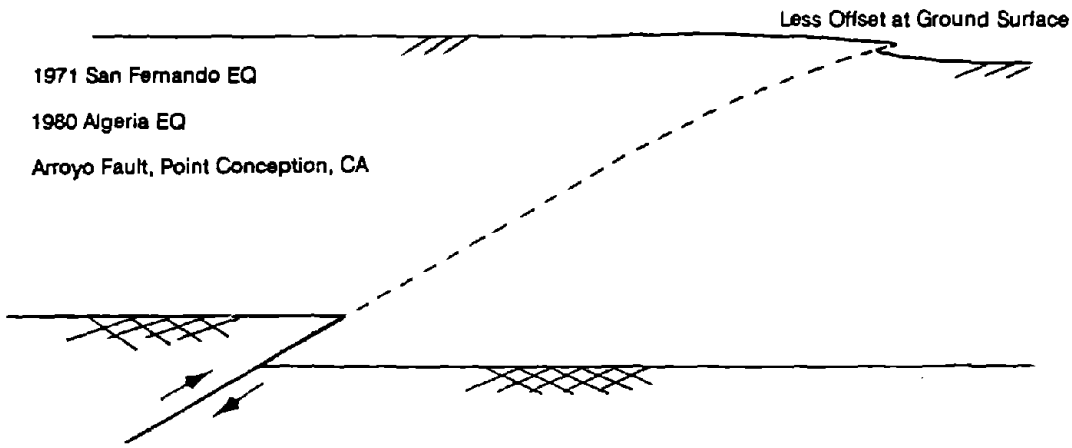

(B) "Stiff" Earth Materials - Shallow Dip

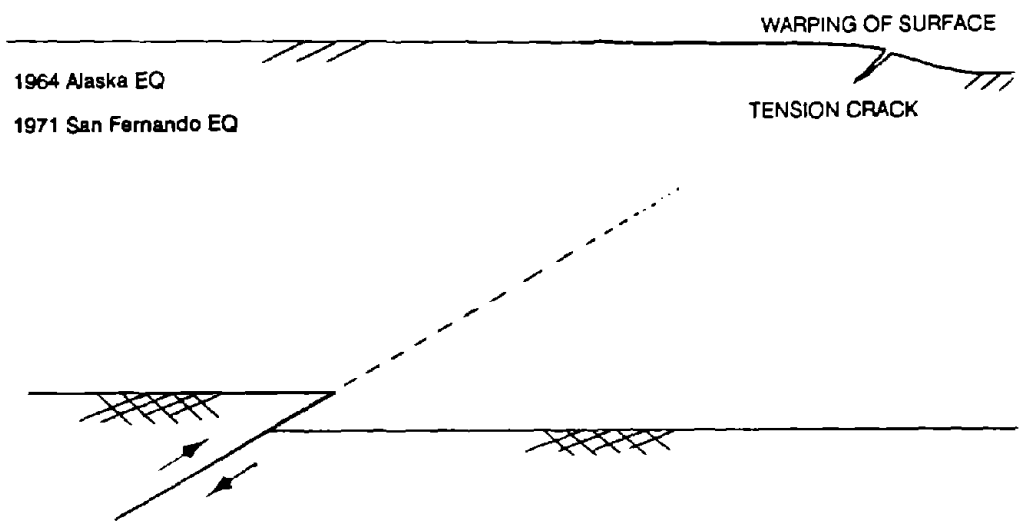

(C) "Ductile" Earth Materials

Figure 3-30: PATH OF THRUST FAULT RUPTURE THROUGH SOIL

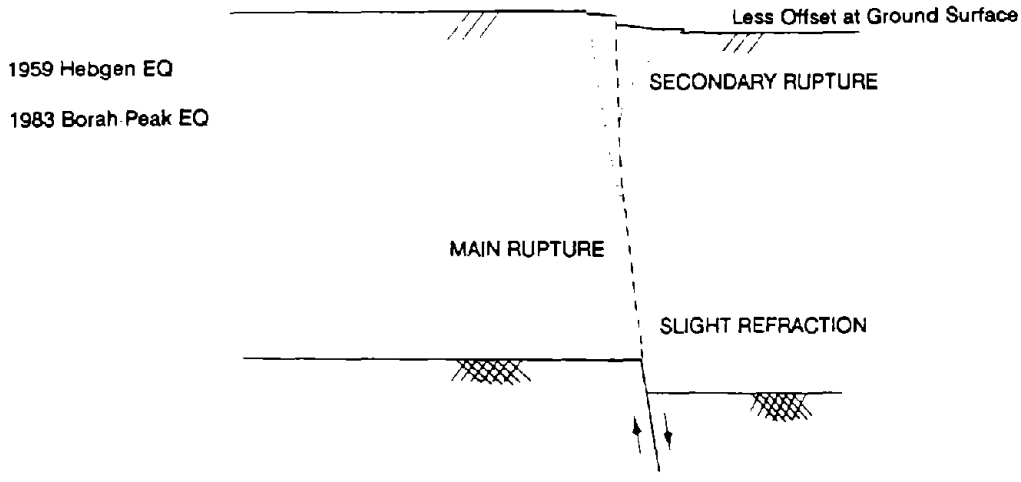

(A) "Stiff" Earth Materials - Steep Dip

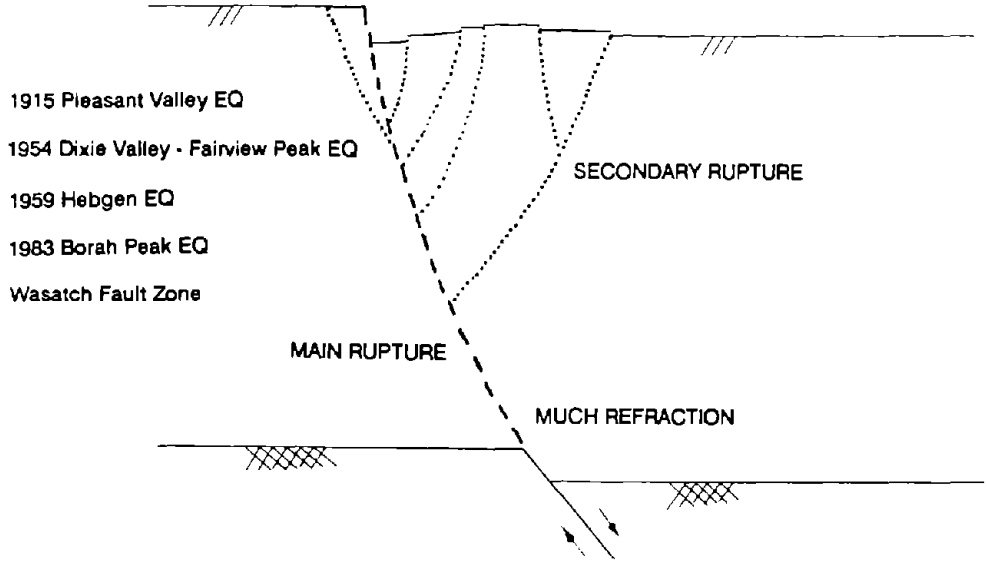

(B) "Stiff" Earth Materials - Shallow Dip

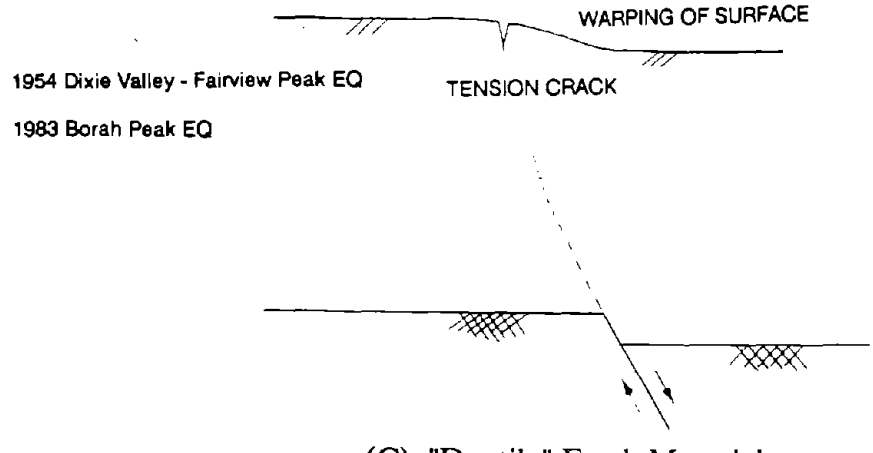

(C) "Ductile" Earth Materials

Figure 3-31: PATH OF NORMAL FAULT RUPTURE THROUGH SOIL

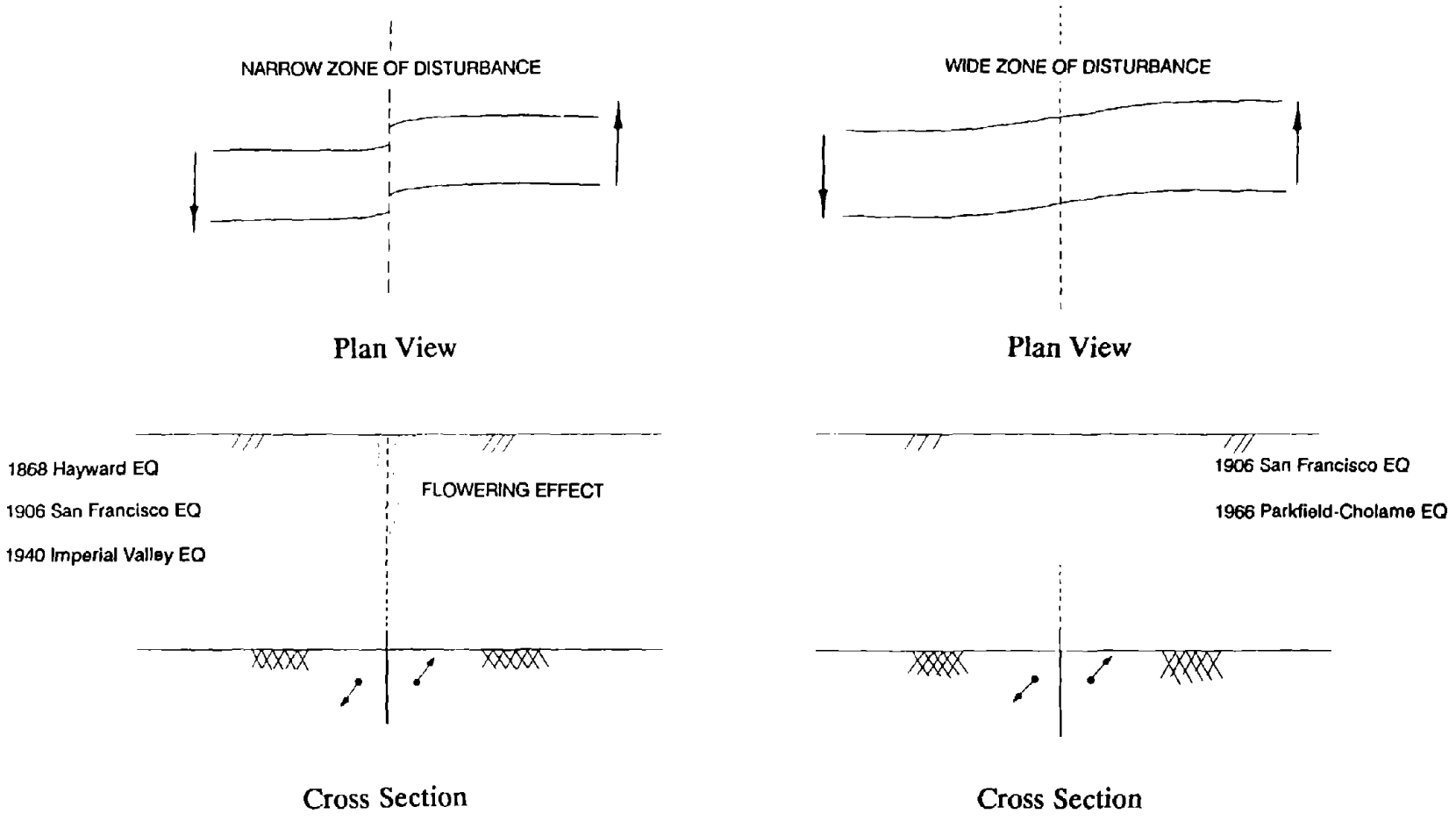

Figure 3-32: PATH OF STRIKE-SLIP FAULT RUPTURE THROUGH SOIL

variations in the depth of soil, irregularities in the movement across or along a fault, irregularities in the orientation of the bedrock fault plane, and excessive secondary movement in or distortion of the adjacent blocks of bedrock.

"Typical" thrust fault travel paths are shown in Figure 3-30. Specific case histories of surface faulting where such behavior was observed are noted. As was discussed in the last section, bedrock fault offsets can be absorbed by deformable mediums, and hence, there may be no clean break observed at the ground surface. Diagram C illustrates this type of behavior. Observation of this type of behavior during the 1964 Alaskan earthquake and 1971 San Fernando earthquake indicates that the absorption of a bedrock fault offset is more likely to occur in compressible organic soils, wet fine grained sediments, and loose granular fills. Diagrams A and B illustrate how a fault rupture might propagate through stiffer earth materials such as dense alluvium or weak sedimentary rocks. Initially, the fault rupture continues along the projection of the bedrock fault plane. As geologic evidence of block faulting in Wyoming and field observations of the 1945 Mikawa, Japan fault movement suggest, the fault rupture gradually begins to bend over the downthrown block. Near the surface this bending becomes more pronounced. The 1964 Alaskan earthquake faults on Montague Island, however, became steeper as they approached the ground surface. This anomaly can be best explained by remembering the extensive down-warping of the Alaskan earthquake's upthrown blocks. This down-warping of the upthrown block near the fault offset mitigates the effects of the kinematic constraints that would be imposed by a sharp offset in two rigid blocks. Kinematic constraints require that a failure surface eventually bends over the downthrown block to allow for the withdrawal of the upthrown block. Figure 3-14 after Prucha et al. (1965) provides another possible explanation. Regional tectonic compression could produce a bedrock thrust fault which steepens as it rises.

Observations made during the 1971 San Fernando earthquake, 1980 Algeria earthquake, and the geoseismic investigation at Point Conception, California indicate that shallow dip thrust faults tend to propagate along the bedrock fault plane until near the surface (See Diagram B of Figure 3-30). Near the surface, the fault gently bends over the downthrown block. This curvature of the fault rupture's travel path may produce local extension zones, which may contain normal fault movements, above the upthrown block. The normal faulting produced during 1980 Algeria earthquake is a good example of this phenomenon.

"Typical" normal fault travel paths are shown in Figure 3-31. Specific case histories of surface faulting where such behavior was observed are noted. Similar to thrust faults, normal faults may warp "ductile" soil deposits and not produce a clean ground break with vertical movement across it (Diagram C of Figure 3-31). At the point of maximum flexure in the warped zone, tension fissures like those formed in the 1983 Borah Peak earthquake may develop. In stiffer materials where a clean ground break develops, the fault plane is generally refracted at the soil-bedrock interface and becomes steeper (Diagram A of Figure 3-31). The dip increases even more near the surface and may become almost vertical. For example, in the 1959 Hebgen earthquake and 1983 Borah Peak earthquake, an extension of the fault plane near the surface draped over the downthrown block and produced a local thrust fault at the surface. In cases where the bedrock fault is more shallow, secondary breaks above the downthrown block can produce gravity grabens similar to those shown in Diagram B of Figure 3-31. The refraction of the fault plane at depth and the curvature of the fault plane near the surface can combine to produce a local extension zone on the downthrown side of the primary fault rupture. Open fissures and complex rupture patterns often develop in these zones. Gravity often exaggerates vertical movements when the ground surface slopes down toward the downthrown block. The earthquake surface rupture case

histories provide a number of dramatic examples of gravity grabens exhibiting these types of features.

"Typical" strike-slip fault travel paths are shown in Figure 3-32. Specific case histories of surface faulting where such behavior was observed are noted. In stiff earth materials a single nearly vertical rupture usually propagates from the bedrock to the ground surface (Diagram A of Figure 3-32). Slight deviations in the strike and dip of the bedrock fault plane and other irregularities can cause the fault planes to move back and forth across the main fault trace. This, of course, will produce a more complicated surface expression of the fault rupture. Moreover, strike-slip faults exposed in exploratory excavations sometimes display a "flowering effect" near the ground surface. This broadening of the zone of fault rupture is a near surface effect and does not usually extend to significant depth. The width of major fault zones like the San Andreas fault zone can be substantial. Movement might be distributed over a multitude of individual fractures within the fault zone. Of course, the resulting multiple fault planes will complicate the pattern of surface faulting. Although the single rupture shown in Figure 3-32 exists quite often in nature, exceptions to this simple rupture pattern should be expected as they are quite common also.

Finally, Diagram B of Figure 3-32 illustrates how a ductile earth material may produce an en echelon surface expression of a bedrock strike-slip fault offset. At the soil-bedrock interface, a "direct shear" mechanism ruptures the soil to produce the usual vertical failure plane. At the surface, a "simple shear" mechanism over a wider distorted zone of soil governs. Instead of developing a failure surface because of kinematic constraints, a stress-induced failure pattern emerges. It appears evident that if only minor horizontal displacements occur on the bedrock fault plane, the offset will be absorped by the overlying deformable earth mass in a zone of general or "simple" shearing deformation without any

actual direct shear failure planes forming at the ground surface. In some cases, the simple shear deformations of the overlying soils produces diagonally oriented fissures or failure surfaces, and this was described by several investigators as "en echelon" cracking or fissures.

3.3 Models of Fault Rupture Propagation

3.3.1 General:

The results from a number of physical and numerical model studies of fault rupture propagation are available in the literature. More than thirty years ago, geologists employed sandbox tests to study the development of fault structures in geologic media. More recently, geotechnical engineers have utilized 1 g small-scale models and centrifuge models to study fault propagation through cohesionless materials. Concurrently, geotechnical engineers and geologists have employed analytical modelling techniques such as the Finite Element Method (FEM) and the Finite Difference Method (FDM) to improve our understanding of the fault rupture propagation phenomenon. The results from these model tests and numerical analyses are summarized in Sections 3.3.2 and 3.3.3, respectively and lessons to be learned regarding these studies are summarized in Section 3.3.4.

3.3.2 Physical Model Studies:

(a) Sanford (1959):

In his work "Analytical and Experimental Study of Simple Geologic Structures", Sanford (1959) utilized elastic theory and sandbox model tests to study the effects of various boundary deformations on a hypothetical 5 km thick layer of sedimentary rock with average stiffness properties. He hoped to learn how large-scale geologic structures were formed, especially discontinuities like faults. Sanford's use of small-scale model experiments to validate his analytical method

was of particular interest. Sanford tested four materials: (1) beach sand, (2) a mixture of 85% beach sand and 15% clay, (3) coarse sand, and (4) fine sand. The materials were compacted at water contents of about 1% and to dry densities of on the order of 106 pcf. Sanford used an experimental method developed by Tschebotarioff (1952) to estimate the following Mohr-Coulomb strength parameters for these materials: $c < 3$ psf and $\phi = 45°$ to $58°$ (varied with material type). The height of the material in the sandbox ranged from 1 to 4 inches.

The results of the sandbox model tests are shown in Figure 3-33. Sanford concluded that the observed displacement fields were largely the same for the different materials. The horizontal displacements increased near the top of the layer, and the vertical displacement was distributed more gradually across a wider zone toward the upper boundary of the layer. Regarding the observed fracture patterns of the slightly cohesive material 2, Sanford stated that tensile cracks at the top and shear fractures at the bottom formed almost simultaneously. The shear fractures eventually propagated to the surface bending over the downthrown block, and normal faults formed in the tension zone at the surface. The curvature of the shear fracture that propagated to the surface depended on the thickness of the sand layer. As the thickness of the layer decreased, the fractures exhibited greater curvature and a lower dip angle at the surface. The cohesionless materials (Types 1 and 4) did not develop tension cracks and the shear failures were not expressed as sharp breaks, but as narrow shear zones. The curvature of the shear zones in different materials was similar. The general path of the shear rupture is shown in Figure 3-33(C). Finally, material 3 (which, unlike materials 1 and 4, was well-sorted and well-rounded) did not appear to fracture. No explanation was provided to explain this difference in behavior.

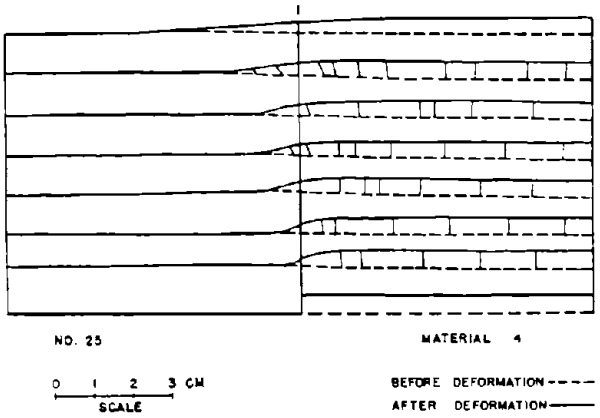

(A) "Typical" Observed Displacement Field

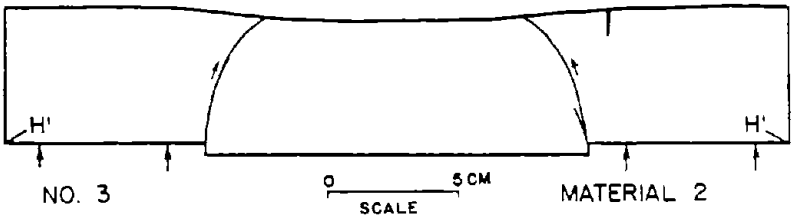

(B) "Typical" Observed Fracture Patterns

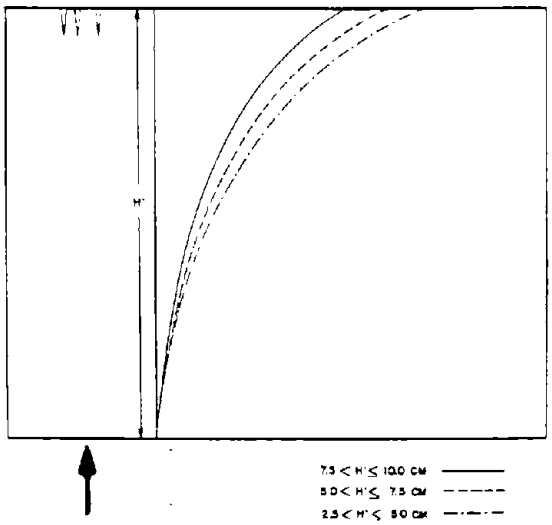

(C) Summarized Results of Fracture Patterns

Figure 3-33: SANFORD'S SANDBOX UPLIFT MODEL TEST RESULTS (after Sanford, 1959)

(b) Belousov (1961):

Belousov (1961) reviewed the work performed by Soviet geologists who employed small-scale models to approximate tectonic processes. To accurately represent rock in these small-scale model experiments, soft materials such as clay or syrup must be used. Because length and time were scaled down in the laboratory experiments, it was necessary to scale down the rigidity of the material used to model the rock. Specific details regarding the properties of the materials used and the size of the models were not provided. One of the results presented, however, was interesting because it illustrated how a soft clay responded to vertical thrust and normal faults.

The pattern of faults that accompanied the block faulting is shown in Figure 3-34. In this experiment, a piston was moved into or out of a box filled with a few inches of "wet" clay. The reader was not informed if this "wet" clay was fully saturated. Nevertheless, the results were informative. Unlike the sandbox tests performed by Sanford (1959), the fault initially propagated over the upthrown block. Belousov felt that these model tests agreed well with geologic fault patterns observed in the field.

(c) Emmons (1969):

Emmons (1969) employed sandbox modeling to study the deformation and rupture patterns created by strike-slip faulting. Emmons filled a box, which was divided in half so one side could move with respect to the other side, with sand vibrated into a dense state. The properties of the sand were not provided. The depth of the sand within the box was typically 14 inches.

The results of his tests are shown in Figure 3-35. Multiple shear fractures consistently developed. Originally, one nearly vertical failure surface formed. Because the failure surface that developed was not planar, however, additional

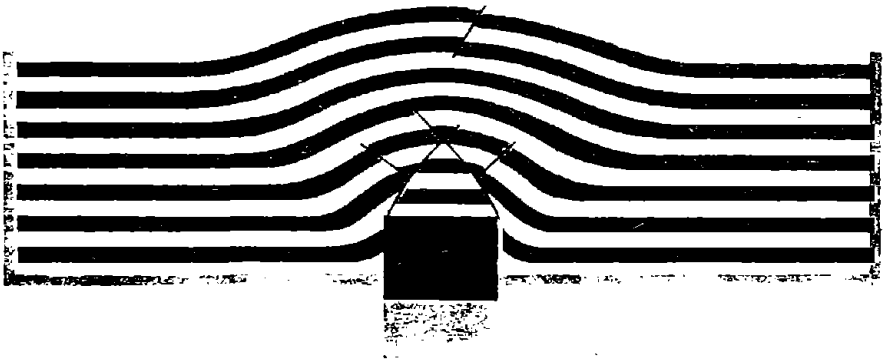

(A) Vertical Thrust Faulting

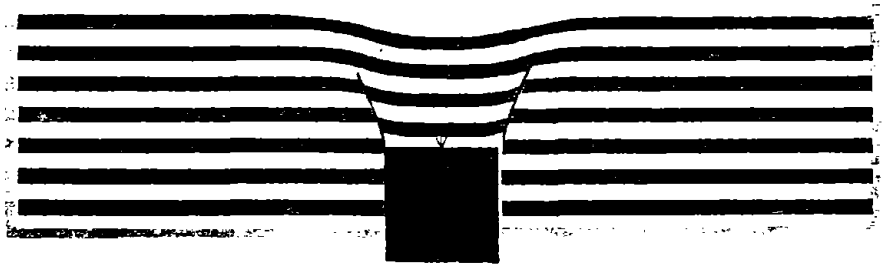

(B) Vertical Normal Faulting

Figure 3-34: BELOUSOV'S CLAY BOX MODEL TEST RESULTS (after Belousov, 1961)

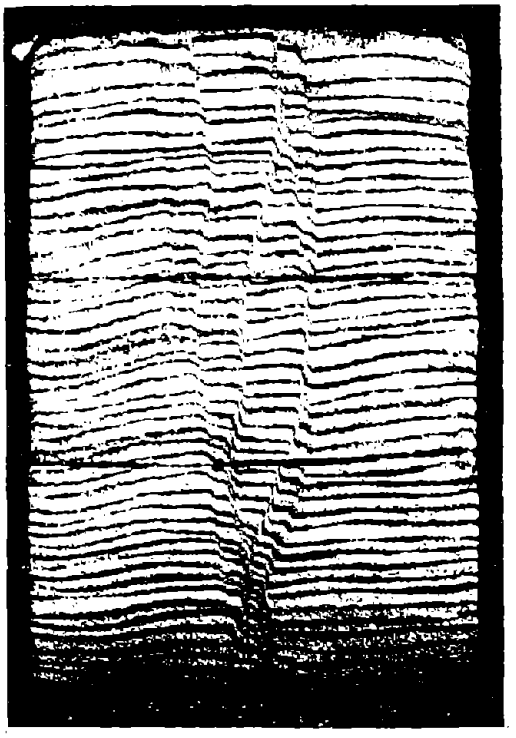

(A) Cross-Section Showing Ruptures Through Horizontal Layers

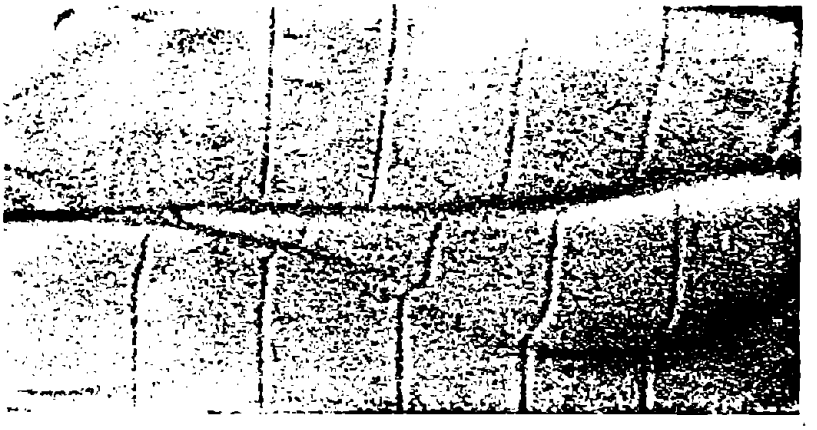

(B) Surface Patterns of Strike-Slip Rupturing in Sand

Figure 3-35: EMMON'S SANDBOX STRIKE-SLIP MODEL TEST RESULTS (after Emmons, 1969)

nonplanar failure surfaces emerged. Differential movement occurred across distinct failure surfaces. Between these established failure planes the sand moved as a fairly "rigid" block. As horizontal deformation of the base continued, these blocks of sand moved vertically as well as horizontally. Hence, horsts and grabens formed. Horizontal offsets measured at the surface were less than those induced at the base of the model. After significant base deformation (i.e. the base has been displaced an eighth to a half of the height of the sand) more complex surface rupture patterns developed. The surface ruptures displayed recognizable geologic features - notably fault drag and branch faulting. Finally, Emmons admitted that these results must be viewed with caution. For instance, these experiments were performed under very low confining pressures. Emmons reasoned that the failure surfaces might be more planar, and hence, produce less flowering over the depth of the sand, if larger models with higher confining stresses were used.

(d) Tchalenko (1970):

Tchalenko (1970) stated,

> Most soils and rocks, when deformed in direct shear, develop narrow shear zones within which the major displacements take place . . . Similarities between shear zones of different scales have been recognized since the earliest days of structural geology and used in model studies of tectonic processes.

Recognizing the similarities between shear zones of different magnitudes, Tchalenko compared the formation of shear zone structures in the shear box test, in the Riedel experiment, and in the ground above a strike-slip fault offset (See Figure 3-36). The Riedel experiment consisted of shearing a 0.4 to 4 inch layer of "plastic" clay by horizontally offsetting two adjoining boards. The Riedel shears shown in Figure 3-36 are similar to the en echelon fractures produced by strike-slip

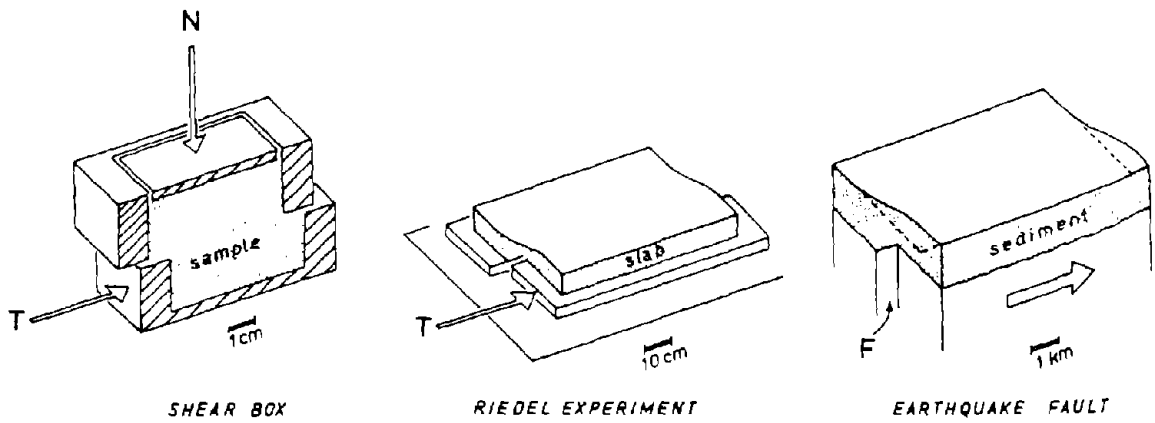

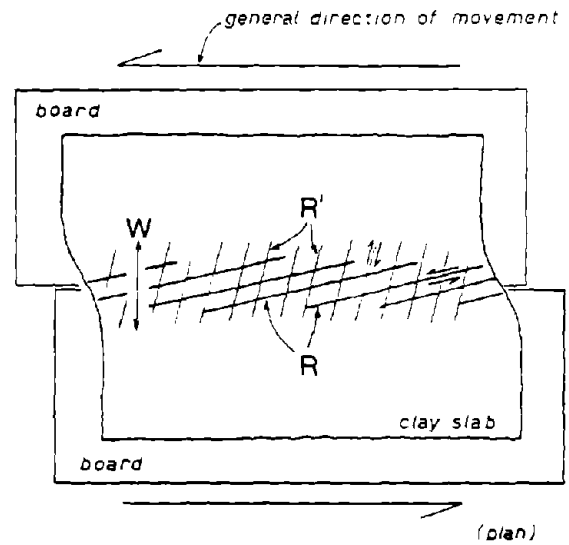

Blow-up of the Riedel experiment showing Riedel Shear (R), conjugate Riedel shear (R'), and width of shear zone (W).

Figure 3-36: SIMILARITIES BETWEEN SHEAR MECHANISMS AT DIFFERENT MAGNITUDES (after Tchalenko, 1970)

fault movements during earthquakes. The conjugate Riedel shears were not observed unless the clay used was at low water contents.

In the Riedel experiment and in the direct shear test, the development of shear fractures was essentially identical. Until some threshold amount of movement occurred, the clay deformed in simple shear without any shear fractures. Just before peak strength was reached, Riedel shears formed. As the deformation continued, these shears were progressively reoriented toward alignment with the direction of movement. When the residual strength was reached, nearly all of the displacement took place along a single principal shear aligned with the direction of movement. Although the sequence of the formation of the shear fractures within a strike-slip fault zone could not be observed, the final shear structures in the direct shear test, the Riedel experiment, and the strike-slip fault zone were very similar, as shown in the photographs of each presented in Figure 3-37. Accordingly, Tchalenko concluded,

> The similarities in structure were interpreted as indicating similarities in the deformation mechanism. At the peak stage, the mechanism is essentially of the simple shear type, at the post-peak stage it is governed by the kinematic restraints inherent in the strain field, and at the residual stage it is of the direct shear type.

Tchalenko made another important observation. He found that the Mohr-Coulomb failure criterion satisfactorily predicted the peak stage structures. The Mohr-Coulomb failure criterion predicted that the failure surfaces would be oriented at an angle of $\beta = 45° - \phi'/2$ to the major principal stress. Using a value of ϕ' of about 23° for the kaolin clay used in the direct shear tests and Riedel experiments and a value of ϕ' between 35° and 40° for the earth materials above the Dasht-e-Bayaz earthquake fault, Tchalenko found that the orientation of the Riedel shears observed in the lab and in the field agreed well with those predicted by the Mohr-Coulomb failure criterion.

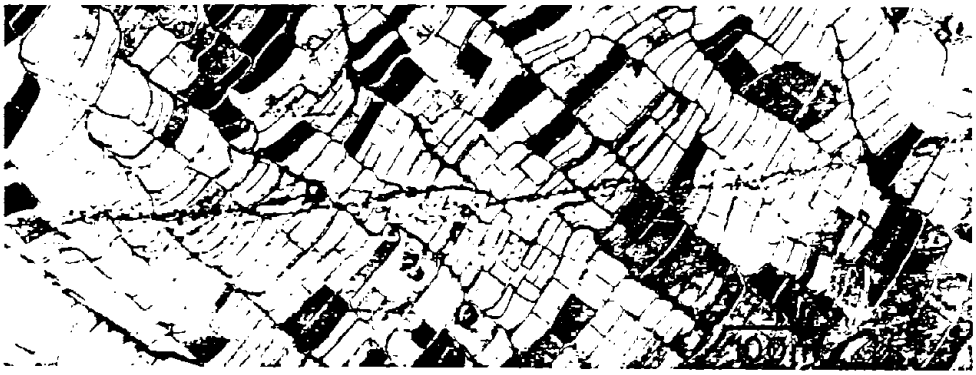

(A) Dasht-e Bayaz earthquake fault: Displacement = 250 cm

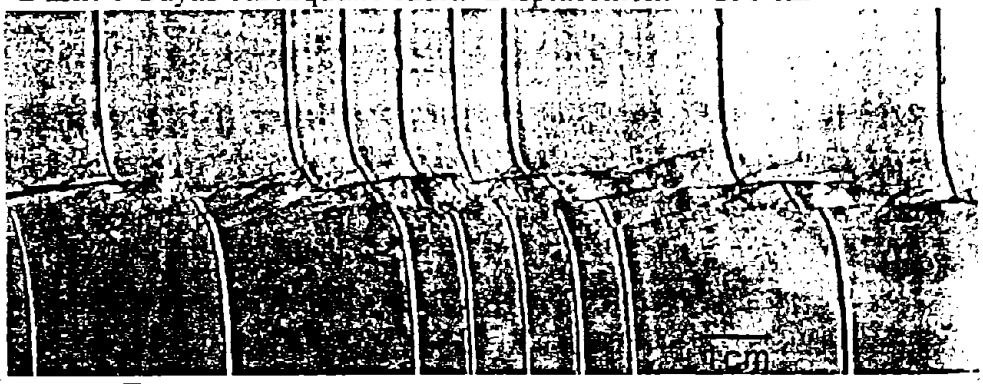

(B) Riedel Experiment: Displacement = 1.95 cm

(C) Direct Shear Box Test: Displacement = 0.8 cm

(D) Magnification of the Shear Zone Developed in the Direct Shear Box Test: Displacement = 0.3 cm

Figure 3-37: SHEAR ZONES OF DIFFERENT MAGNITUDES (after Tchalenko, 1970)

(e) Duncan and Lefebvre (1973):

In this work, Duncan and Lefebvre (1973) presented the results from a series of strike-slip fault movement model tests performed by the Bechtel Corporation. The objective of the model testing program was to observe how a soil deposit which had a rigid inclusion embedded in the top of it responded to a strike-slip bedrock fault movement below the rigid inclusion. No specific details of the modeling material were provided. This test was similar to a Riedel experiment, except that a rigid inclusion was partially embedded in the soft clay material. Figure 3-38 shows how the surface fault rupture diverted around the embedded structure, with separate fault branches passing on opposite sides of the structure. The diagram accompanying the photograph illustrated the earth pressures that developed on the structure in response to the fault offset in the strike-slip bedrock fault below. The active and passive pressure zones were oriented approximately 45° to the free field strike of the surface fault rupture. The passive earth pressure zone could be identified by the rising of the ground surface against the structure, whereas the active earth pressure zone could be identified by the dropping of ground surface against the structure. If the structure was designed to resist these earth loads, it would remain intact and not be damaged by the fault offset below.

(f) Friedman et al. (1976):

As discussed, geologists have used weaker materials like sand or clay in small-scale models to simulate stronger rock materials in the field. Friedman et al. (1976), however, studied the development of shear rupture propagation through sandstone, limestone, and rock salt under high confining pressures (up to 4×10^6 psf). They hoped to avoid many of the pitfalls of small-scale model testing. Samples were approximately 0.4 inches high and the base rock thrust fault was oriented between 30° and 90°.

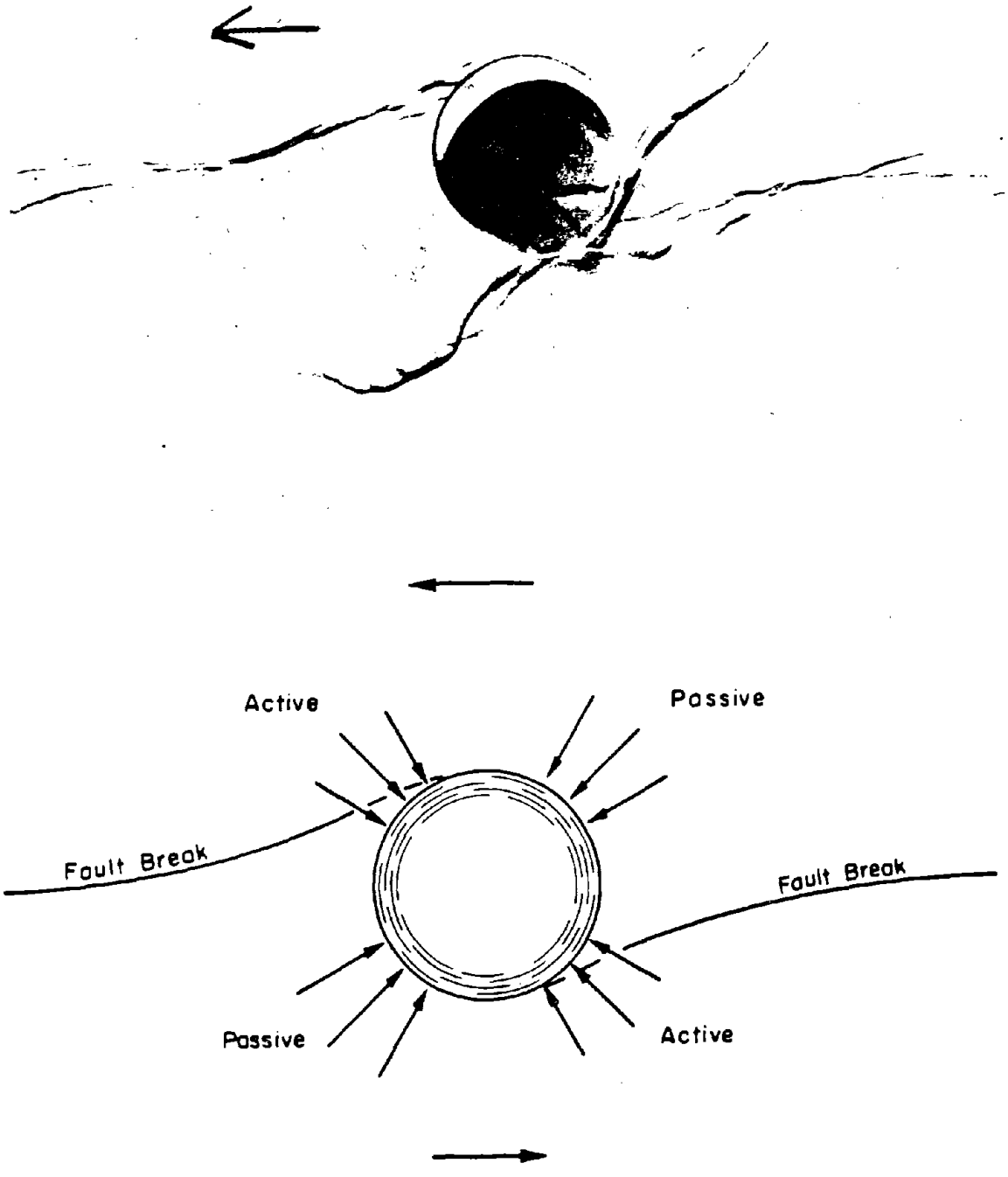

Figure 3-38: PHOTOGRAPH AND DIAGRAM OF EARTH MOVEMENTS AROUND AN EMBEDDED RIGID STRUCTURE (after Duncan and Lefebvre, 1973)

Results from microscopic studies of the tested samples at incremental levels of displacement are shown in Figure 3-39. The fault rupture propagated to reach the surface of the sample when the base deformation was about 15% to 20% of the sample height. For all orientations of the base rock thrust fault, the continuation of the thrust fault bent over the downthrown block with its dip decreasing as it rose toward the top of the sample. Additional fracturing occurred where the change in dip was largest. At large displacements, normal faults formed in an extension zone above the upthrown block. Once the reverse fault was established, deformation in the downthrown block ended. Finally, Friedman and his colleagues observed the formation of microfractures before the development of macroscopic shear fractures. They concluded that these microfractures, which were oriented normal to the minor principal stress, were probably extension fractures. Thus, at the microscopic scale, the deformed rock material actually initially failed in tension.

(g) Horsfield (1977):

Horsfield (1977) performed a series of sandbox model tests to provide insights into the formation of normal fault structures in the North Sea. He hoped to establish a geometrical relationship between basement rock faulting and overburden faulting. The basement faults could have controlled the location and the geometry of the overburden faults which now exist in the oil bearing sediments of the North Sea. The soft sea sediments were modeled using dry, uniformly graded sand compacted to medium density ($e \approx 0.67$) in a sandbox. After working through the scaling relationships presented by Hubbert (1937), Horsfield concluded, "Hence, proper scaling requires the cohesive strength to be scaled down by the same factor as stresses and lengths." With a length reduction of 1×10^{-4} to 1×10^{-5}, the prototype material which had a cohesive strength of on the order of 100,000 psf would have to be modeled using a material which had a cohesive

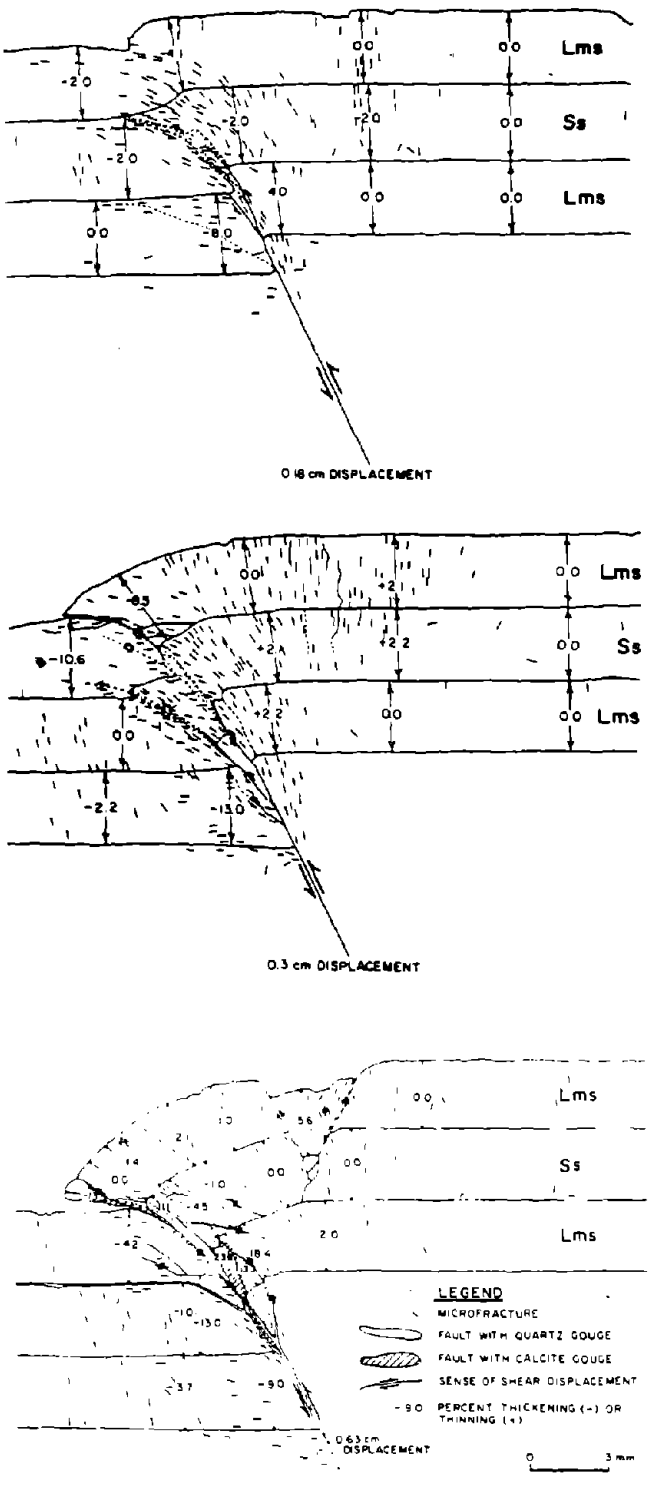

Figure 3-39: RESULTS OF MODEL TESTING OF FAULTING IN ROCKS UNDER HIGH CONFINING STRESSES (after Friedman et al., 1976)

strength of on the order of 5 psf. Since the required model strength value was so low, Horsfield hypothesized that it was reasonable to use a dry cohesionless material to represent the sea sediments.

Representative sandbox model test results are shown in Figure 3-40. Two stages of fault development were observed. Initially, "precurser" faults which overlay and were concave towards the downthrown block formed. These "precurser" faults could actually produce a thrust fault at the surface. Later, more planar normal faults were formed. Movement on low-angle basement faults (30° - 60°) produced antithetic as well as synthetic normal faults creating a graben. Horsfield noted that in some of the experiments the fault intersection with the free surface was slightly bowed. This indicated that the sidewalls of the sandbox restrained sand movement to some degree. Nevertheless, Horsfield concluded that the later stages of the experimental faulting were representative of geologic fault structures observed in the field. On the other hand, this writer observed that the "precurser" faults appeared to represent the development of the thrust mole-tracks observed in the 1959 Hebgen and 1983 Borah Peak earthquakes.

(h) Roth, Scott, and Austin (1981):

In conjunction with the geoseismic investigation for a critical facility near Point Conception, California, a series of centrifuge model tests were performed to validate the numerical model used in subsequent fault propagation analyses. The centrifuge testing was fully described in a report prepared by the geotechnical consulting firm of Dames & Moore (1980). In this article, Roth, Scott and Austin (1981) presented a summary of the results from these centrifuge tests. The goal of the research program was to better understand the behavior of alluvial deposits subjected to bedrock fault movements. Because of the difficulties involved in developing a 1 g small-scale model material which truly represented the prototype

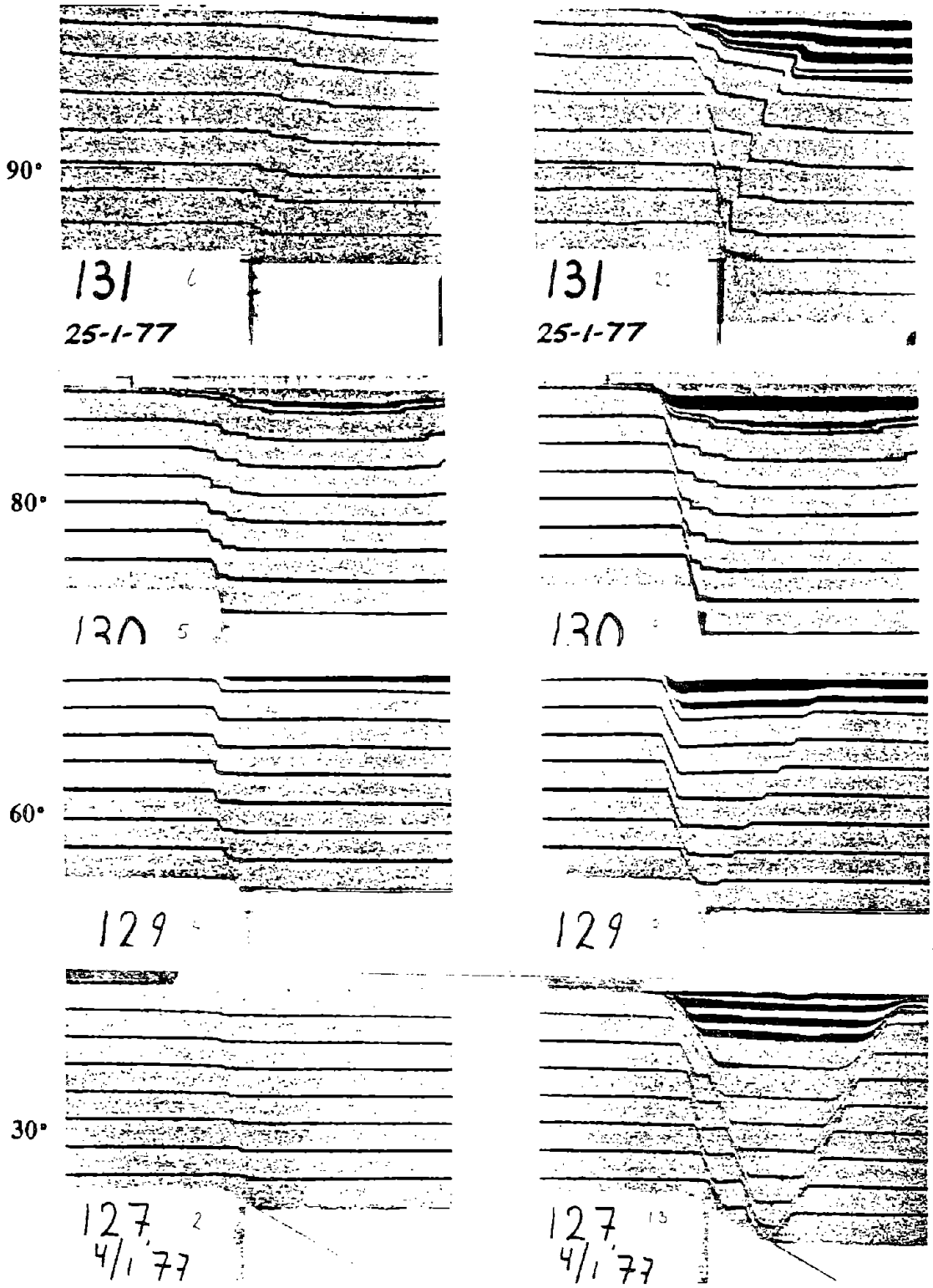

Figure 3-40: DEVELOPMENT OF FAULTS IN DRY SAND OVERLYING BASEMENT FAULTS AT VARIOUS ORIENTATIONS. THE LEFT-HAND AND RIGHT-HAND PHOTOGRAPHS SHOW INITIAL AND LATER FAULT DEVELOPMENT, RESPECTIVELY (after Horsfield, 1977)

material, these researchers turned to centrifuge modeling. If the prototype soil was used in the model tests, the scaling laws required that the soil model be subjected to a higher gravitational force than the prototype. The centrifuge, which could produce accelerations of up to 150 g's, could be employed to create the high gravitational field required for proper modeling. The authors, however, noted one significant drawback. The relative contributions of frictional strength and cohesive strength to a soil's behavior depended on the acceleration field. At high accelerations, the behavior of a cohesive soil would be dominated by the frictional component, whereas at 1 g, the opposite would be true.

Except for one test, the centrifuge model tests were conducted at 50 g's. At this level of acceleration, a prototype soil depth of 30 feet with a vertical bedrock offset of 4 feet was modeled. Because of the excessive weight of the soil at 50 g's, the 45° thrust fault had to be modeled by dropping the downthrown block. Two testing speeds were employed, fast (≈ 0.01 sec) and slow (≈ 5 sec), to investigate the effects of inertia on faulting patterns. Loose sand (γ_d = 88 pcf), dense sand (γ_d = 107 pcf) and the remolded fine sandy silt site material (ϕ = 32°, c = 1000 psf) were tested.

Some of the results from these tests are shown in Figure 3-41. All the sand tests showed the fault decreasing in dip as it approached the surface. The failure plane was more distinct, however, in the dense sand than in the loose sand. Moreover, the dense sand ruptured at a more shallow dip than the loose sand. Overall, slow displacements in both sand samples produced more distinct offsets and shallower ruptures than fast displacements, and the ruptures propagated to the surface at smaller basal offset or displacement.

The cohesive material behaved differently. In the 50 g's tests, more warping occurred across the shear zone before a sharp discontinuity formed, and a secondary shear plane formed at a shallow angle. Because of the inability of the

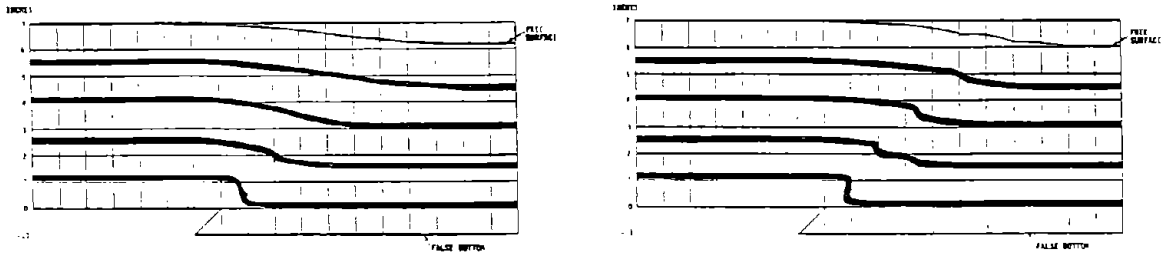

Fast Displacement (50 g's) Slow Displacement (50 g's)

(A) Loose Ottawa #30 Sand (γ_d = 88 pcf)

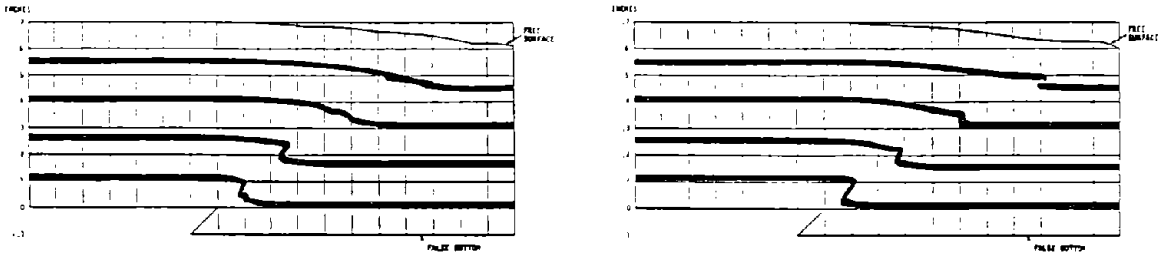

Fast Displacement (50 g's) Slow Displacement (50 g's)

(B) Dense Ottawa #30 Sand (γ_d = 108 pcf)

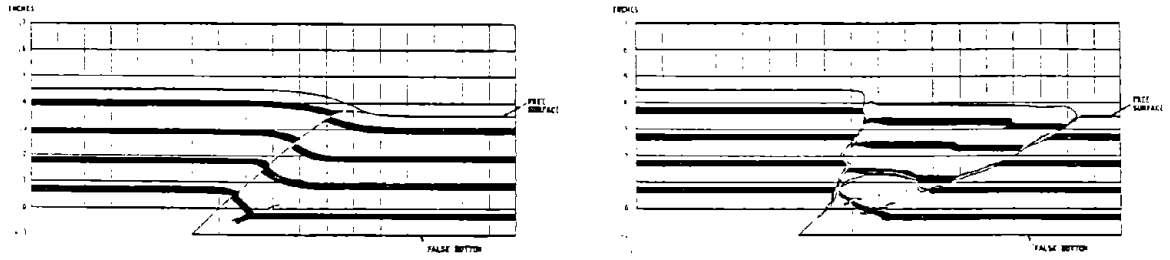

Fast Displacement (50 g's) Fast Displacement (10 g's)

(C) Remolded Fine Sandy Silt (ϕ = 32°, C = 1000 psf)

Figure 3-41: CENTRIFUGE MODELING OF FAULT PROPAGATION THROUGH SOILS (after Dames & Moore, 1980)

centrifuge test to accurately model the relative contributions of the cohesive soil's frictional and cohesive components of strength at high accelerations, a 10 g's test was conducted with the site material. Now, only 4 feet of soil depth was modeled. At this scale, with the cohesive component of strength dominating, the failure pattern was very different. Both a very shallow shear rupture and a nearly vertical tension fissure developed. In summary, the centrifuge testing program highlighted the importance of the soil properties in determining the failure pattern that developed in a soil deposit overlying a bedrock fault.

(i) Walters and Thomas (1982):

Using an experimental set-up similar to that employed by Horsfield (1977), Walters and Thomas (1982) studied the development of shear zones in granular materials above a vertical thrust basement fault. Their test used a uniformly graded sand with a sorted grain size distribution between 0.3 - 0.6 mm. The height of the sand layer was approximately 8 inches. The density of the sand was not given. One of the test results is shown in Figure 3-42. Small displacements of the uplifted basement block produced a shear rupture confined to the lower part of the sand layer. Additional movement of the center block propagated the shear zone to the surface of the sand layer. The failure surface bent over the downthrown block decreasing in dip as it approached the top of the sand. Further movement created a second, more nearly vertical shear zone where most of the subsequent differential displacement within the sand sample occurred.

(j) Lade and Cole (1984):

Lade and Cole completed a comprehensive 1 g sandbox model testing program to learn how bedrock fault ruptures propagated through overlying deposits of alluvium (Lade and Cole, 1984; Lade et al., 1984). Knowing the travel path of a fault rupture as it rises to the surface in an alluvial deposit can be

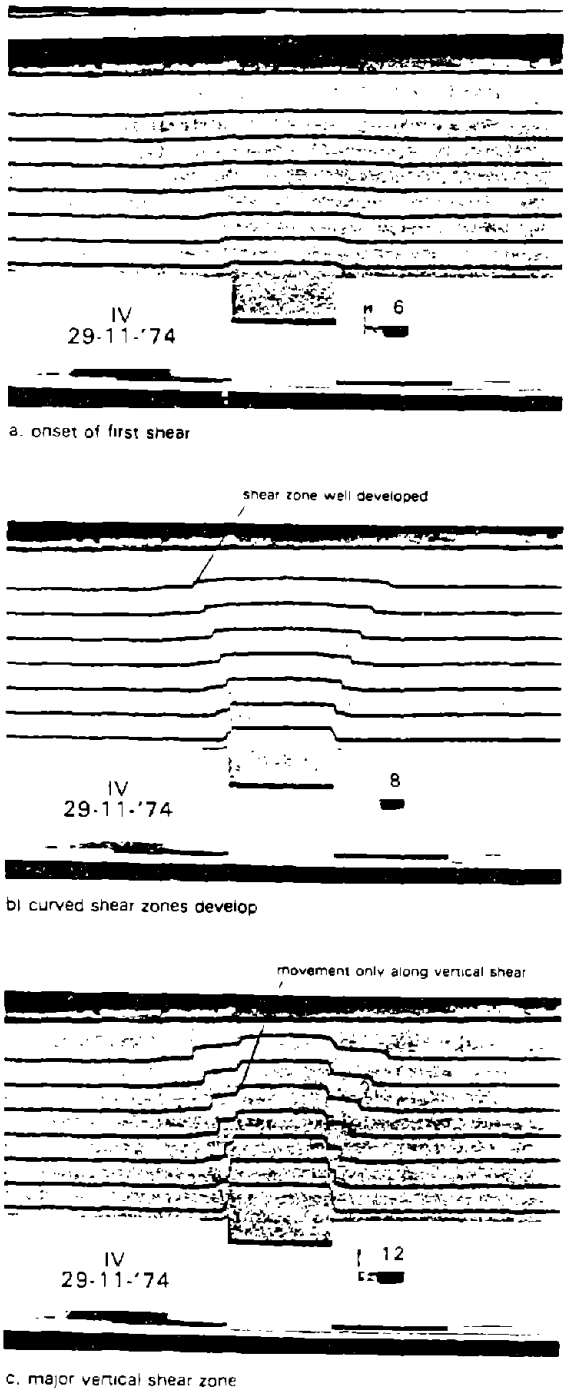

Figure 3-42: CHRONOLOGICAL DEVELOPMENT OF SHEAR ZONES IN SANDBOX EXPERIMENT (after Walters and Thomas, 1982)

important in siting critical facilities. Their study concentrated on understanding "the mechanics of deformation and failure in dry cohesionless material above a fault as it relates to soil mechanics." The static behavior of the dry cohesionless soil was studied without regard to the dynamic and time-related effects accompanying an earthquake event. One of the major goals of the testing program was to decide if stress characteristics as described by the plane strain angle of internal friction (ϕ_{ps}) or kinematic characteristics as described by the plane strain angle of dilation (v_{ps}) determined the shape of the failure surfaces developed in the alluvium above the bedrock faults. Hence, tests were performed on two contrasting cohesionless materials - a dense uniform course sand ($\phi_{ps} = 58°$, $v_{ps} = 30°$) and a mixture of the sand and 1.0 mm diameter styrofoam beads ($\phi_{ps} = 30°$, $v_{ps} = 6°$). The sand layer was around 16 inches high. The tests modeled dip-slip fault movements at several orientations.

Figure 3-43 provides an illustration of the fault rupture propagation process during the conduct of one of the tests. Note that the thrust fault rupture propagation reached the surface at a vertical base deformation between 0.4 to 0.8 inches or 2% to 4% of the height of the dense sand layer. Normal faults propagated to the surface of the dense sand, however, at vertical base deformations of 1% to 3% of the height of the sand layer. "Larger vertical movements were required to develop failure surfaces in the more compressible, loose sand." Additionally, the failure surfaces in the loose sand were not often discernable. Figure 3-44 illustrates two more important points. Initially, the soil in the shear zone warped to accommodate the bedrock fault offset. When the failure surface was fully developed, however, the warped zone rebounded and nearly all of the differential movement occurred across the shear rupture. Furthermore, once the ground surface was broken, the ratio of the additional (incremental) local scarp height to the additional (incremental) vertical bedrock movement was essentially

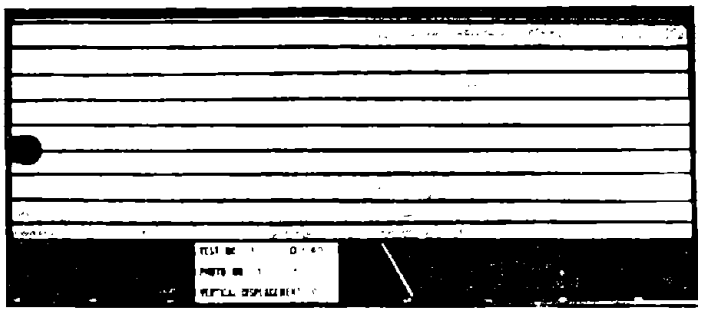

(A) Undeformed

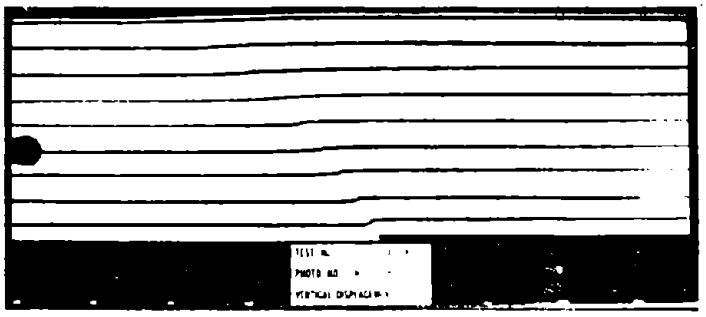

(B) Initiation Of Failure Surface At Bedrock Fault

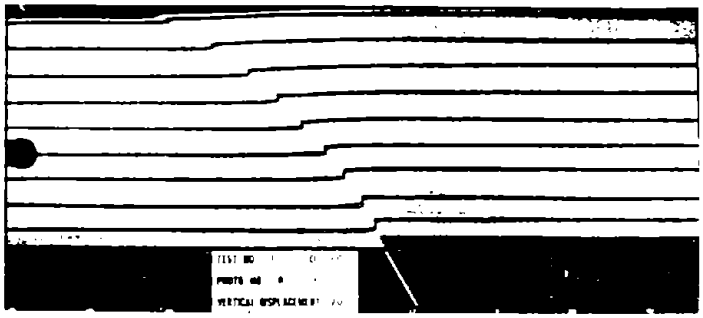

(C) Fully Developed Failure Surface

Figure 3-43: PHOTOGRAPHS OF THREE STAGES IN 60° THRUST FAULT TEST ON DENSE SAND (after Lade and Cole, 1984)

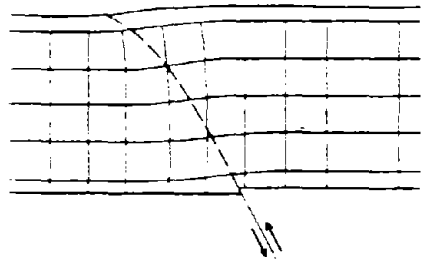

(A) Before the Failure Surface Has Ruptured the Ground Surface

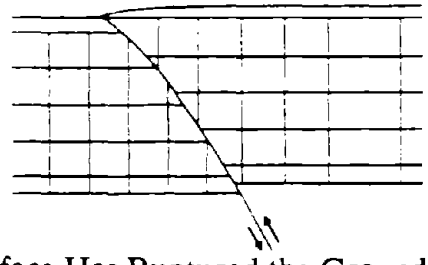

(B) After the Failure Surface Has Ruptured the Ground Surface

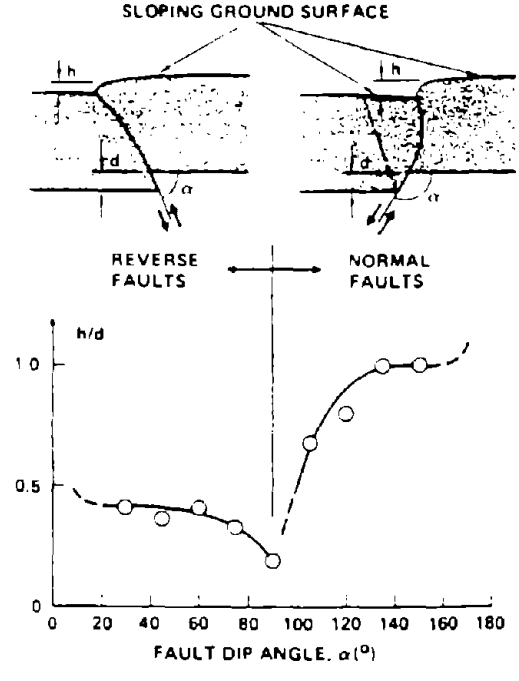

(C) Observed Ratio of Scarp Height to Vertical Bedrock Movement as Function of Fault Dip Angle

Figure 3-44: OBSERVED DEFORMATION OF SAND MASS; TESTS ON DENSE SAND (after Lade et al., 1984)

constant. Hence, warping of the surface of the sand layer continued to accommodate part of the base movement.

A summary of the test results and a proposed relationship to be used to predict the location of surface ruptures in alluvium over dip-slip bedrock faults are presented in Figure 3-45. All of the failure surfaces bent over toward the side of the downthrown block. Normal faults refracted at the soil-bedrock interface. The slight difference in the shape of the failure surfaces formed by the 90° thrust and normal fault offsets indicated that the effects of friction along the side wall of the sandbox were minor.

The experimental results formed the basis for a theoretical model which could predict the shape of the failure surface formed by bedrock faults. A log spiral expression with the input parameters: fault dip angle, height of the soil, and angle of dilation of the soil, described the observed failure surfaces. This relationship could be used to calculate the horizontal distance from the surface rupture to a point on the surface vertically above the point where the bedrock fault intersected the soil-bedrock interface. Figure 3-45(B) could be used to predict where a fault rupture produced by a bedrock fault broke the ground surface. The only soil property required in this calculation was the angle of dilation. Lade and Cole concluded that the soil's kinematic characteristics as described by the angle of dilation of the soil determined the shape of the failure surface as it propagated upwards through the soil.

Finally, Lade and Cole evaluated the applicability of these lab results to field cases. For the three case studies presented, their experimental results agreed reasonably well with the observations made in the field. Again, the angle of dilation was the only soil parameter that their theoretical model required. If the material's angle of dilation was properly re-evaluated at the confining stresses which existed in the field, Lade and Cole felt that the results from these

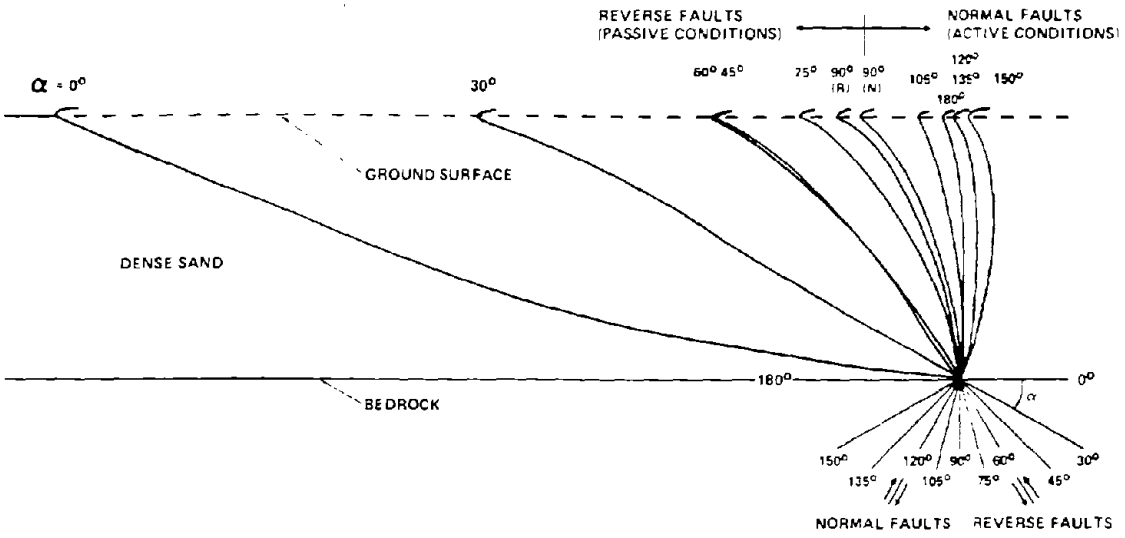

(A) Observed Primary Failure Surfaces

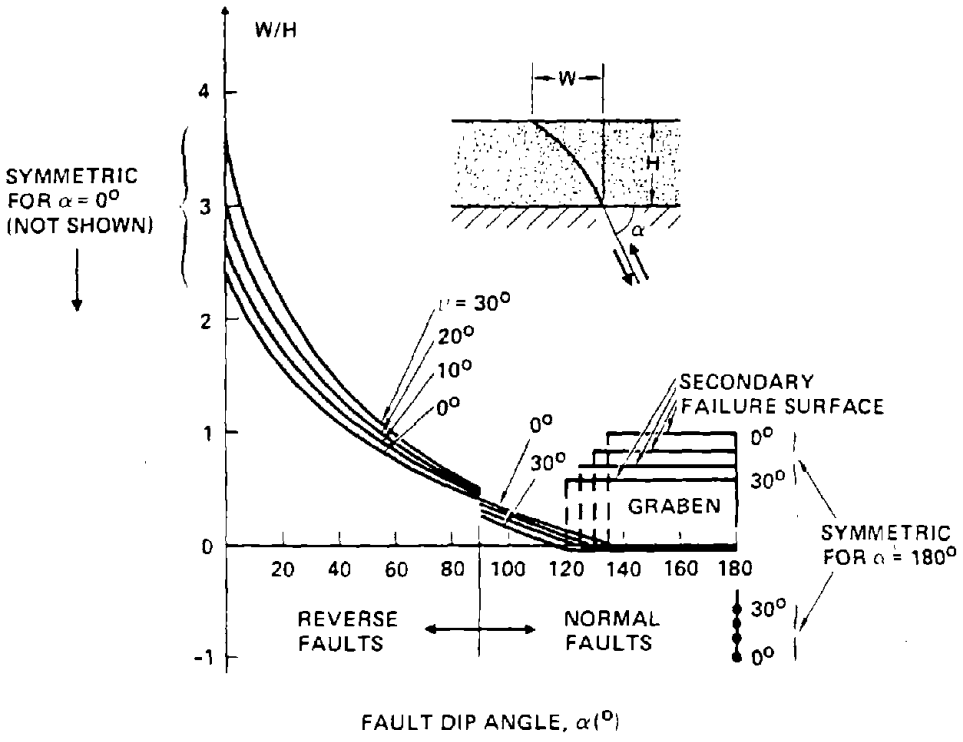

(B) Location of Surface Rupture

Figure 3-45: PRIMARY FAILURE SURFACES OBSERVED IN TESTS ON DENSE SAND (A) AND PROPOSED VARIATION OF W/H FOR LOCATION OF SURFACE RUPTURE IN ALLUVIUM AS A FUNCTION OF DIP ANGLE AND ANGLE OF DILATION (B) (after Lade and Cole, 1984)

experiments performed at low confining stresses were applicable to field conditions. Furthermore, since the alluvium's strength parameters were apparently unimportant, Lade and Cole hypothesized that these results may be applicable to cohesive materials. They did warn, however, that if the deposit was shallow and the soil was relatively strong in cohesion, the soil layer may behave as a beam and fail in tension. Of course, anisotropic soil properties might affect the location of the surface rupture, and the researchers surmised that a dip-slip fault movement with a strike-slip component passing through "typical" soils in the field might form a failure surface located more centrally above the bedrock fault.

3.3.3 Numerical Model Studies:

(a) Duncan and Lefebvre (1973):

In conjunction with the model testing described previously in Section 3.3.2(e), Duncan and Lefebvre (1973) employed the finite element method (FEM) to predict the magnitude of earth pressures on a full size structure that straddled a strike-slip fault offset. Both plane stress analyses of horizontal planes through the soil deposits and the embedded structure, and plane strain analyses of a vertical plane along the strike of the strike-slip bedrock fault were performed. No slip was allowed at the soil-structure interface and the initial coefficient of at rest earth pressure was assumed to be 0.5. The cylindrical structure was 180 feet in diameter and was embedded 80 feet into a 200 foot thick deposit of loose or dense sand. The loose and dense sand materials were modeled by the incremental, nonlinear, stress dependent hyperbolic soil behavior model proposed by Duncan and Chang (1970).

Representative results from the FEM analyses are presented in Figure 3-46. For the plane strain analysis of the loose sand case, the increase in the passive earth pressure against the structure with depth as displacement along the fault increased is shown in Figure 3-46(A). For a plane stress analysis of the loose sand

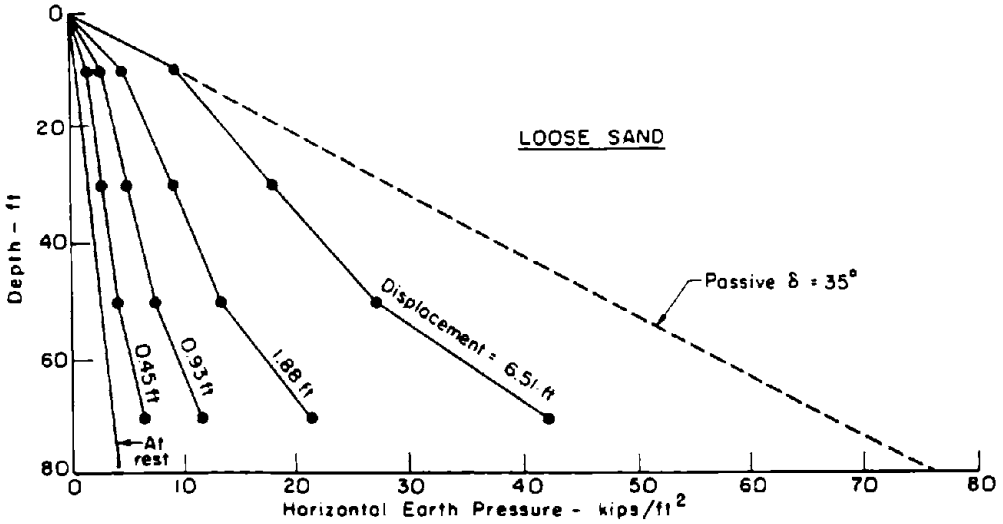

(A) Earth Pressure on Passive Side of Structure

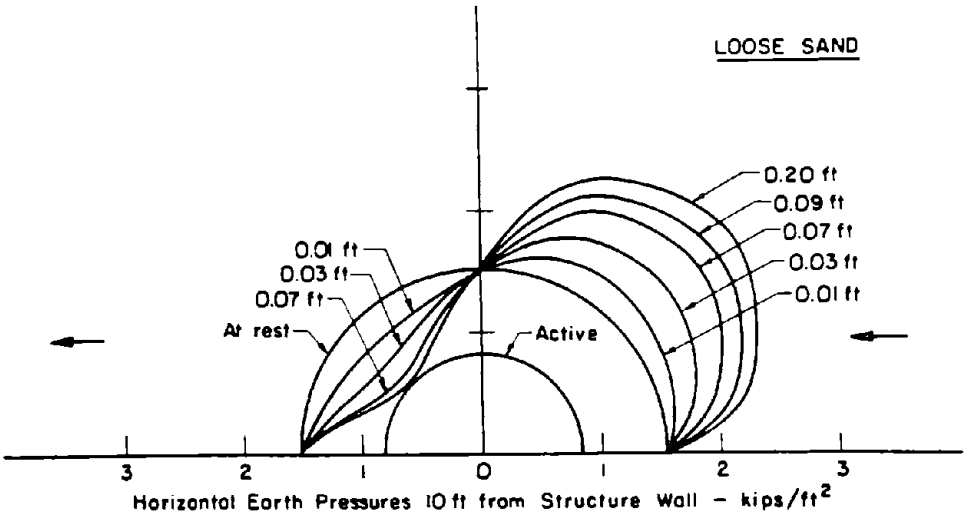

(B) Distribution of Earth Pressures at 30 Foot Depth

Figure 3-46: RESULTS FROM FEM ANALYSES OF EARTH PRESSURES DEVELOPED AGAINST A RIGID STRUCTURE EMBEDDED IN A SOIL DEPOSIT OFFSET BY A STRIKE-SLIP BEDROCK FAULT (after Duncan and Lefebvre, 1973)

case, the variation of the distribution of earth pressures against the structure as the fault movement progressed is shown in Figure 3-46(B). Notice the development of the passive earth pressure zone and active earth pressure zone at orientations of approximately 45° to the direction of fault movement. The results from the plane strain and plane stress analyses agreed within about 30% and compared favorably with the results of the model tests described in Section 3.3.2(e). As expected, the maximum earth pressures against the embedded structure were considerably higher for the stiffer, stronger dense sand case. Most importantly, these studies showed that a proper finite element analysis employing a soil constitutive law which correctly modeled the nonlinear, stress dependent stress-strain and volumetric strain behavior of the soil could be successfully applied to this class of problem.

(b) Scott and Schoustra (1974):

In siting a nuclear power plant in a deep alluvial valley, the researchers were asked what magnitude of bedrock fault movement would be necessary to produce a surface rupture at the ground surface. Scott and Schoustra (1974) employed the finite element method to answer this question. They analyzed a two-dimensional (2-D) plane strain vertical section through alluvium overlying a vertical dip-slip bedrock fault. The boundary displacement imposed, the soil parameters used, and the finite element mesh with yield zones developed at various levels of base fault offset are shown in Figure 3-47. These FEM analyses employed a linear elastic-perfectly plastic constitutive law which used the modified Von Mises yield criterion to model soil behavior. The presence of water was not considered in the analyses. It took approximately 50 meters of vertical differential offset across the bedrock fault to cause the failure zone in the alluvium to propagate up to the surface. This was roughly 6% of the height of the alluvial

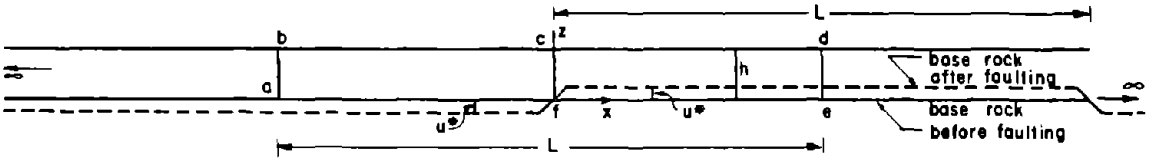

(h = 800 m, L = 9000 m, γ = 1.7 t/m^3, ϕ = 25°, ν = 0.4, and E = 17.7 σ_x)

(A) Faulting Mechanism to be Considered

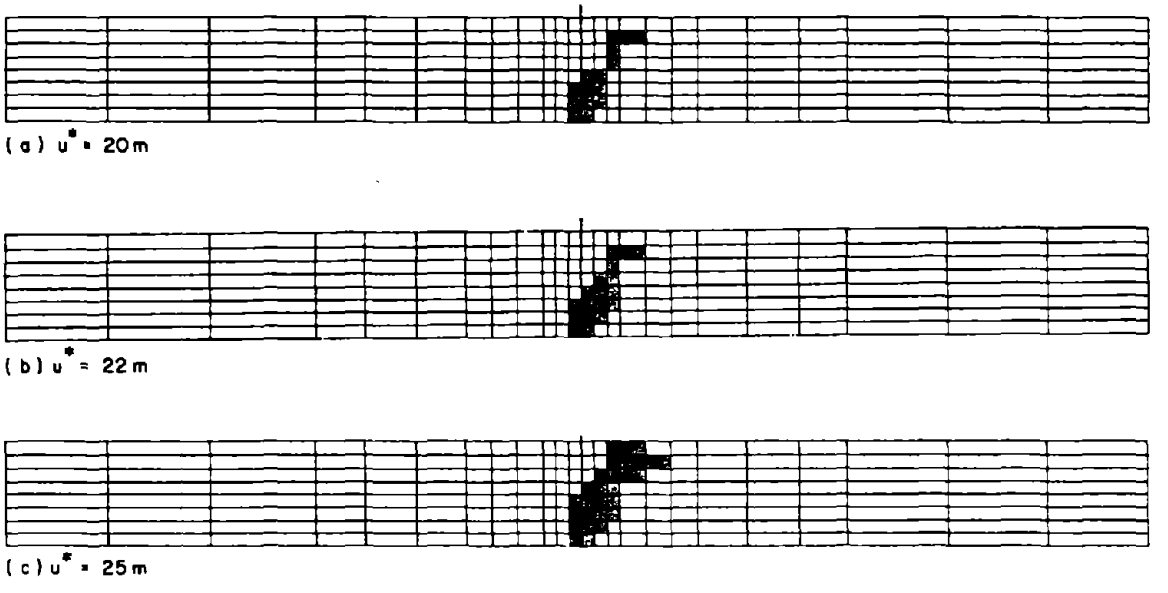

(B) Development of Yield Zone as a Result of Bedrock Fault Offset

Figure 3-47: FEM STUDY OF FAULT PROPAGATION THROUGH A DEEP ALLUVIAL VALLEY (after Scott and Schoustra, 1974)

deposit. The results, however, showed the failure zone in the alluvium bending over the upthrown block as the bedrock fault displaced vertically. In contrast, results from applicable physical model tests discussed in Section 3.3.2 indicated that the surface rupture bent over the downthrown block. Furthermore, Scott and Schoustra realized that in reality the broad failure zone developed in the FEM analyses represented a thin failure surface. The authors felt the results from the FEM analyses, however, justified their conclusion that "Fault displacement in bedrock beneath a deep alluvium must be of considerable magnitude relative to the soil depth in order to cause yielding of the soil at ground surface."

(c) Reddy et al. (1982):

Roth, Stein and Wickham (1982) adopted a novel approach in their study of the application of the finite element method to modeling geologic phenomena such as folding and faulting. Whereas previous studies had employed the equations of elasticity, these researchers applied a penalty-finite element model based on the assumption that rocks behaved as viscous incompressible Newtonian fluids. Their two-dimensional multilayered FEM model of a generalized stratigraphic section of the Paleozoic and Mesozoic strata of the Wyoming Province was 25 km long and 5.5 km high. The rock properties varied over the section and ranged from viscosities between 1.6×10^{20} and 7.5×10^{20} poises with the one exception of 3.2×10^{22} poises, and densities between 2.20 and 2.60 g/cm^3. Once failure as defined by the Mohr-Coulomb failure criterion occurred, the viscosity of these elements was reduced by a factor of 100. The problem was solved iteratively for each small increment of time.

The results from the FEM analyses are shown in Figure 3-48. The bottom and third layers represented brittle rock so fracturing extended laterally along these layers. Another simplified analysis of a homogeneous rock mass did not

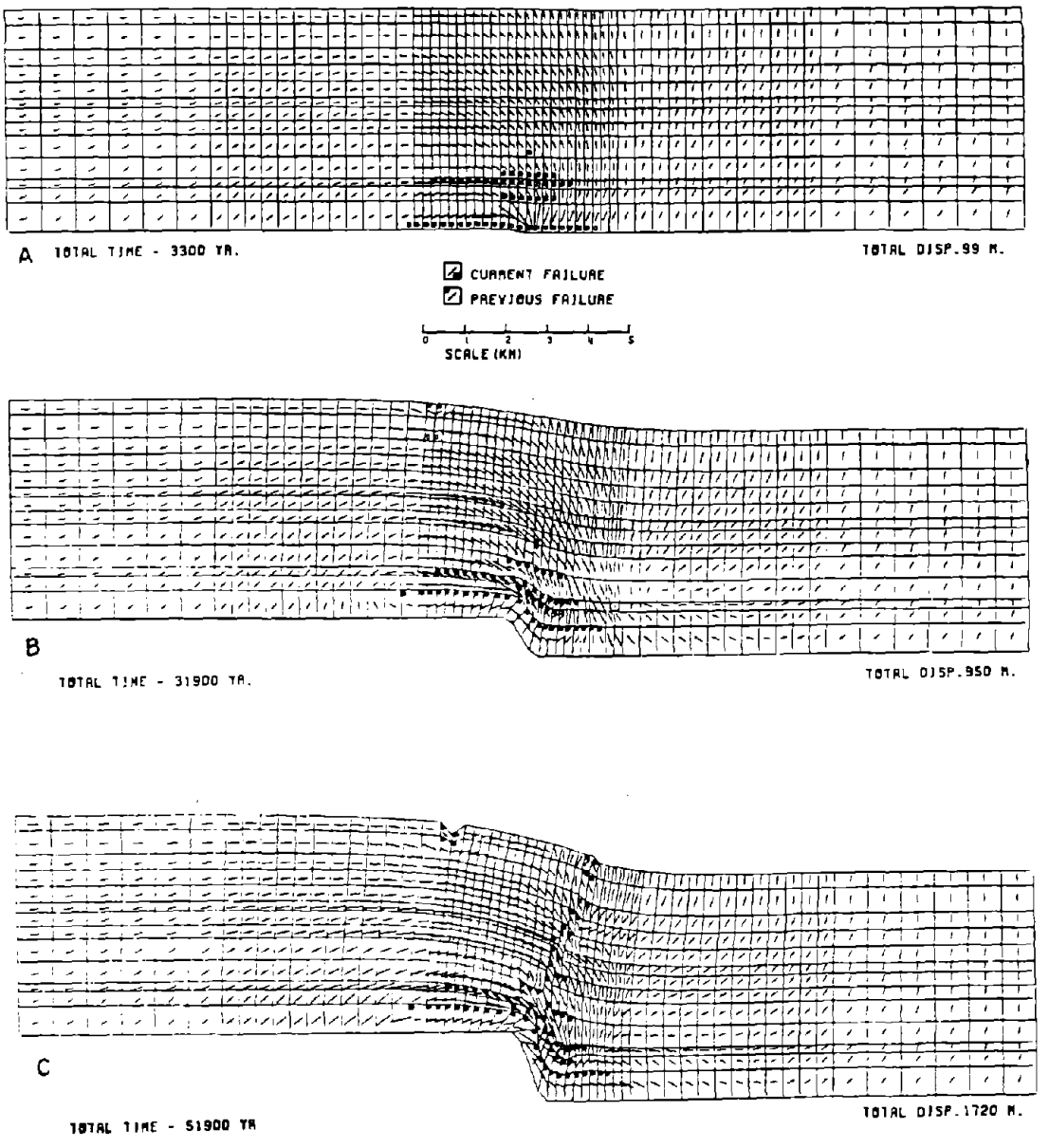

Figure 3-48: PENALTY-FEM EMPLOYING VISCOUS NEWTONIAN FLUID MODEL RESULTS OF BASEMENT ROCK FAULTING: RELATIVE VELOCITY OF 3 CM/YEAR (after Reddy et al., 1982)

display this lateral spreading of fracturing. Otherwise, the results from these analyses were similar. Note that the rupture zone propagated up over the downthrown block and that a small extension zone formed at the ground surface over the upthrown block. Roughly 1700 meters of bedrock offset was necessary to propagate the failure up to the surface. This represented a base displacement of nearly 31% of the height of the rock mass. Finally, the authors remarked that the numerical model results could help explain the geologic structures observed in the field by Prucha et al. (1965) (See Section 3.2.2(a)).

(d) Roth et al. (1982):

In this article, Roth et al. (1982) summarized the results of the numerical analyses performed in conjunction with the centrifuge model tests and geoseismic investigation from the Dames & Moore (1980) site evaluation study of the proposed Liquefied Natural Gas facilities near Point Conception, California (See Sections 3.2.2(a) and 3.3.2(h)). The researchers employed a version of the finite difference computer code SAGE (Geognesis, 1980; Cundall, 1976). The code utilized an explicit finite difference formulation in a Lagrangian frame of reference. An incremental solution technique allowed for the proper handling of large strains, nonlinearities and hysteresis effects. Within each increment, imposed boundary velocities were used to estimate strains which, in turn, were used to calculate stresses. These estimates of stresses were used to update velocities within the region. This sequence was repeated until convergence was obtained. In this study, the soil was modeled as a "no-tension, elasto-plastic material with a Drucker-Prager yield surface determined by a bi-linear Mohr-Coulomb failure envelope, and nonassociated flow rule."

The numerical method was first applied to the centrifuge model tests described in Section 3.3.2(h) to validate its legitimacy. Results were presented in

the form of deformed meshes as shown in Figure 3-49. These results should be compared to the centrifuge model test results shown in Figure 3-41. The authors found the agreement between the numerical results and centrifuge test results "encouraging". The FDM analyses indicated that the shear zones were narrower and flatter in the dense sand and in the case of slow failure conditions. The same behaviors were exhibited in the centrifuge model tests. This writer, however, finds it difficult to identify differences in the deformed meshes presented in the study. For example, how is the width of the shear zone defined? Are there differences in the width of the shear zones in the results presented? The numerical model did, however, indicate that increasing the angle of dilation of the soil flattened the trajectory of the fault rupture. Additionally, the analyses of the cohesive remolded sandy silt material did indicate tension development and a sharper curvature of the ground surface. Similar patterns of behavior were observed in the centrifuge model tests of the field material.

Finally, these numerical methods were employed to analyze the development of the shear fractures exposed in the exploratory trench shown in Figure 3-11. From these analyses, the authors concluded that strength parameters, not elastic parameters, were important. The results were sensitive to the no-tension criterion established. Although the authors concluded that numerical results (which showed a shear zone that increased in dip towards the surface) represented the general trends of the fault exposure, this writer disagrees that the complex fault morphology shown in Figure 3-11 (with its longest shear fracture actually decreasing in dip as it approached the surface) can be characterized as a broad shear zone that increased in dip as it approached the ground surface.

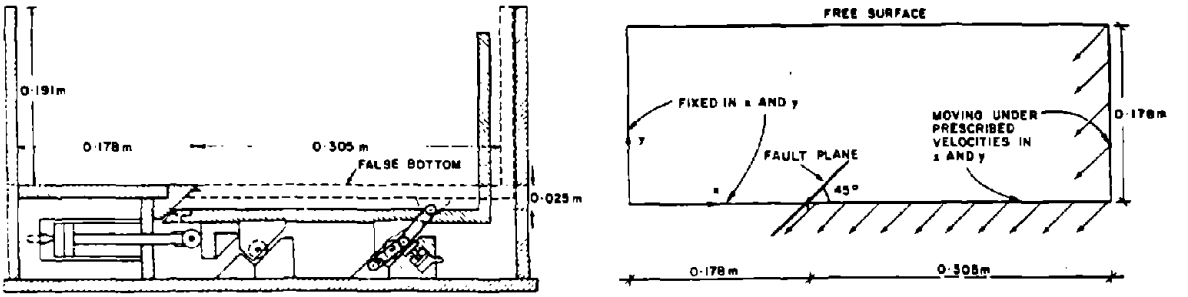

(A) Centrifuge Test Boundary Conditions

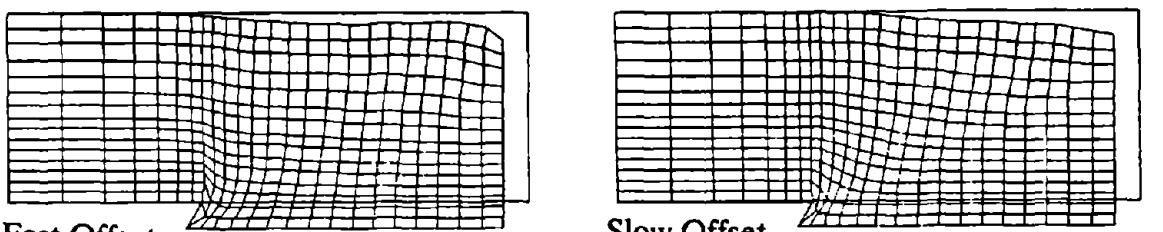

Fast Offset

Slow Offset

(B) Loose Ottawa #30 Sand (γ_d = 88 pcf & Dilation α = 0°)

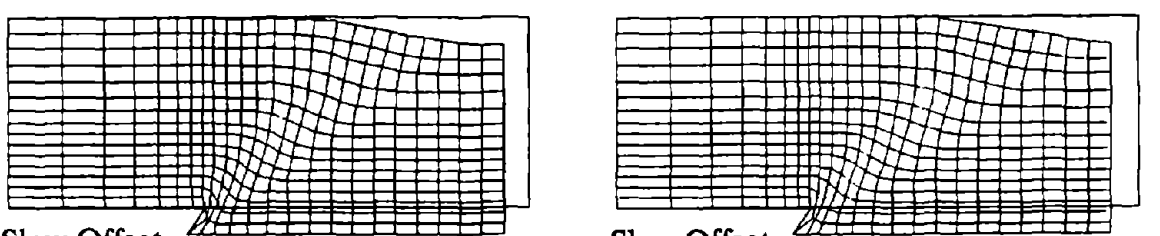

Slow Offset

Slow Offset

(C) Dense Ottawa #30 Sand (γ_d = 107 pcf & Dilation α = 0°)

(D) Dense Ottawa #30 Sand (γ_d = 107 pcf & Dilation α = 10°)

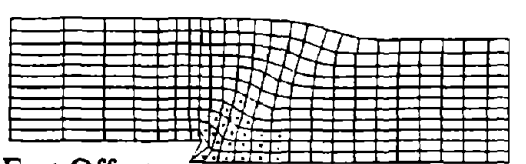

Fast Offset

• Denotes Tension Failure

(E) Remolded Fine Sandy Silt (ϕ = 32° , c = 1000 psf & Dilation α = 5°)

Figure 3-49: FINITE DIFFERENCE METHOD RESULTS. MODELING OF THE CENTRIFUGE TESTS DESCRIBED IN SECTION 2.5.2(H) (after Roth et al., 1982)

(e) Walters and Thomas (1982):

As discussed in Section 3.3.2(i), Walters and Thomas (1982) studied the development of shear zones in granular materials by performing sandbox model experiments. The primary objective of their study, however, was to validate the use of a sophisticated numerical model which could analyze the shear rupture propagation phenomenon in greater detail. The finite element method utilized an incremental elasto-plastic constitutive law with a Drucker-Prager yield criterion. Variable nonassociated post yield flow behavior with frictional strain softening was incorporated into the soil model. If an associated flow rule was used with the Drucker Prager or Mohr-Coulumb yield criterion, the dilatancy rate would always be positive, and continued shearing past failure would produce an ever increasing dilation. Laboratory tests on granular materials have shown that past peak strength the dilation rate actually decreases.

The right half of an 8-inch high by 39-inch long region of the sandbox shown in Figure 3-42 was modeled using 180 eight-node isoparametric plane strain elements. Results from analyses first employing an associated flow rule and then employing a variable nonassociated flow rule are shown in Figure 3-50. Both analyses modeled the development of the first shear zone properly. The first shear zone propagated to the surface, however, at a base uplift of only 6×10^{-4} inches or less than 0.008% of the height of the sand layer; whereas in the sandbox experiments, the first shear zone propagated to the surface at a base uplift of at least 0.1 inches, or at least 1.25% of the height of the sand layer. Only the analyses utilizing the variable nonassociated flow rule could correctly model the subsequent development of the final vertical shear zone. In the analyses performed using the variable and nonassociative flow rule, there was a general reduction in the mean stress after the first shear zone developed which reoriented some of the stress trajectories allowing for the progressive development of steeper shear zones with

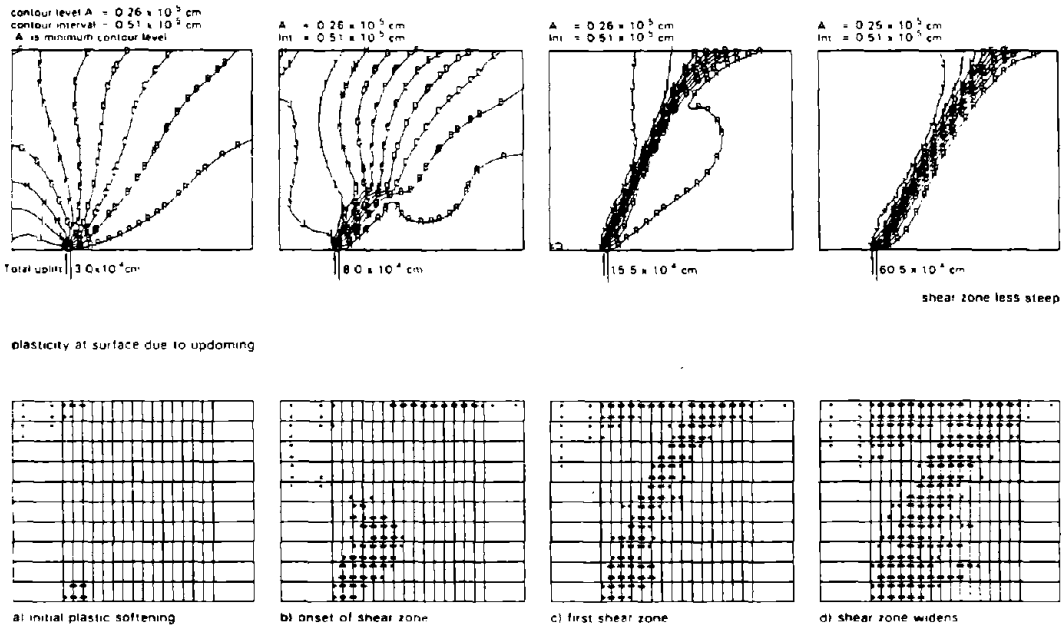

(A) With Associated Flow Rule

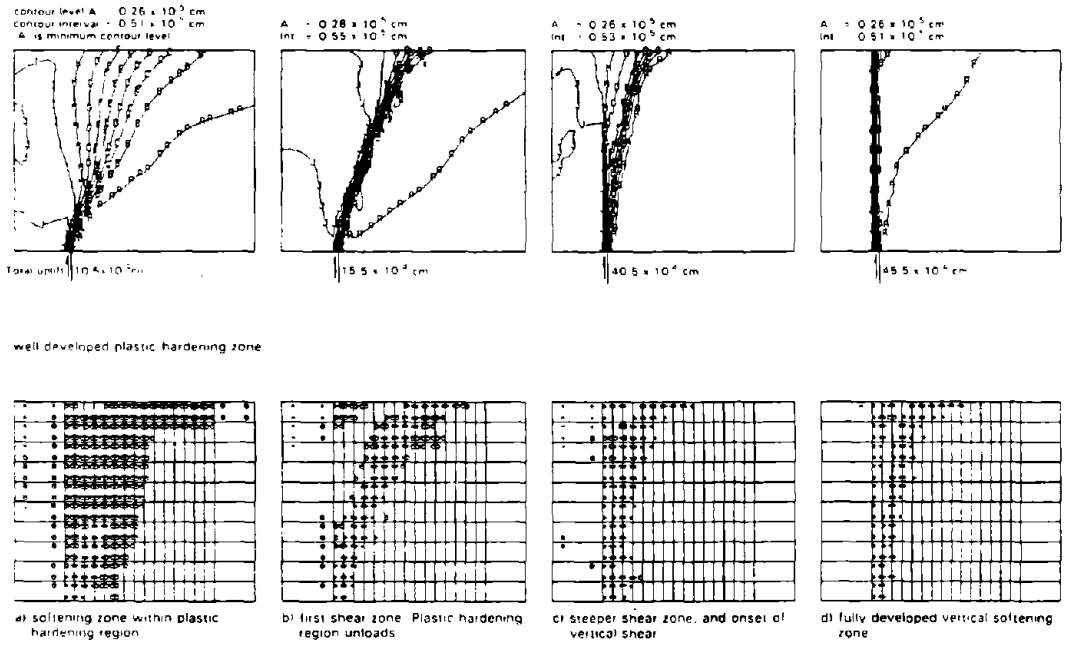

(B) With Variable NonAssociated Flow Rule

Figure 3-50: FE MESH: CIRCLES DENOTE PLASTIC HARDENING ZONE; CROSSES DENOTE PLASTIC GROWTH ZONE AND INCREMENTAL ABSOLUTE DISPLACEMENT CONTOURS FOR NUMERICAL MODEL OF SHEAR ZONE DEVELOPMENT IN GRANULAR MATERIAL (after Walters and Thomas, 1982)

continued base uplift. The displacement contours identified a fairly narrow shear zone indicating that the ability to model strain softening was critical in the localization of the failure zone. One final note: a similar analysis (except that the coefficient of at rest earth pressure was assumed to be 0.7 instead of 1.0) indicated that, even with this sophisticated soil model, a change in just one critical soil parameter could produce significantly different results.

(f) Scott (1987):

In the twenty-seventh Rankine Lecture, Scott (1987) presented an enlightening discussion of "Failure". One of his points of discussion was fault propagation, and in particular, numerical modeling of fault propagation. Scott compared the results from the analyses performed by Scott and Schoustra (1974) and Roth et al. (1982) (See Sections 3.3.3(b) and (d), respectively). Regarding his work with Schoustra, Scott now commented, "A disturbing feature of these analyses of the fault problem was that the failure region did not propagate in the correct way." Instead, the slip-line should have bent over the downthrown block as demonstrated in anchor pull-out model tests. Scott wondered if the use of a more "complex and descriptive constitutive model for the soil" would have improved the FEM results. In contrast, analyses performed using the finite difference method, but employing a nonlinear soil model, produced numerical results that exhibited "a reasonable match to the experimental results."

In his Rankine Lecture, Scott noted a project where a fault in a deep alluvial valley was detected by seismic profiling. The fault rupture did not offset the near surface deposits. Instead, it showed a gradually decreasing offset until it died out several hundred feet short of the ground surface. One could have interpreted this to mean that the fault was older than the undisturbed deposits above it, and hence, the fault was inactive. On the other hand, the bedrock fault

could have displaced an amount insufficient to produce a surface rupture. In this case, the fault may have been active and a larger fault offset in the future could propagate the slip-line all the way to the ground surface. Scott asked, ". . . how much displacement would be required at bedrock to cause rupture just to reach the surface of the soil of a specified depth?" His 1974 paper had attempted to answer this question.

Scott identified a number of limitations of the finite element method in the analysis of failure. The propagation of failed elements depended on the shape, type, and arrangement of the elements employed. Results were only as accurate as the soil's constitutive model, and none of the models currently used incorporated all of the important aspects of the behavior of soil. When an attempt was made to do so, the constitutive models became incredibly complex. Scott offered two alternatives to the finite element method. Cundall's discrete element program, UDEC2, circumvented the need to model a granular material as a continuum, and thus eliminated the need for sophisticated soil constitutive models (Cundall, 1976). Interparticle forces and kinematic constraints controlled the solution. Because of the number of particles required, the computer solution time, however, was prohibitive. Another possibility was the finite difference method with dynamic relaxation (similar to the FDM technique described in Section 3.3.3(d)). Within each load step, newly applied forces induced accelerations which through double integration produced displacements, and hence, strains. At this point, any unstable, nonlinear constitutive law could be employed to calculate stresses. From stresses, forces were calculated. The pattern continued until convergence was obtained. In work performed by Scott's doctoral student Burridge (1987), this FDM technique was employed to analyze the development of slip-lines in slope stability problems. Although the deformed meshes and displacement contour plots indicated the correct general patterns of development of the failure surfaces, often

two or more times the gravitational force applied in centrifuge tests had to be applied to the numerical models of these tests to initiate failure. Additional work was thus required to refine this numerical method.

3.3.4 Lessons to be Learned from Physical and Numerical Modeling of Fault Rupture Propagation:

Comparing the results of the physical model tests with the numerical model tests and with the fault rupture case histories presented on Section 3.2, one sees a number of similarities. In fact, finding agreement in a few critical points in such a diverse group of model tests should provide some level of confidence in the lessons learned from these tests. The principal lessons to be learned from the review of the physical and numerical model tests which examined the fault rupture propagation phenomenon are presented herein.

Lade and Cole (1984) provide the most complete picture of the fault rupture propagation problem. Their results agree well with the results from other model tests and field studies, and their Figure 3-45(A) thus appears to summarize the characteristics of the failure patterns that develop in dry alluvium above dip-slip bedrock faults. Regarding strike-slip fault movements, Tchalenko (1970) presented the clearest picture of the behavior of soil above these fault movements. In summary, dip-slip faults tend to bend over the downthrown block. Normal faults refract at the soil-bedrock contact. Additionally, low-angle normal faults usually produce graben structures. Thrust faults tend to propagate along the orientation of the bedrock fault, but they do usually decrease in dip as they approach the ground surface. The continuations of strike-slip faults are nearly vertical as they propagate upwards through overlying soils, though flowering may occur near the ground surface. In ductile materials the direct shear offset at the base of the deposit can be transformed into a distorted zone of simple shear which produces en echelon

cracks. Shear zones at different scales (e.g. shear test and earthquake faulting) possess similar characteristics. Individual shear planes are usually narrow, although, loose, more compressible materials may accommodate distinct bedrock offsets by broad warped zones.

It is important to characterize the soil properly in model tests. Researchers disagree as to whether strength parameters (e.g. friction angle and cohesion) or kinematic parameters (e.g. angle of dilation) determine soil behavior during fault rupture propagation through soils. There is no reason why both cannot be considered important. The results of different model tests appear to support this reasoning. Both strength parameters and kinematic parameters have been employed by researchers to successfully predict the location and expression of the rupture zone as it propagates upwards through overlying soils.

Soil characteristics are instrumental in determining how much base deformation or offset is required to propagate a shear zone from the base of the soil to the ground surface. In model tests employing dry sand, base deformations of on the order of 1% to 15% of the height of the overlying soil deposit are required to propagate a base shear rupture to the ground surface. Loose, more compressible materials require more base deformation, while dense, less compressible materials require less base deformation. Normal fault ruptures propagate faster (i.e. require less base offset to propagate to the ground surface) than thrust fault ruptures, which in turn propagate faster than strike-slip fault ruptures.

Physical model tests were performed at low confining stresses using relatively weak materials, except for the experiments conducted by Friedman et al. (1976). The results from their work using rocks under high confining pressures, however, were remarkably similar to the results published for the other physical model tests. None of the physical model tests dealt directly with the issue of dip-

slip base fault rupture propagation through saturated clay. Similarly, none of these tests modeled saturated sand sheared under undrained conditions.

Finally, numerical modeling of the fault rupture propagation phenomenon can be successful provided that the soil's nonlinear stress-strain behavior is properly or at least adequately modeled. Linear elastic-perfectly plastic constitutive laws, however, produce inconsistent results when employed in the finite element method. Although based on continuum mechanics, the finite element method can model the development of the shear and tension zones in the soil overlying a base rock fault offset. It is difficult to localize shear failure within narrow zones and it is even more difficult to ensure that secondary shear zones are modeled correctly. The results from the reviewed finite element analyses indicated that the coefficient of at rest earth pressure was possibly a critical soil parameter. The discrete element method, and to lesser extent, the finite difference method with dynamic relaxation, look very promising, but refinements are necessary before these techniques can be routinely applied to this class of problem.

3.4 Summary and Findings

This chapter has presented a comprehensive review of previous studies of the propagation of fault ruptures through earth materials. The general observations by a number of geologists and seismologists regarding earthquakes and the fault rupture propagation phenomenon have been presented. Moreover, eighteen indicative fault rupture propagation field studies were reviewed and evaluated. In addition, ten physical model studies and six numerical model studies of the fault rupture propagation phenomenon have been examined, and lessons to be learned from these studies have been summarized. The field studies and model studies of fault rupture propagation brought forth a number of salient observations.

Foremost, the fault rupture propagation phenomenon is rather complex. A number of variables influence the fault rupture process. Given the complexity of the fault rupture propagation phenomenon, it is surprising that consistent patterns of behavior emerged during the review of the field studies and the physical and numerical model studies. Although exceptions to these general patterns of behavior may be found, the preponderance of evidence justifies making generalized observations regarding "typical" patterns of behavior.

Depending primarily on the magnitude of the earthquake and the type of fault movement, the maximum surface offset from known earthquake events ranged from less than an inch to at most around 35 feet. Because the average surface fault offset was only 50% of the maximum offset along the fault and since dams would not typically be sited across major faults, the dam engineer (in most cases) would have to incorporate defensive design features that would accommodate only a few inches to at most 5 to 10 feet of differential movement. The site specific value of expected fault offset, however, could be assessed only after a comprehensive geologic study of the dam site and the surrounding region was conducted. In most cases, the majority of fault movement appears to occur along a single rupture plane, with the remainder of the movement being distributed over a wider distorted zone. Displacement on secondary fault features located some distance away from the primary fault trace can, however, be significant, and thus, the total surface displacement generated during an earthquake event may be distributed over a zone up to tens of miles wide.

Field observations of surface faulting indicate that, in general, the bedrock behaves as shown in Figures 3-27, 3-28, and 3-29. Down-warping of the upthrown block during thrust faulting creates tension fissures in the bedrock surface. Subsidence of the normal fault's hanging wall may produce secondary fractures. Secondary bedrock deformations are less likely to occur in strike-slip faulting.

Nevertheless, some amount of movement should be expected to occur on existing planes of weakness in the foundation rock for all types of fault movement.

Field observations of surface faulting and the results of physical model tests of fault rupturing indicate that differential movement across the fault rupture dissipates as the fault rupture propagates to the surface in unconsolidated earth materials. In the 1964 Alaska earthquake, a fault offset roughly 1.5% of the height of the overlying fractured rock medium was locally absorbed and did not propagate to the surface. The character of the soil determined the amount of base movement necessary to propagate the fault rupture to the surface. In a number of model tests, it was found that a base displacement or offset of between 1% and 15% of the height of the overlying sand layer was necessary to propagate the rupture to the surface.

Field observations of surface faulting indicate that, in general, fault ruptures in unconsolidated earth materials behave as shown in Figures 3-30, 3-31 and 3-32. The rupture path depends on the orientation of the fault plane, the types of fault movement, the amount of fault displacement, and the depth and character of the overlying earth deposit. Typically, dip-slip fault surfaces are concave toward the downthrown block. Thrust faults gradually decrease in dip near the surface. Normal faults refract at the soil-bedrock contact and gradually increase in dip as they approach the ground surface. The refraction and the variation of the dip of the fault plane helps produce gravity grabens. Strike-slip faults tend to follow the almost vertical orientation of the underlying bedrock fault.

Field observations of surface faulting and the results of physical model tests of fault rupturing indicate that the great majority of the soil overlying the bedrock adjacent to the fault does not participate in the rupture process. Most of the soil deposit remains relatively undisturbed. Relative motion is primarily concentrated within a fairly narrow zone above the bedrock fault. Once failure

occurs, differential movement is usually localized to a thin, distinct failure plane. Ductile materials, however, may accommodate significant fault movement by warping without actually breaking.

Physical model tests, particularly 1 g small-scale model experiments, produced consistent results in studies of dip-slip fault propagation through dry cohesionless soils. The Lade and Cole (1984) study results, as shown in Figure 3-45(A), summarized the characteristic of the failure patterns that develop in dry alluvium above dip-slip bedrock faults.

The finite element method can be applied to the fault rupture propagation problem provided that the soil's nonlinear stress-dependent stress-strain behavior is properly or at least adequately modeled. Linear elastic-perfectly plastic constitutive laws produced inconsistent results when employed in the finite element method, but nonlinear stress-deformation behavioral models provided significantly better predictions of observed behavior. Although based on continuum mechanics, the finite element method appears to be capable of modeling the development of shear and tension zones during fault rupture propagation with sufficient accuracy as to represent a useful engineering tool.

Field observations, physical model test results, and numerical analyses indicate that both stress characteristics and kinematic constraints combine to control the behavior of the soil above the bedrock fault movement. The Mohr-Coulomb strength failure criterion with the parameters of angle of friction and cohesion has been used successfully to numerically model soil behavior observed during fault rupture propagation. Conversely, the kinematic parameter of the soil's angle of dilation has also been employed successfully to predict the shape of the fault rupture plane in soils overlying a base rock fault offset.

The review of the earthquake fault rupture propagation field studies and the physical and numerical model studies of fault rupture propagation also

identified critical shortcomings in our current level of understanding of this phenomenon. Although the review of fault rupture propagation field studies provided valuable insights, no well-documented case history exists which fully describes how a deep soil deposit (i.e. greater than 50 feet) responds to a base rock fault displacement. Previous studies have focused on surface expressions of faulting, relatively shallow exploratory trenches (i.e. less than 20 feet in depth), and interpretations of surficial geologic evidence.

Furthermore, results from fault rupture propagation model tests of saturated clay or saturated sand under undrained conditions are not available. Likewise, no analyses have been performed to study fault rupture propagation through saturated clay or saturated sand under undrained conditions. Finally, the results from two studies: the Belousov (1961) model tests and the Scott and Schoustra (1974) finite element analyses, differed from the results of the majority of the physical and numerical model studies. In these two studies, the vertical base fault rupture propagated over the upthrown block, whereas the other studies showed that the final failure surface formed over the downthrown block during a vertical bedrock fault offset. It thus appears that there are inconsistencies leaving questions to be answered based on the Belousov (1961) and Scott and Schoustra (1974) study results.

Given the shortcomings in our current state of knowledge regarding the fault rupture propagation phenomenon, the literature review was once again extended to explore two additional closely related topics: anchor pull-out behavior and mining subsidence, in the hope that soil behavior analogous to the modes of behavior involved in fault rupture propagation through soils could be observed. In particular, information describing the behavior of saturated clay subjected to a base deformation under undrained conditions will be sought. Anchor pull-out studies and mining subsidence will be examined in the next chapter.

CHAPTER FOUR:
REVIEW AND EVALUATION OF PREVIOUS STUDIES OF TWO ANALOGIES TO THE FAULT RUPTURE PROPAGATION PHENOMENON

4.1 Introduction

The review of previous studies which modeled the fault rupture propagation phenomenon either physically or numerically brought forth a number of important lessons. Some questions, however, remained unanswered. The soft clay model tests presented by Belousov (1961) and the fault propagation finite element analyses by Scott and Schoustra (1974) found that the primary failure zone formed above the upthrown block adjacent to a vertical bedrock fault offset. Whereas, other physical model and numerical model studies showed that the failure surface formed over the downthrown block during a vertical bedrock fault offset. Fault rupture field studies suggest and kinematic constraints require that the fully developed final failure zone ruptures the ground surface over the downthrown block. It therefore appears that there are inconsistencies leaving questions to be answered based on the Belousov (1961) and Scott and Schoustra (1974) study results.

Furthermore, nearly all of the fault rupture propagation studies performed to date have employed dry cohesionless materials in their research. As discussed previously, the work completed by Lade and Cole (1984) appears to summarize the characteristics of the failure patterns that develop in dry, cohesionless materials overlying dip-slip bedrock faults. Yet, the critical component of an earth dam is its core. The core material retains the reservoir water, and the majority of earth dams possess cores of saturated compacted clayey materials. Only the Belousov (1961) study could be used to examine the development of fault ruptures in clay above dip-slip fault movements, and the results of his model tests differed from the

results of the sandbox model tests as described in the previous paragraph. Moreover, it was not clear if the clay material used in the Belousov (1961) experiments was fully saturated.

Given the shortcomings in our current level of understanding of the fault rupture propagation phenomenon, it might be useful to identify well-documented problems which display behavior analogous to the fault rupture propagation problem. Chapter Four presents a review and evaluation of two closely related problems: anchor pull-out behavior and mining subsidence, in the hope that soil rupture behavior closely analogous to the modes of behavior involved in fault rupture propagation through soils might be observed. The principal lessons to be learned from the anchor pull-out problem and the mining subsidence problem with respect to fault rupture propagation through soils are discussed in the summary section.

4.2 Anchor Pull-Out Studies

4.2.1 The Anchor Pull-Out/Fault Rupture Propagation Analogy:

The anchor pull-out problem proved to be a good analogy to the fault rupture propagation problem. Considerable effort has been devoted toward improving the profession's understanding of the anchor pull-out problem. In addition, the withdrawal of a horizontal anchor plate embedded in a soil deposit was thought to be analogous to the uplift of the upthrown bedrock block adjacent to a vertical dip-slip fault. The primary emphasis in anchor pull-out studies has been to determine the pull-out resistance of the anchor. This review, however, would focus on the pattern of shear fractures that develop while the anchor is being pulled out of the ground.

The principal methods of determining an anchor's pull-out resistance are shown in Figure 4-1. Each method assumes different failure planes through the

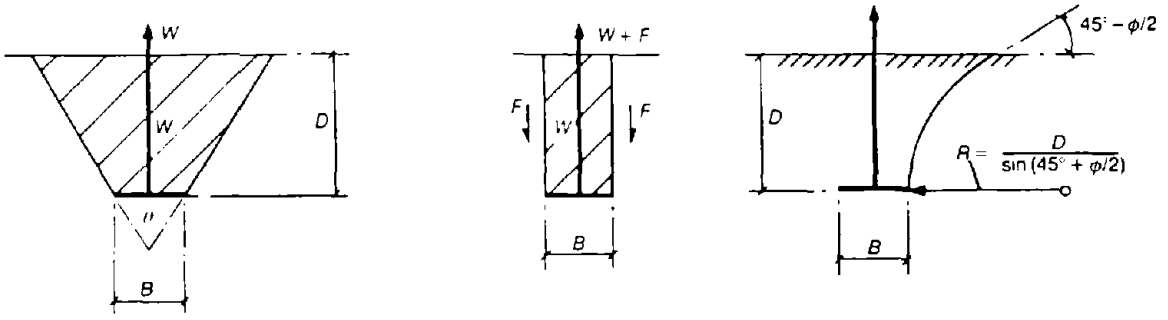

(A) Cone Method (B) Cylinder Method (C) Balla Method

Figure 4-1: METHODS USED TO ESTIMATE ANCHOR PULL-OUT RESISTANCE (after Sutherland, 1988)

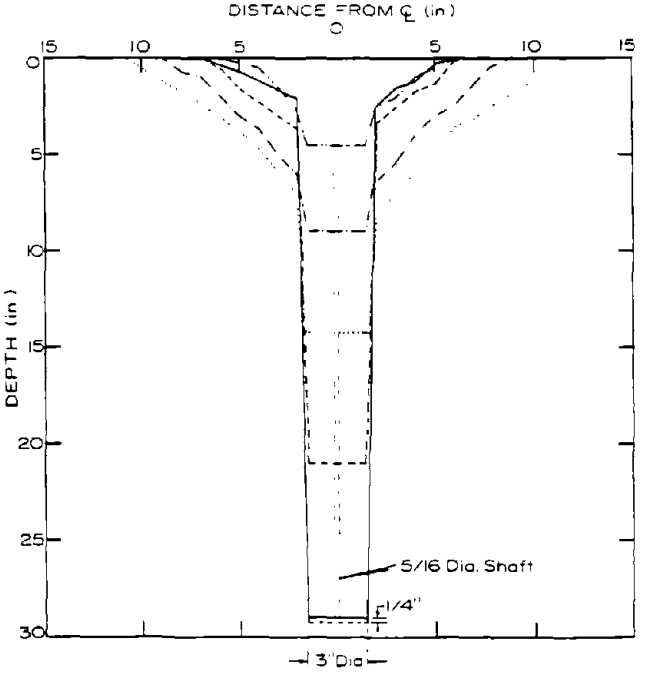

Figure 4-2: OBSERVED SHAPES OF SLIP SURFACES CAUSED BY WITHDRAWAL OF CIRCULAR PLATES FROM STIFF SILTY CLAY (after Vesic, 1971)

overlying soil, and hence, each method produces slightly different estimates of the anchor's pull-out resistance. All of the methods show the final failure zone rupturing the ground surface either vertically above or to the outside of the edge of the uplifted anchor plate. The failure surfaces delineated in each of these methods were simplifications of slip-lines observed in model tests conducted in the laboratory and in prototype anchor tests performed in the field. Vesic (1971) commented,

> Observations in small-scale model tests with anchor plates and anchor piles at Duke University proved that the shape shown in [Figure 4-1(c)] occurs only in the case of relatively shallow anchors in dense sand or stiff silty clay. For shallow anchors in loose sand or soft clay, the slip surface, though not clearly established, is closer to being a vertical cylinder around the perimeter of the anchor. Note that very deep anchors do not fail in general shear such as that shown in [Figure 4-1(c)], regardless of the relative density of the soil. Experiments indicate that they can be moved vertically for considerable distances by producing a failure pattern similar to punching shear failure in deep foundations.

The observed shapes of slip surfaces shown in Figure 4-2, as well as similar conclusions made by Meyerhoff (1973), confirmed Vesic's comments.

One of the difficulties to utilizing the anchor pull-out/fault rupture propagation analogy was the difference between the behavior of shallow and deep anchors. The anchor's critical normalized depth, $(D/B)_{CRIT}$, was defined as the ratio of the depth of the anchor to the width of the anchor plate that distinguished when an anchor behaved as a shallow or deep anchor. The critical normalized depth for most anchors ranged from around 2 in loose materials to more than 10 in very dense soil deposits. Since the width of the upthrown block in the fault rupture propagation problem is relatively large (in essence, close to infinite), the typical shallow anchor failure pattern might then be expected to "best" represent the behavior of soil overlying a vertical dip-slip bedrock fault. Yet, does the soil

directly above the vertical bedrock fault "know" that the uplifted block is theoretically close to infinite when the bedrock fault displaces some small amount? Perhaps, the critical normalized depth parameter used to describe anchor pull-out behavior does not apply to the fault rupture propagation problem. Instead, in this case, the conditions of shallow or deep embedment might be better defined by the conditions of low or high confining stresses, or better yet, dilatant soil behavior or contractive soil behavior. Where soils behave contractively, failure patterns might form like those observed in deep anchor pull-out studies. Where soils behave dilatantly, failure patterns might form like those observed in shallow anchor pull-out studies.

Two other differences between the anchor pull-out problem and the fault rupture propagation problem must be considered. If soil is allowed to fall into or to be pulled into the void created when the anchor plate displaces upward, the boundary conditions for these two problems become significantly different. Thus, results from anchor pull-out tests which allow such soil movement will be ignored in this study. Finally, if the soil is very compressible and the anchor plate width is relatively narrow, failure patterns that develop around one edge of the anchor plate might interact with the failure patterns that develop around the other edge of the anchor plate. Again, the boundary conditions for the two problems (anchor pull-out and fault rupture propagation) become excessively different. Thus, it would be difficult to use results from anchor pull-out tests under these conditions to illustrate how soil responds to a bedrock fault rupture.

In Section 4.2 the results of physical model tests and numerical analyses of anchor pull-out are presented in the hope that information from these studies will improve our understanding of the fault rupture propagation phenomenon. Lessons to be learned from the anchor pull-out studies regarding the fault rupture propagation problem are discussed in the last part of this section.

4.2.2 Physical Model Studies:

(a) Anchor Pull-Out in Sand:

Much of the early work in studying the anchor pull-out problem concentrated on understanding how frictional materials responded to anchors under various applied loadings. Anchors were primarily embedded in frictional materials to provide adequate support at relatively small deformations. Thus, the majority of model tests have been performed to date using dry, cohesionless materials. The results from a number of these physical model tests are presented to compare with the results from the physical fault rupture model tests. It is hoped that this review will validate the usefulness of the anchor pull-out/fault rupture analogy and will provide additional insights into the fault rupture propagation problem.

The results of model tests performed by Balla (1961), which became the experimental basis for the Balla method for calculating anchor pull-out capacities, are shown in Figure 4-3. The final rupture surface, which was easily discernable, curved away from the centerline of the withdrawn anchor. The soil above the inside edge of the anchor appeared to participate in the failure also. The right photograph of Figure 4-3 shows this clearly. In the left photograph, the final rupture surface appeared to actually move up over the anchor plate before deflecting away from the anchor centerline. Khadilkar et al. (1971) agreed,

> With increase in pull-out the soil lying just above the enlarged base gets compressed. A further increase in load results in heaving of the soil at top. Additional pull-out load overcomes the shear strength of the soil and finally cracks are observed to extend through the soil mass and ultimate rupture is established.

Work by Dickin (1988) illustrates this point further. As shown in Figure 4-4, multiple failure surfaces develop above and to the outside of the uplifted anchor

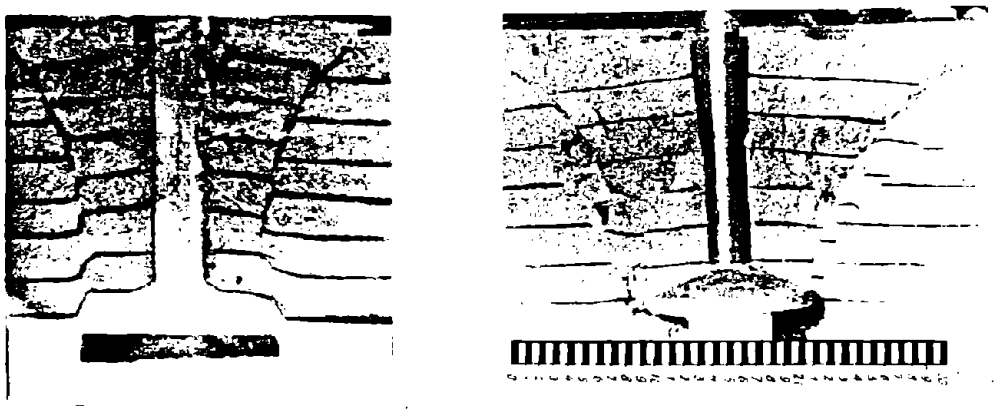

Figure 4-3: SHAPE OF THE BREAKING OUT EARTH MASS (after Balla, 1961)

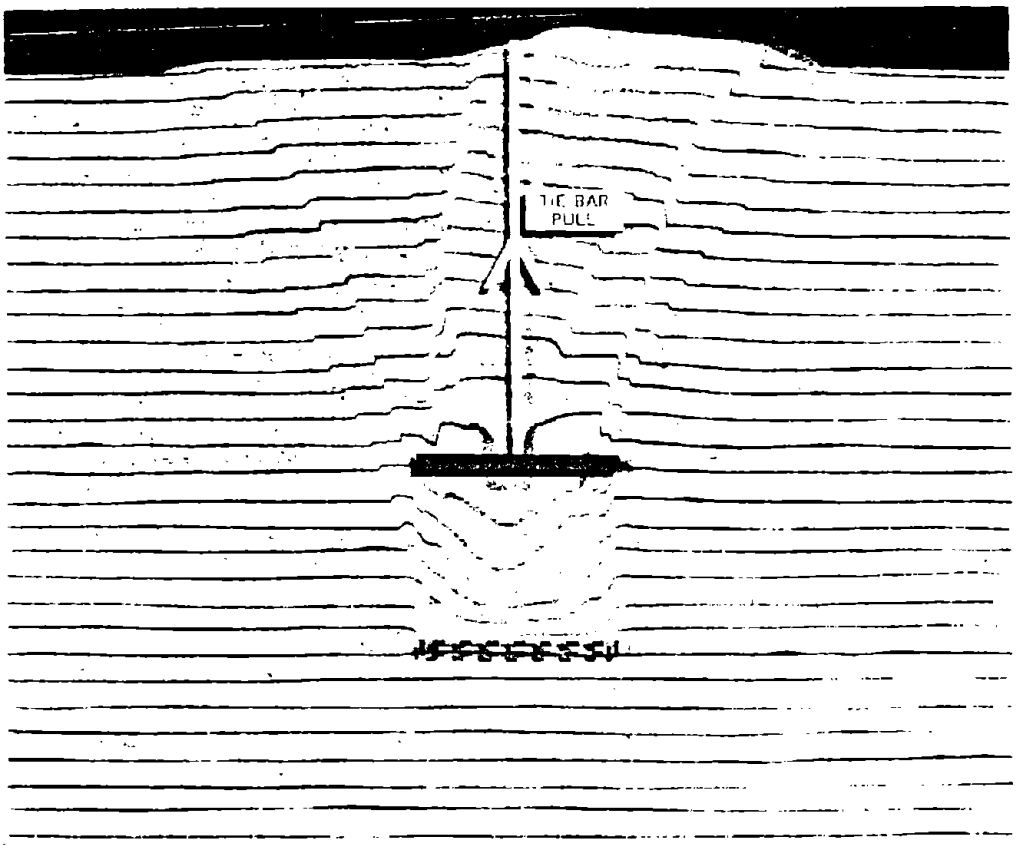

Figure 4-4: FAILURE MECHANISM AROUND 75 MM ANCHOR AT D/B = 3 IN DENSE SAND (after Dickin, 1988)

plate. On both sides of the anchor, some failure planes developed over the anchor for a short distance while the final shear zones moved out into the sand away from the anchor centerline. Additional photographs of anchor pull-out tests in sand presented by Meyerhof and Adams (1968) confirmed that the slip surface was more cylindrical in loose sand than it was in dense sand. In dense sand, the slip surfaces immediately began to deflect away from the center of the anchor plate. Finally, precise measurements by Vardonlakis et al. (1981) indicated that a trap-door uplift movement of roughly 10% of the height of the dry, dense sand was necessary to cause the failure surface to propagate to the ground surface. The trap-door uplift model tests displayed failure patterns similar to those described in the fault rupture model tests and in the anchor pull-out model tests.

(b) Anchor Pull-Out in Clay:

A number of publications authored by Sutherland and Davie have addressed the problem of understanding the uplift resistance of soils (Davie, 1973; Davie and Sutherland, 1977; Davie and Sutherland, 1978; Sutherland, 1988). In fact, in the twenty-eighth Rankine Lecture, Sutherland (1988) presented a comprehensive review of this problem. The doctoral thesis by Davie (1973), however, was the basis for the majority of Sutherland and Davie's original work in this area. In this document, detailed descriptions and results are provided for a series of 65 model anchor pull-out tests using saturated clay as the testing material. Their testing program brought forth a number of important points.

Reasonable modeling of the prototype anchor and soil required that clays of low shear strength be employed in the 1 g small-scale model tests. Davie and Sutherland (1977) found that the ratio of soil shear strength to the product of the soil's unit weight and width or depth of the anchor ($C/\gamma B$ or $C/\gamma D$) should usually be at least approximately equivalent in the model and in the prototype. Hence, 1 g

small-scale model tests required the use of weak clay materials. Sutherland (1988) warned that if the prototype clay was very soft, it could only be modeled with either large models or with soils of negligible shear strength. Large models, however, are not usually feasible and "the failure characteristics of extremely soft clays can be quite different from those of stiffer clays because of their viscous nature." It was considered important that model tests employed to predict failure loads should adequately model the prototype soil's failure characteristics.

In the 1 g small-scale model tests performed by Sutherland and Davie, they judged that these extreme conditions did not exist, and hence, the prototype soil could be modeled with low shear strength soils believed to possess similar failure characteristics. Two clays were prepared in the laboratory. A mixture of bentonite and glycerine (referred to as glyben) possessed shear strengths of on the order of 100 to 400 psf. A mixture of a natural occurring silty clay and a soft clay (referred to as silty clay) possessed shear strengths of on the order of 185 to 225 psf. The majority of tests were actually push-out tests modeling shaft-raising in tunnel construction. Hence, the soil above the horizontal plate was not disturbed by an anchor rod and suction under the uplifted plate was typically not allowed. These conditions actually improved the similarity between these model tests and the fault rupture propagation model tests. The width of the model anchors ranged from 1 to 8 inches. The anchors were embedded 1.5 to 12 inches into the soil. "Nonlayered" samples were prepared by kneading together small balls of material to eliminate preferred lines of weakness. "Layered" samples were prepared by manually kneading the material in layers. Volume change tests on the clay materials estimated Poisson's ratio at 0.48, which indicated that the clay was very close to full saturation.

Representative results from three of the anchor plate push-out tests are shown in Figure 4-5. These photographs illustrate the different modes of crack and

(A) Shallow Anchor Case, D/B = 1.5

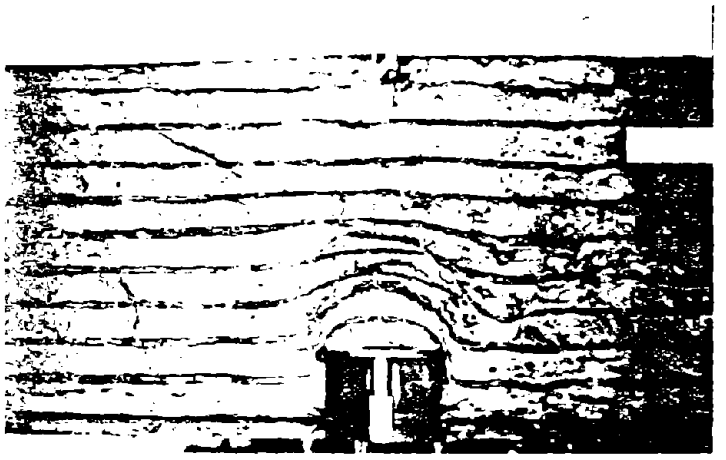

(B) Intermediate Anchor Case, D/B = 3.0

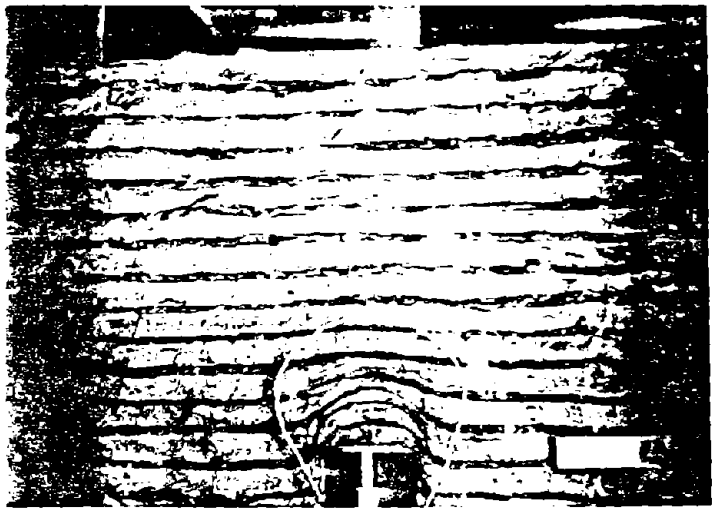

(C) Deep Anchor Case, D/B = 4.5

Figure 4-5: DEFORMATION AND CRACKING AT ULTIMATE UPLIFT RESISTANCE OF HORIZONTAL PLATE IN SOFT CLAY (after Sutherland, 1988)

failure patterns for anchors at various depth to width ratios (D/B). In the shallow anchor case (D/B = 1.5), numerous tension cracks were observed when the failure condition was achieved; whereas, in the deep anchor case (D/B = 4.5), a plastic zone above the uplifted plate was apparent when the failure load was obtained. Upon closer inspection of these test results, however, a number of similarities could be found. Even in the shallow anchor case, a zone of highly stressed clay material appeared to form above the inside edge of the anchor plate. In fact, this shear zone appeared to move slightly over the uplifted plate until tension cracks formed and changed the predominant failure mechanism. This initial shear zone and its tendency to move toward the center of the anchor plate could be seen more clearly in the intermediate and deep anchor cases. In the deep anchor case, as well as in intermediate and shallow anchor cases, a zone of extension or reduced stress formed to the outside of the edge of the uplifted plate. Tension cracks clearly defined this zone in the intermediate and shallow cases. The glyben did not seem to develop distinct shear failure planes. Instead, a wider zone of distorted clay accommodated the anchor plate movement.

The Sutherland and Davie studies focused on understanding the load-deformation behavior of uplifted horizontal plates in soft clay, and in particular, the ultimate resistance of the anchor. The focus of this writer's research, however, is understanding the failure patterns that develop in soil as a result of base deformation. The model test data provided by Davie (1973) provided an excellent opportunity to check one of this writer's hypotheses. Unconfined triaxial compression test data on each material was provided. The glyben material reached the maximum deviatoric stress at approximately 20% axial strain. The silty clay failed at approximately 28% axial strain. If the ratio of the plate displacement at failure to the depth of the anchor (d_f/D) was calculated for each of the 58 applicable anchor push-out model tests (tests which allowed suction to

develop beneath the anchor plate were not included), an interesting point could be made. In the 47 plate push-out tests in glyben, the base displacement required to cause failure in the overlying soil averaged around 23% of the depth of anchor embedment ($d_f/D = 0.23$). On the other hand, in the 11 plate push-out tests in the silty clay material, the base displacement required to produce failure averaged around 35% of the depth of anchor embedment ($d_f/D = 0.35$). The axial strain at failure in the silty clay unconfined triaxial compression tests was roughly 40% higher than that of the glyben, and the base deformation (normalized as a percentage of the depth of embedment) required to produce failure in the silty clay was roughly 50% higher than that of the glyben. It appeared that the amount of base deformation necessary to produce the failure condition in the overlying soil was roughly proportional to the failure strain of the overlying soil. Therefore, it would appear that the rate of growth of the shear rupture zone above a bedrock fault offset might be primarily a function of the failure strain of the overlying earth material.

A number of other works in this area were reviewed, but the details of the test conditions and the test results were either not given, or when provided, the test conditions described did not match the test conditions necessary to allow for the application of the anchor pull-out/fault rupture analogy (Meyerhof and Adams, 1968; Ali, 1968; Bhatnager, 1969; Vesic, 1971; Meyerhof, 1973; Rowe and Davis, 1982a). The Sutherland and Davie work, however, did provide useful insights.

4.2.3 Numerical Model Studies:

(a) Anchor Pull-Out in Sand:

A number of studies have employed the finite element method to analyze the problem of anchor pull-out in cohesionless materials and the results from four studies are discussed herein. Rowe and Davis (1982b) used an elasto-plastic

constitutive model for soil which employed a Mohr-Coulomb failure criterion and either an associated or nonassociated flow rule. The authors claimed that results from their finite element analyses agreed reasonably well with the results from their model testing program. Their study emphasized the importance of the sand's angle of dilation parameter. Velocity fields at collapse loads indicated that increasing the value of the angle of dilation parameter caused the failure surface to become less steep.

Ito and Kitahara (1982) successfully applied the finite element method to this problem by using a nonlinear, incremental elastic, stress-dependent soil constitutive law which accurately modeled the sandy soil's stress-strain behavior. The predicted ultimate pull-out load was around 15% higher than the value estimated in large-scale model tests, and at working loads, the load-deformation behavior exhibited in the FEM analyses and in the model tests agreed within 5%. Furthermore, the authors noted, ". . . the failure zone obtained by numerical analysis has a shape likely to envelop the final slip surface observed by the experiment."

On the other hand, in the 1988 Rankine Lecture, Sutherland admitted that,

> Attempts by the Glasgow research students to date have not been particularly successful when the finite element approach has been applied to the uplift resistance problem, and especially so when the predictions were compared with the field tests at Sizewell in the shaft raising operations . . . As far as the finite element analyses were concerned, the predictions for clay were reasonable, but conservative compared with model tests and other methods of analysis. The finite element predictions for cohesionless soils, however, were most unsatisfactory. They gave highly conservative results for other than loose sands and could not have formed the basis for the successful shaft raising design at Sizewell as a design for failure case.

As Scott (1987) pointed out in the 1987 Rankine Lecture, which was later confirmed by Sutherland (1988) in the 1988 Rankine Lecture, it was difficult to develop an accurate soil constitutive model for dense sands. Most current practical

FEM soil constitutive models do not model dilative volumetric strain behavior well.

Finally, Tagaya et al. (1983) performed a relatively exhaustive FEM soil parameter sensitivity study regarding anchor pull-out behavior in dry, cohesionless materials. In his analyses of the anchor pull-out problem, Tagaya and his colleagues investigated the effects of changing various factors on the results calculated by the finite element method. The authors employed the nonlinear elasto-plastic soil constitutive model developed by Lade (1972). The FEM analyses utilized 4-node isoparametric elements and an incremental load solution technique. The FEM results were validated against results from centrifuge model tests. This study provided a number of important lessons.

The predicted pull-out load decreased as more elements were employed in the finite element analyses. A small number of elements produced a larger failure zone and hence, required more energy to develop failure. To better model the actual narrow failure zones that developed in the physical model tests, a refined mesh (e.g. elements 1/6 to 1/4 of the anchor width) was employed along anticipated failure planes to minimize energy dissipation. As expected, a solution technique which employed small load increments modeled observed soil behavior more realistically. Tagaya et al. (1983) found that up to two-thirds of the failure load, larger load increments could be used. Then, gradually decreasing load increments should be used as the failure load was approached. The left and right vertical boundaries of the finite element mesh should extend to at least three times the anchor width away from the edge of the anchor. Nodes along this boundary should be fixed in the horizontal direction, but should be free to displace in the vertical direction.

The soil parameter sensitivity study identified four characteristics of the cohesionless soil that should be modeled adequately to successfully employ the

FEM in the analysis of the anchor pull-out problem. The initial state of stress as described by the parameter K_O, the coefficient of lateral earth pressure at rest, played an integral role. The lower the K_O value, the closer the initial soil condition was to failure, and hence, the predicted pull-out load was lower. The volume-change parameters were also important. Increasing the soil's tendency to dilate, increased the predicted pull-out load. Of course, increasing the stiffness of the soil produced a more brittle load-deformation behavior, and increasing the strength of the soil increased the pull-out load capacity of the anchor. In review, however, the results of the FEM analyses of the anchor pull-out problem in cohesionless soils were typically most sensitive to variations in the parameter K_O and to variations in the volume change parameters (e.g. Poisson's ratio) .

(b) Anchor Pull-Out in Clay:

As was previously pointed out by Sutherland (1988), whereas, it has been difficult to successfully use the finite element method to analyze anchor pull-out in cohesionless materials, FEM predictions of anchor pull-out resistance in cohesive materials have been reasonably correct. Thus, an adequate finite element analysis provides sufficient accuracy to be used as an engineering tool in the study of anchor pull-out behavior in cohesive soils.

In his doctoral research program, Davie (1973) employed the FEM to analyze the anchor pull-out model tests already discussed in Section 4.2.2(b). In this study, he employed an axi-symmetric linear elastic-perfectly plastic soil constitutive model with a Von Mises yield criterion. The FEM analyses were performed with 180 to 200 4-node isoparametric elements and with 15 to 20 displacement increments. The value of the key soil parameters were: modulus of elasticity = 15,000 psf; Poisson's ratio = 0.495; yield stress = 375 psf; coefficient of

lateral earth pressure at rest = 1.0; and the unit weight = 0 pcf. Tension was allowed to develop in the soil mass.

Representative results from Davie's FEM analyses are shown in Figure 4-6. Note that the shaded zones denote regions of tensile stresses. Even in the deep anchor cases, these tension zones were extensive. It appeared that employing elements which could sustain tensile stresses reduced the reliability of the FEM results. In the shallow anchor case shown, the failure zone propagated up vertically from the edge of the anchor plate. In the intermediate and deep cases, the failure zone initially propagated up vertically, but soon began to bend over the uplifted anchor plate. As displacement of the anchor plate continued, the yield zone again grew vertically until the failed zone reached the surface at a point just outside of the edge of the anchor. The final slip-line in all three cases was cylindrical. The physical model tests indicated, however, that for the shallow anchor case the final slip-line should bend over away from the anchor near the ground surface. The predicted ultimate pull-out loads, however, were considered to be reasonable.

4.2.4 Lessons to be Learned from Anchor Pull-Out Studies Regarding Fault Rupture Propagation:

The results from the anchor pull-out model tests agreed quite closely with the results from the fault rupture propagation model tests discussed in Section 3.3.2. The final slip-lines which developed in each group of model tests were similar. They formed at the edge of the uplifted anchor plate or base section and propagated up toward the surface vertically, although near the surface the slip-line bent over away from the uplifted soil. The anchor pull-out model tests, however, clearly showed a zone of highly compressed soil above and to the inside of the edge of the anchor plate. In sand, sometimes a distinct failure plane formed in this

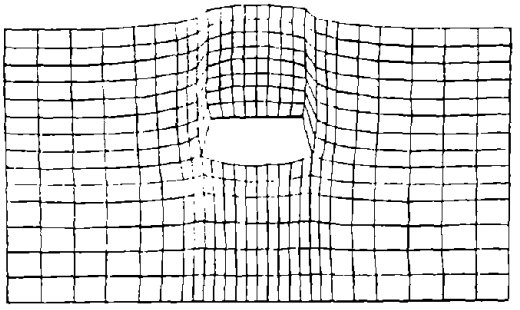

(A) Deformed Mesh (Displacements x 8)

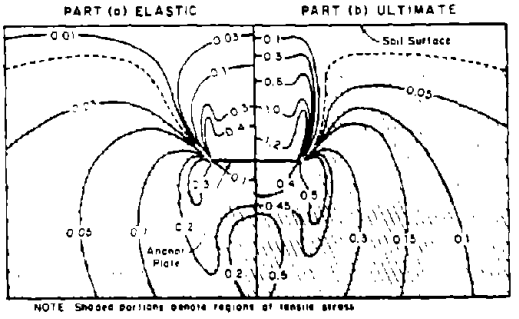

(B) Distribution of Vertical Normal Stress

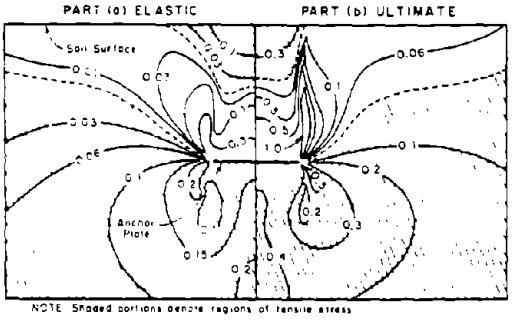

(C) Distribution of Radial Normal Stress

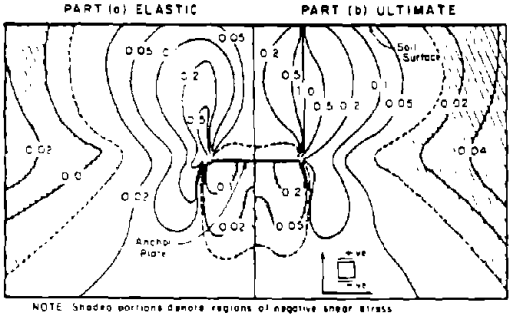

(D) Distribution of Shear Stress

Figure 4-6: RESULTS FROM LINEAR ELASTIC-PERFECTLY PLASTIC FINITE ELEMENT ANALYSES WHERE THE ANCHOR DEPTH TO WIDTH RATIO EQUALED 1.5 (after Davie, 1973)

compressed region. In clay, a plastic zone of highly stressed soil typically developed above the anchor plate. This appeared to confirm what had been surmised earlier in Section 3.3 about the behavior of soil overlying a displaced base section. As shown in Figure 4-7, when the uplifted block initially displaced vertically, an "inverted footing" type of failure appeared to begin to develop. A zone of highly stressed or failed soil formed vertically above the edge of the uplifted block and tended to move up and over the uplifted block. With further base displacement, the failure zone once again propagated more in a vertical direction. This initiated the final phase or the "anchor pull-out" type of failure. To comply with kinematic constraints, the final slip-line must allow the uplifted block to be removed out of the soil deposit. Thus, a vertical failure zone or a failure zone which bends over the downthrown block developed. Near the ground surface there was a tendency for all the final failure planes to bend over the downthrown block.

This two-phase development of the shear failure zone in the soil overlying a displaced vertical thrust fault possibly explained the deviations observed in the Belousov (1961) model tests in soft clay and the Scott and Schoustra (1974) finite element analyses of fault propagation in an alluvial valley. Both of these models appeared to only show the first phase of failure or the "inverted footing" type of failure. Anchor pull-out model tests and FEM analyses often displayed this type of failure initially. If the Belousov (1961) model test would have continued with additional uplift of the base section, the final phase of failure or the "anchor pull-out" type of failure would have occurred. Kinematic constraints require this to be true. Likewise, the FEM was not inherently deficient because the Scott and Schoustra (1974) analyses predicted only the first phase of failure. Instead, a number of FEM studies of fault rupture propagation and anchor pull-out have shown that the FEM could reasonably predict the final phase of failure or the

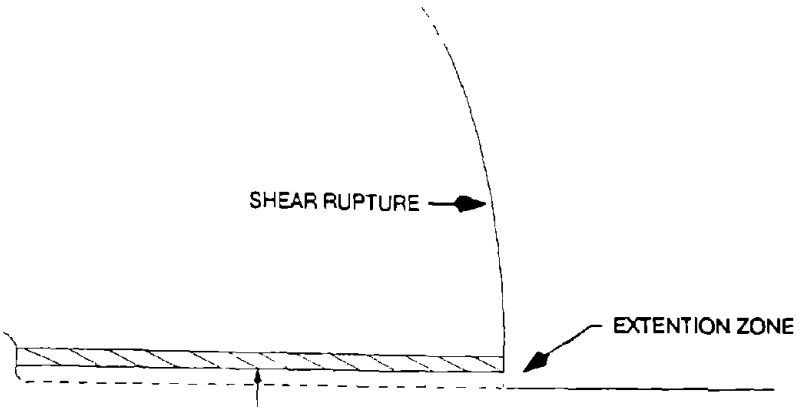

(A) "Inverted Footing" Type of Failure

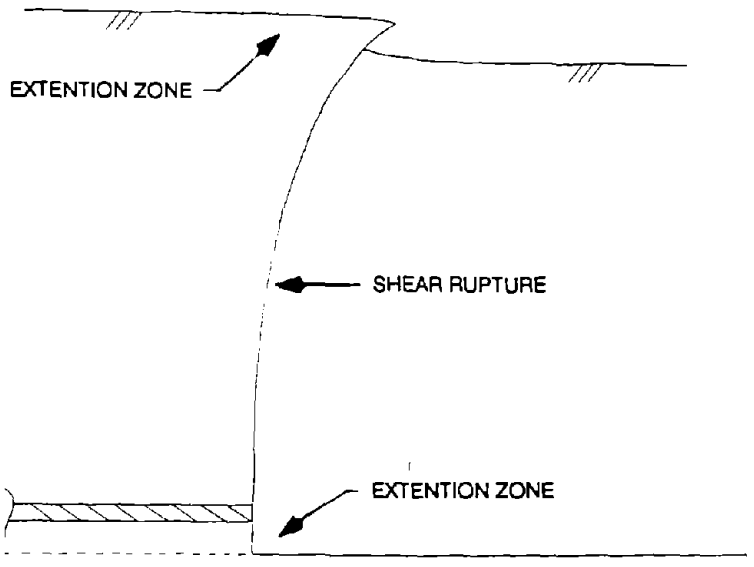

(B) "Anchor Pull-Out" Type of Failure

Figure 4-7: DEVELOPMENT OF FAILURE ZONES IN THE SOIL OVERLYING A VERTICAL THRUST FAULT MOVEMENT

"anchor pull-out" type of failure. The successful FEM studies employed soil constitutive laws which adequately modeled the nonlinear stress-strain behavior of the soil overlying the anchor. In contrast, linear elastic-perfectly plastic soil models appeared to be deficient. When various nonlinear soil models were employed, however, the finite element results were much improved. Greater sophistication in soil constitutive models was required when modeling medium to dense sand which tended to dilate when sheared. Simpler nonlinear soil constitutive laws could satisfactorily model non-dilatant materials.

Besides the shear zones which develop in soils because of base deformation, the physical model tests and numerical model analyses indicated that tension zones could develop adjacent to the edge of the uplifted anchor plate and at the ground surface over the uplifted anchor. These possible tension zones or extension zones are shown also in Figure 4-7. The possibility of tension zones forming in the core of a dam which crosses a dip-slip fault would be a source of grave concern to the dam engineer. It is not known if tension would actually develop in deep soil deposits which overlie bedrock faults. The physical model tests and FEM analyses were performed on soils under relatively low confining pressures. These results, however, do clearly indicate that zones of local extension would probably develop. Even if these extension zones did not become tension zones, the minor principal stress might drop to a value low enough to permit hydraulic fracturing. The development of regions of stress reduction in soils that overlie bedrock faults requires further study.

Sutherland (1988) recognized the difficulties in modeling soft clay prototype materials. Large-scale models or models employing extremely soft, weak clays which might behave differently than the prototype clays would be necessary to satisfy scaling laws. Likewise, it should be recognized that large prototype structures such as earth dams would require large-scale models which might not be

economically feasible or models with soil materials with negligible shear strength and possibly different failure characteristics. It is important to recognize the potential difficulties in physical model testing and to ensure that modeling inaccuracies are for the most part satisfactorily reduced.

One of the most critical lessons to be learned in the review and evaluation of anchor pull-out studies was the demonstration of the importance of the soil's failure strain in determining the rate of fault rupture propagation. Manipulation of the data presented by Davie (1973) appeared to indicate that the magnitude of base movement necessary to cause the shear rupture zones to propagate up to the ground surface of the soil deposit was primarily dependent on the failure strain of the soil. Furthermore, the axial strain at failure (i.e. at the maximum deviatoric load) in a standard unconfined triaxial compression test could be used to describe the failure strain of the soil in the fault rupture propagation problem. The Davie (1973) test data implied that of all the soil parameters used to describe the soil, the most critical parameter may well be the failure strain of the soil.

The FEM studies brought forth a number of salient points. The finite element method can be successfully applied to this boundary deformation problem. Although limitations exist, FEM analyses can provide valuable insights into the anchor pull-out problem, as well as the fault rupture propagation problem. Localization of shear failure in narrow zones is difficult to achieve as the failed zone usually widens as it propagates toward the ground surface. Yet, at least the zone within which the distinct failure planes develop is predicted reasonably well by adequate FEM analyses. An adequate FEM analysis appears to require employment of a nonlinear stress-strain soil model. Linear elastic or linear elastic-perfectly plastic soil models have not consistently produced acceptable results. Furthermore, modeling the dilatant behavior of dense, cohesionless materials is

important; whereas, nondilatant materials have been modeled quite well with simpler soil constitutive laws.

The anchor pull-out FEM results are somewhat sensitive to some of the soil parameters. The coefficient of lateral earth pressure at rest appears to be an important soil parameter. Of course, the soil parameters which most significantly describe the soil's stress-strain behavior and volume-change behavior influence the development of failure in the soil. As one might expect, it is important to model the soil as a "no-tension" material. All of the numerical models reviewed utilized an incremental load solution technique. Once the soil approaches the failure condition, gradually decreasing load or displacement increments should be imposed to maintain accuracy. Finally, smaller elements should be concentrated in the expected zone of shear failure to minimize the overestimation of the width of the actual shear failure zones.

4.3 Mining Subsidence Studies

Numerous well-documented case histories of mining subsidence exist. Because of the long history of mining in Europe, often under towns, many detailed studies of the movement of the ground surface as a result of ore or coal extraction can be found in the literature. In fact, a number of mining subsidence theories based on the ground movements observed in the field have been developed to predict the shape and the magnitude of the subsidence bowl created at the ground surface. These experience-based theories predict the general pattern of ground deformation reasonably well. Since the dropping of the roof of a mined seam produces a base deformation in the overlying bedrock which might be analogous to the base deformation produced by a nearly vertical normal fault movement, studies of mining subsidence were examined to determine their usefulness as an analogy to the earthquake fault rupture propagation phenomenon.

The pattern of ground subsidence resulting from underground mining operations is summarized in Figure 4-8. In this diagram, a typical subsidence profile and strain profile above a mined out seam is shown. Critical mining subsidence parameters are defined. At first glance, it might appear that well-documented case histories of mining subsidence could be used to illustrate how ground above a bedrock fault might look after fault movement. Figure 4-9 illustrates why this is not the case. The mechanics of mining subsidence differ greatly from the mechanics of fault rupture propagation through overlying soils. For instance, in mining subsidence case histories, the extracted seams were often hundreds to thousands of feet below the ground surface. Hence, the principles of rock mechanics, not soil mechanics, often governed. As Figure 4-9 indicates, the height of the void created by the excavated seam was distributed among a number of different movements in various rock beds. Stress reduction uplifted the mine floor. Caving and bulking of roof materials typically filled the majority of the underground space created by mineral extraction. Bending of overlying rock beds and slippage between these beds accommodated some of the roof deformation. Shear fracturing on distinct failure planes did occur, but in general, the other movements accommodated most of the total vertical movement. By the time the rock beds near the ground surface displaced, much of the total movement had already been absorbed through bulking of fractured rock materials and rock bed separation. Normally, these rock beds near the ground surface deformed in the gentle shape of the subsidence bowl shown in Figure 4-8. Thus, the overlying soil "saw" nothing resembling a fault offset on a distinct bedrock fault plane. Additionally, no well-documented case histories of mining subsidence could be found in this review of literature where the bedrock was overlain by at least fifty or more feet of soil.

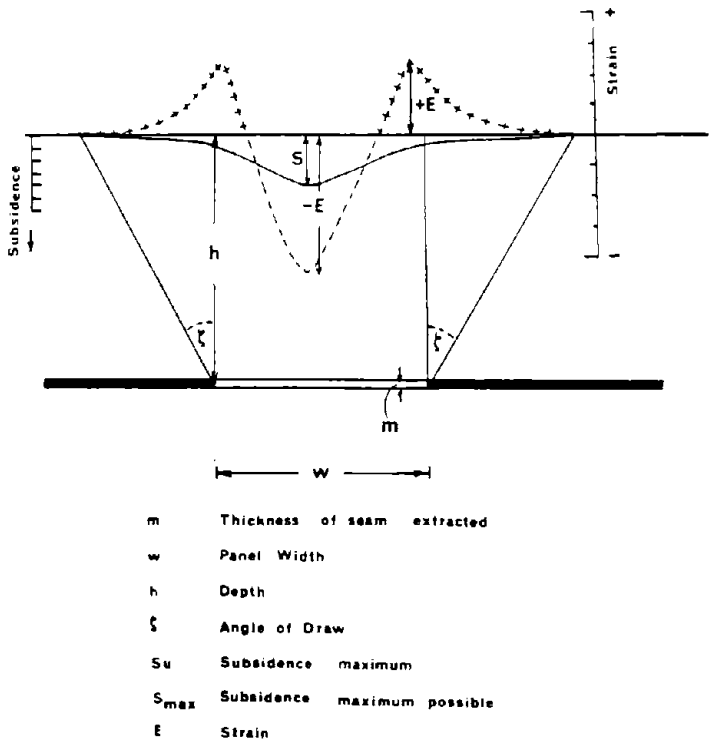

Figure 4-8: STRAIN PROFILE SUPERIMPOSED ON TYPICAL MINING SUBSIDENCE PROFILE (after Geddes, 1977)

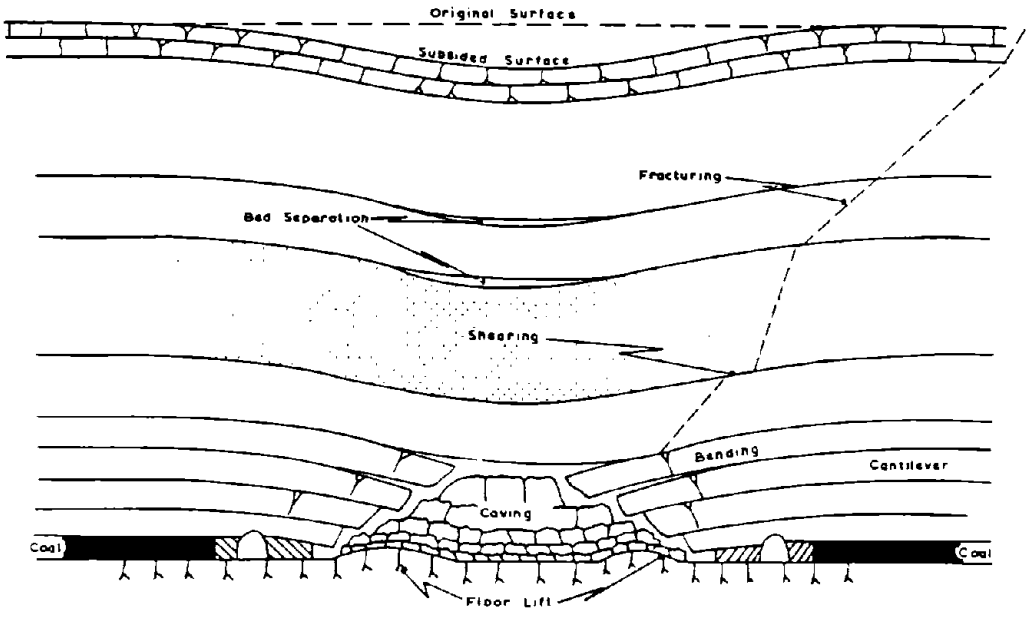

Figure 4-9: STRATA MOVEMENTS RESULTING FROM UNDERGROUND MINING (after Shadbolt, 1977)

An exception to the development of a gentle subsidence bowl was fault-controlled subsidence (Lee, 1966; Bell, 1975; Kratzsch, 1983; Dunrud, 1984). Faults provided existing planes of weakness which could localize vertical subsidence movements. Hence, in a small number of documented cases, sharp offsets as much as a few feet ruptured the ground surface on distinct failure planes through the soil. Dunrud (1984) noted that extraction in a 2300 foot deep room-and-pillar mine near Sunnyside, Utah created a graben in the overburden as much as 150 feet wide and 8 feet deep adjacent to an existing bedrock fault plane. The ground ruptured as much as 1 foot along a 500 foot long section of a pre-existing bedrock fault in another case where mine operations resumed approximately 900 feet below the ground surface. Yet, in the cases of fault-controlled subsidence where the bedrock displaced across a distinct failure plane, the overlying soil deposit was either very shallow or its depth and character were not described in detail.

Therefore, this reasonably comprehensive review of mining subsidence case histories did not uncover one well-documented field case history which could be used to illustrate fault rupture propagation through soil or to validate any proposed numerical or physical model of fault rupture propagation through soil. A few lessons, however, could be learned. First, of course, that the mechanics of mining subsidence and earthquake fault rupture differ significantly. Second, base rock movements produce a gentle bowl shaped subsidence profile with local tension and compression zones at the ground surface. Base offsets could occur without rupturing the ground surface. Finally, it was clearly shown that the bulking of originally dense earth materials could fill voids created by mining extraction. The mining subsidence case histories thus appeared to confirm the view by Leps (1989) that a dense cobble zone above a bedrock fault could bulk and accommodate some of the differential movement across the fault during an earthquake.

4.4 Summary and Findings

In Chapter Four, previous studies of anchor pull-out behavior in both cohesionless soils and cohesive soils were reviewed and evaluated. The anchor pull-out problem provided critical insights into the fault rupture propagation phenomenon. Similarly, works in the field of mining subsidence were reviewed in the hope that soil behavior analogous to how a soil responds to an earthquake base rock fault movement might be observed. The mining subsidence problem, however, proved to be a tenuous analogy to the phenomenon of fault rupture propagation through overlying soils. The studies of anchor pull-out and mining subsidence did bring forth a number of salient observations.

The anchor pull-out analogy proved to be extremely useful. 1 g small-scale model testing of anchors in soft saturated clay indicates that the amount of anchor plate displacement necessary to produce failure in the soil above the anchor is principally proportional to the soil's failure strain. Moreover, the soil's axial strain at failure (e.g. maximum deviatoric stress) in an unconfined triaxial compression test appears to define the soil's failure strain during soil rupturing reasonably well.

The results of anchor pull-out model tests indicate that both stress characteristics and kinematic constraints combine to control the behavior of the soil overlying the bedrock fault movement. A highly stressed region initially forms above the edge of the uplifted base section and stress reduction occurs to the side of the edge of the uplifted base section during the anchor plate movement. Although failure may occur in these zones of stress increase and stress reduction, the final failure surface must be kinematically admissible, and hence, it must bend over the downthrown block. These two phases of the development of the shear failure zone in the soil overlying a displaced vertical thrust fault (i.e. the "inverted

footing" type of failure and the "anchor pull-out" type of failure) are illustrated in Figure 4-7.

The finite element method is judged to not be inherently deficient because the Scott and Schoustra (1974) analyses predicted only the first phase of failure (the "inverted footing" type of failure). Instead, a number of FEM studies of the anchor pull-out problem have shown that the FEM can reasonably predict the final phase of failure (the "anchor pull-out" type of failure). The finite element analyses are much improved when nonlinear soil constitutive models are employed. Additionally, numerical analyses of the anchor pull-out problem indicate that the coefficient of lateral earth pressure at rest is possibly a critical soil parameter.

Mining subsidence, in general, cannot be used as a direct analogy to fault rupture propagation through overlying soils. The mechanics of mining subsidence differ greatly from the mechanics of earthquake fault rupture propagation through soil. Namely, the majority of the vertical deformation in mining subsidence is accommodated by the caving and bulking of the roof rock materials and by the bending and slippage of the overlying rock beds, not shear rupturing of overlying earth materials.

On the other hand, the use of the anchor pull-out/fault rupture propagation analogy also posed some potential problems. For instance, the effects of various base rock fault plane orientations could not be studied since the anchor pull-out analogy only modeled a vertical thrust/normal fault offset. Furthermore, the majority of the previous anchor pull-out model studies employed dry, cohesionless soils or extremely soft clays possessing a viscous type of soil behavior at failure. Moreover, many model tests allowed suction to develop underneath the anchor plate, which, in turn, destroyed the similarity between the boundary conditions in the anchor pull-out and earthquake fault rupture scenarios. Finally, the potential development of regions of stress reduction in soils that overlie displaced base

sections requires further study. Overall, however, the anchor pull-out analogy provided key insights into the fault rupture propagation phenomenon.

CHAPTER FIVE:
SUMMARY, FINDINGS, AND SHORTCOMINGS OF THE CURRENT LEVEL OF UNDERSTANDING

5.1 Summary of the Review and Evaluation of Case Histories and Previous Studies

An extensive review of literature has been performed to assimilate information which might improve our understanding of the behavior of earth embankments offset by a fault movement in their foundation. The literature review included a survey of previous studies of the effects of bedrock fault rupture on the performance of earth dams. In addition, a small group of full-scale earth dam/fault rupture case histories were examined. Without clear guidance from the full-scale earth dam case histories, earthquake fault rupture propagation case histories were investigated to provide critical insights into the fault rupture propagation phenomenon. Although these field investigations provided general patterns of soil behavior during fault rupture propagation, previous model studies of faulting (both physical and numerical) were reviewed to examine the behavior of the soil overlying base rock fault movements in greater detail. Finally, two analogous classes of problems, anchor pull-out and mining subsidence, were reviewed and evaluated to obtain additional information on how soils, particularly saturated cohesive soils, respond to base deformations or offsets. The findings of this review and evaluation of literature, as well as the shortcomings in the present understanding of this topic, are presented herein.

5.2 Findings from the Review and Evaluation of Case Histories and Previous Studies

Based on the field observations, laboratory data, and numerical results currently available, these findings can be made regarding the effects of tectonic movements on the stresses and deformations in earth embankments:

1. Casagrande's concept of multiple lines of defense should be employed in the design of all dams built over potentially active faults. Experts agreed that particular attention must be devoted to controlling the hazards of concentrated leaks through the dam and its foundation. The stability of the foundation must be guaranteed. A thick, ductile core protected upstream by thick 'crackstopper' zones and downstream by thick filter and transition zones were considered desirable. These zones must be backed up by a drainage system that extends the full height and length of the dam. All zones must be wider than the maximum anticipated potential fault offset. The crest width and the freeboard of the dam should be maximized, whereas the required reservoir capacity should be minimized. Of course, if possible, a dam site traversed by potentially active faults should be avoided. Spillways and outlet control works should not traverse potentially active fault traces. Finally, the experts concluded that rigid dam structures such as concrete gravity dams should not be constructed over potentially active faults.
2. Pure reasoning was shown to have limitations. In 1974, Sherard reasoned that a broadly graded gravel-sand mixture was the best material to use in the core of an earth dam built over a potentially active fault because of the material's "self-healing" tendency. Just five

years later, when investigating the development of sinkholes in earth dams constructed of broadly graded soils, Sherard concluded that these materials were prone to soil migration even without base differential movement, and hence, broadly graded soils were potentially unstable with regard to internal erosion.

3. A proper geologic investigation must be conducted in the early planning stages of any dam sited in a seismic region. The study should include a geologic survey of a large area surrounding the dam site and a detailed study of fault traces and secondary fractures which cross the dam site. Some amount of movement on these fault traces and secondary fractures throughout the seismic region should be anticipated. In most cases, the amount of displacement across even a major fault would be less than 5 to 10 feet.
4. Field observations of surface faulting indicate that, in general, the bedrock behaves as shown in Figures 3-27, 3-28 and 3-29. Down-warping of the upthrown block during thrust faulting creates tension fissures in the bedrock surface. Subsidence of the normal fault's hanging wall may produce secondary fractures. Secondary bedrock deformations are less likely to occur in strike-slip faulting. Nevertheless, some amount of movement should be expected to occur on existing planes of weakness in the foundation rock during all types of fault movement.
5. Field observations of surface faulting and the results of physical model tests of fault rupturing indicate that differential movement across the fault rupture dissipates as the fault rupture propagates to the surface in unconsolidated earth materials. The character of the soil determined the amount of base movement necessary to propagate the fault rupture

to the surface. In a number of model tests, it was found that a base displacement or offset of between 1% and 15% of the height of the overlying sand layer was necessary to propagate the rupture to the ground surface.

6. Field observations of surface faulting indicate that, in general, fault ruptures in unconsolidated earth materials behave as shown in Figures 3-30, 3-31 and 3-32. The rupture path depends on the orientation of the fault plane, the types of fault movement, the amount of fault displacement, and the depth and character of the overlying earth deposit. Typically, dip-slip fault surfaces are concave toward the downthrown block. Thrust faults gradually decrease in dip near the ground surface. Normal faults refract at the soil-bedrock contact and gradually increase in dip as they approach the ground surface. The refraction and the variation of the dip of the fault plane helps produce gravity grabens. Strike-slip faults tend to follow the almost vertical orientation of the underlying bedrock fault.
7. Field observations of surface faulting and the results of physical model tests of fault rupturing indicate that the great majority of the soil overlying the bedrock adjacent to the fault does not participate in the rupture process. Most of the soil deposit remains relatively undisturbed. Relative motion is primarily concentrated within a fairly narrow zone above the bedrock fault. Once failure occurs, differential movement is usually localized to a thin, distinct failure plane. Ductile materials, however, may accommodate significant fault movement by warping without actually breaking.

8. Physical model tests, particularly 1 g small-scale model experiments, produced consistent results in studies of dip-slip fault propagation through dry cohesionless soils.
9. The finite element method can be applied to the fault rupture propagation problem provided the soil's nonlinear stress-dependent stress-strain behavior is properly or at least adequately modeled. Linear elastic-perfectly plastic soil constitutive models produced inconsistent results when employed in the finite element method, but nonlinear stress-deformation behavioral models provided significantly better predictions of observed behavior. Although based on continuum mechanics, the finite element method appears to be capable of modeling the development of shear and tension zones during fault rupture propagation with sufficient accuracy as to represent a useful engineering tool.
10. The anchor pull-out analogy proved to be extremely useful. Model testing of anchors in soft clay indicate that the amount of anchor plate displacement necessary to predict failure in the soil above the anchor was primarily dependent on the soil's failure strain. Moreover, the soil's axial strain at failure (maximum deviatoric stress) in an unconfined triaxial compression test appears to define the soil's failure strain during soil rupturing reasonably well.
11. Numerical analyses of the boundary deformation problem indicated that the coefficient of lateral earth pressure at rest was likely to be an important soil parameter.
12. Mining subsidence, in general, cannot be used as an analogy of fault rupture propagation. The mechanics of mining subsidence and earthquake fault rupture propagation differ significantly.

13. Field observations, laboratory data, and numerical analyses indicate that both stress characteristics and kinematic constraints combine to control the behavior of the soil above the bedrock fault movement. A highly stressed region forms above the edge of the upthrown block and stress reduction occurs to the side of the edge of the upthrown block during dip-slip fault movement. Although failure may occur in these zones of stress increase and stress reduction, the final failure surface must be kinematically admissible, and hence, it must bend over the downthrown block. Figure 4-7 illustrates this two-phase development of the shear rupture zones in the soil overlying a dip-slip bedrock fault.

5.3 Shortcomings in the Current Level of Understanding

The review of the field observations, laboratory data, and numerical results currently available identified these shortcomings in the current level of understanding of the effects of tectonic movements on stresses and deformations in earth embankments:

1. No well-documented case history exists which describes how earth dams respond to base rock fault displacements.
2. No well-documented case study exists which describes how a deep soil deposit (i.e. depth greater than 50 feet) responds to a base rock fault displacement. Previous studies have focused on surface expressions of faulting, relatively shallow exploratory trenches (i.e. less than 20 feet in depth), and interpretations of surficial geologic evidence.
3. Results from model tests of earth dams of substantial height offset by fault movements are not available. To date only homogeneous

prototype earth embankments less than 20 feet high have been modeled in the laboratory.

4. Results from fault rupture propagation model tests of saturated clay or saturated sand under undrained conditions are not available.
5. No reliable analyses have been performed to study the effects of tectonic movements on stresses and deformations in earth dams.
6. Likewise, no analyses have been performed to study fault rupture propagation through saturated clay or saturated sand under undrained conditions.
7. Finally, the hydraulic conductivity along newly formed shear fractures in earth materials is not known.

Considerable effort, therefore, must be devoted to items 2, 3, 4, 5, 6 and 7 above until well-documented full-scale earth dam/fault rupture propagation case histories become available. The studies presented in subsequent chapters are directed towards development of analytical procedures suitable for evaluating the stresses and deformations in earth embankments generated by tectonic movements. Of course, tectonic vibrations accompany tectonic movements. Because of the inherent complexity of this dynamic, as well as static, problem, only one part of the problem will be addressed here. Relatively much attention has been devoted to understanding the dynamic response of earth embankments to seismic loadings. It is hoped that an improved understanding of the static boundary deformation problem will assist the engineer who must design against the simultaneous application of static and dynamic loads on an earth embankment.

CHAPTER SIX:
MODEL TESTING OF FAULT RUPTURE PROPAGATION THROUGH SATURATED CLAY

6.1 Introduction

The review of literature presented in Chapters Two through Five showed that results from prior model tests of fault rupture propagation through saturated clay under undrained conditions are not available. Although the results from previous studies involving testing of dry sands provide valuable insights, the applicability of these results to saturated clay is questionable. Yet, the saturated clay core is the critical component of an earth dam. Accordingly, it would be useful to explore the effect of base rock fault movement on the integrity and serviceability of the saturated clay core of an earth dam. To isolate critical parameters for a more in-depth study of their influence on the response of overlying, saturated clay materials to a base rock fault displacement, a program of controlled laboratory model testing was performed. The results of these tests, performed using 1 g small-scale models composed of a weak saturated clay mixture, are presented herein. Finally, lessons learned regarding the performance of earth dams built over active faults from the model testing of fault rupture propagation through saturated clay are discussed.

6.2 1 g Small-Scale Modeling of Saturated Clay

6.2.1 Review of Previous Studies:

A number of researchers have employed 1 g small-scale model testing to study the behavior of saturated clay under undrained loading conditions. The anchor pull-out work by Davie and Sutherland (1977) discussed previously in Section 4.2 is just one example. Likewise, a considerable amount of 1 g small-scale

model testing has been performed at the University of California at Berkeley over the past thirty years (Seed and Clough, 1963; Sultan and Seed, 1967; Kovacs, 1968; Kovacs et al., 1971; Arango-Greiffenstein, 1971). This previous research, principally under the direction of Dr. H. Bolton Seed, has shown that observations of the performance of 1 g small-scale models can provide valid insights into the performance of prototype earth structures.

The mechanical requirements of model similitude must be satisfied in order for the results of small-scale model tests to be adequately representative of the performance of the prototype earth structure. A number of studies have analyzed this problem and found that mechanical similitude requirements can be met in 1 g scale models if the conditions delineated in Table 6-1 are fulfilled (Hubbert, 1937; Clough and Pirtz, 1958; Seed and Clough, 1963; Roscoe, 1968). If the unit weight of the model and prototype soil are essentially the same, the mechanical similitude requirements will be satisfied provided the model-to-prototype ratios of length, modulus of elasticity, and undrained shear strength equals λ, the geometric scale ratio. In cases where all of the quantities listed in Table 6-1 cannot be simultaneously satisfied in the model, the quantities most significantly affecting the performance of the prototype should be satisfied. For example, if elastic deformations are important, then the ratio of the modulus of elasticity of the model to that of the prototype must be satisfied; whereas, if inelastic deformations in a soil mass at or near failure are important, then the clay's undrained shear strength must be modeled properly.

In modeling earth embankments, previous researchers at the University of California at Berkeley identified four additional factors that can influence the validity of the extrapolation of observations of 1 g small-scale model tests to predict the performance of the full-scale prototype earth structure. In general, the major problems are: (1) pore-pressure changes in cohesionless materials may

Table 6-1: 1 g SCALE MODEL SIMILITUDE REQUIREMENTS

Quantity	Required Model-to-Prototype Proportions
Unit Weight of Soil	1
Lengths	λ
Forces	λ^2
Times	$\sqrt{\lambda}$
Accelerations	1
Modulus of Elasticity	λ
Angle of Internal Friction	1
Undrained Shear Strength	λ

Where λ is the Geometric Scale Ratio

differ in the small-scale model and in the prototype; (2) capillary forces may overly influence the behavior of small-scale soil models; (3) soil load-deformation behavior may be significantly different at the extremely low confining stresses in the small-scale model; and (4) the different rates of loading in the field and in the laboratory may alter the soil strength characteristics of the prototype and model soils. Regarding their work on models composed of saturated clay materials, these researchers found that: (1) in contrast to cohesionless materials, the low permeability of the types of clay materials used in these studies adequately ensures that drainage is not allowed during shearing; furthermore, test data indicates that pore pressure changes in weak clays appear to be about the same (to scale) as those measured in natural clays; (2) capillary forces do not significantly affect the behavior of small-scale models if the clay is completely saturated at a high water content and the models are "sufficiently large"; models at least 6 inches in height are considered "sufficiently large" for the types of materials and conditions employed in the model tests described in this chapter; (3) additionally, "sufficiently large" soil models ensure that special soil strength characteristics which need to be considered at extremely low confining pressures can be ignored; and (4) the effects of the rate of loading on the undrained strength of saturated clays can be included by adjusting the strength of the model clay for rates of loading different from the field conditions. Therefore, careful 1 g small-scale model testing of saturated clay can provide valuable insights into the performance of prototype earth embankments.

Considerable effort was devoted to finding a clay material suitable for use in 1 g small-scale model testing. Early model studies employed a kaolinite material having a water content of approximately 125%, but this material was found to consolidate excessively before and during testing. The model clay must exhibit a very low rate of consolidation so the water content, and hence, the

strength of the clay, would remain constant during testing. In addition, the model clay should exhibit a stress-strain behavior similar in form to that of the prototype soil, and should have a low undrained shear strength which can be varied and controlled so as to satisfy the scaling requirements. Investigation of a variety of clay mixtures identified a mixture of three parts kaolinite to one part sodium montmorillonite (based on dry weight) as the most suitable model clay material. This clay mixture exhibits a low rate of consolidation, suitable stress-strain behavior, and can be mixed to various water contents resulting in a wide (and controllable) range of undrained shear strengths. The principal engineering index characteristics of this clay mixture, as well as of its components, are provided in Table 6-2. The grain size distribution curves of the kaolinite and the sodium montmorillonite or bentonite, as determined by means of hydrometer analysis, are presented in Figure 6-1. This clay mixture (hereinafter referred to as model clay) was successfully employed in a number of model studies of earth embankments (Seed and Clough, 1963; Sultan and Seed, 1967; Kovacs, 1968; Arango-Greiffenstein, 1971).

As shown in Figure 6-2, the undrained shear strength of the model clay can be adjusted in a controlled fashion over a wide range by manipulation of the model clay's water content. As shown in this figure, the work performed by previous researchers in evaluating and documenting this relationship between water content and undrained shear strength has been updated with additional data developed in this study. Varying the water content of the model clay from 230% to 80% produced clay materials with undrained shear strengths of on the order of 2 psf to 100 psf. Unconfined triaxial compression tests by Kovacs (1968) indicated that the stress-strain behavior of the model clay was relatively brittle with failure as defined by the maximum deviatoric stress occurring at or before 5% axial strain. Although not stated, it is believed that the unconfined compression tests were performed on

Table 6-2: PROPERTIES OF THE CLAY MATERIALS USED

Property	Kaolinite	Montmorillonite	3:1 Mixture
Brand Name	Huber-45	Volclay Premium Gel	--
Specific Gravity	2.60	2.78	2.64
Liquid Limit	38%	516%	140%
Plastic Limit	24%	34%	22%
Plastic Index	14%	482%	118%
Natural Moisture	0.7%	15%	--

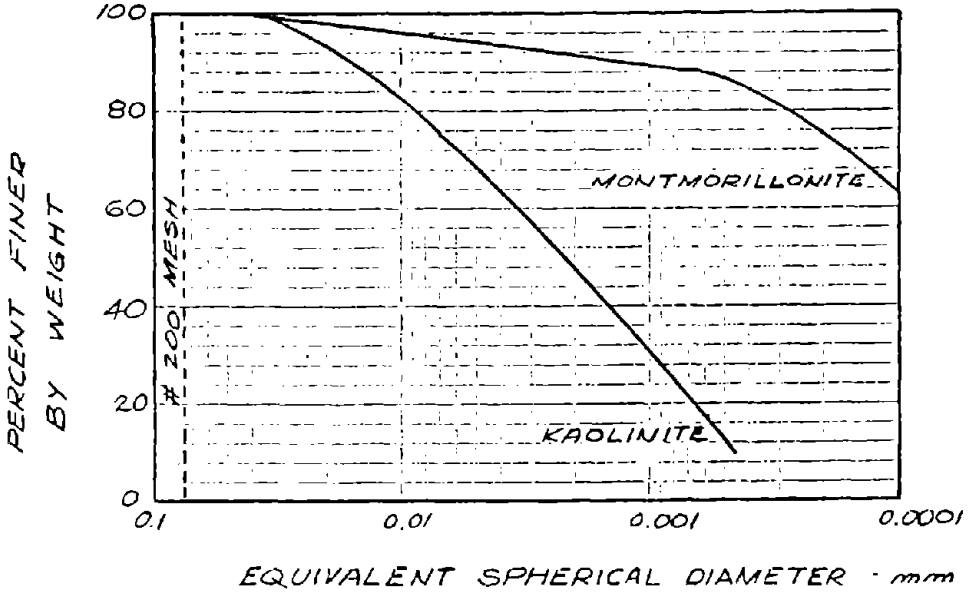

Figure 6-1: GRAIN SIZE DISTRIBUTION CURVE OF CLAY MATERIALS (after Kovacs, 1968)

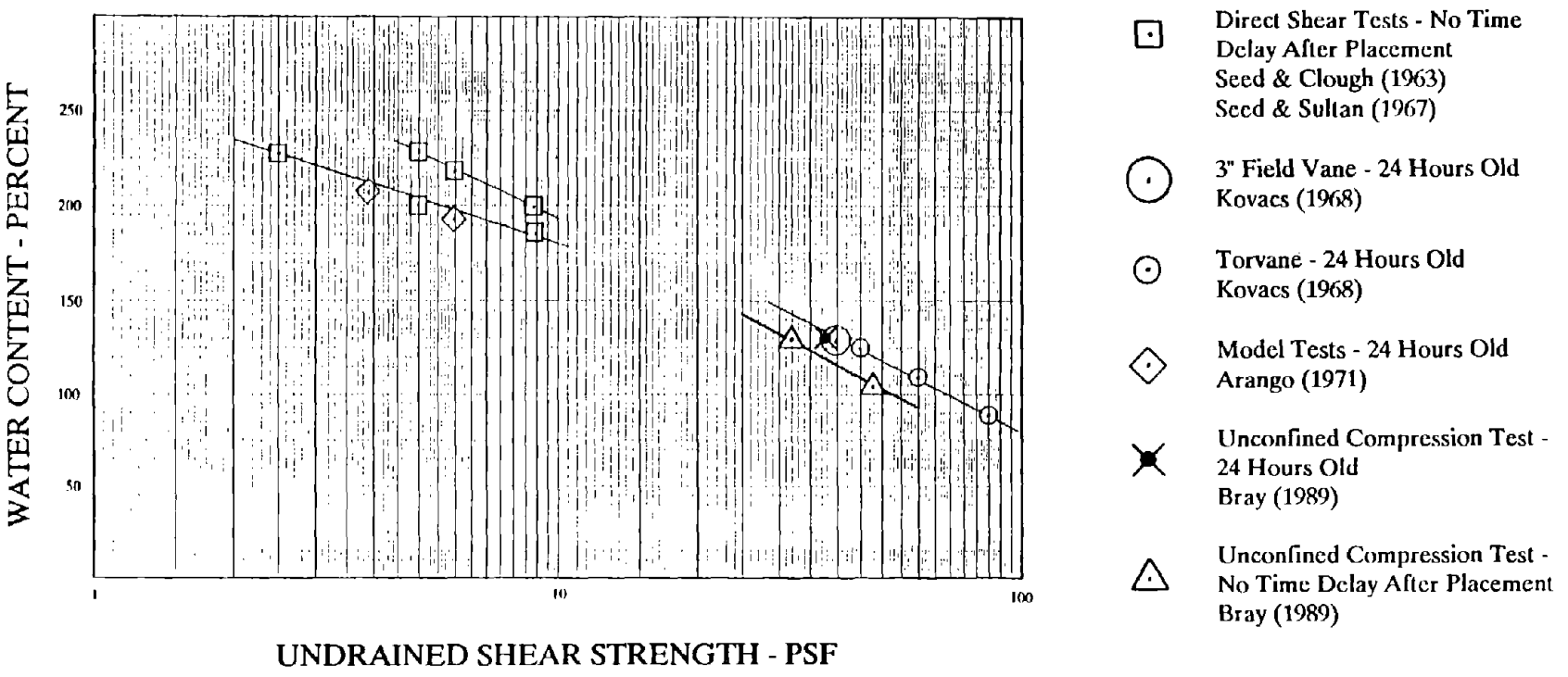

Figure 6-2: UNDRAINED SHEAR STRENGTH AND WATER CONTENT RELATIONSHIP OF KAOLINITE-BENTONITE CLAY

model clays at low water contents since a cylindrical sample with a height of several inches would not stand unsupported at higher water contents. In addition, these model clay triaxial samples were cured for 24 hours prior to shearing, because the actual 1 g small-scale model tests were conducted 24 hours after placement of the model clay.

Large direct-shear box tests (12 x 12 inches) were conducted to determine the load-deformation behavior of the clay. Results from a series of large direct-shear tests are presented in Figure 6-3. Three characteristics of the clay are illustrated in these stress-deformation curves: (1) The model clay is highly thixotropic, gaining strength over time; (2) The soil exhibits a post-peak reduction in strength ("sensitivity" or "strain softening"), especially after being allowed to cure for some time (The model clay is, however, only slightly sensitive and the reduction from peak to residual undrained shear strength appears to represent a strength decrease on the order of only 5% to 15%); and (3) The deformation at failure (analogous to the soil's failure strain) depends on the water content and the age of the model clay. In general, it was felt that the load-deformation behavior of the model clay was reasonably similar (to scale) to that of the prototype clays.

On the other hand, the use of the model clay in 1 g small-scale model experiments also posed some potential problems. First, as portrayed in Figure 6-3, the model clay displayed pronounced thixotropic effects. A series of tests were performed to quantify the effects of thixotropic gains in strength. As shown in Figure 6-4, the model clay exhibited a gain in peak undrained shear strength of around 30% after a period of just one day. However, for model clay mixtures at water contents below approximately 130%, it was found that the thixotropic strength gain would be less than 10% after a period of one hour. Due to this thixotropic effect, it was necessary to remold the model clay before use to ensure its strength could be reliably determined. Boundary effects significantly affected

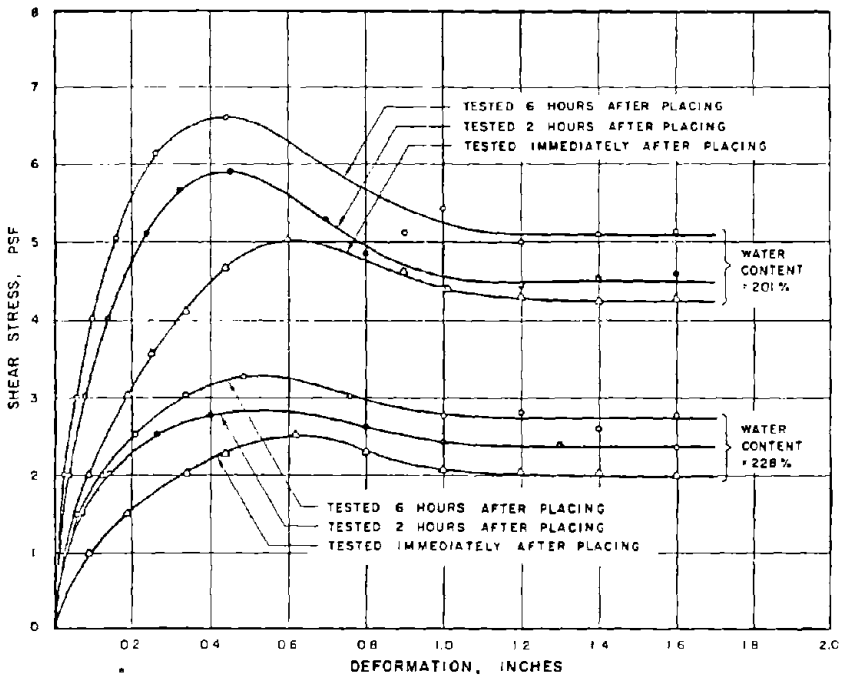

Figure 6-3: LOAD-DEFORMATION BEHAVIOR OF KAOLINITE-BENTONITE CLAY (after Seed and Clough, 1963)

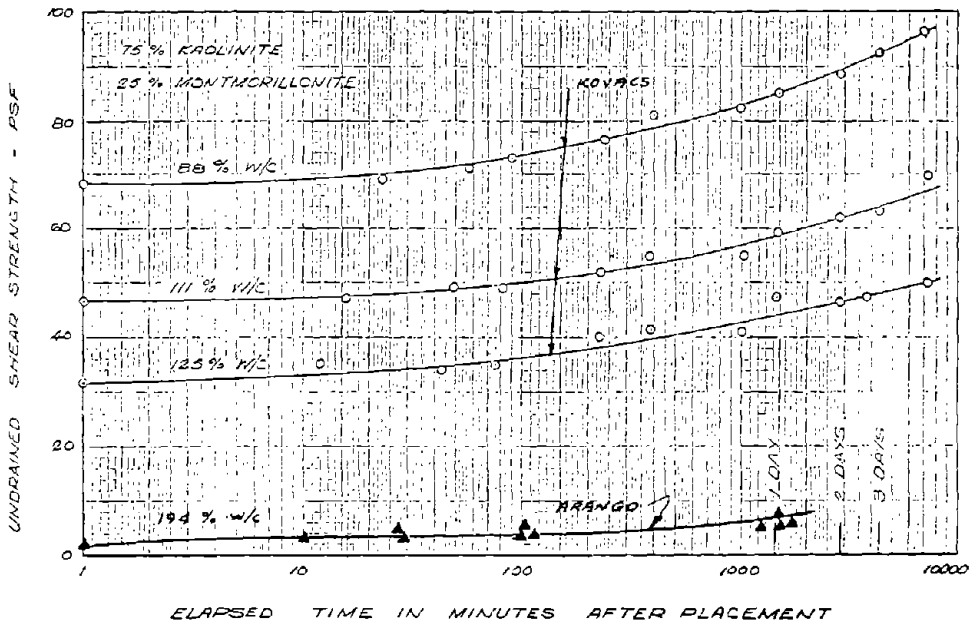

Figure 6-4: UNDRAINED SHEAR STRENGTH VARIATION WITH TIME (after Arango-Greiffenstein, 1971)

the results from actual model tests utilizing the model clay because of the high adhesion between the model clay and the walls of the box used for the model tests. The model clay was sticky and difficult to handle. In fact, the clay had to be placed by throwing it into the model box. Volume change tests, however, indicated that the placed model clay was nearly saturated and that even with some air bubbles entrapped, the placed material behaved as an incompressible saturated clay. A special displacement pump was required to adequately mix the clay mixture at high water contents and a large rotary mixer was required at lower water contents. It took eight hours to prepare 6 cubic feet of model clay. Nevertheless, the model clay proved to be an excellent modeling material because of its generally suitable stress-strain, strength, and volume-change characteristics.

6.2.2 Properties of the Clay Employed in 1 g Small-Scale Model Tests:

The work performed by most of the previous researchers appears to indicate that the most critical characteristic of the clay employed in 1 g small-scale model testing of the fault rupture propagation phenomenon was its strength. Clearly, the disturbed soil mass deformed inelastically during the fault rupture process. To satisfy similitude requirements in modeling large prototype earth embankments, 1 g small-scale models required weak clay materials. Previous model studies typically employed clays with water contents above 200% so undrained shear strengths were less than 10 psf. Trial base deformation model tests utilizing high water content/low shear strength clay mixtures, however, produced unreasonable results. The model clay "flowed" around the displaced base section without creating a clearly defined failure surface. Failure did not propagate to the surface of the clay model without excessive base deformation. It appeared that the model clay at high water contents and extremely low shear strengths possessed the viscous type of failure behavior that Sutherland had warned

about in his 1988 Rankine Lecture (See Section 4.2.2). Of course, in modeling fault rupture propagation, the failure behavior of the model clay must be similar to that of the prototype clay.

One of the interesting results from the previous model studies of earth embankments was an observation made by Arango-Greiffenstein (1971) regarding slope failure in clay embankments. He found that the locus of points of maximum shear strain in the model clay bank seemed to best define the extent and geometric characteristics of the yielding soil mass. It was not surprising that the failure planes developed within the zones of maximum shear strains, and this serves to illustrate the importance of using a material which can, with suitably "scaled" shear strength, still "fail" at a representative shear strain. The clay material used in these studies should satisfy this important modeling criterion.

The examination of the results from the anchor pull-out tests conducted by Davie (1973) further highlighted the importance of the stress-strain behavior of the material employed in the small-scale model including, in particular, the failure strain of the clay. Although unconfined compression tests conducted after 24 hours of thixotropic hardening of clay mixtures at low water contents indicated that the model clay failed at or below 5% axial strain, similar strength test data was not available for the softer clay material at higher water contents. Large direct-shear tests were conducted on the wetter clay mixtures, but it was difficult to assess whether the nonuniform distributions of stress and deformation across the large, soft samples affected the observed load-deformation behavior. The large direct-shear tests of high water content clays did, however, show that the deformation required to produce failure decreased as the water content decreased and as the time after placement increased (See Figure 6-3). Proper modeling of fault rupture propagation should be performed using a clay with a failure strain similar to that of

the prototype soil. Additional testing was thus required to ensure that this stipulation could be satisfied.

Since trial base deformation model tests employing high water content clay mixtures (e.g. water contents greater than 200%) produced behavior inconsistent with that observed in the field, models employing the clay at lower water contents were constructed. At lower water contents, and thus, higher strengths, however, the 1 g small-scale models could not represent large prototype earth embankments. Moreover, at low water contents, the model clay was extremely difficult to handle and to place without excessive entrapment of air. The trial base deformation model tests found, however, that the clay mixture at medium water contents (e.g. water contents between 100% and 150%) exhibited reasonable failure characteristics, and that it could be satisfactorily "placed" in the model box. Upon base deformation in the actual model tests, the model clay initially warped slightly, but then ruptured on distinct, visible failure planes. A base deformation of on the order of 5% to 20% of the height of the clay sample was necessary to propagate the rupture to the top surface of the sample. Additionally, since the undrained shear strength of the model clay at the medium water contents was on the order of 20 to 60 psf, 1 g small-scale models of about one foot in height could be employed to represent prototype earth embankments on the order of 50 to 200 feet high (This was true provided the undrained shear strength of the prototype clay material was on the order of 2000 to 4000 psf). Most importantly, the failure strain of the soil at the medium water contents appeared to be in a range that was reasonably suitable for modeling earth dams composed of saturated compacted clay cores (i.e. 5% to 20% axial strain at failure in triaxial tests).

As mentioned earlier, additional strength testing was necessary to define the stress-strain behavior of the model clay at water contents of between 100% and 150% and to validate the use of this clay in fault rupture propagation model tests.

Thus, a series of nine stress-controlled unconfined triaxial compression tests were performed to define the stress-strain characteristics of the model clay over the range of water contents to be employed in the 1 g small-scale fault rupture propagation model tests performed as part of this study. The results of these triaxial tests are presented in Figures 6-5, 6-6 and 6-7. Photographs of two of these unconfined compression tests are shown in Figure 6-8.

The results from the unconfined compression tests were fairly consistent (e.g. the 5 test results shown in Figure 6-5 agree quite closely). Because of the clay's extremely low strength, the 1.4 inch test samples failed at applied axial deviatoric loads of only three quarters of a pound. A special triaxial test apparatus was developed to test the model clay at low strengths. Test samples were formed in split molds lined with plastic wrap greased on the outside with the commercially available "PAM" nonstick cooking spray for easy removal. The plastic wrap could then be carefully peeled away before testing. A special lightweight acrylic top cap was used and a ball bearing replaced the usual loading rod. The load was applied by gradually adding decreasing amounts of small weights at regular intervals to maintain a fairly constant strain rate. Axial deformations were measured with a LVDT and recorded by a data acquisition program running on an IBM PC-AT microcomputer with A/D capacity. As shown in the photographs in Figure 6-8, the samples failed in the lower half of the sample because the self-weight of the sample significantly increased the stress in this region. Hence, half of the weight of the sample was assumed to be included in the applied axial load. The consistency of the test results provides good support for the reliability of the unconfined compression testing procedure as a basis for evaluation of material strength and stress-deformation characteristics. Furthermore, as shown in Figure 6-2, the strengths determined by the nine stress-controlled unconfined triaxial compression tests compared favorably with the strengths determined in previous studies.

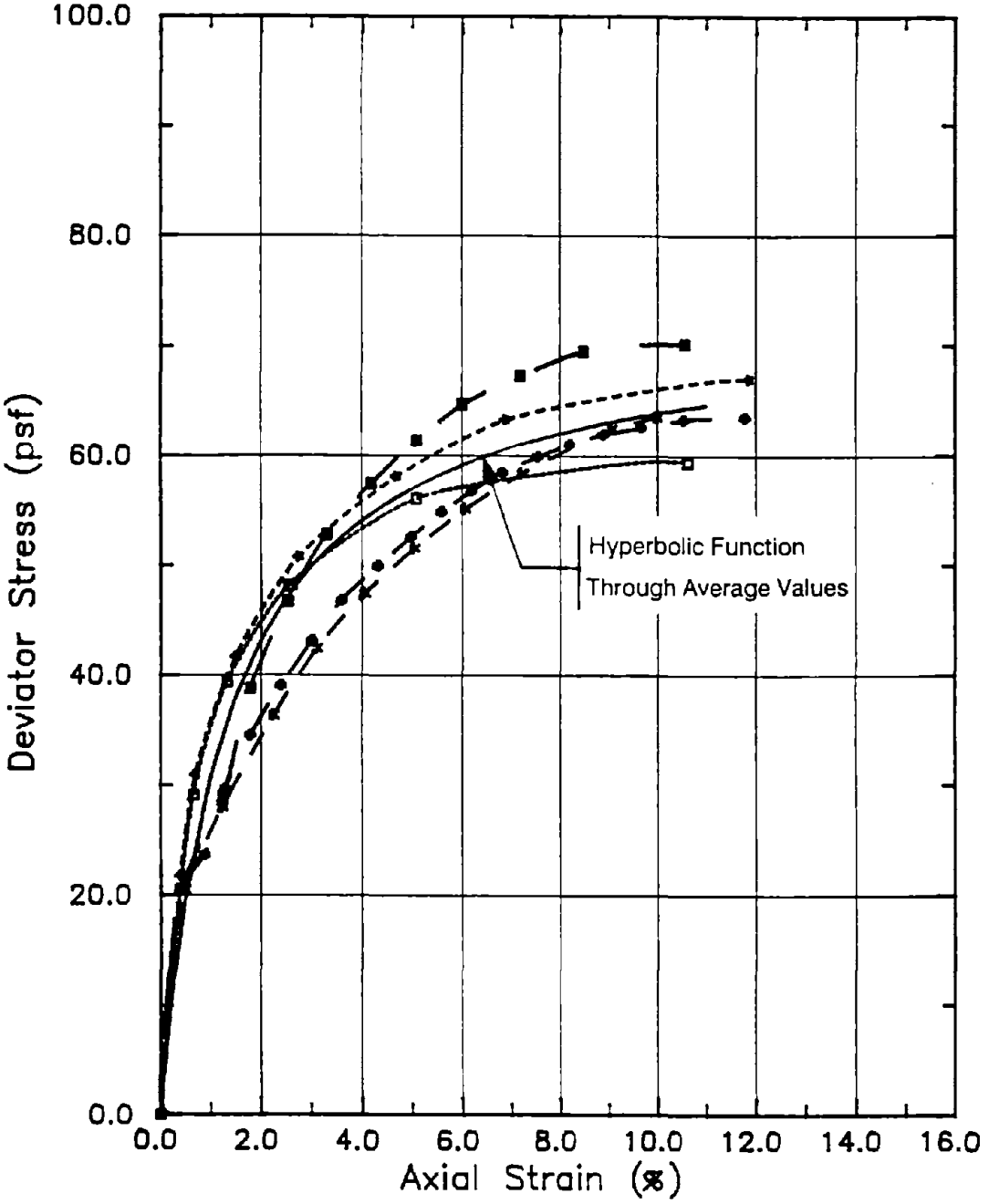

Figure 6-5: STRESS-STRAIN BEHAVIOR OF KAOLINITE-BENTONITE CLAY AT WATER CONTENT OF APPROXIMATELY 130%. TEST CONDUCTED IMMEDIATELY AFTER PLACEMENT

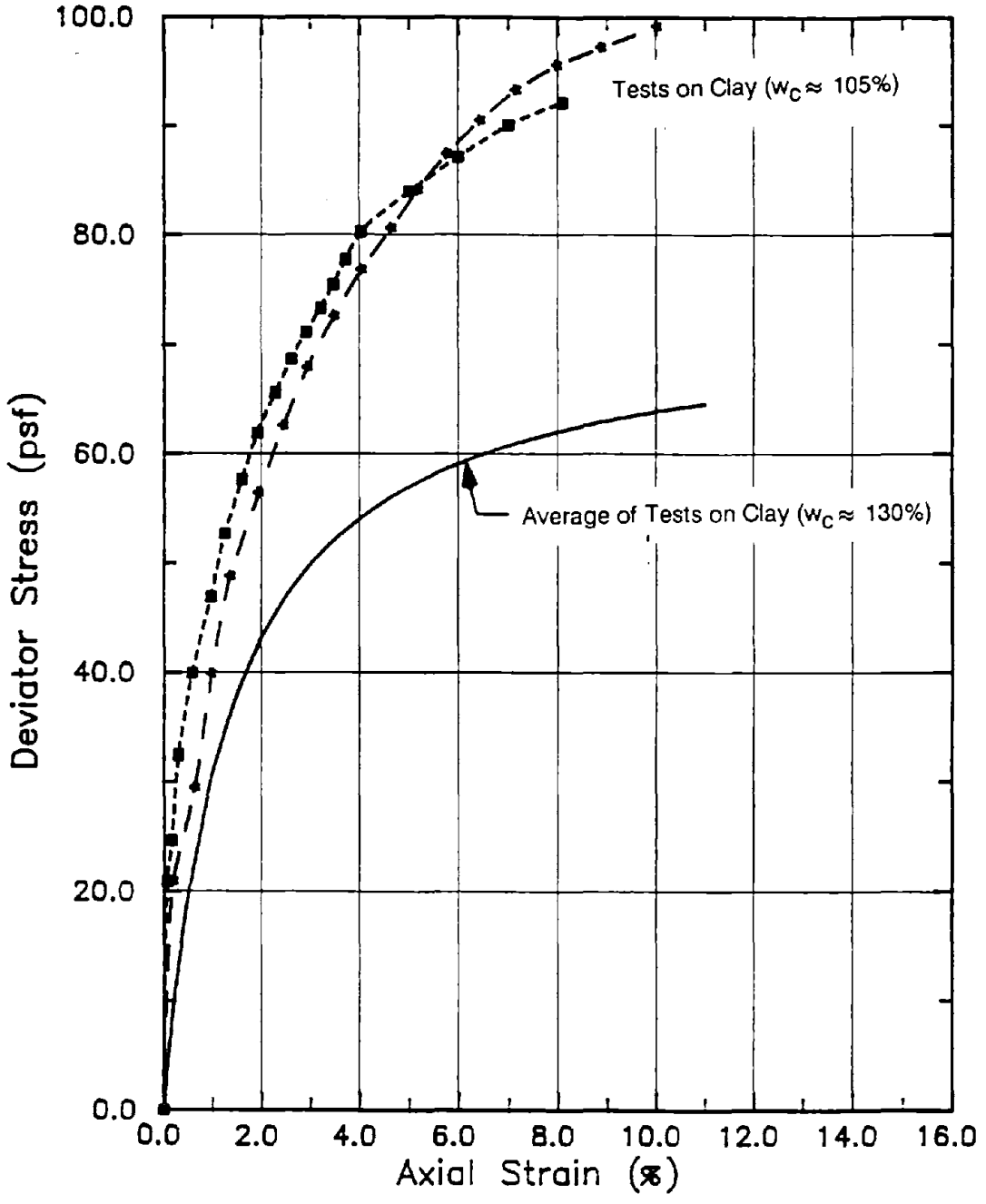

Figure 6-6: STRESS-STRAIN BEHAVIOR OF KAOLINITE-BENTONITE CLAY AT WATER CONTENT OF APPROXIMATELY 105%. TEST CONDUCTED IMMEDIATELY AFTER PLACEMENT

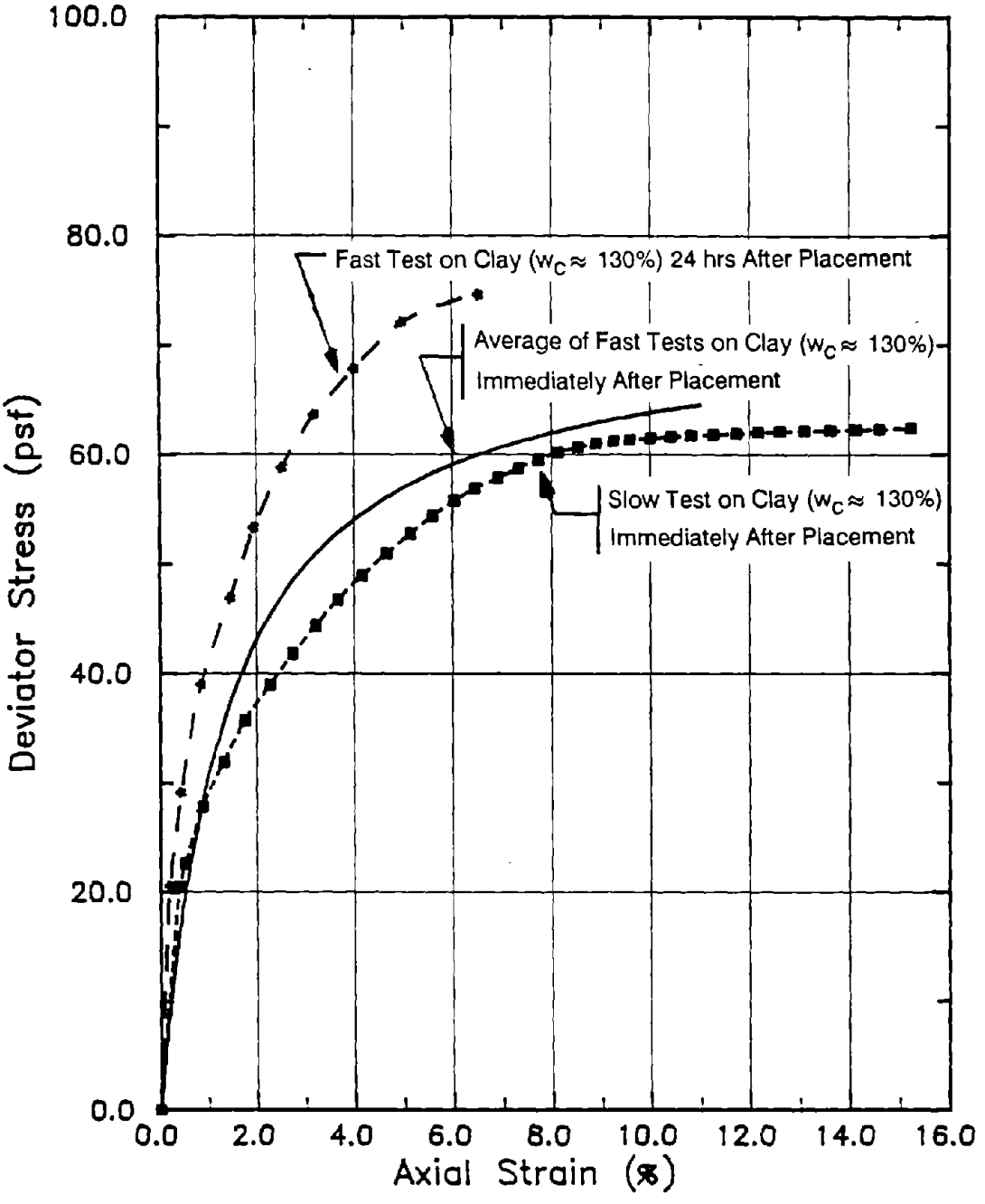

Figure 6-7: STRESS-STRAIN BEHAVIOR OF KAOLINITE-BENTONITE CLAY AT WATER CONTENT OF APPROXIMATELY 130%. TESTS CONDUCTED AT DIFFERENT STRAIN RATES AND AT DIFFERENT TIMES AFTER PLACEMENT. NOTE THE VARIATION IN THE MATERIAL'S FAILURE STRAIN

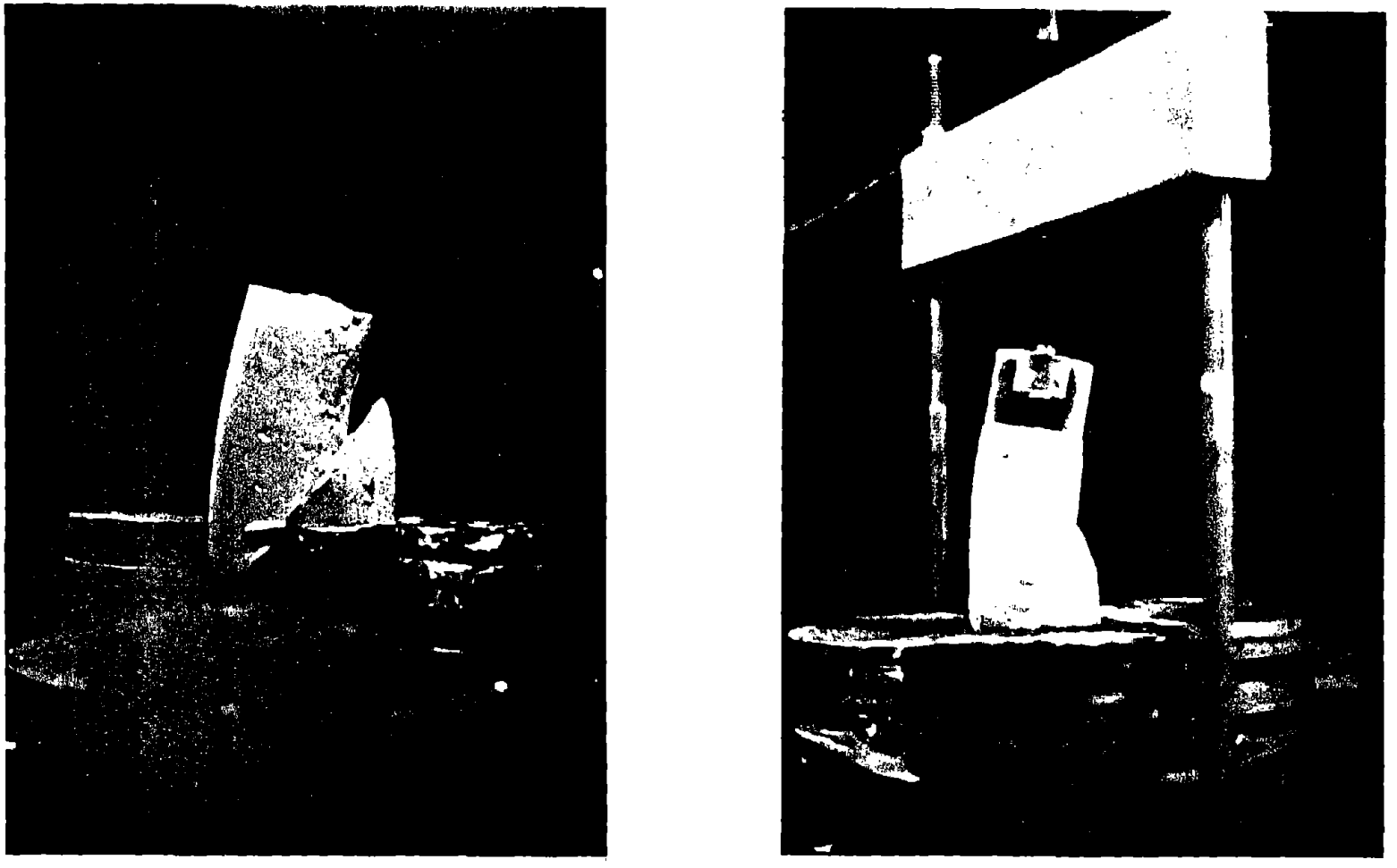

(A) Time to Failure = 1 min.

(B) Time to Failure = 3 min.

Figure 6-8: CLAY SAMPLE AFTER FAILURE IN UNCONFINED COMPRESSION TESTS. THE WATER CONTENT OF THE CLAY WAS APPROXIMATELY 130%. TESTS CONDUCTED IMMEDIATELY AFTER PLACEMENT

Test results on the clay at water contents of approximately 130% and tested immediately after placement are shown in Figure 6-5. The undrained shear strength of the model clay at this water content varied from 30 to 35 psf, with the majority of the tests failing at 32 to 33 psf. The stress-strain behavior of the model clay resembled that of natural soils. The shape of each of the stress-strain curves mirrored the traditional hyperbolic shape of the stress-strain curves of natural soils. Finally, the model clay consistently failed at an axial strain of between 10% and 12%. This level of strain at failure is in reasonable agreement with "typical" results of undrained triaxial compression tests of soft, saturated natural clays and compacted clays.

The capability of varying the model clay's failure strain in a controlled fashion was a desirable property of the clay in this study. Realizing the potential importance of a soil's failure strain, the model clay was tested under different conditions to note the resulting variations in the clay's failure strain. Figure 6-6 shows that the axial failure strain in unconfined compression tests reduced from between 10% and 12% to between 8% and 10% when the water content of the clay dropped from 130% to 105%. At a water content of 105%, however, the model clay was quite stiff and difficult to place without large pockets of entrapped air. Moreover, this relatively slight reduction in the failure strain was not judged to be large enough to cause significant variations in the performance of the clay. In previous studies when the model clay was allowed to sit before testing, the failure strain of the soil decreased. Hence, the model clay at a water content of 130% was tested 24 hours after placement. As shown in Figure 6-7, the failure behavior was significantly more brittle with failure occurring at around 6% to 7% axial strain. The thixotropic strength gain, however, was less than 15%. On the other hand, slowing the imposed shearing or strain rate by an order of three, was found to increase the failure strain to between 14% and 16%. The model clay's strength

remained at around 32 pcf. At the slower strain rate, the clay's creep behavior became more dominant, as shown in Figures 6-7 and 6-8, and the clay displayed more ductile stress-strain and failure behavior. These variations in the material's failure strain could be used in small-scale model tests to investigate the hypothesis that a soil's failure strain is a major factor in determining the rate at which a base rock fault rupture propagates through overlying soil deposits.

6.2.3 Description of the Clay-Box Model Test Apparatus:

The clay-box model test apparatus is shown in Figure 6-9. The box was 42 inches long, 12 inches wide, and 24 inches high. The left half of the box could be moved up or down either vertically or at angles of 60° and 45°. The box was composed of half-inch thick stiff acrylic glass so that maximum deflections of the glass bottom and walls would be less than 0.05 inches, or 0.4% of the box dimensions, under the loading applied by the clay within the box. In addition, rigid steel and aluminum stiffening angles and beams were added to further reduce deflections of the walls of the box and especially the movable base section. The movable base section could be moved up or down through a displacement of 5 inches at a constant rate of deformation with good control by means of a sensitive hydraulic jack.

The major difficulty in the fault rupture propagation model testing program was the high adhesion of the clay material to the walls of the testing box. Previous studies had shown that these boundary effects could be significant. A wide clay-box could be used to reduce the damaging effects of side friction at the clay-wall interface, but the growth of the rupture zone within the middle of the clay could not be observed during testing. Furthermore, cutting of the model clay at water contents greater than 100% smeared the failure planes that developed within the clay. As a result, the propagation of the fault rupture through the clay could only

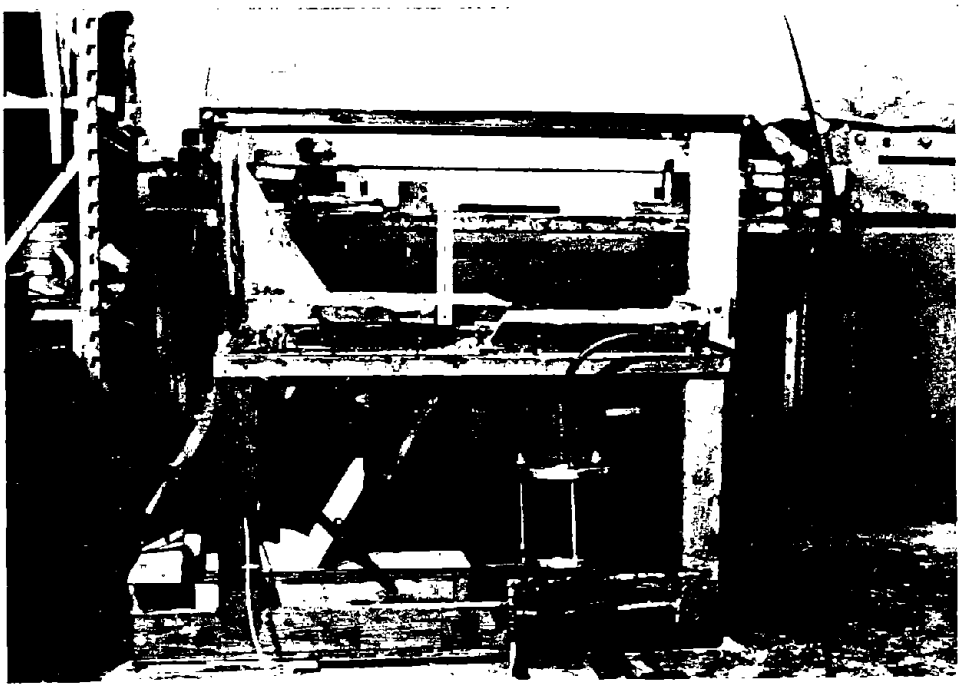

Figure 6-9: THE CLAY-BOX MODEL TESTING APPARATUS. THE BOX WAS 42 INCHES LONG, 12 INCHES WIDE, AND 24 INCHES HIGH. THE LEFT HALF OF THE BOX COULD MOVE UP OR DOWN AT SELECTED ANGLES

be "observed" near the glass walls of the clay-box. Hence, an exhaustive search for a suitable low-friction interface material was conducted. Trial fault rupture propagation model tests found that the "PAM" nonstick cooking spray adhered to the acrylic glass during clay placement and formed a low-friction interface between the clay-box walls and the sticky clay mixture. The "PAM" was sprayed onto the side walls of the acrylic glass box 24 hours before the model clay was placed in the box, and was very effective in reducing clay/wall adhesion. The effectiveness of the "PAM" low-friction interface will be demonstrated by the model test results.

As in previous studies, the model clay was placed into the clay-box testing apparatus using techniques designed to reduce the amount of the air voids in the clay and to reduce disturbance of the "PAM" low-friction interface. Volume measurements of the clay before and after base deformation indicated that even with a few air voids in the clay the soil deformed essentially without volume change. Hence, the clay properly modeled the incompressible saturated clay prototype material under undrained loading conditions. Numerous attempts were made to install horizontal markers of different colored soil to assist in the observation of rupture planes. Installing multiple horizontal marker layers of soil, however, often disturbed the "PAM" low-friction interface. Hence, markers were usually not installed in the model tests. When installed, these markers varied in width and were only approximately horizontal.

Before the "PAM" low-friction interface proved effective, attempts were made to turn the high wall adhesion of the model clay into an advantage. Bray and Goodman (1981) have shown that horizontal base friction models employing a sand-flour-oil mixture could approximate the increased gravitational field developed in a centrifuge machine. Since trial tests indicated that the model clay's wall adhesion was approximately equal to its undrained shear strength, it was hoped that a top and base friction machine employing clay at shear strengths of

around 60 psf sandwiched between two closely spaced horizontal plates of acrylic glass could represent a vertical deposit of clay with a gravitational load of 120 pcf. As the base section was forced into the model clay sandwiched between the horizontal plates which were about a quarter of an inch apart, the wall adhesion of 60 psf on the top and bottom plates applied a combined load of 120 psf on the clay. Hence, the soil's unit weight could be approximated by the skin-friction developed on the top and bottom plates as the base section pushed the soil in a horizontal direction.

Results from trial tests utilizing the horizontal top and base clay friction model are shown in Figure 6-10. Figure 6-10(A) shows a failure pattern similar to that observed for shallow anchor pull-out tests. Figure 6-10(B) shows how application of the "PAM" low-friction interface material destroys the top and base friction effect and produces unreasonable behavior. Whereas the horizontal top and base clay friction apparatus could model thrust fault movements at orientations of 90°, the testing apparatus could not model movements on base faults dipping at other angles. The orientation of the side friction force would always be parallel to the movement of the base section. For example, a model of a 45° thrust fault would incorrectly produce a situation where the gravitational force of the soil's weight acts at an orientation parallel to the 45° thrust movement, whereas, in reality, gravity in a vertical soil deposit acts vertically downward or at an angle of 45° to the direction of this thrust fault movement. Nonetheless, these brief "pilot" studies suggest that, the horizontal top and base clay friction model could be useful in other studies where the gravitational force is aligned with the principal direction of the soil movement.

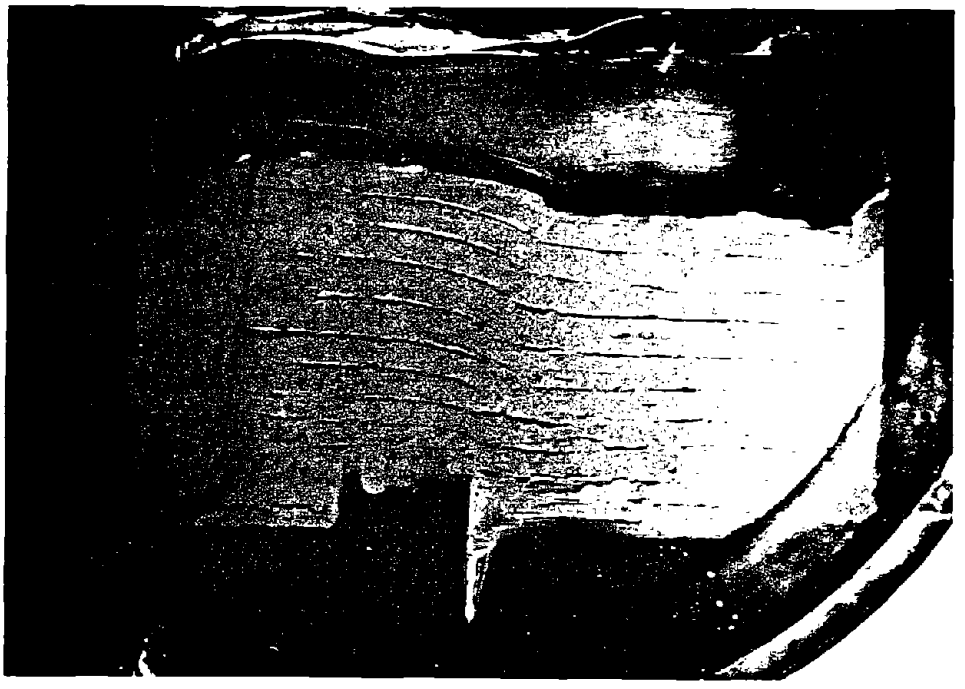

(A) Vertical Thrust Movement with Gravity

(B) Vertical Thrust Movement without Gravity
("PAM" applied to the top and base friction plates)

Figure 6-10: RESULTS OF TRIAL TESTS UTILIZING THE HORIZONTAL TOP AND BASE CLAY FRICTION MODEL

6.3 1 g Small-Scale Model Tests of Fault Rupture Propagation through Saturated Clay

6.3.1 Overview of Clay-Box Model Testing Program:

The details of the clay-box model tests of fault rupture propagation through saturated clay are described in Table 6-3. A total of eleven tests were conducted over a period of three weeks. Models subjected to the 90° thrust/normal fault displacements investigated the performance of saturated clay materials overlying bedrock faults at nearly vertical orientations. These bedrock faults could be high angle thrust or normal faults, or strike-slip faults with a significant vertical component of movement. Moreover, this series of model tests allowed for the observation of the development of the "inverted footing" type of failure followed by the "anchor pull-out" type of failure hypothesized to occur above uplifted horizontal anchor plates as described in Section 4.2 (See Figure 4-7). Furthermore, the effectiveness of the "PAM" low-friction interface could be ascertained by observing differences between the 90° thrust fault and 90° normal fault model tests. Additionally, a series of model tests were conducted for 60° normal fault movements and 60° thrust fault movements. In these experiments, the effect of the orientation of the fault plane could be examined. Finally, the failure strain of the clay employed in the 60° thrust fault models was varied to note the significance of this parameter in the rate of fault rupture propagation.

The model clay was mixed in a large rotary mixer and stored in an airtight 55 gallon drum lined with a rubber bag. The model clay not contaminated by the "PAM" interface material was reused in the model tests. During the testing period, the water content of the model clay slightly decreased but remained within the range of 130% to 136%. The undrained shear strength and the failure strain values of the model clay reported in the study were believed to be correct to within ± 10%. Typically, the model tests reached the failure condition in about one minute.

Table 6-3: SATURATED CLAY-BOX DIP SLIP FAULT RUPTURE PROPAGATION TESTING PROGRAM

			SATURATED CLAY PROPERTIES			
Test	Base Fault	Soil Depth (inches)	w_c (%)	S_u (psf)	ϵ_f (%)	Shearing Rate
1	90° Thrust	10.6	136	30	11.5	Fast
2	90° Thrust	10.6	136	30	11.5	Fast
3	90° Thrust	11.0	136	30	11.5	Fast
4	90° Normal	10.6	134	31	11	Fast
5	90° Normal	6.9	134	31	11	Fast
6	60° Normal	7.9	132	31	11	Fast
7	60° Normal	9.4	132	31	11	Stage 1: Slow Stage 2: Fast
8	60° Normal	9.4	132	31	11	Fast
9	60° Thrust	9.4	130	32	11	Fast
10	60° Thrust	9.8	130	32	6.5	Fast (Clay cured 24 hours)
11	60° Thrust	6.3	130	32	15	Slow

Note: Fast Tests were completed in 30 - 60 seconds
Slow Tests were completed in 120 - 180 seconds

As stated earlier, the clay-box tests modeled the behavior of a prototype saturated clay profile which was on the order of 50 to 150 feet deep. The results of the model tests are presented in the following sections. The results are presented in the form of sketches of the observed failure patterns. The development of the failure patterns as well as the amount of base deformation necessary to propagate the fault rupture to the surface of the clay sample are noted.

6.3.2 90° Thrust Fault:

The results from three model tests where half of the base displaced upwards along a vertical fault plane are presented in Figures 6-11, 6-12, 6-13, and 6-14. The results of these three tests were in close agreement with each other. Initially, the rupture propagated over the upthrown block. At larger base deformations, the rupture zone was expressed as a series of nearly vertical shear planes. Finally, the main rupture bent over the downthrown block and broke the surface at a base displacement (offset) of around 10% to 16% of the depth of the clay layer. At this later stage, tension zones developed at the base of the stationary block near the fault and at the surface of the clay above the uplifted block. In two of the tests, nearly horizontal shear planes were observed in the rupture zone region before the development of the nearly vertical main shear rupture. Since the model clay was thrown into place and not rolled into place in distinct soil layers, these horizontal shear planes did not form because of existing planes of weakness in the soil. Instead, these failure planes appeared to be the complementary shear planes of the nearly vertical main shear rupture plane. Again, in the top of the clay layer, the horizontal shear planes formed before the vertical shear planes formed.

6.3.3 90° Normal Faults:

The results from two model tests where half of the base displaced downward along a vertical fault plane are presented in Figures 6-15 and 6-16. The

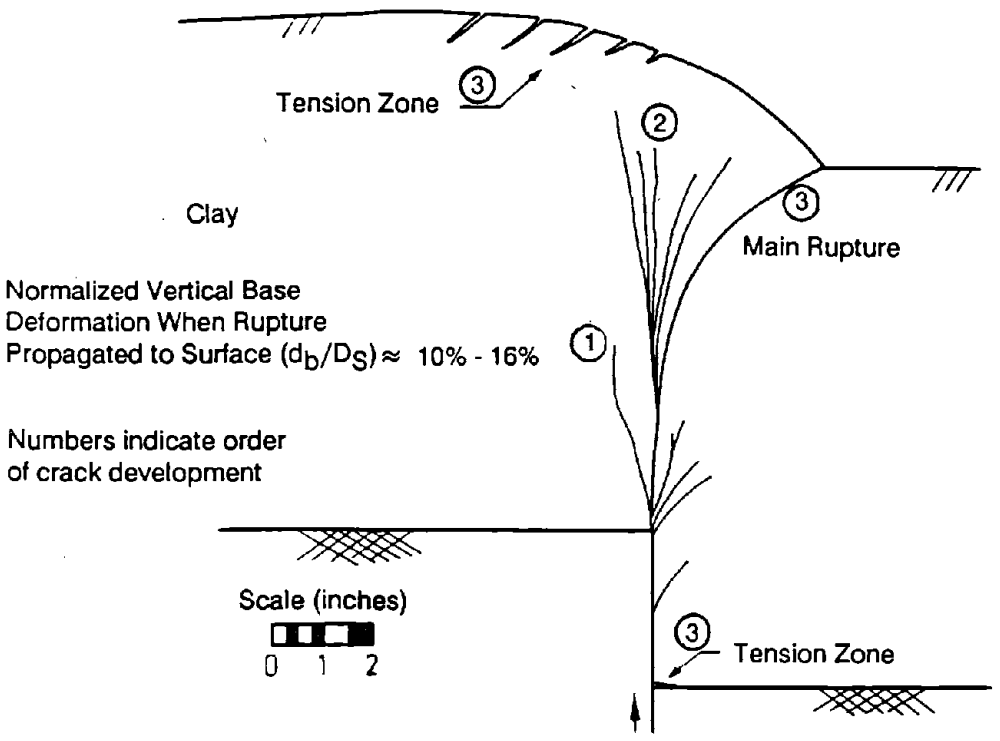

Figure 6-11: RESULTS OF MODEL TEST #1: 90° THRUST FAULT

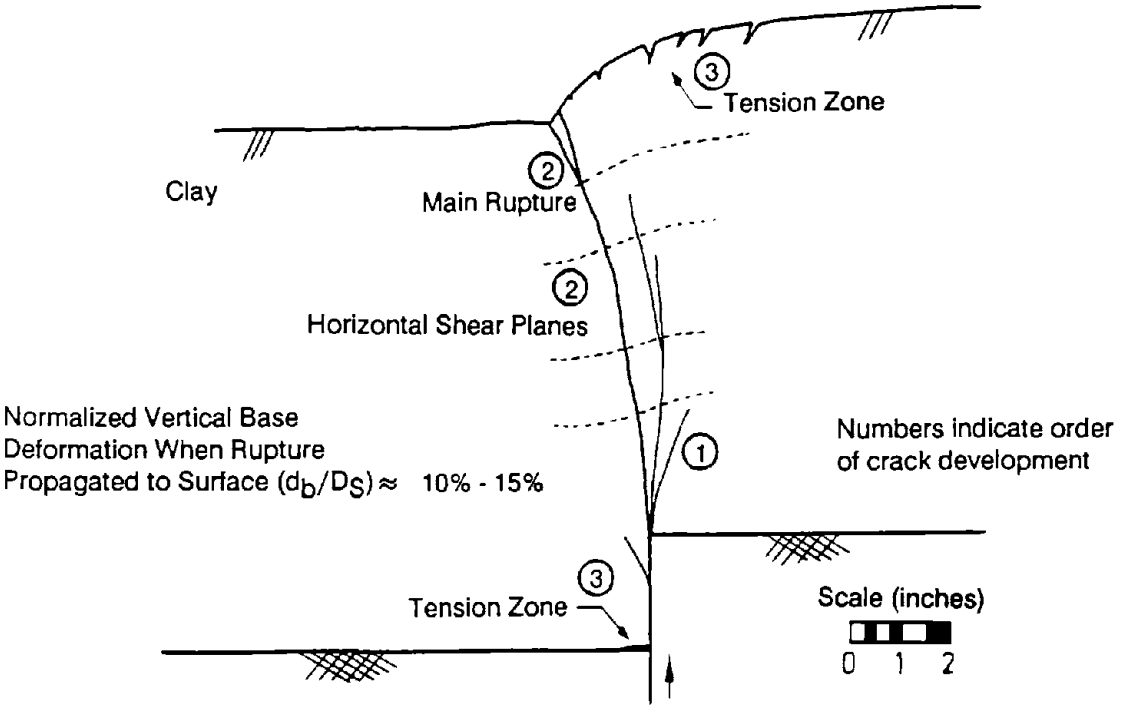

Figure 6-12: RESULTS OF MODEL TEST #2: 90° THRUST FAULT

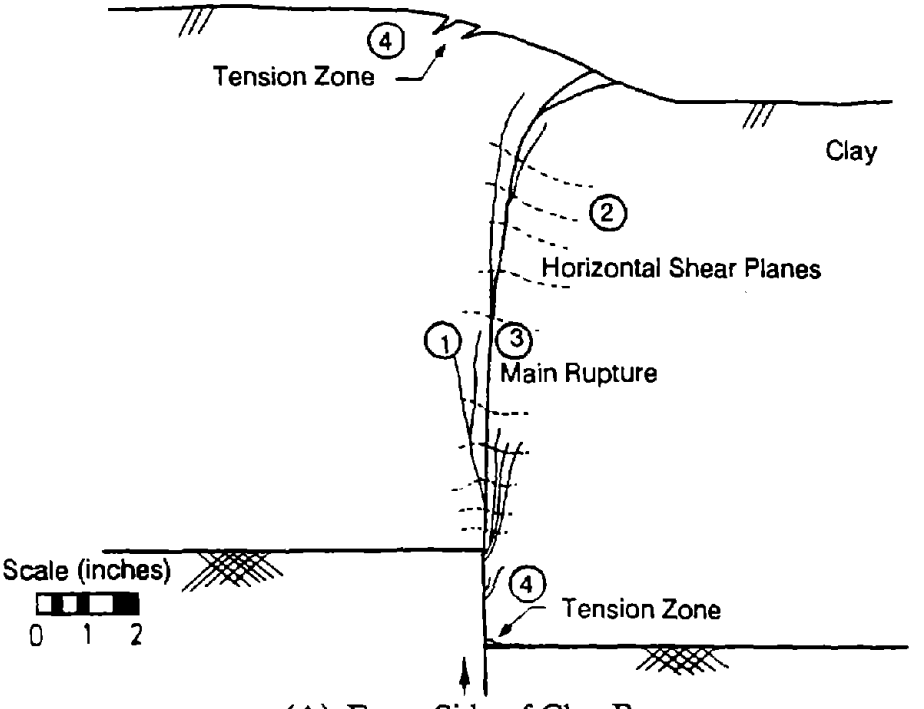

(A) Front Side of Clay-Box

Normalized Vertical Base Deformation When
Rupture Propagated to Surface (d_b/D_S) ≈ 10% - 16%

Numbers indicate order of crack development

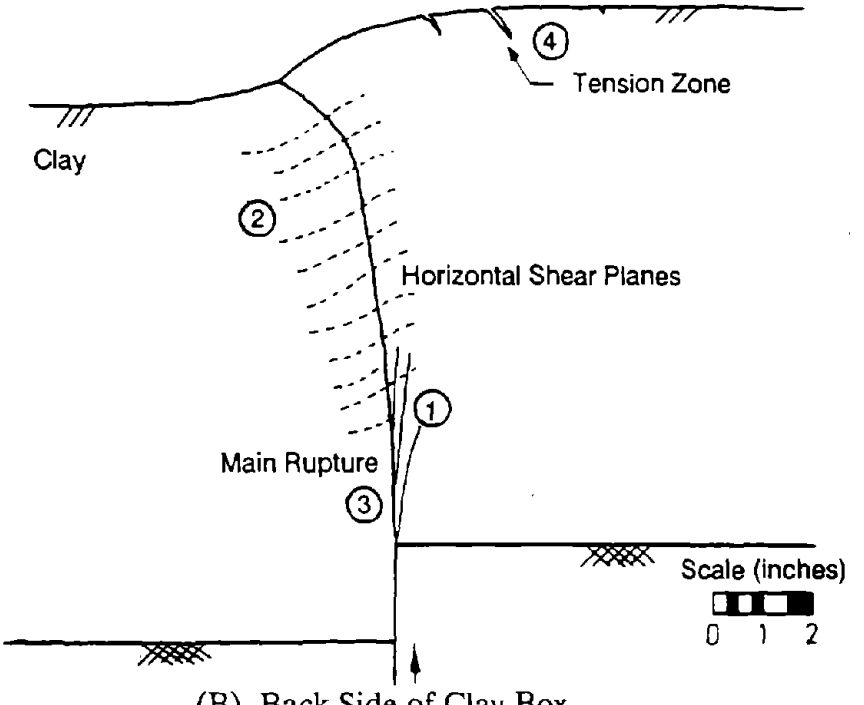

(B) Back Side of Clay-Box

Figure 6-13: RESULTS OF MODEL TEST #3: 90° THRUST FAULT

Figure 6-14: PHOTOGRAPH OF MODEL TEST #2: 90° THRUST FAULT

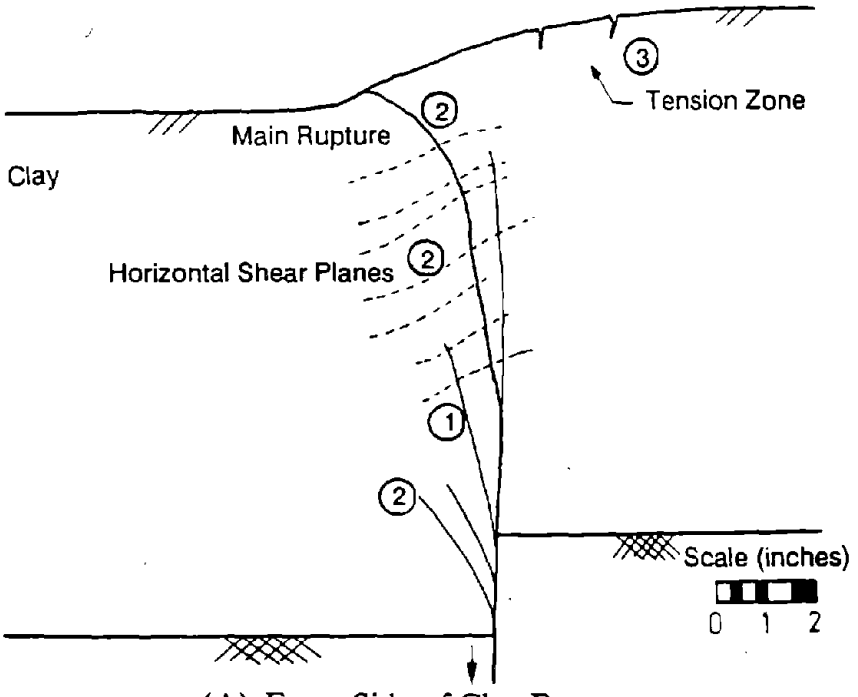

(A) Front Side of Clay-Box

Normalized Vertical Base Deformation When Rupture Propagated to Surface $(d_b/D_S) \approx$ 14% - 18%

Numbers indicate order of crack development

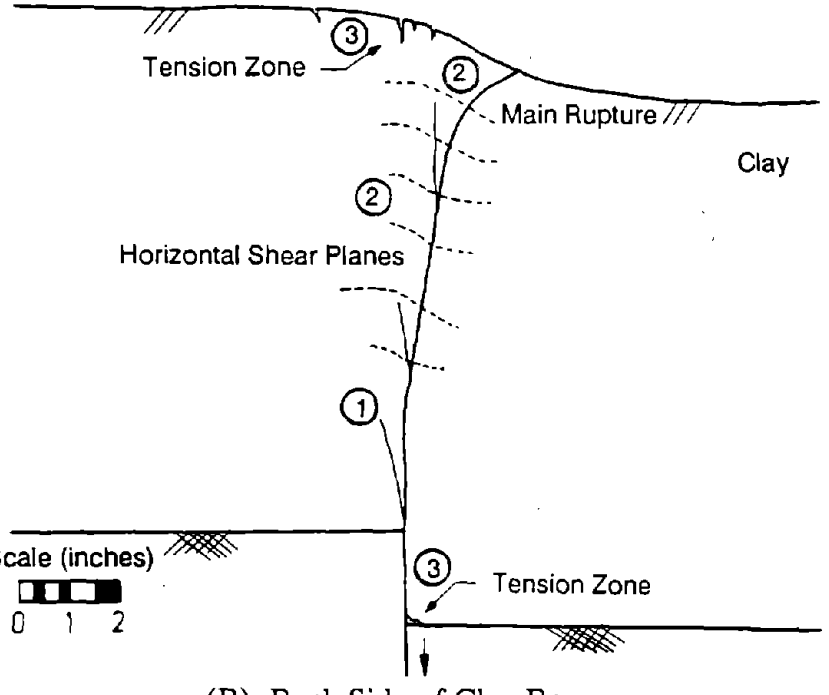

(B) Back Side of Clay-Box

Figure 6-15: RESULTS OF MODEL TEST #4: 90° NORMAL FAULT

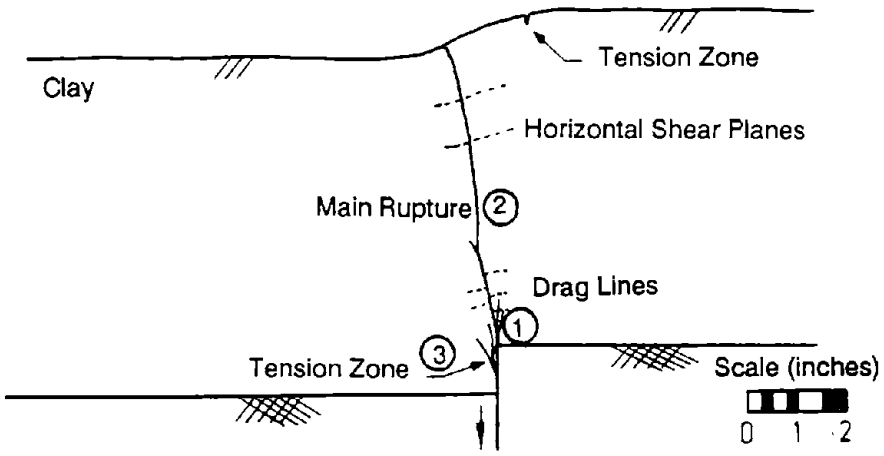

(A) Front Side of Clay-Box

Normalized Vertical Base Deformation When
Rupture Propagated to Surface $(d_b/D_S) \approx$ 11% - 14%

Numbers indicate order of crack development

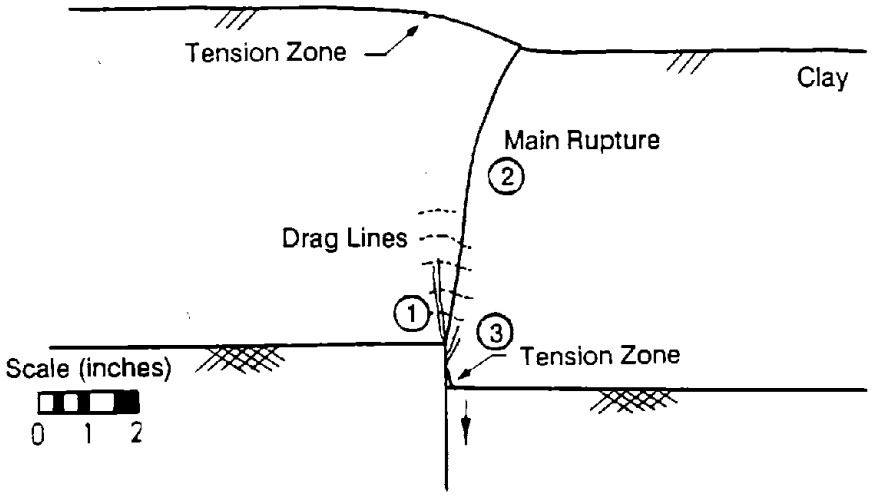

(B) Back Side of Clay-Box

Figure 6-16: RESULTS OF MODEL TEST #5: 90° NORMAL FAULT

results of these two tests were in close agreement with each other and with the results of the 90° thrust fault model tests. The development of the shear planes and tension zones in the clay overlying the vertical normal fault movements was essentially identical to the development of failure planes in the 90° thrust fault model tests. Hence, the "PAM" low-friction interface appeared to dramatically reduce the potentially deleterious effects of the otherwise high wall adhesion of the clay mixture. If wall friction significantly affected the development of the failure planes in the model clay, the normal and thrust fault model tests would have displayed inconsistent results. Furthermore, the main rupture broke the clay surface along a relatively straight line across the width of the sample. The model clay away from the side walls behaved like the model clay adjacent to the side wall "PAM" interface. Finally, after the test, when the model clay was being removed from the clay-box, the clay readily fell away from the side walls coated with "PAM". Therefore, the effect of side friction on the results of these model tests was judged to be fairly minor.

The height of the clay layer was reduced from approximately 10½ inches to less than 7 inches in model test 5 to determine if variations in the height of the soil layer affected results. Overall, the failure patterns observed in model tests of different heights were similar. The occurrence of horizontal shear planes at the top of the clay layer, however, was more pronounced in the model test conducted on the thicker clay layer. In general, model tests conducted with depths of the clay layer from 6 inches to 12 inches displayed similar patterns of behavior.

6.3.4 60° Normal Fault:

The results from three model tests where half of the base displaced downward along a normal fault plane dipping at an angle of 60° are presented in Figures 6-17, 6-18, 6-19, 6-20, and 6-21. The failure pattern formed in the clay

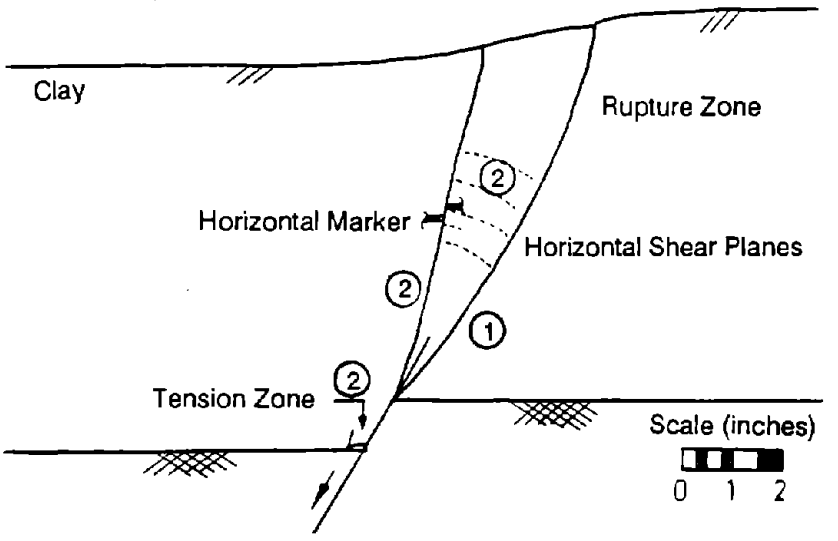

(A) Front Side of Clay-Box

Normalized Vertical Base Deformation When
Rupture Propagated to Surface (d_b/D_S) ≈ 11% - 13%

Numbers indicate order of crack development

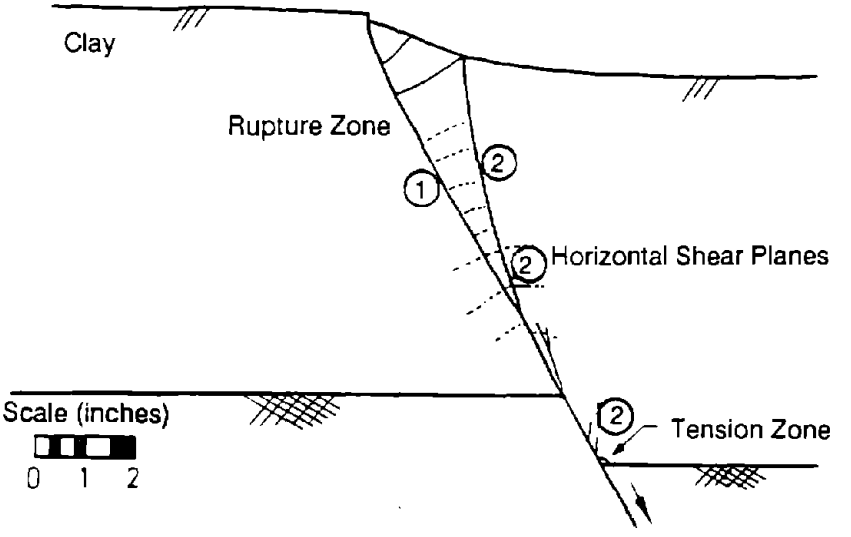

(B) Back Side of Clay-Box

Figure 6-17: RESULTS OF MODEL TEST #6: 60° NORMAL FAULT

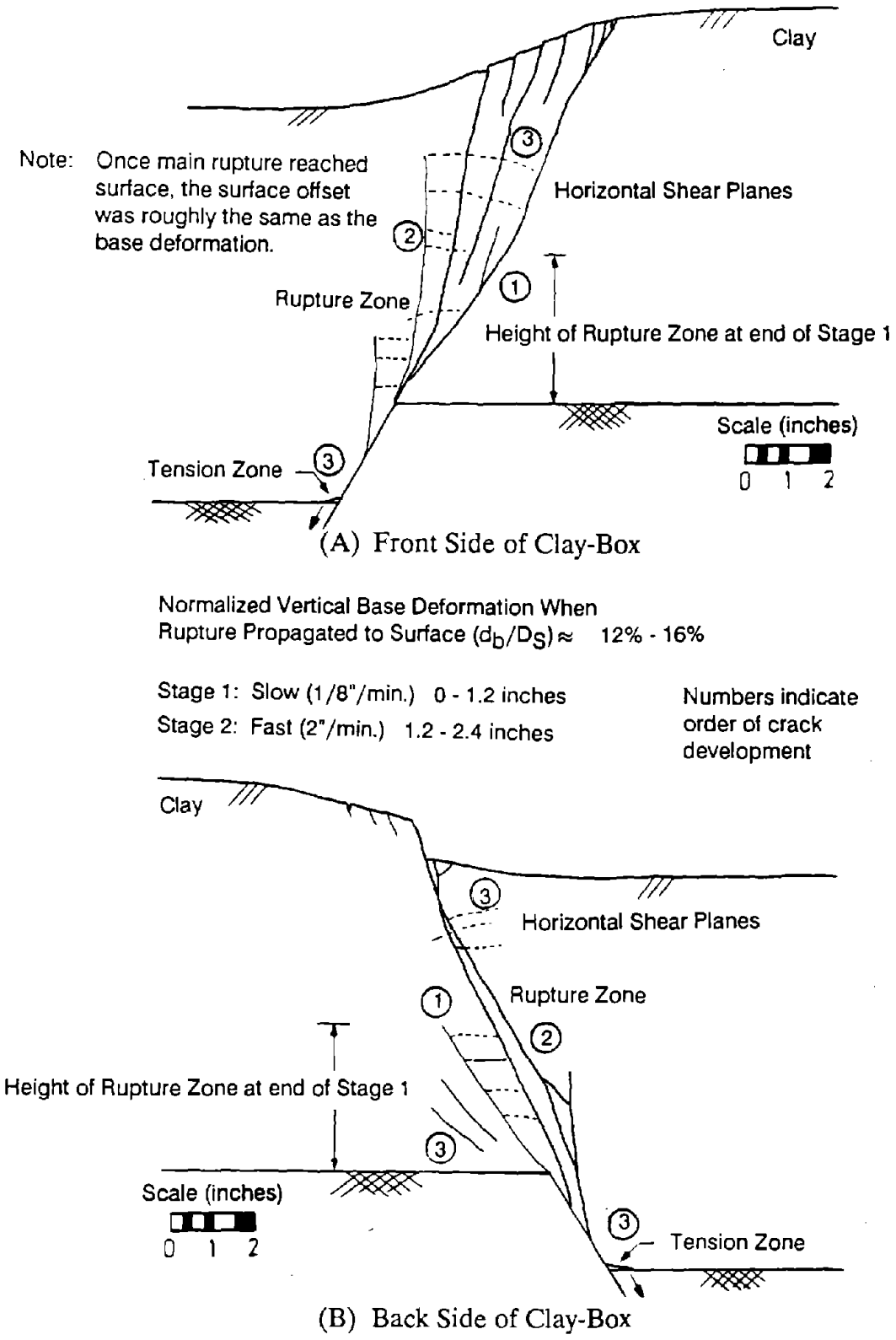

Figure 6-18: RESULTS OF MODEL TEST #7: 60° NORMAL FAULT; TEST CONDUCTED IN TWO STAGES: STAGE 1 - SLOW STRAIN RATE AND STAGE 2 - FAST STRAIN RATE

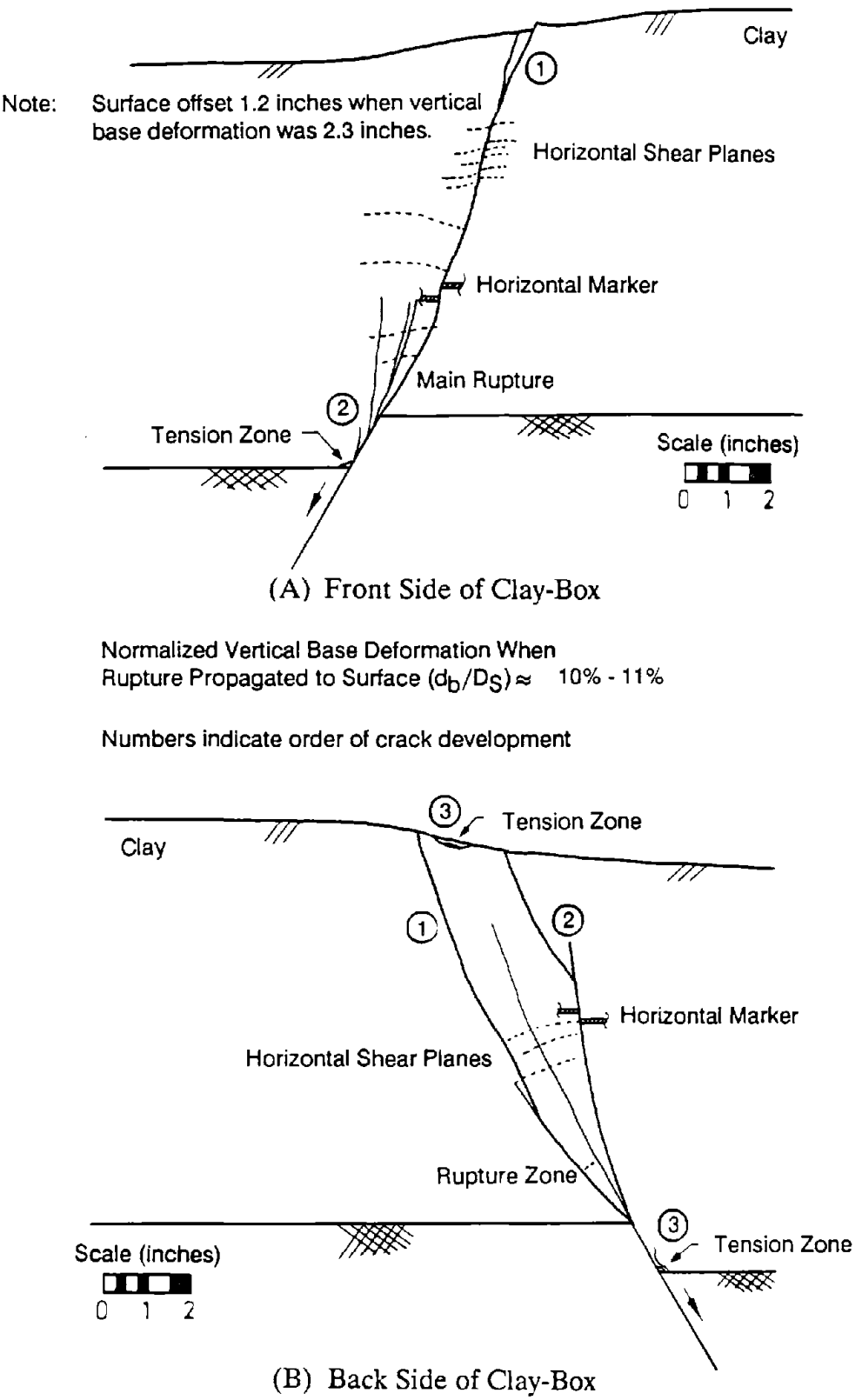

Figure 6-19: RESULTS OF MODEL TEST #8: 60° NORMAL FAULT

Figure 6-20: DEVELOPMENT OF GRABEN ABOVE THE DOWNTHROWN BLOCK DUE TO A 60° NORMAL BASE FAULT DISPLACEMENT

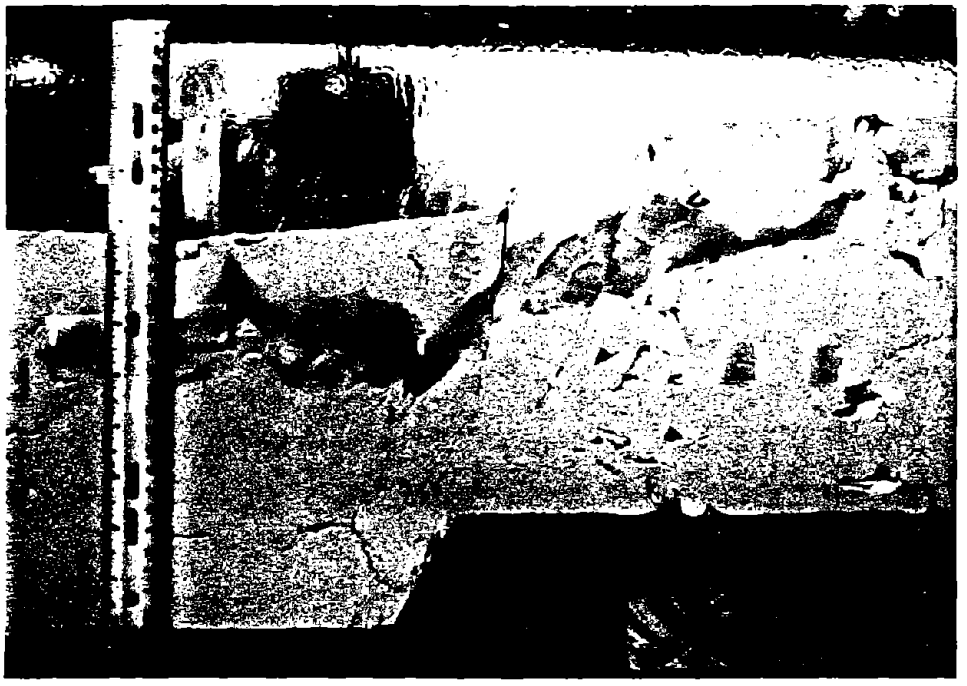

(A) Model Test #6: Typical Failure Pattern

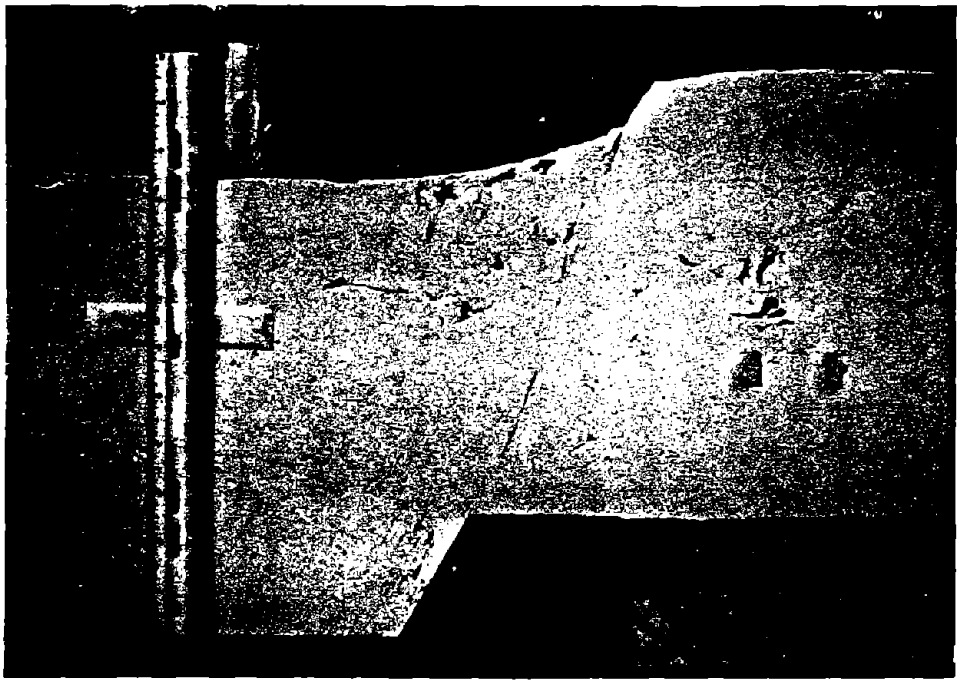

(B) Model Test #8: Case Where Only One Main Rupture Formed

Figure 6-21: PHOTOGRAPHS OF TWO 60° NORMAL FAULT MODEL TESTS

overlying a 60° normal fault movement was more complex than those previously observed in the vertical fault displacement model tests. Typically, the base deformation produced two main rupture planes with a zone of highly disturbed soil between the primary ruptures. The rupture zone was located on the downthrown block side of the projection of the 60° base fault. The primary rupture planes surrounding the rupture zone increased in dip as they propagated to the surface of the clay layer. The dip of rupture planes in the model clay increased to around 80° as they broke the surface.

The sequence of the development of the individual shear planes in the model clay overlying a 60° normal fault movement was similar to that observed in the vertical fault movement model tests. Initially, a shear plane formed over the upthrown block just inside the projection of the base fault. Rather than terminating as the base deformation continued, this failure plane, however, began to bend back toward the downthrown block, increasing in dip as it rose to the surface. Meanwhile, the second main rupture plane formed on the downthrown block side of the first shear plane. This second shear plane refracted at the soil-base contact and propagated to the surface increasing in dip as it rose. During the development of the two main rupture planes, secondary vertical and horizontal shear planes formed in the rupture zone between the two main rupture planes. With additional base movement, a tension zone developed over the downthrown block adjacent to the base fault.

In model tests 6 and 8, a vertical base deformation (offset) of around 10% to 13% of the depth of the soil was required to propagate the main rupture zone to the surface of the clay layer. Whereas, in model test 7, a vertical base deformation (offset) of between 12% and 16% of the depth of the soil was required to produce a shear rupture at the top of the clay layer. Model test 7 was initially conducted at a slow base deformation rate to allow for easier observation of the development of

the shear rupture zone. At the slower rate of base deformation, however, the behavior of the clay appeared to be notably different than that observed when failure was produced in only 30 to 60 seconds. As unconfined compression tests confirmed (see Figure 6-7), the model clay exhibited a more ductile behavior at slower rates of strain. Creep effects became apparent. The failure strain of the model clay increased. Hence, slightly more base deformation was required to propagate the shear rupture to the surface of the clay layer. In Stage 2 of model test 7, the rate of base deformation was increased to the usual speed and the model clay behaved similarly to that observed in the other model tests. Thus, the ductility or the brittleness of the overlying soil seemed to significantly affect the rate of fault rupture propagation.

The model tests furnished a number of other pertinent observations of the fault rupture propagation phenomenon in saturated clay soils. The sketches clearly showed that the amount of differential movement across the distinct failure planes formed in the soil decreased as the fault rupture propagated to the surface. For example, in model test 6 (Figure 6-17), when the vertical offset was nearly 1 inch, the vertical offset in a marker which crossed the shear plane at midheight was approximately 0.2 inches. At the surface, the vertical offset across the failure plane was less than 0.1 inches. Once the rupture plane was fully formed, however, the amount of additional vertical offset at the surface of the clay layer was almost as much as the additional amount of additional vertical offset at the base. The multiple shear planes which increased in dip as they approached the surface produced graben features in the surface of the clay layer. The photograph in Figure 6-20 shows the graben created above the downthrown block during a 60° normal base fault displacement in model test 6.

6.3.5 60° Thrust Fault:

The results from three model tests where half the base displaced upwards along a fault plane dipping at an angle of 60° are presented in Figures 6-22, 6-23, and 6-24. The development of the shear rupture through the clay and the down-warping of the clay surface with increasing base deformation are shown in Figures 6-25 and 6-26. The shape of the shear rupture through the soil was remarkably similar in these three tests. In all three experiments, the main fault rupture initially propagated up over the upthrown block just on the upthrown block side of the projection of the base fault plane. As the main fault rupture approached the top surface, it began to decrease in dip, bending over the downthrown block and breaking the surface on the downthrown block side of the straightline projection of the base fault. At larger base deformations (offsets), tension zones were observed at the top surface in a zone of extension above the upthrown block. Similar to the other model tests results, the differential movement across the fault plane decreased as the shear plane propagated to the surface of the clay layer. After the rupture reached the surface of the clay layer, the offset across the rupture remained less than the additional offset across the rupture at the base and at midheight of the clay layer. Much of the differential movement across the base fault was accommodated by the extensive down-warping of the surface of the clay above the upthrown block. Notice the surface expression of the 60° thrust base fault movement in Figure 6-26.

Although the general characteristics of the shape of the rupture zone were remarkably similar in the three model tests, the results differed significantly in one important aspect. Different magnitudes of base deformation were required to propagate the fault rupture to the surface of the saturated clay layer. The different rates of fault rupture propagation were produced by employing materials in each of the tests with different stress-strain properties, in particular, different failure

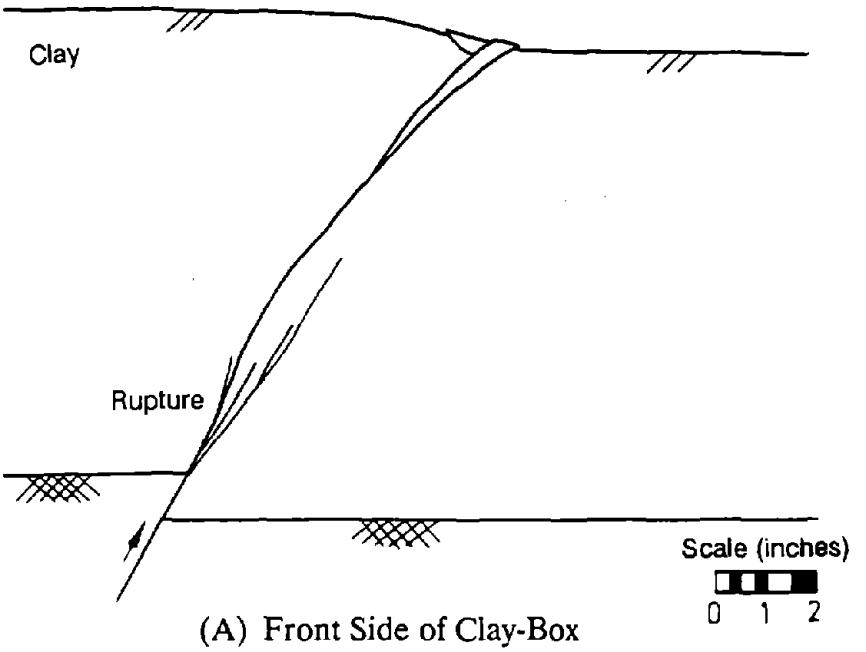

(A) Front Side of Clay-Box

Normalized Vertical Base Deformation When Rupture Propagated to Surface (d_b/D_S) ≈ 10% - 11%

Failure Strain of Soil ≈ 10% - 12%

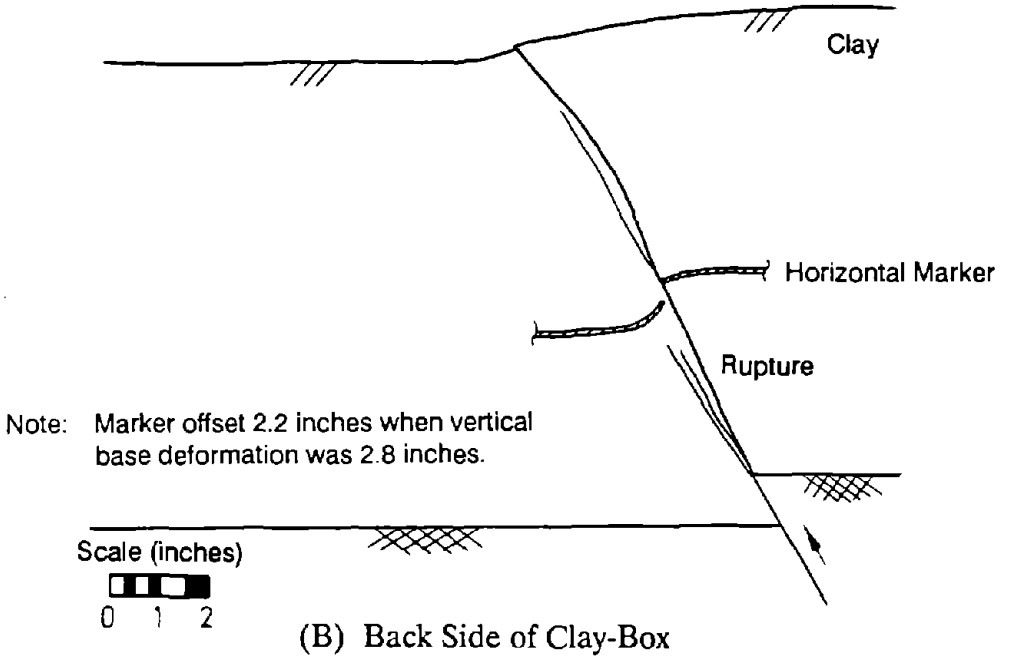

(B) Back Side of Clay-Box

Figure 6-22: RESULTS OF MODEL TEST #9: 60° THRUST FAULT; CLAY WITH AVERAGE FAILURE STRAIN

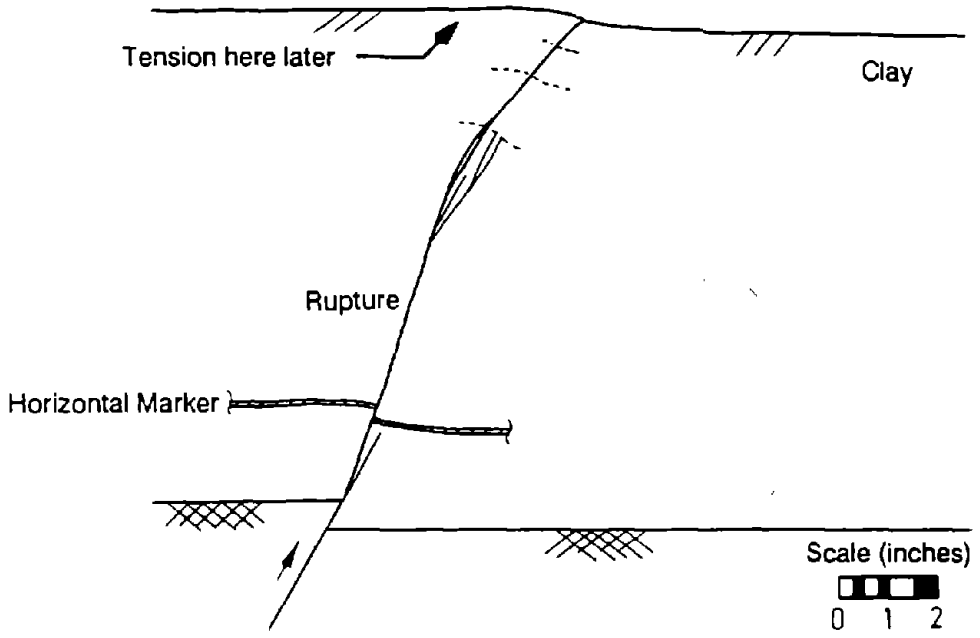

(A) Front Side of Clay-Box

Normalized Vertical Base Deformation When Rupture Propagated to Surface $(d_b/D_S) \approx$ 6%

Failure Strain of Soil ≈ 6% - 7%

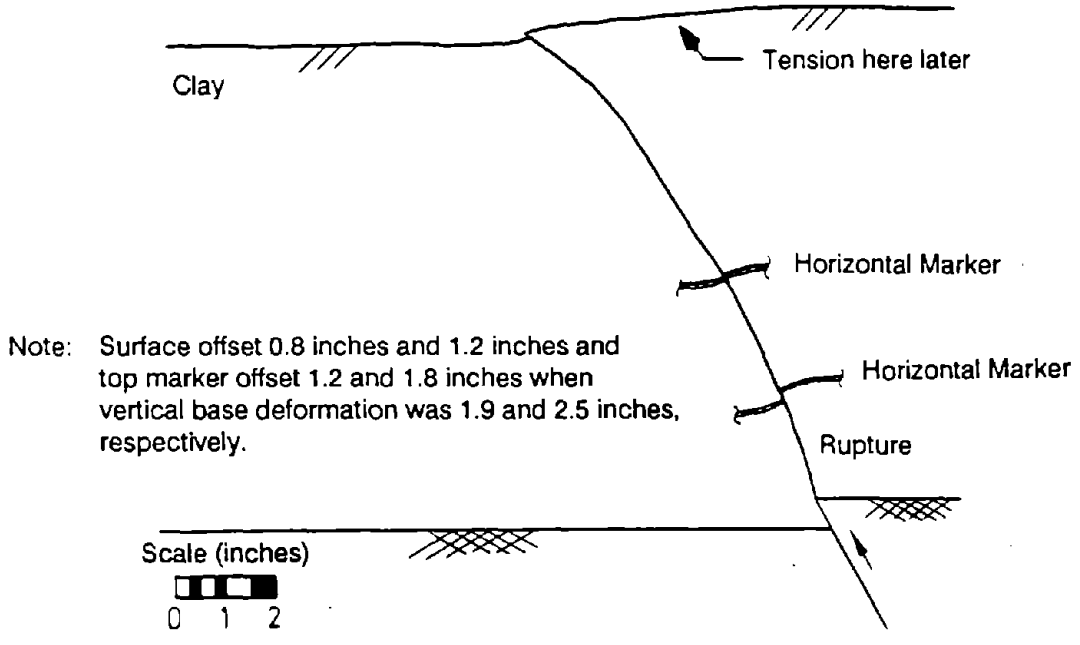

Note: Surface offset 0.8 inches and 1.2 inches and top marker offset 1.2 and 1.8 inches when vertical base deformation was 1.9 and 2.5 inches, respectively.

(B) Back Side of Clay-Box

Figure 6-23: RESULTS OF MODEL TEST #10: 60° THRUST FAULT; CLAY WITH LOW FAILURE STRAIN

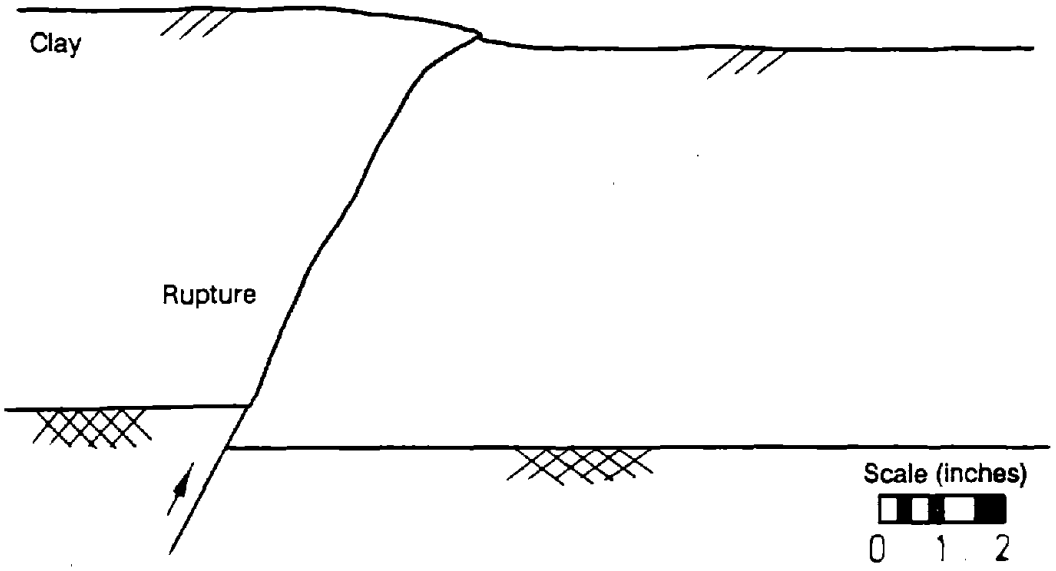

(A) Front Side of Clay-Box

Normalized Vertical Base Deformation When Rupture Propagated to Surface (d_b/D_S) ≈ 11% - 13%

Failure Strain of Soil ≈ 14% - 16%

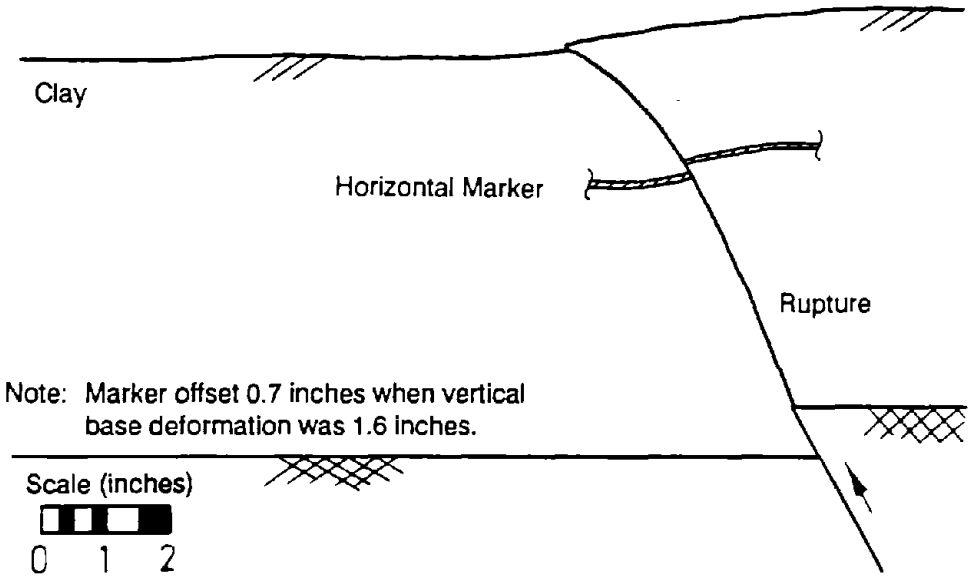

(B) Back Side of Clay-Box

Figure 6-24: RESULTS OF MODEL TEST #11: 60° THRUST FAULT; CLAY WITH HIGH FAILURE STRAIN

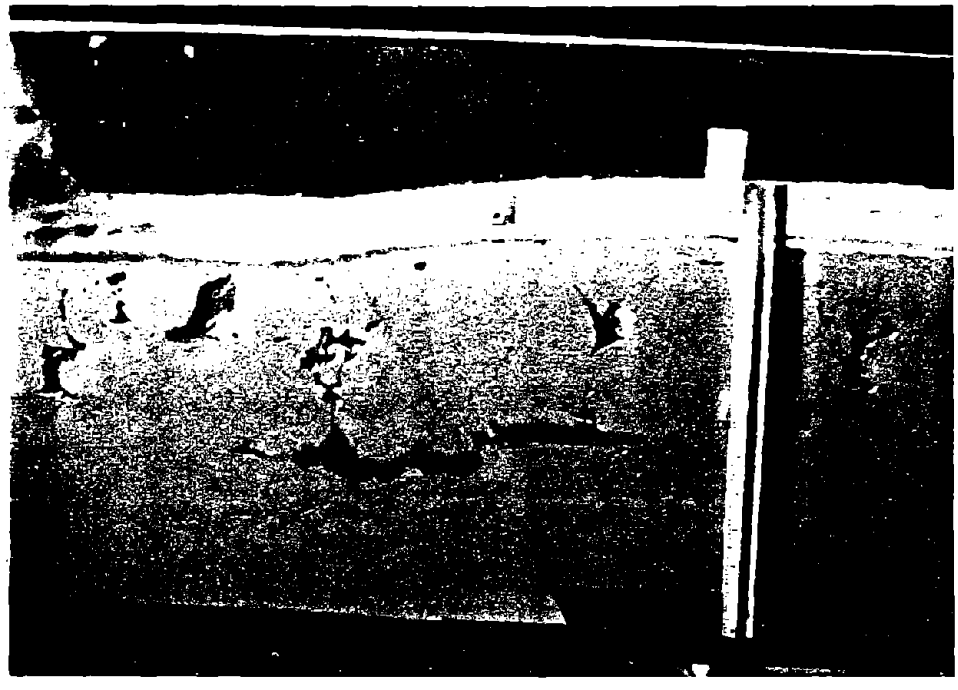

(A) 1.4 inches of Vertical Base Displacement

(B) 2.8 inches of Vertical Base Displacement

Figure 6-25: FAULT RUPTURE PROPAGATION THROUGH SATURATED CLAY. MODEL TEST #9: 60° THRUST FAULT

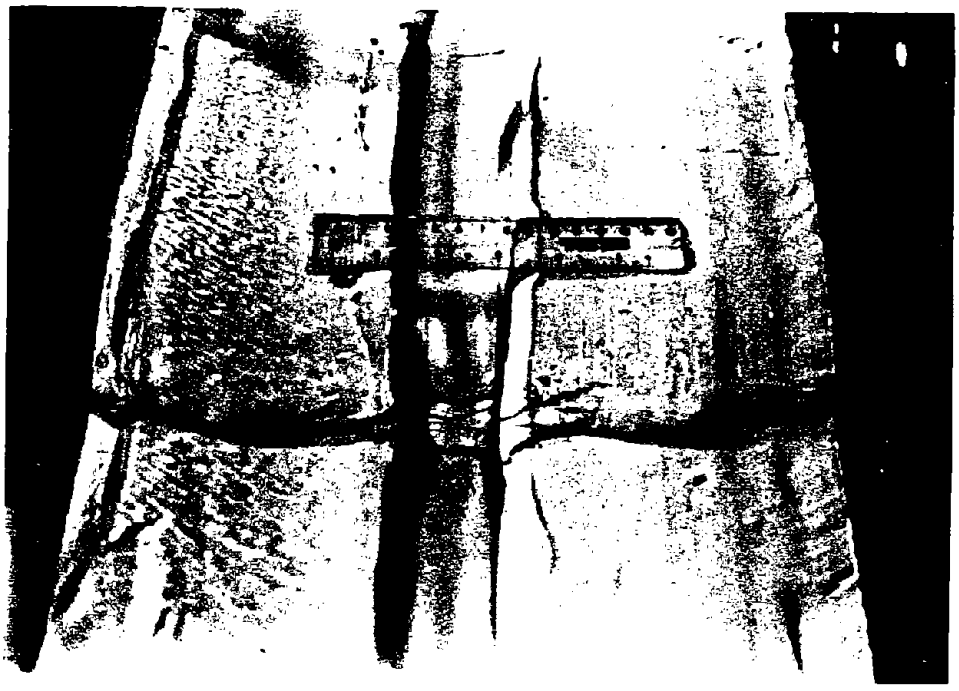

(A) Stage 1

(B) Stage 2

Figure 6-26: DISTURBANCE OF THE CLAY SURFACE WITH INCREASING BASE DEFORMATION. MODEL TEST #9: 60° THRUST FAULT

strains. Model test 9 was performed under conditions similar to those of the previous eight model tests. The clay under these conditions failed in shear in unconfined compression tests at axial strains of 10% to 12%. A vertical base deformation (offset) of 10% to 11% of the depth of the clay layer was required to propagate the rupture to the top surface. Model test 10 was performed under essentially identical test conditions except that the model clay was left undisturbed for 24 hours before testing (without a reduction in water content). As shown in Figure 6-7, the model clay stiffened when allowed to sit undisturbed for a period of 24 hours. Under these conditions, the model clay failed in the unconfined compression test at an axial strain of 6% to 7%. Likewise, a vertical base deformation (offset) of only 6% of the depth of the clay layer was required to propagate the rupture through the more brittle clay material employed in model test 10. Finally, model test 11, which was performed at a slow rate of base deformation, required a vertical base deformation (offset) of 11% to 13% of the depth of the clay to form a shear rupture through the saturated clay overlying the base fault. Unconfined compression test data indicated that the model clay behaved in a more ductile manner at slower rates of strain.

Figure 6-27 illustrates the previous points more clearly. In this graph, the results from the model tests (#9, #10, #11) utilizing materials with different failure strains are plotted. The magnitude of the vertical base offset required to propagate the shear rupture zone through the soil to the ground surface divided by the height of the clay layer is plotted against the axial failure strain of the clay materials in unconfined compression tests. The data indicates that as the soil overlying the bedrock fault displacement becomes more brittle (i.e. the failure strain decreases), the shear rupture zone in the soil propagates further at a given magnitude of base offset (i.e. the normalized base offset required to propagate the shear rupture zone to the ground surface decreases). Although additional work is

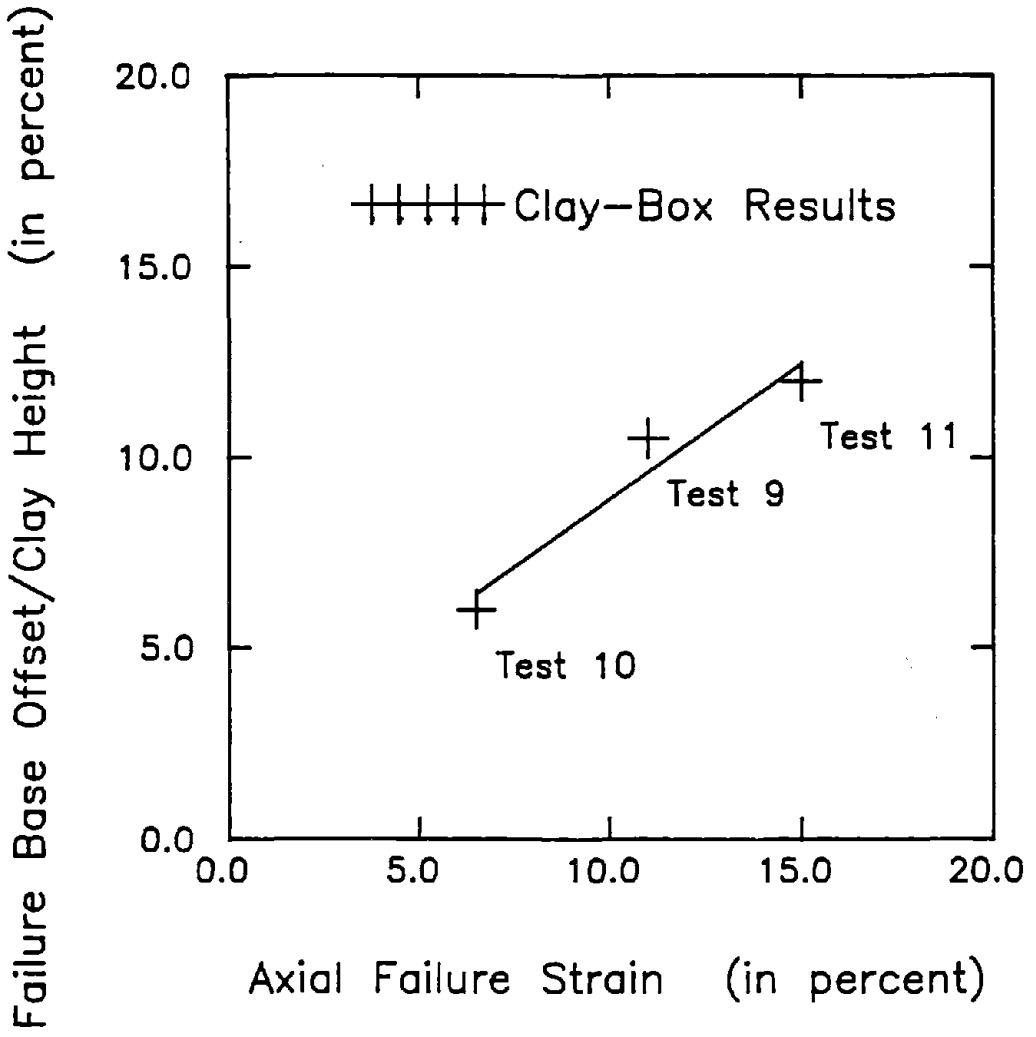

Figure 6-27: RELATIONSHIP BETWEEN THE NORMALIZED BASE OFFSET REQUIRED TO PROPAGATE THE SHEAR RUPTURE ZONE TO THE GROUND SURFACE AND THE FAILURE STRAIN OF THE SOIL

required to validate the use of such a graph, the general trends of the plotted model test results seem appropriate.

6.4 Lessons to be Learned from 1 g Small-Scale Model Testing of Fault Rupture Propagation through Saturated Clay

In the past, a number of 1 g small-scale models employing a weak kaolinite-bentonite clay mixture have reasonably portrayed the essential characteristics of the performance of full-size prototype earth structures. It is therefore not surprising that in this application, the 1 g small-scale model tests provided valuable insights into the base deformation problem. The results of the model tests of fault rupture propagation through saturated clay compared favorably with the general behavior of fault rupture propagation phenomenon as documented in the reviewed field studies described in Chapter Three. Furthermore, the results from these model tests agreed with the published results of other model studies of fault rupture and anchor pull-out described in Chapters Three and Four. Therefore, the 1 g small-scale model experiments were judged to reasonably correctly represent the behavior of a natural saturated clay soil overlying a displaced bedrock fault.

The kaolinite-bentonite clay mixture satisfied the principal mechanical requirements of model similitude. The critical properties of the clay could be controlled to provide a model material with reproducible, consistent characteristics of behavior. The model clay's water content clearly defined its undrained shear strength. Moreover, the model clay and testing procedures could be adjusted to vary the stress-strain behavior of the model material, in particular, its failure strain. The model clay performed best in the fault rupture model tests at water contents from 110% to 150%. At lower water contents, the clay was difficult to handle. At higher water contents, the clay exhibited a more viscous type of behavior at failure and distinct failure planes were difficult to observe. Models which were 6 to 12

inches in height provided good results. Given the undrained shear strength of the model clay material (i.e. around 30 psf), the clay-box model tests represented average strength prototype clay deposits (i.e. 2000 to 4000 psf) which were on the order of 50 to 150 feet deep. The "PAM" low-friction interface material successfully eliminated the problem of the clay's high wall adhesion and sufficiently reduced the disturbance caused by side wall boundary effects. Hence, the development of the shear rupture zone and tension zones in the clay overlying a displaced bedrock fault could be readily observed.

Unconfined triaxial compression tests adequately defined the clay's stress-strain characteristics. The undrained shear strength values from carefully performed unconfined compression tests agreed with the strength values reported in previous studies. The laboratory testing program showed that the stress-strain behavior of the clay mixture was not necessarily brittle as reported in previous studies. Instead, at different water contents, at different times between placement and testing, and at different strain rates, the model clay exhibited both brittle and ductile behavior. In studying fault rupture propagation with eventual application to the problem of fault rupture propagation through earth dams with core sections composed of saturated compacted clay materials, the model clay was judged to adequately represent the prototype material when its axial strain to failure remained within the range of 5% to 15%. Hence, the majority of the tests were performed with the model clay exhibiting a failure strain of around 10%.

The results from the 1 g small-scale model tests indicated the following. Initially, a highly stressed region of soil formed above the upthrown block. Shear fractures were typically observed in this region. This constituted the "inverted footing" stage of failure described in Section 4.2 and illustrated in Figure 4-7. At larger base deformations (offsets), kinematics began to control the development of the rupture zone. The main rupture typically propagated up along the projection

of the underlying base fault plane and bent over toward the downthrown block as the rupture approached the surface of the clay. This constituted the "anchor pull-out" stage of failure illustrated in Figure 4-7. In summary, thrust faults decreased in dip near the ground surface, and normal faults increased in dip near the ground surface.

In several of the model tests, nearly horizontal shear fractures formed in the shear rupture zone during base deformation. These horizontal shear fractures were oriented roughly perpendicular to the main rupture planes. Hence, they appeared to be the complementary shear planes of the primary shear planes. They were more common in the top half of the thicker clay layers. Often the horizontal complementary shear fractures developed before the main rupture reached the top of the clay layer. This is potentially very important. Because an earth dam is constructed in layers of compacted soil, horizontal planes of weakness already exist throughout the core section. Higher rates of seepage typically occur along these earth "bedding planes". The displacement of a bedrock fault might produce shear failure along these established horizontal planes of weakness, and hence, create a potentially serious condition where significant leakage initiates along the contact between compacted layers. Further study of this problem is warranted.

Another grave concern is the potential development of tension zones in the core of an earth dam. In fact, zones of extension are of concern because if the minor principal stress is sufficiently reduced, hydraulic fracturing can occur. At large base deformations, tension fractures were clearly observed in an extension zone at the clay surface which developed above the upthrown block. Sufficient freeboard could accommodate these open tension fractures without threatening the stability of the earth dam. The potential development of extension zones or tension zones within the clay core section is of greater concern. Although difficult to observe, a number of model test results indicated that a local extension or

tension zone formed above the downthrown block adjacent to the bedrock fault. Tension was not apparent in this region until larger base deformations occurred (i.e. base deformations (offsets) sufficient to propagate the shear rupture up near the surface of the clay layer). Further study of this problem is warranted.

The fault rupture propagation model tests clearly indicate that the amount of differential movement across a distinct failure plane decreases as the rupture propagates through the soil. The remainder of the base offset is accommodated by the down-warping of the ground surface above the upthrown block, and internal deformations within the soil. Since the saturated clay under undrained loading conditions deforms at constant volume, the surface of the clay away from the rupture zone moves up or down an amount equal to the upthrown or downthrown base movement. Similarly, the change in elevation of the crest section above the saturated clay core of an earth dam away from the fault zone must equal the change in elevation of the bedrock. Thus, the earth dam design must provide enough freeboard to handle the potential decrease in the crest elevation.

One of the primary findings of the model study is the realization that the rate of fault rupture propagation through soil is strongly influenced by the failure strain of the soil. The bedrock fault does not instantaneously produce a rupture zone through the overlying soil deposit. As described earlier, the rupture propagates up toward the ground surface with increasing base deformation (offset). The rate at which it propagates, however, is determined principally by the failure strain of the soil. Moreover, the axial failure strain of unconfined triaxial compression tests adequately defines the saturated clay's failure strain. As shown in Figure 6-27, the normalized base offset required to propagate the shear rupture zone to the ground surface of the clay layer increases as the failure strain of the clay employed in the model tests increases. Further work is warranted to validate and extend this finding. This relationship could be used by engineers to develop

preliminary estimates of the extent of the zone of saturated clay materials overlying a bedrock fault disturbed by a given displacement across the base rock fault.

Although not useful in this study of fault rupture propagation of base rock faults at various orientations, the horizontal top and base clay friction model described in Section 6.3.3 could prove extremely useful in simple model studies of problems where the principal direction of soil movement is aligned with the gravitational force. The 1 g small-scale model study, however, provided important insights to improve the level of understanding of the effect of tectonic movements on stresses and deformations in earth embankments.

CHAPTER SEVEN:
PRELIMINARY EVALUATION AND SELECTION OF THE NUMERICAL ANALYSIS METHOD

7.1 Introduction

The 1 g small-scale physical model tests of fault rupture propagation through saturated clay provided valuable insights into this class of problem. The physical model testing, however, had some limitations. For example, it took a considerable amount of time and care to perform the physical model tests; hence, a large number of tests could not feasibly be performed. The clay used in the model tests was fairly homogeneous. In many cases, however, the clay in an earth embankment might tend to increase in strength and stiffness with increasing depth below the ground surface . Although controlling the conditions of the model tests allowed for a more in-depth study of some of the parameters influencing the process of fault rupture propagation, a number of details could not be explored adequately. For instance, the physical model tests could not reasonably determine when the minor principal stress within the clay material might be reduced to a value low enough to permit the initiation of hydraulic fracturing.

Numerical analyses of the fault rupture propagation phenomenon might provide answers to a number of the questions not resolved through the physical 1 g small-scale model testing program. In most numerical analyses, the values of the critical soil parameters which define the load-deformation and volume-change behavior of the soil can be precisely controlled. The soil parameters can usually be varied spatially to adequately represent the characteristics of the actual soil profile. The magnitude of induced stresses and deformations can be calculated. Multiple analyses with slightly different values of the critical soil parameters can determine the sensitivity of the results to variations in these soil parameters. Appropriate

numerical analyses might thus provide important insights into the fault rupture propagation phenomenon.

In Chapter One, a number of specific questions were identified as critical to understanding the effects of tectonic movements on stresses and deformations in earth embankments. These six critical questions are repeated here as they will be the principal focus of the numerical studies of fault rupture propagation through soil:

(1) What is the extent of the likely shear rupture zone with increasing magnitudes of base deformation (or offset)?
(2) What will be the extent of tension zones or zones of hydraulic fracturing with increasing magnitudes of base deformation?
(3) How much reservoir water could leak through disturbed core and filter zones or through a disturbed foundation, and might this result in uncontrolled internal erosion?
(4) How might the base deformation damage the slopes and crest of the earth dam?
(5) Given the potential hazards associated with fault rupture propagation through an earth dam, what are the characteristics of the dam core material which can best mitigate these hazards?
(6) What other steps or design features are necessary for the safe construction of a dam over a potentially active fault?

In this chapter, the results of the preliminary finite element analyses of the fault rupture propagation phenomenon will be presented. Initially, a number of numerical analysis techniques will be explored to note the advantages and disadvantages of applying various numerical methods to this class of problem. The limitations of the finite element method will become apparent. Nevertheless, it

will be shown that the finite element method can be applied to this class of problem provided that the soil's nonlinear, stress-dependent, stress-strain behavior is adequately modeled. Linear elastic analyses were first performed to identify the critical characteristics of fault rupture propagation through overlying soils without the bias produced when employing a complex soil constitutive model with its predetermined failure criterion and rules for soil behavior. Next, a linear elastic-perfectly plastic constitutive model was employed in the finite element method to ascertain its suitability. The Scott and Schoustra (1974) finite element study, which Scott (1987) later concluded to be incorrect, utilized a linear elastic-perfectly plastic soil constitutive model. Finally, incremental, nonlinear elastic analyses were performed which provided significantly better predictions of observed behavior. Initially, the nonlinear finite element method was employed to analyze the behavior of dry, cohesionless materials since most previous well-documented physical model tests employed dry cohesionless materials. In the next chapter, the nonlinear finite element analyses will be used to study fault rupture propagation through saturated clay. In the final section of this chapter, Section 7.6, lessons to be learned from the preliminary numerical analyses of fault rupture propagation through soil are discussed.

7.2 The Numerical Analysis Approach

Numerical methods allow the engineer to investigate a number of aspects of the fault rupture propagation phenomenon which are difficult to study from the examination of case histories or the conduct of physical model tests. Whereas, in physical model studies, the boundary conditions and the prototype material are represented by a small-scale testing apparatus and materials which model the critical characteristics of the behavior of the prototype soil, numerical analyses employ mathematical models of the problem's boundary conditions and the

prototype soil to define the problem. The boundary conditions and the soil constitutive model help produce a system of equations which can be solved by various solution algorithms. The system of equations is established by satisfying some combinations of force equilibrium, displacement compatibility, and the appropriate force-displacement relationship for the material in question. The numerical analysis approach allows for the precise control of the model used to represent the behavior of the soil and the imposed boundary conditions. Of course, the accuracy and the reliability of any numerical approach depends on the validity of the mathematical conceptualization of the critical aspects of the problem. If the limitations of the assumptions imposed in the problem definition are understood, the numerical analyses can assist the engineer in attempting to understand the problem in question.

Three numerical approaches were reviewed in the course of this research to determine their suitability for the analysis of fault rupture propagation through overlying soils. They were: the finite element method, the finite difference method with dynamic relaxation, and the discrete element method. Each of these numerical analysis methods were described previously during the review of literature (See Section 3.3.3). In the early stages of this research program, each method was considered for possible use in the analysis of the fault rupture propagation problem.

The discrete element approach intuitively looks promising. A soil mass is not a continuum. Instead, it is an assemblage of finite-sized particles. Interparticle forces fundamentally determine the observed macroscopic behavior of soil. Moreover, once a shear or tension crack (i.e. a discontinuity) develops within the soil mass it typically becomes difficult to reliably apply a numerical approach based on the principles of continuum mechanics. Although the discrete element method might become quite useful in the future, currently it cannot be practically applied

to the fault rupture propagation problem. This analytical technique is new, and hence, not well-validated. To realistically model a soil mass, a large number of discrete elements are necessary, and even with the use of a mainframe computer, the computational effort is considerable. Finally, the discrete element procedures reviewed could be used to predict deformation patterns, but they did not provide reliable stress information (e.g. locate regions where the minor principal stress was reduced to a value low enough to allow for the initiation of hydraulic fracturing). Therefore, it was judged that the discrete element method cannot be practically applied to the fault rupture propagation problem at this time.

Scott (1987) felt that the explicit finite difference method with dynamic relaxation was potentially superior to the implicit finite element method in the analysis of soil failure. Dynamic relaxation is a technique which assumes that a static equilibrium solution can be found by computing the large-time limit of a damped dynamic problem (Otter et al., 1966). Scott reasoned that since unstable stress-strain relationships could be employed in the finite difference method with dynamic relaxation, and because the system of equations could be solved explicitly, the strain softening post-peak strength behavior of some soils could be readily handled without the numerical instabilities which often occur in the more popular finite element method. The finite difference method with dynamic relaxation produced deformed meshes which agreed reasonably well with the deformation patterns observed in centrifuge model tests of failed slopes and fault rupture propagation, but the numerical approach possessed critical shortcomings. As discussed previously in Section 3.3.3, this numerical method often predicted failure to occur at gravitational loads 2 to 4 times larger than that observed in the centrifuge model tests. Hence, in these cases, calculated stress distributions would be erroneous. Being a relatively novel approach to the solution of geotechnical problems, the finite difference method with dynamic relaxation is also not well-

validated. Thus, it was judged that this numerical method cannot be practically applied to the fault rupture propagation problem at this time.

The finite element method thus became the leading choice for the numerical method to be employed in this research. The finite element method has its merits. Because of its relative simplicity, availability, and flexibility, the finite element method has been applied to a wide range of geotechnical problems. Hence, its use in many areas is well-validated. In fact, the large majority of the previous studies of the fault rupture propagation phenomenon employed the finite element method. In addition, the large majority of the previous studies of topics closely related to fault rupture through soils (such as the anchor pull-out problem) have employed the finite element method.

The finite element method has been described in detail in a number of text books (e.g. Zienkiewicz, 1977). In the finite element method, the continuum is "discretized" into a number of individual finite elements. Within each of these finite elements, a displacement function is assumed to define the variation of displacements across the element in terms of nodal displacements. Hence, the displacements at the nodal points become the unknown variables of the problem. Given the constitutive relationship used to describe the material, the force-displacement relationships at the nodes of the finite element are formulated. The principle of virtual displacement can then be used to develop the element stiffness matrix for each finite element. In the displacement approach, the equilibrium equations at the nodes are assembled to form a global stiffness matrix. The boundary conditions (established nodal forces, displacements, or constraints) are imposed, and the global force-displacement equations which utilize the global stiffness matrix can be solved to determine the unknown nodal displacements. From the nodal displacements, the element strains, and, in turn, the element stresses can be calculated from the derivative of the assumed displacement

function and the defined stress-strain constitutive relationship, respectively. Finally, but most importantly, the results must be interpreted to provide the engineer with an approximate solution (but, hopefully, a practically acceptable solution) to a defined problem which, in turn, can be used to provide insights into a more complex field problem.

At this time, it is worthwhile to note the lessons learned from the review of previous studies which employed the finite element method to analyze fault rupture propagation or closely related topics. First of all, despite its limitations, the finite element method can be successfully applied to analyze the development of failure in a soil mass overlying a displaced base section. Although exact representation of all of the aspects of the soil's behavior may not be possible, the finite element analyses can be used as a tool to improve our understanding of the problem. In the finite element model, the left and right vertical boundaries need only extend a distance of three times the height of the soil layer away from the location of the base rock fault. All of the numerical models reviewed utilized an incremental solution technique. As the soil approached the failure condition, gradually decreasing load or displacement increments were imposed to maintain accuracy. Smaller elements were concentrated in the expected zone of failure to minimize the overestimation of the width of the actual failure planes. Localization of failure in narrow zones was difficult to achieve in the finite element method as the failed zone usually widened as it propagated upward toward the ground surface. In fact, it appears that the soil must be modeled as a strain softening material to localize the failure in the soil mass (Rousselier, 1979). In the finite element method, however, it is difficult to model strain softening soil behavior because this often leads to numerical instability during the solution of the equilibrium equations. At least the zone within which the distinct failure planes develop can be predicted reasonably well by proper FEM analyses.

The selection of the soil constitutive model to be employed in the finite element method appeared to be one of the most important considerations in performing sound FEM analyses. Results of finite element analyses of fault rupture propagation or closely related topics (e.g. anchor pull-out behavior) employing nonlinear stress-strain soil models agreed reasonably well with observed behavior. Linear elastic-perfectly plastic soil models did not consistently produce acceptable results. Modeling the dilatant behavior of dense, cohesionless materials was important to obtaining reasonable finite element results for this special case. Nondilatant materials, however, could be modeled satisfactorily with simpler soil constitutive models. The previous finite element studies showed that it was relatively important to model the soil as a "no-tension" material, and that the finite element results were somewhat sensitive to the tension failure criterion selected.

The finite element results were also sensitive to the soil parameters employed in the soil constitutive model. The coefficient of lateral earth pressure at rest appeared to be a sensitive parameter. In fact, results from finite element analyses by Walters and Thomas (1982) (See Section 3.3.3(e)) showed that even with a very sophisticated, complex soil constitutive model, minor variations in the coefficient of lateral earth pressure at rest parameter produced significant variations in the results of the analyses. Hence, it may not be productive to employ a complex soil constitutive model with a large number of soil parameters if the results are sensitive to basic parameters such as K_o which the engineering profession cannot typically determine within an accuracy of better than about ± 20%. In addition to the coefficient of lateral earth pressure at rest, the soil parameters which most significantly describe the soil's stress-strain behavior and volume-change behavior influence the development of failure in the finite element analyses. Sufficient care should then be exercised in modeling the soil's stress-strain behavior (e.g. failure strain, strength, and variation of soil stiffness at

different stress levels) and the soil's volume-change behavior (e.g. Poisson's ratio and angle of dilation).

Given what was learned from this review and evaluation of previous studies employing the finite element method, it is evident that the selection of the soil constitutive model to be employed in the numerical method is rather important. The soil constitutive model employed in the numerical analyses should be as simple as possible, yet it should model the essential characteristics of the behavior of the soil in base rock fault rupture propagation through overlying soils. A number of soil constitutive models were reviewed for possible use in the finite element analyses of this study of fault rupture propagation. They can be categorized under four general headings: (1) linear elastic; (2) linear elastic-perfectly plastic; (3) nonlinear hyperbolic elastic; and (4) nonlinear elasto-plastic with work hardening plasticity. Each soil constitutive model has advantages and disadvantages which will be discussed later in more detail.

Two important distinctions, however, will be made now. The soil's load-deformation behavior can be modeled with either a linear or nonlinear stress-strain relationship. A linear stress-strain relationship is obviously easier to implement, but it is well known that the typical soil's load-deformation behavior is highly nonlinear at or near failure. Secondly, the soil can be modeled as elastic or plastic. With elastic deformation, the principal axes of the strain increment coincide with the principal axes of the stress increment; whereas, with plastic deformation, the principal axes of the strain increment coincide with the principal axes of the overall stress (not the stress increment). Soil strength tests have shown that soils deform elastically at lower stress levels and deform plastically at or near failure (Roscoe et al., 1967; Roscoe, 1970; Hong and Lade, 1989). In selecting a soil constitutive model, these two important distinctions should be considered.

Another important consideration in the selection of a soil constitutive model is the choice of the failure criterion to be employed in the soil constitutive model. Traditionally, the Mohr-Coulomb failure criterion has been the criterion most frequently employed in the analysis of geotechnical problems. As the review of previous studies of fault rupture propagation revealed, however, there is much debate regarding the validity of the Mohr-Coulomb failure criterion in determining the orientation of the shear rupture surface through soil. As Roscoe pointed out in the Tenth Rankine Lecture (Roscoe, 1970), the Mohr-Coulomb failure criterion relies on stress characteristics (e.g. the angle of friction, ϕ) to define the orientation of the shear rupture plane. The failure plane is oriented at an angle $\beta = 45^\circ - \phi/2$ to the major principal stress, σ_1. Through his research, however, Roscoe found that for experiments employing models composed of dry sand, velocity characteristics (e.g. the angle of dilation, v) more accurately predict the orientation of the shear rupture plane. Shear rupture planes develop along zero extension lines which are oriented at an angle of $\beta = 45^\circ - v/2$ to the major principal strain rate, $\dot{\epsilon}_1$. Thus, if the axes of the major principal stress and of the major principal strain increment coincide (which is believed to be essentially true for soils at failure, "plasticity"), the angle, Θ, between the stress characteristics and the velocity characteristics in the soil mass is: $\Theta = \frac{1}{2}(\phi - v)$.

Attempts to resolve the debate as to whether stress characteristics or velocity characteristics best predict the orientation of the shear rupture surface have been inconclusive. For example, several articles published in the Proceedings of the Roscoe Memorial Symposium (Parry, 1972), attempted to resolve the debate without success. More recently, Vardoulakis, Goldscheider and Gudehus (1978) and Vardoulakis (1980) have claimed that neither of these criteria govern (that is, neither the stress characteristic: $\beta = 45^\circ - \phi/2$ oriented to the major principal stress, or the velocity or kinematic characteristic: $\beta = 45^\circ - v/2$ oriented to the

major principal strain rate actually predict the orientation of the shear failure plane in dry sand). Instead, their experimental evidence suggests that the truth lies between the two predictions with the stress characteristics overestimating the angle β, and the velocity characteristics underestimating the angle β, where β is the orientation of the failure plane relative to the major principal stress and the major principal strain increment which are believed to coincide in a soil mass at failure (plasticity).

In tests of dry, dense sands where most of the studies reviewed have focused, the difference between the angle of friction, ϕ, and the angle of dilation, v, can be significant. It follows that the difference between predictions from stress characteristics and kinematic characteristics ($\Theta = \frac{1}{2} (\phi - v)$) can be significant. For most cases, however, the differences between the angle of friction and angle of dilation may not be significant relative to the limits of accuracy in the determination of these two soil parameters. In addition, most of the authors who criticized the consequence of accepting the Mohr-Coulomb failure criterion, namely, that the shear rupture planes are oriented at an angle $\beta = 45° - \phi/2$ to the major principal stress, never questioned if the Mohr-Coulomb failure criterion adequately predicted when failure in any element of soil did occur (Roscoe, 1970; Harkness, 1972; Frydman, 1974). Therefore, it appears to be reasonable, especially for the case of an undrained analysis of saturated clay, to employ the Mohr-Coulomb failure criterion.

As Louderback (1937) asserted (See Section 2.2.2), in seismic regions such as California, the most satisfactory topographic features for a dam are typically fault-controlled valleys. In the fault-controlled valleys, the river often follows the predominant plane of weakness, the fault trace. For example, in the majority of the examples of earth dams built across potentially active faults presented in Table 1-1, the fault is oriented perpendicular to the longitudinal axis of the dam. Given

the fact that the fault will often traverse the dam's longitudinal axis, three dimensional (3-D) effects might be significant in the analysis of fault rupture propagation through earth embankment dams. On the other hand, since reliable analyses of fault rupture propagation through either saturated clay or earth embankment dams have not been performed, it might be prudent to initially analyze the simpler two-dimensional (2-D) case. For instance, previous analyses of fault rupture propagation (all 2-D analyses) have found that a large number of elements must be employed, with smaller elements concentrated in the region above the bedrock fault, to obtain satisfactory results from the finite element analyses. A 3-D finite element analysis would then require an even larger number of elements to define the problem, and hence, result in an inordinate amount of computational effort. Furthermore, the interpretation of the results would be difficult.

Two-dimensional finite element analyses of fault rupture propagation through overlying soils might provide practical insights in many cases. In situations where the dam length to height ratio is relatively large (i.e. $L/H > 6$) and the dip-slip fault traverses the dam near the middle section of the dam length, a 2-D plane strain analysis of a vertical plane through the core section parallel to the dam's longitudinal axis might provide acceptable results. Of course, 2-D plane strain analysis of the dam's cross section would be appropriate in cases where a dip-slip fault is oriented parallel to the dam's longitudinal axis (as is the case for the Cedar Springs Dam). Moreover, the 2-D analyses of dip-slip fault movements would address what the engineering community believes to be the most dangerous situation - dip-slip fault offsets (Swiger, 1978). 2-D plane strain analyses were thus judged to be suitable for gaining insight into the general problem of fault rupture propagation through overlying saturated clays. Therefore, 2-D finite element analyses were performed, realizing that additional research would be required to

extend the findings from this study to problems where 3-D effects were significant (e.g. a strike-slip fault movement which is oriented perpendicular to the dam's longitudinal axis where the dam is situated in a steep, narrow canyon).

The finite element formulation employed in this research is based upon the usual assumption that strains are infinitesimal. The exact definition of strain contains second-order nonlinear terms which for most problems are typically small, and hence, can be ignored in the small strain approach. Additionally, the small strain approach calculates the strain using the original undeformed geometry of the finite element mesh. The small strain approach has been shown to be acceptable in the majority of geotechnical problems. A refinement of the small strain approach is obtained by approximating the finite strain solution by loading the mesh incrementally (using the infinitesimal strain formulation to solve for each increment) and updating the geometry of the mesh after each increment. In this method, the natural strain or logarithmic strain, which is the summation of strain increments each of which is calculated on the deformed mesh geometry, is now used. Second-order nonlinear terms of the exact strain-displacement definition are still ignored. A number of studies have found that this approach gives acceptable solutions to most geotechnical problems (Davis and Booker, 1975; Carter et al., 1977; Britto and Gunn, 1987; Pender, 1989). The refined small strain approach based on the natural strain definition will also be employed in this study to examine differences from analyses employing the infinitesimal strain formulation. A more exact finite strain formulation which incorporates the second-order nonlinear terms of the strain-displacement relationship should be necessary only when very large strains occur (e.g. solution of a pile driving problem where strains are greater than roughly 100%; Pender, 1989). Since previous small-scale model studies and the clay-box model tests of this study have shown that a base deformation of on the order of 1% to 15% of the height of the soil overlying the

base fault is required to propagate the shear rupture upwards to the ground surface of the soil, an exact large strain formulation in the finite element method may not be required to analyze fault rupture propagation through overlying soil.

One of the important lessons to be learned from the application of a numerical method to any geotechnical problem is the value of a graphic post-processor. Since up to 80% of an analyst's time during finite element studies can be required to check a finite element mesh and to interpret the results from the analysis, the graphic post-processor can dramatically improve the finite element analyst's effectiveness and efficiency. For instance, in the same amount of time, a large number of finite element analyses may be performed when using a graphic post-processor allowing time for a larger number of parameter sensitivity analyses. During this research, the author has helped develop two graphic post-processors which will be used to present some of the results from the finite element analyses. In particular, a modification of Dr. R. L. Taylor's PCFEAP computer program, named FEAPPLOT, proved invaluable during the course of this research.

7.3 Linear Elastic Analyses of Fault Rupture Propagation

As discussed previously in Section 7.2, there has been considerable debate as to which soil constitutive model and which failure criterion are most appropriate for use in the finite element method when analyzing geotechnical problems. The results from any finite element analysis will necessarily depend on the soil constitutive model employed in the finite element method. So as not to unduly bias the preliminary finite element analyses of fault rupture propagation through overlying soils, a simple linear elastic soil constitutive model was first employed. The linear elastic analyses employed no failure criterion and the principal limitations of a linear elastic soil model are clearly known. It is often useful to first analyze complex geotechnical problems with very simple models of soil behavior to

ensure that the problem is defined properly, and that further refinements of the soil constitutive model do not produce unknown or undesirable deviations from the simpler analyses. In this study, the primary purpose of the linear elastic finite element analyses was to perform an unbiased search for a way to predict the development and orientation of the shear rupture zone in the soil overlying a base rock fault which had displaced.

Dr. Taylor's powerful finite element analysis computer program, PCFEAP, was utilized in the linear elastic analyses of fault rupture propagation (Taylor, 1987(a); Taylor, 1987(b)). The program PCFEAP was modified for these studies to employ the standard geotechnical sign convention (e.g. compressive stresses are positive) in lieu of the usual structural mechanics sign convention, and to include initial at rest earth stresses in the analyses. Additionally, the graphics post-processor was modified so additional results such as strain values and the principal stress ratio could be plotted. The modified PCFEAP program was re-validated, and its results were shown to agree closely with the results from a validated computer program, FEADAM (Duncan et al., 1984), and with known elastic solutions to well-defined problems.

Again, the primary aim of the linear elastic analyses of fault rupture propagation was to perform an unbiased search for a way to predict the orientation of the shear rupture zone in the deformed soil mass. Figure 7-1 illustrates how the linear elastic finite element analyses might be used to predict the orientation of a shear rupture zone in a deformed soil specimen. In this instance, a simple analysis of a triaxial compression test is performed. The soil was arbitrarily defined by the following parameters: E = 300,000 psf, ν = 0.4, and σ_i = 100 psf (except for one weakened element which was used to initiate failure where E = 250,000 psf). As shown in Figure 7-1, the contour plots of maximum shear stress, maximum shear strain, and the principal stress ratio all indicate the expected orientation of the

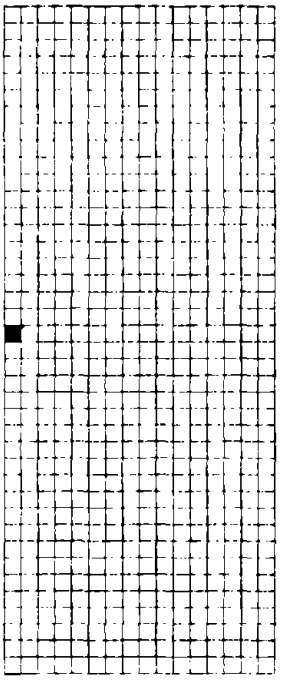

(A) Finite Element Mesh (solid element indicates location of weakened element)

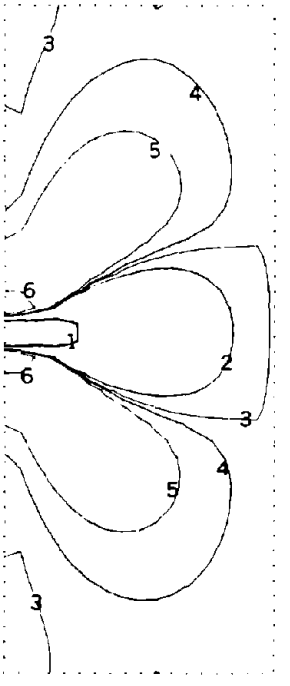

(B) Principal Stress Ratio at ϵ_a = 1%

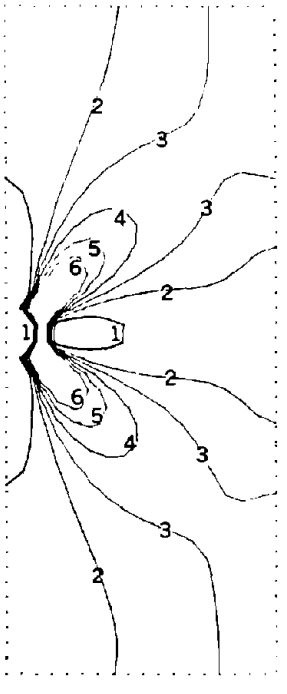

(C) Maximum Shear Stress (psf) at ϵ_a = 1%

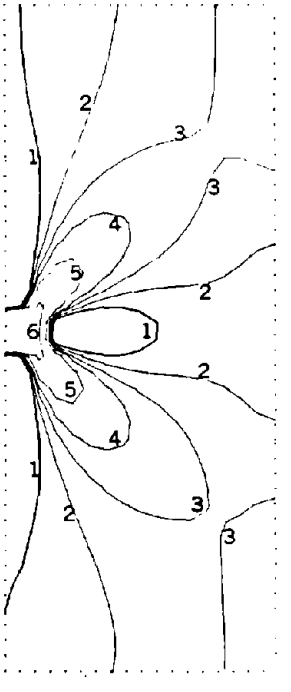

(D) Maximum Shear Strain at ϵ_a = 1%

Figure 7-1: ELASTIC FINITE ELEMENT ANALYSIS OF A TRIAXIAL COMPRESSION TEST

failure plane in a nonfrictional material (i.e. the angle of the failure plane to the direction of major principal axial strain in the specimen, $\beta = 45°$). Additionally, contour plots of the major principal stress increment and the major principal strain increment found that $\beta = 45°$.

The remaining linear elastic finite element analyses studied the change in stresses and strains in the soil overlying these typical bedrock faults: 90° thrust fault, 90° normal fault, 60° normal fault, and 45° thrust fault. For these analyses, the soil was defined by these parameters: E = 200,000 psf, $\nu = 0.4$, $\gamma = 120$ pcf, and $K_0 = 0.5$. In some of the analyses, the modulus of elasticity, E, increased linearly with depth ($E \approx 17\sigma_3$; Vesic and Clough, 1968). A soil deposit 400 feet deep was modeled with 433 4-node isoparametric plane strain elements. The length of the finite element mesh in the analyses varied from 1200 feet to 2400 feet to note the effect of moving the vertical boundaries of the finite element mesh. The vertical boundaries were free to displace in the vertical direction but fixed in the horizontal direction. The bottom horizontal boundary was fixed in both the vertical and horizontal direction, except prescribed displacements of half of the bottom boundary could be enforced to simulate a base deformation.

In Figure 7-2(A), the deformed mesh of a vertical (90°) thrust fault is shown. The contour plots of the maximum shear stress increment resulting from a 5 foot base offset when the finite element mesh has a length to height ratio of 3:1 and 6:1 are shown in Figures 7-2(B) and 7-2(C), respectively. The stress plots are almost identical. It seems clear that sufficient accuracy is obtained by modeling the soil overlying the displaced fault to a horizontal distance of roughly 1.5 times the height of the soil layer away from the fault. Similar results were obtained in the analyses of the 60° normal fault movements and the 45° thrust fault movements with respect to the location of vertical side boundaries. Previous analyses of fault rupture propagation customarily used finite element meshes with

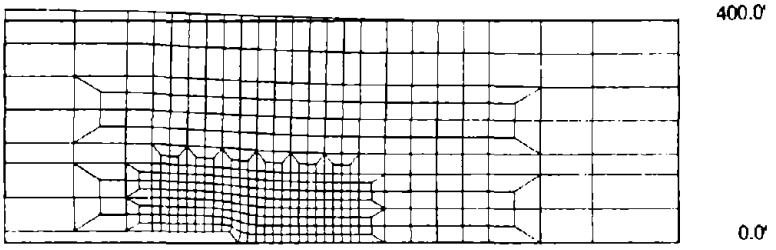

(A) Deformed Mesh: 20' offset

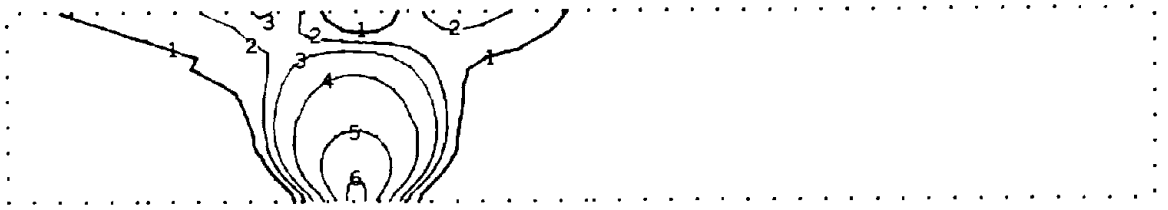

(B) Maximum Shear Stress Increment (psf): 5' offset (L/H = 6:1)

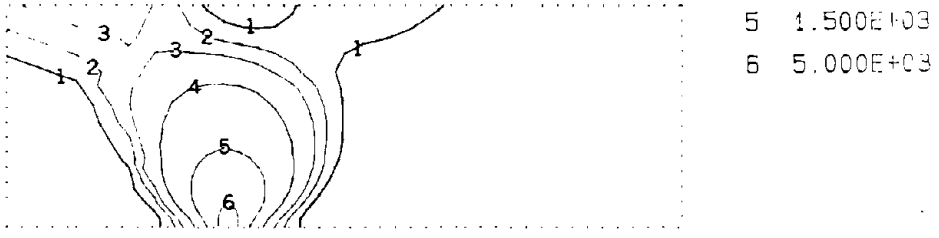

(C) Maximum Shear Stress Increment (psf): 5' offset (L/H = 3:1)

Figure 7-2: ELASTIC FINITE ELEMENT ANALYSES OF A 90° THRUST FAULT MOVEMENT: EFFECTS OF THE LOCATION OF THE VERTICAL BOUNDARIES

length to height ratios of 6:1, 8:1, or even 11:1. In this study, it was found that meshes with length to height ratios of 3:1 provided acceptable results. Thus, without the need for an extensive finite element mesh, more elements can be concentrated within the region of interest directly above the base rock fault and not away from the fault where the soil moves as a fairly "rigid" body.

Similar to the results presented by Scott and Schoustra (1974) (See Section 3.3.3(a)), the maximum shear stress increment plots shown in Figure 7-2 appear to indicate that the shear failure zone would propagate up over the upthrown block during a vertical thrust movement. That is, the higher values of the maximum shear stress increment are located above the upthrown block. Previous model studies and the clay-box model studies suggest, and kinematic constraints require, however, that the final fault rupture zone propagates over the downthrown block. The contour plot of maximum shear stress (Figure 7-3(A)) portrays the same tendency, showing that the maximum shear stresses are located above the inside edge of the upthrown block. Likewise, the contour plots of the maximum shear strain and the principal stress ratio also indicate regions of maximum values located over the upthrown block. It appears that the linear elastic finite element analyses only predict the first phase of shear zone development during fault rupture propagation or the "inverted footing" type of failure. Finally, it is noteworthy that the analyses predicted that a small region of tension would develop at the base of the soil deposit over the downthrown block adjacent to the base fault, and that a larger region of tension would develop near the ground surface over the upthrown block (See Figure 7-3(D)).

The results of the linear elastic finite element analyses of a vertical (90°) normal fault movement are presented in Figure 7-4. In this case, the left side of the mesh drops down vertically instead of displacing upwards. As expected, the contour plots of maximum shear stress, principal stress ratio, and minor principal

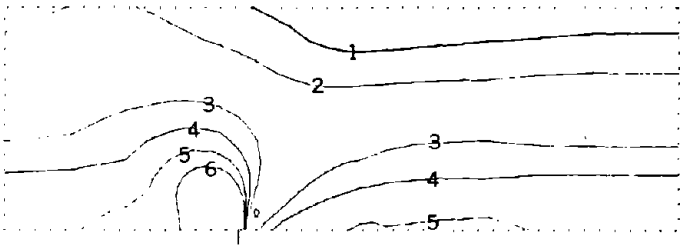

(A) Maximum Shear Stress (psf): 20' offset

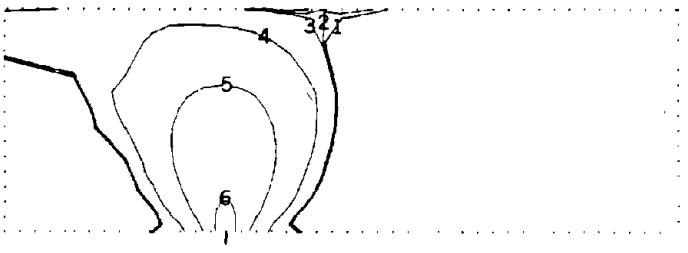

(B) Maximum Shear Strain: 5' offset

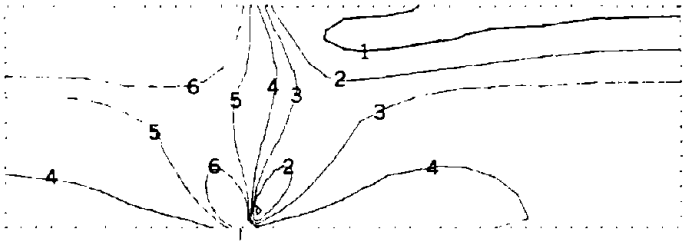

(C) Principal Stress Ratio: 20' offset

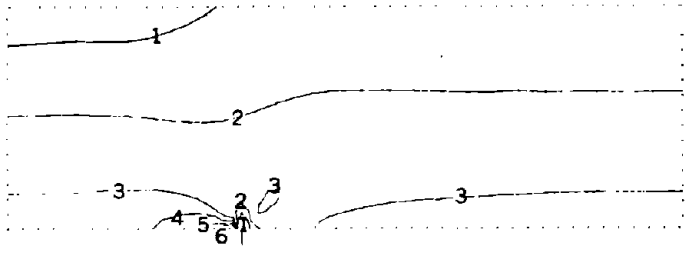

(D) Minor Principal Stress (psf): 20' offset

Figure 7-3: ELASTIC FINITE ELEMENT ANALYSES OF A 90° THRUST FAULT MOVEMENT

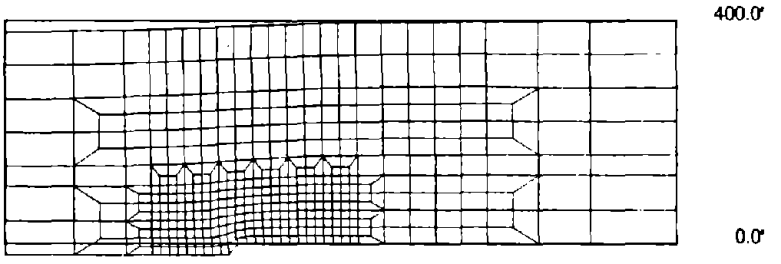

(A) Deformed Mesh: 20' offset

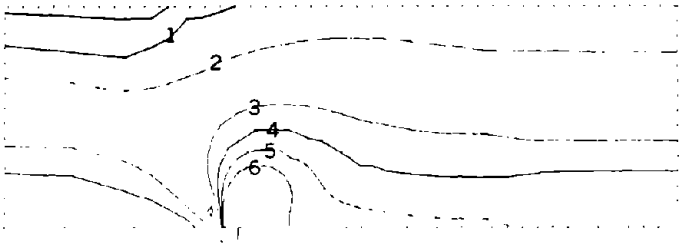

1 1.000E+03
2 3.000E+03
3 7.000E+03
4 9.000E+03
5 1.100E+04
6 1.300E+04

(B) Maximum Shear Stress (psf): 20' offset

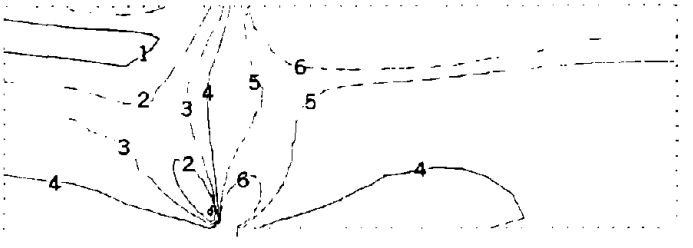

1 1.300E+00
2 1.600E+00
3 1.800E+00
4 2.000E+00
5 2.500E+00
6 3.000E+00

(C) Principal Stress Ratio: 20' offset

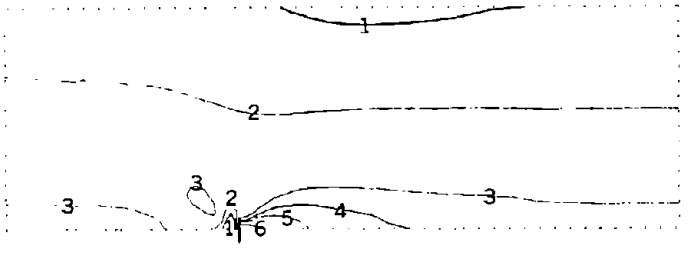

1 .000E+00
2 1.000E+04
3 2.000E+04
4 2.300E+04
5 2.600E+04
6 3.200E+04

(D) Minor Principal Stress (psf): 20' offset

Figure 7-4: ELASTIC FINITE ELEMENT ANALYSES OF A 90° NORMAL FAULT MOVEMENT

stress (See Figure 7-4(B), (C), and (D)) basically mirror the stress plots of the vertical (90°) thrust fault analyses (See Figure 7-3(A), (C), and (D)). Hence, the finite element analyses calculate only the change in stress resulting from the relative displacement of the base sections (the absolute displacements of the base sections are irrelevant). Additional analyses were performed where the soil deposit was not homogeneous; instead, the modulus of elasticity increased linearly with depth (i.e. from $E \approx 50{,}000$ psf near the ground surface to $E \approx 400{,}000$ psf near the soil-bedrock contact). The results from the analyses of the nonhomogeneous soil deposit were essentially identical to those of the homogeneous soil deposit. Hence, for the remainder of the study of elastic analyses, the soil deposit was assumed to be homogeneous.

The results of the linear elastic finite element analyses of a 60° normal fault movement and a 45° thrust fault movement are shown in Figures 7-5 and 7-6, respectively. The elastic analyses appear to be more appropriate for the 60° normal fault movement than the 45° thrust fault movement. For example, the maximum shear stress (Figure 7-5(B)) and the principal stress ratio (not shown) are at maximum values along the projection of the base rock fault plane (the expected failure plane) in the analyses of the 60° normal fault; whereas, the maximum shear stress (Figure 7-6(B)) and the principal stress ratio (not shown) are at minimum values along the projection of the base rock fault plane (the expected failure plane) in the analyses of the 45° thrust fault. Similarly, the maximum shear stress increment and the maximum shear strain contour plots show better agreement with observed behavior in the analyses of the 60° normal fault than in the analyses of the 45° thrust fault (Figures 7-5(C) and (D), and Figures 7-6(C) and (D)). As might be expected, the elastic analyses are more appropriate for the normal fault movement because here the soil overlying the displaced base is unloading, and soils have been found to typically behave more nearly elastically

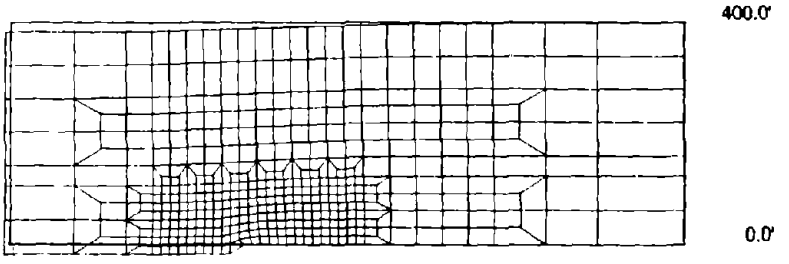

(A) Deformed Mesh: 20' offset

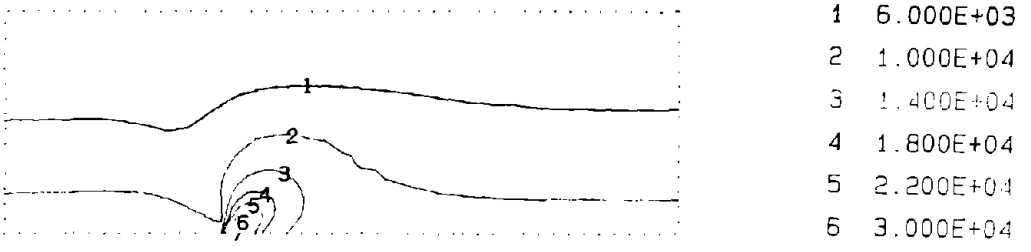

(B) Maximum Shear Stress (psf): 5' offset

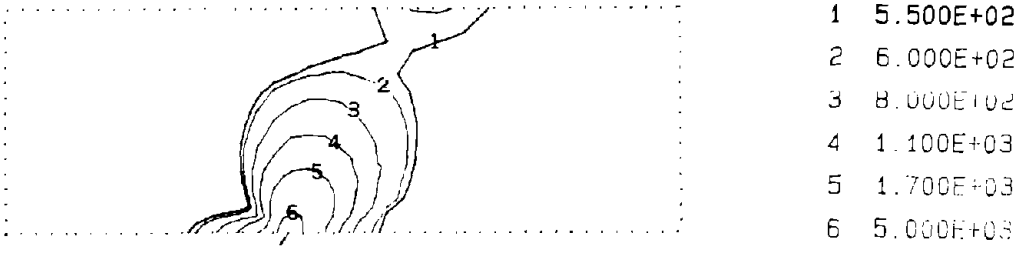

(C) Maximum Shear Stress Increment (psf): 5' offset

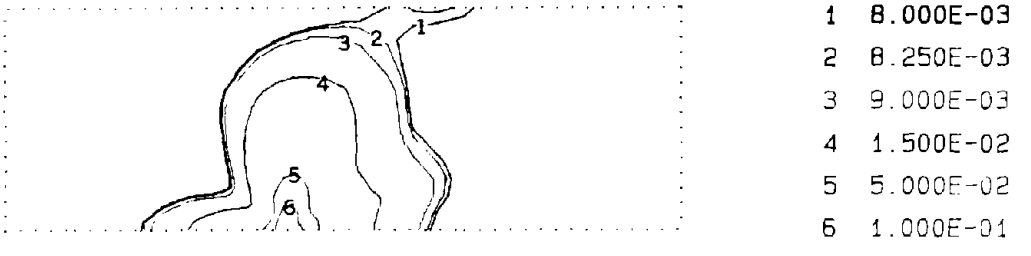

(D) Maximum Shear Strain: 5' offset

Figure 7-5: ELASTIC FINITE ELEMENT ANALYSES OF A 60° NORMAL FAULT MOVEMENT

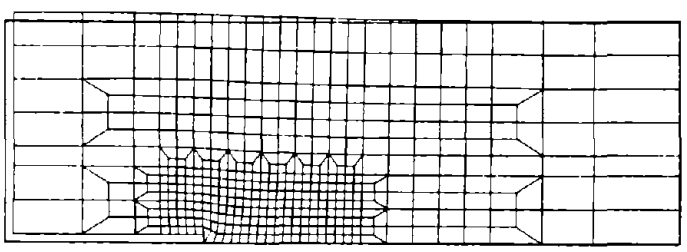

(A) Deformed Mesh: 20' offset

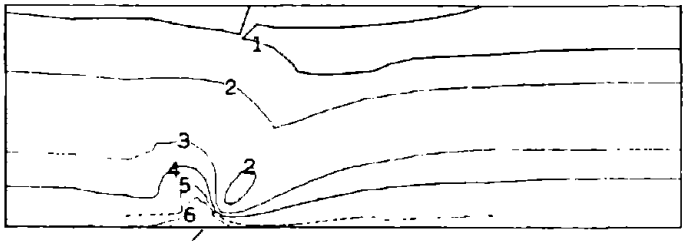

(B) Maximum Shear Stress (psf): 20' offset

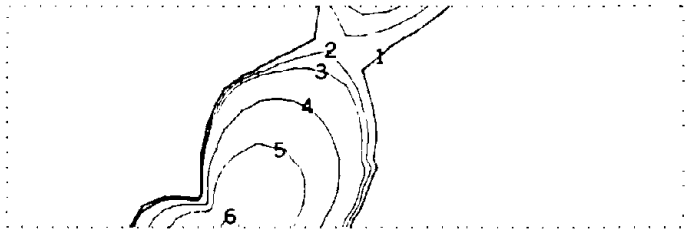

(C) Maximum Shear Stress Increment (psf): 5' offset

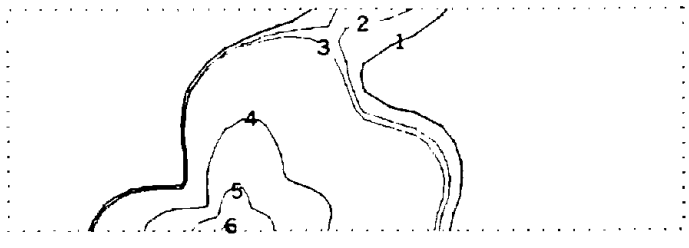

(D) Maximum Shear Strain: 5' offset

Figure 7-6: ELASTIC FINITE ELEMENT ANALYSES OF A 45° THRUST FAULT MOVEMENT

during unloading. On the other hand, soils tend to deform inelastically during primary loading, which is the case for the soil overlying a base rock thrust fault movement.

In summary, the linear elastic finite element analyses did not produce results consistent with observed behavior of fault rupture propagation through soils. Thrust fault movements (45° and 90°) produced highly stressed regions where strains were maximums over the upthrown block, yet kinematic constraints require that the final rupture zone propagates over the downthrown block. It appears that a linear elastic stress analyses cannot determine the location or orientation of the final rupture zone through the soil overlying a displaced bedrock thrust fault. The elastic analyses only show the initial "inverted footing" phase of the shear rupture zone development. In addition, as the deformed meshes presented in Section 7.3 illustrate, the linear elastic analyses do not localize the rupture zone within the soil mass well. At the surface of the soil layer, the vertical differential movement is spread across a wide area. The linear elastic finite element analyses did, however, produce more reasonable results with respect to the location of the suspected failure plane through the soil in the case of normal fault movements (in this case, the soil is unloading). Finally, the linear elastic finite element analyses indicated that the maximum shear strain, the maximum shear stress increment, and displacement plots (deformed meshes which show the effects of kinematic constraints) might be useful in determining the location and orientation of the shear rupture zone through the soil overlying a displaced base rock fault.

7.4 Linear Elastic-Perfectly Plastic Analyses of Fault Rupture Propagation

A linear elastic-perfectly plastic soil constitutive model was believed to be inadequate for the analysis of fault rupture propagation because the results from

previous studies of the shear rupture behavior of soils did not agree with the patterns of failure observed in model tests (Scott and Schoustra, 1974; Davie, 1973). In the Scott and Schoustra (1974) study, the failed zone propagated to the surface over the upthrown block of a vertical base rock fault offset. This, of course, is incorrect as Scott (1987) pointed out since kinematic constraints require that the final rupture zone propagates over the downthrown block. In the Davie (1973) study of anchor pull-out behavior, the linear elastic-perfectly plastic finite element analysis was not able to predict the failure pattern observed in the shallow anchor pull-out tests (i.e. the wedge or Balli shaped failure surface, see Chapter Four). Nevertheless, finite element analyses employing a linear elastic-perfectly plastic soil model were performed as a part of this research to ascertain if this soil constitutive model is actually deficient and to learn what refinements if any are necessary to improve the reliability of the analyses.

Again, Dr. Taylor's PCFEAP program is used to analyze the fault rupture propagation problem. In this case, however, a linear elastic-perfectly plastic soil constitutive law is employed in the finite element analyses. The 300 foot deep layer of saturated clay soil overlying the base rock fault was modeled with a generic mesh (with a length of 1000 feet or L/H = 3.3) of 800 quadrilateral shaped 4-node isoparametric plane strain elements (See Figure 7-7(A)). The soil parameters required to define the behavior of the soil are: the modulus of elasticity, E; Poisson's ratio, ν; and the deviatoric failure stress, 2C. The saturated clay was assumed to be close to normally consolidated (i.e. strength increasing approximately linearly with depth) except for an overconsolidated region with fairly uniform strength near the top of the soil layer. Hence, the undrained shear strength of the clay was varied within each of the 20 soil layers to range from 1000 psf near the surface to nearly 6000 psf at a depth of 300 feet. Accordingly, the stiffness of the clay was increased approximately linearly with depth keeping the

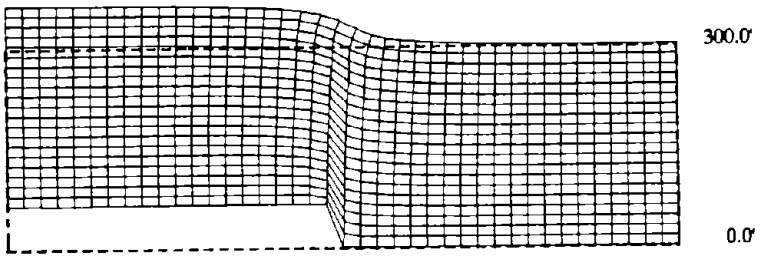

(A) Deformed Mesh (disp. magnified by 5): 12.8' offset

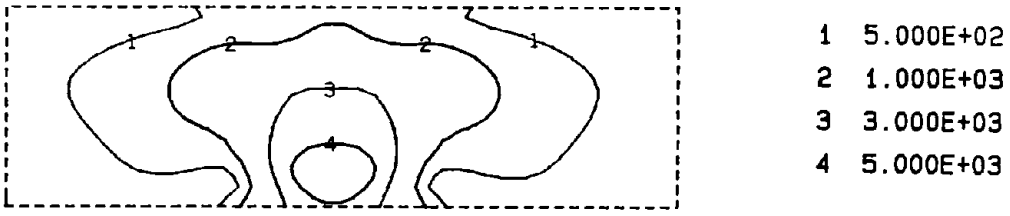

(B) Maximum Shear Stress (psf): 4.0' offset

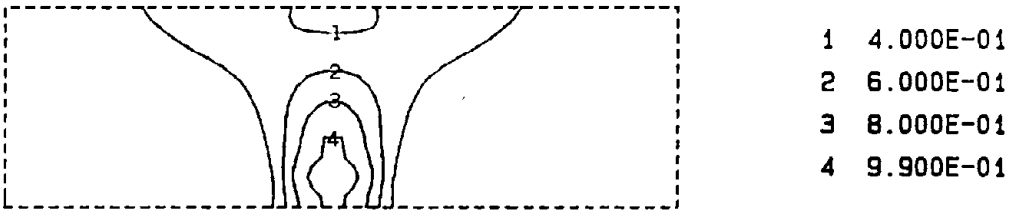

(C) Yield Level (> 0.99 indicates failure): 4.0' offset

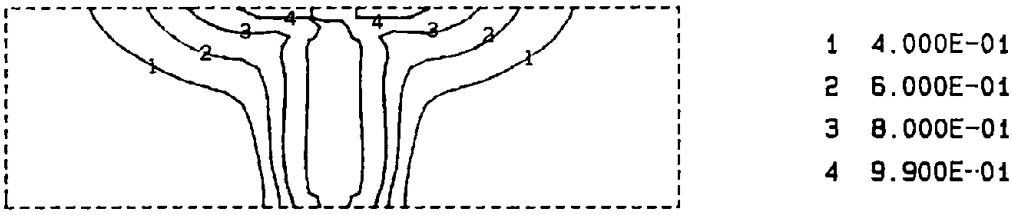

(D) Yield Level (> 0.99 indicates failure): 12.8' offset

Figure 7-7: ELASTIC-PERFECTLY PLASTIC FINITE ELEMENT ANALYSES OF A VERTICAL THRUST FAULT MOVEMENT

axial failure strain of the clay at around ϵ_a = 1%. Poisson's ratio was assumed to be 0.49. In these analyses, K_o was assigned an initial value of 1.0.

Several solution algorithms were employed to note their effectiveness regarding solution of this boundary deformation problem (Taylor, 1977). The Newton-Raphson iteration algorithm where the tangent stiffness matrix (i.e. the global finite element stiffness matrix) is recalculated after each solution of the developed system of equations is found did not consistently converge. A modified Newton-Raphson solution technique which recalculated the tangent stiffness matrix only after a solution of the system of equations was iteratively solved did, however, converge, but it converged very slowly. The incremental load solution technique proved to be most efficient. In this procedure, the total boundary displacements were subdivided into approximately 20 equal displacement increments. Within each displacement (or load) increment, the modified Newton-Raphson solution technique rapidly achieved convergence to a solution of minimum energy. As previous studies had suggested, it appears important to use an incremental solution algorithm to effectively and accurately solve the fault rupture propagation problem.

The results of the linear elastic-perfectly plastic finite element analysis of fault rupture propagation through soil as a result of a vertical thrust fault movement are shown in Figure 7-7. As opposed to the linear elastic analyses conducted in Section 7.3, much better localization of the deformation pattern in the region above the base rock fault is possible (See Figure 7-7(A)). Similar to the elastic analyses, however, the elastic-perfectly plastic analyses produced a broad region of maximum shear stress values (See Figure 7-7(B)). On the other hand, the maximum shear stress plot was now symmetrical about the base rock fault indicating no tendency for the fault plane to move either over the upthrown block or the downthrown block at any stage. Likewise, the contour plot of yield levels

within the elements, which indicates how close an element is to failure (yield level greater than 0.99 denotes plastic shear failure), was symmetrical about the fault at lower base displacements (See Figure 7-7(C)). The plastic zone reaches the ground surface at a base deformation of 12.8 feet or 4.3% of the height of the clay layer ($h_f/d_b \approx 23$). Again, the yield level plot is nearly symmetrical about the vertical base rock fault.. The plastic zone does, however, reach the surface first over the upthrown block. Moreover, by the time the plastic zone reaches the ground surface it is rather wide.

Refinement of the finite element mesh did not alter the results of the analysis appreciably. Furthermore, the strength and stiffness parameters were not sensitive in themselves, but since together they defined the failure strain of the soil, variations in these soil parameters altered the amount of base deformation required to propagate the rupture through the overlying soil to the ground surface. The characteristics of the failure pattern (i.e. size and orientation), however, remained the same for analyses where the failure strain of the soil varied. Previous numerical studies reviewed earlier in Chapters Three and Four had failed to recognize the importance of defining the correct failure strain of the soil overlying a base rock fault offset. Figure 7-8 illustrates this point. If average soil stiffness and strength parameters are used in a linear elastic-perfectly plastic model (which is essentially a bilinear model of the soil's stress-strain curve) that "best fit" the actual stress-strain curve of the soil in question (See Figure 7-8(A)), the failure strain of the soil can be grossly underestimated. Although not intuitively pleasing to the eye, in situations where the soils failure strain is a critical soil parameter (as it appears to be in the rate of fault rupture propagation through soil), the bilinear approximation of the soil's stress-strain curve labeled (B) can well describe the essential characteristics of soil behavior.

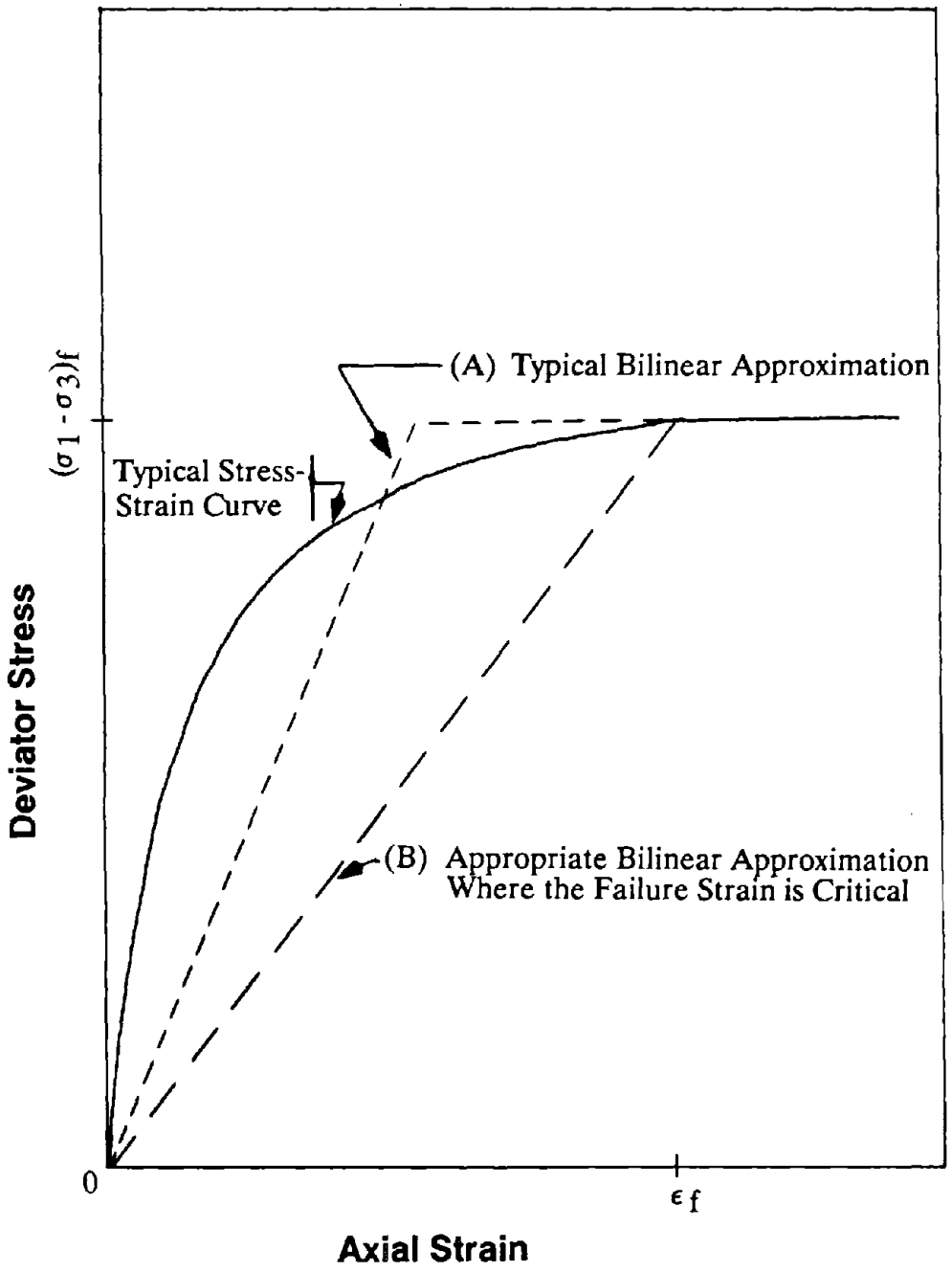

Figure 7-8: THE ELASTIC-PERFECTLY PLASTIC BILINEAR APPROXIMATION OF A SOIL'S STRESS-STRAIN BEHAVIOR

In summary, the results of the linear elastic-perfectly plastic finite element analyses of fault rupture propagation through soil agree more closely with the observed failure patterns that develop in physical model tests than do the results of the linear elastic finite element analyses, but inconsistencies still remain. The linear elastic-perfectly plastic finite element analyses suffer primarily from the assumption that soil deformed linear elastically up to the point of failure. In reality, the stress-strain behavior of soil is generally nonlinear, especially near failure. The soil constitutive model's assumption of a linear pre-failure stress-strain behavior of the soil may be responsible for the predicted symmetrical, broad contours of maximum shear stress in the soil mass, the symmetrical plastic zone which predicts neither an "inverted footing" type of failure nor an "anchor pull-out" type of failure, and the prediction that the plastic zone first reaches the ground surface over the upthrown block. The elastic-perfectly plastic finite element analyses of fault rupture propagation did, however, localize the failure zone within the displacement field better than the linear elastic finite element analyses could. Furthermore, the importance of the soil's failure strain was re-emphasized. Finally, refinements to the linear elastic-perfectly plastic model employed in these finite element analyses might improve its reliability (e.g. allow for K_o values other than 1.0, and develop a tension cut-off failure criterion).

7.5 Incremental Nonlinear Elastic Analyses of Fault Rupture Propagation

7.5.1 General:

Linear elastic and linear elastic-perfectly plastic soil constitutive models produced inconsistent results when employed in the finite element method. In a number of cases, the finite element analyses based on these two soil constitutive models failed to adequately predict the essential characteristics of soil behavior observed in small-scale model tests and in field studies of fault rupture propagation

through soils. It appeared that both soil constitutive models were deficient because of the assumption that the stress-strain behavior of the soil overlying the displaced base rock fault was linear elastic up to the point of failure. Since it is generally acknowledged that typical soils exhibit highly nonlinear stress-strain behavior at or near failure, the fault rupture propagation problem was re-analyzed employing a soil constitutive law in the finite element method which could model the soil's nonlinear stress-strain behavior.

7.5.2 Duncan et al. (1984) Hyperbolic Soil Model:

One of the simpler means of modeling a soil's nonlinear stress-strain behavior is the incremental nonlinear hyperbolic elastic approach. The Duncan et al. (1984) hyperbolic stress-strain model has been widely used in a large number of finite element analyses of different types of "static" (non-vibratory or non-cyclically loaded) geotechnical problems. A full description of the Duncan hyperbolic soil model, along will the most recent developments of the method are described in Duncan et al. (1980) and Duncan et al. (1984).

The Duncan hyperbolic soil model assumes that the stress-strain behavior for typical soils can be approximated by a hyperbolic function as shown in Figure 7-9(a). The instantaneous slope of the hyperbolic stress-strain curve is the tangent modulus (E_t). This tangent modulus is a function of the soil's current confining stress ($\sigma 3$) and stress level (SL) and is expressed as:

$$E_t = (1 - R_f \cdot SL)^2 K \cdot P_a \cdot (\sigma_3 / P_a)^n \qquad (7\text{-}1)$$

where SL = Stress Level = $(\sigma_1 - \sigma_3)/(\sigma_1 - \sigma_3)_f$ (7-2)

which describes how close the soil is to failure.

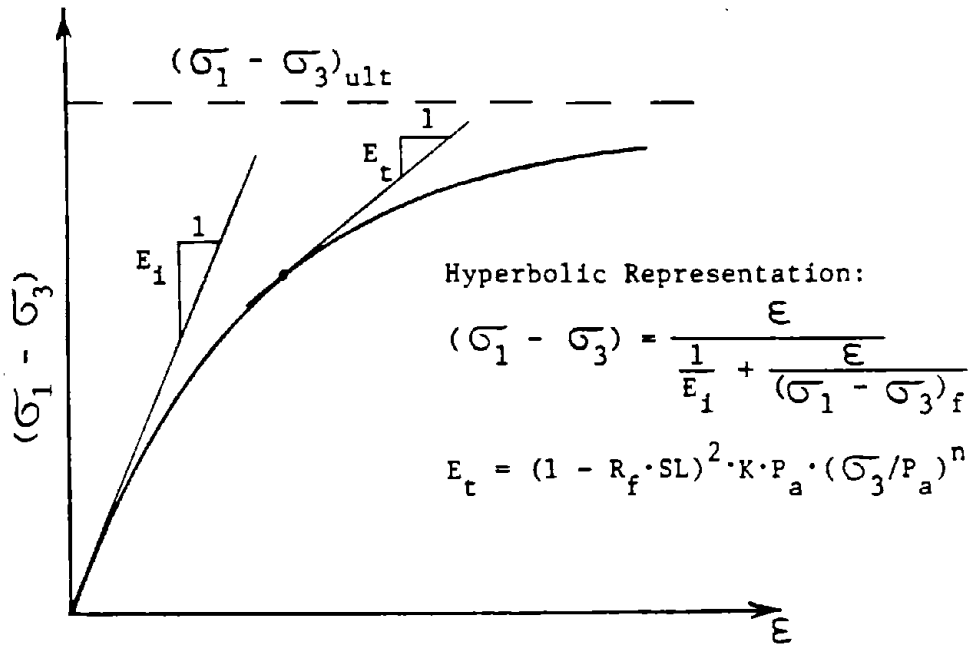

(a) Hyperbolic Representation of Stress-Strain Curve for Primary Loading.

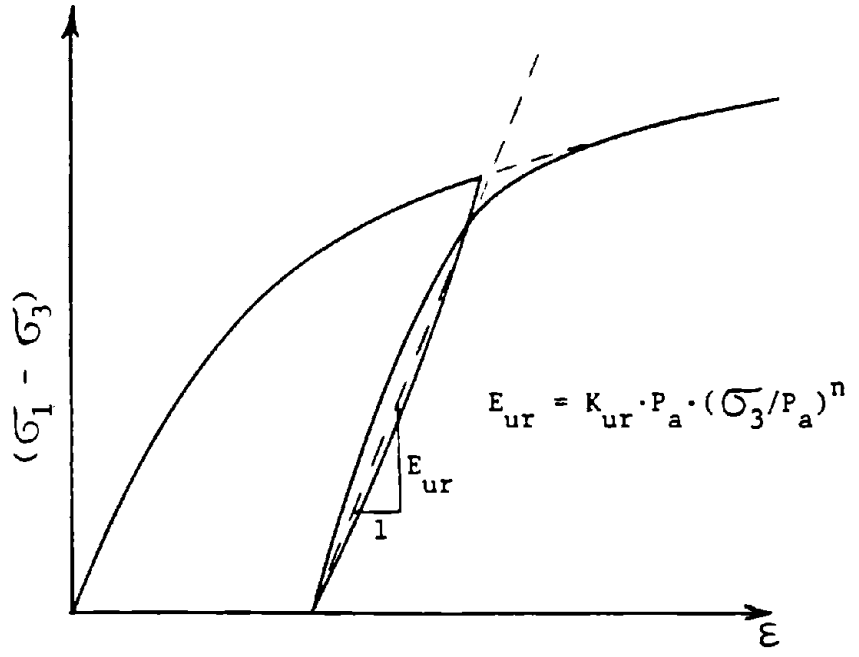

(b) Linear Unloading-Reloading Stress-Strain Relationship.

Figure 7-9: HYPERBOLIC MODEL OF STRESS-STRAIN BEHAVIOR (after Seed and Duncan, 1984)

$$(\sigma_1 - \sigma_3)_f = (2C \cdot \cos\phi + 2\sigma_3 \cdot \sin\phi)/(1 - \sin\phi) \quad (7\text{-}3)$$

which is the deviatoric stress at failure as determined by the traditional Mohr-Coulomb failure criterion.

K,n = Model parameters (constants) relating the initial modulus, E_i, to the confining stress σ_3 as:

$$E_i = K \cdot P_a \cdot (\sigma_3/P_a)^n \quad (7\text{-}4)$$

P_a = Atmospheric pressure, introduced into the model in order to make K and n dimensionless numbers.

$$R_f = (\sigma_1 - \sigma_3)_f/(\sigma_1 - \sigma_3)_{ult} \quad (7\text{-}5)$$

which is a model parameter (constant) used to help describe the curvature of the hyperbolic function ($(\sigma_1 - \sigma_3)_{ult}$ is the theoretical asymptote of the hyperbolic function). R_f is typically between 0.6 to 0.9 for most soils.

In general, during primary loading, the soil's stiffness or tangent modulus (E_t) increases with increasing confining stress (σ_3) and decreases with increasing stress level (SL).

As shown in Figure 7-9(b), the model incorporates a linear stress-dependent unloading-reloading stress-strain relationship for instances when the current stress state (SS) is less than the maximum previous stress state ($SS_{max\ past}$). The stress state (SS) is defined as:

$$SS = SL \cdot \sqrt[4]{(\sigma_3/P_a)} \quad (7\text{-}6)$$

The 1984 slightly modified version of the original 1980 model utilizes the new parameter, stress state, which is a function of stress level and confining stress, to

distinguish between primary loading and unloading-reloading instead of relying solely on the original criterion of maximum previous stress level. The unloading-reloading modulus (E_{ur}) is modeled as a function of confining stress (σ_3) according to the equation:

$$E_{ur} = K_{ur} \cdot (\sigma_3/P_a)^n \tag{7-7}$$

where K_{ur} is typically 1.2 to 3 times greater than K (the modulus parameter determining E_i). The other model parameters in this equation have been previously defined.

Finally, the bulk modulus (B) of the soil is expressed as a function of only σ_3 as:

$$B = K_b \cdot P_a \cdot (\sigma_3/P_a)^m \tag{7-8}$$

where K_b and m are dimensionless model parameters (constants). Since Poisson's ratio (ν) can be expressed as:

$$\nu = 1/2 - E/6B \tag{7-9}$$

modeling the bulk modulus (B) as being independent of stress level and modeling the tangent modulus (E_t) as a function that decreases with increasing stress level, effectively results in modeling Poisson's ratio (ν) as increasing with increasing stress level. The bulk modulus is constrained so that the permissible values of Poisson's ratio range from roughly 0.15 ($\nu_{min} = (1 - \sin\phi)/(2 - \sin\phi)$) to 0.49.

Thus, the soil modulus (E_t or E_{ur}) defines the stress-strain behavior of the soil material, and together, the soil modulus (E_t or E_{ur}) and the bulk modulus (B) defines the volumetric strain behavior of the soil material. This relatively simple hyperbolic soil model may be applied in terms of either total stress or effective stress by using input parameters appropriate for either a total stress or an effective

stress analysis. A total of nine independent model parameters ($C, \phi, \Delta\phi$, K, K_{ur}, n, R_f, K_b, m) are necessary in the hyperbolic soil model to reasonably describe the nonlinear stress-strain and volumetric strain behavior of most soils.

The Duncan et al. (1984) hyperbolic soil model is employed in the computer program SSCOMP: a plane strain, incremental load finite element program for evaluation of soil-structure interaction and compaction-induced lateral stresses and deflections (Seed and Duncan, 1984). The program SSCOMP is currently installed on a Digital Micro-VAX mini-computer at the University of California at Berkeley. The computer program SSCOMP was utilized in this research to model the nonlinear stress-strain behavior of the soil overlying the displaced base rock fault.

The computer program SSCOMP calculates stresses, strains and displacements in soil elements by means of an analytical technique which simulates the total deformation of a displaced base section in a number of displacement increments. The nonlinear and stress-dependent stress-strain and volumetric strain properties of the soils are approximated by varying the values of the soil's elastic modulus and bulk modulus in accordance with the calculated stresses, using the Duncan et al. (1984) hyperbolic soil model. An increment of the analysis of the fault rupture propagation problem is a specified displacement of part of the base section below the overlying soil deposit. Each increment is analyzed twice. In the first iteration, soil elastic modulus and Poisson's ratio values based on the stress conditions in each soil element at the beginning of the increment are used, and in the second iteration, the average of the stresses calculated at the end of the first iteration and the original stresses at the beginning of the increment are used. The two-iteration solution procedure thus allows modeling of the nonlinear stress and stress-history dependent soil element properties. The results of the second iteration of each increment are retained, and the changes in stress and strain in the soil are added to the values at the beginning of the increment. After each

increment is successfully solved and the incremental element stresses and strains are calculated and added to the current solution, the final solution is reached.

During each iteration of each increment in the program SSCOMP, each soil element can be in one of four possible states as defined by the hyperbolic soil model: primary loading, unloading-reloading, shear failure, or tensile failure. The conditions for determining whether a soil element is in a state of primary loading or in a state of unloading-reloading has been described previously. If the current stress state (SS) is greater than or equal to the maximum previous stress state ($SS_{max\ past}$), the element is in a state of primary loading, otherwise, it is in a state of unloading-reloading. Shear failure occurs when the stress level of an element exceeds 95% of its shear strength (i.e. $SL = (\sigma_1 - \sigma_3)/(\sigma_1 - \sigma_3)_f > 0.95 \cdot (\sigma_1 - \sigma_3)_f$). The soil element which fails in shear is effectively modeled as an "incompressible fluid" with a very low elastic modulus and a Poisson's ratio near 0.5. Tensile failure occurs when the minor principal stress (σ_3) is negative. The soil element which fails in tension is effectively modeled as an "air element" with an extremely low elastic modulus which limits additional tensional stresses to very low magnitudes. Hence, this soil model achieves a near "no-tension" soil element which is invaluable in realistic analyses of geotechnical problems.

Initially, during these preliminary analyses of the fault rupture propagation problem, the computer program SSCOMP, which employs the incremental nonlinear hyperbolic elastic soil model described previously, was used to analyze fault rupture propagation through dry, cohesionless materials. As the review of literature found, the vast majority of physical and numerical model studies of fault rupture propagation through soils to date have employed dry, cohesionless soil materials. Thus, these preliminary nonlinear finite element analyses will study the behavior of dry, cohesionless materials since the previous well-documented physical model tests employed dry, cohesionless materials. The primary objective

of these preliminary finite element studies of fault rupture propagation through soils, however, is to evaluate the suitability of the incremental nonlinear elastic hyperbolic stress-strain soil model in finite element studies of fault rupture propagation through soils. Additionally, it is hoped that these preliminary nonlinear finite element studies will determine the sensitivity of the results of the FEM analyses to possibly critical soil model parameters.

7.5.3 Incremental Nonlinear Elastic Analyses of Fault Rupture Propagation through Dry Sand:

In these preliminary incremental nonlinear finite element analyses of fault rupture propagation through soil, the soil overlying the displaced bedrock fault was assumed to be a typical, well-graded, medium dense, dry sand. Appropriate hyperbolic stress-strain, strength, and bulk modulus soil model parameters were used to characterize the sand material (i.e. γ_m = 120 pcf, ϕ' = 36°, $\Delta\phi'$ = 5°, C = 0, K = 300, K_{ur} = 600, n = 0.4, R_f = 0.7, K_b = 75, m = 0.2). K_o was estimated in these analyses to be either 0.5 or 1.0. In one set of analyses, the bulk modulus (B) was made to be very large to constrain Poisson's ratio (ν) to be very close to 0.5. Ordinarily, the value of Poisson's ratio during the analyses ranged from 0.35 to 0.45.

Manipulation of the hyperbolic representation of the soil's stress-strain behavior shown in Figure 7-9(a):

$$(\sigma_1 - \sigma_3) = \epsilon / [1/E_i + \epsilon / (\sigma_1 - \sigma_3)_f] \qquad (7\text{-}10)$$

produces an equation useful for calculating the strain of the soil at various stress levels:

$$\epsilon = (\sigma_1 - \sigma_3)_f / [E_i \cdot (1/SL - R_f)] \qquad (7\text{-}11)$$

It follows that the soil's shear failure strain which occurs at a stress level of 95% in the program SSCOMP can be estimated as:

$$\epsilon_f = (\sigma_1 - \sigma_3)_f/[E_i \cdot (1.05 - R_f)] \qquad (7\text{-}12)$$

Given the hyperbolic soil material properties used to describe the well-graded, medium dense, dry sand employed in these preliminary finite element analyses, the shear failure strain of the sand was on the order of 4% to 10% depending on the confining stress acting within the soil element at the time of failure. Since the deviatoric stress at failure, $(\sigma_1 - \sigma_3)_f$, and the initial tangent modulus, E_i, both depend on the confining stress, σ_3, the shear failure strain necessarily depends on the magnitude of the confining stress currently acting within a particular soil element ($\epsilon_f \approx f(\sigma_3)$).

Similar to the linear elastic-perfectly plastic finite element analyses discussed previously in Section 7.4, a soil deposit 300 feet deep was modeled with a fairly regular finite element mesh (384 isoparametric 4-node plane strain elements) which possessed a length to height ratio of approximately 4:1. "Typical" base rock faults of a vertical thrust fault, a thrust fault dipping at an angle of 45°, and a normal fault dipping at an angle of 60° were studied.

Initial nonlinear finite element analyses of fault rupture propagation indicated that relatively simple finite element models of the soil overlying the displaced base rock fault (i.e. finite element meshes which had less than around 250 soil elements) could not reasonably model the development of shear rupture zones or tension zones within the soil mass. In fact, a relatively refined mesh was required in the vicinity of the base rock fault to model the proper initiation of shear failure in the soil, and especially, the development of tensile failure in the soil. In addition, if relatively large displacement increments were imposed (i.e. increments of base displacement (or offset) greater than around 0.5% of the height

of the soil overlying the base fault), the results of the incremental nonlinear finite element analyses of fault rupture propagation were inconsistent. To allow the nonlinear incremental elastic hyperbolic soil model to adequately represent the true nonlinear stress-strain behavior of typical soils at or near failure, a larger number of displacement increments had to be imposed. In the following preliminary analyses of dry, cohesionless materials, approximately 20 displacement increments were imposed before the final shear rupture zone propagated up to the ground surface.

Results of the incremental nonlinear elastic finite element analyses of the propagation of a vertical base rock thrust fault through the overlying well-graded, medium dense, dry sand are shown in Figures 7-10, 7-11, and 7-12. In the first case (Figure 7-10), the coefficient of lateral earth pressure at rest (K_o) was estimated to be 0.5. In the second case (Figure 7-11), K_o was estimated to be 1.0. In the third case (Figure 7-12), K_o was again estimated to be 0.5, but Poisson's ratio (ν) was constrained to be close to 0.5 (hence, the sand was neither contractive nor dilative during shearing, but instead, deformed at nearly constant volume). The Duncan et al. (1984) hyperbolic soil model cannot model dilatant soil behavior, so the use of this model in situations where soils tend to dilate when sheared is open to question.

The deformed mesh and displacement vector plot (Figures 7-10(a) and (b), respectively) clearly show that in comparison to the results of the linear elastic finite element analyses (See Section 7.3), the nonlinear finite element analyses predicted much greater localization of the vertical differential movement within the soil overlying the base rock fault. In fact, the displacement vector plot (Figure 7-10(b)) shows that a majority of the soil above the base rock away from the location of the base rock fault deforms as a fairly "rigid" block. In addition, the displacement plot appears to indicate that the final rupture zone as defined by the locus of points at each originally horizontal level in the soil mass where the change

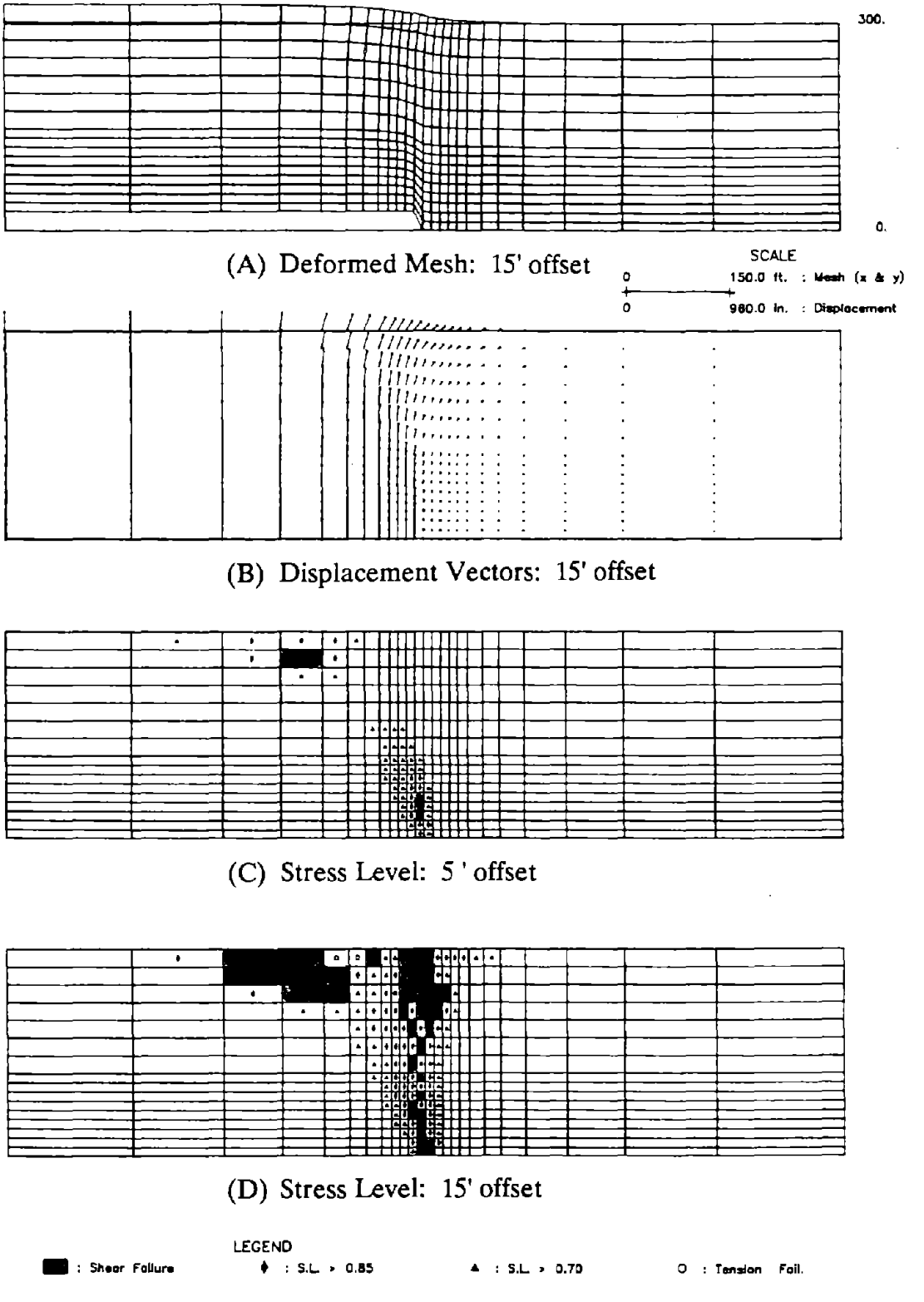

Figure 7-10: RESULTS OF NONLINEAR FINITE ELEMENT ANALYSES OF DRY SAND (K_o = 0.5) WITH A 90° THRUST FAULT MOVEMENT

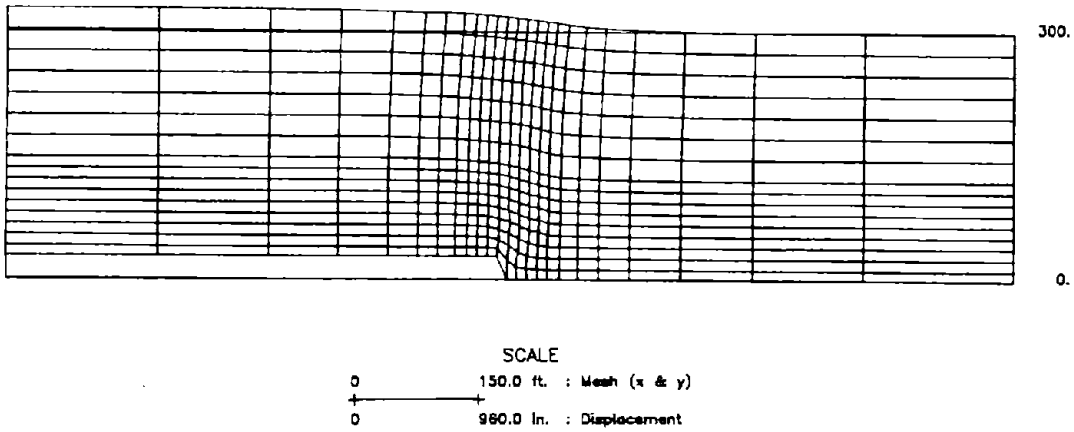

(A) Deformed Mesh: 15' offset

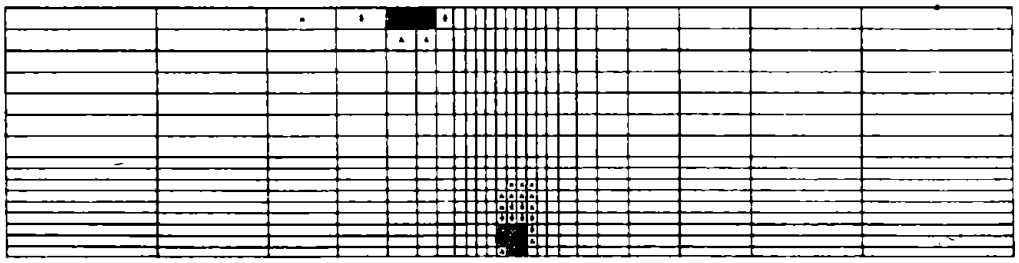

(B) Stress Level: 5' offset

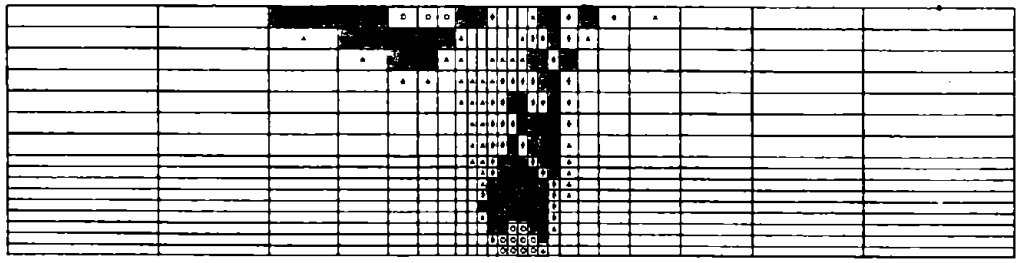

(C) Stress Level: 15' offset

LEGEND
: Shear Failure ♦ : S.L. > 0.85 ▲ : S.L. > 0.70 ○ : Tension Fail.

Figure 7-11: RESULTS OF NONLINEAR FINITE ELEMENT ANALYSES OF DRY SAND (K_o = 1.0) WITH A 90° THRUST FAULT MOVEMENT

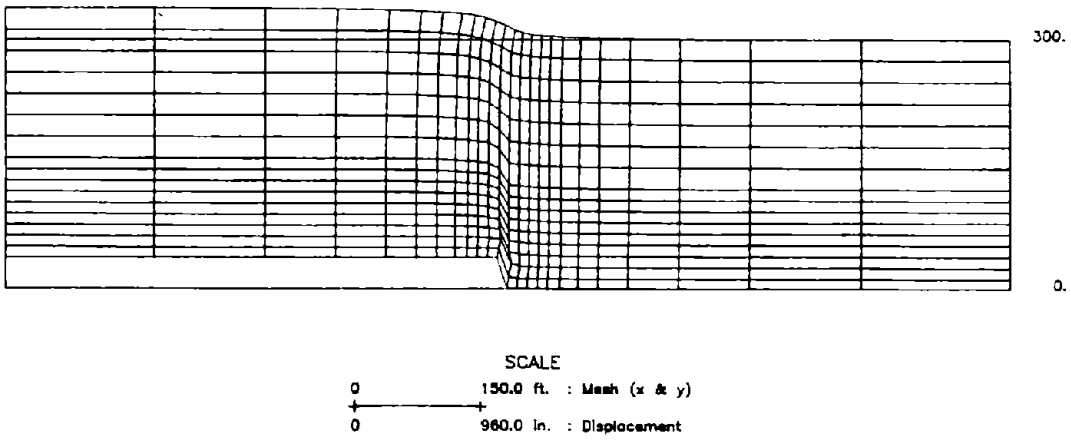

(A) Deformed Mesh: 20' offset

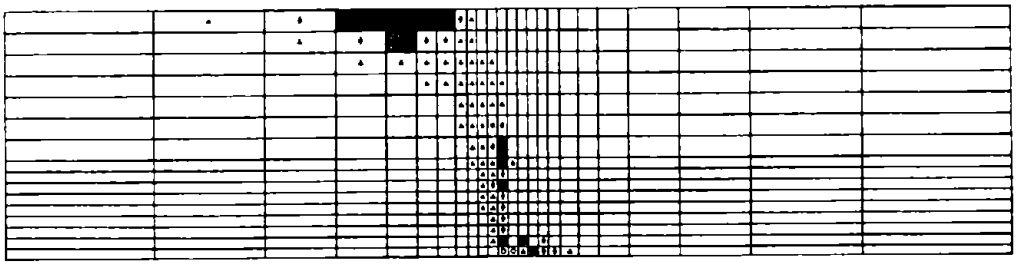

(B) Stress Level: 5' offset

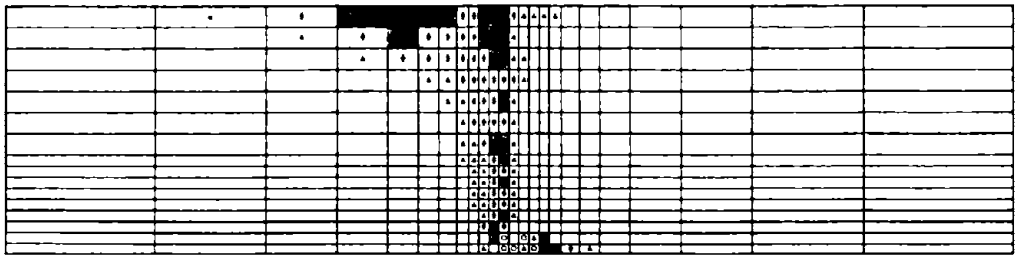

(C) Stress Level: 10' offset

LEGEND
: Shear Failure : S.L. > 0.85 : S.L. > 0.70 : Tension Fail.

Figure 7-12: RESULTS OF NONLINEAR FINITE ELEMENT ANALYSES OF DRY SAND (K_o = 0.5 & ν = 0.49) WITH A 90° THRUST FAULT MOVEMENT

in the magnitude of deformation along each originally horizontal level is a maximum agrees reasonably well with the final rupture surface observed in the sandbox model tests previously described in Section 3.3.2 (the "anchor pull-out" type of failure pattern).

The stress level plots shown in Figures 7-10(c) and (d) appear to reasonably predict the hypothesized two-phase development of the shear rupture zones in the soil overlying a vertical base fault offset. Initially, a zone of highly stressed soil forms above the upthrown block indicating the "inverted footing" type of failure. As the base deformation increases, however, the actual shear failure zone (identified by shaded elements) propagates up toward the ground surface along the projection of the vertical base rock fault below. Hence, the final solution is kinematically admissible. In this case, the fault rupture reaches the ground surface at a base offset of 15 feet (roughly 5% of the depth of the soil deposit overlying the displaced base section). Similar to observations made in fault rupture field studies, previous laboratory physical model tests, and previous finite element studies (See Chapter Three), a zone of local extension (as evidenced by elements that fail in tension as well as by elements that fail in shear because of the reduction of the minor principal stress) forms at or near the ground surface in a region above the upthrown block.

The deformed mesh and the stress level plots shown in Figure 7-11 indicate that as the coefficient of lateral earth pressure at rest (K_O) is increased from 0.5 to 1.0 (the other hyperbolic model parameters remained the same as those used in the first case), the failure surface predicted by the incremental nonlinear elastic finite element analyses moves to a position over the downthrown block portraying more curvature of the shear failure zone near the ground surface. In these finite element analyses of fault rupture propagation through a dry, cohesionless material, the results appear to be fairly sensitive to the value of the soil parameter K_O

chosen. Published results of previous finite element studies of fault rupture propagation through dry, cohesionless materials sometimes showed this same sensitivity to the K_o soil parameter (e.g. Walters and Thomas, 1982; Section 3.3.3(e)), but previous investigators did not clearly acknowledge the significant effects that variations in the K_o parameter had on their finite element results. The anchor pull-out finite element study by Tagaya et al. (1983) did, however, show that the pull-out capacity of anchors in dry, cohesionless materials was sensitive to the value of K_o. The other significant difference between these preliminary finite element results where K_o equaled 1.0 and the results where K_o equaled 0.5 was the development of a zone of tension located just above the downthrown block adjacent to the vertical base rock fault in the finite element analyses where K_o equaled 1.0. The magnitude of base offset necessary to propagate the rupture zone to the ground surface, however, remained on the order of 15 feet or roughly 5% of the depth of the soil overlying the displaced base section for both K_o conditions.

In the third case, where the soil parameters are identical to those used in the first case except that Poisson's ratio was constrained to be 0.49 so that the soil deformed at essentially constant volume, the failure pattern that developed in the soil was significantly different than that which developed in the first case. The deformed mesh shown in Figure 7-12(a) appears to indicate that the differential vertical movement is more localized when the soil deforms at constant volume. The highly stressed region (SL > 0.70) and the actual shear failure zone depicted in the stress plots shown in Figures 7-12(b) and (c) are also narrower in case three where the soil deforms at essentially constant volume. The stress plots still portray the initial "inverted footing" type of failure pattern as well as the final "anchor pull-out" type of failure pattern as shown in the first analyses, but now only approximately 10 feet of base fault offset is required to propagate the rupture zone to the ground surface. Hence, a base offset of only 3.3% of the depth of the

overlying sand layer is required to propagate the shear rupture zone to the ground surface in case three; whereas, a base offset of 5% of the depth of the overlying sand layer is required in the first case. It appears that when the soil deforms at constant volume the base deformation (or offset) required to propagate the rupture zone to the ground surface may decrease relative to that necessary when the soil contracts during shear deformation. Finally, the constant volume analyses predict the development of a tension zone at the bottom of the soil layer near the base rock fault at a smaller magnitude of base offset than in the case where Poisson's ratio remained between 0.35 and 0.45 (contractive soil behavior). A number of analyses were performed with Poisson's ratio (ν) equal to values between 0.45 and 0.49 to determine if "mesh locking" affected the results of the analyses (i.e. a numerical problem which sometimes occurs in a displacement based finite element approach), and "mesh locking" when $\nu \approx 0.5$ was not judged to be a concern in these analyses.

The transition from the initial phase of the shear rupture zone development (the "inverted footing" type of failure) to the final phase of the shear rupture zone development (the "anchor pull-out" type of failure) can be seen more clearly by examining changes in the pattern of maximum shear strains that develop in the soil overlying the displaced base rock fault. In Figures 7-13(a-c), the shaded elements indicate the zone of maximum shear strain at each level in the soil layer at increasing magnitudes of base deformation (or offset) during the first set of finite element analyses. Figure 7-13(d) (results from the second finite element analyses where $K_O = 1.0$) illustrates one of the effects of increasing the value of K_O from 0.5 to 1.0. Figures 7-13(a-c) clearly show that as the magnitude of base deformation (or offset) increases, the zone of maximum shear strain changes from a position which is concave over the upthrown block to a position which is slightly concave over the downthrown block near the ground surface. Figure 7-13(d) shows that

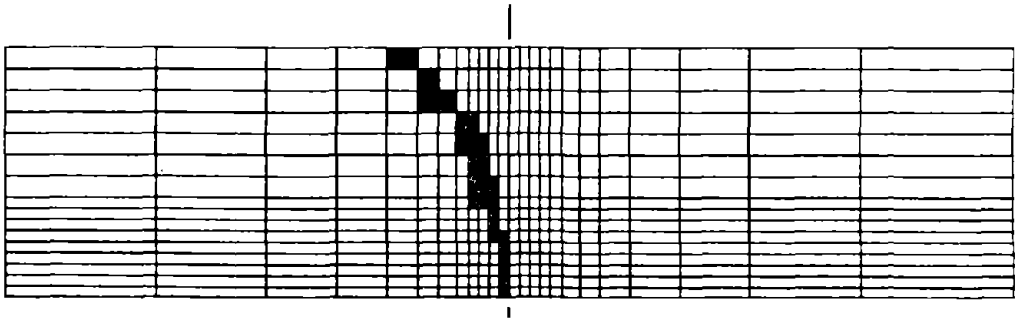

(A) Maximum Shear Strain (K_o = 0.5): 5' offset

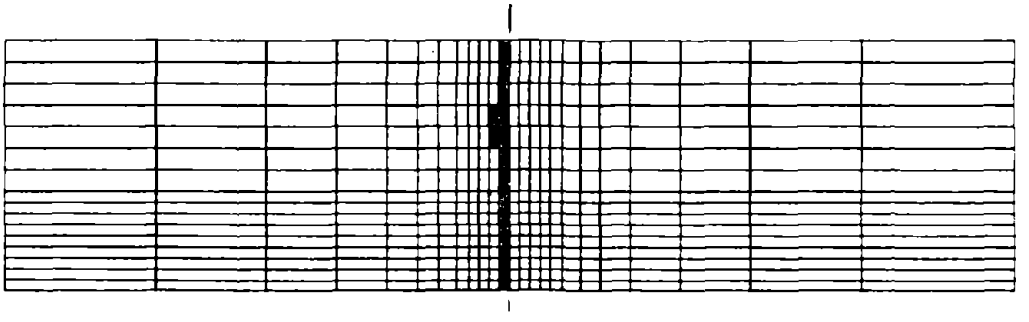

(B) Maximum Shear Strain (K_o = 0.5): 15' offset

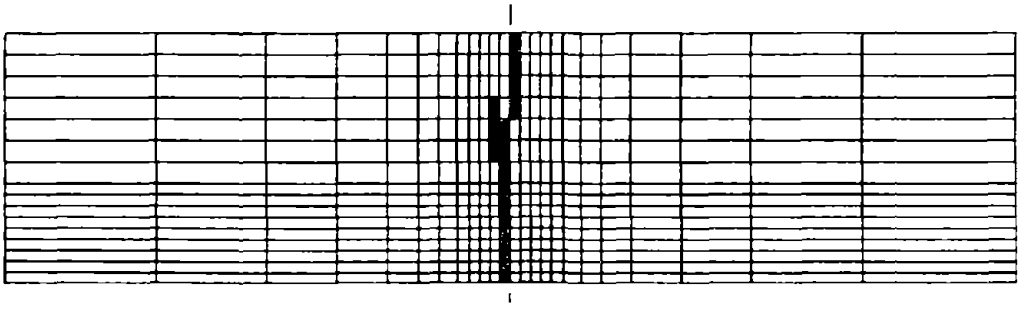

(C) Maximum Shear Strain (K_o = 0.5): 20' offset

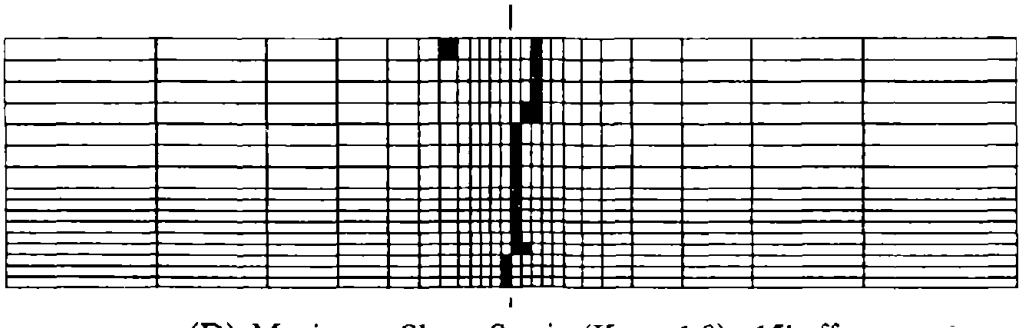

(D) Maximum Shear Strain (K_o = 1.0): 15' offset

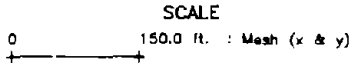

Figure 7-13: RESULTS OF NONLINEAR FINITE ELEMENT ANALYSES OF DRY SAND WITH A 90° THRUST FAULT MOVEMENT: MAXIMUM SHEAR STRAIN

increasing the value of K_o moves the shear rupture zone farther over the downthrown block at the same magnitude of base offset (i.e. 15 feet of base offset).

Additional finite element analyses of fault rupture propagation through dry, cohesionless materials were performed with the base rock fault expressing a thrust fault movement dipping at an angle of 45° and a normal fault movement dipping at an angle of 60° . The results of two of these analyses are shown in Figures 7-14 and 7-15. In these two analyses, the well-graded, medium dense, dry sand overlying the base fault was modeled with essentially the same hyperbolic model parameters employed in the finite element analyses previously described in this section. The coefficient of lateral earth pressure at rest was assumed to be 1.0 for this FEM analysis of the 45° thrust fault, and K_o was assumed to be 0.5 for this FEM analyses of the 60° normal fault. Both sets of the FEM results appeared to agree fairly well with the results of the sandbox experiments described in Section 3.3.2. The rupture zone produced by the 45° thrust fault movement reached the ground surface at a vertical base deformation (or offset) of 14 feet (4.7% of the depth of the overlying sand deposit); whereas, the rupture zone produced by the 60° normal fault movement reached the ground surface at a vertical base deformation (or offset) of 9 feet (3% of the depth of the overlying sand deposit). The Cole and Lade (1984) fault rupture propagation sandbox model tests also indicated that the rupture zone through the dry, cohesionless materials employed in their study propagated faster when the base rock fault movement was a normal dip-slip offset instead of a thrust dip-slip offset.

In the finite element analyses of fault rupture propagation through dry, cohesionless materials, the rupture zone widened as it propagated upwards toward the ground surface. Hence, when the rupture zone reached the ground surface, it was often excessively wide. In physical model tests, the majority of differential movement was concentrated on distinct failure planes. The wider shear failure

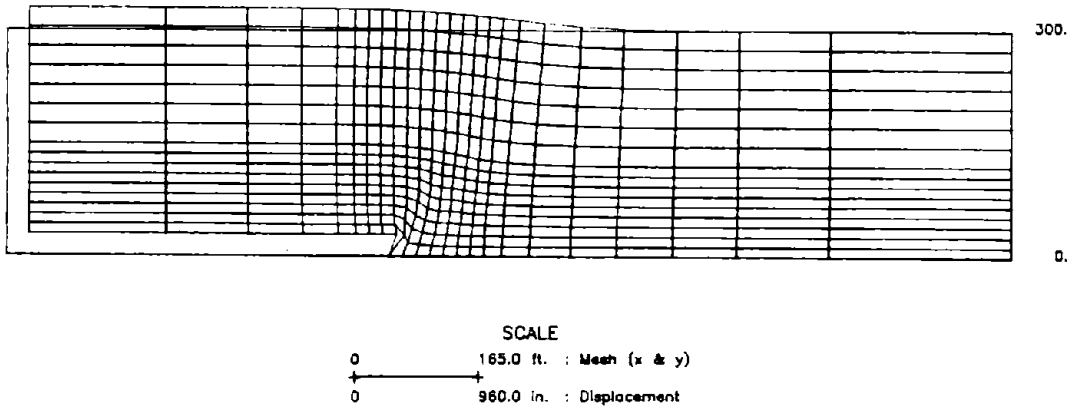

(A) Deformed Mesh: 20' offset

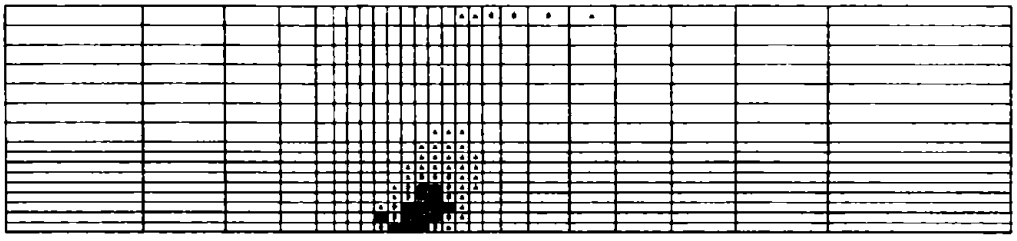

(B) Stress Level: 10' offset

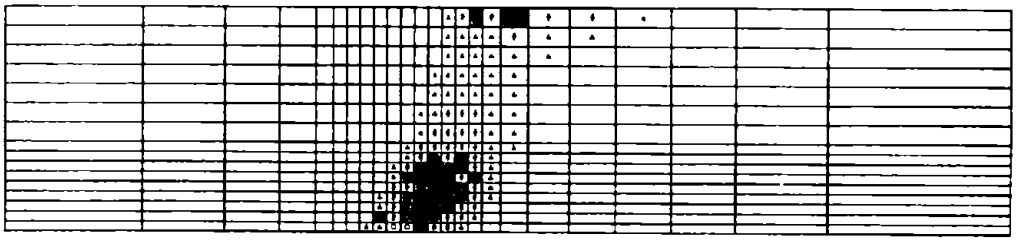

(C) Stress Level: 15' offset

LEGEND
: Shear Failure ♦ : S.L. > 0.85 ▲ : S.L. > 0.70 ○ : Tension Fail.

Figure 7-14: RESULTS OF NONLINEAR FINITE ELEMENT ANALYSES OF DRY SAND (K_o = 1.0) WITH A 45° THRUST FAULT MOVEMENT

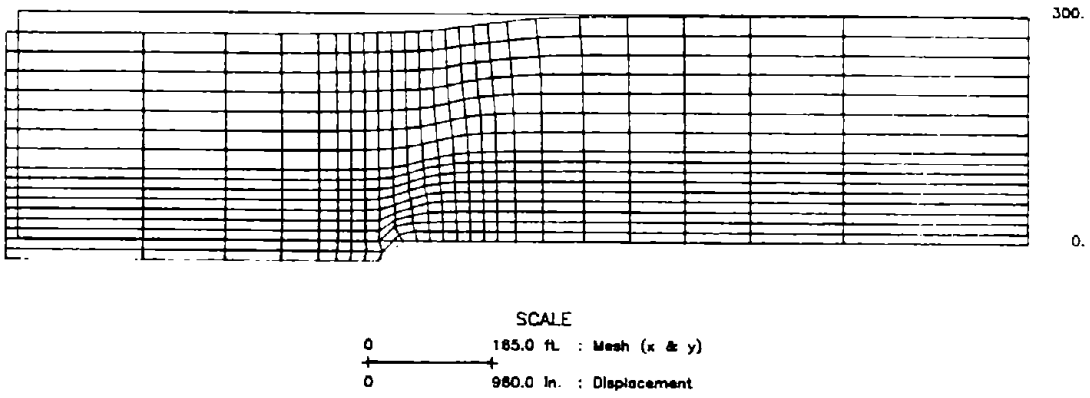

(A) Deformed Mesh: 15' offset

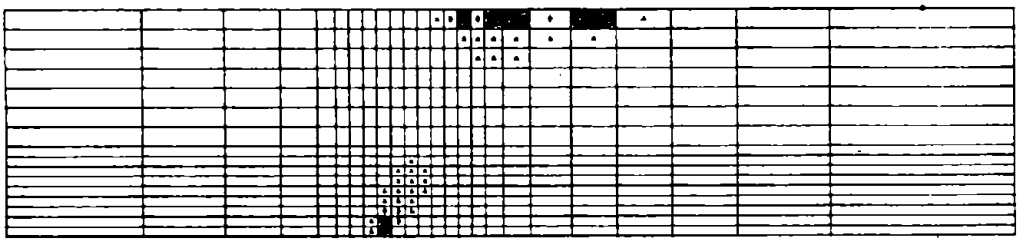

(B) Stress Level: 2.5' offset

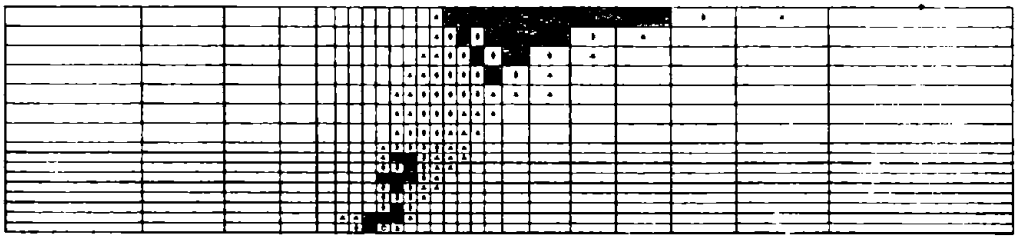

(C) Stress Level: 5.0' offset

Figure 7-15: RESULTS OF NONLINEAR FINITE ELEMENT ANALYSES OF DRY SAND (K_o = 0.5) WITH A 60° NORMAL FAULT MOVEMENT

zone produced in these finite element analyses was, however, likely to envelop the distinct shear failure planes that actually formed in the physical model tests. Furthermore, the base deformation (or offset) required to propagate the shear rupture zone (although it was wider than that produced in the physical model tests) to the ground surface in the finite element models was on the same order of magnitude of that required to propagate the rupture zone to the ground surface in the physical model tests (i.e. base offset of on the order of 2% to 6% of the depth of the overlying sand layer). Moreover, the general characteristics of the failure pattern that developed in the soil overlying a displaced base rock fault predicted by these incremental nonlinear elastic finite element analyses appeared to agree reasonably well with those shown to occur in fault rupture propagation and anchor pull-out physical model tests. Therefore, an appropriate finite element analysis which employs a nonlinear, stress-strain soil behavioral model appears to be capable of modeling the development of shear rupture zones during fault rupture propagation through soil with sufficient accuracy as to represent a useful engineering tool.

7.5.4 Summary:

The results of the preliminary incremental nonlinear elastic finite element analyses of fault rupture propagation through dry, cohesionless soils agree in a general sense with the observed failure patterns that develop in physical model tests. Hence, it appears that the computer program SSCOMP which employs the Duncan et al. (1984) hyperbolic soil model can be used to provide insights into the fault rupture propagation phenomenon. This application of the finite element method did, however, illustrate some of the shortcomings of this numerical approach. For example, these finite element analyses typically predicted a shear failure zone through the soil overlying the displaced bedrock fault that was

excessively wide. On the other hand, the critical characteristics of the development of shear and tension zones in the soil agreed suitably well with observations made during physical model tests so as to provide some level of confidence that the application of the program SSCOMP in the analyses of fault rupture propagation through soil was reasonable.

These preliminary incremental nonlinear elastic finite element analyses brought forth a number of important observations. To improve the accuracy and reliability of these analyses, it is relatively important to employ a large number of smaller sized elements located in the expected region of shear and tension failure. Furthermore, it is relatively important to use a reasonable number of displacement (or load) increments in the solution technique to ensure that the nonlinear stress-strain behavior of the deforming soil can be adequately modeled. The coefficient of lateral earth pressure at rest (K_o) was shown to be a critical soil parameter in analyses of dry, cohesionless materials. Increasing the magnitude of the K_o parameter used to define the soil's initial stress state causes the rupture zone to move farther over the downthrown block. Decreasing the soil's tendency to contract in volume during shear deformation causes the shear rupture zone to propagate upwards toward the ground surface at a faster rate. In addition, when the soil deforms at essentially constant volume, the shear rupture zone becomes significantly narrower than if the soil displayed contractive volume-change behavior during shear deformation. The stress level plots and the maximum shear strain plots both clearly illustrate the two-phase development of the shear rupture zone in the soil overlying a displaced vertical base rock thrust fault. Initially, a zone of highly stressed soil forms over the upthrown block during a vertical base rock fault offset (the "inverted footing" type of failure). As base deformation (or offset) continues, the orientation of the shear rupture zone becomes more vertical, and in the final stages of base deformation, the shear rupture zone forms either

vertically above the vertical base rock fault or slightly bent over toward the downthrown block (the "anchor pull-out" type of failure). Hence, the incremental nonlinear elastic finite element results were kinematically admissible and agreed reasonably well with observations made during physical model tests of fault rupture propagation and anchor pull-out.

7.6 Lessons to be Learned from the Preliminary Numerical Analyses Regarding Fault Rupture Propagation

In Chapter Seven, a number of numerical methods, and consequently, a number of soil constitutive models, were reviewed and evaluated to determine their respective suitability in the study of fault rupture propagation through soil. A number of important lessons were learned from this preliminary review, evaluation, and selection of the numerical analysis method to be applied in this study of the fault rupture propagation phenomenon.

Although the use of the discrete element method looks promising in the analysis of dry soil masses within which shear and tension discontinuities form during deformation, it is a relatively recent approach which requires further development and validation before it can be routinely applied to complex geotechnical problems. The finite difference method with dynamic relaxation also appears to require additional work before this numerical method can be routinely applied in the study of the fault rupture propagation problem. On the other hand, although the finite element method (displacement approach) has limitations, especially in the analysis of the development of failure patterns in soil masses because it is based on the principles of continuum mechanics, it has been successfully utilized to analyze the process of soil rupturing in previous fault rupture propagation studies and in previous anchor pull-out behavior studies. Moreover, this study's preliminary finite element analyses of fault rupture

propagation through soil indicated that the finite element method could provide valuable insights into the fault rupture propagation phenomenon provided that the soil's nonlinear stress-dependent, stress-strain behavior was adequately modeled.

The selection of the soil constitutive model to be employed in the numerical method used to analyze the fault rupture propagation problem proved to be crucial. Linear elastic and linear elastic-perfectly plastic constitutive models produced inconsistent results when employed in the finite element method, but the incremental nonlinear elastic hyperbolic soil model provided significantly better predictions of observed behavior.

The linear elastic analyses of fault rupture propagation did emphasize the importance of monitoring relative nodal displacements (deformed meshes or displacement vector plots) during the fault rupture process for locating the probable rupture zone through the overlying soil. In fact, it appeared that plots of the distribution of maximum shear strain within the soil overlying the displaced base rock fault predicted the region in which the fault rupture zone would most likely develop fairly well. The linear elastic finite element analyses failed, however, to reliably predict the final phase of the development of the shear rupture zone through the disturbed soil (the "anchor pull-out" type of failure). Often, the results from these analyses were not kinematically admissible.

The linear elastic-perfectly plastic finite element analyses of fault rupture propagation through soils were better able to predict observed behavior. The zone of differential displacement in the soil was much more localized when the linear elastic-perfectly plastic soil constitutive model was employed. This soil constitutive model still suffered, however, from the assumption that the pre-failure load-deformation behavior of the soil was linear elastic. Plots of maximum shear stress contours in the disturbed soil overlying the displaced base rock fault were broad and symmetrical, and hence, did not agree reasonably well with observations made

during physical model studies and previous finite element studies of the process of soil rupturing. Moreover, stress level plots, which depicted the development of the shear zone with increasing magnitudes of base deformation (or offset), did not predict the two-phase development of the shear rupture zone above an uplifted base section (i.e. the "inverted footing" and the "anchor pull-out" phases of failure). Furthermore, the linear elastic-perfectly plastic finite element analyses incorrectly predicted that the rupture zone would first reach the ground surface over the upthrown block. Finally, these analyses re-emphasized the importance of adequately modeling the soil's failure strain in this class of problem. It appeared that it was important to correctly represent the soil's actual failure strain in the finite element analyses of fault rupture propagation.

The hyperbolic soil model, which adequately represents the nonlinear stress-strain behavior of soil during shear deformation, appeared to provide acceptable results when employed in an incremental finite element approach. Results of the computer program SSCOMP, which employs the Duncan et al. (1984) hyperbolic soil constitutive model, agreed reasonably well with the results of a number of sandbox and clay-box physical model experiments involving fault rupture propagation and anchor pull-out. The hyperbolic soil constitutive model utilized the traditional Mohr-Coulomb failure criterion which was found to be acceptable in previous studies of this class of problem. Opinions differed as to whether a soil constitutive model employed to study the development of failure in a soil should include velocity characteristics such as the angle of dilation as well as the usual stress characteristics such as the angle of friction. In the majority of cases, it was judged that the difference between the stress characteristics (e.g. the angle of friction) and the velocity characteristics (e.g. the angle of dilation) of the deforming soil mass would be relatively small and would, in fact, be even less

significant in a total stress analysis of a saturated clay under undrained conditions where dilation would not occur.

The preliminary incremental nonlinear elastic finite element analyses of fault rupture propagation through dry, cohesionless materials were judged to indicate that this numerical approach appears to be capable of modeling the development of shear and tension zones during fault rupture propagation with sufficient accuracy as to represent a useful engineering tool. The analyses provided a number of useful observations of the rupturing of soil as a result of a base rock fault offset. Increasing the value of the soil parameter K_o caused the rupture zone to move to a position more over the downthrown block. In addition, decreasing the soil's tendency to contract in volume during shear deformation decreased the magnitude of base offset necessary to propagate the rupture zone to the ground surface. In general, a vertical base deformation (or offset) of on the order of 2% to 6% of the depth of the soil overlying the displaced base rock fault was required to propagate the rupture surface to the ground surface for the cases analyzed (i.e. 300 foot deep deposit of well-graded, medium dense, dry sand with typical engineering soil properties).

The incremental nonlinear elastic finite element analyses of fault rupture propagation required relatively refined finite element meshes (on the order of 400 soil elements to represent a 2-D plane strain condition where the length to height ratio was approximately 4:1) to adequately model the development of shear zones and especially tension zones in the vicinity of the base rock fault. In addition, a larger than usual number of displacement (or load) increments had to be imposed in the computer program SSCOMP (20 instead of the usual 5 to 10) to allow the hyperbolic soil model to adequately represent the nonlinear stress-strain behavior of soil at or near failure. In so doing, the Duncan et al. (1984) hyperbolic soil model appeared to reasonably accurately model the decrease in a soil element's

stiffness as that soil element approached shear failure (maximum deviatoric stress). Finally, the incremental nonlinear elastic analyses correctly predicted the two-phase development of the shear rupture zone in the soil overlying a displaced vertical dip-slip base rock fault (i.e. initially, the "inverted footing" type of failure; followed by the "anchor pull-out" type of failure; See Figure 4-7). In the next chapter, the results of a reasonably comprehensive finite element study of fault rupture propagation through saturated clay using a modified version of the program SSCOMP employing a revised Duncan hyperbolic soil model will be presented and discussed.

CHAPTER EIGHT:
FINITE ELEMENT ANALYSES OF FAULT RUPTURE PROPAGATION THROUGH SATURATED CLAY

8.1 Introduction

The preliminary finite element analyses of fault rupture propagation through soil presented in Chapter Seven suggest that the finite element method can be successfully applied to this class of problem provided that the soil's nonlinear stress-dependent, stress-strain behavior is adequately modeled. The computer program SSCOMP, which employs the Duncan et al. (1984) hyperbolic soil model, appears to be capable of producing results which agree reasonably well with the patterns of soil behavior observed in sandbox model tests of fault rupture propagation. In addition, the preliminary finite element study presented in Chapter Seven provided a number of observations of the sensitivity of the results of the numerical analyses to variations in critical soil parameters. The preliminary evaluation and selection of an appropriate numerical method to be utilized in the study of fault rupture propagation also highlighted a number of deficiencies in the finite element method. Overall, appropriate nonlinear finite element analyses such as the incremental nonlinear elastic finite element approach employed in SSCOMP were judged to be capable of modeling the development of shear and tension zones during fault rupture propagation with sufficient accuracy as to provide a good basis for engineering analyses.

Previous numerical studies of fault rupture propagation described in Section 3.3.3 and the preliminary nonlinear finite element analyses described in Section 7.5 indicate that the finite element method can, at least in a general way, analyze the development of failure in a dry, cohesionless material under certain circumstances. The reasonably comprehensive review of literature performed during the course of

this research found, however, that few previous numerical analyses of fault rupture propagation through saturated clay under undrained conditions had been performed. As discussed previously, the core section of the earth dam is critical to the stability and safe performance of the earth dam built across a potentially active fault. Although a number of other hazards are associated with the rupturing of a fault which passes through the foundation of the earth dam, the hazards associated with the destabilization or failure of the core section of the earth dam pose the gravest dangers to the overall stability of the earth dam. Since the majority of core sections of earth dams are constructed of clayey soils, which in time become saturated, there is a real need to analyze fault rupture propagation through saturated clayey materials under undrained conditions. This will be the focus of the finite element studies presented in Chapter Eight.

In Section 8.2, a slightly modified version of the Duncan et al. (1984) hyperbolic soil model will be developed for use in the computer program SSCOMP to analyze a number of problems involving fault rupture propagation through saturated clay under undrained conditions. In Section 8.3, to validate the use of this incremental nonlinear elastic finite element program, an attempt will be made to predict the results of the fault rupture propagation clay-box model tests performed as a part of this research program and described previously in Chapter Six. In addition, the Davie (1973) anchor pull-out tests in saturated clay materials will be analyzed in Section 8.4. The results of a general finite element study of fault rupture propagation through saturated clay under undrained conditions will then be presented in Section 8.5. The applicability of these two-dimensional, plane strain finite element analyses to the study of the performance of an earth dam core section composed of clayey materials will also be discussed. Finally, in Section 8.6, the lessons to be learned from the incremental nonlinear elastic finite element

analyses regarding fault propagation through saturated clay under undrained conditions will be presented.

8.2 Incremental Nonlinear Elastic Analyses of Saturated Clays

The operation of the computer program SSCOMP which employs the Duncan et al. (1984) hyperbolic soil model has been described previously in Section 7.5.2. The equations presented in Section 7.5.2, as well as Figure 7-9 which illustrates the Duncan hyperbolic stress-strain relationship, describe how the hyperbolic soil model parameters combine to represent the stress-strain and volumetric strain behavior of typical soils. One of the principal assumptions inherent in the Duncan hyperbolic soil model is that the stiffness and the strength of the soil are functions of the minor principal stress. Equations 7-1 and 7-3 (See Section 7.5.2) show that the soil's stiffness and strength increase as the minor principal stress increases during incremental loading. In the analyses of dry, cohesionless sand described previously in Section 7.5, where no porewater pressure exists, the total stresses calculated by the finite element method are equal to the effective stresses within the soil element ($\sigma = \sigma' + u$; $u = 0$), and thus, if effective strength soil parameters are used (c', ϕ'), the Duncan hyperbolic soil model reasonably adjusts the soil's stiffness and strength with calculated variations of the minor principal stress. Therefore, in a drained analysis of a soil mechanics problem, the Duncan hyperbolic soil model can be employed in a straightforward manner in an incremental finite element program such as SSCOMP provided that the appropriate soil parameters are used.

In an undrained analysis of a geotechnical problem, however, the Duncan hyperbolic soil model cannot always be applied in such a straightforward manner. If the undrained analysis is to be performed in terms of effective stresses, then changes in the porewater pressure at points within the soil mass will produce

corresponding changes in the effective stress within the soil mass. But changes in a soil's porewater pressure during shear deformation or loading are not explicitly incorporated into the hyperbolic soil model. As discussed in the previous paragraph, the hyperbolic soil model's governing equations modify the soil's stiffness and strength in terms of changes in the calculated minor principal stress, but within the program SSCOMP, the calculated changes in the minor principal stress are made with respect to global (or total) changes in stress due to external force equilibrium. No attempt is made in the program or in the soil constitutive model to directly adjust the calculated minor principal stress (which is, in essence, the total minor principal stress) for possible changes in the porewater pressure within the soil mass. Thus, in an effective stress analysis of an undrained loading of a soil mass, the Duncan hyperbolic model requires that changes in the porewater pressure at each stage of the incremental loading be reasonably predicted and the calculated minor principal stress (which is a total stress) be adjusted correspondingly so that the model consistently utilizes only effective stresses within the soil constitutive model. The application of the Duncan hyperbolic soil model in this case (an effective stress analysis of an undrained loading) appears to be quite cumbersome and suspect in the sense that it will only be as accurate as the predictions of the incremental changes in porewater pressure at each point in the deforming soil mass.

It appears more reasonable to perform an undrained analysis with the Duncan hyperbolic soil model by utilizing a total stress approach. In a total stress analysis, changes in the total minor principal stress which occur during shear deformation do not produce changes in the soil's stiffness or strength. Instead, the strength of the soil at a point (or within a soil element) would depend only on its initial state and it would not change as the total stress variables changed during the incremental loading. Likewise, the stiffness of the soil at a point (or within a soil

element) would depend only on its initial state and its current stress level (or how close the soil was to failure), and it would not change as the total minor principal stress variable changed during incremental loading. Hence, soil strength in a total stress analysis utilizing the incremental nonlinear finite element program SSCOMP, which employs the Duncan et al. (1984) hyperbolic soil model, would be defined as a constant parameter which did not depend on changes in the calculated minor principal stress. In addition, soil stiffness in a SSCOMP total stress analysis would be defined as a function which depended only on changes in the calculated stress level during incremental loading. Of course, the assumption inherent in this total stress approach is that the total stress hyperbolic soil model parameters adequately represent the behavior of the soil in the field. It is assumed that the excess porewater pressures generated in the field respond similarly to the excess porewater pressures generated during the laboratory tests employed to estimate the hyperbolic soil model parameters.

In mathematical terms (see Equation 7-3 of Section 7.5.2), for the soil strength to be independent of changes in the minor principal stress in the framework of the Duncan hyperbolic soil model, the model's soil strength parameter "ϕ" must be set equal to 0 (so that $2 \cdot \sigma 3 \cdot \sin \phi = 0$). Likewise, examining equation 7-1 (See Section 7.5.2), for soil stiffness to be independent of changes in the minor principal stress in the framework of the hyperbolic soil model, the soil parameter "n" must be set equal to 0 (so that $(\sigma 3/P_a)^n = 1$). Thus, in a total stress analysis, the hyperbolic soil model Equations 7-3 and 7-1 can be simplified as follows:

$$(\sigma 1 - \sigma 3)_f = 2C \qquad (8\text{-}1)$$

$$E_t = (1 - R_f \cdot SL)^2 K \cdot P_a \qquad (8\text{-}2)$$

Similarly, Equations 7-4 and 7-7 (See Section 7.5.2) can be simplified to:

$$E_i = K \cdot P_a \tag{8-3}$$

$$E_{ur} = K_{ur} \cdot P_a \tag{8-4}$$

Another consideration in a total stress analysis of an undrained loading of saturated clay is the need to adequately model the constant volume behavior of the soil mass during shear deformation. To achieve constant volume behavior, Poisson's ratio (ν) must be constrained to be 0.5 or close to 0.5 (in the Duncan hyperbolic soil model, ν = 0.49 to represent constant volume behavior). Because ν = 1/2 - E/6B (Equation 7-9), Poisson's ratio (ν) can be made to be equal to 0.49 by setting the bulk modulus equal to roughly seventeen (17) times the tangent modulus (E_t). In fact, the program SSCOMP currently constrains the bulk modulus (B) in such a manner (e.g. $B = 17 \cdot E_t$) when the Mohr-Coulomb friction angle strength parameter "ϕ" is less than 2.3°. Hence, the values of the model parameters "K" and "m" described in Equation 7-8 (See Section 7.5.2) are irrelevant in these total stress analyses where "ϕ" has already been set equal to 0. Finally, the initial ratio of σ_3 to σ_1 in terms of total stress must be calculated to be input into the program SSCOMP in lieu of $K_o = \sigma_3'/\sigma_1'$, which is in terms of effective stress.

These considerations can be satisfied with the Duncan et al. (1984) hyperbolic soil model currently employed in the computer program SSCOMP by direct manipulation of the values of the soil parameters input into the model. The hyperbolic soil model's current tension failure criteria, however, had to be modified to permit a reasonable total stress analysis of an undrained loading of a typical geotechnical problem. Currently, the program SSCOMP defines tensile failure in a soil element when the minor principal stress (σ_3) is negative. The bulk

modulus (B) assigned to represent a soil element which undergoes tensile failure is computed with Equation 7-8 (See Section 7.5.2) using $\sigma 3$ equal to 0.02 times the atmospheric pressure, and the soil's tangent modulus (E_t) is set equal to one-tenth of the bulk modulus. In cases where the model parameter "m" equals 0, as is the case in a total stress analysis of an undrained loading of saturated clay (actually, in any analysis where the parameter "m" equals 0, which may occur in effective stress analyses involving cohesionless soils, this manner of defining tensile failure does not work as intended), the bulk modulus assigned to an element which fails in tension does not become an extremely small number as intended because with the exponent "m" equal to 0, the value of $(\sigma 3/P_a)^m$ always equals 1.0 and $B = K \cdot P_a$ (which can be a number of substantial magnitude). Consequently, since the soil's tangent modulus equals only one-tenth of the bulk modulus, the stiffness assigned to the soil element which fails in tension is not reduced to an extremely low value as intended, but instead, it can also be a number of substantial magnitude. Hence, the soil element that fails in tension continues to take on additional negative stresses and the soil does not behave as a "no-tension" material. This can produce significant discrepancies in analyses where the "no-tension" criteria is critical to the proper analysis of a geotechnical problem.

To remedy the computer program's inability to achieve the desired "no-tension" soil behavior when a soil element's minor principal stress is negative, SSCOMP has been modified to automatically set the soil's stiffness (or tangent modulus, E_t) to a relatively low value by employing the following equation when the model parameter "m" equals 0:

$$E_t = K \cdot P_a \cdot 0.0001 \qquad (8\text{-}5)$$

The factor (0.0001) reduces E_t when $m = 0$ by roughly the same order of magnitude as the original Duncan et al. (1984) algorithm reduced E_t when $m \neq 0$.

The results of the analyses of the fault rupture propagation problem were essentially insensitive to reasonable variations in this factor (0.0001). The bulk modulus (B) is set equal to seventeen (17) times the tangent modulus (E_t) to maintain Poisson's ratio at approximately 0.49. With this algorithm, the soil stiffness of a soil element which undergoes tensile failure is extremely low so that the soil element does not take on significant additional tensile stresses. Hence, the "no-tension" soil behavior which is critical to properly modeling fault rupture propagation through soil is maintained.

In summary, for the special case of employing the program SSCOMP, which employs the Duncan et al. (1984) hyperbolic soil model, to perform a total stress analysis of saturated clay under undrained loading conditions, the general equations describing the soil constitutive model described previously in Section 7.5.2 are simplified as follows:

$$E_t = (1 - R_f \cdot SL)^2 K \cdot P_a \qquad (8\text{-}6)$$

$$SL = (\sigma_1 - \sigma_3) / (\sigma_1 - \sigma_3)_f \qquad (8\text{-}7)$$

$$(\sigma_1 - \sigma_3)_f = 2C \qquad (8\text{-}8)$$

$$E_i = K \cdot P_a \qquad (8\text{-}9)$$

$$R_f = (\sigma_1 - \sigma_3)_f / (\sigma_1 - \sigma_3)_{ult} \qquad (8\text{-}10)$$

$$E_{ur} = K_{ur} \cdot P_a \quad (K_{ur} \approx (1.5 - 2.0) \cdot K) \qquad (8\text{-}11)$$

$$B = 17 \cdot E_t \quad (\text{i.e.} \nu = 0.49) \qquad (8\text{-}12)$$

In all, effectively only four soil parameters (C, K, K_{ur}, R_f) are required to define the stress-strain and volumetric strain behavior of the soil at a particular point in a soil mass. Since strength and stiffness are a function of the initial state of the saturated clay in a total stress analysis, however, these parameters (C, K, K_{ur}, R_f) should be uniquely defined within each soil element within the finite element

model to adequately represent the earth mass to be modeled. For example, in the case of level ground where the soil's strength and stiffness typically vary as some function of the depth with the soil mass, sufficient horizontal layers of soil elements should be employed in the finite element mesh to adequately model the variation of soil properties (strength and stiffness) with depth. Once incremental loading initiates, while an element is in a state of primary loading, its strength will remain constant and its stiffness will decrease as the stress level increases (i.e. as the soil element approaches failure; failure being defined as the maximum deviatoric stress). If the element is in a state of unloading/re-loading the stiffness is defined by Equation 8-11.

Finally, the results of the clay-box model tests and the preliminary finite element analyses of this research described previously in Chapters Six and Seven, respectively, as well as findings from the review and evaluation of previous studies (Chapters Two through Five), have all emphasized the potential importance of adequately describing the soil's failure strain in studies of fault rupture propagation through soils. In defining the hyperbolic soil model parameters used to represent the stress-strain behavior of the clay soil overlying a bedrock fault, it is essential that the combined effect of establishing values for the model parameters C, K, K_{ur}, and R_f be understood, since together they uniquely define the soil's shear failure strain (ϵ_f). Simplifying Equation 7-12 (See Section 7.5.2) for the special case where $(\sigma_1 - \sigma_3)_f = 2C$, the saturated clay's axial failure strain during undrained loading is defined by:

$$\epsilon_f = 2C/K \cdot P_a(1.05 - R_f) \qquad (8\text{-}13)$$

where P_a equals the atmospheric pressure. Since in the majority of geotechnical problems, the strength parameter "C" is usually known with the highest level of

confidence, for a given value of C, the model parameters K and R_f should be controlled to ensure that the critical soil parameter "ϵ_f" is properly defined.

8.3 Analyses of Fault Rupture Propagation in the Clay-Box Model Tests

In Chapter Six, the results from a series of eleven clay-box model tests of fault rupture propagation through saturated clay were presented. In this section, the computer program SSCOMP, which employs the modified version of the Duncan et al. (1984) hyperbolic soil model described previously in Section 8.2, is applied to the known conditions of these clay-box model tests to examine the capability of this numerical method to reasonably predict the observed results of the fault rupture propagation clay-box model tests. The results of the clay-box model tests will be used to validate the use of the program SSCOMP in a more in-depth study of fault rupture propagation through saturated clay.

The conduct of the clay-box model tests was described in detail in Chapter Six. The stress-strain behavior of the saturated kaolinite-bentonite model clay under undrained conditions has been described by the results of a number of stress-controlled unconfined triaxial compression tests (See Figures 6-5 and 6-7). The majority of the clay-box tests (tests 1-9) were conducted at a relatively fast rate of base displacement (time to failure = 30 - 60 seconds) immediately after placement of the model clay with the model clay at a water content of approximately 130%. The model clay under these conditions behaved as shown in Figure 6-5. Under these conditions, the undrained shear strength of the model clay was approximately 32 psf and the axial failure strain of the clay was on the order of 11%. The hyperbolic stress-strain relationship which "best" describes the general behavior of the model clay under these circumstances is shown as the solid line in Figure 6-5. The hyperbolic soil model parameters that produce this hyperbolic stress-strain relationship are:

$C = 34$ psf (in SSCOMP, shear failure occurs at SL = 95%)

$K = 2.5$

$K_{ur} = 1.5\,K = 3.75$

$R_f = 0.935$

($\epsilon_f = 11\%$)

($\phi = \Delta\phi = 0$; $m = n = 0$; $K_b = 17 \cdot K$)

In addition, the unit weight (γ) of the model clay was roughly 100 pcf, and the initial coefficient of lateral earth pressure at rest (K_o; which is in terms of initial effective stress) was assumed to be 0.7 (i.e. in total stress, $\sigma_3/\sigma_1 \approx 0.89$). In earlier finite element studies of soil rupture through cohesionless materials, the results of the finite element analyses were found to be sensitive to variations in the parameter K_o. In these analyses of the clay-box model tests (undrained loading of saturated clay), however, varying the value of K_o within the range of 0.6 to 0.9 did not significantly affect the finite element results.

Hyperbolic model parameters were also developed to represent the behavior of the model clay under the conditions of clay-box model tests 10 and 11 (See Figure 6-7). In model test 10, the clay-box test was performed at a relatively rapid rate of base displacement after the model clay was allowed to set up over a period of 24 hours after placement of the model clay, which maintained a constant water content of approximately 130%. Under these conditions, the undrained shear strength of the model clay was now approximately 37 psf and the axial failure strain of the clay was on the order of 6% to 7%. The hyperbolic soil model parameters that "best" represent the stress-strain behavior of the model clay material under these conditions are:

$C = 39$ psf

$K = 3.6$

$K_{ur} = 1.5\ K = 5.4$

$R_f = 0.895$

($\epsilon_f = 6.5\%$)

In model test 11, the clay-box test was performed at a relatively slow rate of base displacement (time to failure = 120 - 180 seconds) immediately after placement of the model clay, which had a water content of approximately 130%. Under these conditions, the undrained shear strength of the model clay was now approximately 31 psf and the axial failure strain of the clay was on the order of 14% to 16%. The hyperbolic soil model parameters that "best" represent the stress-strain behavior of the model clay under these conditions are:

$C = 33$ psf

$K = 1.85$

$K_{ur} = 1.5\ K = 2.78$

$R_f = 0.941$

($\epsilon_f = 15\%$)

The finite element model of the clay-box tests was a two-dimensional, plane strain model of a vertical section through the clay-box oriented perpendicular to the strike of the base fault plane. The finite element mesh employed nearly 470 4-node isoparametric soil elements with the majority of smaller elements concentrated in the region directly above the base fault. Similar to the clay-box model testing apparatus, the left half was displaced up or down along prescribed base fault plane orientations. To ensure that the nonlinear incremental elastic finite element approach adequately represented the nonlinear stress-strain

behavior of the model clay material, approximately 50 base displacement increments were utilized to propagate the shear rupture zone to the ground surface of the clay layer. Although preliminary finite element analyses suggested that only 20 to 30 displacement increments were necessary to ensure that the nonlinear stress-strain behavior of the soil was adequately modeled, the additional displacement increments were employed because the additional computational effort was not significant. In fact, the program SSCOMP required only approximately 4 hours of total time on a Digital Micro-VAX mini-computer to perform a 50 displacement increment solution of a finite element model with nearly 470 elements and more than 550 nodal points.

Results of the incremental nonlinear finite element analyses of clay-box model test 9 (60° base thrust fault movement; model clay's failure strain equals 11%) are shown in Figure 8-1. In a general sense, the deformation of the ground surface of the clay layer shown in the deformed mesh of Figure 8-1(a) agrees fairly well with the ground deformation which occurred during the clay-box model test (See Figures 6-22 and 6-25). Within the soil mass, the finite element method employed does not show the distinct failure planes which develop in the clay-box model test, instead a wider zone of distortion indicates the region within which the distinct failure planes might occur.

The upward propagation of the shear rupture zone and the development of tension at the base of the clay layer adjacent to the base fault offset are shown in Figures 8-1(b) and 8-1(c). Initially, the shear rupture zone tends to propagate straight up above the upthrown base section (the "inverted footing" type of failure). With additional base offset, the shear rupture zone bends over toward the downthrown block and ruptures the ground surface roughly along the projection of the 60° base thrust fault satisfying kinematic constraints (the "anchor pull-out" type of failure). The shear rupture zone reaches the ground surface at a vertical base

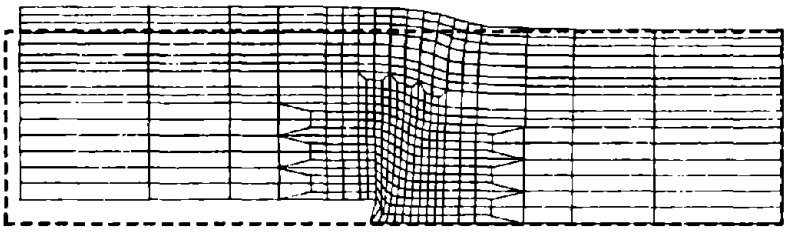

(A) Deformed Mesh: 0.1' vertical offset (12% D_S)

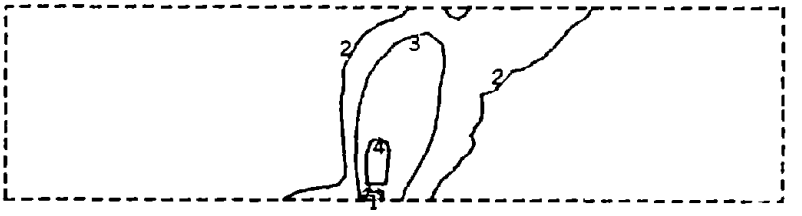

(B) Stress Level: 0.033' vertical offset (4% D_S)

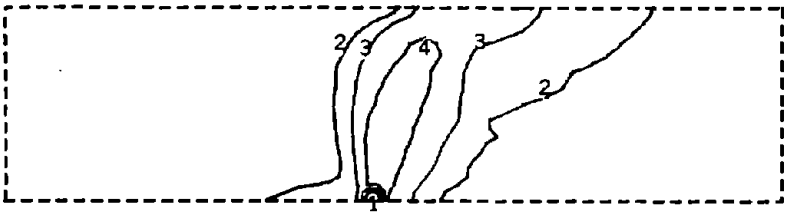

(C) Stress Level: 0.065' vertical offset (8% D_S)

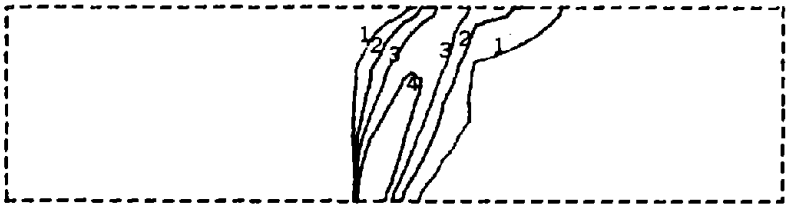

(D) Maximum Shear Strain: 0.1' vertical offset (12% D_S)

Figure 8-1: RESULTS OF NONLINEAR FINITE ELEMENT ANALYSES OF CLAY-BOX 60° THRUST FAULT MODEL TEST 9: ϵ_f = 11%

offset of roughly 0.085 feet or 11% of the depth of the overlying clay layer, which agrees reasonably well with the results of clay-box model test 9 where a vertical base deformation of between 10% to 11% of the depth of the overlying clay layer was required to propagate the rupture zone to the ground surface. Again, in this finite element approach, the shear rupture is not localized to a distinct failure plane, but instead a wider zone of shear failure. Accepting this limitation of the finite element method, the finite element analyses predict at least in a general way the zone within which distinct shear failure planes form. Figure 8-1(d) shows that the plot of maximum shear strain contours is also useful in identifying the most likely location of the shear failure planes which actually develop in the clay-box model test. Finally, Figure 8-1(b) appears to indicate that a small, local zone of tension develops in the vicinity of the base fault. It was difficult to see the development of tension zones at the base of the clay-box during the 60° thrust fault movement model tests.

Results of the incremental nonlinear finite element analyses of clay-box model tests 10 and 11 (60° base thrust fault movement; model clay's failure strain equals 6.5% and 15% in model tests 10 and 11, respectively) are shown in Figures 8-2 and 8-3. Whereas, it took a vertical base offset of roughly 11% of the depth of the clay layer to propagate the shear rupture zone to the ground surface in the finite element analysis of clay-box model test 9 where the failure strain of the clay was in the order of 11%; the finite element analyses of model test 10 predict that a vertical base offset of only 0.055 feet or 7% of the depth of the clay layer is required to propagate the shear rupture zone to the ground surface when the model clay's failure strain has been reduced to only 6.5%. The finite element prediction of the magnitude of base offset necessary to propagate the rupture zone to the ground surface (7% D_S) agrees reasonably well with the result of the clay-box model test (6% D_S). In addition, the formation of the shear rupture zone in

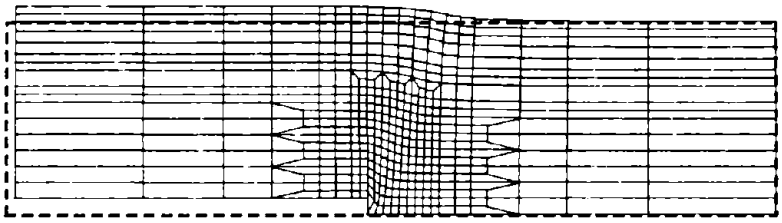

(A) Deformed Mesh: 0.065' vertical offset (8% D_S)

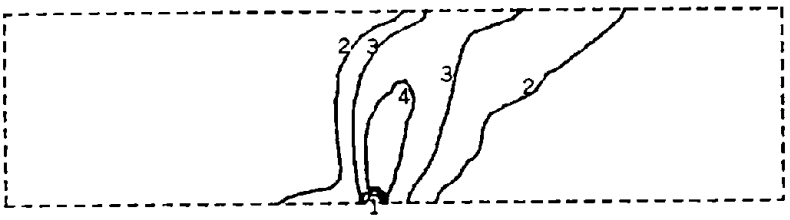

(B) Stress Level: 0.033' vertical offset (4% D_S)

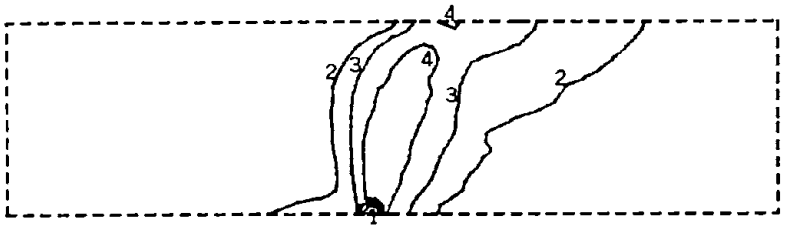

(C) Stress Level: 0.046' vertical offset (6% D_S)

(D) Maximum Shear Strain: 0.065' vertical offset (8% D_S)

Figure 8-2: RESULTS OF NONLINEAR FINITE ELEMENT ANALYSES OF CLAY-BOX 60° THRUST FAULT MODEL TEST 10: ϵ_f = 6.5%

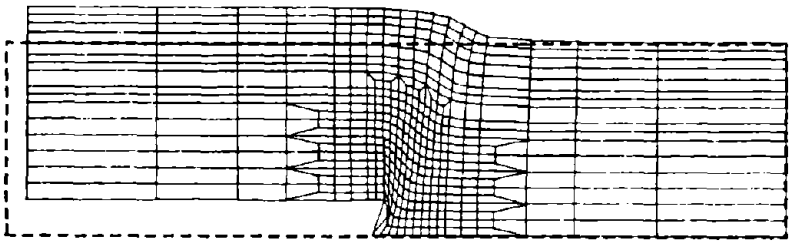

(A) Deformed Mesh: 0.1' vertical offset (20% D_S)

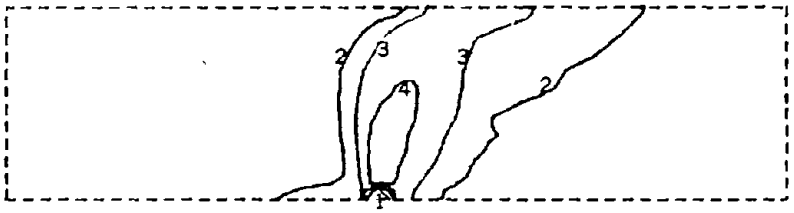

(B) Stress Level: 0.046' vertical offset (9% D_S)

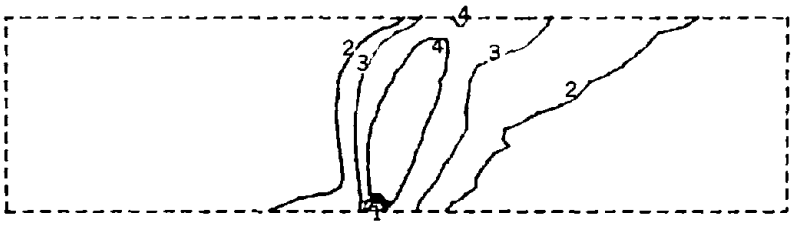

(C) Stress Level: 0.065' vertical offset (12% D_S)

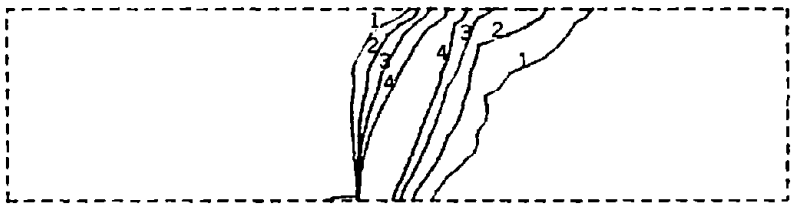

(D) Maximum Shear Strain: 0.1' vertical offset (20% D_S)

Figure 8-3: RESULTS OF NONLINEAR FINITE ELEMENT ANALYSES OF CLAY-BOX 60° THRUST FAULT MODEL TEST 11: ϵ_f = 15%

clay-box model test 10 is predicted reasonably well by this nonlinear finite element analysis.

The finite element analyses of model test 11 predict that a vertical base offset of 0.075 feet or 14% of the depth of the clay layer is necessary to propagate the shear rupture zone to the ground surface, and this agrees fairly well with the results of clay-box model test 11 where a vertical base offset of between 11% to 13% of the depth of the overlying clay layer was required to propagate the rupture zone to the ground surface. In all three finite element analyses of the 60° thrust fault model tests (as well as in the actual clay-box model tests), the shapes of the shear rupture zones in the soil mass are fairly similar. Figure 8-4, which shows the agreement between the nonlinear finite element analyses' prediction of the rate of growth of the shear rupture zone with respect to the observed rate of growth of the rupture zone during the clay-box model tests, appears to indicate that the incremental nonlinear elastic finite element program SSCOMP (which employs a modified version of the Duncan et al. (1984) hyperbolic soil model) is capable of predicting the general development of failure in the soil overlying a base fault movement. It appears that the ability of the hyperbolic soil model to adequately represent the essential characteristics of the soil's stress-strain behavior, particularly, the soil's failure strain, is the primary reason for this numerical method's success in satisfactorily predicting fault rupture propagation through saturated clay.

Results of the finite element analyses of clay-box model test 8 (See Figure 8-5: 60° normal fault movement; failure strain of the model clay equals 11%) also appear to agree fairly well with the observed behavior of the saturated clay material during the 60° normal fault model tests described previously in Section 6.3.4. The shear rupture zone in the clay soil in both the numerical analyses and the clay-box tests appears to generally follow the projection of the underlying base

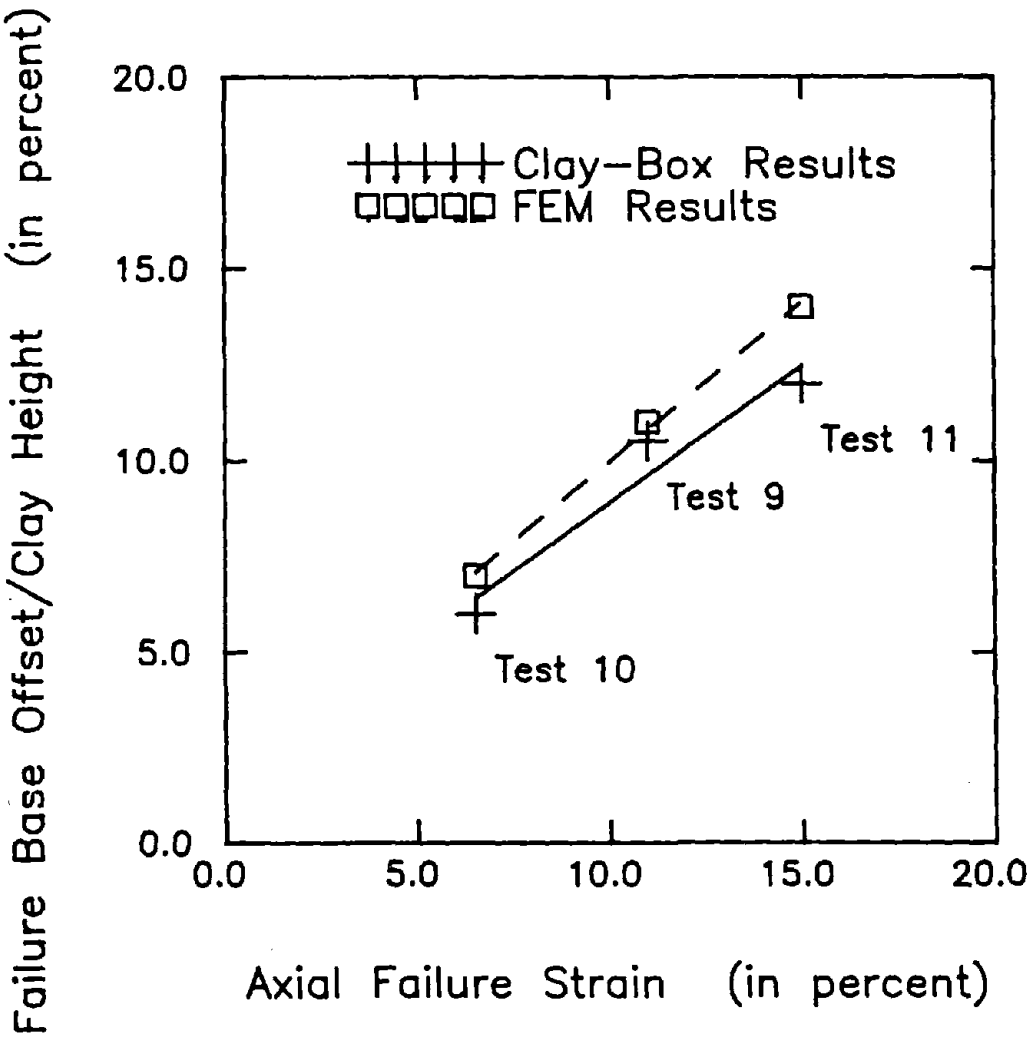

Figure 8-4: NONLINEAR FINITE ELEMENT PREDICTION OF THE RELATIONSHIP BETWEEN THE NORMALIZED BASE OFFSET REQUIRED TO PROPAGATE THE SHEAR RUPTURE ZONE TO THE GROUND SURFACE AND THE FAILURE STRAIN OF THE SOIL

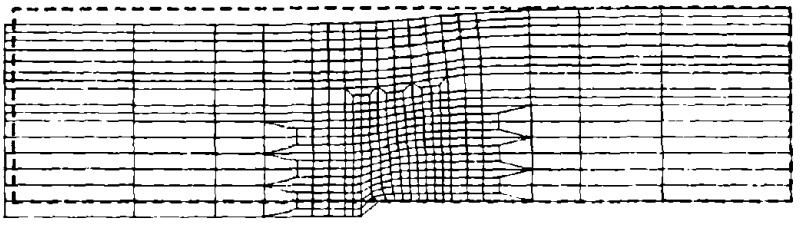

(A) Deformed Mesh: 0.065' vertical offset (8% D_S)

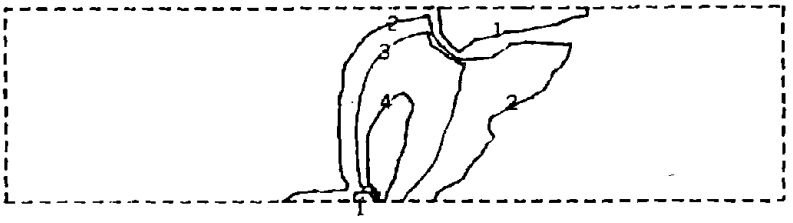

(B) Stress Level: 0.046' vertical offset (6% D_S)

(C) Stress Level: 0.065' vertical offset (8% D_S)

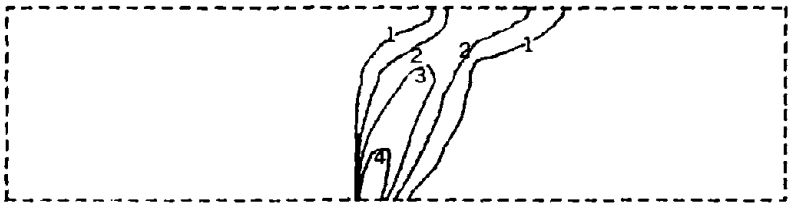

(D) Maximum Shear Strain: 0.065' vertical offset (8% D_S)

Figure 8-5: RESULTS OF NONLINEAR FINITE ELEMENT ANALYSES OF CLAY-BOX 60° NORMAL FAULT MODEL TEST 8: ϵ_f = 11%

fault. The rupture zone reaches the ground surface in the finite element analyses at a vertical base offset of around 8% to 9% of the depth of the clay; whereas, the rupture zone propagates up to the ground surface in the clay-box tests at a vertical base offset of on the order of 10% to 11% of the depth of the clay.

The results of these nonlinear finite element analyses appear to be somewhat sensitive to the tension failure criteria employed in the numerical model. The rupture zone reaches the ground surface earlier in the finite element analyses of the 60° normal fault movement because the finite element analyses predict that tension develops at the ground surface as the shear rupture is propagating up from the base offset. Hence, a complete rupture zone through the saturated clay is formed through the clay layer at a lower magnitude of base deformation with shear failure occurring in the lower three-quarters of the clay layer and tension failure occurring in the top one-quarter of the clay layer. In the clay-box model tests, it was difficult to observe the development of tension zones, and the development of a zone of tension near the clay surface was not clearly observed until the base offset was of sufficient magnitude to propagate the shear rupture to the top of the clay.

The kaolinite-bentonite model clay's apparent unusually high tensile strength (to scale) might also partially explain this slight discrepancy in the results of the finite element analyses and the clay-box model tests. In the majority of natural soils, it is assumed that tension develops in a soil mass the moment that the minor principal stress becomes negative; whereas, the sticky model clay material employed in this study appears to be able to sustain tensile stresses (at least in the short-term). In simple tensile tests of the model clay material, where the model clay was rolled into a thin, relatively uniform strand of soil (similar to the procedure employed in the standard plasticity index test, except the water content of the model clay is above the soil's liquid limit) and then held up to see if the

strand of soil can sustain the tensile stresses imposed by the soil's self-weight, the model clay was shown (at least qualitatively) to possess some amount of tensile strength in the short-term. Accordingly, the program SSCOMP was modified in the analyses of the clay-box model tests to allow tensile stresses to develop in the model clay material up to the point where the minor principal stress exceeded the new tension cut-off stress of "-C" (where C = undrained shear strength of the model clay). This adjustment of the program's tension cut-off criterion improved the ability of the finite element analyses to predict the general behavior of the saturated clay during base fault movement. It was judged reasonable to employ the tension cut-off criterion of "-C" because this tensile failure criterion has been shown to be appropriate in a number of more sophisticated tensile tests of saturated clay soils (e.g. Davie, 1973), and the simple tensile tests of this study could not be used as a basis for clearly establishing that this model clay's tensile capacity was greater than "-C". As previous finite element studies had suggested, the definition of tensile failure in the soil mass appears to affect the results of the analyses of small-scale models where the original stresses throughout the soil mass are low and zones of possible tension are extensive.

The results of the nonlinear finite element analyses of the fault rupture propagation clay-box experiments where either a 90° thrust fault movement or a 90° normal fault movement was imposed agree reasonably well with the results of the vertical fault clay-box tests. The deformed meshes (Figures 8-6(a) and 8-7(a)) of both types of fault movements predict the warped shape of the ground surface fairly well. The development of the shear rupture zone through the model clay layer is similar in shape and in rate of growth in both the finite element analyses and the clay-box tests (Compare the finite element results shown in Figures 8-6 (b-d) and 8-7(b-c) with the results of the clay-box model tests shown in Figures 6-11 through 6-16). The final shear rupture zone in the finite element analyses

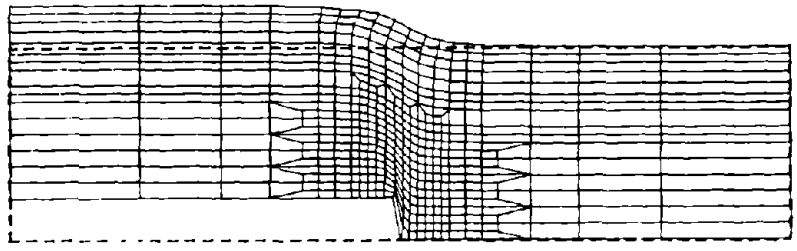

(A) Deformed Mesh: 0.2' vertical offset (22% D_S)

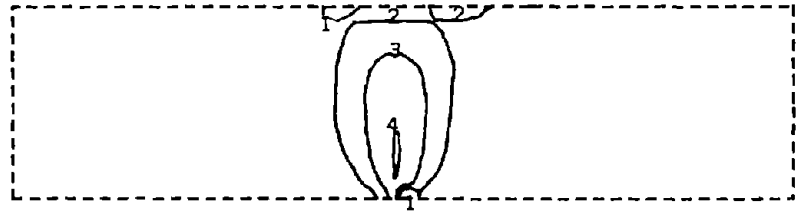

1 Tension Failure
2 Stress Level = 50%
3 Stress Level = 75%
4 Shear Failure

(B) Stress Level: 0.033' vertical offset (4% D_S)

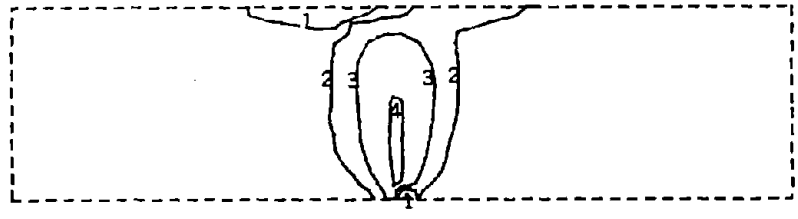

1 Tension Failure
2 Stress Level = 50%
3 Stress Level = 75%
4 Shear Failure

(C) Stress Level: 0.046' vertical offset (5% D_S)

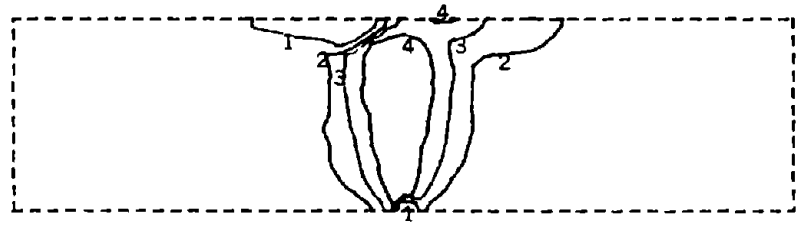

1 Tension Failure
2 Stress Level = 50%
3 Stress Level = 75%
4 Shear Failure

(D) Stress Level: 0.16' vertical offset (18% D_S)

Figure 8-6: RESULTS OF NONLINEAR FINITE ELEMENT ANALYSES OF CLAY-BOX 90° THRUST FAULT MODEL TESTS 1, 2, & 3: ϵ_f = 11%

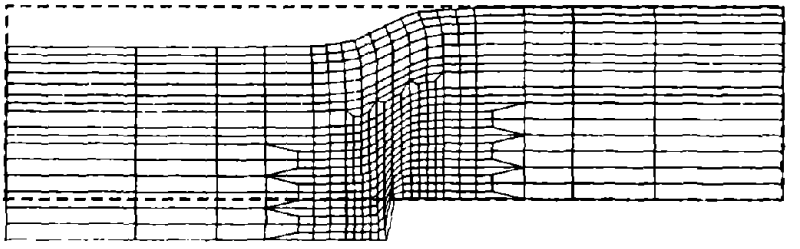

(A) Deformed Mesh (Test 4): 0.2' vertical offset (22% D_S)

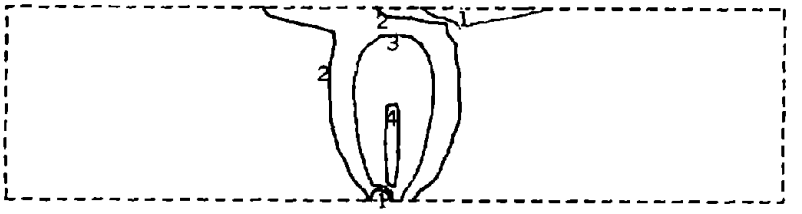

(B) Stress Level (Test 4): 0.046' vertical offset (5% D_S)

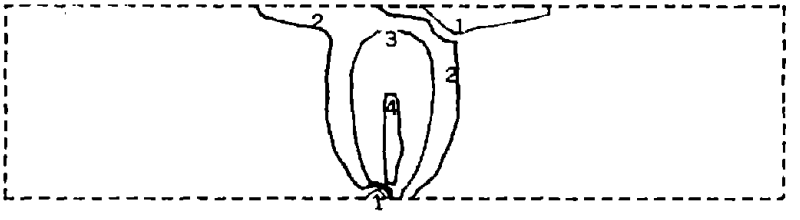

(C) Stress Level (Test 5): 0.033' vertical offset (5% D_S)

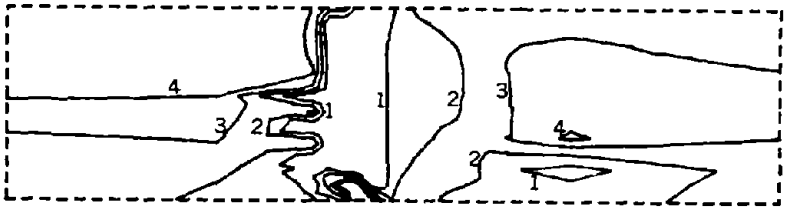

(D) Orientation of the Minor Principal Stress to the Horizontal (Test 4): 0.046' vertical offset (5% D_S)

Figure 8-7: RESULTS OF NONLINEAR FINITE ELEMENT ANALYSES OF CLAY-BOX 90° NORMAL FAULT MODEL TESTS 4 & 5: ϵ_f = 11%

propagates straight up from the vertical base fault and bends over toward the downthrown block side near the ground surface (the "anchor pull-out" type of failure). Hence, the final solution of the incremental nonlinear elastic finite element analyses of fault rupture propagation through saturated clay is kinematically admissible. In addition, the finite element prediction that the shear rupture zone propagates to the ground surface in the vertical base fault clay-box model tests at a normalized vertical base deformation (d_b/D_s) of on the order of 16% to 18% agrees fairly well with the results of the actual clay-box tests where a normalized vertical base deformation (d_b/D_s) of between 10% to 18% was required to propagate the rupture zone to the ground surface.

Moreover, the development of tension zones predicted by the finite element analyses agrees reasonably well with the sequence of tension failure in the clay-box model tests. In both, at higher magnitudes of base deformation (or offset), a small, local zone of tension develops at the base of the clay layer adjacent to the base fault over the downthrown block, and a larger tension zone develops near the ground surface of the clay above the upthrown block. Similar to the results of the clay-box tests, the finite element results indicate that regardless of whether the vertical fault movement displays a normal fault or thrust fault movement and regardless of whether the depth of the clay layer is close to 6 inches or 12 inches, the characteristics of the failure patterns that develop in the saturated clay soil overlying the displaced base fault are essentially the same.

The nonlinear finite element analyses provide the opportunity to investigate how the stress distribution changes throughout the clay layer at different magnitudes of base offset, and to note the potential ramifications of the resulting stress states in the soil. In some of the clay-box tests, nearly horizontal shear or tensile cracks were observed in the rupture zone region before the full development of the nearly vertical main shear rupture. These cracks or failure

planes appeared to be either the complementary shear planes of the nearly vertical main shear rupture plane through the clay layer or local tensile cracks in the clay soil. Figure 8-7(d) shows that at relatively small base offsets, the stress distribution within the clay layer overlying a displaced vertical fault is modified so that the minor principal stress, which was initially oriented horizontally, is oriented more in a nearly vertical direction in the rupture zone region. This re-orientation of the minor and major principal stresses might help produce the nearly horizontal shear or tension cracks that appear to develop in the rupture zone region directly overlying the displaced base fault. For example, the formation of nearly horizontal tension cracks would be more likely to occur in this region where the minor principal stress tends to act on these nearly horizontal planes of failure. On the other hand, a 45° re-orientation of the principal stresses would help explain the development of the vertical and horizontal shear failure planes in the rupture zone. In any case, it is important to note how the stresses within the soil mass change during the process of base rock fault rupture propagation, and the nonlinear finite element method appears to be capable of providing pertinent insights.

Another interesting aspect of these nonlinear finite element analyses of the clay-box model tests was the re-emphasis of the relative importance of the soil's failure strain. If hyperbolic soil model parameters were selected to model the stress-strain behavior of the model clay at a water content of approximately 105% (where the clay's undrained shear strength was roughly 50 psf or more than 1.5 times the strength of the clay at a water content of approximately 130% (32 psf), but the clay's axial failure strain was only around 10% instead of 11%; see Figure 6-6), the nonlinear finite element method predicted that the rate of shear rupture growth in the stronger, lower water content model clay material (C = 50 psf) was only slightly less than the rate of growth of the shear rupture zone in the weaker, higher water content model clay material (C = 32 psf). The results of the finite

element analyses were found to be much more sensitive to variations in the soil's failure strain than in larger variations in the soil's undrained shear strength. Hence, these analyses suggest that the failure strain of the soil, not its strength, is the most important parameter to model in analyses of fault rupture propagation through soil.

In summary, the reasonable agreement between the results predicted by the nonlinear finite element analyses and the actual results of the clay-box model tests provide a basis for concluding that the incremental nonlinear elastic finite element program SSCOMP, which employs a slightly modified version of the Duncan et al. (1984) hyperbolic soil model, is capable of being used as an engineering tool in the study of fault rupture propagation through saturated clay. If the hyperbolic model parameters are properly fitted to adequately represent the nonlinear stress-strain behavior of the model clay material under the conditions imposed by the clay-box experiment (fast or slow base displacement rate; testing immediately after placement of the model clay or after a delay of 24 hours), in particular, if the hyperbolic soil model parameters are "fitted" to adequately represent the failure strain of the model clay, the program SSCOMP provides reasonably accurate predictions of the observed behavior of the soil overlying the displaced base fault. Figure 8-4 clearly suggests that these nonlinear finite element analyses can reasonably predict the development of fault rupture propagation through soil observed in the clay-box model tests.

The incremental nonlinear elastic finite element approach, however, was also shown to possess some shortcomings. The finite element method tended to exaggerate the width of the rupture zone, and the results of the analyses were shown to be somewhat sensitive to the selection of the tensile failure criteria. Yet, the nonlinear finite element method was able to model the principal characteristics of the development of failure in the saturated clay soil overlying the displaced base

fault so the application of this analytical method to the study of fault rupture propagation was judged to be reasonable in terms of the expected accuracy of engineering analyses of the complex phenomenon of fault rupture propagation. Therefore, the use of the program SSCOMP in the study of fault rupture propagation through saturated clay is judged to be reasonably validated based on its agreement with the results of the clay-box model tests.

8.4 Analyses of the Davie (1973) Anchor Pull-Out Clay-Box Model Tests

In Section 4.2.2(b), a series of 1g small-scale clay-box model tests which studied anchor pull-out behavior were discussed. In this section, the results of these anchor pull-out model tests will be used to investigate the capability of the incremental nonlinear elastic finite element program SSCOMP, which employs a slightly modified version of the Duncan et al. (1984) hyperbolic soil model, to reasonably predict the general characteristics of the failure patterns (both shear and tension) that develop in the saturated clay overlying the displaced anchor plate. Davie (1973) showed that the finite element method could be used to predict the ultimate pull-out capacity of the model anchors embedded in clay reasonably well. In this study, the emphasis, however, will be on the capability of the finite element method to predict the nature of the failure patterns that develop in the saturated clay soil that overlies the displaced base section.

The results of three "typical" anchor pull-out model tests were described in detail in Section 4.2.2(b) and shown in Figure 4-5. The soil overlying the displaced anchor plate displayed three general forms of behavior at or near "failure" (failure is defined as the base displacement necessary to produce the maximum anchor pull-out capacity): shallow, intermediate, and deep anchor behavior. In the shallow anchor case, tension failure zones within the soil mass were extensive. In the deep anchor case, a local shear failure zone or plastic zone formed above the

displaced anchor plate. In the intermediate anchor case, the soil exhibited both tensile and shear failure. It is hoped that the incremental nonlinear finite element approach will be able to predict these three distinctive forms of soil behavior at the appropriate depth of anchor embedment and at the appropriate level of anchor displacement.

The computer program SSCOMP was utilized to analyze a two-dimensional (2-D) plane strain vertical cross section through the center of the anchor plate. The depth of the clay overlying the base anchor plate was approximately 6 inches for the shallow anchor case (D/B = 1.5), 8 inches for the intermediate anchor case (D/B = 3), and 12 inches for the deep anchor case (D/B = 4.5). The length to depth ratios of the finite element meshes employed in these analyses ranged from 2.5:1 for the deep anchor case to 6:1 for the shallow anchor case. Nearly 300 4-node isoparametric elements were used to model the soil overlying the anchor in the shallow anchor case and nearly 470 4-node isoparametric elements were employed in the analyses of the intermediate and deep anchors. Approximately 50 gradually increasing displacement increments were imposed to produce the ultimate failure condition for the uplifted anchor.

Davie (1973) provided unconfined triaxial compression test data for the saturated clay soil employed in the clay-box model tests described in Section 4.2.2.(b). For the three tests shown in Figure 4-5, the undrained shear strength was roughly 175 psf for the shallow and deep anchor cases and 205 psf for the intermediate anchor case. In all three tests, the axial failure strain of the glyben (a mixture of bentonite and glycerine) was on the order of 20%. Appropriate hyperbolic soil model parameters were selected to reasonably represent the nonlinear stress-strain behavior and the constant volume behavior of the glyben. In the finite element analyses of the shallow and deep anchor cases, these hyperbolic soil model parameters were assigned:

$C = 175$ psf

$K = 14.5$

$K_{ur} = 1.5\,K = 21.8$

$R_f = 0.995$

($\epsilon_f = 20\%$)

In the intermediate anchor case, these hyperbolic soil model parameters were assigned:

$C = 205$ psf

$K = 14.5$

$K = 1.5\,K = 21.8$

$R_f = 0.985$

($\epsilon_f = 20\%$)

In all three analyses, the unit weight of the clay (γ) was 106 pcf and the coefficient of lateral earth pressure at rest (K_o) was assumed to be 0.9 (in total stress, $\sigma 3/\sigma 1 = 0.96$). In this total stress analysis of a saturated clay under undrained loading conditions, the remaining hyperbolic soil model parameters were assigned as follows: $\phi = \Delta\phi = 0$, $m = n = 0$, and $K_b = 8.33 \cdot K$ (i.e. $\nu \approx 0.48$).

The results of the nonlinear finite element analyses are presented in Figures 8-8, 8-9, and 8-10. In part (a) of each of these figures, the deformed meshes of the finite element models of the shallow, intermediate, and deep anchor cases at the magnitude of anchor displacement shown in Figure 4-5 are presented. There appears to be fairly good agreement between the observed patterns of displacement in the clay-box model tests and the patterns of displacement predicted in the finite element analyses. In the shallow anchor case, the clay directly above the anchor plate is fairly undeformed, whereas the top surface of the clay layer is greatly deformed. On the other hand, in the deep anchor case, the clay

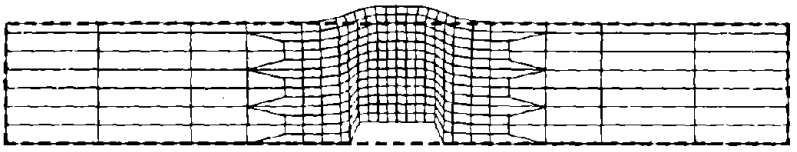

(A) Deformed Mesh: 0.1' vertical uplift (18% D)

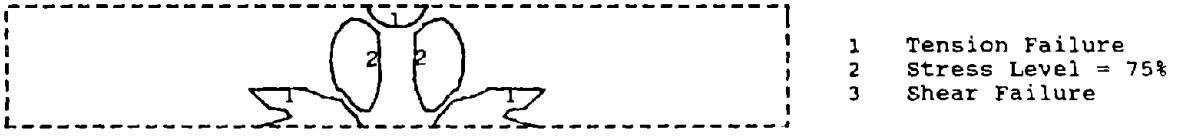

(B) Stress Level: 0.035' vertical uplift (7% D)

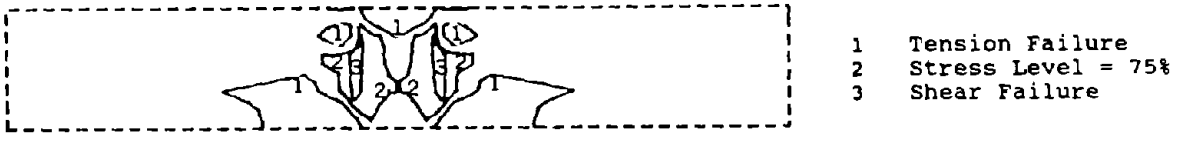

(C) Stress Level: 0.060' vertical uplift (12% D)

Figure 8-8: RESULTS OF NONLINEAR FINITE ELEMENT ANALYSES OF DAVIE (1973) ANCHOR PULL-OUT MODEL TESTS: D/B = 1.5

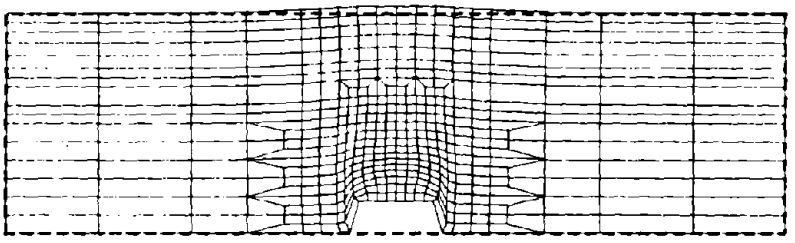

(A) Deformed Mesh: 0.1' vertical uplift (15% D)

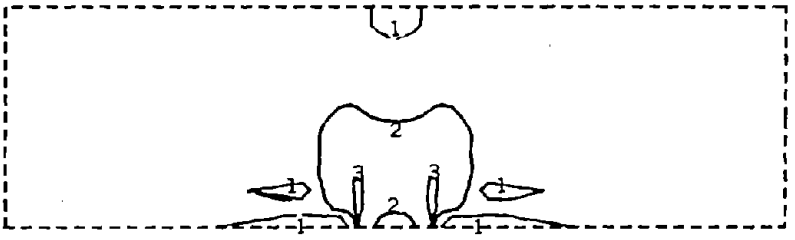

(B) Stress Level: 0.035' vertical uplift (6% D)

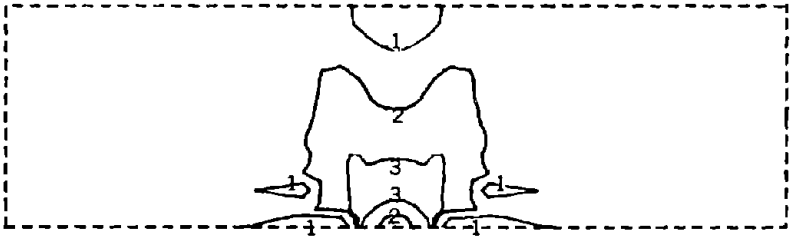

(C) Stress Level: 0.060' vertical uplift (9% D)

Figure 8-9: RESULTS OF NONLINEAR FINITE ELEMENT ANALYSES OF DAVIE (1973) ANCHOR PULL-OUT MODEL TESTS: D/B = 3.0

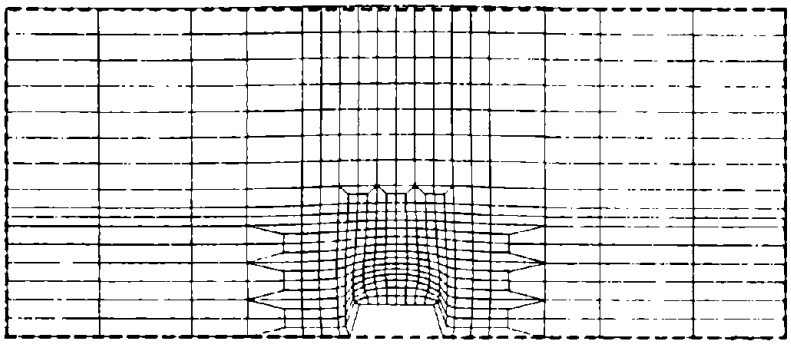

(A) Deformed Mesh: 0.1' vertical uplift (10% D)

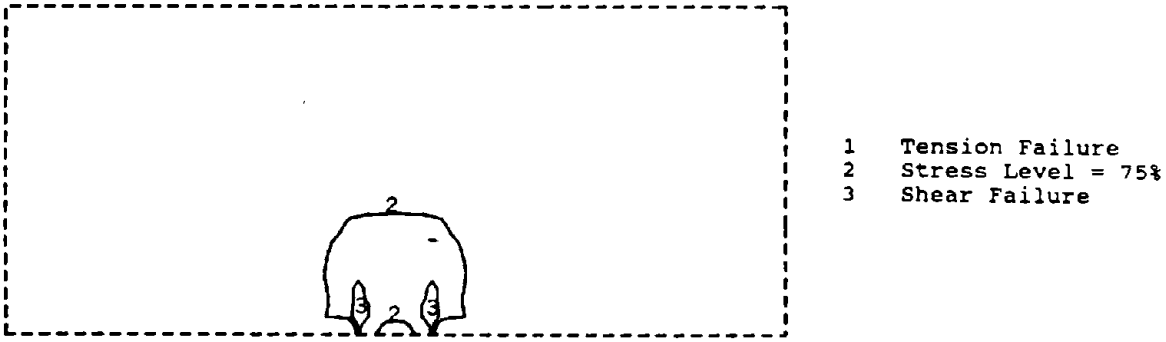

(B) Stress Level: 0.035' vertical uplift (4% D)

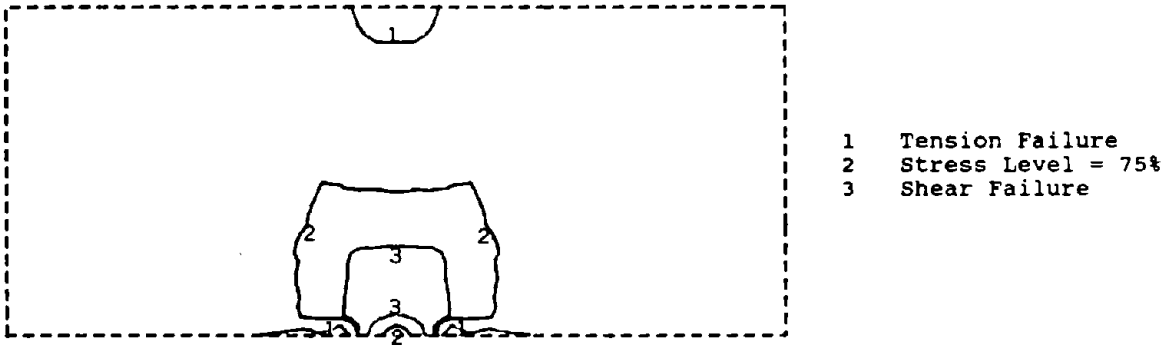

(C) Stress Level: 0.1' vertical uplift (10% D)

Figure 8-10: RESULTS OF NONLINEAR FINITE ELEMENT ANALYSES OF DAVIE (1973) ANCHOR PULL-OUT MODEL TESTS: D/B = 4.5

directly above the anchor plate shows much deformation, whereas the deformation of the top surface of the clay layer is barely noticeable.

Likewise, each of the respective finite element results shows the correct development of failure in the soil mass overlying the uplifted anchor plate for the shallow, intermediate, and deep anchor cases. The shallow anchor finite element results indicate that tensile failure in the soil mass is pervasive. As shown in Figure 8-8(b), tension zones form at the base of the clay-box in the regions adjacent to the edge of the anchor plate and at the top surface of the clay layer directly above the anchor plate. At larger anchor plate displacements (Figure 8-8(c)), these tension zones grow and additional tension zones develop in the clay layer near the ground surface. In addition, nearly vertical shear failure zones form above the edge of the uplifted anchor plate. These results of the nonlinear finite element analyses shown in Figure 8-8 agree reasonably well with the pattern of failure that developed in the actual clay-box model test shown in Figure 4-5(a). Finally, the magnitude of anchor plate displacement required to produce failure in the soil in the clay-box model tests (i.e. the amount of anchor plate uplift at or near ultimate pull-out capacity) was on the order of 0.5 to 1.0 inch, which agrees fairly well with the magnitude of anchor plate displacement that produces failure in the finite element analyses (which was 0.6 to 1.1 inches). The magnitude of the anchor plate displacement required to produce "failure" in the soil overlying the anchor could only be roughly estimated because of the highly nonlinear load-deformation behavior of the anchor at or near failure (i.e. maximum pull-out load). Hence, the point of failure is not clearly defined, rather it is estimated as the magnitude of anchor plate displacement when the anchor pull-out load is within 10% of the maximum anchor pull-out load during the test.

Comparing the results of the finite element analyses of the intermediate and deep anchor cases shown in Figures 8-9(b-c) and 8-10(b-c) with the results of the

anchor pull-out model tests shown in Figure 4-5(b-c), it appears that the nonlinear finite element analyses reasonably predict the development of failure in the saturated clay soil overlying the uplifted anchor plate. In the intermediate anchor case, the analyses properly show the development of tension zones to the outside of the edge of the anchor plate and at the ground surface above the anchor plate. The plastic zone directly above the anchor plate looks similar in both the results of the analyses and the model tests. In the deep anchor case, tensile failure develops only after larger magnitudes of anchor plate displacement, and the tension zones remain smaller. Failure in the soil overlying the uplifted anchor occurs principally in the form of a small, local plastic shear failure zone directly above the displaced anchor plate. The magnitude of anchor plate displacement necessary to produce the shear and failure zones in the finite element analyses agrees reasonably well with that required to produce a similar state of failure in the model tests. In the intermediate anchor case, 0.5 to 1.3 inches of anchor uplift produces the ultimate pull-out load in the model test, whereas 0.5 to 1.0 inch of anchor uplift was required to produce failure in the soil in the finite element analyses. In the deep anchor case, 0.8 to 2.0 inches of anchor uplift produced the ultimate pull-out load in the model test, whereas 1.0 to 1.5 inches of anchor uplift was required to produce failure in the soil in the finite element analyses.

In summary, it appears that the incremental nonlinear elastic finite element approach employed in the program SSCOMP adequately predicts the general form of the failure patterns that developed in the Davie (1973) anchor pull-out model tests. The location and extent of tensile failure zones within the saturated clay overlying the displaced anchor plate predicted by the nonlinear finite element analyses compare favorably with those observed in the model tests. In addition, the analyses reasonably predict the correct development of shear failure zones or plastic zones in the soil overlying the displaced anchor. In the deep anchor case,

the soil primarily fails in shear. In the shallow anchor case, the soil primarily fails in tension. The finite element method was able to roughly predict the level of anchor plate displacement necessary to produce the failure condition in the soil (i.e. maximum pull-out capacity). In fact, a number of finite element analyses were performed where the saturated clay's failure strain was roughly 50% higher ($\epsilon_f \approx$ 29% in lieu of 20%), and as occurred in the model tests (see Section 4.2.2(b)), roughly 50% more anchor plate displacement was required to produce "failure" in the soil overlying the uplifted anchor plate. Hence, the nonlinear finite element analyses properly show the importance of the overlying soil's failure strain.

Because of the overall agreement between the results of these analyses and the clay-box anchor pull-out model tests, the incremental nonlinear elastic finite element program SSCOMP, which employs a slightly modified version of the Duncan et al. (1984) hyperbolic soil model, is judged to be of sufficient accuracy so as to represent a useful engineering tool in the study of the rupturing of soil overlying a displaced base section.

8.5 Analyses of Fault Rupture Propagation through Saturated Clay

8.5.1 General:

In this section, the validated incremental nonlinear elastic finite element program SSCOMP will be used to provide additional insights into the process of fault rupture propagation through saturated clay. The results of two-dimensional (2-D), plane strain finite element analyses of two profiles of saturated clay soil (an 80 foot and 300 foot depth of normally consolidated to slightly over-consolidated saturated clay) will be presented. The focus of the investigation is to study the development of shear rupture zones and tension zones (or zones where the minor principal stress is reduced to a low enough value to permit the initiation of hydraulic fracturing) in the saturated clay overlying a base rock fault which

undergoes increasing magnitudes of displacement (or offset). In addition, a soil parameter sensitivity study will be performed to note the sensitivity of the results of the analyses to variations in the soil parameters which describe the stress-strain and volumetric strain behavior and the initial stress state of the saturated clay. The purpose of the parameter sensitivity study is to understand which of the characteristics of the saturated clay material which can best mitigate the potential hazards associated with fault rupture propagation through saturated clay. An improved understanding of this phenomenon would assist engineers in the design and construction of earth dams with saturated clay cores built across potentially active faults.

8.5.2 Analyses of an 80 Foot Deep Deposit of Saturated Clay:

The 2-D plane strain finite element model represents a vertical section through a typical saturated clay soil deposit which is oriented perpendicular to the strike of the dip-slip base rock fault. Additionally, the finite element model might represent a vertical section through a saturated clay core which is either oriented parallel to the longitudinal axis of an earth dam traversed by a dip-slip bedrock fault whose strike is perpendicular to the dam's longitudinal axis, or oriented perpendicular to the longitudinal axis of an earth dam overlying a dip-slip bedrock fault whose strike is parallel to the dam's longitudinal axis. As previously mentioned, a relatively "typical" profile of clay soil is to be studied. The characteristics of the normally consolidated to slightly overconsolidated 80 foot deep deposit of saturated clay can be described by the Duncan et al. (1984) hyperbolic soil model parameters which "best" represent the stress-strain and volumetric strain behavior and the initial stress state of the saturated clay soil. They are:

C = 22 · z, except C = 440 when z < 20

K = 4.2 · z, except K = 84 when z < 20

K_{ur} = 1.5 K = 6.3 z, except K_{ur} = 126 when z < 20

R_f = 0.953

K_o = 0.7 (in total stress, $\sigma 3/\sigma 1$ = 0.86), except K_o = 0.9 (in total stress, $\sigma 3/\sigma 1$ = 0.95) in selected analyses

γ = 120 pcf

[ϵ_f = 5%]

($\phi = \Delta\phi = 0$; m = n = 0; K_b = 17 · K (i.e. $\nu \approx 0.49$))

where z = depth in feet

It is assumed reasonable that the strength and stiffness of the clay increased roughly linearly with depth except for an overconsolidated region of clay of nearly constant strength and stiffness near the top of the soil profile. Hence, the clay's undrained shear strength increases from approximately 400 psf near the ground surface to roughly 1800 psf at a depth of 80 feet, and the clay's initial Young's Modulus ranges from 180,000 psf to 710,000 psf. The failure strain of the clay is on the order of 5%. The development of these soil model parameters will be discussed in greater detail in the next section. Up to 10 feet of vertical base fault offset is imposed through approximately 40 gradually decreasing increments of displacement.

Results of a number of finite element analyses of the 80 foot deep deposit of saturated clay overlying either a 45° thrust fault, a 60° normal fault, or a vertical thrust/normal fault in the base rock are presented in Figures 8-11 and 8-12. The deformed mesh resulting from the 45° thrust bedrock fault offset (Figure 8-11(a)) indicates that the majority of shear distortion is concentrated in a relatively narrow zone along the projection of the base rock fault plane. The stress

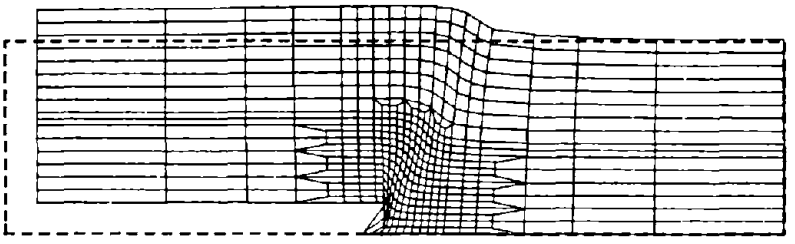

(A) Deformed Mesh (Displacements magnified by a factor of 5): 2.6' vertical offset

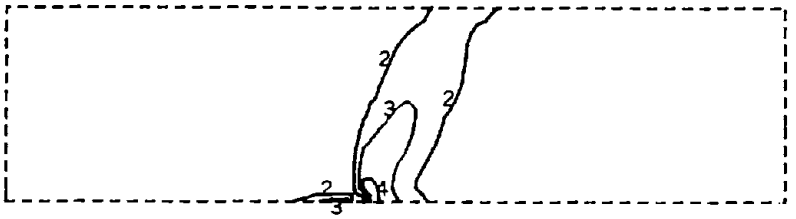

(B) Stress Level: 1' vertical offset (1.2% D_S)

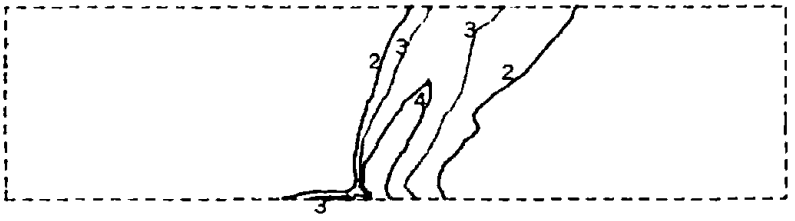

(C) Stress Level: 2' vertical offset (2.5% D_S)

(D) Maximum Shear Strain (%): 2' vertical offset (2.5% D_S)

Figure 8-11: RESULTS OF NONLINEAR FINITE ELEMENT ANALYSES OF 45° THRUST FAULT MOVEMENT: DEPTH OF SOIL (D_S) = 80'

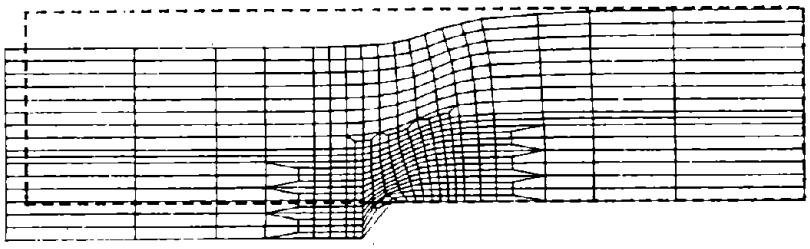

(A) 60° Normal Fault - Deformed Mesh (5 x Disp): 3' vertical offset (3.8% D_S)

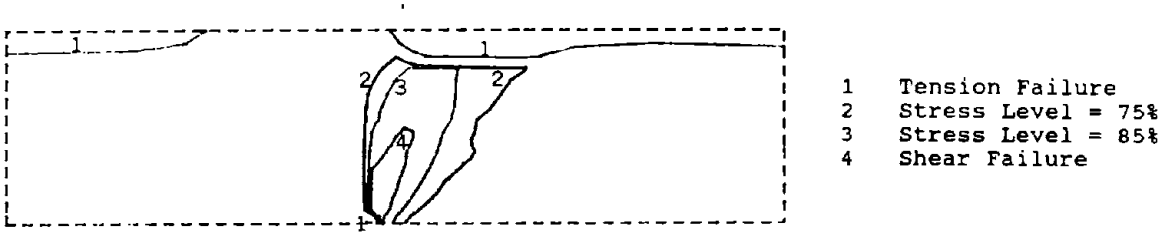

(B) 60° Normal Fault - Stress Level: 2' vertical offset (2.5% D_S)

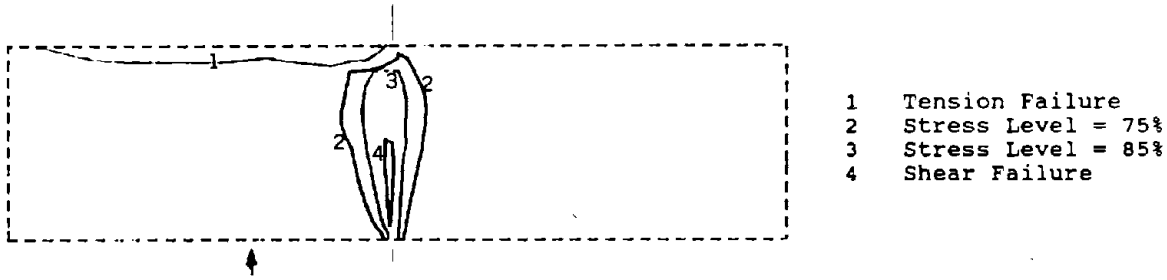

(C) Vertical Fault - Stress Level: 2' vertical offset (2.5% D_S)

Figure 8-12: RESULTS OF NONLINEAR FINITE ELEMENT ANALYSES OF 60° NORMAL FAULT MOVEMENT AND VERTICAL FAULT MOVEMENT: DEPTH OF SOIL (D_S) = 80'

level plots at increasing magnitudes of base offset (Figure 8-11(b-c)) show the progressive development of the shear rupture zone in the overlying clay soil. Initially (Figure 8-11(b)), the "inverted footing" type of failure pattern develops with the shear zone propagating over the uplifted base rock section. At larger base offsets (Figure 8-11(c)), however, kinematic constraints force the shear rupture zone to propagate roughly along the projection of the base rock fault plane (the "anchor pull-out" type of failure pattern). In this case, the transition from a stress controlled shear failure pattern (the "inverted footing" type of failure) to a kinematics controlled rupture pattern (the "anchor pull-out" type of failure) occurs between 1.0 and 2.0 feet of vertical base fault displacement (or at a vertical base offset of roughly 1.2-2.5% of the depth of the overlying saturated clay layer). The plot of maximum shear strain contours (Figure 8-11(d)) is also useful in identifying the most likely location of the primary rupture zone in the clay. Roughly 3.0 feet of vertical base rock fault offset is necessary to propagate the fault rupture zone through the entire depth of the soil. In fact, throughout the analysis it appears that the height of the shear rupture zone during base deformation is on the order of 18 to 26 times the magnitude of the vertical base rock fault displacement.

The development of tensile failure in these analyses is found to be somewhat sensitive to the configuration of the finite element mesh employed. In particular, it appears that the size of the soil elements adjacent to the base rock fault can significantly affect whether the soil element directly adjacent to the base rock fault over the downthrown base section fails first in shear or in tension. Hence, it is difficult in these analyses to note any consistent relationship between the initiation of tensile failure at the soil-bedrock contact, and the characteristics of the overlying soil deposit and the direction of the base rock fault movement. The development of a larger zone of minor principal stress reduction in this region is found, however, to be relatively insensitive to normal variations in the finite

element model and analyses. Only the behavior of the soil element directly adjacent to the base rock fault over the downthrown block appears sensitive to the analytical procedures. Thus, it is more useful to investigate the development of a zone where the minor principal stress is reduced to a low enough value to permit the initiation of hydraulic fracturing (i.e. if the 80 foot deep saturated clay soil represents the core section of an earth dam with water impounded behind it, hydraulic fracturing of the core might be possible if the minor principal stress (σ_3) is less than the reservoir porewater pressure at a depth of around 80 feet or $u \approx 62.4 \text{ pcf} \cdot 80 \text{ ft} \approx 5000$ psf). At a vertical base rock fault offset of 3 feet, the size of the zone near the soil-bedrock interface where σ_3 is less than roughly 5000 psf is on the order of 6 to 8 ft^2.

The development of failure in the saturated clay overlying the bedrock fault planes at various orientations appears to agree reasonably well with that observed in the physical model tests and in the field studies of surface fault rupture. Figure 8-12 shows typical results from some of the finite element analyses. The deformed mesh and a stress level contour plot are shown for a 60° normal fault movement (Figure 8-12(a-b)) and for a vertical dip-slip fault movement (Figure 8-12(c-d)). Again, the stress level contour plots appear reasonable indicating the development of relatively narrow shear rupture zones that propagate principally along the projection of the base rock fault plane. As in the previous case of a 45° thrust fault movement, in these cases, the fault rupture propagates to the ground surface at a vertical base rock fault offset of roughly 3 feet (or 4% of the depth of the overlying clay layer). During increasing magnitudes of base deformation (or offset), the height of the shear rupture zone appears to be on the order of 18 to 26 times the magnitude of the base rock fault offset.

On the other hand, the development of zones of potential hydraulic fracturing ($\sigma_3 < 5000$ psf) near the soil-bedrock contact differs significantly, and it

appears that the extent of these zones depends largely upon the type of fault movement. Normal dip-slip fault movements appear to produce larger zones of potential hydraulic fracturing than do thrust fault movements. In fact, the magnitude of the FEM predicted zone of potential hydraulic fracturing appears to increase as the bedrock fault movement changes from a low angle thrust fault movement to a steep angle thrust fault movement, and from a steep angle normal fault movement to a shallow angle normal fault movement. For example, at a vertical base offset of 3 feet, the 45° thrust fault movement produces a 6 to 8 ft^2 zone of potential hydraulic fracturing; the vertical thrust/normal fault movement produces a 18 to 24 ft^2 zone; and the 60° normal fault movement produces a 42 to 56 ft^2 zone of potential hydraulic fracturing.

The 80 foot deep deposit of saturated clay analyzed in these finite element studies is on the order of magnitude modeled by the 1 g small-scale model tests performed as a part of this research program and described previously in Chapter Six. It is noteworthy that both the numerical model and the physical model of the saturated clay deposit, which is on the order of a hundred feet deep, provided fairly similar results. Each approach has its particular limitations. The physical model tests portrays the clay as being relatively homogenous; while the numerical approach portrays the actual distinct rupture planes that develop in the soil overlying a base rock fault offset as a wider zone of shear distortion and failure. Yet, both the physical and numerical models provide useful insights which are fairly consistent with one another. These model predictions, which are similar to the general trends observed in field studies of surface fault rupture, should provide a higher level of confidence that both approaches (the 1 g small-scale model tests and the incremental nonlinear elastic finite element analyses) can be used as engineering tools in the study of fault rupture propagation through saturated clay.

8.5.3 Sensitivity Study and Analyses of a 300 Foot Deep Deposit of Saturated Clay:

To extend the findings of these model tests and numerical analyses, a relatively comprehensive investigation of the phenomenon of fault rupture propagation through a 300 foot depth of saturated clay soil will now be performed. The capability of performing an in-depth study of the process of fault rupture propagation through a soil deposit of such depth is one of the real advantages of the numerical approach. For example, the 1 g small-scale model tests of this study were not able to adequately represent a deposit of such a large depth, because to satisfy the necessary scaling requirements, a model clay with an extremely low undrained shear strength would be required, and the model clay at these low strengths was shown to exhibit a viscous type of failure behavior not representative of typical field conditions. In addition, it will be relatively easy to modify critical soil parameters to note their effect on the behavior of the overall soil mass and to approximately model the distribution of soil strength and load-deformation behavior throughout the soil mass.

The nonlinear stress-strain behavior of the normally consolidated to slightly overconsolidated saturated clay soil was varied as shown in Table 8-1 to determine the sensitivity of the finite element analyses to variations in critical soil parameters. These values of soil strength, stiffness, and failure strain are reasonable for typical deposits of soft to medium saturated natural clay soils. The baseline case undrained shear strength variation of $C = 22 \cdot z$ (where z = depth in feet and C is expressed in the units of psf) is felt to be reasonable as it suggests that $C/p' \approx 0.35$ and that the initial stress level (SL) of the clay is on the order of 60%. The initial stiffness hyperbolic soil model parameter (K) is more difficult to estimate as the variation of Young's Modulus (E) with depth in a saturated clay soil is known with much less certainty. A number of widely accepted works in the field of soil mechanics suggest that Young's Modulus increases either linearly with depth or as

Table 8-1: HYPERBOLIC SOIL MODEL PARAMETERS EMPLOYED TO DESCRIBE THE STRESS-STRAIN BEHAVIOR OF THE SATURATED CLAY

Case	Description	C (psf)	K	R_f	K_o	ϵ_f (%)
1	Baseline	22 · z	8.32 · z	0.95	0.5	2.4
2	2 · ϵ_f & 0.5 · E_i	22 · z	4.16 · z	0.95	0.5	4.9
3	0.9 · ϵ_f & 0.8 · C	17.6 · z	8.32 · z	0.96	0.5	2.2
4	1.4 · K_o	22 · z	8.32 · z	0.95	0.7	2.4
5	1.35 · ϵ_f & 0.5 E_i	22 · z	4.16 · z	0.90	0.5	3.3
6	1.2 ϵ_f & 1.5 · C	33 · z	8.32 · z	0.925	0.5	2.9
7	2 · ϵ_f & 0.25 E_i	22 · z	2.08 · z	0.847	0.5	4.9

Note 1: $\phi = \Delta\phi = 0$; $m = n = 0$; $K_b = 17 \cdot K$(i.e. $\nu \approx 0.49$); & $K_{ur} = 1.5 \cdot K$

Note 2: z = depth in feet

Note 3: The undrained shear strength (C) and the initial stiffness hyperbolic soil model parameter (K) are actually constant within the top 30 feet of the clay deposit with C = 500 psf and K = 190 in the baseline case 1. In the other cases, these values are constants but adjusted according to the description provided.

Note 4: γ = 120 pcf

Note 5: K_o is provided in terms of effective stress since by definition $K_o = \sigma'_3/\sigma'_1$. If $K_o = 0.5$, $\sigma_3/\sigma_1 = 0.76$ (total stress). If $K_o = 0.7$, $\sigma_3/\sigma_1 = 0.86$ (total stress).

Note 6: $\epsilon_f = 2C/[K \cdot P_a (1.05 - R_f)]$
where P_a = 2116.2 psf

the square root of the depth. In the range of depths from 100 feet to 300 feet, the variation of the model stiffness parameter is of the same order of magnitude whether it is made to vary linearly with depth or as the square root of the depth.

Since it is important in these studies to maintain control of the critical soil failure strain parameter, it was decided that the initial Young's Modulus of the soil would vary linearly with depth. This, in conjunction with varying the clay's undrained shear strength linearly with depth, maintains the failure strain as a constant over the depth of the clay (See Note 6 of Table 8-1). The failure strain of the soil in the cases analyzed ranges from approximately 2% to 5%. Finally, the initial coefficient of lateral earth pressure at rest (K_o) varies within the range of 0.5 and 0.7 (in total stress, $\sigma 3/\sigma 1$ = 0.76 and 0.86, respectively) to note the effect of variations in this soil parameter.

In summary, in the baseline case 1, the normally consolidated to slightly overconsolidated saturated clay's undrained strength (C) increases from around 500 psf near the ground surface to 6500 psf at a depth of 300 feet. The clay's initial tangent modulus (E_i) ranges from 7 x 10^4 psf to 9 x 10^5 psf. The clay's failure strain is approximately 2.5%. These values are increased or decreased by as much as a factor of 4 in the other cases to note the sensitivity of the results to variations in the critical soil parameters.

The 2-D plane strain finite element model incorporated nearly 500 4-node isoparametric finite elements to represent the 300 foot deep clay deposit. Nearly 400 of the model's finite elements were located between the depths of 150 feet and 300 feet with over 200 of the soil elements concentrated in the region directly overlying the base rock fault. The finite element mesh used in these studies is shown in Figure 8-13(a). Preliminary analyses found that around 20 to 40 displacement increments were required to allow the incremental nonlinear finite element model to adequately represent the highly nonlinear stress-strain behavior

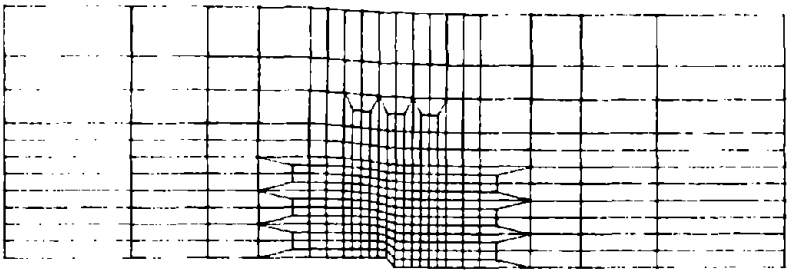

(A) Deformed Mesh (z = 150' - 300'): 6' vertical offset

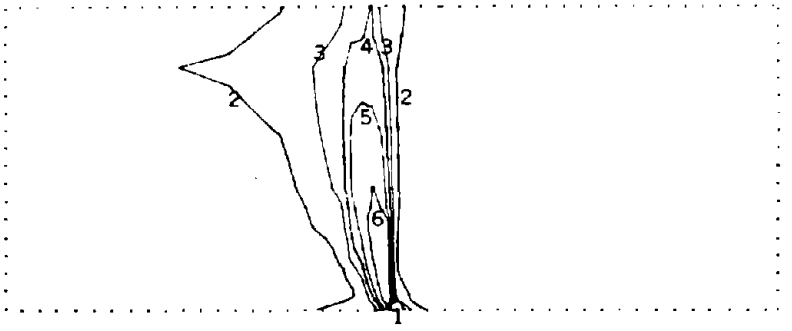

(B) Stress Level (L/H = 3:1): 5' vertical offset

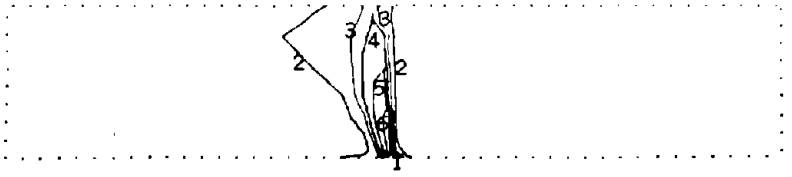

(C) Stress Level (L/H = 6:1): 5' vertical offset

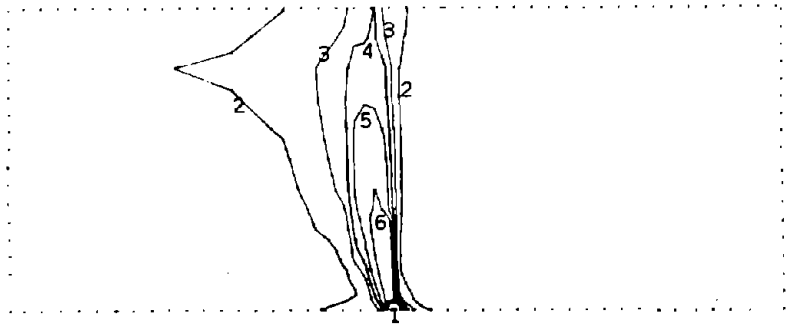

(D) Stress Level (Incremental Remeshing): 5' vertical offset

Figure 8-13: RESULTS OF NONLINEAR FINITE ELEMENT ANALYSES OF VERTICAL FAULT MOVEMENT: EFFECTS OF L/H RATIO OF MESH AND INCREMENTAL REMESHING: D_S = 300'

of the saturated clay soil at or near failure. If only 5 to 15 displacement increments were employed to propagate the shear rupture zone from the base rock fault to the ground surface, inconsistent soil behavior occurred with shear failure, and especially tensile failure, initiating and developing erratically. In the region of interest (between 150 and 300 feet deep), the length to height ratio of the finite element mesh was approximately 3:1. The stress level contour plot shown in Figure 8-13(b) illustrates the development of shear failure and tensile failure in the clay overlying a vertical base rock dip-slip fault offset of 5 feet. The shear failure zone is confined to a relatively narrow region. A number of analyses were performed with the finite element mesh's length to height ratio increased to 6:1 in the region of interest. Comparing Figure 8-13(c) with Figure 8-13(b), it is evident that increasing the length to height ratio of the mesh beyond 3:1 is not necessary in the analysis of this problem.

In Section 7.2, the merits of incrementally remeshing to calculate the natural strain (or logarithmic strain which is the summation of strain increments each of which is calculated on the deformed mesh geometry) was discussed. To ascertain the effect of employing this modification to the infinitesimal strain approach (which in many problems approximates the large strain formulation) the computer program SSCOMP was modified to automatically remesh after each solution increment. The results of these analyses utilizing the natural strain approach, however, were not significantly different than the analyses performed based on the usual infinitesimal strain assumption (Compare Figure 8-13(d) with Figure 8-13(b)). As suggested in Section 7.2, the small strain approach is suitable for this class of problem because base deformations of on the order of only 1% to 15% of the depth of the soil overlying the base rock fault are required to propagate the shear rupture zone upwards to the ground surface. The difference between calculating strains relative to the undeformed mesh geometry or the deformed

mesh geometry does not appear significant, especially up to the point of failure within each soil element which actually fails in shear. After an element fails, the tip of the shear rupture zone propagates upward away from this element so its effect on the future development of the shear rupture zone is limited. Furthermore, after an element fails, its stiffness is reduced to an extremely low value so its effect on the distribution of stress near the tip of the shear rupture zone is also limited. It appears that these analyses suggest that adequately modeling the behavior of soil up to the point of failure in this class of problem might be as important, if not more important, than properly modeling the behavior of the soil past "failure" (that is, if the soil does not exhibit a significant reduction in its post-peak strength; which is hopefully the case for a compacted clay soil comprising the core of an earth dam).

In an attempt to achieve better localization of the shear rupture zone to properly model the development of distinct shear rupture planes, interface soil elements of negligible thickness were employed to represent shear planes in the deforming soil mass. The use of an interface soil element which utilizes a hyperbolic soil model similar to that already discussed to represent the nonlinear shear deformation behavior of the soil parallel to the orientation of the interface, and a linear elastic soil model to represent the load-deformation behavior of the soil normal to the orientation of the interface element is discussed thoroughly in the SSCOMP user manual (Seed and Duncan, 1984). Initially, as shown in Figure 8-14(a), the interface element properly localized the differential movement across the base rock fault offset to a distinct shear plane. At larger base rock fault movements, when the exact location of the continuation of the shear rupture plane cannot be determined apriori (i.e. the shear rupture zone deviates from its initial vertical orientation and exhibits the "inverted footing" type of failure pattern), the

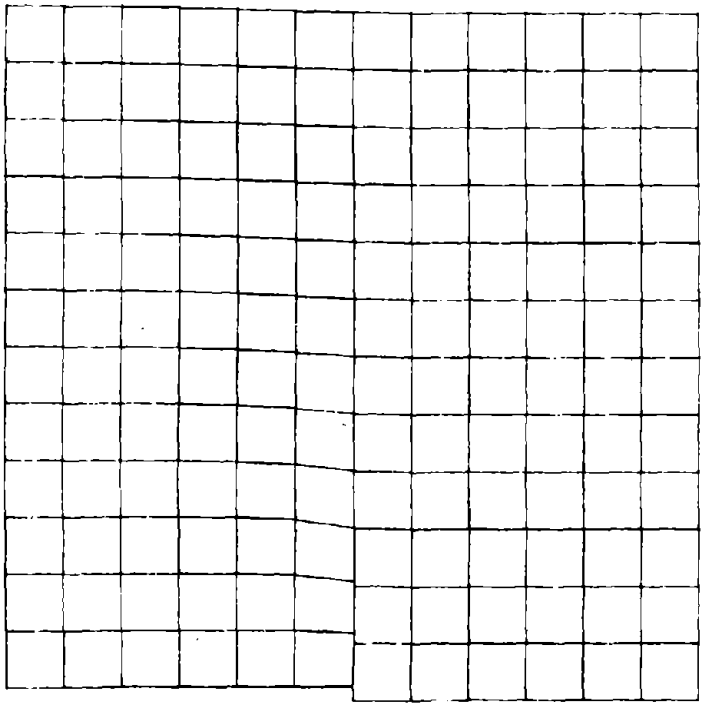

(A) Blow-up of Deformed Mesh (z = 240' - 300'): 1.25' vertical offset

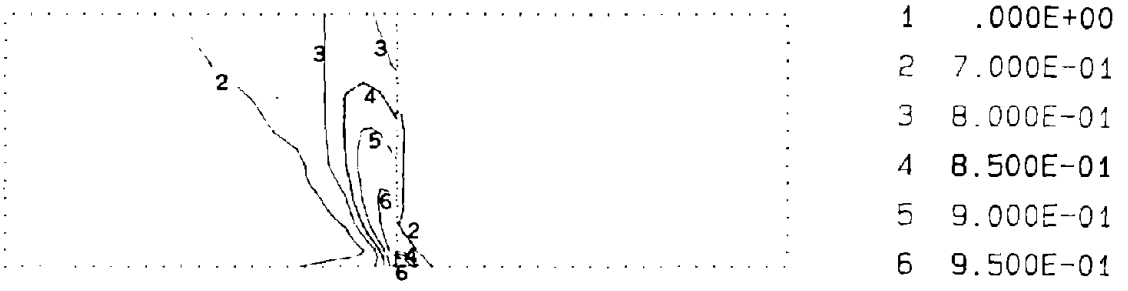

(B) Stress Level (z = 150' - 300'): 2.5' vertical offset

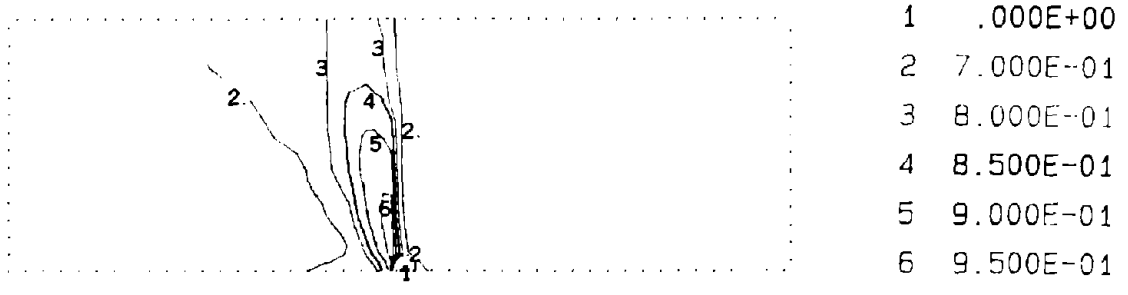

(C) Stress Level w/o interface element (z = 150' - 300'): 2.5' vertical offset

Figure 8-14: RESULTS OF NONLINEAR FINITE ELEMENT ANALYSES OF VERTICAL FAULT MOVEMENT: EFFECTS OF THE USE OF THE INTERFACE ELEMENT: D_S = 300'

use of the interface element does not alter the development of the primary shear rupture zone.

The results of the analyses, which incorporated a series of vertical soil interface elements aligned end to end along the projection of the vertical thrust/normal base rock fault (See Figure 8-14(b)), can be compared to the results of the analyses where no interface elements are employed (Figure 8-14(c)). At the 2.5 foot base offset, both analyses indicate that the shear rupture zone was roughly 50 feet high and slightly inclined toward the upthrown block side. In addition, the distributions of maximum shear strain, maximum shear stress, and minor principal stress were essentially the same in both of these analyses. Attempts were made to adjust the location and the orientation of the soil interface elements to align them with the predicted shear rupture zone at each stage of incremental displacement, but this scheme was very complex and cumbersome, and was judged to not significantly affect the rate at which the shear rupture zone propagated or the distribution of the minor principal stress which indicated zones of potential hydraulic fracturing. The characterization of the distinct shear rupture planes observed in the model tests and field studies as a relatively narrow shear rupture zone which was likely to envelop these distinct shear planes did not appear to significantly affect the development of shear and tension zones in the saturated clay overlying a displaced base rock fault. Hence, for the purpose of this research the use of interface elements to represent distinct shear rupture planes was not considered necessary in maintaining the suitability of the nonlinear finite element method for use as an engineering tool in the study of the process of fault rupture propagation through saturated clay.

The displacement vectors shown in Figure 8-15(a) further indicate that the zone of shear distortion was relatively narrow even if the soil mass was modeled with 4-node isoparametric elements. The majority of the soil does not participate

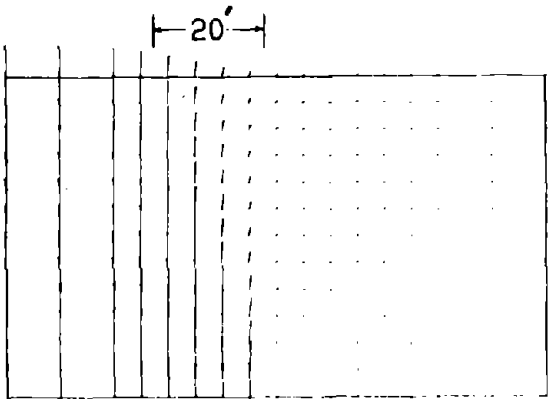

(A) Case 1 Displacement Vectors
(z = 240' - 300'): 2.5' vertical offset

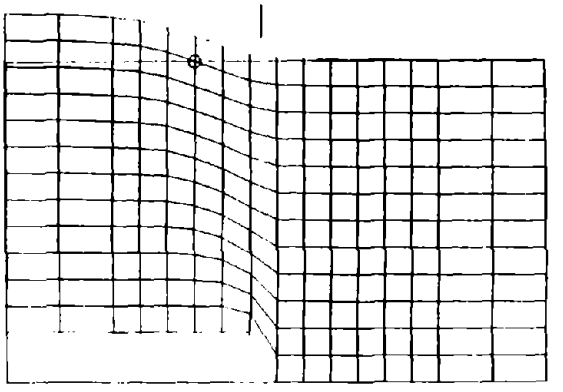

(B) Case 1 Deformed Mesh
(z = 240' - 300'): 3.75' vertical offset

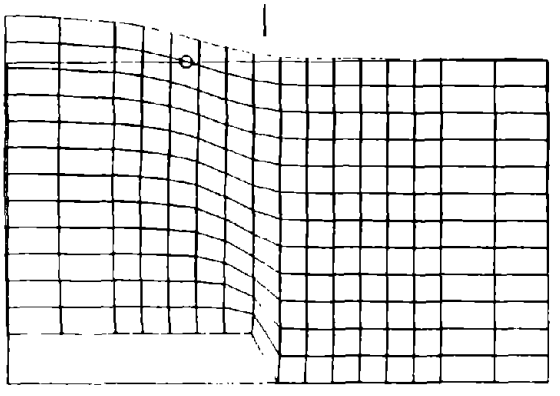

(C) Case 2 Deformed Mesh
(z = 240' - 300'): 3.75' vertical offset

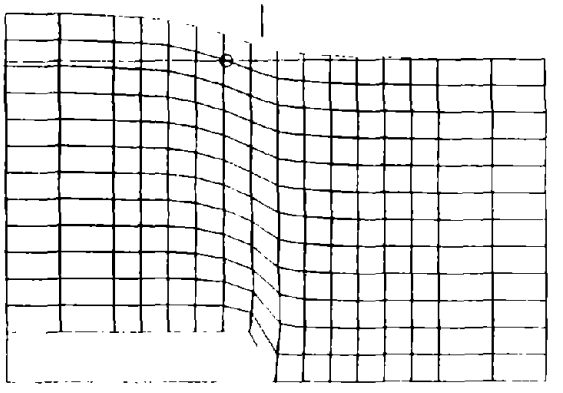

(D) Case 4 Deformed Mesh
(z = 240' - 300'): 3.75' vertical offset

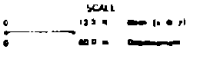

Figure 8-15: RESULTS OF NONLINEAR FINITE ELEMENT ANALYSES OF VERTICAL FAULT MOVEMENT: DISPLACEMENT PATTERNS: D_S = 300'

in the development of the shear rupture zone through the overlying soil mass. Instead, the large majority of the differential movement across the vertical thrust fault plane is accommodated in a relatively narrow zone directly above the base rock fault between two extensive zones of soil overlying the upthrown and downthrown blocks which effectively behave as fairly "rigid" blocks of soil that deform uniformly.

The blow-ups (enlarged views) of the deformed meshes shown in Figure 8-15(b-d) illustrate some of the effects of variations in some of the critical soil parameters. Figure 8-15(b) shows a blow-up of the deformed mesh in the vicinity of the base fault at a base offset of 3.75 feet for the baseline case 1 (See Table 8-1). If the stiffness of the soil is reduced by half and the failure strain of the soil is doubled producing a clay with a more ductile stress-strain behavior, the zone of shear distortion appears wider with more distortion occurring over the upthrown block (See Figure 8-15(c)). The more ductile material accommodates much of the differential movement across a broader zone of shear distortion. The higher failure strain of the soil allows the soil to accommodate more differential base deformation before a shear rupture zone develops. Finally, Figure 8-15(d) shows that increasing the coefficient of lateral earth pressure at rest from 0.5 to 0.7 (a 40% increase) moves the zone of shear distortion over more toward the downthrown block. Although not nearly as dramatic as what occurred in the studies involving dry, cohesionless materials, these results suggest that the K_o soil parameter is a relatively important soil parameter in the study of fault rupture propagation through saturated clay as it affects the location of the shear rupture zone which develops in the clay overlying the displaced base rock fault.

As discussed previously, a series of incremental nonlinear finite element analyses were performed employing the characterization of the saturated clay overlying the vertical base rock fault as described in Table 8-1. Representative

results of this series of analyses are illustrated in Figures 8-16 and 8-17. In these figures, the region of interest of the finite element mesh from a depth of 150 feet to 300 feet is shown for several of the cases described in Table 8-1 for a vertical base rock fault offset of 2.5 feet. Comparing the baseline case 1 (Figure 8-16(b)) with case 2 (Figure 8-16(c)) where the soil's failure strain has been doubled and its stiffness halved, the height of the shear rupture zone in the baseline case 1 at the same magnitude of base offset is roughly twice the height of the shear rupture zone in case 2. In addition, tensile failure is observed in the soil element adjacent to the base rock fault on the downthrown side in the baseline case 1, but not in case 2. Figure 8-17 illustrates the effect of modifying the soil parameters as described in cases 3, 4 and 5. For example, the shear rupture zone is located closer to the downthrown block when K_O is increased from 0.5 to 0.7. These figures also illustrate that by far the most significant soil parameter in these analyses is the failure strain of the soil. Increasing the failure strain of the soil decreases the height of the shear rupture zone at this magnitude of base offset.

The results of this parameter study are described in greater detail in Table 8-2. These results clearly indicate the importance of the soil's failure strain. Again, comparing case 1 and case 2, the soil's failure strain in case 2 is twice that in case 1, and in case 2 the shear rupture zone in the soil produced by the base rock fault offset is roughly half of the height of the rupture zone in case 1. On the other hand, in cases 2 and 7, where the soil's failure strain is the same and the initial stiffness in case 7 is half of that in case 2, the height of the shear rupture zones at increasing magnitudes of base offset are essentially the same. Examining case 4 where K_O equals 0.7 instead of 0.5, the initiation of the shear rupture zone is delayed until the base deformation is at least 2.5 feet. Once the shear rupture zone forms, however, its height at equal vertical base offsets appears to be essentially the same as that for the baseline case.

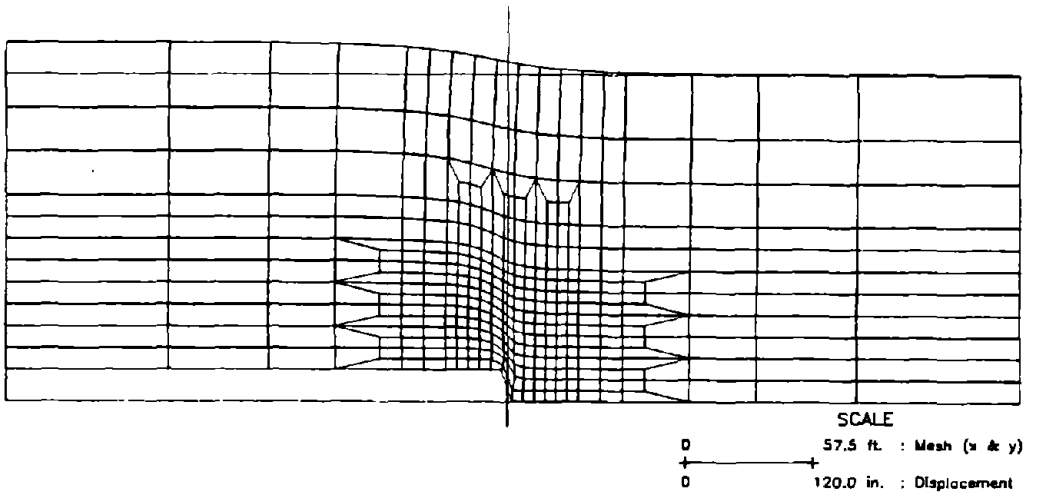

(A) Deformed Mesh (5x Disp) (z = 150' - 300'): 2.5' vertical offset

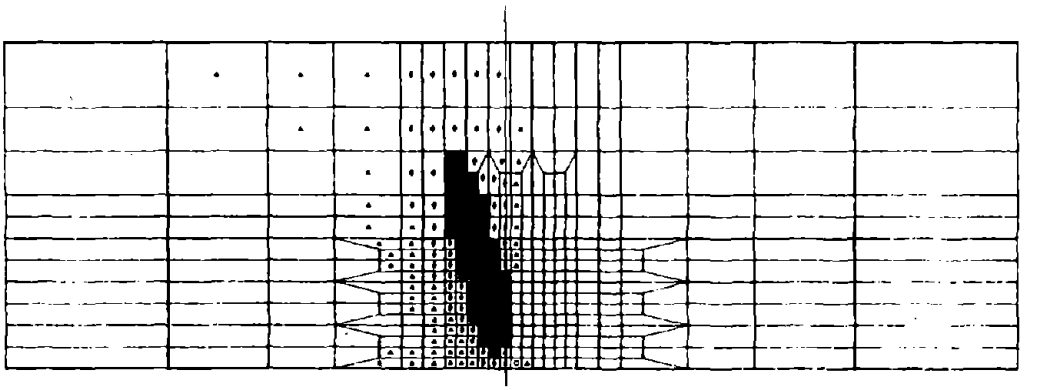

(B) Case 2 Shear Failure Zone (z = 150' - 300'): 2.5' vertical offset

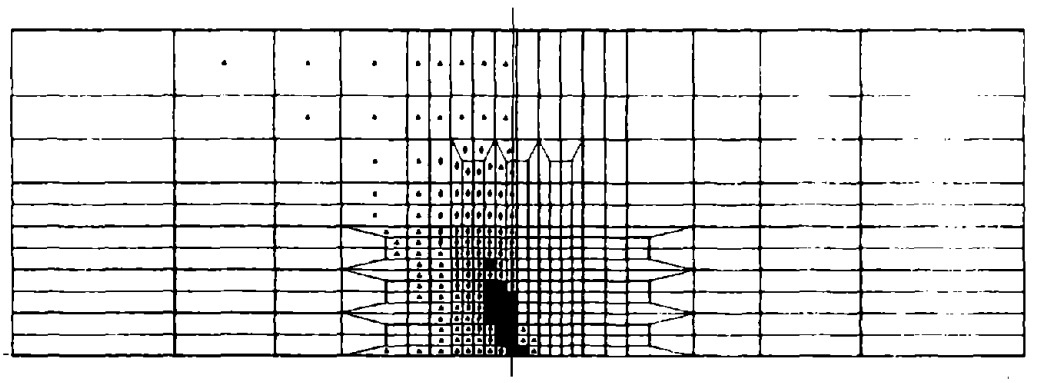

(C) Case 3 Shear Failure Zone (z = 150' - 300'): 2.5' vertical offset

Figure 8-16: RESULTS OF NONLINEAR FINITE ELEMENT ANALYSES OF VERTICAL FAULT MOVEMENT: VARIATION IN THE HEIGHT OF THE SHEAR FAILURE ZONE; CASE 1 & 2: D_S = 300'

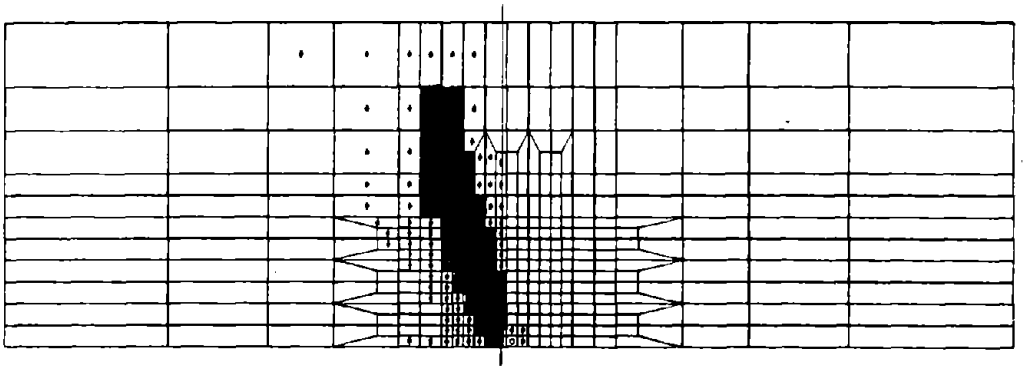

(A) Case 3 Shear Failure Zone (z = 150' - 300'): 2.5' vertical offset

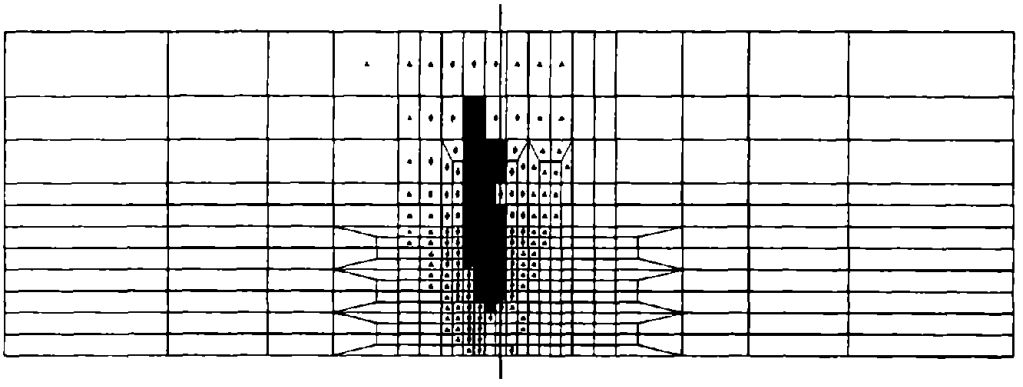

(B) Case 4 Shear Failure Zone (z = 150' - 300'): 2.5' vertical offset

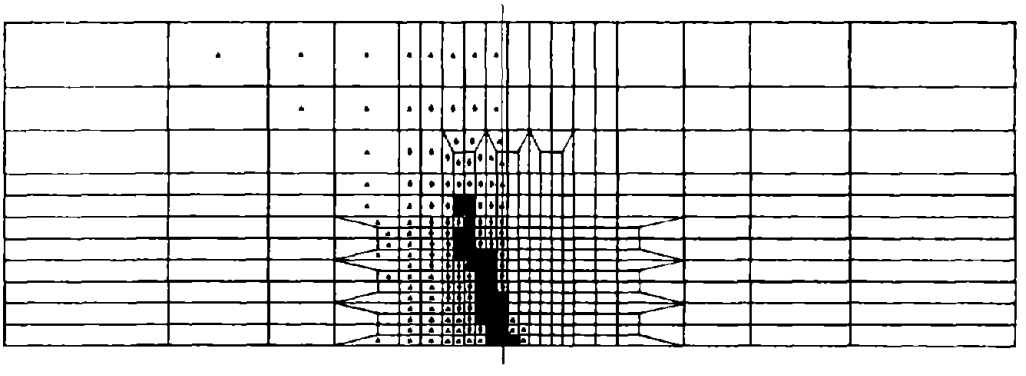

(C) Case 5 Shear Failure Zone (z = 150' - 300'): 2.5' vertical offset

Figure 8-17: RESULTS OF NONLINEAR FINITE ELEMENT ANALYSES OF VERTICAL FAULT MOVEMENT: VARIATION IN THE HEIGHT OF THE SHEAR FAILURE ZONE: CASE 3, 4 & 5: D_S = 300'

Table 8-2: Results of the Soil Parameter Sensitivity Study of the Vertical Dip-Slip Fault Movement

CASE	1 (Baseline)	2	3	4	5	6	7	8
Description	$C = 22 \cdot z$; $E_i = 17{,}500 \cdot z$ $K_o = 0.5$; $\epsilon_f = 2.4\%$	$2 \cdot \epsilon_f$ & 0.5 E_i	$0.9 \cdot \epsilon_f$ & $0.8 \cdot C$	$1.4 \cdot K_o$	$1.35 \cdot \epsilon_f$ & 0.5 E_i	$1.2 \cdot \epsilon_f$ & $1.5 \cdot C$	$2 \cdot \epsilon_f$ & $0.25 \cdot E_i$	case 2 except $\nu \approx 0.45$ instead of $\nu \approx 0.49$
Failure Strain (%)	2.4	4.9	2.2	2.4	3.3	2.9	4.9	4.9
Height of Shear Rupture Zone (h_f) vs. Vertical Base Offset (d_b) in feet & (h_f/d_b):								
Vertical Base Offset (d_b) = 0.312'	0'	0'	10' (32 x d_b)	0'	0'	0'	0'	0'
d_b = 0.625'	5' (8 x d_b)	0'	15' (24x)	0'	0'	0'	0'	0'
d_b = 1.25'	40' (32x)	10' (8 x d_b)	50' (40x)	0'	25' (20 x d_b)	30' (24 x d_b)	5' (4 x d_b)	10' (8 x d_b)
d_b = 2.50'	100' (40x)	45' (18x)	120' (48x)	120' (48 x d_b)	80' (32x)	80' (32x)	45' (18x)	35' (14x)
d_b = 3.75'	160' (43x)	80' (21x)	160' (43x)	160' (43x)	120' (32x)	120' (32x)	70' (19x)	60' (16x)
d_b = 5.00'	--	120' (24x)	--	--	120' (24x)	160' (32x)	120' (24x)	100' (20x)
Vertical Base Offset (d_b) when Tensile Failure Occurs in feet	2.5'	3.75'	2.5'	> 5.0'	3.75'	1.25'	3.75'	> 5.0'
Extent of Zone of Potential Hydraulic Fracturing (σ_3 < 20,000 psf) in square feet	≈ 325 sf	≈ 300 sf	≈ 125 sf	≈ 75 sf	≈ 325 sf	≈ 1000 sf	≈ 275 sf	≈ 400 sf

Increasing the value of K_O appears to delay the initiation of tensile failure in the soil adjacent to the base rock fault. Tensile failure appeared to develop earliest in case 6 where the clay's undrained shear strength was approximately 50% greater than that in the baseline case 1. The more brittle stress-strain behavior of the stronger clay material might be partially responsible for this effect. Conversely, tensile failure appeared to develop later in cases where the initial tangent modulus of the soil was reduced helping to produce a clay which exhibits a more ductile stress-strain behavior (e.g. cases 2, 5, 7).

A relatively comprehensive study of the sensitivity of the results to variations in the volume change behavior of the clay as characterized by Poisson's ratio was performed. In the finite element program SSCOMP, constant volume behavior was approximated by assuming Poisson's ratio was a value close to 0.5, but not actually 0.5, because in the displacement finite element formulation employed in SSCOMP, $\nu = 0.5$ created numerical instabilities. In the program SSCOMP, Poisson's ratio was assumed to be 0.49 when the soil deformed at constant volume. To note the effects of slight variations in the actual value of Poisson's ratio employed in the finite element calculations, the program was modified to enforce Poisson's ratio to remain constant and be either 0.49, 0.48, 0.47, or 0.45. It was also judged important to check the sensitivity of the results to variations in Poisson's ratio because initially the clayey material comprising the core of an earth dam might not be fully saturated and the nearly saturated clay might be, for example, better characterized as a $\nu = 0.45$ material.

The in-depth sensitivity study of the effect of variations in Poisson's ratio found that, in general, within the range of $\nu = 0.45 - 0.49$, the results are not significantly affected by slight variations in the value of Poisson's ratio. For example, examining the results from the analyses of case 8 where the soil model parameters are defined identical to those employed in case 2, except Poisson's ratio

now equals 0.45 instead of approximately 0.49, the development of the shear rupture zone is fairly similar to that observed during the analyses of case 2. The analyses do, however, clearly identify a trend that suggests that slightly decreasing the value of Poisson's ratio from 0.49 to 0.45 produces a slight decrease in the height of the shear rupture zone at each magnitude of base offset. In addition, the development of tension in the soil appears to be delayed as the value of Poisson's ratio decreases. In actuality, the soil element directly adjacent to the base rock fault on the downthrown side of the fault is the only element that is highly sensitive to the value of Poisson's ratio employed regarding the initiation of tensile failure. Overall, the zone of potential hydraulic fracturing (the zone where the minor principal stress is reduced to a value low enough to permit the initiation of hydraulic fracturing; in this case, σ_3 < 20,000 psf) is not highly sensitive to slight variations in the Poisson's ratio parameter within the range of 0.45 to 0.49. If the clay in question is very fully saturated or nearly saturated, it appears reasonable to use a value of Poisson's ratio of on the order of 0.47 - 0.49.

In addition to these analyses of the response of a saturated clay soil mass overlying a vertical dip-slip fault movement, a number of nonlinear finite element analyses were performed with various orientations of the base rock fault plane and different types of fault movements (either thrust or normal). The development of shear and tension zones in the 300 foot deep saturated clay deposit overlying these base rock fault movements was, in general, similar to those patterns observed in the finite element analyses of the 80 foot deep clay deposit described previously in Section 8.5.2. The height of the shear rupture zone in the soil above the base rock fault rupture was primarily related to the amount of vertical base offset and the stress-strain behavior of the clay (particularly, the failure strain of the clay). For example, within the limits of accuracy of these analyses of fault rupture propagation through soil, the vertical height of the shear zone in the clay produced

by a 45° thrust fault movement, a 60° normal fault movement, or a vertical thrust/normal fault movement was roughly the same at identical magnitudes of vertical base fault displacement (or offset). Of course, the orientation of the shear rupture zone through the overlying soil depended largely on the orientation of the underlying base rock fault plane. The final shear rupture zone through the overlying saturated clay tended to follow the projection of the base rock fault plane, although there was a tendency for the shear rupture zones produced in the clay by normal fault movements to slightly increase in dip as the rupture zone approached the ground surface and to be slightly wider. The development of tensile failure in the saturated clay appeared to be somewhat sensitive to the type of base rock fault movement as well as to the finite element model (or mesh). Tensile failure developed earlier in the analyses of the nonvertical dip-slip fault movements.

The development of zones of potential hydraulic fracturing in the saturated clayey material comprising the core section of an earth dam, however, was of greater interest in this study. As discussed previously, the development of tensile failure in these analyses was often inconsistent, and, as well as other factors, depended on the characteristics of the finite element mesh and the incremental solution technique employed. The development of zones where the minor principal stress was reduced to a value low enough to permit the initiation of hydraulic fracturing was, however, fairly insensitive to these numerical approach-related factors. In the analyses of the saturated clay core of an earth dam constructed over a potentially active fault, the development of zones of potential hydraulic fracturing would be of great concern to the design engineer as such zones could initiate instability in the core through uncontrolled leakage and internal erosion.

A few representative results of the nonlinear finite element analyses of the cases previously described (where the vertical base movement was 5 feet) which show the characteristics of the zones of minor principal stress reduction where hydraulic fracturing could possibly occur (σ_3 < 20,000 psf) are shown in Figure 8-18. The 45° thrust fault movement (Figure 8-18(c)) appears to produce very limited zones where the minor principal stress is reduced below the 20,000 psf threshold value. On the other hand, the normal fault movement (Figure 8-18(d)) produces a larger zone of potential hydraulic fracturing at the soil-bedrock contact near the base rock fault. In addition, it appears that the minor principal stress is significantly reduced throughout the entire depth of the clay and at vertical base offsets greater than 5 feet this zone could become quite extensive. The vertical dip-slip fault movement produced the most extensive zone of potential hydraulic fracturing at a vertical base offset equal to or less than 5 feet. Figure 8-18(a-b) shows the results of the analyses of case 2 described previously in Table 8-2.

At the bottom of Table 8-2, estimates of the relative magnitude of the zone of potential hydraulic fracturing are shown for each of the respective cases employed in the soil parameter sensitivity study. It appears that the extent of the zones of potential hydraulic fracturing principally depends on the soil model parameters that describe the saturated clay's initial stress state (K_o) and its undrained shear strength (C). To a lesser degree, the soil model parameters ϵ_f (the failure strain), ν (Poisson's ratio) and E_i (the initial stiffness parameter that helps describe the general shape of the hyperbolic stress-strain relationship) appear to affect the development of tension zones and zones of potential hydraulic fracturing in the saturated clay overlying a displaced base rock fault. Reduction in the clay's minor principal stress in the region near the base rock fault appears to be more pervasive in the results of the analyses of case 6 where the clay possesses the highest undrained shear strength. Conversely, the results of the analyses of case 5

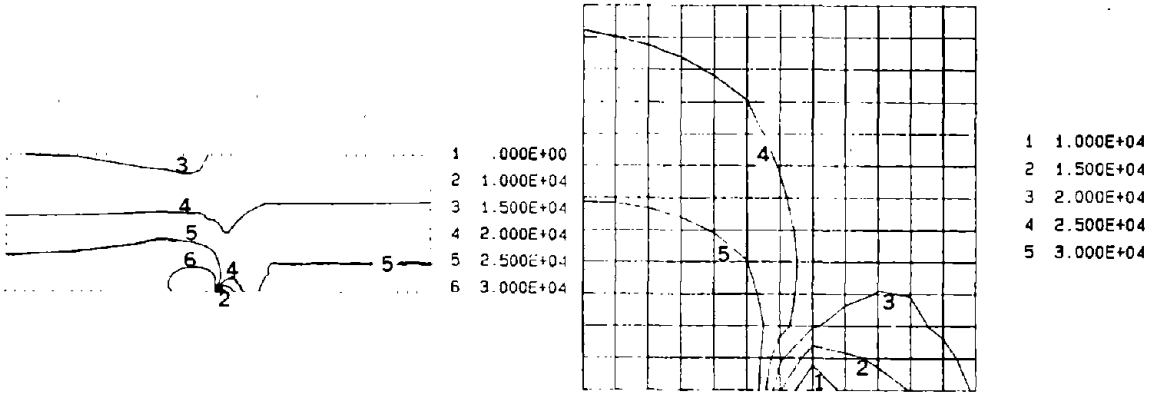

(A) Vertical Fault - Minor Principal Stress (psf; z = 150' - 300') 5' vertical offset

(B) Vertical Fault - Minor Principal Stress (psf; z = 240' - 300') 5' vertical offset

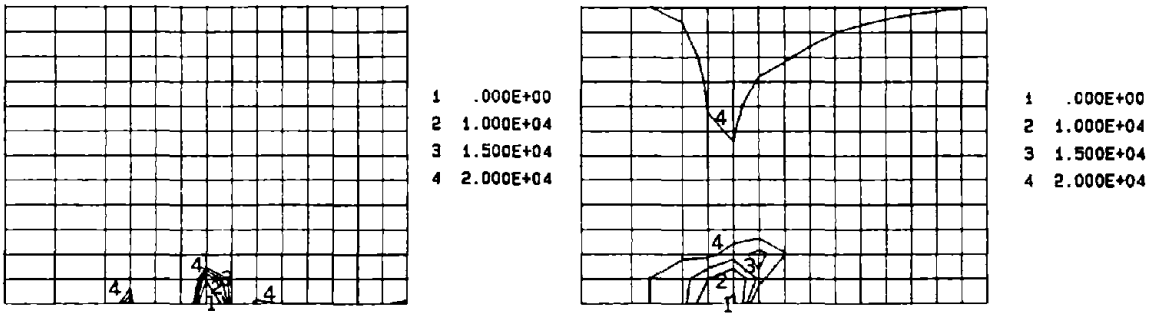

(C) 45° Thrust Fault - Minor Principal Stress (psf; z = 240' - 300') 5' vertical offset

(D) 60° Normal Fault - Minor Principal Stress (psf; z = 240' - 300') 5' vertical offset

Figure 8-18: RESULTS OF NONLINEAR FINITE ELEMENT ANALYSES OF VARIOUS FAULT MOVEMENTS AND CASE 2 CLAY PARAMETERS: ZONES OF POTENTIAL HYDRAULIC FRACTURING (σ_3 < 20,000 PSF): D_s = 300'

where the value of K_o was highest suggest that higher initial lateral earth pressures in the saturated clay minimize the extent of the zone of potential hydraulic fracturing. The importance of the other soil model parameters are less clear, although there appears to be a general trend which indicates that reducing the initial stiffness of the clay (and hence, the brittleness of the clay's stress-strain behavior) helps reduce the extent of zones of potential hydraulic fracturing.

8.5.4 Summary:

The incremental nonlinear elastic finite element program SSCOMP, which employs a slightly modified version of the Duncan et al. (1984) hyperbolic soil model, provided valuable insights into the phenomenon of fault rupture propagation through saturated clay. The nonlinear finite element analyses found that the rate at which the shear rupture zone propagates through the saturated clay overlying a displaced base rock fault appears to depend primarily on the failure strain of the soil. In fact, the analyses described in this section appear to suggest that the normalized height of the shear rupture zone (h_f/d_b: the height of the shear rupture zone divided by the magnitude of the vertical base offset) is roughly inversely proportional to the failure strain of the saturated clay. Other hyperbolic soil model parameters which help to describe the general shape of the clay's stress-strain relationship are of lesser importance in determining the development of the shear rupture zone through the soil.

It appears that the parameters: K_o (the coefficient of lateral earth pressure at rest), C (the undrained shear strength), ν (Poisson's ratio), and E_i (the initial tangent modulus of the stress-strain relationship which helps to define the stiffness of the soil during load-deformation) also affect the development of failure (shear and tensile) in the soil mass but not to the extent of the failure strain parameter. Increasing K_o delays the initiation of shear and tensile failure in the clay. To a

lesser degree, it appears that decreasing the undrained shear strength (C) of the clay delays the initiation of tension. Decreasing Poisson's ratio (ν) to a value slightly lower than 0.49 delays the initiation of tensile failure and slightly decreases the normalized height of the shear ruture zone (all other factors remaining the same). Decreasing E_i appears to spread the differential base movement across a wider zone of shear distortion and to slightly delay the initiation of tensile failure. The orientation of the shear rupture zone through the soil appears to be primarily dependent on the orientation of the base rock fault plane and on the value of K_o used to describe the initial stress state of the saturated clay soil. The use of interface elements to localize shear failure to distinct rupture planes and the use of incremental remeshing in the solution technique are quite cumbersome and do not significantly alter the results of these analyses regarding the development of shear and tensile failure in the clay.

8.6 Lessons to be Learned from the Finite Element Analyses Regarding Fault Rupture Propagation through the Saturated Clay Core of an Earth Dam

The results from these numerical analyses of fault rupture propagation through saturated clayey materials suggest that the finite element method can be applied to this class of problem provided that the soil's nonlinear, stress-dependent stress-strain behavior is adequately modeled. The incremental nonlinear elastic finite element program SSCOMP which employs a slightly modified version of the Duncan et al. (1984) hyperbolic soil model is capable of adequately modeling the nonlinear stress-strain behavior of the saturated clay overlying a displaced base rock fault, and hence, these nonlinear finite element analyses provide good predictions of observed behavior. The results of the finite element analyses of the clay-box model tests described previously in Chapter Six agree reasonably well with the patterns of failure observed in the model clay overlying the deformed base

sections. In addition, the results from the FE analyses of the Davie (1973) anchor pull-out clay-box model tests compare favorably with the observed behavior of the saturated clay soil overlying the uplifted anchor plate. The good agreement between the observed behavior of the soil in these clay-box model tests and the soil behavior predicted using the incremental nonlinear elastic finite element method provides good support for the application of this numerical approach in the study of the effects of tectonic movements on stresses and deformations in earth dams constructed of core sections composed of saturated clayey materials.

These studies provide strong evidence that the most critical soil parameter in the numerical modeling of fault rupture propagation through saturated clay is the failure strain of the clay. Although these analyses emphasize the importance of adequately modeling the general shape of the saturated clay's nonlinear stress-strain relationship, which includes reasonable representations of the clay's undrained shear strength, its ductility or brittleness (stiffness), and its initial stress state (i.e. the value of the coefficient of lateral earth pressure at rest and the initial vertical stress), the results of these analyses were most sensitive to variations in the soil's failure strain. The physical model tests performed in the course of this research, as well as a number of previous sandbox and clay-box model tests described in the review of literature, similarly suggested that the development of the shear rupture zone in the soil overlying a displaced base rock fault depends primarily on the failure strain of the soil. In particular, the magnitude of the vertical base offset required to propagate the shear rupture zone up to the ground surface is principally a function of the clay's failure strain. Figure 8-19 which depicts the results of the nonlinear finite element analyses of fault rupture propagation through saturated clay which were performed as a part of this research program clearly shows the relative importance of the soil's failure strain parameter. There is almost a linear relationship between the normalized base offset required

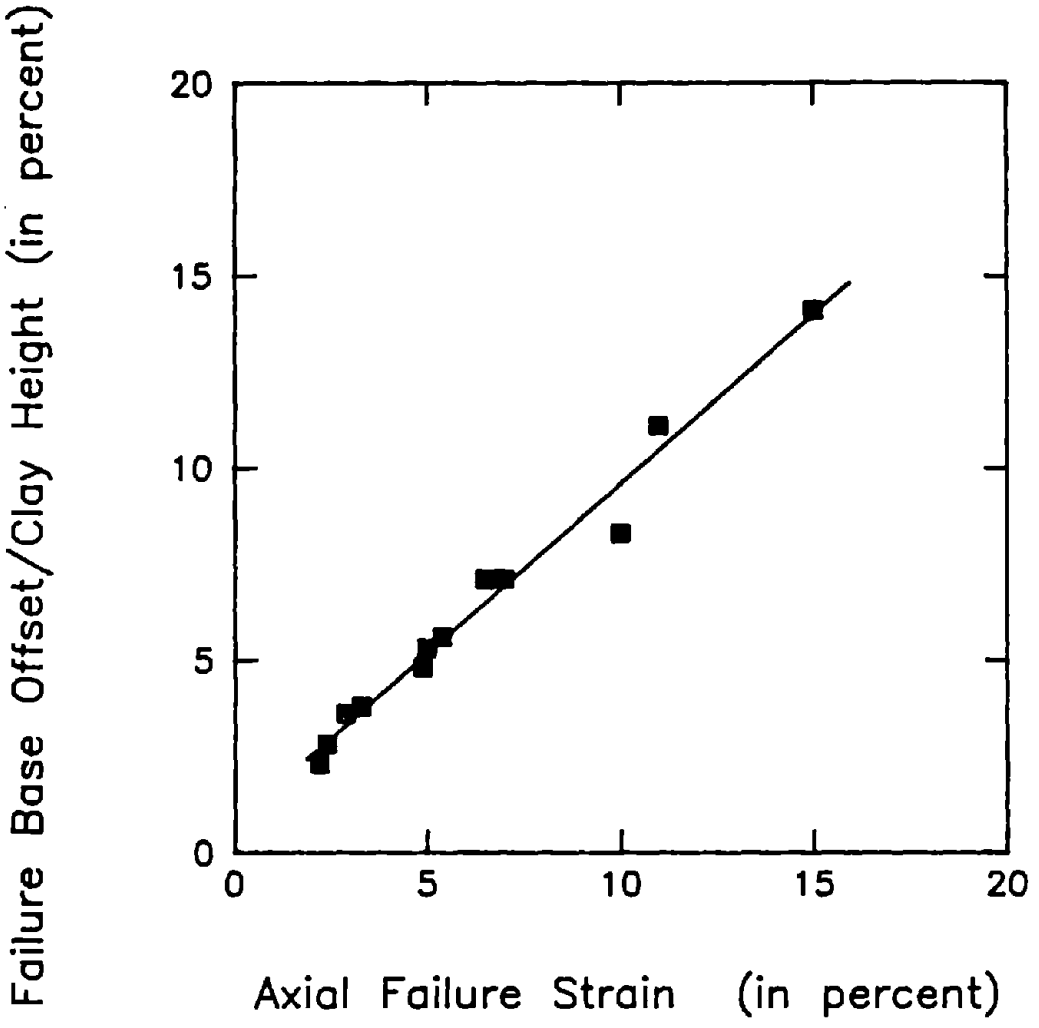

Figure 8-19: NONLINEAR FINITE ELEMENT PREDICTION OF THE RELATIONSHIP BETWEEN THE NORMALIZED BASE OFFSET REQUIRED TO PROPAGATE THE SHEAR RUPTURE ZONE TO THE GROUND SURFACE AND THE FAILURE STRAIN OF THE SOIL

to propagate the shear rupture zone through the clay and the axial failure strain of the saturated clay. The soil behavior illustrated in Figure 8-19 compares favorably with that shown previously in Figures 6-27 and 8-4.

As mentioned previously in Chapter Three, in most cases, earth dams would be planned at sites where fault movements were at the lower end of the ranges of possible fault displacements, as dams would not typically be sited across major faults considered capable of producing major earthquakes. In any case, the records of observed maximum surface fault displacements presented in Figure 3-2 suggest that there is a reasonable magnitude of maximum fault offsets that one would have to consider in an analysis of base rock fault rupture propagation through overlying soils. Depending primarily on the magnitude of the earthquake and the type of fault movement, the maximum surface offset from known earthquake events ranges from less than an inch to at most 35 feet. In most cases, however, the typical expected reasonable range of differential movement across faults overlain by man-made earth embankments would be only a few inches to at most 5 to 10 feet. Of course, the site-specific value of expected fault offset could be assessed only after a comprehensive geologic study of the project site and the surrounding region. In general, the usual expected base rock fault offsets encountered in the design of typical earth structures might not be of sufficient magnitude to produce a shear rupture that propagates all the way up to the ground surface.

It is more practical then to refer to the height of the shear rupture zone in the soil at specified expected base rock fault offsets. A review of the intermediate results of the incremental nonlinear finite element analyses of fault rupture propagation through saturated clay performed in this study provides such data as shown in Figure 8-20. In this graph, the normalized height of the shear rupture zone (i.e. the height of the shear rupture zone in the clay overlying the base rock fault divided by the current magnitude of vertical base offset) is plotted as a

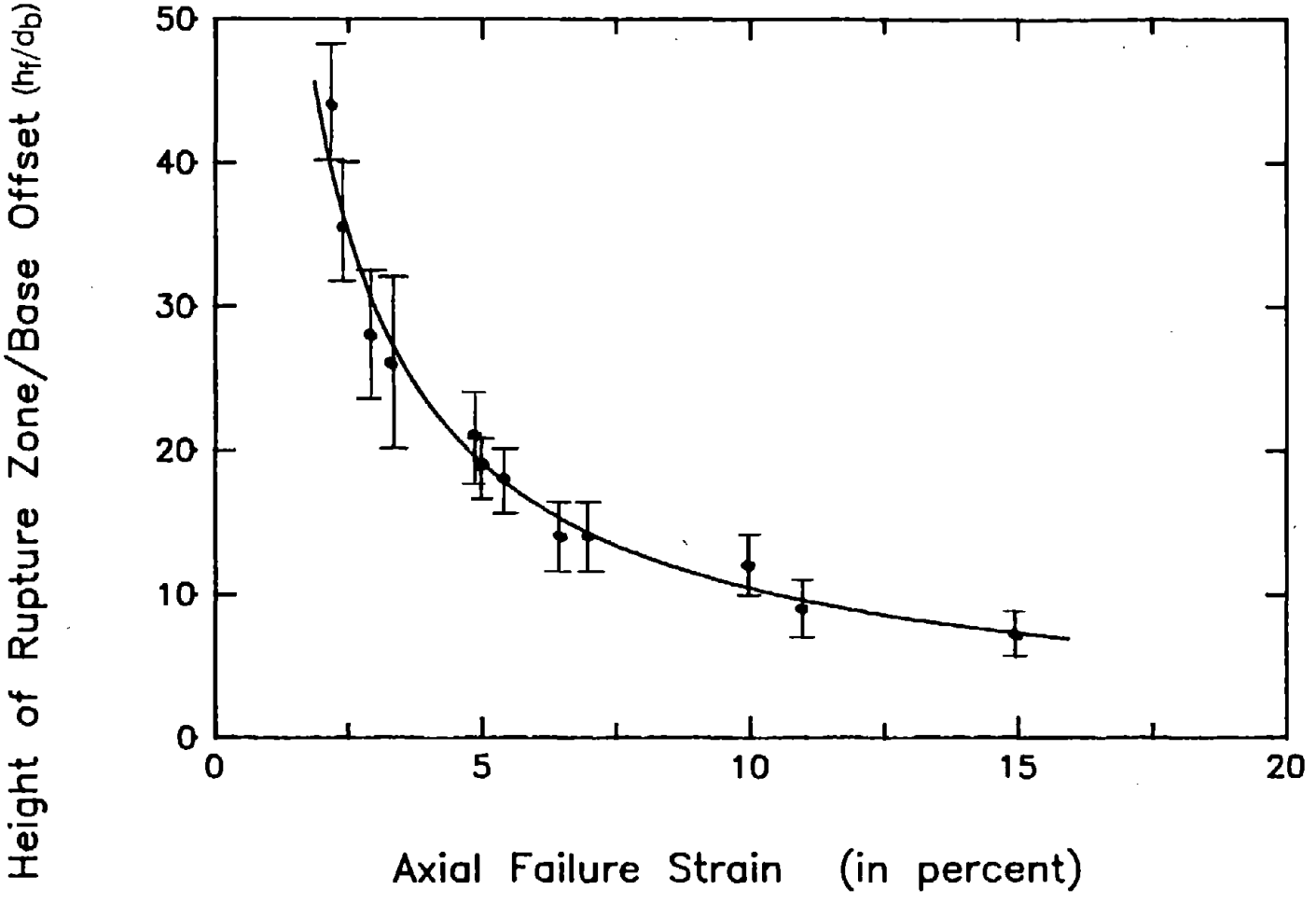

Figure 8-20: RELATIONSHIP BETWEEN THE NORMALIZED HEIGHT OF THE SHEAR RUPTURE ZONE ABOVE THE BASE ROCK FAULT OFFSET AND THE FAILURE STRAIN OF THE SATURATED CLAY OVERLYING THE FAULT

function of the axial failure strain of the clay. The error bars depict the variation in the normalized height of the shear rupture zones at different levels of vertical base rock fault offsets. Overall, the data is fairly consistent showing that the rupture zone propagates farther in saturated clayey materials that exhibit brittle stress-strain behavior (i.e. low values of failure strain), and that the rupture zone propagates least in the saturated clayey materials that exhibit a more ductile stress-strain behavior (i.e. high values of failure strain).

This data provides the engineer with an improved understanding of the relative importance of the overlying soil's failure strain and the potential effects of placing the soil in such a manner as to achieve brittle or ductile soil shear deformation behavior. Moreover, this data provides the engineer with a preliminary estimate of the anticipated magnitude of the shear rupture zone in a particular soil overlying a base rock fault which is expected to produce a specified fault offset, and at least, a sense of the scale of the problem. Of course, given the complexity of the fault rupture propagation phenomenon, additional site, material and project specific in-depth studies should be performed and a sufficient factor of safety should be employed in the design of earth dams built across potentially active faults. Nevertheless, the data provided in Figure 8-20, in at least a qualitative way, provides information useful in answering the first of the critical questions delineated in the introductory chapter (See Chapter 1: (1) What is the extent of the likely shear rupture zone with increasing magnitudes of base deformation?).

The results of the sensitivity study presented previously in Section 8.5 provides valuable insights into the effects of the soil's stress-strain and volumetric strain behavior on the development of tension zones or zones of potential hydraulic fracturing in saturated clayey materials overlying a displaced base rock fault. Regarding the potential of the saturated clayey soil of an earth dam core

section to develop hydraulic fracturing under the water pressure of the impounded reservoir (i.e. $\sigma_3 < u$), it appears that the failure strain of the clay is a less important factor. Instead, the soil parameters K_o (the coefficient of the lateral earth pressure at rest), C (the undrained shear strength), and E_i (the initial tangent modulus or stiffness) are relatively more important in the development of tension zones or zones of potential hydraulic fracturing. As the value of K_o increases, the clay's initial minor principal stress increases and the development of tensile failure in the soil is delayed. Correspondingly, the potential for zones of hydraulic fracturing and the extent of such zones are significantly reduced. The soil parameter "C" appears to affect the development of potential zones of hydraulic fracturing in the opposite sense. As the undrained shear strength of the clay increased in these nonlinear finite element analyses, the extent of the zone of potential hydraulic fracturing also increased. The results from these analyses suggest that a stronger clay soil would be more likely to develop zones where the minor principal stress was reduced to a low enough value to permit the initiation of hydraulic fracturing. The cause of this observation is not entirely clear. Finally, to a much lesser degree than the K_o and C soil parameters, the value of the initial stiffness of the clay soil (E_i), which helps describe the general shape of the clay's stress-strain relationship, affects the development of zones of potential hydraulic fracturing. As the value of E_i decreased, the extent of the zones of potential hydraulic fracturing by the finite element analyses predicted also decreased.

The incremental nonlinear finite element analyses performed as a part of this research program, thus, help answer the second critical question delineated in the Introduction (See Chapter One: (2) What will be the extent of tension zones or zones of potential hydraulic fracturing with increasing magnitudes of base deformation?) The analyses suggest that the extent of zones of potential hydraulic fracturing depends primarily on the initial stress state of the soil as described by

the coefficient of lateral earth pressure at rest, the undrained shear strength of the soil, and the magnitude and the orientation of the base rock fault movement.

These nonlinear finite element studies of a 2-D, plane strain, level ground section (where the depth of the soil equals 80 feet or 300 feet) through the saturated clay core of an earth dam or through a generic deposit of natural saturated clay soil also help answer the critical questions 3, 4 and 5 delineated in Chapter One. Regarding question 3 (See Chapter One), the amount of reservoir water that might leak through shear rupture zones, tension zones, or zones of potential hydraulic fracturing appears to be related to the nonlinear stress-strain behavior of the saturated clay, the initial stress state of the clay, and the magnitude and the orientation of the base rock fault movement. On the other hand, regarding question 4 (See Chapter One), these analyses confirm the observations made during small-scale physical model studies of fault rupture propagation through soils, as well as observations reported in surface fault rupture field studies, that the differential movement across the distinct shear rupture planes dissipates as the base rock fault rupture propagates upward through the overlying soil. Hence, the damage produced in the slopes and crest of the earth dam would principally depend on the nonlinear stress-strain behavior of the saturated clay and the magnitude and the orientation of the base rock fault movement (Question (4) of Chapter One).

Finally, this relatively comprehensive study of the sensitivity of the results of the nonlinear finite element analyses to variations in the soil model parameters employed to describe the stress-strain and volumetric strain behavior of the clay and the initial stress state of the clay provides suggestions as to the characteristics of the dam core material which can "best" mitigate the potential hazards associated with fault rupture propagation through typical earth dams. Of course, specific suggestions can only be put forth after conducting a comprehensive geotechnical

study of the earth dam in question. This investigation should include a comprehensive geologic study of the dam site and the surrounding region, and a comprehensive geotechnical study of the earth embankment which includes extensive laboratory and field testing of soils and in-depth analyses of the dam. In general, however, these studies suggest that the "best" dam clay core material should exhibit ductile stress-strain behavior (i.e. sufficiently large strain at failure in the clay, without a significant post-peak drop in the strength of the clay). It also appears beneficial to adequately place and compact the clay in the earth dam core section in a manner which increases the initial lateral earth pressures or minor principal stress in the soil. All in all, this numerical study helped develop an improved knowledge and understanding of the effect of tectonic movements on stresses and deformations in earth embankments.

CHAPTER NINE:
SUMMARY AND CONCLUSIONS

9.1 Summary

This study was undertaken to further develop the understanding of how an earth dam responds to a fault offset in its foundation (See Chapter One, Questions 1-6). Since many earth dams are constructed with nearly saturated clay core sections, one of the principal objectives of this program of research was to improve our current level of understanding of fault rupture propagation through overlying saturated clay soils. An improved understanding of this phenomenon would also assist engineers in siting and designing critical buildings, facilities, and utility and transportation systems to be constructed in regions where cohesive soils overlie potentially active faults.

The results of this research have led to the development of analytical techniques for modeling fault rupture propagation through overlying saturated clays, and to the development of preliminary recommendations for design provisions to minimize the resulting potentially adverse effects on dam stability and integrity. In this study, a relatively comprehensive review, evaluation and synthesis of previous works which improve the current level of understanding of fault rupture propagation through overlying soils was performed. Previous studies of the effects of fault rupture on the performance of earth dams and some indicative full-scale earth dam/fault offset case studies were reviewed in Chapter Two. The literature review was extended in Chapter Three to investigate available earthquake surface rupture field case histories. Additionally, physical and numerical model studies of the fault rupture propagation phenomenon were reviewed and evaluated. In Chapter Four, illustrative studies of a closely related problem, anchor pull-out behavior, were examined, and soil behavior analogous to

that displayed during fault rupture propagation through saturated clay was observed. Findings from this review, evaluation and synthesis of available case histories and related previous studies were summarized in Chapter Five.

In Chapter Six, the results from 1 g small-scale model tests of fault rupture propagation through saturated clay were presented and were found to be in fairly close agreement with the observations made during field studies and previous sandbox model tests. The model clay material exhibited well-scaled stress-deformation behavior for small-scale model testing without the need for a centrifuge apparatus.

A number of numerical methods and soil behavior models were evaluated through the preliminary analyses performed in Chapter Seven. Finally, the results of an in-depth nonlinear finite element study of fault rupture propagation through saturated clay were discussed in Chapter Eight. The results from the numerical analyses suggest that the finite element method can be successfully applied to this class of problem provided that the soil's nonlinear stress-dependent stress-strain behavior is adequately modeled (in this case, by the use of a hyperbolic nonlinear elastic soil model). The results of these studies have led to the development of modeling and analytical techniques for investigating the phenomenon of fault rupture propagation through overlying clays, and an improved understanding of some of the factors controlling this phenomenon.

9.2 Fault Rupture Propagation through Soil

Case histories often provide the most reliable source of information with regard to how physical events occur, and the use of case histories as a basis for the development of both insights and engineering judgment has long been a cornerstone of geotechnical practice. Field studies of either surface fault ruptures or fault planes exposed in exploratory trenches exhibit considerable variability in

fault rupture propagation behavior because of the complexities of the geologic materials, their stratigraphy, and processes involved. Although the majority of differential movement across a fault trace is typically confined to one or more distinct rupture planes within a wider overall zone of shear deformation, often a more complex, discontinuous pattern of fault ruptures develops within a zone varying in width along the fault trace. Warping of the bedrock adjacent to the primary fault, as well as movement on secondary breaks, can complicate the surface expression of the bedrock fault offset. Given the complexity of the fault rupture process, it is somewhat surprising that any reasonably consistent patterns of behavior emerged during the review of the case histories, but such trends were observed. Although exceptions to these general patterns of behavior may be found, the preponderance of evidence justifies making a number of salient observations regarding "trends" or "typical" patterns of behavior.

Recent work by Wells et al. (work in progress) provides insight into the scale of the fault rupture problem. Their review of nearly 90 field cases of observed surface fault ruptures shows, as illustrated in Figure 3-2, that depending primarily on the magnitude of the earthquake and the type of fault movement, the maximum surface offset ranges from less than an inch to at most approximately 35 feet. Moreover, researchers have found that the average surface fault offset in any given event is usually not more than 50% of the maximum offset at one point along the fault. Hence, in most cases, the magnitude of potential surface fault offsets along most of the ruptured fault length would be at most 5 to 15 feet. Of course, the site-specific value of the expected fault offset can be assessed only after a comprehensive geologic study of the project site and the surrounding region.

A number of geologists have found that the principal factors controlling the general characteristics of surface faulting are: (a) the type of fault movement (thrust, normal, or strike-slip), (b) the inclination of the fault plane, (c) the amount

of displacement on the fault, (d) the depth and geometry of the earth materials overlying the bedrock fault, and (e) the nature of the overlying earth materials. Examples which illustrate characteristics of fault rupture propagation through overlying soils are shown in Figures 3-30, 3-31 and 3-32. These figures focus on only three of the more important variables - the type of fault movement, the inclination of the fault plane, and the nature of the overlying soil deposit.

Typically, thrust faults tend to gradually decrease in dip near the ground surface. Normal faults tend to refract at the soil-bedrock contact and increase in dip as they approach the ground surface. This refraction and variation of the dip of the normal fault plane may produce gravity grabens. Strike-slip faults tend to follow the almost vertical orientation of the underlying bedrock fault, although the rupture zone may spread or "flower" near the ground surface. Relative motion is primarily concentrated within a relatively narrow zone above the bedrock fault. Once failure occurs, differential movement is usually localized to thin, distinct failure planes. Ductile materials, however, may accommodate significant fault movement by warping without actually developing distinct shear surfaces.

Field observations of surface faulting indicate that, in general, the bedrock behaves as shown in Figures 3-27, 3-28 and 3-29. Down-warping of the upthrown block during thrust faulting creates tension fissures in the bedrock surface. These tension fissures in the bedrock would probably produce tension zones in the soil overlying the deformed bedrock. Subsidence of the normal fault's hanging wall may produce secondary fractures. Secondary bedrock deformations are less likely to occur in strike-slip faulting. Nevertheless, some amount of movement should be expected to occur on existing planes of weakness in the foundation rock during all types of fault movement.

Differential movement across the fault rupture typically diminishes as the rupture propagates up toward the ground surface. For example, an 8 foot offset

was locally absorbed in a 500 foot high fractured rock cliff during the 1964 Alaska earthquake, producing no surface rupture. The 1930 Idu, Japan earthquake created an 8 foot offset in a tunnel located at a depth of 500 feet, but less than 3 feet of this offset appeared at the ground surface. Within one region, the 1954 Dixie Valley - Fairview Peak earthquake produced a scarp 3 to 4 feet in height which was continuous, except for a quarter mile gap where the fault "disappeared" under an alluvial fan composed of looser granular materials.

One of the principal shortcomings in this review of earthquake fault rupture case histories was the lack of well-documented case studies which fully described how a deep soil deposit (i.e. greater than 50 feet) responded to a base rock fault offset. Geologic field studies relied primarily on surface expressions of faulting, relatively shallow exploratory trenches (i.e. less than about 20 feet in depth) and interpretations of surficial geologic evidence. Few studies were found in which both the surficial faulting features and the underlying bedrock displacements were well-documented.

For this reason, as well as to reduce the apparent variability inherent in the field studies, previous physical and numerical model studies of the fault rupture propagation phenomenon were also reviewed. No widespread agreement has been reached, however, as to the "best" way to model the fault rupture propagation process. Furthermore, the majority of these previous studies (both physical and numerical) of the process of fault rupture propagation involved the modeling of dry, cohesionless materials. The work by Lade and Cole (1984) (See Figure 3-45(a)) appears to summarize the characteristics of the failure patterns observed to develop in dry alluvium overlying dip-slip bedrock faults. Of course, the applicability of these results to saturated clay is limited. Few results of model tests and numerical analyses of fault rupture propagation through saturated clay under undrained conditions are available.

9.3 Fault Rupture Propagation through Saturated Clay

These studies have led to the development of physical modeling procedures and analytical techniques for investigating the process of fault rupture propagation through saturated clay. The 1 g small-scale models composed of a weak, saturated kaolinite-bentonite clay mixture proved valuable in providing insight into the study of fault rupture propagation through saturated clay. The model clay with undrained shear strengths on the order of 10-100 psf and well-scaled stress deformation behavior could be employed in reasonable small-scale model testing without the need for a centrifuge apparatus. The scale models tested demonstrated failure behavior in close agreement to that observed in the field and in previous physical model studies employing dry sand. It was found that the height of the shear zone in the saturated clay above the base rock fault rupture was related to the amount of base movement and the stress-strain behavior of the soil (in particular, the failure strain of the soil).

The results from the numerical analyses suggest that the finite element method can be applied to this class of problem provided that the soil's nonlinear stress-strain behavior is adequately modeled. Linear elastic and linear elastic-perfectly plastic constitutive laws produced inconsistent results when employed in the finite element method, but the incremental nonlinear elastic hyperbolic soil model provided significantly better predictions of observed behavior. The predicted rupture zone enveloped the actual rupture planes which formed in the clay-box model tests. In addition, the finite element method was able to reasonably predict the magnitude of base offset required to propagate the shear rupture up to the top of the clay surface. The ability of the hyperbolic soil model to adequately represent the essential characteristics of the clay's stress-strain behavior, especially the clay's failure strain, appears to be the primary reason for

this numerical method's success in satisfactorily predicting the effects of fault rupture propagation through saturated clay.

The anchor pull-out/fault rupture analogy also proved to be extremely useful. Model testing of anchors in soft clay indicate that the amount of anchor plate displacement necessary to produce failure in the soil above the anchor was also primarily dependent on the soil's failure strain. These studies of anchor pull-out behavior (both physical and numerical), as well as field observations of surface fault ruptures and the results of the 1 g small-scale clay-box model tests and the nonlinear finite element analyses of fault rupture propagation through overlying cohesive soils, indicate that both stress characteristics and kinematic constraints combine to control the behavior of the soil above the bedrock fault movement. A highly stressed region forms above the inside edge of the upthrown block and stress reduction occurs to the side of the edge of the upthrown block during dip-slip fault movement. Although shear failure may occur in the zone of stress increase, the final shear failure surface must be kinematically admissible, and hence, it must bend over the downthrown block. Figure 4-7 illustrates this two-phase development of the shear rupture zones in the soil overlying a dip-slip bedrock fault.

One of the principal findings of this study is the realization that the rate of fault rupture propagation through soil depends in large part on the failure strain of the soil. The bedrock fault does not instantaneously produce a rupture zone through the overlying soil deposit. Instead, the rupture propagates up toward the ground surface with increasing base rock fault offset. The rate at which it propagates (i.e. how far it propagates in the overlying soil at a specified base rock fault offset), however, is determined principally by the failure strain of the saturated clay soil. Moreover, the axial failure strain of unconfined triaxial compression tests appears to define the saturated clay's failure strain. As shown in

Figure 8-20 (where the normalized height of the shear rupture zone (h_f/d_b) is plotted as a function of the axial failure strain of the clay), the shear rupture zone propagates farther in saturated clayey materials that exhibit brittle stress-strain behavior (i.e. low values of failure strain), and the shear rupture zone propagates least in the saturated clayey materials that exhibit a more ductile stress-strain behavior (i.e. high values of failure strain). This data provides the engineer with an improved understanding of the relative importance of the overlying soil's failure strain and the potential effects of brittle or ductile soil shear deformation behavior. Moreover, this data provides the engineer with a preliminary estimate of the anticipated magnitude of the shear rupture zone in a particular soil overlying a base rock fault which is expected to produce a specified fault offset, and at least a sense of the scale of the problem. Of course, given the complexity of the fault rupture propagation phenomenon, additional in-depth studies which consider the site characteristics, the material properties, and the details of the project in question, should be performed and a sufficient factor of safety should be employed in estimates of the development of the shear rupture zone in the saturated clay soil overlying a potentially active base rock fault.

The results of the soil parameter sensitivity study provide valuable insights into the effects of the soil's stress-strain and volumetric strain behavior on the development of shear rupture or tension zones (or zones of potential hydraulic fracturing) in the saturated clayey soil overlying a displaced base rock fault. Whereas the failure strain of the clay appears to be the principal factor controlling the height of the shear rupture zones at specified magnitudes of base offset, the analyses suggest that the shape and the orientation of the shear rupture zone depend primarily on the initial stress state of the soil as described by the coefficient of the lateral earth pressure at rest, and on the magnitude and the orientation of the base rock fault movement. Increasing the value of K_o appears to move the

shear rupture zone slightly more over the downthrown block. The final shear rupture zone tends to follow the projection of the base rock fault plane, although normal fault planes tend to sometimes increase in dip as they approach the ground surface.

Regarding the development of tension zones ($\sigma 3 < 0$) or zones of stress reduction where the minor principal stress is reduced to a value low enough to permit the initiation of hydraulic fracturing ($\sigma 3 <$ u), it appears that the axial failure strain of the clay is a less important factor than it is in the development of shear rupture zones. Instead, the clay's initial stress state (as described by K_o and the initial vertical stress), its undrained shear strength (C), its volume change behavior (e.g. the value of ν), and the stiffness of the clay (E_i) appear to be more important factors in the development of tension zones or zones of potential hydraulic fracturing. In a general sense, the development of tensile failure in the soil is delayed, and correspondingly, the potential for zones of hydraulic fracturing and the extent of such zones are significantly reduced if the value of K_o increases and the values of C and E_i decrease. The effect of variations in the value of Poisson's ratio (ν) was inconsistent. Increasing the value of ν appeared to reduce the extent of the zone of potential hydraulic fracturing, but conversely, increasing ν appeared to produce tensile failure at lower magnitudes of base deformation. These studies also suggest that the extent of the zone of potential hydraulic fracturing is significantly smaller in soils overlying base rock thrust faults than in soils overlying base rock normal faults. Overall, the analyses suggest that the extent of zones of potential hydraulic fracturing depends primarily on the initial stress state of the soil, the undrained shear strength and stiffness of the soil, and the magnitude and type of the base rock fault movement.

These studies help to answer the first two critical questions delineated in the introductory chapter (See Chapter One: (1) What is the extent of the likely

shear rupture zone with increasing magnitudes of base deformations? and (2) What will be the extent of tension zones or zones of potential hydraulic fracturing with increasing magnitudes of base deformation?). Furthermore, the modeling and analytical techniques developed as a part of this research program (the 1 g small-scale model tests and the incremental nonlinear elastic finite element analyses of fault rupture propagation through overlying saturated clay), shown to provide good agreement with previous field studies, will assist the engineer in future investigations of the fault rupture propagation phenomenon.

9.4 The Effects of Tectonic Movements on Stresses and Deformations in Earth Embankments

Despite its potential limitations, engineering judgment based on the observations and the study of the performance of soils during well-documented field case histories provides one of the most reliable means of evaluating the potential effects of tectonic movements on stresses and deformations in earth embankments. Few case histories exist, however, which describe how earth dams respond to base rock fault displacements, and these indicative full-scale earth dam/fault rupture propagation case histories are not well-documented. Nevertheless, a number of earth dams have been designed to safely accommodate fault offsets in the foundation rock, and a review, evaluation, and synthesis of previous studies in this area, of the indicative full-scale earth dam/fault rupture propagation case histories, and of previous studies of closely related topics such as surface fault rupture and anchor pull-out behavior brings forth a number of salient observations.

Casagrande's concept of multiple lines of defense should be employed in the design of all dams built over potentially active faults. Experts agree that particular attention must be devoted to controlling the hazards of concentrated leaks through

the dam and its foundation. The stability of the foundation must be guaranteed. A thick, ductile core protected upstream by thick 'crackstopper' zones and downstream by thick filter and transition zones were considered desirable. These zones should be backed up by a drainage system that extends the full height and length of the dam. All zones must be wider than the maximum anticipated potential fault offset. The crest width and the freeboard of the dam should be maximized, whereas the required reservoir capacity should be minimized. Of course, if possible, a dam site traversed by potentially active faults should be avoided. Spillways and outlet control works should not traverse potentially active fault traces. Finally, the experts concluded that rigid dam structures such as concrete gravity dams should not be constructed over potentially active faults.

Pure reasoning based on engineering judgment, however, was shown to have limitations. For example, an experienced engineer had reasoned that the "best" material to use in the core of an earth dam built over a potentially active fault was a broadly graded gravel-sand mixture because of the material's supposed "self-healing" tendency, only to discover later that these materials were, in fact, prone to soil migration (internal erosion) even without base differential movement. Considerable effort, therefore, should be devoted towards the development of modeling and analytical techniques that help improve our understanding of this problem until nature provides full-scale earth dam/fault rupture propagation case histories which can be well-documented. The good agreement between the results of the 1 g small-scale clay-box model tests and the incremental nonlinear elastic finite element analyses performed in this study, the results of previous physical and numerical studies of closely related topics, and field observations of surface fault rupture documented in case histories provides good support for the application of these clay-box model tests and nonlinear finite element analyses in the study of the

effects of tectonic movements on stresses and deformations in earth dams constructed of core sections composed of saturated clayey materials.

These 1 g small-scale model studies and nonlinear finite element studies of a 2-D, plane strain, level ground section or through the saturated clay core of an earth dam help answer the critical questions (1-5) delineated in Chapter One. As discussed previously in Section 9.3, the extent of the likely shear rupture zone in the saturated clay soil overlying the displaced base rock fault at specified magnitudes of offset (See Chapter One, Question 1) is determined principally by the soil's axial failure strain (See Figure 8-20). On the other hand, these studies suggest that the extent of zones of potential hydraulic fracturing (See Chapter One, Question 2) depends primarily on the initial stress state of the soil, the undrained shear strength and stiffness of the soil, and the magnitude and type of the base rock fault movement.

Regarding Question 3 (See Chapter One), the amount of reservoir water that might leak through shear rupture zones, tension zones, or zones of potential hydraulic fracturing appears to be related to the nonlinear stress-strain behavior of the saturated clay, the initial stress state of the clay, and the magnitude and the orientation of the base rock fault movement. Regarding Question 4 (See Chapter One), these studies confirm the observations reported in surface fault rupture field studies that the differential movement across the distinct shear rupture planes dissipates as the base rock fault rupture propagates upward through the overlying soil. Hence, the damage produced in the slopes and crest of the earth dam would principally depend on the nonlinear stress-strain behavior of the saturated clay and the magnitude and the orientation of the base rock fault movement (and, of course, the geometry of the embankment).

Finally, this study of the sensitivity of the results of the nonlinear finite element analyses to variations in the soil model parameters employed to describe

the stress-strain and volumetric strain behavior of the clay and the initial stress state of the clay provides insight regarding the characteristics of the dam core material which can "best" mitigate the potential hazards associated with fault rupture propagation through typical earth dams (See Chapter One, Question 5). Of course, specific suggestions can only be put forth after conducting a comprehensive geotechnical study of the earth dam in question. This investigation should include a comprehensive geologic study of the dam site and the surrounding region, and a comprehensive geotechnical study of the earth embankment which includes extensive laboratory and field testing of soils and in-depth analyses of the dam. The investigation should address concerns with respect to overall earthquake-resistant design, as well as other design considerations. In general, however, these studies suggest that (with respect to mitigating the potential hazards associated with fault rupture propagation through an earth dam) the earth dam's clay core material should exhibit ductile stress-strain behavior (i.e. sufficiently large strain at failure in the clay, without a significant post-peak drop in the strength of the clay). It also appears beneficial to adequately place and compact the clay in the earth dam core section in a manner which increases the initial lateral earth pressures or minor principal stress in the soil. Overall, this study helped develop an improved knowledge and understanding of the effects of tectonic movements on stresses and deformations in earth embankments.

9.5 Suggestions for Future Research

Based on the field observations, laboratory data, and numerical results currently available, the models and analytical procedures developed during these studies appear to provide a suitable basis for the evaluation of a number of the effects of tectonic movements on the stresses and deformations in earth embankments for many situations. Given the complexity of the fault rupture

propagation phenomenon and the lack of well-documented full-scale earth dam/fault rupture propagation case histories, further study would be useful in a number of areas as follows:

1. Case Histories: There is a need to take advantage of the information provided by well-documented case histories of fault rupture propagation through earth embankments. It is important now to identify potential case histories and to instrument the selected dam sites with acceleration and deformation measurement devices to capture this critical data when it becomes available. In addition, since few well-documented field studies exist which describe how a deep soil deposit (i.e. depth greater than 50 feet) responds to a base rock fault offset, the sites of potentially active faults should be instrumented and deeper exploratory trenches should be planned at known sites of surface fault rupture.

2. Modeling: Additional physical and numerical model studies of fault rupture propagation through soils are warranted. There is a need to perform incremental nonlinear elastic-plastic finite element studies to note the effect of not only modeling the soil element behavior adequately up to the point of failure, but also past failure, especially in situations where the clay soil may exhibit a significant post-peak drop in strength. Analyses of the saturated, cohesionless materials comprising the filter and transition zones of the earth dam are still required. 3-D finite element analyses should be performed to study the effect of an oblique-slip fault movement (e.g. strike-slip) in the foundation of an earth dam. Likewise, additional 1 g small-scale model testing of the performance of an earth embankment which traverses a

strike-slip fault offset would be beneficial. Of course, in the long run, it is hoped that modeling techniques will be developed to investigate the simultaneous application of static and dynamic loads on an earth embankment.

3. Properties: To adequately answer Question 3 (How much reservoir water could leak through disturbed core and filter zones or through a disturbed foundation, and might this result in uncontrolled internal erosion?), the hydraulic conductivity along newly formed shear fractures in earth materials must be investigated. Further studies to investigate localized stress reduction, tensile failure, or potential hydraulic fracture would also be useful. Additionally, the performance of filter materials disturbed by tectonic movements remains uncertain.

These are only some of the most significant shortcomings of the current level of understanding of the effects of tectonic movements on stresses and deformations in earth embankments. Further study of this class of problem would be desirable.

REFERENCES

Ali, M. S. (1968). "Pullout Resistance of Anchor Plates and Anchor Piles in Soft Bentonite Clay," Duke University, Soil Mechanics Series No. 17, pp. 1-53.

Ambraseys, N. N. (1960). "On the Seismic Behaviour of Earth Dams," Proceedings of the Second World Conference on Earthquake Engineering, Vol. 1, Japan, pp. 331-358.

Ambraseys, N. and Jackson, J. (1984). "Seismic Movements." In Ground Movements and their Effects on Structures. Ed. P.B. Attewell and R. K. Taylor. New York: Surrey University Press, pp. 353-380.

Arango-Grieffenstein, I. (1971). "Seismic Stability of Slopes in Saturated Clay," thesis submitted to the University of California, Berkeley, California, in partial satisfaction of the requirements for the degree of Doctor of Philosophy, June.

Asquith, D. O. and Leighton, F. B. (1973). "Earth Rupture and Structural Damage by San Fernando Earthquake in North Sylmar Housing Development." In San Fernando, California, Earthquake of February 9, 1971. Ed. L. M. Murphy. Washington, D.C.: U.S. Department of Commerce, pp. 207-212.

Balla, A. (1961). "The Resistance to Breaking Out of Mushroom Foundations for Pylons," Proceedings of the Fifth International Conference on Soil Mechanics and Foundation Engineering, Paris, July 17-22, pp. 569-576.

Barrientos, S. E., Ward, S. N., Gonzalez-Ruiz, J. R., and Stein, R. S. (1985). "Inversion for moment as a function of depth from geodetic observations and long period body waves of the 1983 Borah Park, Idaho earthquake," U.S. Geological Survey Open-File Report 85-290, pp. 485-518.

Barrows, A. G., Kahle, J. E., Weber, F. H., Jr. and Saul, R. B. (1973). "Map of Surface Breaks Resulting from San Fernando, California Earthquake of February 9, 1971." In San Fernando, California, Earthquake of February 9, 1971. Ed. L. M. Murphy. Washington, D.C.: U.S. Department of Commerce.

Bell, F. G. (1975). Site Investigations in Areas of Mining Subsidence. London: Newnes-Butterworths.

Belousov, V. V. (1961). "Experimental Geology," Scientific American, February, pp. 96-106.

Bhatnagar, R. S. (1969). "Pullout Resistance of Anchors in Silty Clay," Duke University, Soil Mechanics Series No. 18, pp. 1-62.

Bolt, B. A. (1972). "San Fernando Rupture Mechanism and the Pacoima Strong-Motion Record," Bulletin of the Seismological Society of America, Vol. 62, No. 4, August, pp. 1053-1061.

Bonilla, M. G. (1967). "Historic Surface Faulting in Continental United States and Adjacent Parts of Mexico," United States Department of the Interior, Geological Survey, TID-24124, pp. 1-36.

Bonilla, M. G. (1970). "Surface Faulting and Related Effects." In Earthquake Engineering. Ed. R. L. Wiegel. New Jersey: Prentice Hall, pp. 47-74.

Bonilla, M. G. (1973). "Trench Exposures Across Surface Fault Ruptures Associated with San Fernando Earthquake." In San Fernando, California, Earthquake of February 9, 1971. Ed. L. M. Murphy. Washington, D.C.: U.S. Department of Commerce, pp. 173-182.

Bonilla, M. G. (1982). "Evaluation of Potential Surface Faulting and Other Tectonic Deformation," prepared for U.S. Nuclear Regulatory Commission, NUREG/CR-2991, RA, October.

Bonilla, M. G. (1988a). "Faulting and Seismic Activity." In The Heritage of Engineering Geology: The First Hundred Years. Ed. G. A. Kiersch. Boulder, Colorado, Geological Society of America, Centennial Special Volume 3.

Bonilla, M. G. (1988b). "Minimum Earthquake Magnitude Associated with Coseismic Surface Faulting," Bulletin of the Association of Engineering Geologists, Vol. XXV, No. 1, February, pp. 17-29.

Bonilla, M. G. (1988c). Discussion of the General Behavior of Soil and Rock During Fault Movement, Private Communication.

Bonilla, M. G. and Lienkaemper, J. J. (1988). "The Visability of Active Faults Exposed in Exploratory Trenches [abstr.]," Geological Society of America, No. 2503.

Bray, J. W. and Goodman, R. E. (1981). "The Theory of Base Friction Models [abstr.]," Int. Jour. Rock Mech. Min. Science & Geomech., Vol. 18, pp. 453-468.

Briggs, H. (1929). Mining Subsidence. London: Edward Arnold & Co.

Briggs, H. and Morrow, J. (1927). "An Attempt at the Rationale of Faulting and Subsidence," Transactions of The Institution of Mining Engineers, Vol. LXXIII, Part 5, August, pp. 465-500.

Britto, A. M. and Gunn, M. J. (1987). Critical State Soil Mechanics via Finite Elements. Chichester: Ellis Horwood.

Brune, J. N. and Allen, C. R. (1967). "A low-stress-drop, low-magnitude earthquake with surface faulting. The Imperial, California, Earthquake of March 4, 1966," Bulletin of the Seismological Society of America, 57, pp. 501-514.

Bureau of Reclamation, U.S. Department of the Interior (1940). All-American Canal Project Report File, Denver, Colorado.

Burridge, P. B. (1987). "Failure of Slopes," thesis submitted to the California Institute of Technology, Pasadena, California, in partial fulfillment of the requirements for the degree of Doctor of Philosophy, March.

Butterfield, R. and Harkness, R. M. (1972). "The Kinematics of Mohr-Coulomb Materials." In Stress-Strain Behavior of Soils. Ed. R.H.G. Parry. Oxfordshire: G. T. Foulis & Co., Ltd., pp. 220-233.

Buwalda, J. P. and St. Amand, P. (1955). "Geological Effects of the Arvin-Tehachapi Earthquake," California Division of Mines, Bulletin 171, pp. 41-56.

Carter, J. P., Small, J. C. and Booker, J. R. (1977). "A Theory of Finite Elastic Consolidation," Int. Jour. Solids and Structures, Vol. 13, pp. 467-478.

Casagrande, A. (1937). "Seepage through Dams," Journal of the New England Water Works Association, Vol. LI, No. 2, June, pp. 296-336.

Casagrande, A. and Hirschfield, R. C. (1960). "Stress-Deformation and Strength Characteristics of a Clay Compacted to a Constant Dry Unit Weight," Research Conference on Shear Strength of Cohesive Soils, Soil Mechanics and Foundations Division, ASCE, Boulder, Colorado, June, pp. 359-418.

Chen, W. F. and Baladi, G. Y. (1985). Soil Plasticity: Theory and Implementation. New York: Elsevier.

Cheney, J. A., Shen, C. K. and Ghorayeb, F. (1984). "Fault Movement: Its Potential Damage to Embankment Dams," Eighth World Conference on Earthquake Engineering, San Francisco, California, pp. 341-347.

Clark, T. A. (1940). "Report of Earthquake Damage in Imperial Valley, May 18, 1940," U.S. Department of Interior, Bureau of Reclamation, Office Report, July, pp. 24-27.

Clough, R. W. and Pirtz, D. (1958). "Earthquake Resistance of Rock-Fill Dams," Transactions, ASCE, Vol. 123.

Cluff, L. S. (1988). Discussion of the General Behavior of Soil and Rock During Fault Movement, Private Communication.

Cluff, L. S., Slemmons, D. B. and Waggoner, E. B. (1970). "Active Fault Zone Hazards and Related Problems of Siting Works of Man," Proceedings of the Symposium on Earthquake Engineering, Indian Society of Earthquake Technology, University of Roorkee, Roorkee, November 14-16, pp. 401-410.

Cole, D. A., Jr. and Lade, P. V. (1984). "Influence Zones in Alluvium Over Dip-Slip Faults," Journal of Geotechnical Engineering, ASCE, Vol. 110, No. 5, May, pp. 599-615.

Compton, R. R. (1985). Geology in the Field. 2nd ed. New York: John Wiley & Sons.

Crone, A. J., Machette, M. N., Bonilla, M. G., Lienkaemper, J. J., Pierce, K. L., Scott, W. E. and Bucknam, R. C. (1985). "Characteristics of Surface Faulting Accompanying the Borah Peak Earthquake, Central Idaho," U.S.G.S. Open-File Report 85-290-A.

Crone, A. J., Machette, M. N., Bonilla, M. G., Lienkaemper, J. J., Pierce, K. L., Scott, W. E. and Bucknam, R. C. (1987). "Surface Faulting Accompanying the Borah Peak Earthquake and Segmentation of the Lost River Fault, Central Idaho," Bulletin of the Seismological Society of America, Vol. 77, No. 3, June, pp. 739-770.

Cundall, P. (1976). "Explicit Finite-Difference Methods in Geomechanics," Proceedings of the Second International Conference on Numerical Methods in Geomechanics, Blacksburg, Virginia, June 20-26, pp. 132-150.

Dames & Moore (1980). Report: Final Geoseismic Investigation, Proposed LNG Terminal, Little Cojo Bay, California, Vols. 1-8, for Western LNG Terminal Associates, October.

Davie, J. R. (1973). "Behaviour of Cohesive Soils under Uplift Forces," thesis submitted to the University of Glasgow for the degree of Doctor of Philosophy, July.

Davie, J. R. and Sutherland, H. B. (1977). "Uplift Resistance of Cohesive Soils," Journal of the Geotechnical Engineering Division, ASCE, Vol. 103, No. GT9, September, pp. 935-952.

Davie, J. R. and Sutherland, H. B. (1978). "Modeling of Clay Uplift Resistance," Journal of the Geotechnical Engineering Division, ASCE, Vol. 104, No. GT6, June, pp. 755-759.

Davis, E. H. and Booker, J. R. (1975). "Application of Plasticity Theory to Foundations," Proceedings of the General Session of the Symposium on Soil Mechanics: Recent Developments, The University of New South Wales, Australia, July 14-18, pp. 83-112.

Department of Water Resources of the State of California (1974). "Proceedings of the Conference on Earthquake Engineering for Water Projects," Meeting at Sacramento, January 15-16.

Dewey, J. W. (1985). "Instrumental seismicity of central Idaho," U.S. Geological Survey, Open-File Report 85-290, pp. 264-284.

Dickin, E. A. (1988). "Uplift Behavior of Horizontal Anchor Plates in Sand," Journal of Geotechnical Engineering, Vol. 114, No. 11, November, pp. 1300-1317.

Doser, D. I. and Smith, R. B. (1988). "Source parameters of the 28 October 1983 Borah Peak, Idaho, earthquake from body wave analysis," Bulletin of the Siesmological Society of America, 75, pp. 1041-1051.

Duncan, J. M., Byrne, P., Wong, K. S. and Mabry, P. (1980). "Strength, Stress-Strain and Bulk Modulus Parameters for Finite Element Analyses of Stresses and Movements in Soil Masses," College of Engineering, University of California, Berkeley, California, Report No. UCB/GT/80-01, August.

Duncan, J. M. and Chang, C-Y. (1970). "Nonlinear Analysis of Stress and Strain in Soils," Journal of the Soil Mechanics and Foundation Division, ASCE, Vol. 96, No. SM5, September, pp. 1629-1653.

Duncan, J. M. and Lefebvre, G. (1973). "Earth Pressure on Structures Due to Fault Movement," Meeting Preprint #1949, ASCE National Structural Engineering Meeting, San Francisco, April 9-13, pp. 1-24.

Duncan, J. M., Seed, R. B., Wong, K. S. and Ozawa, Y. (1984). "FEADAM84: A Computer Program for Finite Element Analysis of Dams," Department of Civil Engineering, Stanford University, Research Report No. SU/GT/84-03, November.

Dunrud, C. R. (1984). "Coal Mine Subsidence-Western United States," Geological Society of America, Reviews in Engineering Geology, Vol. VI, pp. 151-193.

Emmons, R. C. (1969). "Strike-Slip Rupture Patterns in Sand Models," Tectonophysics, Vol. 7, No. 1, pp. 71-87.

Friedman, M., Handin, J., Logan, J. M., Min, K. D. and Stearns, D. W. (1976). "Experimental Folding of Rocks under Confining Pressure: Part III. Faulted Drape Folds in Multilithologic Layered Specimens," Bulletin of the Geological Society of America, Vol. 87, July, pp. 1049-1066.

Frydman, S. (1974). "Yielding of Sand in Plane Strain," Journal of the Geotechnical Engineering Division, ASCE, Vol. 100, No. GT5, May, pp. 491-501.

Gates, G. O. (1969). "Earthquake Hazards," Conference on Geologic Hazards and Public Problems, Office of Emergency Preparedness, Region Seven, Santa Rosa, California, pp. 19-52

Geddes, J. D. (1977). Large Ground Movements and Structures. New York: John Wiley & Sons.

Geddes, J. D. (1984). "Structural Design and Ground Movements." In Ground Movements and their Effects on Structures. Ed. P. B. Attewell and R. K. Taylor. New York: Surrey University Press, pp. 243-267.

Geognosis (1980). User's Handbook for Program SAGE. Report submitted to Dames & Moore, October.

Gilbert, G. K. (1890). "Lake Bonneville," U.S. Geological Survey Mon. 1.

Gudehus, G. (1976). "On Constitutive Laws for Soils and Rocks," Proceedings of the Second International Conference on Numerical Methods in Geomechanics, Blacksburg, Virginia, June 20-26, pp. 1305-1320.

Hadley, J. B. (1964). "Landslides and related phenomena accompanying the Hebgen earthquake of August 7, 1959," U.S. Geological Survey, Paper 435.

Hafner, W. (1951). "Stress Distributions and Faulting," Bulletin of the Geological Society of America, Vol. 62, April, pp. 373-398.

Harkness, R. M. (1972). "An Essay on 'Mohr-Coulomb'." In Stress-Strain Behaviour of Soils. Ed. R.H.G. Parry. Oxfordshire: G. T. Foulis & Co., Ltd., pp. 212-219.

Heath, E. G. and Leighton, F. B. (1973). "Subsurface Investigation of Ground Rupturing during San Fernando Earthquake." In San Fernando, California, Earthquake of February 9, 1971. Ed. L. M. Murphy. Washington, D.C.: U.S. Department of Commerce, pp. 165-172.

Hoek, E. (1983). "Strength of Jointed Rock Masses," Geotechnique, Vol. 33, No. 3, pp. 187-223.

Hong, W. P. and Lade, P. V. (1989). "Strain Increment and Stress Directions in Torsion Shear Tests." Journal of the Geotechnical Engineering Division, ASCE, Vol. 115, No. 10, October, pp. 1388-1401.

Horsfield, W. T. (1977). "An Experimental Approach to Basement-Controlled Faulting," Geologie En Mijnbouw, Vol. 56, No. 4, pp. 363-370.

Hubbert, M. K. (1937). "Theory of Scale Models as Applied to the Study of Geologic Structures," Bulletin of the Geological Society of America, Vol. 48, October, pp. 1459-1520.

Hubbert, M. K. (1951). "Mechanical Basis for Certain Familiar Geologic Structures," Bulletin of the Geological Society of America, Vol. 62, April, pp. 355-372.

Institution of Civil Engineers (1977). Ground Subsidence. London: The Institution.

Ito, H. and Kitahara, Y. (1982). "Pulling-Out Resistance of Electronic Transmission Tower Footing Partially Penetrating into the Surrounding Ground at its Bottom Slab," International Symposium on Numerical Models in Geomechanics, Zurich, September 13-17, pp. 677-686.

James, R. G. and Bransby, P. L. (1971). "A Velocity Field for Some Passive Earth Pressure Problems," Geotechnique, Vol. 21, No. 1, pp. 61-83.

Jones, J. C. (1915). "The Pleasant Valley, Nevada, Earthquake of October 2, 1915," Bulletin of the Seismological Society of America, V. 5, No. 4, pp. 190-205.

Khadilkar, B. S., Paradkar, A. K. and Golait, Y. S. (1971). "Study of Rupture Surface and Ultimate Resistance of Anchor Foundations," Proceedings of the Fourth Asian Regional Conference on Soil Mechanics and Foundation Engineering, Vol. I, Bangkok, Thailand, July, pp. 121-127.

Kinner, E. B. and Ladd, C. C. (1970). "Load-Deformation Behavior of Saturated Clays during Undrained Shear," Massachusetts Institute of Technology, Department of Civil Engineering Research Report R70-27, Soils Publication No. 259, May.

Kovacs, W. D. (1968). "An Experimental Study of the Response of Clay Embankments to Base Excitation," thesis submitted to the University of California, Berkeley, California, in partial satisfaction of the requirements for the degree of Doctor of Philosophy, June.

Kovacs, W. D., Seed, H. B. and Chan, C. K. (1971). "Dynamic Moduli and Damping Ratios for a Soft Clay," Journal of the Soil Mechanics and Foundations Division, ASCE, Vol. 97, No. SM1, January, pp. 59-75.

Kratsch, Helmut (1983). Mining Subsidence Engineering. New York: Springer-Verlag.

Ladd, C. C. (1965). "The Influence of Stress System on the Behavior of Saturated Clays during Undrained Shear," Soil Mechanics Division, Department of Civil Engineering, Massachusetts Institute of Technology, Research Report R65-11, July.

Lade, P. V. (1972). "The Stress-Strain and Strength Characteristics of Cohesionless Soils," thesis submitted to the University of California, Berkeley in partial fulfillment of the requirements for the degree of Doctor of Philosophy.

Lade, P. V. and Cole, D. A., Jr. (1984). "Influence Zones in Alluvium Over Dip-Slip Faults," Journal of Geotechnical Engineering, ASCE, Vol. 110, No. 5, May, pp. 599-615.

Lade, P. V., Cole, D. A., Jr. and Cummings, D. (1984). "Multiple Failure Surfaces Over Dip-Slip Faults," Journal of Geotechnical Engineering, ASCE, Vol. 110, No. 5, May, pp. 616-627.

Lambe, T. W. and Whitman, R. V. (1969). Soil Mechanics. New York: John Wiley & Sons.

Lawson, A. C., et al. (1908). "The California Earthquake of April 18, 1906," Report of the State Earthquake Investigation Commission, Carnegie Institution of Washington, Vol. I, Washington, D.C.

Lee, A. J. (1966). "The effect of faulting on mining subsidence," The Mining Engineer, 125(71), pp. 735-745.

Lee, F. H., Lo, K. W. and Lee, S. L. (1988). "Tension Crack Development in Soils," Journal of Geotechnical Engineering, ASCE, Vol. 114, No. 8, August, pp. 915-929.

Lee, I. K. (1974). "Stability and Earth Pressures." In Soil Mechanics - New Horizons. Ed. I. K. Lee. New York: American Elsevier Publishing Company, Inc., 1974, pp. 206-236.

Lee, I. K. (1975). "Application of Plasticity Theory to the Prediction of Earth Pressures," Proceedings of the General Session of the Symposium on Soil Mechanics: Recent Developments, The University of New South Wales, Australia, July 14-18, pp. 27-81.

Lee, K. L. and Shen, C. K. (1969). "Horizontal Movements Related to Subsidence," Journal of the Soil Mechanics and Foundations Division, ASCE, Vol. 94, No. SM1, January, pp. 139-166.

Leonards, G. A. (1987). Dam Failures. Proceedings of the International Workshop on Dam Failures, Purdue University, West Lafayette, Indiana, August 6-8, 1985, New York: Elsevier, pp. 7-172.

Leps, T. M. (1987). "Failure of Baldwin Hills Reservoir, 1963 - Interpretation of Step-By-Step Failure Sequence; Invited Discusser's Responses to Prepared Questions; Comments on Paper Entitled: Baldwin Hills Reservoir Failure; and Ground Subsidence Analysis Prior to the Baldwin Hills Reservoir Failure," Engineering Geology, Vol. 24, pp. 83-102 and 143-154.

Leps, T. M. (1989). "The Influence of Possible Fault Offsets on Dam Design," Water Power & Dam Construction, April, pp. 36-43.

Louderback, G. D. (1937). "Characteristics of Active Faults in the Central Coast Ranges of California, with Application to the Safety of Dams," Bulletin of the Seismological Society of America, Vol. 27, No. 1, January, pp. 1-27.

Louderback, G. D. (1950). "Faults and Engineering Geology," The Geological Society of America, Engineering Geology (Berkeley) Volume, November, pp. 125-150.

McCalpin, J. (1987). "Recommended Setbacks from Active Normal Faults," Proceedings of the 23rd Symposium on Engineering Geology & Soils Engineering, Logan, Utah, April 6-8, pp. 35-56.

Malde, H. E. (1987). "Quaternary Faulting Near Arco and Howe, Idaho," Bulletin of the Seismological Society of America, Vol. 77, No. 3, June, pp. 847-867.

Manning, J. C. (1973). "Field Trip to Areas of Active Faulting and Shallow Subsidence in the Southern San Joaquin Valley," Spring Meeting, Far West Section, National Association of Geology Teachers, April 21-22.

Meyers, W. B. and Hamilton, W. (1964). "Deformation Accompanying the Hebgen Lake Earthquake of August 17, 1959," U.S. Geological Survey Professional Paper 435-I, pp. 55-138.

Meyerhof, G. G. (1973). "Uplift Resistance of Inclined Anchors and Piles," Proceedings of the Eighth International Conference on Soil Mechanics and Foundation Engineering, Moscow, Vol. 2, pp. 167-172.

Meyerhof, G. G. and Adams, J. I. (1968). "The Ultimate Uplift Capacity of Foundations," Canadian Geotechnical Journal, Vol. V, No. 4, November, pp. 225-244.

Mitchell, J. K. (1976). Fundamentals of Soil Behavior. New York: John Wiley & Sons.

Nasu, N. (1931). "Comparative Studies of Earthquake Motions Above-Ground and in a Tunnel (Part I)," Tokyo University Earthquake Research Institute, Vol. 9, pp. 454-472.

National Academy of Science (1980). "Earthquake Research for the Safer Siting of Critical Facilities," National Research Council Publication, 3082-x, Washington, D.C.

Niccum, M. R., Cluff, L. S., Chamorro, F., and Wyllie, L. (1976). "Banco Central de Nicaragua: A case history of a high-rise building that survived surface fault rupture," in Humphrey, C. B., ed., Engineering Geology and Soils Engineering Symposium, no. 14, Boise, Idaho, Idaho Transportation Department, Division of Highways, pp. 133-144.

Oakeshott, G. B. (1973). "Patterns of Ground Ruptures in Fault Zones Coincident with Earthquakes: Some Case Histories," the Association of Engineering Geologists, Reprinted from Geology, Seismicity, and Environmental Impact, Special Publication, October, pp. 287-312.

Otter, J. R. H., Cassell, A. C. and Hobbs, R. E. (1966). "Dynamic Relaxation," Proc. Instn. Civil Engineers 35, pp. 633-656.

Ozawa, Y. and Duncan, J. M. (1976). "Elasto-Plastic Finite Element Analyses of Sand Deformations," Proceedings of the Second International Conference on Numerical Methods in Geomechanics, Blacksburg, Virginia, June 20-26, pp. 243-263.

Parker, T. J. and McDowell, A. N. (1955). "Model Studies of Salt-Dome Tectonics," Bulletin of the Geological Society of America, Vol. 39, No. 12, December, pp. 2384-2470.

Parry, R. H. G. (1972). Stress-Strain Behavior of Soils. Oxfordshire: G. T. Foulis & Co., Ltd.

Patton, T. L. (1983). "Stress Failure in an Isotropic Layer Overlying Reverse, Vertical, and Normal Faults [abstr.]," The Geological Society of America, South-Central Section, 17th Annual Meeting, Abstracts with Programs, Volume 15, No. 1, January, p. 39.

Patton, T. L. and Fletcher, R. C. (1983). "Simple Rheological Model for Rock with Multiple Fracture Sets; Application to the Deformation of a Fractured Surface Layer above a Deep Basement Fault [abstr.]," The Geological Society of America, 96th Annual Meeting, Abstracts with Programs, Volume 15, No. 6, September, p. 659.

Patton, T. L., Fletcher, R. C. and Logan, J. M. (1982). "Upward Propagation of Normal Faults through a Sedimentary Sequence [abstr.]," The Geological Society of America, 95th Annual Meeting, Abstracts with Programs, Volume 14, No. 7, August, p. 584.

Pender, M. J. (1989). Course notes, CE 298-4: Constitutive Modeling of Geotechnical Materials, University of California, Berkeley, California, Spring Semester.

Plafker, G. (1967). "Surface Faults on Montague Island Associated with the 1964 Alaska Earthquake," Geological Survey Professional Paper 543-G.

Potts, D. M., Dounias, G. T. and Vaughan, P. R. (1987). "Finite Element Analysis of the Direct Shear Box Test," Geotechnique, Vol. 37, No. 1, pp. 11-23.

Prucha, J. J., Graham, J. A. and Nickelsen, R. P. (1965). "Basement-Controlled Deformation in Wyoming Province of Rocky Mountains Foreland," Bulletin of the American Association of Petroleum Geologists, Vol. 49, No. 7, July, pp. 966-992.

Reddy, J. N., Stein, R. J. and Wickham, J. S. (1982). "Finite-Element Modelling of Folding and Faulting," International Journal for Numerical and Analytical Methods in Geomechanics, Vol. 6, pp. 425-440.

Reid, H. F. (1910). "The California Earthquake of April 18, 1906," Report of the State Earthquake Investigation Commission, Carnegie Institution of Washington, Vol. II, Washington, D.C.

Richter, C. F. (1958). Elementary Seismology. San Francisco: W. H. Freeman and Company.

Roscoe, K. H. (1968). "Soils and Model Tests," Journal of Strain Analysis, Vol. 3, No. 1, pp. 57-64.

Roscoe, K. H. (1970). "The Influence of Strains in Soil Mechanics," Geotechnique, Vol. 20, No. 2, pp. 129-170.

Roth, W. H., Kalsi, G., Papastamatiou, O. and Cundall, P. A. (1982). "Numerical Modelling of Fault Propagation in Soils," Proceedings of the Fourth International Conference on Numerical Methods in Geomechanics, Edmonton, Canada, May 31-June 4, pp. 487-502.

Roth, W. H., Scott, R. F. and Austin, I. (1981). "Centrifuge Modeling of Fault Propagation through Alluvial Soils," Geophysical Research Letters, Vol. 8, No. 6, May, pp. 561-564.

Roth, W. H., Sweet, J. and Goodman, R. E. (1982). "Numerical and Physical Modeling of Flexural Slip Phenomena and Potential for Fault Movement," Rock Mechanics, Suppl. 12, pp. 27-46.

Rousselier, G. (1979). "Numerical Treatment of Crack Growth Problems," Proceedings of a Seminar held at the Joint Research Commission of the European Communities, Ispra, Italy, April 2-6, pp. 165-189.

Rowe, R. K. and Davis, E. H. (1982a). "The Behaviour of Anchor Plates in Clay," Geotechnique, Vol. 32, No. 1, pp. 9-23.

Rowe, R. K. and Davis, E. H. (1982b). "The Behaviour of Anchor Plates in Sand," Geotechnique, Vol. 32, No. 1, pp. 25-41.

Sanford, A. R. (1959). "Analytical and Experimental Study of Simple Geologic Structures," Bulletin of the Geological Society of America, Vol. 70, January, pp. 19-52.

Schad, H. (1985). "Computing Costs for FEM Analysis of Foundation Engineering Problems and Possible Ways of Increasing Efficiency," International Journal for Numerical and Analytical Methods in Geomechanics, Vol. 9, pp. 261-275.

Schmertmann, J. H. and Osterberg, J. O. (1960). "An Experimental Study of the Development of Cohesion and Friction with Axial Strain in Saturated Cohesive Soils," Research Conference on Shear Strength of Cohesive Soils, Soil Mechanics and Foundations Division, ASCE, Boulder, Colorado, June, pp. 643-681.

Schussler, H. (1909). "The Water Supply of San Francisco," Journal of Electricity, Power and Gas, Vol. XXIII, No. 24, San Francisco, December 11.

Scott, R. F. (1987). "Failure," Geotechnique, Vol. 37, No. 4, pp. 423-466.

Scott, R. F. and Schoustra, J. J. (1974). "Nuclear Power Plant Siting on Deep Alluvium," Journal of the Geotechnical Engineering Division, ASCE, Vol. 100, No. GT4, April, pp. 449-459.

Seed, H. B. (1983). "The Role of Case Studies in the Development of Geotechnical Engineering Practice," Proceedings of the 7th Pan American Conference on Soil Mechanics and Foundation Engineering, Vancouver, British Columbia, June.

Seed, H. B. (1987). Course notes, CE 276: Earth Dam Engineering, University of California, Berkeley, California, Spring Semester.

Seed, H. B. and Clough, R. W. (1963). "Earthquake Resistance of Sloping Core Dams," Journal of the Soil Mechanics and Foundations Division, ASCE, Vol. 89, No. SM1, February, pp. 209-241.

Seed, H. B., Mitchell, J. K. and Chan, C. K. (1960). "The Strength of Compacted Cohesive Soils," Research Conference on Shear Strength of Cohesive Soils, Soil Mechanics and Foundations Division, ASCE, Boulder, Colorado, June, pp. 877-953.

Seed, R. B. and Duncan, J. M. (1984). "SSCOMP: A Finite Element Analysis Program for Evaluation of Soil-Structure Interaction and Compaction Effects," Department of Civil Engineering, University of California, Berkeley, California, Report No. UCB/GT/84-02, February.

Shadbolt, C. H. (1977). "Mining Subsidence-Historical Review and State of the Art." In Large Ground Movements and Structures. Ed. J. D. Geddes. New York: John Wiley & Sons, pp. 705-748.

Sherard, J. L. (1966). "A Study of the Influence of the Earthquake Hazard on the Design of Embankment Dams," report submitted to the California Department of Water Resources, July, 1966.

Sherard, J. L. (1967). "Earthquake Considerations in Earth Dam Design," Journal of the Soil Mechanics and Foundations Division, ASCE, Vol. 93, No. SM4, July, pp. 377-401.

Sherard, J. L. (1979). "Sinkholes in Dams of Coarse, Broadly Graded Soils," Thirtieth International Congress on Large Dams, New Delhi, pp. 25-35.

Sherard, J. L. (1986). "Hydraulic Fracturing in Embankment Dams," Journal of Geotechnical Engineering, ASCE, Vol. 112, No. 10, October.

Sherard, J. L., Cluff, L. S. and Allen, C. R. (1974). "Potentially Active Faults in Dam Foundations," Geotechnique, Vol. 24, pp. 367-427.

Sherard, J. L., Dunnigan, L. P., and Talbot, J. R. (1984a). "Basic Properties of Sand and Gravel Filters," Journal of Geotechnical Engineering, Vol. 110, No. 6, June, pp. 684-700.

Sherard, J. L., Dunnigan, L. P., and Talbot, J. R. (1984b). "Filters for Silts and Clays," Journal of Geotechnical Engineering, Vol. 110, No. 6, June, pp. 701-718.

Sherard, J. L., Woodward, R. J., Gizienski, S. F. and Clevenger, W. A. (1963). Earth and Earth Rock Dams. New York: John Wiley & Sons, Inc.

Slemmons, D. B. (1957). "Geological Effects of the Dixie Valley-Fairview Peak, Nevada, Earthquakes of December 16, 1954," Bulletin of the Seismological Society of America, Vol. 47, No. 4, pp. 353-375.

Sohn, J. S. (1987). "Crack Propagation in Earth Embankments Subjected to Fault Movement," thesis submitted to the University of California, Davis in partial fulfillment of the requirements for the degree of Doctor of Philosophy.

Spitzley, J. (1984). "Stress Analysis of Fracture Patterns Found in Quaternary Faults," Proceedings of the Twenty-First Annual Engineering Geology and Soils Engineering Symposium, Moscow, Idaho, April 5-6, pp. 45-57.

State of California, Department of Water Resources (1967). "Earthquake Damage to Hydraulic Structures in California," Bulletin No. 116-3, June.

State of California, Division of Safety of Dams (1988). Drawings and correspondence from the files of the Los Angeles Dam. Personal Communication.

Stein, R. S. and Barrientos, S. E. (1985). "The 1983 Borah Peak, Idaho, earthquake-Geodetic evidence for deep rupture on a planar fault," U.S. Geological Survey, Open-File Report 85-250, pp. 459-484.

Steinbrugge, K. V. and Cloud, W. K. (1962). "Epicentral Intensities and Damage in the Hebgen Lake, Montana, Earthquake of August 17, 1959," Bulletin of the Seismological Society of America, Vol. 52, No. 2, April, pp. 181-234.

Sture, S. and Ko, H. Y. (1978). "Strain-Softening of Brittle Geologic Materials," International Journal for Numerical and Analytical Methods in Geomechanics, Vol. 2, pp. 237-253.

Sultan, H. A. and Seed, H. B. (1967). "Stability of Sloping Core Earth Dams," Journal of the Soil Mechanics and Foundations Division, ASCE, Vol. 93, No. SM4, July, pp. 45-67.

Sutherland, H. B. (1988). "Uplift Resistance of Soils," Geotechnique, Vol. 38, No. 4, pp. 493-516.

Suyehiro, K. (1932). "Engineering Seismology - Notes on American Lectures," ASCE Proceedings, 58(4), pp. 1-43.

Swan, F. H., III, Schwartz, D. P. and Cluff, L. S. (1980). "Recurrence of Moderate to Large Magnitude Earthquakes Produced by Surface Faulting on the Wasatch Fault Zone, Utah," Bulletin of the Seismological Society of America, Vol. 70, No. 5, October, pp. 1431-1462.

Swiger, W. F. (1978). "Specialty Session on Design for Fault Displacement," ASCE Specialty Conference: Earthquake Engineering and Soil Dynamics, June 19-21.

Tagaya, K., Tanaka, A. and Aboshi, H. (1983). "Application of Finite Element Method to Pullout Resistance of Buried Anchor," Soils and Foundations, Japanese Society of Soil Mechanics and Foundation Engineering, Vol. 23, No. 3, September, pp. 91-104.

Taylor, C. L., Cline, K. M., Page, W. D. and Schwartz, D. P. (1985). "The Borah Peak, Idaho Earthquake of October 28, 1983 - Surface Faulting and Other Phenomena," Earthquake Spectra, Vol. 2, No. 1, pp. 23-49.

Taylor, C. L. and Cluff, L. S. (1977). "Fault Displacement and Ground Deformation Associated with Surface Faulting," ASCE Specialty Conference on Lifeline Earthquake Engineering, Los Angeles, pp. 338-353.

Taylor, C. L., Messinger, D. L. and Peshon, H. (1982). "Alameda County Fairmont Hospital - Juvenile Hall Complex," Conference on Earthquake Hazards in the San Francisco Bay Area, California State University, Hayward, California, March 24-27, pp. 61-77.

Taylor, R. L. (1977). "Computer Procedures for Finite Element Analysis." In The Finite Element Method by D. C. Zienkiewicz, 3rd Ed. London: McGraw-Hill Book Company (UK) Limited.

Taylor, R. L. (1987a). "PCFEAP -- A Personal Computer Finite Element Analysis Program," Department of Civil Engineering, University of California, Berkeley, California, March 22.

Taylor, R. L. (1987b). "Finite Element Tools for Computational Mechanics Instruction," IBM ACIS University Conference, Boston, Massachusetts, June 27-30.

Tchalenko, J. S. (1970). "Similarities Between Shear Zones of Different Magnitudes," Bulletin of the Geological Society of America, Vol. 81, June, pp. 1625-1640.

Terzaghi, K. (1936). "Stress Distribution in Dry and in Saturated Sand above a Yielding Trap-Door," Proceedings of the International Conference on Soil Mechanics and Foundation Engineering, Cambridge, Massachusetts, June 22-26, Vol. I, pp. 307-311.

Terzaghi, K. and Peck, R. B. (1967). Soil Mechanics in Engineering Practice. 2nd ed., New York: John Wiley & Sons.

Tibbetts, F. H. (1936). "Earthquake-Proof Earth Dams," Engineering News Record, V. 117, July 2, pp. 10-13.

Tocher, D. (1958). "Earthquake Energy and Ground Breakage," Bulletin of the Seismological Society of America, Vol. 48, April, pp. 147-153.

Vagneron, J., Lade, P. V. and Lee, K. L. (1976). "Evaluation of Three Stress-Strain Models for Soils," Proceedings of the Second International Conference on Numerical Methods in Geomechanics, Blacksburg, Virginia, June 20-26, pp. 1329-1351.

Vallejo, L. E. (1982). "Development of a Shear Zone Structure in Stiff Clays," Proceedings of the Fourth International Conference on Numerical Methods in Geomechanics, Edmonton, Canada, May 31 - June 4, Vol. I, pp. 255-274.

Valliappan, S. (1975). "Application of the Finite Element Method to Soil Deformation," Proceedings of the General Session of the Symposium on Soil Mechanics: Recent Developments, The University of New South Wales, Australia, July 14-18, pp. 113-142.

Vardoulakis, I. (1980). "Shear Band Inclination and Shear Modulus of Sand in Biaxial Tests," International Journal for Numerical and Analytical Methods in Geomechanics, Vol. 4, pp. 103-119.

Vardoulakis, I., Goldscheider, M. and Gudehus, G. (1978). "Formation of Shear Bands in Sand Bodies as a Bifurcation Problem," International Journal for Numerical and Analytical Methods in Geomechanics, Vol. 2, pp. 99-128.

Vardoulakis, I., Graf, B. and Gudehus, G. (1981). "Trap-Door Problem with Dry Sand: A Statical Approach Based upon Model Test Kinematics," International Journal for Numerical and Analytical Methods in Geomechanics, Vol. 5, pp. 57-78.

Vesic, A. S. (1971). "Breakout Resistance of Objects Embedded in Ocean Bottom," Journal of the Soil Mechanics and Foundations Division, ASCE, Vol. 97, No. SM9, September, pp. 1183-1205.

Vesic, A. S. and Clough, G. W. (1968). "Behavior of Granular Materials under High Stresses," Journal of Soil Mechanics and Foundation Division, ASCE, Vol. 94, No. SM3, Proc. Paper 5954, May, pp. 661-688.

Walters, J. V. and Thomas, J. N. (1982). "Shear Zone Development In Granular Materials," Proceedings of the Fourth International Conference on Numerical Methods in Geomechanics, Edmonton, Canada, May 31 - June 4, Vol. I, pp. 263-274.

Walton, G. and Cobb, A. E. (1984). "Mining Subsidence." In Ground Movements and their Effects on Structures. Ed. P. B. Attewell and R. K. Taylor. New York: Surrey University Press, pp. 216-242.

Wells, D., Coppersmith, K., Slemmons, D. B. and Zhang, X. (work in progress). "Relationships between the Maximum Surface Displacements and the Earthquake Magnitude," private communication.

Whitfield, L. M. (1984). "Ground Movements from Coal Extraction in the Vicinity of Dams and Storages in New South Wales, Australia." In Ground Movements and Structures. Ed. J. D. Geddes. New York: John Wiley & Sons.

Witkind, I. J. (1964). "Reactivated Faults North of Hebgen Lake," U.S. Geological Survey Professional Paper 435-6, pp. 37-50.

Witkind, I. J., Myers, W. B., Hadley, J. B., Hamilton, W. and Fraser, G. D. (1962). "Geologic Features of the Earthquake at Hebgen Lake, Montana, August 17, 1959," Bulletin of the Seismological Society of America, Vol. 52, No. 2, April, pp. 163-180.

Wong, K. S. (1978). "Elasto-Plastic Finite Element Analyses of Passive Earth Pressure Tests," thesis submitted to the University of California, Berkeley in partial fulfillment of the requirements for the degree of Doctor of Philosophy, June 16, 1978.

Wroth, C. P. (1984). "The Interpretation of In Situ Soil Tests," Geotechnique, Vol. 34, No. 4, pp. 449-489.

Yerkes, R. F. (1973). "Effects of San Fernando Earthquake as Related to Geology." In San Fernando, California, Earthquake of February 9, 1971. Ed. L. M. Murphy. Washington, D.C.: U.S. Department of Commerce.

Yerkes, R. F. (1974). "Geologic Environment of the Van Norman Reservoir Area," U.S. Geological Survey Circular 691-A, B.

Youd, T. L., Yerkes, R. F. and Clark, M. M. (1978). "San Fernando Faulting Damage and Its Effect on Land Use," Proceedings of the ASCE Geotechnical Engineering Division Specialty Conference on Earthquake Engineering and Soil Dynamics, Vol. II, Pasadena, California, June 19-21, pp. 1111-1125.

Zienkiewicz, O. C. (1976). "Plasticity and Some of Its Corollaries in Soil Mechanics. Collapse and Continuing Deformation under Load Repetition," Proceedings of the Second International Conference on Numerical Methods in Geomechanics, Blacksburg, Virginia, June 20-26, pp. 1275-1303.

Zienkiewicz, O. C. (1977). The Finite Element Method. 3rd ed. London: McGraw-Hill Book Company (UK) Limited.

EARTHQUAKE ENGINEERING RESEARCH CENTER REPORT SERIES

EERC reports are available from the National Information Service for Earthquake Engineering(NISEE) and from the National Technical Information Service(NTIS). Numbers in parentheses are Accession Numbers assigned by the National Technical Information Service; these are followed by a price code. Contact NTIS, 5285 Port Royal Road, Springfield Virginia, 22161 for more information. Reports without Accession Numbers were not available from NTIS at the time of printing. For a current complete list of EERC reports (from EERC 67-1) and availablity information, please contact University of California, EERC, NISEE, 1301 South 46th Street, Richmond, California 94804.

UCB/EERC-80/01 "Earthquake Response of Concrete Gravity Dams Including Hydrodynamic and Foundation Interaction Effects," by Chopra, A.K., Chakrabarti, P. and Gupta, S., January 1980, (AD-A087297)A10.

UCB/EERC-80/02 "Rocking Response of Rigid Blocks to Earthquakes," by Yim, C.S., Chopra, A.K. and Penzien, J., January 1980, (PB80 166 002)A04.

UCB/EERC-80/03 "Optimum Inelastic Design of Seismic-Resistant Reinforced Concrete Frame Structures," by Zagajeski, S.W. and Bertero, V.V., January 1980, (PB80 164 635)A06.

UCB/EERC-80/04 "Effects of Amount and Arrangement of Wall-Panel Reinforcement on Hysteretic Behavior of Reinforced Concrete Walls," by Iliya, R. and Bertero, V.V., February 1980, (PB81 122 525)A09.

UCB/EERC-80/05 "Shaking Table Research on Concrete Dam Models," by Niwa, A. and Clough, R.W., September 1980, (PB81 122 368)A06.

UCB/EERC-80/06 "The Design of Steel Energy-Absorbing Restrainers and their Incorporation into Nuclear Power Plants for Enhanced Safety (Vol 1a): Piping with Energy Absorbing Restrainers: Parameter Study on Small Systems," by Powell, G.H., Oughourlian, C. and Simons, J., June 1980.

UCB/EERC-80/07 "Inelastic Torsional Response of Structures Subjected to Earthquake Ground Motions," by Yamazaki, Y., April 1980, (PB81 122 327)A08.

UCB/EERC-80/08 "Study of X-Braced Steel Frame Structures under Earthquake Simulation," by Ghanaat, Y., April 1980, (PB81 122 335)A11.

UCB/EERC-80/09 "Hybrid Modelling of Soil-Structure Interaction," by Gupta, S., Lin, T.W. and Penzien, J., May 1980, (PB81 122 319)A07.

UCB/EERC-80/10 "General Applicability of a Nonlinear Model of a One Story Steel Frame," by Sveinsson, B.I. and McNiven, H.D., May 1980, (PB81 124 877)A06.

UCB/EERC-80/11 "A Green-Function Method for Wave Interaction with a Submerged Body," by Kioka, W., April 1980, (PB81 122 269)A07.

UCB/EERC-80/12 "Hydrodynamic Pressure and Added Mass for Axisymmetric Bodies.," by Nilrat, F., May 1980, (PB81 122 343)A08.

UCB/EERC-80/13 "Treatment of Non-Linear Drag Forces Acting on Offshore Platforms," by Dao, B.V. and Penzien, J., May 1980, (PB81 153 413)A07.

UCB/EERC-80/14 "2D Plane/Axisymmetric Solid Element (Type 3-Elastic or Elastic-Perfectly Plastic)for the ANSR-II Program," by Mondkar, D.P. and Powell, G.H., July 1980, (PB81 122 350)A03.

UCB/EERC-80/15 "A Response Spectrum Method for Random Vibrations," by Der Kiureghian, A., June 1981, (PB81 122 301)A03.

UCB/EERC-80/16 "Cyclic Inelastic Buckling of Tubular Steel Braces," by Zayas, V.A., Popov, E.P. and Mahin, S.A., June 1981, (PB81 124 885)A10.

UCB/EERC-80/17 "Dynamic Response of Simple Arch Dams Including Hydrodynamic Interaction," by Porter, C.S. and Chopra, A.K., July 1981, (PB81 124 000)A13.

UCB/EERC-80/18 "Experimental Testing of a Friction Damped Aseismic Base Isolation System with Fail-Safe Characteristics," by Kelly, J.M., Beucke, K.E. and Skinner, M.S., July 1980, (PB81 148 595)A04.

UCB/EERC-80/19 "The Design of Steel Energy-Absorbing Restrainers and their Incorporation into Nuclear Power Plants for Enhanced Safety (Vol.1B): Stochastic Seismic Analyses of Nuclear Power Plant Structures and Piping Systems Subjected to Multiple Supported Excitations," by Lee, M.C. and Penzien, J., June 1980, (PB82 201 872)A08.

UCB/EERC-80/20 "The Design of Steel Energy-Absorbing Restrainers and their Incorporation into Nuclear Power Plants for Enhanced Safety (Vol 1C): Numerical Method for Dynamic Substructure Analysis," by Dickens, J.M. and Wilson, E.L., June 1980.

UCB/EERC-80/21 "The Design of Steel Energy-Absorbing Restrainers and their Incorporation into Nuclear Power Plants for Enhanced Safety (Vol 2): Development and Testing of Restraints for Nuclear Piping Systems," by Kelly, J.M. and Skinner, M.S., June 1980.

UCB/EERC-80/22 "3D Solid Element (Type 4-Elastic or Elastic-Perfectly-Plastic) for the ANSR-II Program," by Mondkar, D.P. and Powell, G.H., July 1980, (PB81 123 242)A03.

UCB/EERC-80/23 "Gap-Friction Element (Type 5) for the Ansr-II Program," by Mondkar, D.P. and Powell, G.H., July 1980, (PB81 122 285)A03.

UCB/EERC-80/24 "U-Bar Restraint Element (Type 11) for the ANSR-II Program," by Oughourlian, C. and Powell, G.H., July 1980, (PB81 122 293)A03.

UCB/EERC-80/25 "Testing of a Natural Rubber Base Isolation System by an Explosively Simulated Earthquake," by Kelly, J.M., August 1980, (PB81 201 360)A04.

UCB/EERC-80/26 "Input Identification from Structural Vibrational Response," by Hu, Y., August 1980, (PB81 152 308)A05.

UCB/EERC-80/27 "Cyclic Inelastic Behavior of Steel Offshore Structures," by Zayas, V.A., Mahin, S.A. and Popov, E.P., August 1980, (PB81 196 180)A15.

UCB/EERC-80/28 "Shaking Table Testing of a Reinforced Concrete Frame with Biaxial Response," by Oliva, M.G., October 1980, (PB81 154 304)A10.

UCB/EERC-80/29 "Dynamic Properties of a Twelve-Story Prefabricated Panel Building," by Bouwkamp, J.G., Kollegger, J.P. and Stephen, R.M., October 1980, (PB82 138 777)A07.

UCB/EERC-80/30 "Dynamic Properties of an Eight-Story Prefabricated Panel Building," by Bouwkamp, J.G., Kollegger, J.P. and Stephen, R.M., October 1980, (PB81 200 313)A05.

UCB/EERC-80/31 "Predictive Dynamic Response of Panel Type Structures under Earthquakes," by Kollegger, J.P. and Bouwkamp, J.G., October 1980, (PB81 152 316)A04.

UCB/EERC-80/32 "The Design of Steel Energy-Absorbing Restrainers and their Incorporation into Nuclear Power Plants for Enhanced Safety (Vol 3): Testing of Commercial Steels in Low-Cycle Torsional Fatigue," by Spanner, P., Parker, E.R., Jongewaard, E. and Dory, M., 1980.

UCB/EERC-80/33 "The Design of Steel Energy-Absorbing Restrainers and their Incorporation into Nuclear Power Plants for Enhanced Safety (Vol 4): Shaking Table Tests of Piping Systems with Energy-Absorbing Restrainers," by Stiemer, S.F. and Godden, W.G., September 1980, (PB82 201 880)A05.

UCB/EERC-80/34 "The Design of Steel Energy-Absorbing Restrainers and their Incorporation into Nuclear Power Plants for Enhanced Safety (Vol 5): Summary Report," by Spencer, P., 1980.

UCB/EERC-80/35 "Experimental Testing of an Energy-Absorbing Base Isolation System," by Kelly, J.M., Skinner, M.S. and Beucke, K.E., October 1980, (PB81 154 072)A04.

UCB/EERC-80/36 "Simulating and Analyzing Artificial Non-Stationary Earth Ground Motions," by Nau, R.F., Oliver, R.M. and Pister, K.S., October 1980, (PB81 153 397)A04.

UCB/EERC-80/37 "Earthquake Engineering at Berkeley - 1980," by , September 1980, (PB81 205 674)A09.

UCB/EERC-80/38 "Inelastic Seismic Analysis of Large Panel Buildings," by Schricker, V. and Powell, G.H., September 1980, (PB81 154 338)A13.

UCB/EERC-80/39 "Dynamic Response of Embankment, Concrete-Gavity and Arch Dams Including Hydrodynamic Interation," by Hall, J.F. and Chopra, A.K., October 1980, (PB81 152 324)A11.

UCB/EERC-80/40 "Inelastic Buckling of Steel Struts under Cyclic Load Reversal.," by Black, R.G., Wenger, W.A. and Popov, E.P., October 1980, (PB81 154 312)A08.

UCB/EERC-80/41 "Influence of Site Characteristics on Buildings Damage during the October 3,1974 Lima Earthquake," by Repetto, P., Arango, I. and Seed, H.B., September 1980, (PB81 161 739)A05.

UCB/EERC-80/42 "Evaluation of a Shaking Table Test Program on Response Behavior of a Two Story Reinforced Concrete Frame," by Blondet, J.M., Clough, R.W. and Mahin, S.A., December 1980, (PB82 196 544)A11.

UCB/EERC-80/43 "Modelling of Soil-Structure Interaction by Finite and Infinite Elements," by Medina, F., December 1980, (PB81 229 270)A04.

UCB/EERC-81/01 "Control of Seismic Response of Piping Systems and Other Structures by Base Isolation," by Kelly, J.M., January 1981, (PB81 200 735)A05.

UCB/EERC-81/02 "OPTNSR- An Interactive Software System for Optimal Design of Statically and Dynamically Loaded Structures with Nonlinear Response," by Bhatti, M.A., Ciampi, V. and Pister, K.S., January 1981, (PB81 218 851)A09.

UCB/EERC-81/03 "Analysis of Local Variations in Free Field Seismic Ground Motions," by Chen, J.-C., Lysmer, J. and Seed, H.B., January 1981, (AD-A099508)A13.

UCB/EERC-81/04 "Inelastic Structural Modeling of Braced Offshore Platforms for Seismic Loading," by Zayas, V.A., Shing, P.-S.B., Mahin, S.A. and Popov, E.P., January 1981, (PB82 138 777)A07.

UCB/EERC-81/05 "Dynamic Response of Light Equipment in Structures," by Der Kiureghian, A., Sackman, J.L. and Nour-Omid, B., April 1981, (PB81 218 497)A04.

UCB/EERC-81/06 "Preliminary Experimental Investigation of a Broad Base Liquid Storage Tank," by Bouwkamp, J.G., Kollegger, J.P. and Stephen, R.M., May 1981, (PB82 140 385)A03.

UCB/EERC-81/07 "The Seismic Resistant Design of Reinforced Concrete Coupled Structural Walls," by Aktan, A.E. and Bertero, V.V., June 1981, (PB82 113 358)A11.

UCB/EERC-81/08 "Unassigned," by Unassigned, 1981.

UCB/EERC-81/09 "Experimental Behavior of a Spatial Piping System with Steel Energy Absorbers Subjected to a Simulated Differential Seismic Input," by Stiemer, S.F., Godden, W.G. and Kelly, J.M., July 1981, (PB82 201 898)A04.

UCB/EERC-81/10 "Evaluation of Seismic Design Provisions for Masonry in the United States," by Sveinsson, B.I., Mayes, R.L. and McNiven, H.D., August 1981, (PB82 166 075)A08.

UCB/EERC-81/11 "Two-Dimensional Hybrid Modelling of Soil-Structure Interaction," by Tzong, T.-J., Gupta, S. and Penzien, J., August 1981, (PB82 142 118)A04.

UCB/EERC-81/12 "Studies on Effects of Infills in Seismic Resistant R/C Construction," by Brokken, S. and Bertero, V.V., October 1981, (PB82 166 190)A09.

UCB/EERC-81/13 "Linear Models to Predict the Nonlinear Seismic Behavior of a One-Story Steel Frame," by Valdimarsson, H., Shah, A.H. and McNiven, H.D., September 1981, (PB82 138 793)A07.

UCB/EERC-81/14 "TLUSH: A Computer Program for the Three-Dimensional Dynamic Analysis of Earth Dams," by Kagawa, T., Mejia, L.H., Seed, H.B. and Lysmer, J., September 1981, (PB82 139 940)A06.

UCB/EERC-81/15 "Three Dimensional Dynamic Response Analysis of Earth Dams," by Mejia, L.H. and Seed, H.B., September 1981, (PB82 137 274)A12.

UCB/EERC-81/16 "Experimental Study of Lead and Elastomeric Dampers for Base Isolation Systems," by Kelly, J.M. and Hodder, S.B., October 1981, (PB82 166 182)A05.

UCB/EERC-81/17 "The Influence of Base Isolation on the Seismic Response of Light Secondary Equipment," by Kelly, J.M., April 1981, (PB82 255 266)A04.

UCB/EERC-81/18 "Studies on Evaluation of Shaking Table Response Analysis Procedures," by Blondet, J. M., November 1981, (PB82 197 278)A10.

UCB/EERC-81/19 "DELIGHT.STRUCT: A Computer-Aided Design Environment for Structural Engineering," by Balling, R.J., Pister, K.S. and Polak, E., December 1981, (PB82 218 496)A07.

UCB/EERC-81/20 "Optimal Design of Seismic-Resistant Planar Steel Frames," by Balling, R.J., Ciampi, V. and Pister, K.S., December 1981, (PB82 220 179)A07.

UCB/EERC-82/01 "Dynamic Behavior of Ground for Seismic Analysis of Lifeline Systems," by Sato, T. and Der Kiureghian, A., January 1982, (PB82 218 926)A05.

UCB/EERC-82/02 "Shaking Table Tests of a Tubular Steel Frame Model," by Ghanaat, Y. and Clough, R.W., January 1982, (PB82 220 161)A07.

UCB/EERC-82/03 "Behavior of a Piping System under Seismic Excitation: Experimental Investigations of a Spatial Piping System supported by Mechanical Shock Arrestors," by Schneider, S., Lee, H.-M. and Godden, W. G., May 1982, (PB83 172 544)A09.

UCB/EERC-82/04 "New Approaches for the Dynamic Analysis of Large Structural Systems," by Wilson, E.L., June 1982, (PB83 148 080)A05.

UCB/EERC-82/05 "Model Study of Effects of Damage on the Vibration Properties of Steel Offshore Platforms," by Shahrivar, F. and Bouwkamp, J.G., June 1982, (PB83 148 742)A10.

UCB/EERC-82/06 "States of the Art and Pratice in the Optimum Seismic Design and Analytical Response Prediction of R/C Frame Wall Structures," by Aktan, A.E. and Bertero, V.V., July 1982, (PB83 147 736)A05.

UCB/EERC-82/07 "Further Study of the Earthquake Response of a Broad Cylindrical Liquid-Storage Tank Model," by Manos, G.C. and Clough, R.W., July 1982, (PB83 147 744)A11.

UCB/EERC-82/08 "An Evaluation of the Design and Analytical Seismic Response of a Seven Story Reinforced Concrete Frame," by Charney, F.A. and Bertero, V.V., July 1982, (PB83 157 628)A09.

UCB/EERC-82/09 "Fluid-Structure Interactions: Added Mass Computations for Incompressible Fluid," by Kuo, J.S.-H., August 1982, (PB83 156 281)A07.

UCB/EERC-82/10 "Joint-Opening Nonlinear Mechanism: Interface Smeared Crack Model," by Kuo, J.S.-H., August 1982, (PB83 149 195)A05.

UCB/EERC-82/11 "Dynamic Response Analysis of Techi Dam," by Clough, R.W., Stephen, R.M. and Kuo, J.S.-H., August 1982, (PB83 147 496)A06.

UCB/EERC-82/12 "Prediction of the Seismic Response of R/C Frame-Coupled Wall Structures," by Aktan, A.E., Bertero, V.V. and Piazzo, M., August 1982, (PB83 149 203)A09.

UCB/EERC-82/13 "Preliminary Report on the Smart 1 Strong Motion Array in Taiwan," by Bolt, B.A., Loh, C.H., Penzien, J. and Tsai, Y.B., August 1982, (PB83 159 400)A10.

UCB/EERC-82/14 "Shaking-Table Studies of an Eccentrically X-Braced Steel Structure," by Yang, M.S., September 1982, (PB83 260 778)A12.

UCB/EERC-82/15 "The Performance of Stairways in Earthquakes," by Roha, C., Axley, J.W. and Bertero, V.V., September 1982, (PB83 157 693)A07.

UCB/EERC-82/16 "The Behavior of Submerged Multiple Bodies in Earthquakes," by Liao, W.-G., September 1982, (PB83 158 709)A07.

UCB/EERC-82/17 "Effects of Concrete Types and Loading Conditions on Local Bond-Slip Relationships," by Cowell, A.D., Popov, E.P. and Bertero, V.V., September 1982, (PB83 153 577)A04.

UCB/EERC-82/18 "Mechanical Behavior of Shear Wall Vertical Boundary Members: An Experimental Investigation," by Wagner, M.T. and Bertero, V.V., October 1982, (PB83 159 764)A05.

UCB/EERC-82/19 "Experimental Studies of Multi-support Seismic Loading on Piping Systems," by Kelly, J.M. and Cowell, A.D., November 1982.

UCB/EERC-82/20 "Generalized Plastic Hinge Concepts for 3D Beam-Column Elements," by Chen, P. F.-S. and Powell, G.H., November 1982, (PB83 247 981)A13.

UCB/EERC-82/21 "ANSR-II: General Computer Program for Nonlinear Structural Analysis," by Oughourlian, C.V. and Powell, G.H., November 1982, (PB83 251 330)A12.

UCB/EERC-82/22 "Solution Strategies for Statically Loaded Nonlinear Structures," by Simons, J.W. and Powell, G.H., November 1982, (PB83 197 970)A06.

UCB/EERC-82/23 "Analytical Model of Deformed Bar Anchorages under Generalized Excitations," by Ciampi, V., Eligehausen, R., Bertero, V.V. and Popov, E.P., November 1982, (PB83 169 532)A06.

UCB/EERC-82/24 "A Mathematical Model for the Response of Masonry Walls to Dynamic Excitations," by Sucuoglu, H., Mengi, Y. and McNiven, H.D., November 1982, (PB83 169 011)A07.

UCB/EERC-82/25 "Earthquake Response Considerations of Broad Liquid Storage Tanks," by Cambra, F.J., November 1982, (PB83 251 215)A09.

UCB/EERC-82/26 "Computational Models for Cyclic Plasticity, Rate Dependence and Creep," by Mosaddad, B. and Powell, G.H., November 1982, (PB83 245 829)A08.

UCB/EERC-82/27 "Inelastic Analysis of Piping and Tubular Structures," by Mahasuverachai, M. and Powell, G.H., November 1982, (PB83 249 987)A07.

UCB/EERC-83/01 "The Economic Feasibility of Seismic Rehabilitation of Buildings by Base Isolation," by Kelly, J.M., January 1983, (PB83 197 988)A05.

UCB/EERC-83/02 "Seismic Moment Connections for Moment-Resisting Steel Frames.," by Popov, E.P., January 1983, (PB83 195 412)A04.

UCB/EERC-83/03 "Design of Links and Beam-to-Column Connections for Eccentrically Braced Steel Frames," by Popov, E.P. and Malley, J.O., January 1983, (PB83 194 811)A04.

UCB/EERC-83/04 "Numerical Techniques for the Evaluation of Soil-Structure Interaction Effects in the Time Domain," by Bayo, E. and Wilson, E.L., February 1983, (PB83 245 605)A09.

UCB/EERC-83/05 "A Transducer for Measuring the Internal Forces in the Columns of a Frame-Wall Reinforced Concrete Structure," by Sause, R. and Bertero, V.V., May 1983, (PB84 119 494)A06.

UCB/EERC-83/06 "Dynamic Interactions Between Floating Ice and Offshore Structures," by Croteau, P., May 1983, (PB84 119 486)A16.

UCB/EERC-83/07 "Dynamic Analysis of Multiply Tuned and Arbitrarily Supported Secondary Systems," by Igusa, T. and Der Kiureghian, A., July 1983, (PB84 118 272)A11.

UCB/EERC-83/08 "A Laboratory Study of Submerged Multi-body Systems in Earthquakes," by Ansari, G.R., June 1983, (PB83 261 842)A17.

UCB/EERC-83/09 "Effects of Transient Foundation Uplift on Earthquake Response of Structures," by Yim, C.-S. and Chopra, A.K., June 1983, (PB83 261 396)A07.

UCB/EERC-83/10 "Optimal Design of Friction-Braced Frames under Seismic Loading," by Austin, M.A. and Pister, K.S., June 1983, (PB84 119 288)A06.

UCB/EERC-83/11 "Shaking Table Study of Single-Story Masonry Houses: Dynamic Performance under Three Component Seismic Input and Recommendations," by Manos, G.C., Clough, R.W. and Mayes, R.L., July 1983, (UCB/EERC-83/11)A08.

UCB/EERC-83/12 "Experimental Error Propagation in Pseudodynamic Testing," by Shiing, P.B. and Mahin, S.A., June 1983, (PB84 119 270)A09.

UCB/EERC-83/13 "Experimental and Analytical Predictions of the Mechanical Characteristics of a 1/5-scale Model of a 7-story R/C Frame-Wall Building Structure," by Aktan, A.E., Bertero, V.V., Chowdhury, A.A. and Nagashima, T., June 1983, (PB84 119 213)A07.

UCB/EERC-83/14 "Shaking Table Tests of Large-Panel Precast Concrete Building System Assemblages," by Oliva, M.G. and Clough, R.W., June 1983, (PB86 110 210/AS)A11.

UCB/EERC-83/15 "Seismic Behavior of Active Beam Links in Eccentrically Braced Frames," by Hjelmstad, K.D. and Popov, E.P., July 1983, (PB84 119 676)A09.

UCB/EERC-83/16 "System Identification of Structures with Joint Rotation," by Dimsdale, J.S., July 1983, (PB84 192 210)A06.

UCB/EERC-83/17 "Construction of Inelastic Response Spectra for Single-Degree-of-Freedom Systems," by Mahin, S. and Lin, J., June 1983, (PB84 208 834)A05.

UCB/EERC-83/18 "Interactive Computer Analysis Methods for Predicting the Inelastic Cyclic Behaviour of Structural Sections," by Kaba, S. and Mahin, S., July 1983, (PB84 192 012)A06.

UCB/EERC-83/19 "Effects of Bond Deterioration on Hysteretic Behavior of Reinforced Concrete Joints," by Filippou, F.C., Popov, E.P. and Bertero, V.V., August 1983, (PB84 192 020)A10.

UCB/EERC-83/20 "Correlation of Analytical and Experimental Responses of Large-Panel Precast Building Systems," by Oliva, M.G., Clough, R.W., Velkov, M. and Gavrilovic, P., May 1988.

UCB/EERC-83/21 "Mechanical Characteristics of Materials Used in a 1/5 Scale Model of a 7-Story Reinforced Concrete Test Structure," by Bertero, V.V., Aktan, A.E., Harris, H.G. and Chowdhury, A.A., October 1983, (PB84 193 697)A05.

UCB/EERC-83/22 "Hybrid Modelling of Soil-Structure Interaction in Layered Media," by Tzong, T.-J. and Penzien, J., October 1983, (PB84 192 178)A08.

UCB/EERC-83/23 "Local Bond Stress-Slip Relationships of Deformed Bars under Generalized Excitations," by Eligehausen, R., Popov, E.P. and Bertero, V.V., October 1983, (PB84 192 848)A09.

UCB/EERC-83/24 "Design Considerations for Shear Links in Eccentrically Braced Frames," by Malley, J.O. and Popov, E.P., November 1983, (PB84 192 186)A07.

UCB/EERC-84/01 "Pseudodynamic Test Method for Seismic Performance Evaluation: Theory and Implementation," by Shing, P.-S.B. and Mahin, S.A., January 1984, (PB84 190 644)A08.

UCB/EERC-84/02 "Dynamic Response Behavior of Kiang Hong Dian Dam," by Clough, R.W., Chang, K.-T., Chen, H.-Q. and Stephen, R.M., April 1984, (PB84 209 402)A08.

UCB/EERC-84/03 "Refined Modelling of Reinforced Concrete Columns for Seismic Analysis," by Kaba, S.A. and Mahin, S.A., April 1984, (PB84 234 384)A06.

UCB/EERC-84/04 "A New Floor Response Spectrum Method for Seismic Analysis of Multiply Supported Secondary Systems," by Asfura, A. and Der Kiureghian, A., June 1984, (PB84 239 417)A06.

UCB/EERC-84/05 "Earthquake Simulation Tests and Associated Studies of a 1/5th-scale Model of a 7-Story R/C Frame-Wall Test Structure," by Bertero, V.V., Aktan, A.E., Charney, F.A. and Sause, R., June 1984, (PB84 239 409)A09.

UCB/EERC-84/06 "R/C Structural Walls: Seismic Design for Shear," by Aktan, A.E. and Bertero, V.V., 1984.

UCB/EERC-84/07 "Behavior of Interior and Exterior Flat-Plate Connections subjected to Inelastic Load Reversals," by Zee, H.L. and Moehle, J.P., August 1984, (PB86 117 629/AS)A07.

UCB/EERC-84/08 "Experimental Study of the Seismic Behavior of a Two-Story Flat-Plate Structure," by Moehle, J.P. and Diebold, J.W., August 1984, (PB86 122 553/AS)A12.

UCB/EERC-84/09 "Phenomenological Modeling of Steel Braces under Cyclic Loading," by Ikeda, K., Mahin, S.A. and Dermitzakis, S.N., May 1984, (PB86 132 198/AS)A08.

UCB/EERC-84/10 "Earthquake Analysis and Response of Concrete Gravity Dams," by Fenves, G. and Chopra, A.K., August 1984, (PB85 193 902/AS)A11.

UCB/EERC-84/11 "EAGD-84: A Computer Program for Earthquake Analysis of Concrete Gravity Dams," by Fenves, G. and Chopra, A.K., August 1984, (PB85 193 613/AS)A05.

UCB/EERC-84/12 "A Refined Physical Theory Model for Predicting the Seismic Behavior of Braced Steel Frames," by Ikeda, K. and Mahin, S.A., July 1984, (PB85 191 450/AS)A09.

UCB/EERC-84/13 "Earthquake Engineering Research at Berkeley - 1984," by , August 1984, (PB85 197 341/AS)A10.

UCB/EERC-84/14 "Moduli and Damping Factors for Dynamic Analyses of Cohesionless Soils," by Seed, H.B., Wong, R.T., Idriss, I.M. and Tokimatsu, K., September 1984, (PB85 191 468/AS)A04.

UCB/EERC-84/15 "The Influence of SPT Procedures in Soil Liquefaction Resistance Evaluations," by Seed, H.B., Tokimatsu, K., Harder, L.F. and Chung, R.M., October 1984. (PB85 191 732/AS)A04.

UCB/EERC-84/16 "Simplified Procedures for the Evaluation of Settlements in Sands Due to Earthquake Shaking," by Tokimatsu, K. and Seed, H.B., October 1984, (PB85 197 887/AS)A03.

UCB/EERC-84/17 "Evaluation of Energy Absorption Characteristics of Highway Bridges Under Seismic Conditions - Volume I and Volume II (Appendices)," by Imbsen, R.A. and Penzien, J., September 1986.

UCB/EERC-84/18 "Structure-Foundation Interactions under Dynamic Loads," by Liu, W.D. and Penzien, J., November 1984, (PB87 124 889/AS)A11.

UCB/EERC-84/19 "Seismic Modelling of Deep Foundations," by Chen, C.-H. and Penzien, J., November 1984, (PB87 124 798/AS)A07.

UCB/EERC-84/20 "Dynamic Response Behavior of Quan Shui Dam," by Clough, R.W., Chang, K.-T., Chen, H.-Q., Stephen, R.M., Ghanaat, Y. and Qi, J.-H., November 1984, (PB86 115177/AS)A07.

UCB/EERC-85/01 "Simplified Methods of Analysis for Earthquake Resistant Design of Buildings," by Cruz, E.F. and Chopra, A.K., February 1985, (PB86 112299/AS)A12.

UCB/EERC-85/02 "Estimation of Seismic Wave Coherency and Rupture Velocity using the SMART 1 Strong-Motion Array Recordings," by Abrahamson, N.A., March 1985, (PB86 214 343)A07.

UCB/EERC-85/03 "Dynamic Properties of a Thirty Story Condominium Tower Building," by Stephen, R.M., Wilson, E.L. and Stander, N., April 1985, (PB86 118965/AS)A06.

UCB/EERC-85/04 "Development of Substructuring Techniques for On-Line Computer Controlled Seismic Performance Testing," by Dermitzakis, S. and Mahin, S., February 1985, (PB86 132941/AS)A08.

UCB/EERC-85/05 "A Simple Model for Reinforcing Bar Anchorages under Cyclic Excitations," by Filippou, F.C., March 1985, (PB86 112 919/AS)A05.

UCB/EERC-85/06 "Racking Behavior of Wood-framed Gypsum Panels under Dynamic Load," by Oliva, M.G., June 1985.

UCB/EERC-85/07 "Earthquake Analysis and Response of Concrete Arch Dams," by Fok, K.-L. and Chopra, A.K., June 1985, (PB86 139672/AS)A10.

UCB/EERC-85/08 "Effect of Inelastic Behavior on the Analysis and Design of Earthquake Resistant Structures," by Lin, J.P. and Mahin, S.A., June 1985, (PB86 135340/AS)A08.

UCB/EERC-85/09 "Earthquake Simulator Testing of a Base-Isolated Bridge Deck," by Kelly, J.M., Buckle, I.G. and Tsai, H.-C., January 1986, (PB87 124 152/AS)A06.

UCB/EERC-85/10 "Simplified Analysis for Earthquake Resistant Design of Concrete Gravity Dams," by Fenves, G. and Chopra, A.K., June 1986, (PB87 124 160/AS)A08.

UCB/EERC-85/11 "Dynamic Interaction Effects in Arch Dams," by Clough, R.W., Chang, K.-T., Chen, H.-Q. and Ghanaat, Y., October 1985, (PB86 135027/AS)A05.

UCB/EERC-85/12 "Dynamic Response of Long Valley Dam in the Mammoth Lake Earthquake Series of May 25-27, 1980," by Lai, S. and Seed, H.B., November 1985, (PB86 142304/AS)A05.

UCB/EERC-85/13 "A Methodology for Computer-Aided Design of Earthquake-Resistant Steel Structures," by Austin, M.A., Pister, K.S. and Mahin, S.A., December 1985, (PB86 159480/AS)A10 .

UCB/EERC-85/14 "Response of Tension-Leg Platforms to Vertical Seismic Excitations," by Liou, G.-S., Penzien, J. and Yeung, R.W., December 1985, (PB87 124 871/AS)A08.

UCB/EERC-85/15 "Cyclic Loading Tests of Masonry Single Piers: Volume 4 - Additional Tests with Height to Width Ratio of 1," by Sveinsson, B., McNiven, H.D. and Sucuoglu, H., December 1985.

UCB/EERC-85/16 "An Experimental Program for Studying the Dynamic Response of a Steel Frame with a Variety of Infill Partitions," by Yanev, B. and McNiven, H.D., December 1985.

UCB/EERC-86/01 "A Study of Seismically Resistant Eccentrically Braced Steel Frame Systems," by Kasai, K. and Popov, E.P., January 1986, (PB87 124 178/AS)A14.

UCB/EERC-86/02 "Design Problems in Soil Liquefaction," by Seed, H.B., February 1986, (PB87 124 186/AS)A03.

UCB/EERC-86/03 "Implications of Recent Earthquakes and Research on Earthquake-Resistant Design and Construction of Buildings," by Bertero, V.V., March 1986, (PB87 124 194/AS)A05.

UCB/EERC-86/04 "The Use of Load Dependent Vectors for Dynamic and Earthquake Analyses," by Leger, P., Wilson, E.L. and Clough, R.W., March 1986, (PB87 124 202/AS)A12.

UCB/EERC-86/05 "Two Beam-To-Column Web Connections," by Tsai, K.-C. and Popov, E.P., April 1986, (PB87 124 301/AS)A04.

UCB/EERC-86/06 "Determination of Penetration Resistance for Coarse-Grained Soils using the Becker Hammer Drill," by Harder, L.F. and Seed, H.B., May 1986, (PB87 124 210/AS)A07.

UCB/EERC-86/07 "A Mathematical Model for Predicting the Nonlinear Response of Unreinforced Masonry Walls to In-Plane Earthquake Excitations," by Mengi, Y. and McNiven, H.D., May 1986, (PB87 124 780/AS)A06.

UCB/EERC-86/08 "The 19 September 1985 Mexico Earthquake: Building Behavior," by Bertero, V.V., July 1986.

UCB/EERC-86/09 "EACD-3D: A Computer Program for Three-Dimensional Earthquake Analysis of Concrete Dams," by Fok, K.-L., Hall, J.F. and Chopra, A.K., July 1986, (PB87 124 228/AS)A08.

UCB/EERC-86/10 "Earthquake Simulation Tests and Associated Studies of a 0.3-Scale Model of a Six-Story Concentrically Braced Steel Structure," by Uang, C.-M. and Bertero, V.V., December 1986, (PB87 163 564/AS)A17.

UCB/EERC-86/11 "Mechanical Characteristics of Base Isolation Bearings for a Bridge Deck Model Test," by Kelly, J.M., Buckle, I.G. and Koh, C.-G., November 1987.

UCB/EERC-86/12 "Effects of Axial Load on Elastomeric Isolation Bearings," by Koh, C.-G. and Kelly, J.M., November 1987.

UCB/EERC-87/01 "The FPS Earthquake Resisting System: Experimental Report," by Zayas, V.A., Low, S.S. and Mahin, S.A., June 1987.

UCB/EERC-87/02 "Earthquake Simulator Tests and Associated Studies of a 0.3-Scale Model of a Six-Story Eccentrically Braced Steel Structure," by Whittaker, A., Uang, C.-M. and Bertero, V.V., July 1987.

UCB/EERC-87/03 "A Displacement Control and Uplift Restraint Device for Base-Isolated Structures," by Kelly, J.M., Griffith, M.C. and Aiken, I.D., April 1987.

UCB/EERC-87/04 "Earthquake Simulator Testing of a Combined Sliding Bearing and Rubber Bearing Isolation System," by Kelly, J.M. and Chalhoub, M.S., 1987.

UCB/EERC-87/05 "Three-Dimensional Inelastic Analysis of Reinforced Concrete Frame-Wall Structures," by Moazzami, S. and Bertero, V.V., May 1987.

UCB/EERC-87/06 "Experiments on Eccentrically Braced Frames with Composite Floors," by Ricles, J. and Popov, E., June 1987.

UCB/EERC-87/07 "Dynamic Analysis of Seismically Resistant Eccentrically Braced Frames," by Ricles, J. and Popov, E., June 1987.

UCB/EERC-87/08 "Undrained Cyclic Triaxial Testing of Gravels-The Effect of Membrane Compliance," by Evans, M.D. and Seed, H.B., July 1987.

UCB/EERC-87/09 "Hybrid Solution Techniques for Generalized Pseudo-Dynamic Testing," by Thewalt, C. and Mahin, S.A., July 1987.

UCB/EERC-87/10 "Ultimate Behavior of Butt Welded Splices in Heavy Rolled Steel Sections," by Bruneau, M., Mahin, S.A. and Popov, E.P., July 1987.

UCB/EERC-87/11 "Residual Strength of Sand from Dam Failures in the Chilean Earthquake of March 3, 1985," by De Alba, P., Seed, H.B., Retamal, E. and Seed, R.B., September 1987.

UCB/EERC-87/12 "Inelastic Seismic Response of Structures with Mass or Stiffness Eccentricities in Plan," by Bruneau, M. and Mahin, S.A., September 1987.

UCB/EERC-87/13 "CSTRUCT: An Interactive Computer Environment for the Design and Analysis of Earthquake Resistant Steel Structures," by Austin, M.A., Mahin, S.A. and Pister, K.S., September 1987.

UCB/EERC-87/14 "Experimental Study of Reinforced Concrete Columns Subjected to Multi-Axial Loading," by Low, S.S. and Moehle, J.P., September 1987.

UCB/EERC-87/15 "Relationships between Soil Conditions and Earthquake Ground Motions in Mexico City in the Earthquake of Sept. 19, 1985," by Seed, H.B., Romo, M.P., Sun, J., Jaime, A. and Lysmer, J., October 1987.

UCB/EERC-87/16 "Experimental Study of Seismic Response of R. C. Setback Buildings," by Shahrooz, B.M. and Moehle, J.P., October 1987.

UCB/EERC-87/17 "The Effect of Slabs on the Flexural Behavior of Beams," by Pantazopoulou, S.J. and Moehle, J.P., October 1987.

UCB/EERC-87/18 "Design Procedure for R-FBI Bearings," by Mostaghel, N. and Kelly, J.M., November 1987.

UCB/EERC-87/19 "Analytical Models for Predicting the Lateral Response of R C Shear Walls: Evaluation of their Reliability," by Vulcano, A. and Bertero, V.V., November 1987.

UCB/EERC-87/20 "Earthquake Response of Torsionally-Coupled Buildings," by Hejal, R. and Chopra, A.K., December 1987.

UCB/EERC-87/21 "Dynamic Reservoir Interaction with Monticello Dam," by Clough, R.W., Ghanaat, Y. and Qiu, X-F., December 1987.

UCB/EERC-87/22 "Strength Evaluation of Coarse-Grained Soils," by Siddiqi, F.H., Seed, R.B., Chan, C.K., Seed, H.B. and Pyke, R.M., December 1987.

UCB/EERC-88/01 "Seismic Behavior of Concentrically Braced Steel Frames," by Khatib, I., Mahin, S.A. and Pister, K.S., January 1988.

UCB/EERC-88/02 "Experimental Evaluation of Seismic Isolation of Medium-Rise Structures Subject to Uplift," by Griffith, M.C., Kelly, J.M., Coveney, V.A. and Koh, C.G., January 1988.

UCB/EERC-88/03 "Cyclic Behavior of Steel Double Angle Connections," by Astaneh-Asl, A. and Nader, M.N., January 1988.

UCB/EERC-88/04 "Re-evaluation of the Slide in the Lower San Fernando Dam in the Earthquake of Feb. 9, 1971," by Seed, H.B., Seed, R.B., Harder, L.F. and Jong, H.-L., April 1988.

UCB/EERC-88/05 "Experimental Evaluation of Seismic Isolation of a Nine-Story Braced Steel Frame Subject to Uplift," by Griffith, M.C., Kelly, J.M. and Aiken, I.D., May 1988.

UCB/EERC-88/06 "DRAIN-2DX User Guide.," by Allahabadi, R. and Powell, G.H., March 1988.

UCB/EERC-88/07 "Cylindrical Fluid Containers in Base-Isolated Structures," by Chalhoub, M.S. and Kelly, J.M., April 1988.

UCB/EERC-88/08 "Analysis of Near-Source Waves: Separation of Wave Types using Strong Motion Array Recordings," by Darragh, R.B., June 1988.

UCB/EERC-88/09 "Alternatives to Standard Mode Superposition for Analysis of Non-Classically Damped Systems," by Kusainov, A.A. and Clough, R.W., June 1988.

UCB/EERC-88/10 "The Landslide at the Port of Nice on October 16, 1979," by Seed, H.B., Seed, R.B., Schlosser, F., Blondeau, F. and Juran, I., June 1988.

UCB/EERC-88/11 "Liquefaction Potential of Sand Deposits Under Low Levels of Excitation," by Carter, D.P. and Seed, H.B., August 1988.

UCB/EERC-88/12 "Nonlinear Analysis of Reinforced Concrete Frames Under Cyclic Load Reversals," by Filippou, F.C. and Issa, A., September 1988.

UCB/EERC-88/13 "Implications of Recorded Earthquake Ground Motions on Seismic Design of Building Structures," by Uang, C.-M. and Bertero, V.V., November 1988.

UCB/EERC-88/14 "An Experimental Study of the Behavior of Dual Steel Systems," by Whittaker, A.S., Uang, C.-M. and Bertero, V.V., September 1988.

UCB/EERC-88/15 "Dynamic Moduli and Damping Ratios for Cohesive Soils," by Sun, J.I., Golesorkhi, R. and Seed, H.B., August 1988.

UCB/EERC-88/16 "Reinforced Concrete Flat Plates Under Lateral Load: An Experimental Study Including Biaxial Effects," by Pan, A. and Moehle, J., October 1988.

UCB/EERC-88/17 "Earthquake Engineering Research at Berkeley - 1988," by EERC, November 1988.

UCB/EERC-88/18 "Use of Energy as a Design Criterion in Earthquake-Resistant Design," by Uang, C.-M. and Bertero, V.V., November 1988.

UCB/EERC-88/19 "Steel Beam-Column Joints in Seismic Moment Resisting Frames," by Tsai, K.-C. and Popov, E.P., November 1988.

UCB/EERC-88/20 "Base Isolation in Japan, 1988," by Kelly, J.M., December 1988.

UCB/EERC-89/01 "Behavior of Long Links in Eccentrically Braced Frames," by Engelhardt, M.D. and Popov, E.P., January 1989.

UCB/EERC-89/02 "Earthquake Simulator Testing of Steel Plate Added Damping and Stiffness Elements," by Whittaker, A., Bertero, V.V., Alonso, J. and Thompson, C., January 1989.

UCB/EERC-89/03 "Implications of Site Effects in the Mexico City Earthquake of Sept. 19, 1985 for Earthquake-Resistant Design Criteria in the San Francisco Bay Area of California," by Seed, H.B. and Sun, J.I., March 1989.

UCB/EERC-89/04 "Earthquake Analysis and Response of Intake-Outlet Towers," by Goyal, A. and Chopra, A.K., July 1989.

UCB/EERC-89/05 "The 1985 Chile Earthquake: An Evaluation of Structural Requirements for Bearing Wall Buildings," by Wallace, J.W. and Moehle, J.P., July 1989.

UCB/EERC-89/06 "Effects of Spatial Variation of Ground Motions on Large Multiply-Supported Structures," by Hao, H., July 1989.

UCB/EERC-89/07 "EADAP - Enhanced Arch Dam Analysis Program: User's Manual," by Ghanaat, Y. and Clough, R.W., August 1989.

UCB/EERC-89/08 "Seismic Performance of Steel Moment Frames Plastically Designed by Least Squares Stress Fields," by Ohi, K. and Mahin, S.A., August 1989.

UCB/EERC-89/09 "Feasibility and Performance Studies on Improving the Earthquake Resistance of New and Existing Buildings Using the Friction Pendulum System," by Zayas, V., Low, S., Mahin, S.A. and Bozzo, L., July 1989.

UCB/EERC-89/10 "Measurement and Elimination of Membrane Compliance Effects in Undrained Triaxial Testing," by Nicholson, P.G., Seed, R.B. and Anwar, H., September 1989.

UCB/EERC-89/11 "Static Tilt Behavior of Unanchored Cylindrical Tanks," by Lau, D.T. and Clough, R.W., September 1989.

UCB/EERC-89/12 "ADAP-88: A Computer Program for Nonlinear Earthquake Analysis of Concrete Arch Dams," by Fenves, G.L., Mojtahedi, S. and Reimer, R.B., September 1989.

UCB/EERC-89/13 "Mechanics of Low Shape Factor Elastomeric Seismic Isolation Bearings," by Aiken, I.D., Kelly, J.M. and Tajirian, F., December 1989.

UCB/EERC-89/14 "Preliminary Report on the Seismological and Engineering Aspects of the October 17, 1989 Santa Cruz (Loma Prieta) Earthquake," by EERC, October 1989.

UCB/EERC-89/15 "Experimental Studies of a Single Story Steel Structure Tested with Fixed, Semi-Rigid and Flexible Connections," by Nader, M.N. and Astaneh-Asl, A., August 1989.

UCB/EERC-89/16 "Collapse of the Cypress Street Viaduct as a Result of the Loma Prieta Earthquake," by Nims, D.K., Miranda, E., Aiken, I.D., Whittaker, A.S. and Bertero, V.V., November 1989.

UCB/EERC-90/01 "Mechanics of High-Shape Factor Elastomeric Seismic Isolation Bearings," by Kelly, J.M., Aiken, I.D. and Tajirian, F.F., March 1990.

UCB/EERC-90/02 "Javid's Paradox: The Influence of Preform on the Modes of Vibrating Beams," by Kelly, J.M., Sackman, J.L. and Javid, A., May 1990.

UCB/EERC-90/03 "Earthquake Simulator Tests of Viscoelastic Dampers for Medium Rise Structures," by Kelly, J.M. and Aiken, I.D., May 1990.

UCB/EERC-90/04 "Damage to the San Francisco-Oakland Bay Bridge During the October 17, 1989 Earthquake," by Astaneh, A., June 1990.

UCB/EERC-90/05 "Preliminary Report on the Principal Geotechnical Aspects of the October 17, 1989 Loma Prieta Earthquake," by Seed, R.B., Dickenson, S.E., Riemer, M.F., Bray, J.D., Sitar, N., Mitchell, J.K., Idriss, I.M., Kayen, R.E., Kroop, A., Harder, L.F., Jr. and Power, M.S., April 1990.

UCB/EERC-90/06 "Models of Critical Regions in Reinforced Concrete Frames Under Seismic Excitations," by Zulfiqar, N. and Filippou, F., May 1990.

UCB/EERC-90/07 "A Unified Earthquake-Resistant Design Method for Steel Frames Using ARMA Models," by Takewaki, I., Conte, J.P., Mahin, S.A. and Pister, K.S., June 1990.

UCB/EERC-90/08 "Soil Conditions and Earthquake Hazard Mitigation in the Marina District of San Francisco," by Mitchell, J.K., Masood, T., Kayen, R.E. and Seed, R.B., May 1990.

UCB/EERC-90/09 "Influence of the Earthquake Ground Motion Process and Structural Properties on Response Characteristics of Simple Structures," by Conte, J.P., Pister, K.S. and Mahin, S.A., July 1990.

UCB/EERC-90/10 "Experimental Testing of the Resilient-Friction Base Isolation Sytsem," by Clark, P.W. and Kelly, J.M., July 1990.

UCB/EERC-90/11 "Seismic Hazard Analysis: Improved Models, Uncertainties and Sensitivities," by Araya, R. and Der Kiureghian, A., March 1988.

UCB/EERC-90/12 "Effects of Torsion on the Linear and Nonlinear Seismic Response of Structures," by Sedarat, H. and Bertero, V.V., September 1989.

UCB/EERC-90/13 "The Effects of Tectonic Movements on Stresses and Deformations in Earth Embankments," by Bray, J. D., Seed, R. B. and Seed, H. B., September 1989.